

2016

Source Mechanism Analysis of Single-Well Microseismic Data Using Full-Wavefield Moment Tensor Inversion

Trudy Watkins

Louisiana State University and Agricultural and Mechanical College

Follow this and additional works at: https://digitalcommons.lsu.edu/gradschool_theses



Part of the [Earth Sciences Commons](#)

Recommended Citation

Watkins, Trudy, "Source Mechanism Analysis of Single-Well Microseismic Data Using Full-Wavefield Moment Tensor Inversion" (2016). *LSU Master's Theses*. 4582.

https://digitalcommons.lsu.edu/gradschool_theses/4582

This Thesis is brought to you for free and open access by the Graduate School at LSU Digital Commons. It has been accepted for inclusion in LSU Master's Theses by an authorized graduate school editor of LSU Digital Commons. For more information, please contact gradetd@lsu.edu.

SOURCE MECHANISM ANALYSIS OF SINGLE-WELL MICROSEISMIC DATA
USING FULL-WAVEFIELD MOMENT TENSOR INVERSION

A Thesis

Submitted to the Graduate Faculty of the
Louisiana State University and
Agricultural and Mechanical College
in partial fulfillment of the
requirements for the degree of
Master of Science

in

The Department of Geology and Geophysics

by
Trudy Lynn Watkins
B.S. Texas Tech University, 2014
May 2017

Acknowledgements

I would like to thank my research advisor, Dr. Juan Lorenzo, and my committee members Dr. Arash Dahi Taleghani and Dr. Karen Luttrell for their guidance. I would also like to give thanks to Joel Le Calvez of Schlumberger for providing the microseismic data for this thesis.

Thank you to past and present members of Dr. Lorenzo's research group including Abigail Maxwell, Marital Morrison, Abah Omale, Ruhollah Keshvardoost, and Derek Goff for their encouragement.

Thank you to the Department of Geology and Geophysics at LSU for providing a teaching assistantship for two years of my Master's degree.

And finally, thank you to my parents, for their continued support throughout my graduate studies.

Table of Contents

Acknowledgements	ii
Abstract	iv
Chapter 1: Introduction	1
1.1 Problem and Objectives	1
1.2 Microseismic Monitoring	3
1.3 Moment Tensors.....	5
1.4 Moment Tensor Inversion	11
1.5 Characteristics of Microseismic Events Occurring During Hydraulic Fracturing	14
1.6 Microseismic Data Acquisition	15
Chapter 2: Methods.....	22
2.1 Synthetic Seismogram Calculation	22
2.2 Moment Tensor Inversion	26
2.3 Microseismic Data Processing and Analysis.....	29
Chapter 3: Results	42
3.1 Full-Wavefield Moment Tensor Inversion of Synthetic Seismograms	42
3.2 Microseismic Event Characteristics	50
Chapter 4: Discussion	58
4.1 Receiver Angular Coverage of Source	58
4.2 Deviatoric Constraint.....	59
4.3 Neglect of Anisotropy in Moment Tensor Inversion.....	59
Chapter 5: Conclusions.....	61
5.1 Recommendations	62
5.2 Future Work	62
References	64
Appendix A: Processing Workflows and Programs	70
Appendix B: Data Tables and Plots.....	267
Appendix C: Full-Wavefield Moment Tensor Inversion Results.....	280
Vita.....	445

Abstract

Receiver angular coverage of microseismic sources occurring during hydraulic fracturing treatments is an important factor to consider when interpreting moment tensor inversion results. A horizontal receiver array can provide greater angular coverage of vertical failure planes than a vertical receiver array. The source orientation can be accurately determined if the array samples both sides of the failure plane. However, the compensated-linear-vector-dipole (CLVD) mechanism can be overestimated by up to $\sim 40\%$ for double-couple (DC) sources and the isotropic mechanism can be overestimated by $\sim 70\%$ for CLVD sources. Source mechanism constraints on the moment tensor inversion are used to mitigate the lack of angular coverage. The use of the deviatoric assumption decreases the error in the source mechanism to $\sim 70\%$ for DC sources and $\sim 50\%$ for CLVD sources however this introduces an error of $\sim 55^\circ$ in the strike of the CLVD source. Moment tensor inversion programs typically assume isotropic velocity models however rocks can have anisotropic seismic velocities. Inversion of sources occurring in anisotropic media but assuming an isotropic velocity model in the inversion results in source orientations with errors $< 15^\circ$ and up to 80% error in the resolved source mechanism.

Chapter 1: Introduction

1.1 Problem and Objectives

The results retrieved from moment tensor inversion of a single vertical array of receivers are inaccurate in the determination of the source mechanism components and source orientation because of the lack of angular coverage of the event (Eaton & Forouhdeh, 2011; Vavryčuk, 2007). Not accounting for anisotropy in the inversion can lead to overestimation of tensile mechanisms and misorientation of the fault plane solution (Sileny & Vavryčuk, 2002; Vavryčuk, 2005). Moment tensor inversions typically only consider the far-field terms and have source constraints applied to compensate for the lack of angular coverage (Vavryčuk, 2007; Warpinski & Du, 2010). Full-wavefield moment tensor inversion, which includes the intermediate- and near-field terms, is used to increase the accuracy of the inversion results for microseismic data with small source-receiver distances (Song & Toksoz, 2011). This thesis aims to answer the following questions:

1. Can accurate source mechanisms be resolved from a single horizontal array of receivers using full-wavefield moment tensor inversion?
2. How does the angular coverage of an event affect the accuracy of the inversion?
3. How does the isotropic velocity model affect the results of the inversion for sources generated in an anisotropic medium?

Horizontal receiver arrays can provide better angular coverage than vertical receiver arrays if they sample the seismic field on both sides of the vertical failure plane of a

hydraulic fracture. The proximity of horizontal arrays to the microseismic events provides small source-receiver distances in which the intermediate- and near-field terms could prove useful in the moment tensor inversion. We expect to see that with increasing angular coverage, there is less error in the moment tensor solution.

Moment tensor inversions are typically used with isotropic velocity models, however, hydraulic fracturing treatments are completed in shaly formations that have anisotropic velocities (Warpinski et al., 2009). An accurate velocity model is necessary to retrieve an accurate result from moment tensor inversion (Jechumtálová & Bulant, 2013). Studying how the isotropic velocity model in the moment tensor inversion affects the results of sources generated in an anisotropic medium increases our understanding of the method and contributes to our interpretation of the results. We expect that the neglect of anisotropy in the moment tensor inversion will introduce errors into the event location and estimated mechanism percentages because of the inaccurate velocity model.

A microseismic data set is provided by Schlumberger for a hydraulic fracturing treatment near a known fault zone in the Barnett Shale. To simulate the field environment of hydraulic fracturing treatments, I use this microseismic data as the reference for the source-receiver geometry and seismic velocities in the study of full-wavefield moment tensor inversion.

1.1.1 Significance

The goal of hydraulic fracturing treatments is to increase the permeability of the reservoir by creating pathways (i.e. fractures) for hydrocarbons to flow from the reservoir to the well (Eisner et al., 2006; Maxwell & Norton, 2012). Identification of microseismic source mechanisms with opening failure types occurring during the treatment contributes to the evaluation of the effectiveness of the treatment (Urbancic et al., 2009; van der Baan et al., 2013).

By locating the origin of multiple microseismic events, a “cloud” of events identifies the extent of fracture growth and orientation (Downie et al., 2010). The size of these clouds estimates the fracture height and length and indicates the extent of the stimulated reservoir volume (van der Baan et al., 2013). The extent of fracture growth aids in the analysis of the efficiency of the treatment by determining if fractures are extending beyond the targeted zone of hydrocarbons (Eisner et al., 2006).

1.2 Microseismic Monitoring

Microseismic monitoring is the process of placing seismic sensors either on (surface arrays) or below (downhole arrays) the Earth’s surface to measure ground movement during a hydraulic fracturing treatment (Clarkson, 2011; Maxwell, 2014). As fluid is pumped into the formation and the hydraulic fractures grow, the rock failure releases energy detected as a microseismic event at the receivers (Figure 1.1a).

During downhole monitoring, receivers are placed on a tool string in a monitoring well near the treatment well (Figure 1.1a). Although the downhole environment is less noisy than the surface environment, the distance between available vertical wells and the microseismic events can result in microseismic monitoring with large source-receiver distances (> 1 km) and limited angular coverage of the events (Maxwell, 2014, pp. 32-40). Surface arrays can be used to have greater angular coverage, but there is a lower signal-to-noise ratio and events at depth are harder to detect (Figure 1.1b) (Duncan & Lakings, 2006; Maxwell, 2014, pp. 32-40).

The receivers used in microseismic monitoring usually consist of three-components (3-C), meaning they detect ground movement in three directions at right angles to each other (i.e. XYZ) (Eisner et al., 2010; Maxwell, 2014, p. 43). 3-C receivers are important for sampling the wavefield from multiple directions and are required for moment tensor inversion.

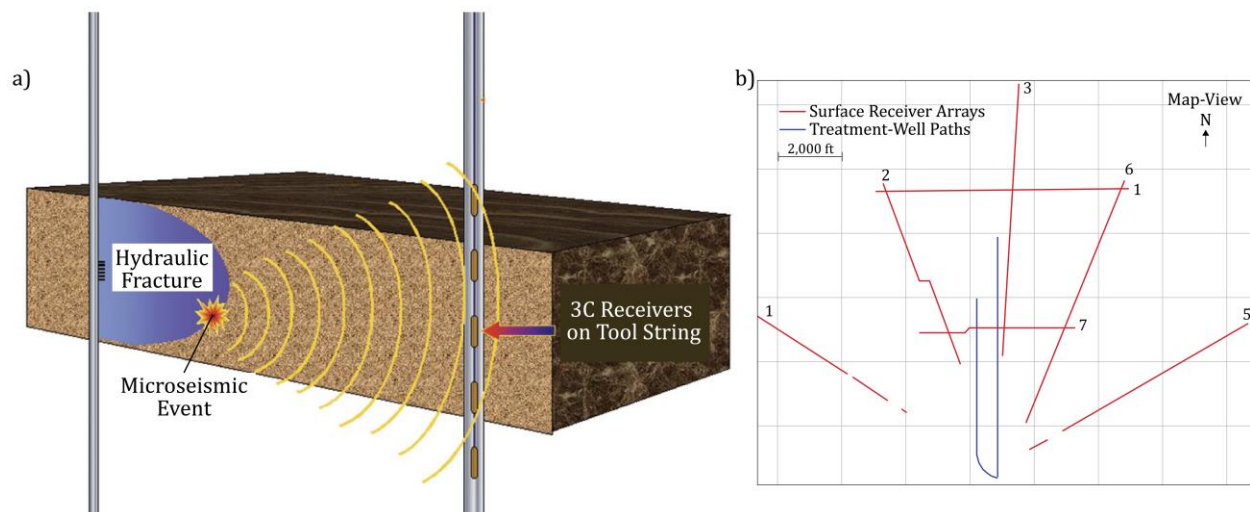


Figure 1.1: a) Microseismic monitoring can be done using vertical wells (monitoring wells) to monitor hydraulic fracture growth in a second nearby vertical well (treatment well) (adapted from Clarkson (2011)). b) Surface arrays of receivers can also be used to monitor hydraulic fracturing treatments (adapted from Drew et al. (2012)).

1.3 Moment Tensors

A moment tensor (M) is the mathematical representation of the orientation of the fault plane and the type of failure (tensile and/or shearing) at the origin of an earthquake (Baig & Urbancic, 2010). The displacement u detected by a seismic receiver is a function of M and the Green's function G (Earth model)

$$u_n(x, t) = M_{pq} * G_{np,q} \quad (1.1)$$

where n is the n th component of displacement and p and q represent the coupled forces acting along the q -axis in the p direction (Figure 1.2) (Aki & Richards, 2002, p. 77; Jost & Hermann, 1989). M is written as the matrix

$$M = \begin{bmatrix} M_{xx} & M_{xy} & M_{xz} \\ M_{yx} & M_{yy} & M_{yz} \\ M_{zx} & M_{zy} & M_{zz} \end{bmatrix} \quad (1.2)$$

and is symmetric ($M_{xy} = M_{yx}$, $M_{xz} = M_{zx}$, and $M_{yz} = M_{zy}$) (Figure 1.2) in order to conserve angular momentum (Forouhideh & Eaton, 2009).

Moment tensors can imply three types of failure mechanisms: double-couple (DC), compensated-linear-vector-dipole (CLVD), and isotropic (ISO). These mechanisms are visually represented on “beach-ball” diagrams, which are lower-hemisphere stereographic projections that represent the directions of motion at the source. The fault plane orientation (strike, dip, and rake) is interpreted from the beach-ball diagram (Figure 1.3) (Warpinski & Du, 2010). Sources can be interpreted as purely DC, CLVD, or ISO or they can

be considered as a combination of the three failure mechanisms with different percentages of strength (i.e. 25% DC, 50% CLVD, 25% ISO).

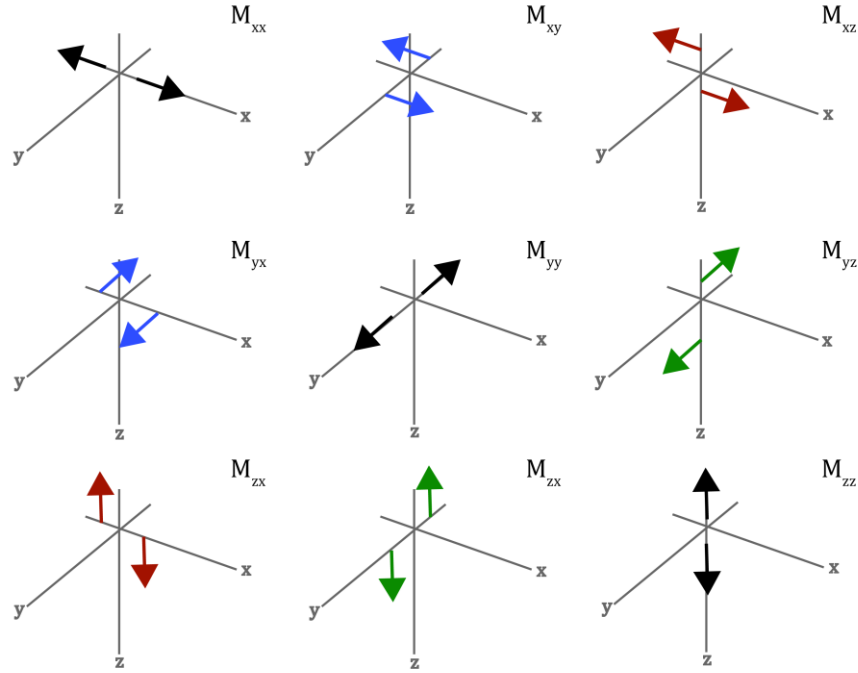


Figure 1.2: Moment tensor M represents the nine double-couples of force acting at a source (adapted from Jost and Hermann (1989)). Because M is symmetric, $M_{xy}=M_{yx}$ (blue), $M_{xz}=M_{zx}$ (red), and $M_{yz}=M_{zy}$ (green) (Forouhdeh & Eaton, 2009). The double-couple forces along the diagonal of M (M_{xx} , M_{yy} , and M_{zz} , black) represent a volumetric change at the source (Stein & Wyssession, 2003, p. 245).

The DC component represents shearing at the source such as fault slip. Shearing can occur as strike-slip (in direction of strike) or dip-slip (in direction of dip) movement (Stein & Wyssession, 2003, pp. 242-244). The radiation pattern of the DC source is symmetric about the origin of the source (Figure 1.3). The plane perpendicular to the fault plane is called the auxiliary plane (i.e., the W-E line in the beach-ball diagram for the DC source in Figure 1.3) (Bormann et al., 2013, p. 59). The CLVD component indicates crack opening or closing (Baig & Urbancic, 2010; Stein & Wyssession, 2003, p. 245). The third component is the ISO

component that represents volumetric change. A positive ISO component is an explosive event whereas a negative ISO component is an implosive event (Baig & Urbancic, 2010).

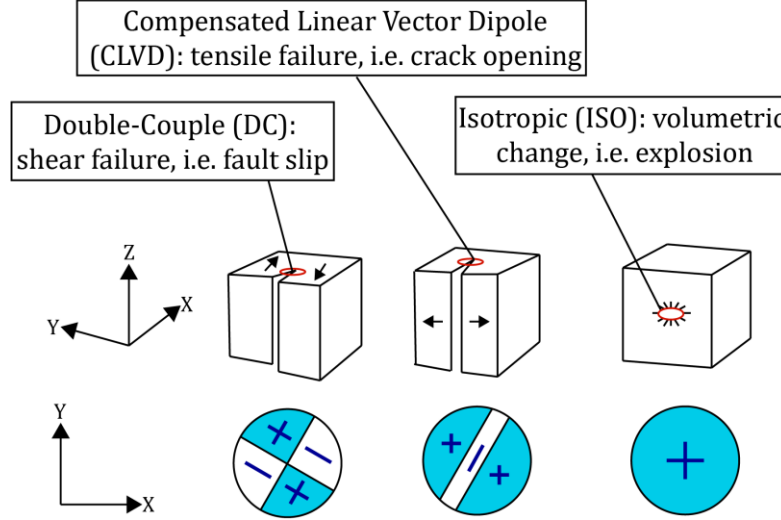


Figure 1.3: Failure mechanisms are represented on beach-ball diagrams (adapted from Baig and Urbancic (2010)). These diagrams indicate the directions in which the medium surrounding the source is moving such that the shaded (blue) areas of the beach-balls (+) represent the surrounding material moving away from the source whereas the non-shaded (white) areas (-) represent the surrounding material moving inward towards the origin of the source.

To interpret the DC, CLVD, and ISO mechanisms from moment tensors, the tensors are decomposed mathematically into an ISO tensor (M_{ISO}) and a deviatoric tensor (M_{DEV}), with M_{DEV} consisting of the DC and CLVD components

$$M = M_{ISO} + M_{DEV} \quad (1.3)$$

$$M_{ISO} = \frac{1}{3} tr(M) \begin{bmatrix} 1 & 0 & 0 \\ 0 & 1 & 0 \\ 0 & 0 & 1 \end{bmatrix} \quad (1.4)$$

where $tr(M)$ is the trace of the original moment tensor (M) (Vavryčuk, 2015). This isotropic tensor represents the volumetric change of the source because it only consists of the double-couple forces along the diagonal of M (Figure 1.2) (Dahm & Krüger, 2014, p. 5). If

the trace of M is zero, such as for pure DC sources, then the strength of the ISO mechanism of the source is zero.

The orientation and relative percentages of the DC and CLVD mechanisms of the source are determined from M_{DEV} . The eigenvector of M_{DEV} with the maximum eigenvalue represents the minimum compressional (\vec{T}) axis of the source mechanism whereas the eigenvector of M_{DEV} with the minimum eigenvalue represents the maximum compressional (\vec{P}) axis of the source mechanism (Song & Toksoz, 2011; Stein & Wysession, 2003, pp. 226-227) The \vec{T} and \vec{P} axes are related to the source orientation by

$$\vec{u} = \frac{1}{\sqrt{2}}(\vec{T} + \vec{P}) \text{ and } \vec{v} = \frac{1}{\sqrt{2}}(\vec{T} - \vec{P}) \quad (1.5)$$

where \vec{u} is the slip vector and \vec{v} is the fault plane normal (Jost & Hermann, 1989). We determine the strike ϕ , dip δ , and rake λ of the source using

$$\vec{u} = \begin{pmatrix} \cos \lambda \cos \phi + \sin \lambda \cos \delta \sin \phi \\ -\cos \lambda \sin \phi + \cos \lambda \cos \delta \cos \phi \\ \sin \lambda \sin \delta \end{pmatrix} \text{ and } \vec{v} = \begin{pmatrix} -\sin \delta \sin \phi \\ -\sin \delta \cos \phi \\ \cos \delta \end{pmatrix} \quad (1.6)$$

(Figure 1.4) (Stein & Wysession, 2003, p. 228).

Lastly, the ratio of the CLVD component relative to the DC component is represented by the parameter ε and calculated from

$$\varepsilon = -\frac{e_{|min|}}{|e_{|max|}|} \quad (1.7)$$

where $e_{|min|}$ and $e_{|max|}$ are the minimum and maximum absolute eigenvalues of M_{DEV} , respectively (Song & Toksoz, 2011; Vavryčuk, 2001).

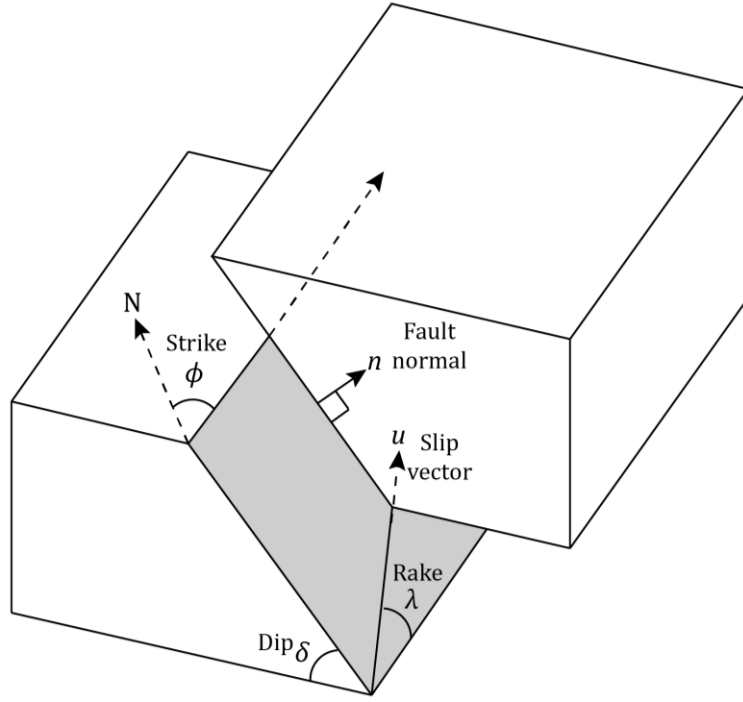








Figure 1.4: Block diagram depicting fault plane terminology (adapted from Song et al. (2014)).

The moment tensor from Eqn. (1.2) can be written as a combination of the six basic moment tensors with

$$M = \begin{bmatrix} -a_5 + a_6 & a_1 & -a_3 \\ a_1 & -a_4 + a_6 & a_2 \\ -a_3 & a_2 & a_4 + a_5 + a_6 \end{bmatrix} \quad (1.8)$$

where a_n is the n th basic moment tensor (Table 1.1) (Warpinski & Du, 2010). All possible moment tensors can be written as this combination of the six basic moment tensors (Sokos & Zahradnik, 2009).

Table 1.1: The six basic moment tensors represent the six basic focal mechanisms identified by their strike, dip, rake, and source mechanism (Sokos & Zahradnik, 2008; Warpinski & Du, 2010). The last column shows the visual representation (beach-ball diagram) of these focal mechanisms (Warpinski & Du, 2010). All possible moment tensors can be written as a combination of these six basic moment tensors (Sokos & Zahradnik, 2008).

Tensor	Focal Mechanism				Beach-ball
	Source Orientation			Source Mechanism	
	Strike	Dip	Rake		
$a_1 = \begin{bmatrix} 0 & 1 & 0 \\ 1 & 0 & 0 \\ 0 & 0 & 0 \end{bmatrix}$	0°	90°	0°	DC (strike-slip)	
$a_2 = \begin{bmatrix} 0 & 0 & 1 \\ 0 & 0 & 0 \\ 1 & 0 & 0 \end{bmatrix}$	90°	90°	-90°	DC (dip-slip)	
$a_3 = \begin{bmatrix} 0 & 0 & 0 \\ 0 & 0 & -1 \\ 0 & -1 & 0 \end{bmatrix}$	0°	90°	90°	DC (dip-slip)	
$a_4 = \begin{bmatrix} -1 & 0 & 0 \\ 0 & 0 & 0 \\ 0 & 0 & 1 \end{bmatrix}$	90°	45°	90°	DC (dip-slip)	
$a_5 = \begin{bmatrix} 0 & 0 & 0 \\ 0 & -1 & 0 \\ 0 & 0 & 1 \end{bmatrix}$	0°	45°	90°	DC (dip-slip)	
$a_6 = \begin{bmatrix} 1 & 0 & 0 \\ 0 & 1 & 0 \\ 0 & 0 & 1 \end{bmatrix}$	--	--	--	ISO	

1.4 Moment Tensor Inversion

Moment tensor inversion solves for M in Eqn. (1.1) using input displacement data (u) from seismic receivers and information (i.e. seismic velocities) about the Earth model (G). The inversion problem is a least-squares fit of the minimization of the difference (Δ) between the input data (u_j) and synthetic seismograms ($a_n G_{jn}$):

$$\Delta = \sum_{j=1}^{N_s} \int \left[u_j(t) - \sum_{n=1}^6 a_n G_{jn}(t) \right]^2 \quad (1.9)$$

where j is the j th receiver, N_s is the number of receivers, and a_n denotes the n th elementary seismogram representing the n th basic moment tensor (Table 1.1) (Kikuchi & Kanamori, 1991; Sokos & Zahradnik, 2008). The moment tensor is calculated with the six best-fit values of a_n using Eqn. (1.8).

Moment tensor inversions are commonly used with only isotropic assumptions, however many geologic formations have anisotropic velocities (Thomsen, 1986). Shale is a vertically transverse isotropic (VTI) medium in which hydraulic fracturing is commonly completed in because of its low permeability (Maxwell & Norton, 2012). In VTI media, the seismic velocities vary vertically as a function of the angle between the vertical axis and the direction of wave propagation (Ikelle & Amundsen, 2005, pp. 530-533; Thomsen, 1986). When inverting events with waveforms generated in anisotropic media but assuming isotropy, the error in the resolved source orientation is low ($< 20^\circ$), however, the CLVD and ISO components are overestimated for pure-DC sources (Sileny & Vavryčuk, 2002).

1.4.1 Full-Wavefield Displacement

If we expand the formula for the Green's function G in Eqn. (1.1), the displacement u at receiver n at time t for an infinite, homogenous, and isotropic medium is

$$\begin{aligned}
 u_n(x, t) = M_{pq} * G_{np,q} = & \left(\frac{15\gamma_n\gamma_p\gamma_q - 3\gamma_n\delta_{pq} - 3\gamma_p\delta_{nq} - 3\gamma_q\delta_{np}}{4\pi\rho} \right) \frac{1}{r^4} \int_{r/\alpha}^{r/\beta} \tau M_{pq}(t - \tau) d\tau \\
 & + \left(\frac{6\gamma_n\gamma_p\gamma_q - \gamma_n\delta_{pq} - \gamma_p\delta_{nq} - \gamma_q\delta_{np}}{4\pi\rho\alpha^2} \right) \frac{1}{r^2} M_{pq} \left(t - \frac{r}{\alpha} \right) \\
 & - \left(\frac{6\gamma_n\gamma_p\gamma_q - \gamma_n\delta_{pq} - \gamma_p\delta_{nq} - 2\gamma_q\delta_{np}}{4\pi\rho\beta^2} \right) \frac{1}{r^2} M_{pq} \left(t - \frac{r}{\beta} \right) \\
 & + \frac{\gamma_n\gamma_p\gamma_q}{4\pi\rho\alpha^3} \frac{1}{r} \dot{M}_{pq} \left(t - \frac{r}{\alpha} \right) - \left(\frac{\gamma_n\gamma_p - \delta_{np}}{4\pi\rho\beta^3} \right) \gamma_q \frac{1}{r} \dot{M}_{pq} \left(t - \frac{r}{\beta} \right)
 \end{aligned} \tag{1.10}$$

where

$\gamma_k =$ k th direction cosine between source and receiver

$\delta_{ab} = \begin{cases} 0 & \text{if } a \neq b \\ 1 & \text{if } a = b \end{cases}$ (Kronecker delta)

$\rho =$ Density of medium

$r =$ Source-receiver distance

$\alpha =$ P-wave velocity of medium

$\beta =$ S-wave velocity of medium

$M_{pq} =$ Moment tensor (Aki & Richards, 2002, p. 77).

The first term represents the amplitudes of the near-field that decays at r^{-4} and has no distinguishable P- and S- wave arrivals (Aki & Richards, 2002, p. 74). The second and third terms represent the intermediate-field amplitudes separated into P- and S-wave terms and

decay at r^{-2} . The final two terms represent the far-field amplitudes with distinguishable P- and S-wave terms. The far-field amplitudes are what is most observed in earthquake data with large source-receiver distances (> 1 km) because of the low attenuation of r^{-1} (Aki & Richards, 2002, p. 73). The intermediate- and near-field amplitudes are most apparent for source-receiver distances less than five times the S-wave wavelength because the amplitudes have not yet attenuated to negligible values (Figure 1.5) (Song & Toksoz, 2011). Beyond this range, the far-field amplitudes dominate, however the intermediate- and near-field amplitudes can contribute ~ 5 -20% of the total wavefield.

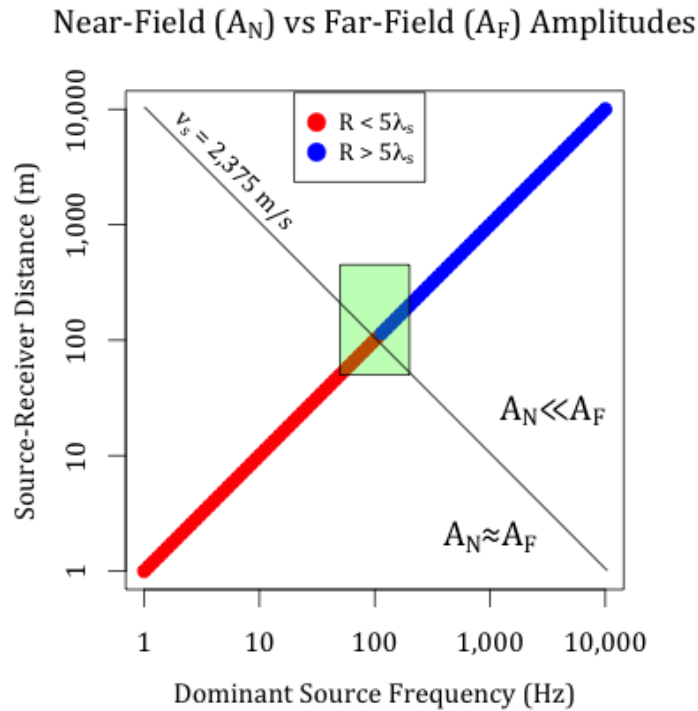


Figure 1.5: Plot of frequency versus source-receiver distance (R) for a medium with shear-wave velocity of 2,375 m/s (derived from shear sonic logs for target formation of this study) (Ichinose et al., 2000; Song & Toksoz, 2011). The green box highlights the range of frequencies (50-200 Hz) and source-receiver distances (50-450 m) studied in this thesis. The red points are where R is less than five times the S-wave wavelength ($5\lambda_s$) and the blue points are where R is greater than $5\lambda_s$ (Song & Toksoz, 2011).

Microseismic events with a vertical array of receivers in the near-field of the source can be inverted for an accurate solution using full-wavefield moment tensor inversion (Song & Toksoz, 2011). Events with larger source-receiver distances, where the source-receiver distance is greater than five times the S-wave wavelength, are inverted by applying constraints to the inversion, such as limiting the ranges of strike and dip or assuming a 0% ISO source (Song & Toksoz, 2011). Constraints reduce the number of variables that are being solved for, but can increase the error in the results, such as overestimation of the shearing mechanism when assuming a pure shear source for an event that contains tensile mechanisms (Vavryčuk, 2007).

1.5 Characteristics of Microseismic Events Occurring During Hydraulic Fracturing

Microseismic events associated with hydraulic fracturing commonly contain high frequencies (> 100 Hz), are of low magnitudes (< -1.5), and are expected to have tensile source mechanisms (Figure 1.6) (Downie et al., 2010; Eaton et al., 2013; Urbancic et al., 2009). These events occur near the treatment well during initial fracture propagation and are oriented in the present-day direction of the maximum horizontal stress (S_{HMAX}) in which hydraulic fractures propagate (Cuenot et al., 2006; Jones & Britt, 2009, p. 4; Urbancic et al., 2009).

Events containing lower frequencies (< 80 Hz) and of higher magnitudes (> -1.5) can occur with DC source mechanisms not striking in the direction of S_{HMAX} (Figure 1.6) (Das & Zoback, 2011; Song et al., 2014; Urbancic et al., 2009). The source of shear failure is interpreted as slippage along natural discontinuities (i.e., faults or natural fractures)

resulting from interaction with hydraulic fractures (Baig & Urbancic, 2010; Downie et al., 2010).

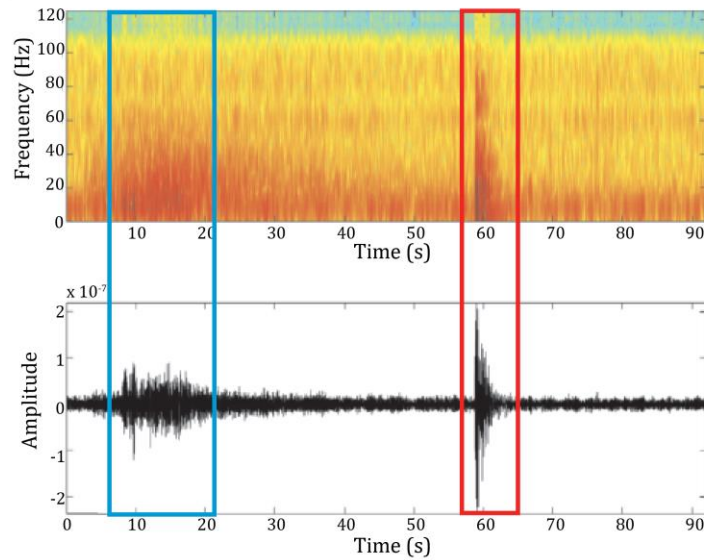


Figure 1.6: Microseismic events with frequencies > 100 Hz (within red rectangle) are what is most commonly observed in hydraulic fracturing treatments (adapted from Eaton et al. (2013)). Lower frequency (within blue rectangle) events are also observed (Eaton et al., 2013).

1.6 Microseismic Data Acquisition

Three horizontal wells approximately 850 m in length and 150 m apart from each other were drilled, perforated, and treated in northeast Texas (Figure 1.8). The treatment was divided into thirteen stages. Each stage represented a reservoir interval (~ 100 m in length) along the wellbore where fluid was being pumped into the formation (Schlumberger, 2016). Four stages were completed in wells 1H and 2H and five stages were completed in well 3H. With the exception of three stages, each stage was perforated with eight perforations in each stage (Table 1.2, Figure 1.7).

Table 1.2: Perforations were spaced every 15.24 m (50 ft) with a density of 1 shot per 6 cm (5 shots per foot, 5 shots total) at each perforation location. Refer to Figure 1.7 for diagram and description of each parameter.

Spacing	15.24 m (50 ft)
Density	1 shot per 6.1 cm (5 shots per foot)
Phasing Angle	60°
Diameter	1.12 cm (0.44 in)
Penetration	79.76 cm (31.4 in)

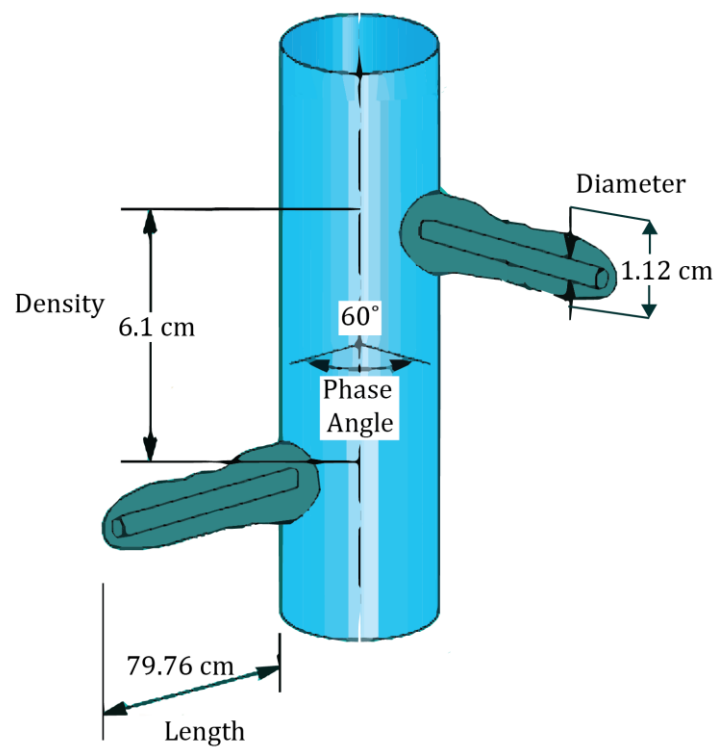


Figure 1.7: Diagram of perforation geometry (adapted from Cosad (1992)). The perforation density is 1 shot per 6.1 cm (5 shots per foot) so that each shot is 6.1 cm (2.4 in) apart. Five shots were fired at each perforation location. The phase angle is the angle between charges on the perforation gun (60°) and the perforation penetration is the length that the charge penetrates into the formation (79.76 cm or 31.4 in) (Schlumberger, 2016). The diameter is the width of the perforation charge.

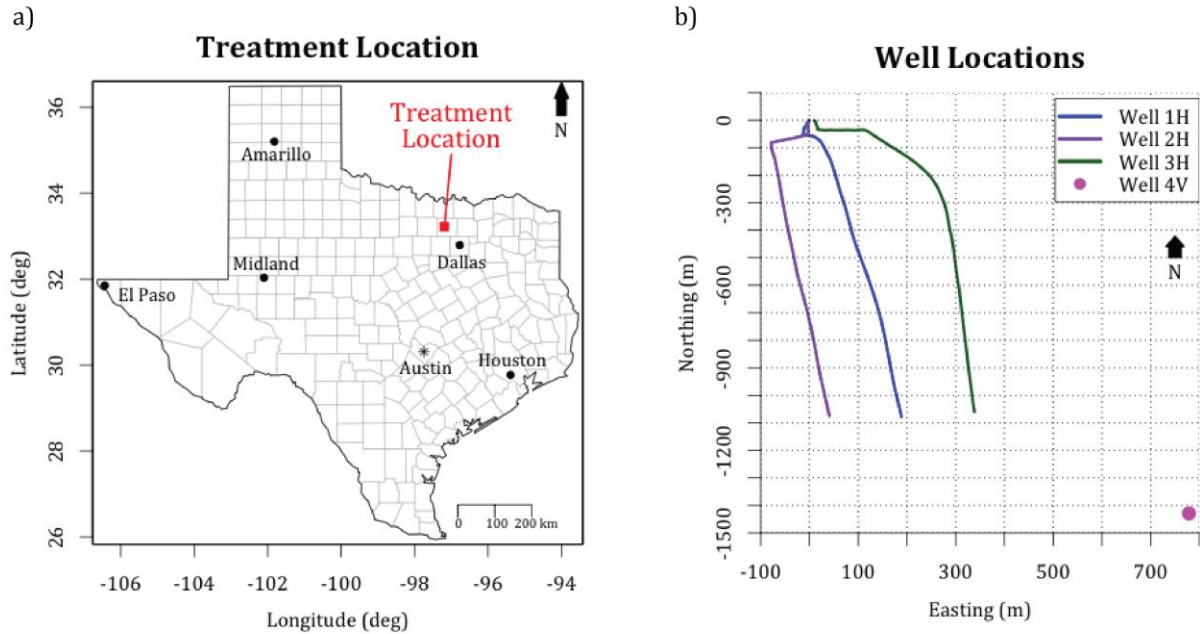


Figure 1.8: a) Map of Texas indicating the location of the hydraulic fracturing treatment in northeast Texas. b) Map view of the horizontal well paths and the location of the vertical well from which compressional and shear sonic logs were collected (Figure 1.9). The reference point of 0,0 is the XY surface location well 1H.

Eight 3-C geophones were placed in well 2H to monitor the perforation and treatment of wells 1H and 3H (Figure 1.10, Table 1.3). After treatment of wells 1H and 3H, the geophones were moved to well 3H to monitor the perforation and treatment of well 2H (Figure 1.11). Compressional-wave and shear-wave sonic logs were collected from the vertical well 4V with a surface location approximately 1,500 m from the surface location of well 1H (Figures 1.8b and 1.9).

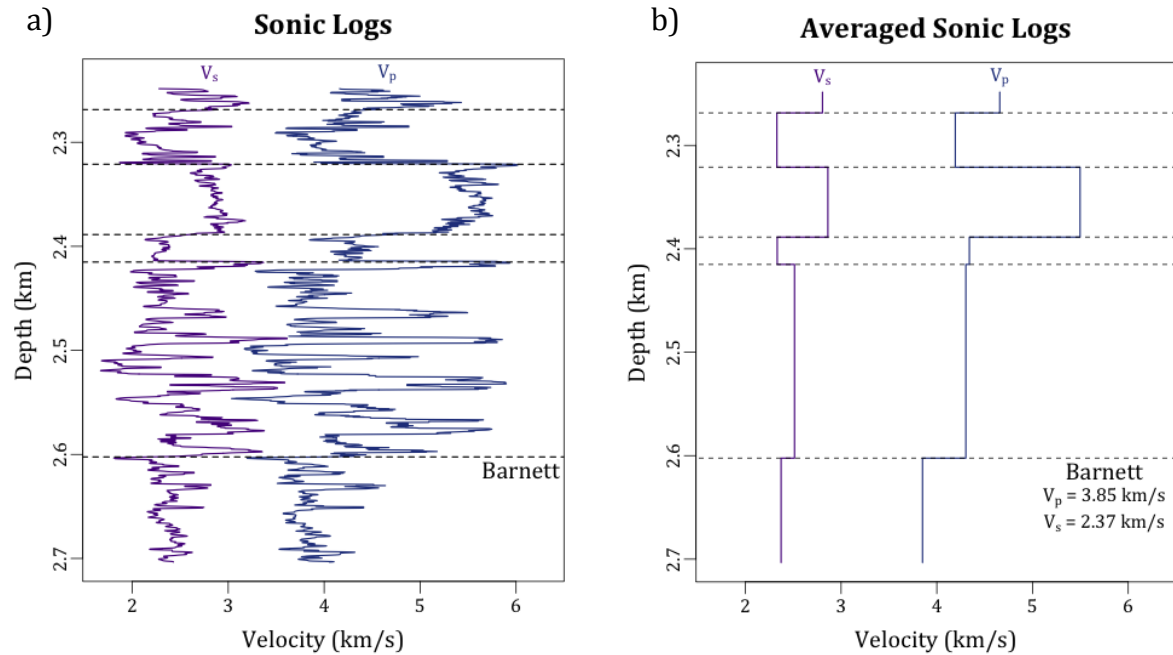


Figure 1.9: a) Compressional- (V_p) and shear-wave (V_s) sonic logs from the vertical well 4V. The sonic data is separated into six layers of depth such that each layer has similar log characteristics to determine the average velocities in each layer. b) Average velocities in each of the six layers. The Barnett Shale is the deepest layer and has an average V_p of 3.85 km/s and an average V_s of 2.37 km/s.

Table 1.3: Table of the seismic sensors, their spacing in the wellbore, and their sample interval used for collection of the microseismic data.

Seismic Sensors	Accelerometers
Sensor Spacing	30.48 m (100 ft)
Sample Interval	0.001 seconds

Well Paths - Map View

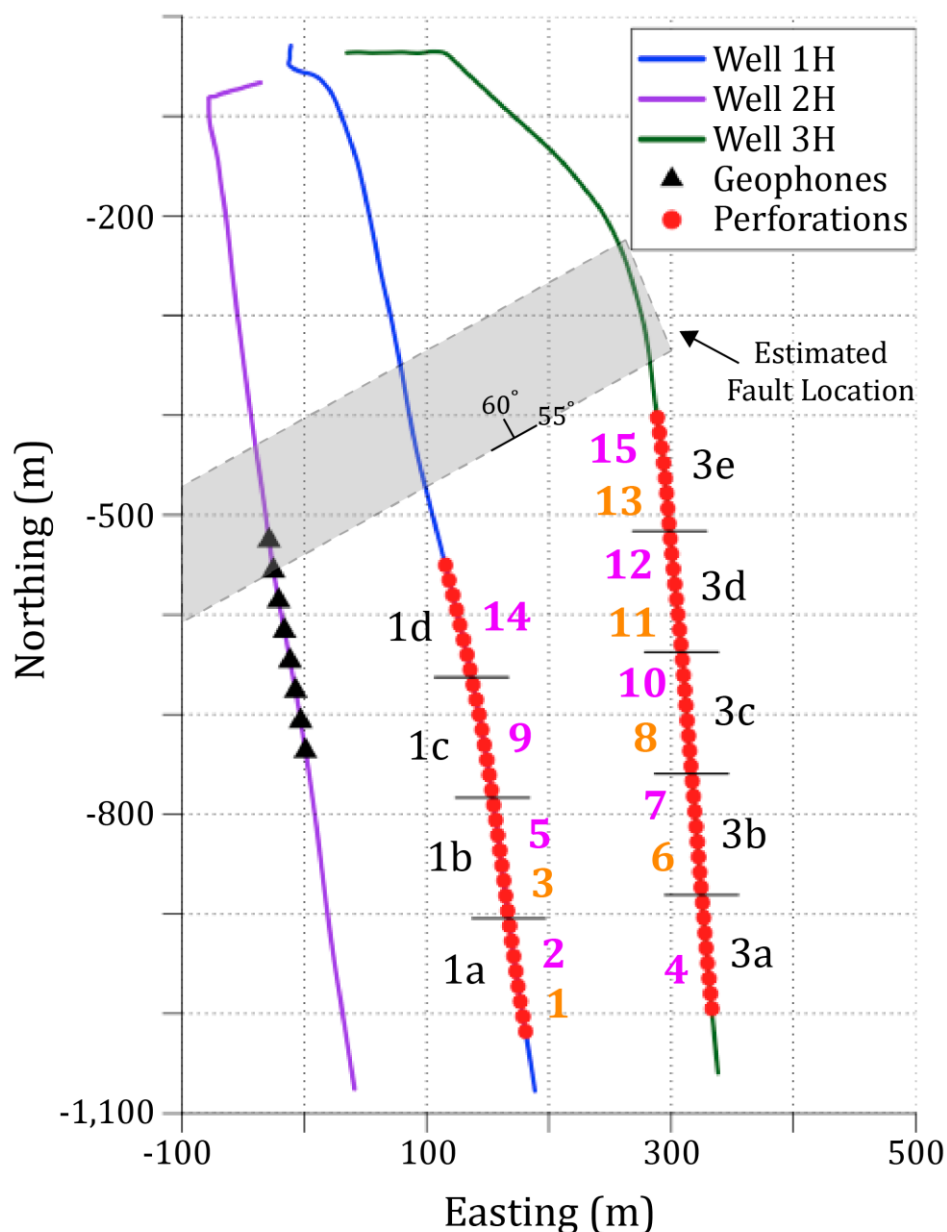


Figure 1.10: Map view of well paths and locations of geophones in monitoring-well 2H and planned perforation locations for each stage for treatment-wells 1H and 3H. The black text labels indicate the treatment-well (1 or 3) and stage (a, b, etc.). The numbers in orange (perforation) and purple (treatment) indicate the order in which the perforations and treatment were completed, i.e. first stage 1a was perforated, then 1a was treated, then 1b was perforated, etc. The reference point of 0,0 is the XY surface location of well 1H. The gray box is the estimated location of a fault in this area.

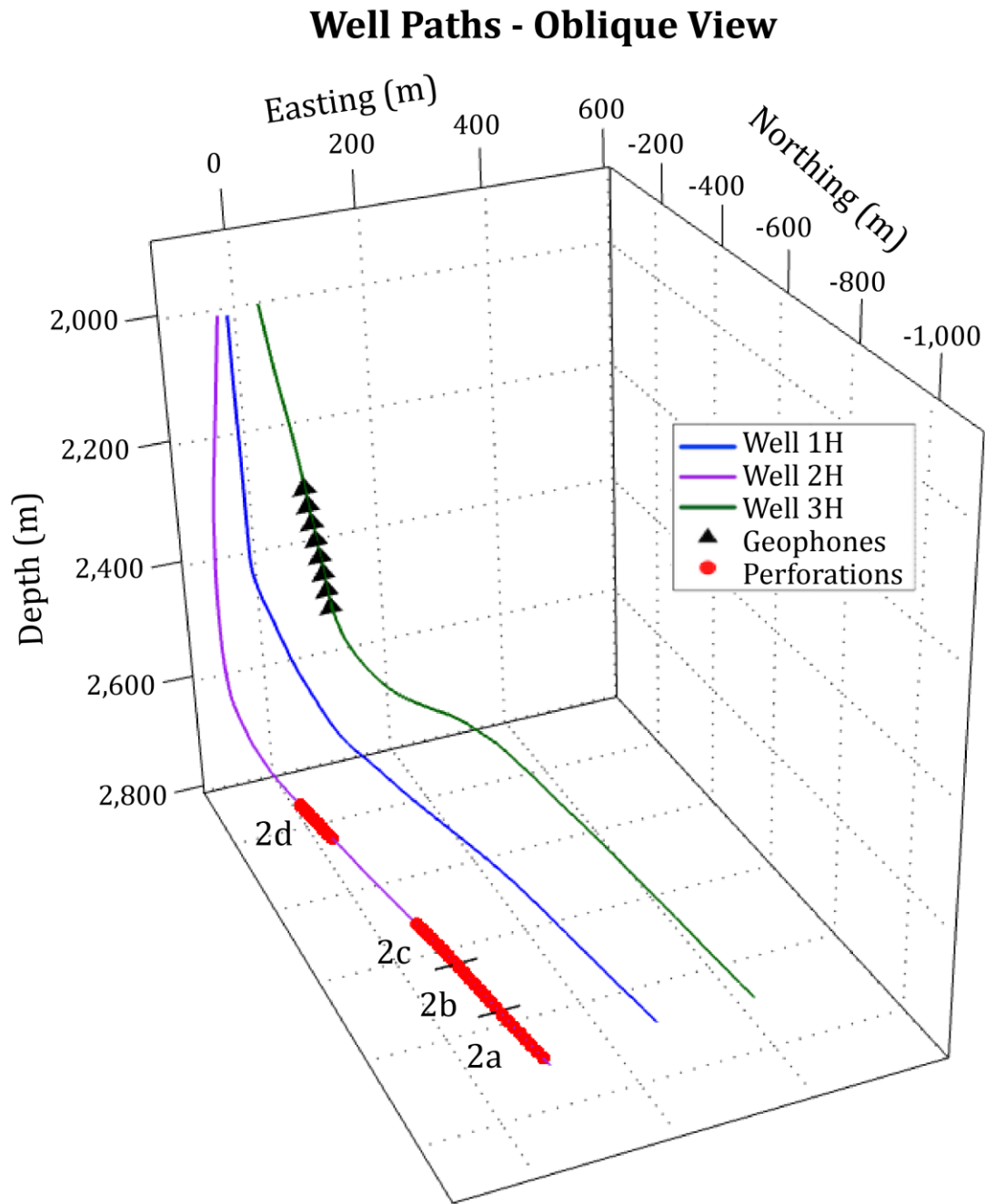


Figure 1.11: Oblique view of well paths with locations of geophones, perforations, and stages for treatment of well 2H. The black text labels indicate the treatment-well (2) and stage (a, b, etc.). Each stage was perforated and treated before moving on to the next stage, i.e. stage 2a was perforated and treated, then stage 2b was perforated and treated, etc. The reference point of 0,0,0 is the XY surface location of well 1H.

1.6.1 Barnett Shale Characteristics

The Barnett Shale is a laminated Mississippian-aged deposit located in the Fort Worth Basin (FWB) in northeast Texas. The FWB has a NE-SW pattern of normal faulting (Figures 1.10 & 1.12) (Pollastro et al., 2007). The present day S_{HMAX} in the FWB is oriented ENE-WSW, which is the orientation of open drilling-induced fractures and hydraulic fractures (Figure 1.12) (Gale et al., 2007). Two sets of calcite-filled natural fractures are present in the Barnett Shale that are not aligned with the S_{HMAX} (Gale et al., 2007). The natural fractures can be reopened during hydraulic fracturing treatments and contribute to the overall fracture network because of the weak contact between the calcite and shale (Gale et al., 2007).

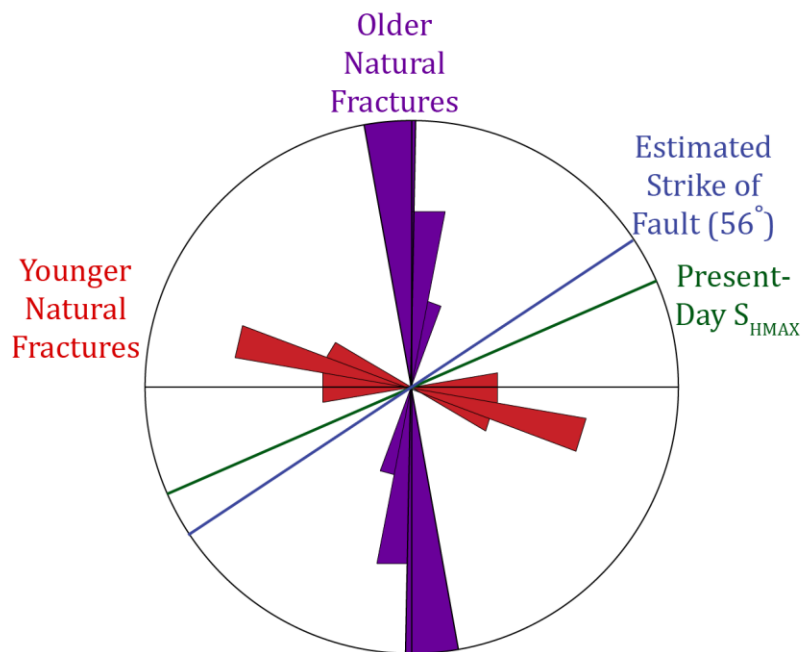


Figure 1.12: The orientation of open fractures is aligned with the present-day S_{HMAX} (green) (adapted from Gale et al. (2007)). The estimated strike of the fault in the treatment area for this thesis is NW-SE (blue). There are two observable sets of calcite-filled natural fractures: an older set oriented N-S (purple) that are cross-cut by a younger set oriented WNW-ESE (orange) (Gale et al., 2007). As indicated by the rose diagram, the older set is more abundant (Gale et al., 2007).

Chapter 2: Methods

2.1 Synthetic Seismogram Calculation

I use synthetic seismograms as the input earthquake data for moment tensor inversion. Synthetic seismograms provide the ideal scenario of noise-free data and I can compare the input parameters of the source to the output results to determine the possible causes of error in the moment tensor inversion. I calculate synthetic seismograms of body waves (P- and S-waves) from Eqn. (1.10) (Aki & Richards, 2002, p. 77) using the program `cartmomtens.m` (Appendix A) with inputs of the source-receiver geometry, seismic velocities, dominant source frequency, and moment tensor.

I consider five scenarios to understand how angular coverage affects the results of full-wavefield moment tensor inversion:

- 1) isotropic medium with dominant source frequency of 125 Hz
- 2) anisotropic (5% VTI) medium with dominant source frequency of 125 Hz
- 3) isotropic medium with dominant source frequency of 125 Hz and 5% random Gaussian noise added to the seismograms
- 4) isotropic medium with dominant source frequency of 50 Hz
- 5) isotropic medium with dominant source frequency of 175 Hz.

The source-time function $s(t)$ is a Ricker wavelet calculated as

$$s(t) = (1 - 2\pi^2 f^2 t^2) e^{-\pi^2 f^2 t^2} \quad (2.1)$$

where f is the peak frequency (Ryan, 1994). The Ricker wavelet is commonly used for synthetic seismogram calculations because it is zero-phase and has only one input frequency which allows for a simple calculation (Ryan, 1994).

The Thomsen parameters ε and γ incorporate VTI anisotropy into the synthetic seismogram calculation. ε and γ represent the variation in the P-wave and S-wave velocities, respectively, by

$$\varepsilon = \gamma = \frac{1 + p_a}{2} \quad (2.2)$$

where p_a is the percent anisotropy of the medium (Ikelle & Amundsen, 2005, pp. 530-533; Thomsen, 1986). Anisotropy is the directional variation of properties of the medium; i.e. in VTI media the seismic velocities are symmetric about the vertical axis and vary as a function of the angle (β) between the direction of wave propagation and the vertical axis:

$$V_p(\beta) = V_{p0}(1 + \varepsilon \sin^4 \beta) \quad (2.3)$$

$$V_s(\beta) = V_{s0}(1 + \gamma \sin^2 \beta) \quad (2.4)$$

where V_{p0} and V_{s0} are the vertical P-wave and S-wave velocities, respectively (Ikelle & Amundsen, 2005, pp. 530-533; Thomsen, 1986).

2.1.1 Input Parameters

All of the input parameters for the synthetic seismogram calculation are selected to resemble inputs for the real field case of the microseismic data presented in section 1.6 (Table 2.1). The source-receiver geometry is of a horizontal array of eight receivers and

three test locations (Figure 2.1a). The three test locations have varying angular coverage and source-receiver distance: 1) 1b has the lowest angular coverage (14°) and smallest average source-receiver distance (~ 300 m), 2) 3d has greater angular coverage (27°) and a larger source-receiver distance (~ 325 m) than 1b, and 3) 3d has the greatest angular coverage (32°) and the largest source-receiver distance (~ 355 m) (Figure 2.1b). Location 1b with the smallest source-receiver distance has the greatest contribution of intermediate- and near-field terms ($\sim 8\%$) to the total amplitude.

I use one pure (100%) DC source, one pure CLVD source, and one pure ISO source in each test case to study the resolvability of the source components for different mechanisms. The DC and CLVD sources have an orientation consistent with the orientation in which vertical fractures open in the Barnett Shale during hydraulic fracturing (Gale et al., 2007) (presented in section 1.6.1, Figure 1.12).

The isotropic velocity model uses the seismic velocities in the Barnett layer of the sonic logs (presented in section 1.6, Figure 1.9). I use a one-layer velocity model and assume the sources and receivers are in the same layer to study the moment tensor inversion results with the simplest velocity model. The anisotropic case has a 5% VTI velocity model, in which the horizontal and vertical seismic velocities differ by up to 5%, to represent the low degree of anisotropy of the Barnett Shale (Song et al., 2014). To study the neglect of anisotropy in the moment tensor inversion, the synthetic seismogram calculation utilizes this anisotropic velocity model and the moment tensor inversion assumes an isotropic velocity model.

This anisotropic velocity model is utilized in the synthetic seismogram calculation and an isotropic velocity

Three of the test cases have a dominant source frequency of 125 Hz because microseismic events occurring during hydraulic fracturing treatments have dominant source frequencies between 100 and 150 Hz (Eaton et al., 2013). I use two other dominant source frequencies of 50 Hz and 175 Hz to determine if events containing lower frequencies are more resolvable than events containing higher frequencies because events containing lower frequencies have less attenuated intermediate- and near-field amplitudes.

Table 2.1: Table of input parameters for synthetic seismogram calculation.

Property	Input Value(s)	
P-wave Velocity	3,850 m/s	
S-wave Velocity	2,375 m/s	
VTI Anisotropy	5%	
Source Frequency	50, 125, 175 Hz	
Source Orientation	Strike	66°
	Dip	90°
	Rake	0°
Source Mechanisms	100% DC	
	100% CLVD	
	100% ISO	
Noise Level	5%	

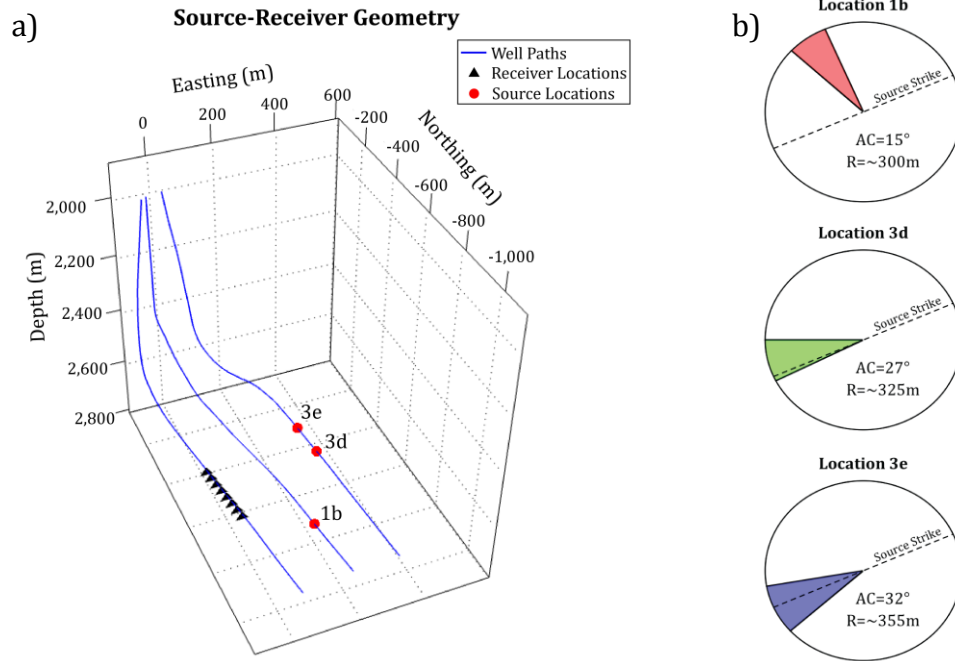


Figure 2.1: a) Oblique 3D view of source-receiver geometry used to calculate synthetic seismograms. There are eight receivers (black triangles) in a horizontal array approximately 300 m west of two of the test event locations (red circles): 3d and 3e. The third tested event location is at 1b. The origin 0,0,0 is the surface location of the middle well. b) Pie charts showing receiver angular coverage of events at locations 1b (top), 3d (middle), and 3e (bottom).

2.2 Moment Tensor Inversion

The computational method of moment tensor inversion is the standard method for determining the source parameters of an earthquake from data recorded at a seismic receiver (Cronin, 2010). ISOLA is a free and open-source moment tensor inversion program that utilizes the full-wavefield in the Green's function and has a user interface (Sokos & Zahradnik, 2009).

2.2.1 ISOLA

ISOLA (ISOLated Asperities) is a moment tensor inversion program written in MATLAB and Fortran 77 that simultaneously searches for the source location and mechanism of a

seismic event (Sokos & Zahradnik, 2008). Other moment tensor inversion software assume pure shear sources associated with large-scale earthquakes and only solve for the orientation of the failure plane whereas ISOLA allows moment tensors to contain non-DC mechanisms (Hardebeck & Shearer, 2008; Sokos & Zahradnik, 2009).

The inputs for ISOLA are velocity seismograms, a one-dimensional (1-D) isotropic velocity model, station coordinates, estimated source coordinates, an estimated origin time, and the approximate frequency content of the event (Figure 2.2) (Sokos & Zahradnik, 2009). ISOLA converts the velocity seismograms into displacement for the moment tensor inversion. The velocity model, source and receiver coordinates, and event frequencies are the inputs for the Green's function calculation.

ISOLA convolves the Green's function with the six basic focal mechanisms to calculate elementary seismograms for the inversion. ISOLA then performs a grid search for a range of input source locations and origin times to find the best correlation as the measure of fit between the input data seismograms and varied combinations of the elementary seismograms (Figure 2.2).

The source location, origin time, and moment tensor with the least difference (greatest correlation) between the input and synthetic seismograms are the final output result from the inversion, along with other properties calculated from the moment tensor (Table 2.2) (Sokos & Zahradnik, 2009).

There are two types of source mechanism constraints available in ISOLA: the deviatoric constraint and the DC constraint (Sokos & Zahradnik, 2008). The deviatoric constraint assumes that the strength of the ISO mechanism of the source is 0% whereas the DC constraint assumes that the sources is 100% DC. To determine the source mechanism using the DC constraint, ISOLA first inverts the seismograms using the deviatoric constraint (Sokos & Zahradnik, 2008). ISOLA then iteratively calculates the minimization while maximizing the DC percentage (Sokos & Zahradnik, 2008). If no solution with a DC percentage greater than 90% and a good correlation to the input data is found within five iterations, the original deviatoric result is outputted (Sokos & Zahradnik, 2008).

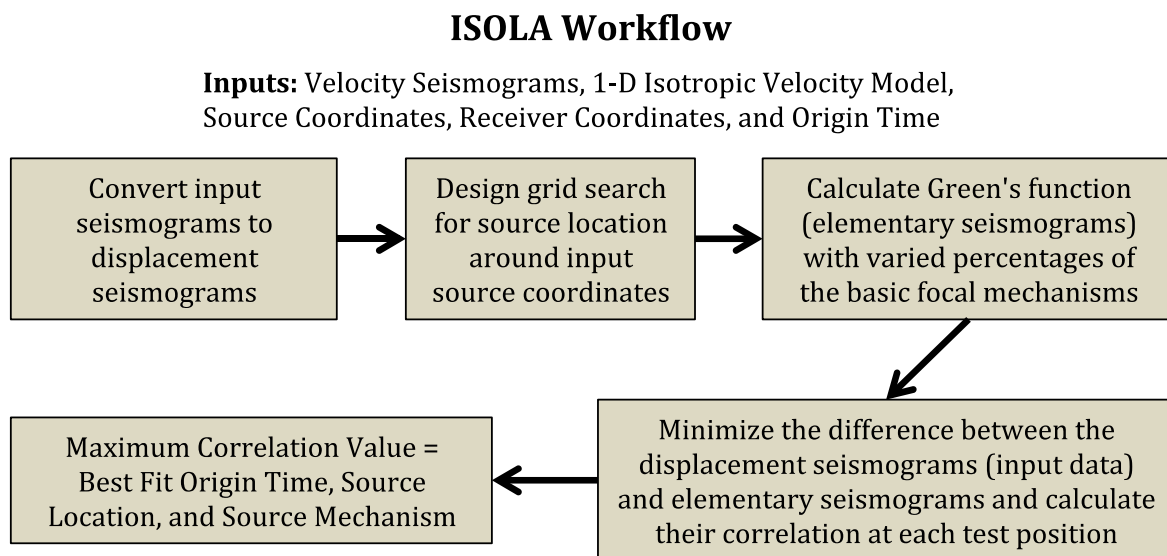


Figure 2.2: Simplified description of the steps for how the ISOLA program inverts for the source mechanism and what inputs are required (Sokos & Zahradnik, 2008).

Table 2.2: Summary of the outputs of ISOLA listed with their definitions (Jost & Hermann, 1989; Sokos & Zahradnik, 2009).

Source Property	Definition
Source location	Latitude ($^{\circ}$), longitude ($^{\circ}$), and depth (km) of source
Origin time	Time of event occurrence (s)
Moment tensor	Matrix representation of focal mechanism
Scalar moment (M_0)	Released seismic energy (N·m)
Mechanism percentages (C_{DC} , C_{CLVD} , C_{ISO})	Percentages of DC, CLVD, and ISO (%)
Orientation	Strike ($^{\circ}$), dip ($^{\circ}$), rake ($^{\circ}$)
P-axis orientation	Direction of maximum compressive motion
T-axis orientation	Direction of minimum compressive (tensile) motion

2.3 Microseismic Data Processing and Analysis

2.3.1 Geophone Reorientation

Each geophone has three sensors that are orthogonal in a right-handed system, but the geophones are not oriented in a common coordinate system. To determine the event location, I first rotate the data at each geophone into the East-North-Up (ENU) coordinate system using the perforation events as calibration points for principal component analysis (PCA).

Particle motion of seismic waves originating from an earthquake source follows the trajectory of a hodograph that can be modeled as the shape of an ellipsoid (Maercklin, 2007). PCA uses the covariance matrix of 3-C seismic data to define this ellipsoid representing the orientation of particle motion (Maercklin, 2007). The largest eigenvalue of this covariance matrix corresponds to the principal axis in which the wave is propagating (Maercklin, 2007). The azimuth ϕ and dip θ of the principal axis identify the direction of

maximum energy detected at the geophone, which corresponds to the direction from which a seismic P-wave is originating (source location) (Figure 2.7) (Maercklin, 2007). For a source with a known location, the azimuth α and dip β between the source and geophone are known. The geophones are reoriented with three Euler angles (E_1, E_2, E_3) in three rotation matrices (R_1, R_2, R_3):

$$E_1 = -\phi \quad E_2 = -(\beta + \theta) \quad E_3 = \alpha \quad (2.5)$$

and

$$R_1 = \begin{bmatrix} \cos E_1 & \sin E_1 & 0 \\ -\sin E_1 & \cos E_1 & 0 \\ 0 & 0 & 1 \end{bmatrix} \quad R_2 = \begin{bmatrix} \cos E_2 & 0 & -\sin E_2 \\ 0 & 1 & 0 \\ \sin E_2 & 0 & \cos E_2 \end{bmatrix} \quad (2.6)$$

$$R_3 = \begin{bmatrix} \cos E_3 & \sin E_3 & 0 \\ -\sin E_3 & \cos E_3 & 0 \\ 0 & 0 & 1 \end{bmatrix}$$

to get

$$\begin{bmatrix} x \\ y \\ z \end{bmatrix} [R_1][R_2][R_3] = \begin{bmatrix} x' \\ y' \\ z' \end{bmatrix} \quad (2.7)$$

where x, y , and z are the original data and x', y' , and z' are the rotated data (Figures 2.3-2.6) (Ikelle & Amundsen, 2005, p. 28).

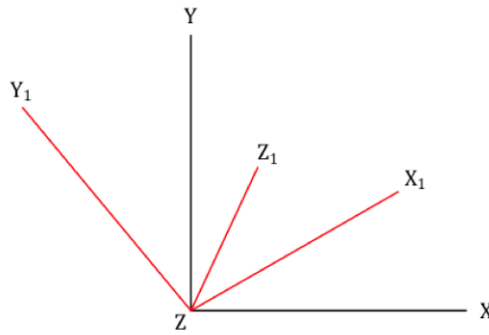


Figure 2.3: Diagram of the axes X_1, Y_1, Z_1 (red) of a randomly oriented 3-C geophone. The goal is to rotate the data using the matrices R_1, R_2 , and R_3 to align the red axes with the black axes ($XYZ=ENZ$). Doing this for each geophone orients all of the microseismic data into a common coordinate system.

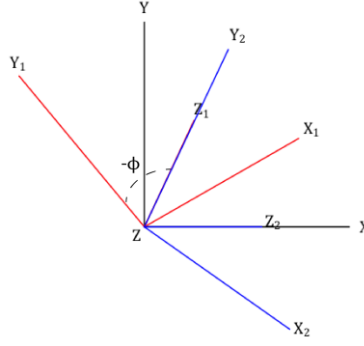


Figure 2.4: Diagram of geophone axes X_2, Y_2, Z_2 (blue) down the Z axis after the first rotation R_1 of the starting randomly oriented axes X_1, Y_1, Z_1 (red). The first rotation is of $-\phi$ about the Z axis (Eqns. (2.5)-(2.6)).

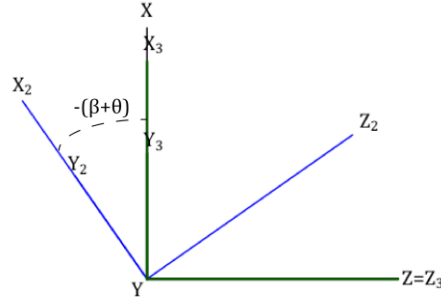


Figure 2.5: Diagram of geophone axes X_3, Y_3, Z_3 (green) down the Y axis after the second rotation R_2 of the X_2, Y_2, Z_2 (blue) axes. The second rotation is $-(\beta+\theta)$ about the Y axis, which aligns the Z_3 axis with the Z axis (Eqns. (2.5)-(2.6)).

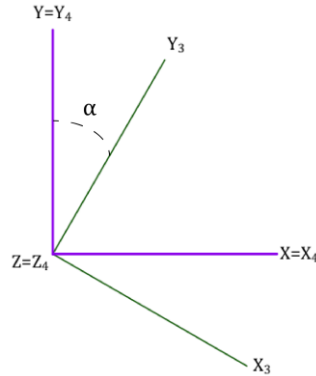


Figure 2.6: Diagram of geophone axes X_4, Y_4, Z_4 (purple) down the Z axis after the third rotation R_3 of the X_3, Y_3, Z_3 (green) axes. The third and final rotation is of angle α about the Z axis which aligns the X_4 and Y_4 axes with the X and Y axes, respectively (Eqns. (2.5)-(2.6)).

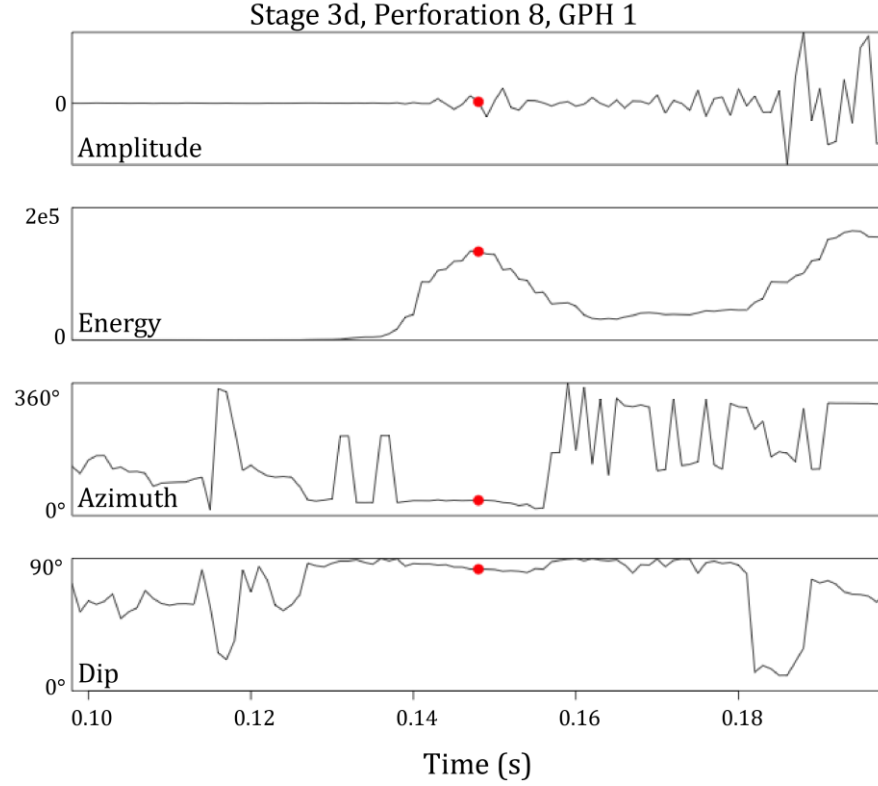


Figure 2.7: Example of the seismogram (top) and PCA results at geophone 1 for perforation 8 of stage 3d. The red circle is the time of the maximum energy (second row) at the P-wave arrival. The azimuth ϕ (third row) and dip θ (bottom row) at the time of the maximum energy (red dot) are used for rotating the microseismic data in Eqns. (2.5)-(2.7). This step is completed at each geophones for each perforation to reorient the microseismic data into the ENU coordinate system.

I rotate the microseismic data for each geophone at each stage with the average Euler angles of that particular geophone and stage to account for possible anomalies in the PCA results for a particular perforation. I use PCA again after the data are rotated to get a new azimuth ϕ and dip θ . The absolute difference between this azimuth ϕ and dip θ and the known azimuth α and dip β is averaged for each geophone for each stage and assigned as the error (Figure 2.8) (Table B.1, Appendix B). If the error is greater than 15 degrees for either azimuth or dip, I do not use the geophone for further data analysis for that stage so that further error is not carried over to the calculation of the event location. I carry out PCA

using the program ReorientGphs.R (Appendix A) (Callahan et al., 2015; Mirai Solutions GmbH, 2015) and *supolar* in the free SeismicUn*x package (Stockwell & Cohen, 2014).

Geophone Reorientation Workflow

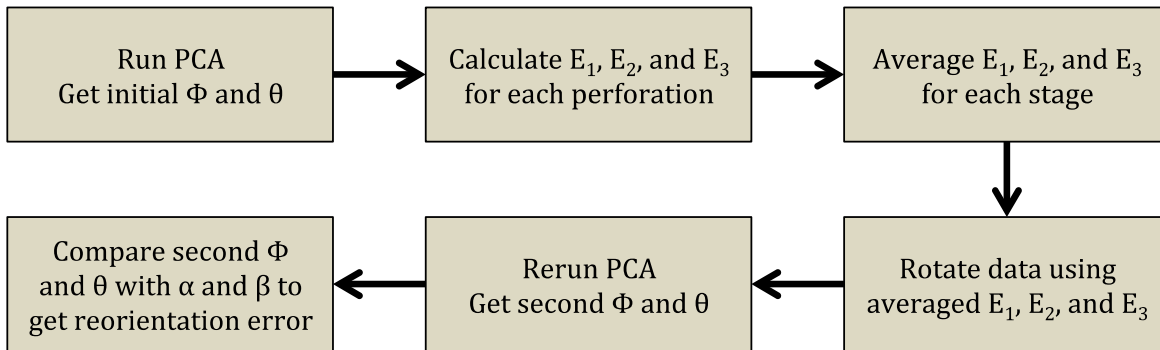


Figure 2.8: Flowchart describing the steps for reorienting the geophones into a common coordinate system. I run the initial PCA on the unrotated data and get the azimuth (Φ) and dip (θ) of the source relative to the receiver. I calculate the three Euler angles (E_1 , E_2 , E_3) using Eqn. (2.5) for each perforation, average E across the stage, and rotate the data using the matrices in Eqn. (2.6). I then run PCA a second time on the rotated data to get the Φ and θ and compare to known values of α and β . The difference between the Φ and α and θ and β is assigned as the error associated with the reorientation of the receivers.

2.3.2 Event Selection from Treatment Data

I use the stages with the greatest number of geophones with reoriented data and the least error in reorientation for event selection (Table B.1, Appendix B). The data are separated into three-second intervals, which is long enough to cover the duration of a single event (~ 0.3 seconds). The root-mean-squared (rms) amplitude is calculated for each three-second interval to find time intervals in the data with the largest amplitudes. For each of the two selected stages, I choose intervals with rms amplitudes greater than two standard deviations away from the mean rms amplitude of the entire stage (Figure 2.9) using EventDetect.R (Appendix A).

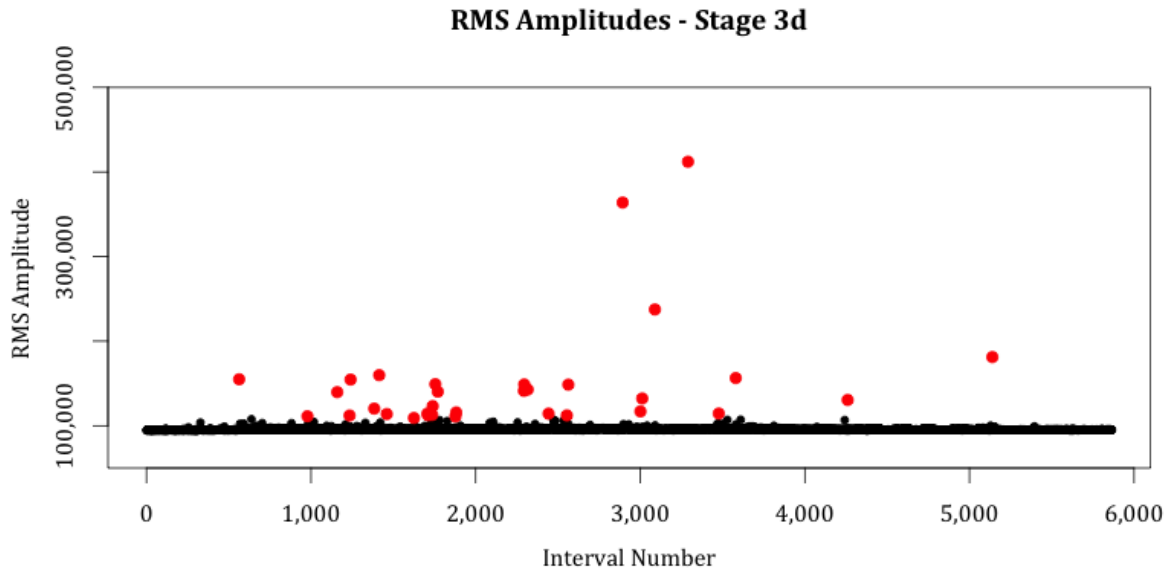


Figure 2.9: Plot of interval number versus the rms amplitude of that interval for stage 3d. Each dot represents a single three-second interval. The dots in red are the intervals that are detected to contain events because the rms amplitude of the interval is greater than two standard deviations plus the mean rms amplitude of the entire stage.

2.3.3 Event Location

Although the horizontal array of receivers has limited angular coverage of the expected source locations, locating the events provides a preliminary determination of whether or not microseismic events are occurring along the estimated fault zone. I use PCA to determine the azimuth and dip of the source relative to the receiver for each event. I then project the azimuth and dip as 3-D lines from the receivers and find the nearest point to these lines using singular value decomposition (SVD) to solve for the event location (Han & Bancroft, 2010).

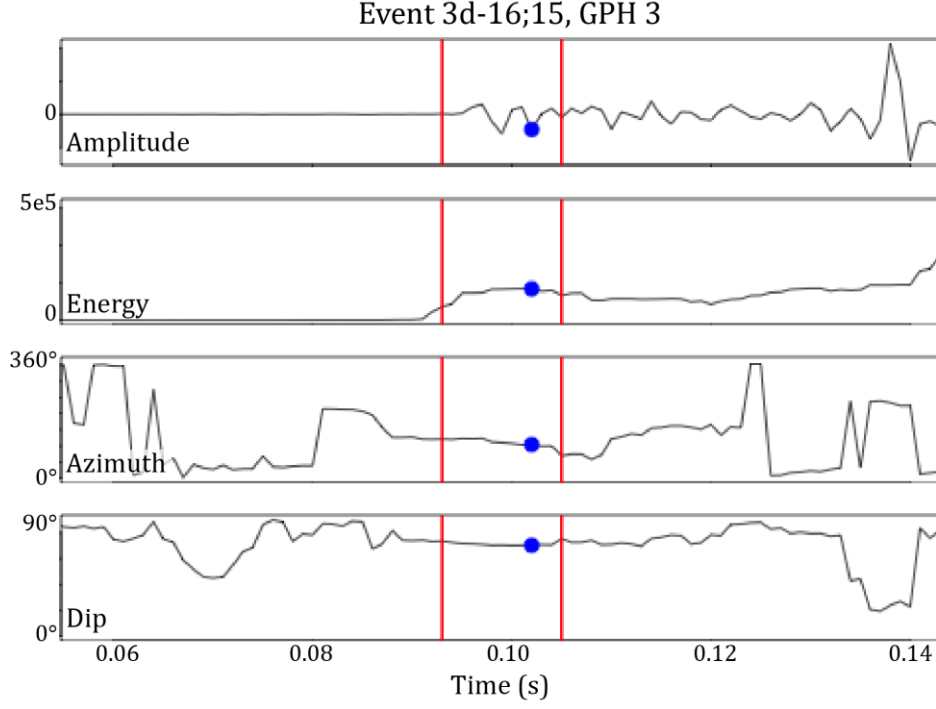


Figure 2.10: Example of window (red lines) defined around P-wave arrival for event 3d-16:15 (stage, hour, and minute in GMT of event occurrence). The first-break (blue point) is the time of the maximum energy detected in the window. I use the azimuth and dip at the time of the first-break and the mean and standard deviation of the azimuth and dip within the window for calculation of the event location in Eqns. (2.8)-(2.9).

For PCA of the selected events, I select a time window of 0.01-0.02 seconds (10-20 samples) around the P-wave arrival (Figure 2.10). I then calculate the mean (μ) and standard deviation (σ) of the azimuths and dips within this window to account for variation of the azimuth (ϕ) and dip (θ) at the first-break (fb) and possible error in first-break picking. I use four test azimuths and four test dips for each geophone:

$$\phi_1 = \mu_\phi \quad \phi_2 = \mu_\phi + \sigma_\phi \quad \phi_3 = \mu_\phi - \sigma_\phi \quad \phi_4 = \phi_{fb} \quad (2.8)$$

$$\theta_1 = \mu_\theta \quad \theta_2 = \mu_\theta + \sigma_\theta \quad \theta_3 = \mu_\theta - \sigma_\theta \quad \theta_4 = \theta_{fb} \quad (2.9)$$

I use the azimuths and dips in Eqns. (2.8) and (2.9) to calculate four sets of direction cosines (u) between the source and each geophone as

$$u_{xn} = \cos \theta_n \sin \phi_n \quad u_{yn} = \cos \theta_n \cos \phi_n \quad u_{zn} = -\sin \theta_n \quad (2.10)$$

where n indicates the geophone number. The direction vector (3-D line) from each geophone to the source is

$$\begin{cases} x - u_{xn}b_n = x_n \\ y - u_{yn}b_n = y_n \\ z - u_{zn}b_n = z_n \end{cases} \quad (2.11)$$

where (x, y, z) is the source location (nearest point), (x_n, y_n, z_n) is the n th geophone location, and b_n is the length of the line between the source and the geophone (source-receiver distance) (Figure 2.11) (Han & Bancroft, 2010).

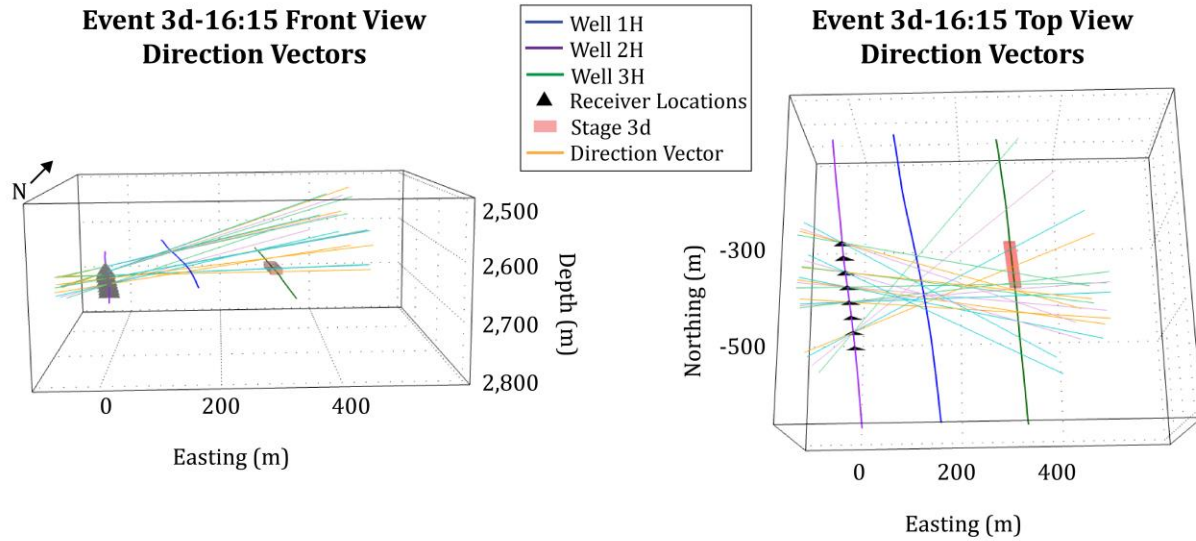


Figure 2.11: Four direction vectors for each geophone are calculated for event 3d-16:15 using the direction cosines in Eqn. (2.10) and Eqn. (2.11). The azimuths and dips from Eqns. (2.8) and (2.9) are those of the first-break (blue point in Figure 2.10, orange lines in this figure), the mean within the window (red lines in Figure 2.10, light purple lines in this figure), the mean minus the standard deviation within the window (light green lines), and the mean plus the standard deviation (light blue lines). The origin 0,0,0 is the XY surface location of well 1H.

The linear system of equations to solve for the nearest point to the 3-D lines between the source and each geophone is

$$d = Gc \quad (2.12)$$

$$d = \begin{bmatrix} x_n \\ y_z \\ z_n \\ \vdots \\ x_m \\ y_m \\ z_m \end{bmatrix} \quad G = \begin{bmatrix} 1 & 0 & 0 & -u_{xn} & 0 \\ 0 & 1 & 0 & -u_{yn} & \dots & 0 \\ 0 & 0 & 1 & -u_{zn} & & 0 \\ & \vdots & & \ddots & & \\ 1 & 0 & 0 & 0 & -u_{xm} \\ 0 & 1 & 0 & 0 & \dots & -u_{ym} \\ 0 & 0 & 1 & 0 & & -u_{zm} \end{bmatrix} \quad c = \begin{bmatrix} x \\ y \\ z \\ b_n \\ \vdots \\ b_m \end{bmatrix} \quad (2.13)$$

I aim to determine the vector c by minimizing b , the distance between the nearest point (x, y, z in c) and the 3-D lines between the source and each geophone (Han & Bancroft, 2010). I use SVD to invert G because G is not a square matrix and thus cannot be directly inverted (Gregorcic, 2001). SVD decomposes G into the matrices U, S , and V such that

$$G = USV^T \quad (2.14)$$

where G is of dimensions $p \times q$ with $p = m * 3$ and $q = m + 3$, U is a $p \times p$ matrix of the left eigenvectors of G , S is a diagonalized $p \times q$ matrix of the singular values of G , and V^T is a transposed $q \times q$ matrix of the right eigenvectors of G (RCoreTeam, 2015). The pseudoinverse of G is

$$G^+ = VS^{-1}U^T \quad (2.15)$$

with S^{-1} as the diagonalized $p \times q$ matrix of the reciprocals of the singular values of G (Gregorcic, 2001). Substituting Eqn. (2.15) into solving for c in Eqn. (2.12) yields

$$d = Gc \leftrightarrow c = G^+d \leftrightarrow c = VS^{-1}U^T d \quad (2.16)$$

with the best fit event location in the first three rows of c .

The rotation of the geophones into the ENU coordinate system can introduce errors associated with geophone misorientation into the determination of the azimuths and dips in the PCA results. I account for geophone misorientation by calculating the event location for all possible combinations of geophones and their azimuths and dips. There are twenty-six possible combinations of geophones (Table B.2, Appendix B) with combinations ranging from two to five geophones. For each combination of n geophones, there are 4^n possible combinations of azimuths and dips. There are ten combinations of two geophones, ten combinations of three geophones, five combinations of four geophones, and one combination of five geophones for each of the two stages. The presented PCA-SVD method of determining event locations is calculated for each of these compounded combinations, which yields 3,104 possible event locations for each selected event (Figure 2.12).

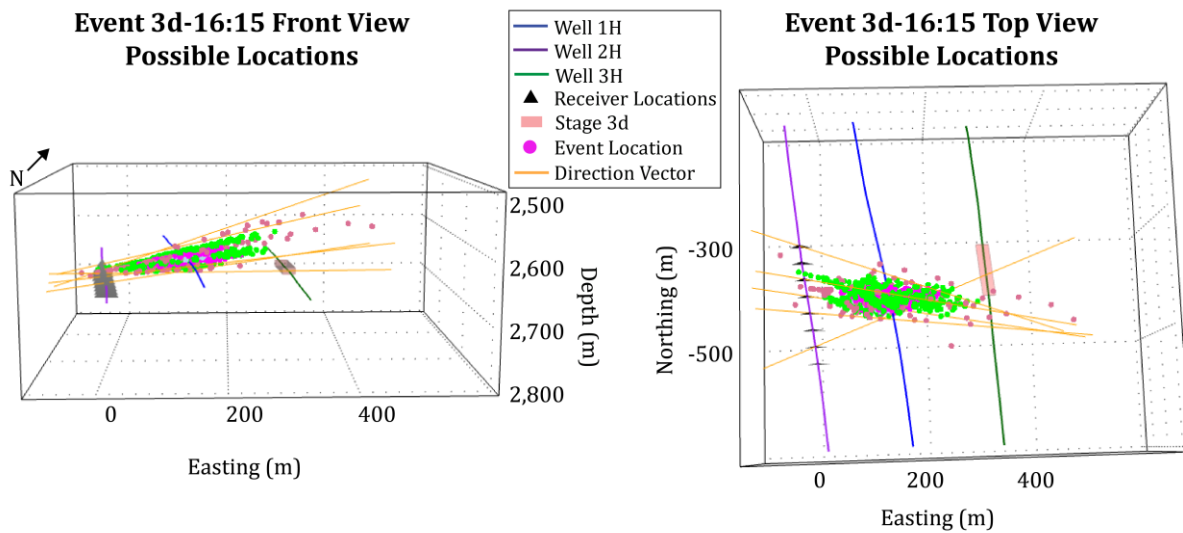


Figure 2.12: Possible event locations calculated for event 3d-16:15. The orange lines are the 3-D direction vectors (lines) between the geophones and source location for the first-break azimuth and dip. The event locations are colored and sized by the number of geophones used in the calculation for that particular location: the smaller pink points are from combinations of two geophones, the green points are from combinations of three geophones, the magenta points are from combinations of four geophones, and the light-blue points (not visible) are from the combination of all five geophones. The origin 0,0,0 is the XY surface location of well 1H.

The limited receiver angular coverage, particularly for stage 1b, increases the error in event location by clustering the possible locations closer to the receivers. To mitigate this directional preference, I remove possible event locations that are located unreasonably close to the geophones and/or outside the expected area of hydraulic fracture growth for that specific stage (Figure 2.13).

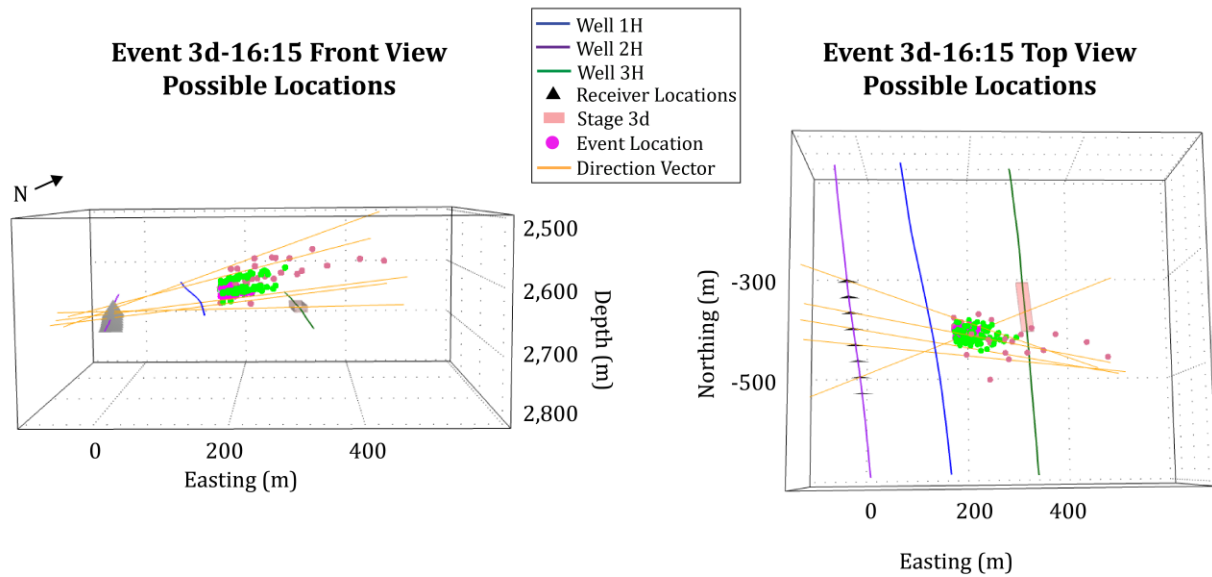


Figure 2.13: Possible event locations for event 3d-16:15 after removing the locations in Figure 2.12 that were located outside the expected area of hydraulic fracture growth for stage 3d. The orange lines are the 3-D direction vectors between the geophones and source location for the first-break azimuth and dip. The event locations are colored and sized by the number of geophones used in the calculation for that particular location: the smaller pink points are from combinations of two geophones, the green points are from combinations of three geophones, the magenta points are from combinations of four geophones, and the light-blue points (not visible) are from the combination of all five geophones. The origin 0,0,0 is the XY surface location of well 1H.

An ellipsoid is fit to the remaining possible event locations (Figure 2.14) (Adler et al., 2015). The center of the ellipsoid is the final calculated event location and the ellipsoid axes lengths are the plus/minus error of the event location in each of the x, y, and z directions (Figure 2.14). This method of event location is completed using the program

EventLocation.R (Appendix A) (Adler et al., 2015; Callahan et al., 2015; Fox et al., 2016; Stockwell & Cohen, 2014).

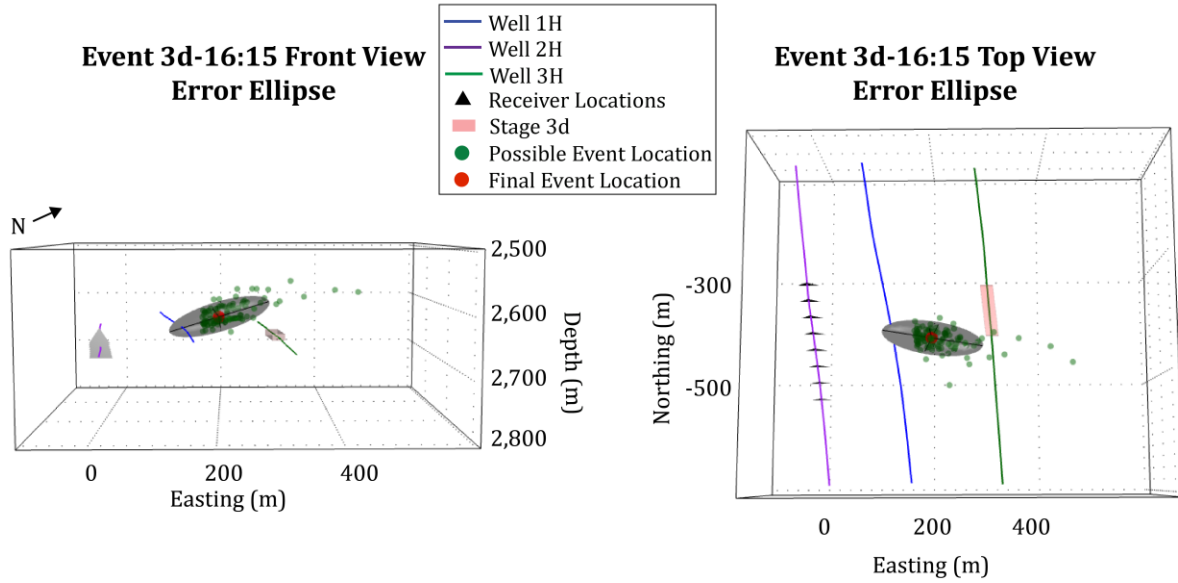


Figure 2.14: A 3-D ellipsoid is fit to the remaining possible event locations (light pink points) for event 3d-16:15. The final event location is the center of this ellipsoid (red point). The ellipsoid axes are the plus/minus error in each of the x, y, and z directions of the event location (Tables B.4-B.5, Appendix B). The origin 0,0,0 is the XY surface location of well 1H.

2.3.4 Magnitude Calculation

I calculate the seismic moment (M_0) for each event in the frequency domain with

$$M_0 = \frac{4\pi\rho v_p r \Omega_0}{R_p} \quad (2.17)$$

where ρ and v_p are the density and P-wave velocity of the medium, respectively, r is the source-receiver distance, Ω_0 is the low-frequency asymptote of the displacement spectrum, and R_p is the average P-wave radiation pattern coefficient (0.52) (Stork et al., 2014). The low-frequency asymptote is equivalent to the area under the displacement signal (Stork et

al., 2014). The program EventMag.R (Appendix A) estimates Ω_0 by fitting Brune's model of the displacement spectrum to the displacement spectrum of the P-wave in the seismograms (Figure 2.15) (Lees, 2015). I use the P-waves instead of the S-waves because the average radiation pattern coefficient and there is less error associated with picking of the P-wave arrival than the S-wave arrival (Boore & Boatwright, 1984; Stork et al., 2014). Finally, I calculate the moment magnitude (M_w) with

$$M_w = \frac{2}{3} \log_{10} M_0 - 6 \quad (2.18)$$

where M_0 is in units of N·m (Stork et al., 2014).

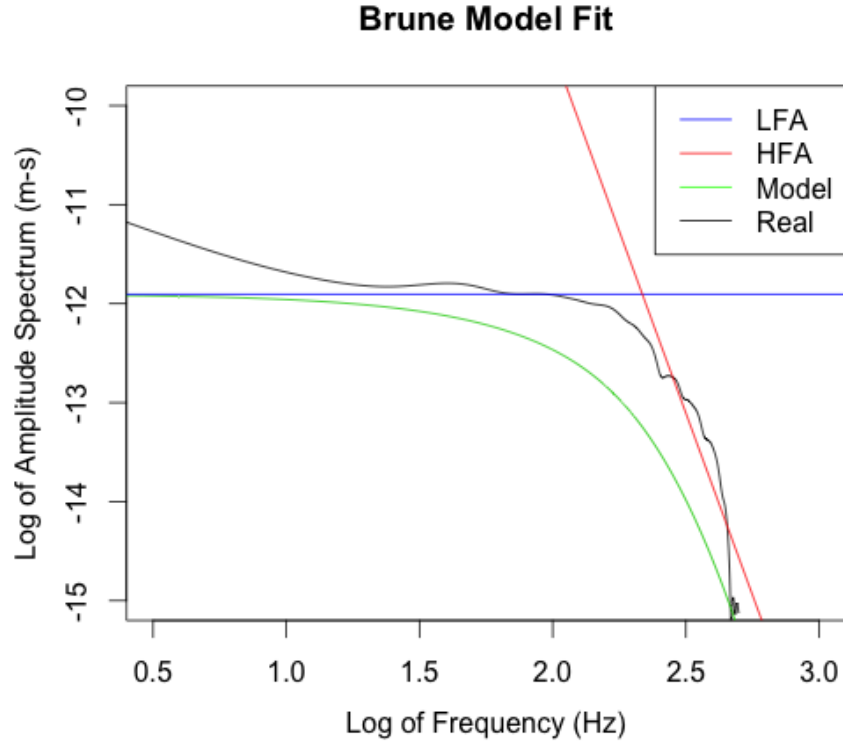


Figure 2.15: Example of how Brune's model (green line) is fit to the displacement spectrum of the real data (black line) showing the low- (LFA, blue line) and high-frequency (HFA, red line) asymptotes. The low-frequency asymptote (Ω_0) is proportional to the seismic moment M_0 (Stork et al., 2014).

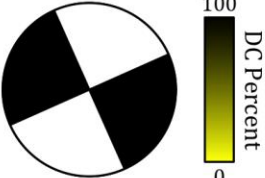

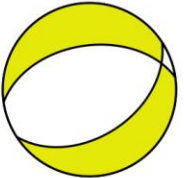
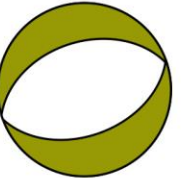
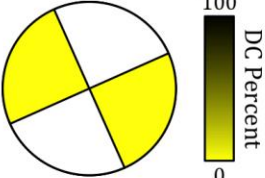
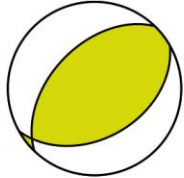
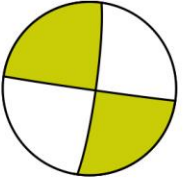
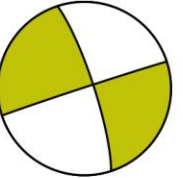
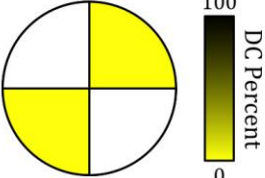
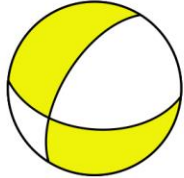
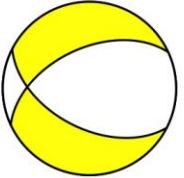
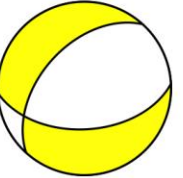
Chapter 3: Results

3.1 Full-Wavefield Moment Tensor Inversion of Synthetic Seismograms

Events with greater angular coverage ($> 25^\circ$) have less error in the resolved source orientations ($< 35^\circ$) than events with less angular coverage (Table 3.1, Figure 3.1). This relationship is apparent regardless of event frequency, indicating that the resolvability of the source orientation is dependent on receiver angular coverage (Figure 3.1). However, it is important to note the relationship between the expected source radiation pattern and receiver angular coverage of that source (Figure 3.2). The angular coverage of events at locations 3d and 3e provides sampling of both sides of the fault planes such that both first-motion up and first-motion down P-wave polarities are detected at the receivers (Figure 3.2b-c). The orientation of the focal mechanism is constrained using these P-wave polarities (Dahm & Krüger, 2014, p. 29). The auxiliary plane is resolved for events at location 1b because of the symmetric radiation pattern of the DC source (Figure 3.2a).

When including the intermediate- and near-field terms in an unconstrained moment tensor inversion, the isotropic source has the least error ($< 13\%$) in the resolved source mechanism because the least-squares minimization is finding a fit to a source with only P-wave amplitudes in the seismograms (Table 3.1).

Table 3.1: Full-wavefield moment tensor inversion results of synthetic seismograms with pure DC (top row), pure CLVD (middle row), and pure ISO (bottom row) sources generated in an isotropic medium and with a dominant event frequency of 125 Hz. The first column shows the input mechanism. The coordinates below each beach-ball indicate the output location from ISOLA where 0 m E, 0 m N is the true source location. The second, third, and fourth columns represent sources occurring at locations 1b, 3d, and 3e, respectively and are in order of increasing angular coverage and decreasing source-receiver distance from left to right. No constraints on the source mechanism are applied to the inversion. The beach-balls are colored by the amount of the resolved DC mechanism such that 100% DC is black and 0% DC is yellow.

Input	Output		
Beach-Ball	Location 1b	Location 3d	Location 3e
DC=100% CLVD=0% ISO=0%  0 m E, 0 m N	DC=62% CLVD=22% ISO=16%  -25 m E, -25 m N	DC=9% CLVD=40% ISO=-51%  25 m E, -50 m N	DC=35% CLVD=42% ISO=-23%  0 m E, 0 m N
CLVD=100% DC=0% ISO=0%  0 m E, 0 m N	CLVD=1% DC=15% ISO=85%  25 m E, 50 m N	CLVD=11% DC=19% ISO=70%  25 m E, -50 m N	CLVD=15% DC=22% ISO=63%  0 m E, 0 m N
ISO=100% DC=0% CLVD=0%  0 m E, 0 m N	ISO=-87% DC=7% CLVD=6%  -50 m E, 0 m N	ISO=91% DC=2% CLVD=7%  25 m E, -50 m N	ISO=91% DC=2% CLVD=8%  0 m E, 0 m N

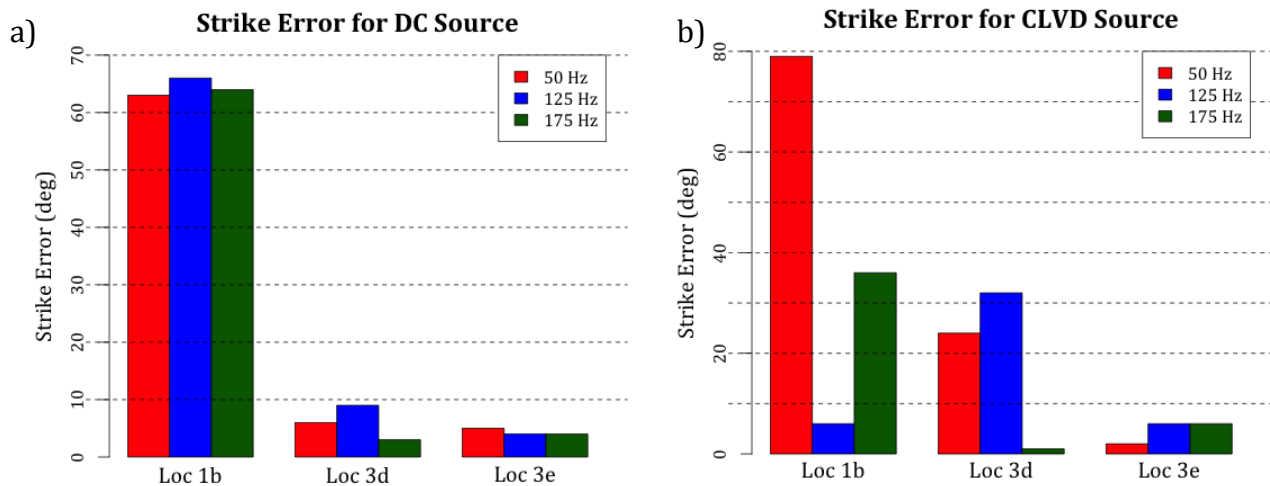


Figure 3.1: Error in source strike from results of full-wavefield moment tensor inversion of synthetic seismograms for a) DC sources and b) CLVD sources. Sources with greater angular coverage (locations 3d and 3e) have less error in the resolved source strike than sources with less angular coverage (location 1b). This relationship is apparent in all three of the tested dominant source frequencies: 50 Hz (red), 125 Hz (blue), and 175 Hz (green).

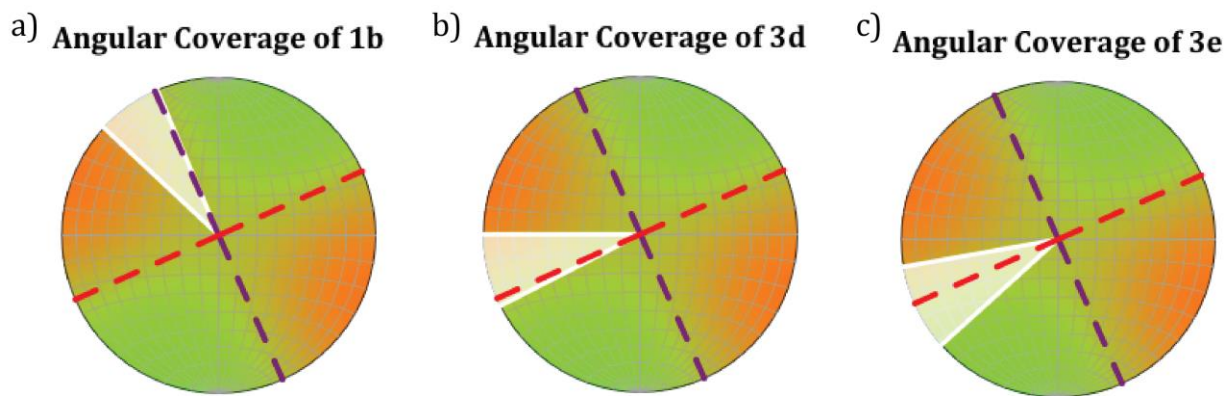


Figure 3.2: Lower-hemisphere stereographic projection of the P-wave radiation pattern of a DC source with strike of 66° , dip of 90° , and rake of 0° (dashed black line) with the angular coverage of the geophones (highlighted in white) relative to the source for an event at a) location 1b, b) location 3d, and c) location 3e. The auxiliary plane is perpendicular to the source orientation with a strike of 156° (purple dashed line). The orange areas represent the surrounding material moving outward from the source and the green areas represent the surrounding material moving inward to the source.

The results of the grid search for the moment tensor inversion of DC and CLVD sources at location 1b show a trade-off between correlation, resolved mechanism, and resolved strike

such that with increasing correlation, there is less error in the resolved mechanism but greater error in the resolved strike (Figure 3.3). This trade-off is only apparent at the location with the least angular coverage (Figure 3.3). The error in calculated source mechanism percentages is less for sources with small source-receiver distances (~ 300 m) and containing lower frequencies because of the less attenuated intermediate- and near-field amplitudes.

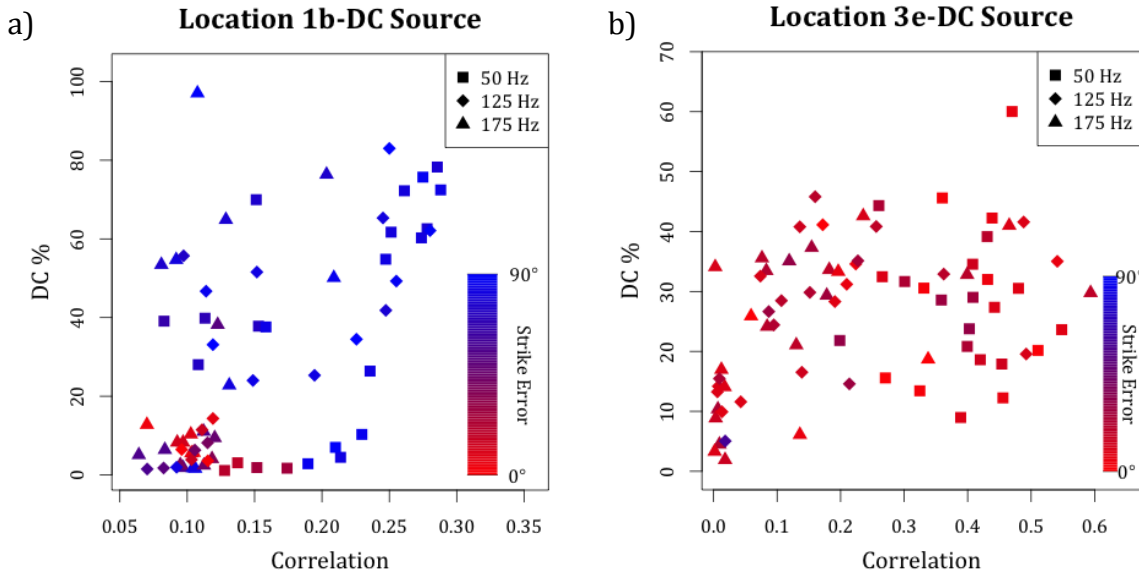


Figure 3.3: Plot of correlation versus resolved mechanism percentage for a DC source occurring at input locations a) 1b and b) 3e for all moment tensor inversion results in the grid search. The squares, diamonds, and triangles represent the results from the moment tensor inversion when the dominant source frequency is 50, 125, and 175 Hz, respectively. The points are colored by the error in the estimated strike where blue is greater error (up to 90°) and red is less error (0°).

The addition of 5% random Gaussian noise to the seismograms does not significantly alter the results of full-wavefield moment tensor inversion from that of the results of the noise-free seismograms (Figure 3.4).

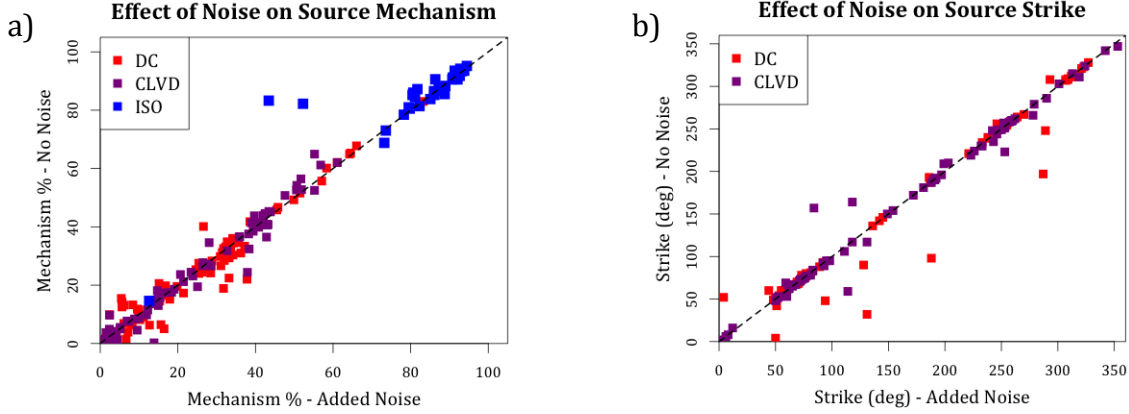


Figure 3.4: Plots of comparison of the full-wavefield moment tensor inversion results for added noise (x-axes) versus noise-free (y-axes) cases for all three tested locations (1b, 3d, and 3e) and all results in the grid search. The addition of 5% random Gaussian noise does not have a significant effect on neither the a) resolved source mechanism nor b) the resolved strike of the source. The dash blacked line is the line with the equation $x=y$.

There is a relationship between event location and angular coverage of the source such that location 3e with the greatest angular coverage always has the minimum location error of zero meters except in the anisotropy and low frequency cases (Figure 3.5). Location 3d consistently has an error in location of approximately 50-55 m (Figure 3.5) and has the moderate angular coverage of the three test locations. Location 1b, with the worst angular coverage, has the most varied error in location (~ 32 -70 m) (Figure 3.5).

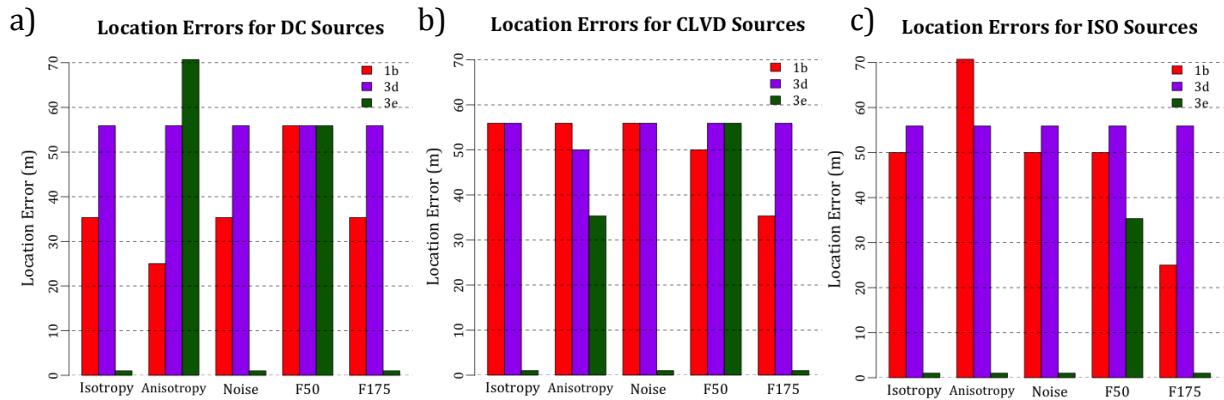




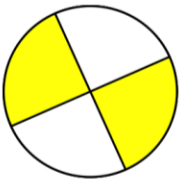





Figure 3.5: Bar plots of location errors for a) DC sources, b) CLVD sources, and c) ISO sources. The five different test cases are plotted along the x-axis in order of: isotropy, anisotropy, noise, frequency of 50 Hz, and frequency of 175 Hz. Each case is separated into three different bars representing each location: 1b (red), 3d (purple), and 3e (green).

3.1.1 Source Constraints

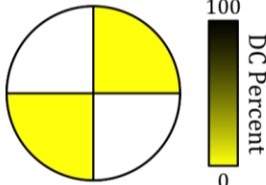



When using full-wavefield moment tensor inversion and applying the deviatoric constraint, the results for CLVD sources with greater angular coverage ($> 25^\circ$) have less error in the estimated source mechanisms than the DC sources (Table 3.2). The source orientation is accurately resolved for the CLVD source located closest to the receivers (location 1b) because of the inclusion of the intermediate- and near-field terms and correct application of the deviatoric constraint (Table 3.2). However, the other two locations (3d and 3e) have greater error in the source orientation with the deviatoric constraint applied than the results of the unconstrained full-wavefield moment tensor inversion (Table 3.1).

Table 3.2: Full-wavefield moment tensor inversion results of synthetic seismograms with pure DC (top row) and pure CLVD (bottom row) sources generated in an isotropic medium and with a dominant event frequency of 125 Hz. The first column shows the input mechanism. The coordinates below each beach-ball indicate the output location from ISOLA where 0 m E, 0 m N is the true source location. The second, third, and fourth columns represent sources occurring at locations 1b, 3d, and 3e, respectively and are in order of increasing angular coverage and decreasing source-receiver distance from left to right. A deviatoric constraint in which the ISO component is assumed to be 0% is applied to the inversion. The beach-balls are colored by the amount of the resolved DC mechanism such that 100% DC is black and 0% DC is yellow.

Input	Output		
Beach-Ball	Location 1b	Location 3d	Location 3e
DC=100% CLVD=0% ISO=0%  0 m E, 0 m N	DC=87% CLVD=13% ISO=0%  -25 m E, -25 m N	DC=32% CLVD=68% ISO=0%  25 m E, -50 m N	DC=28% CLVD=72% ISO=0%  0 m E, 0 m N
CLVD=100% DC=0% ISO=0%  0 m E, 0 m N	CLVD=15% DC=85% ISO=0%  -25 m E, -25 m N	CLVD=40% DC=60% ISO=0%  25 m E, -50 m N	CLVD=52% DC=48% ISO=0%  0 m E, 0 m N

For the ISO source, there is an appearance of non-DC components in the outputted results for the events with greater angular coverage ($> 25^\circ$) with the DC constraint applied (Table 3.3). On the other hand, the location with the least angular coverage (1b) resolves a dominantly DC source. The incorrect application of the DC constraint for moment tensor inversion of tensile sources results in greater error for sources with less angular coverage (14°) than for sources with greater angular coverage ($> 25^\circ$).

Table 3.3: Full-wavefield moment tensor inversion results of synthetic seismograms with a pure ISO source generated in an isotropic medium and with a dominant event frequency of 125 Hz. The first column shows the input mechanism. The coordinates below each beach-ball indicate the output location from ISOLA where 0 m E, 0 m N is the true source location. The second, third, and fourth columns represent sources occurring at locations 1b, 3d, and 3e, respectively and are in order of increasing angular coverage and decreasing source-receiver distance from left to right. A DC constraint in which both the CLVD and ISO components are assumed to be 0% is applied to the inversion. The beach-balls are colored by the amount of the resolved DC mechanism such that 100% DC is black and 0% DC is yellow.

Input	Output		
Beach-Ball	Location 1b	Location 3d	Location 3e
ISO=100% DC=0% CLVD=0%	ISO=0% DC=99% CLVD=1%	ISO=0% DC=31% CLVD=69%	ISO=0% DC=32% CLVD=68%
			
0 m E, 0 m N	-50 m E, 50 m N	25 m E, -50 m N	0 m E, 0 m N

3.1.2 Anisotropy

The majority of the full-wavefield moment tensor inversion results in the entire grid search have less than a 15° difference in the resolved source strike between the isotropic and anisotropic cases (Figure 3.6a). On the other hand, the resolved strength of the DC mechanism has a greater difference of $\sim 25\%$. These differences indicate that the neglect of

anisotropy in the velocity model for moment tensor inversion introduces greater variation in the resolved source mechanism than the resolved source orientation (Figure 3.6b).

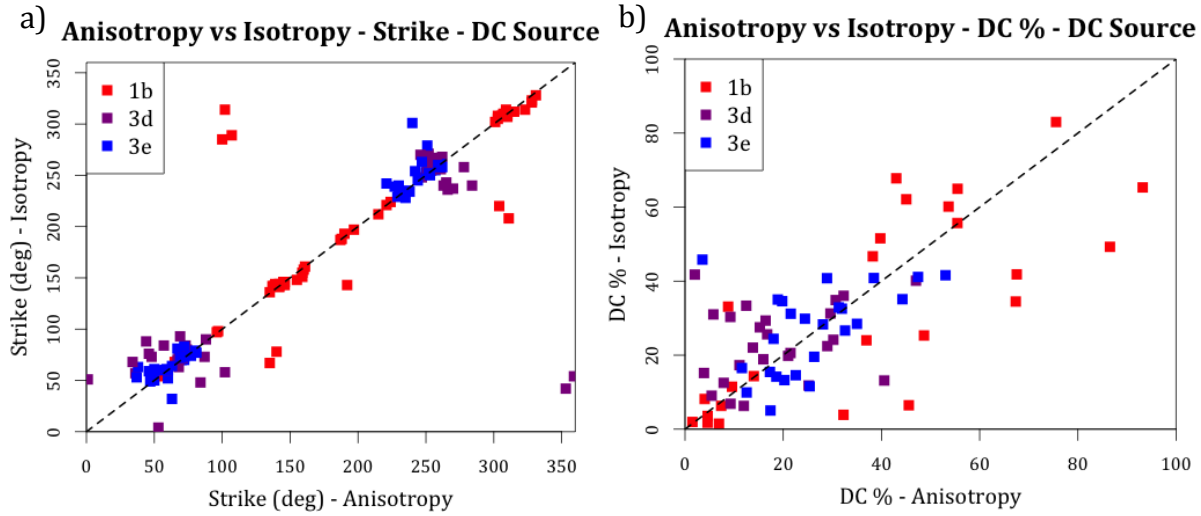


Figure 3.6: Comparison of full-wavefield moment tensor inversion (assumes isotropic seismic velocities) results for sources occurring in anisotropic (x-axes) and isotropic (y-axes) media. a) Comparison of the strike of the DC source shows little variability ($< 15^\circ$) for all locations in the grid search. b) Comparison of the strength of the resolved DC mechanism shows greater variability ($\sim 25\%$). These results indicate that the neglect of anisotropy in the velocity model has a greater effect on the resolved mechanism percentages than the resolved source orientation. The dash blacked line is the line with the equation $x=y$.

The final outputted result for an ISO source at the location with the least angular coverage appears to be dominantly DC. However, the output mechanism is the only result in the entire grid search of the moment tensor inversion with the overestimated DC component (Figure 3.7). The source mislocation is a result of the neglect of anisotropy in the seismic velocities for the moment tensor inversion.

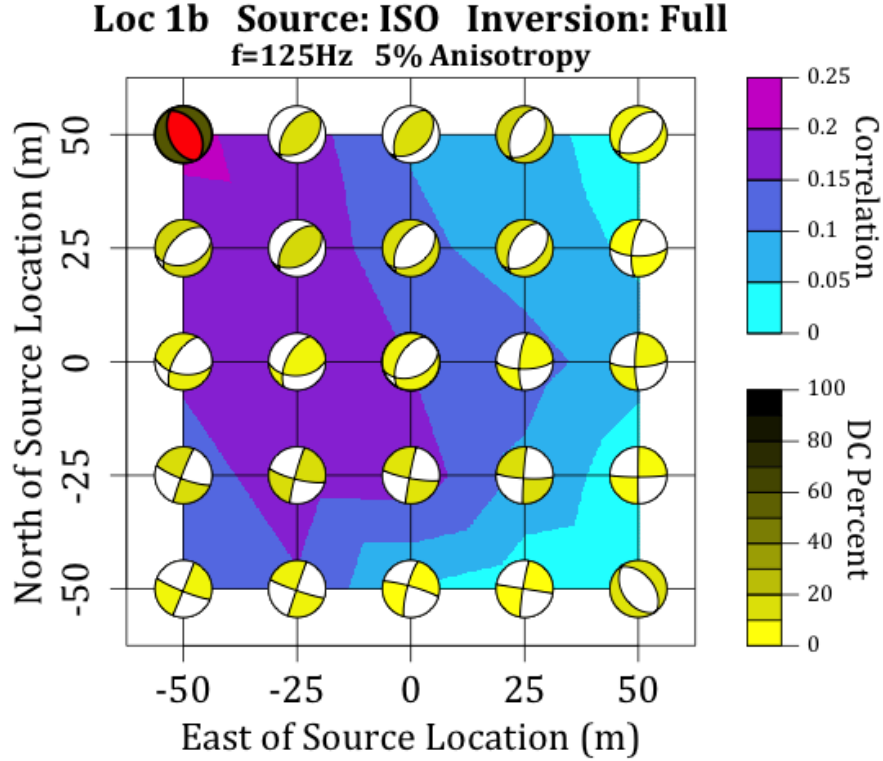


Figure 3.7: Full-wavefield moment tensor inversion results for an isotropic source occurring at location 1b with a dominant source frequency of 125 Hz in a 5% VTI anisotropic medium. The true source location is at 0,0. All locations in the grid search have resolved a high ISO component except for the output location selected as the location with the highest correlation.

3.2 Microseismic Event Characteristics

3.2.1 Event Locations

Events from both stages 1b and 3d are clustered on the west side of their respective treatment wells (Figures 3.8-3.9) and the event location error ellipsoids are oriented NW-SE for stage 1b (Figure 3.10a) and W-E for 3d (Figure 3.10b). The error ellipsoid orientation and event clustering are a result of the limited receiver angular coverage of the treatment area. The lack of receivers to the east of the treatment area limits the resolvability of the W-E coordinate of the event locations thus clustering them towards the west and orienting the error ellipsoids in the direction of the geophones relative to the

stage. Three microseismic events occur outside the expected treatment area for stage 3d and towards the direction of the estimated fault zone (Figure 3.9).

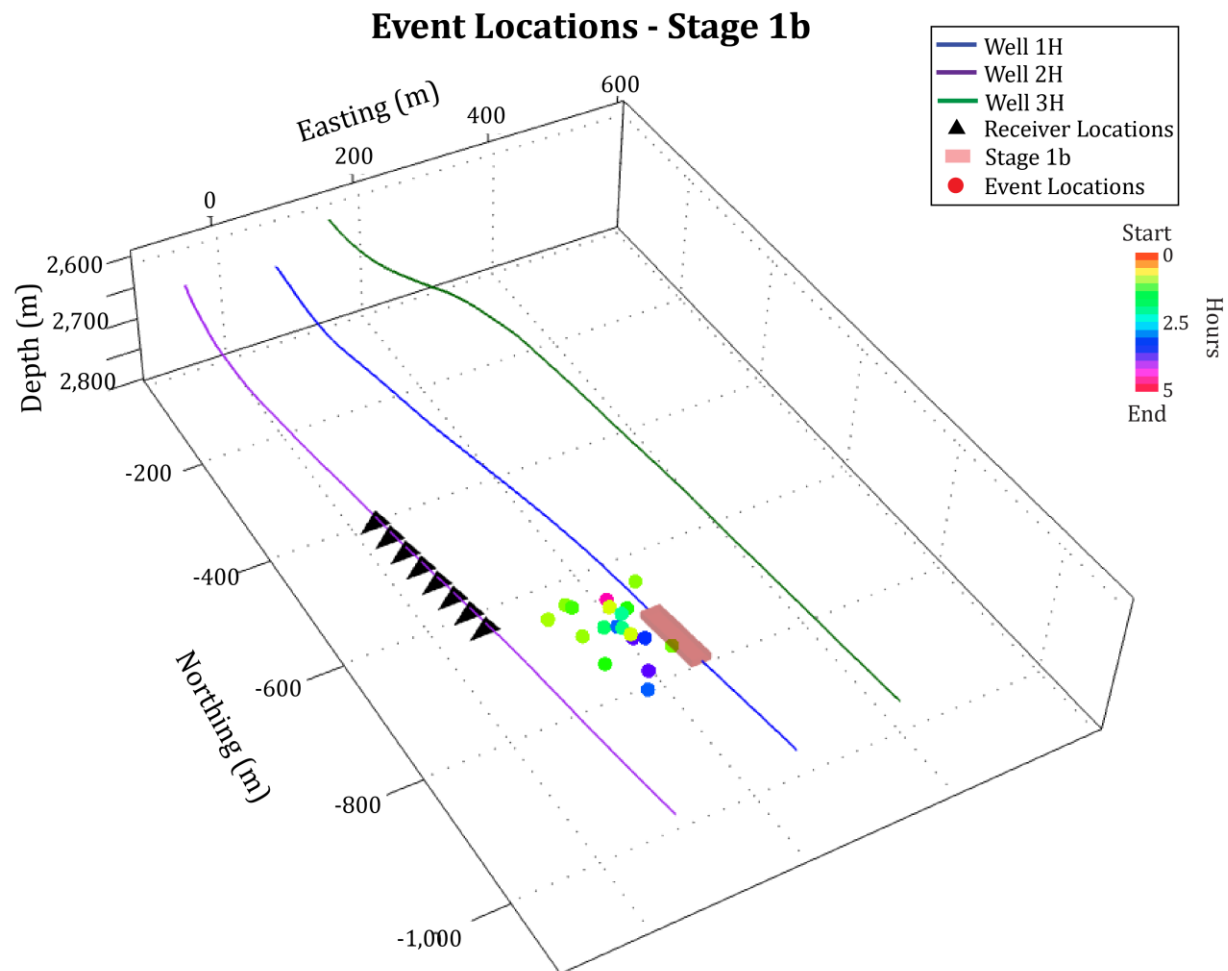


Figure 3.8: Oblique view of well paths, receiver locations (black triangles), and event locations for stage 1b colored by their event time relative to the starting and stopping of the treatment. The origin 0,0,0 is the surface location of well 1H (see Table B.3 in Appendix B for table of X, Y, Z coordinates of locations).

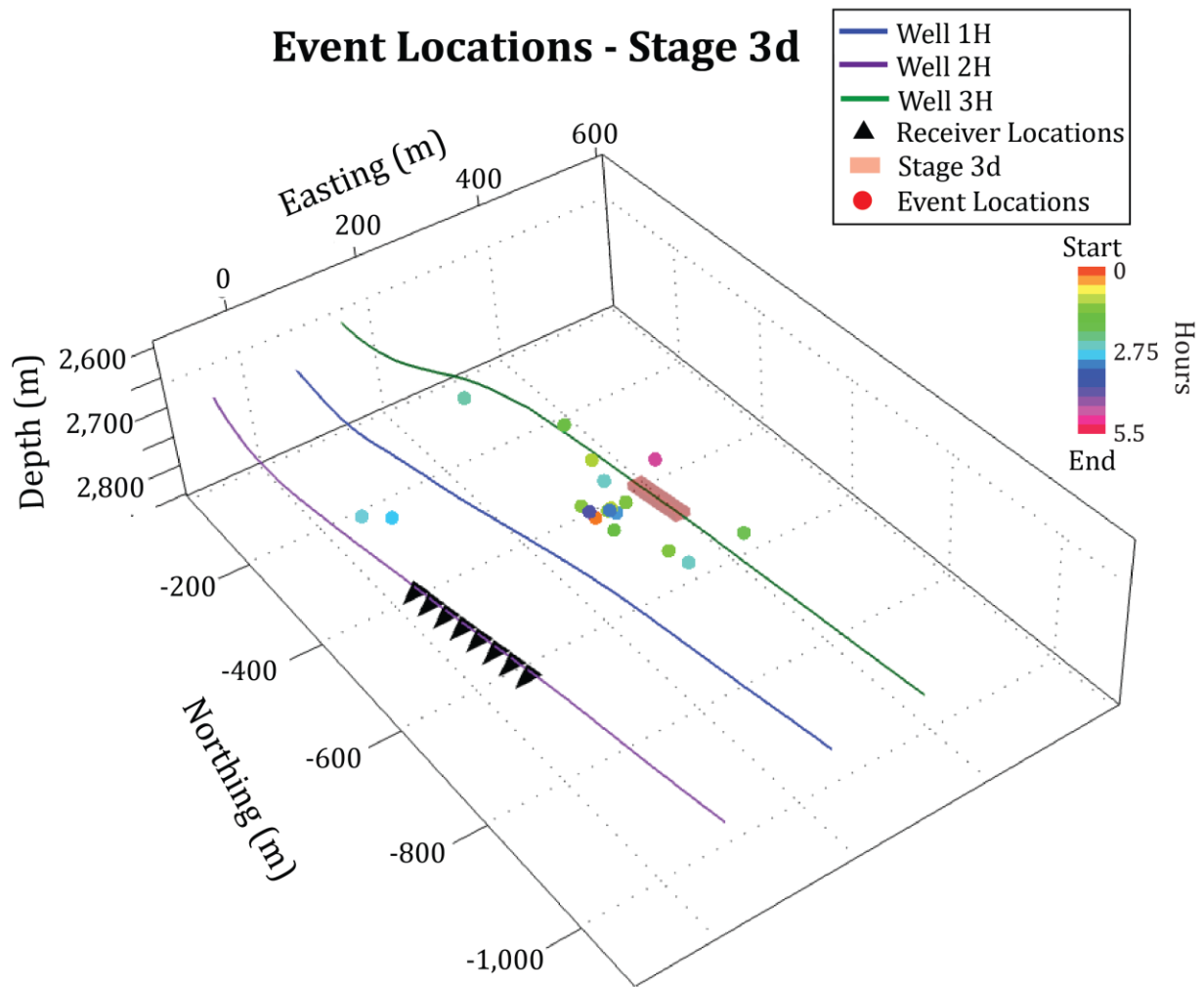


Figure 3.9: Oblique view of well paths, receiver locations (black triangles), and event locations for stage 3d colored by their event time relative to the starting and stopping of the treatment. The origin 0,0,0 is the surface location of well 1H (see Table B.4 in Appendix B for table of X, Y, Z coordinates of locations).

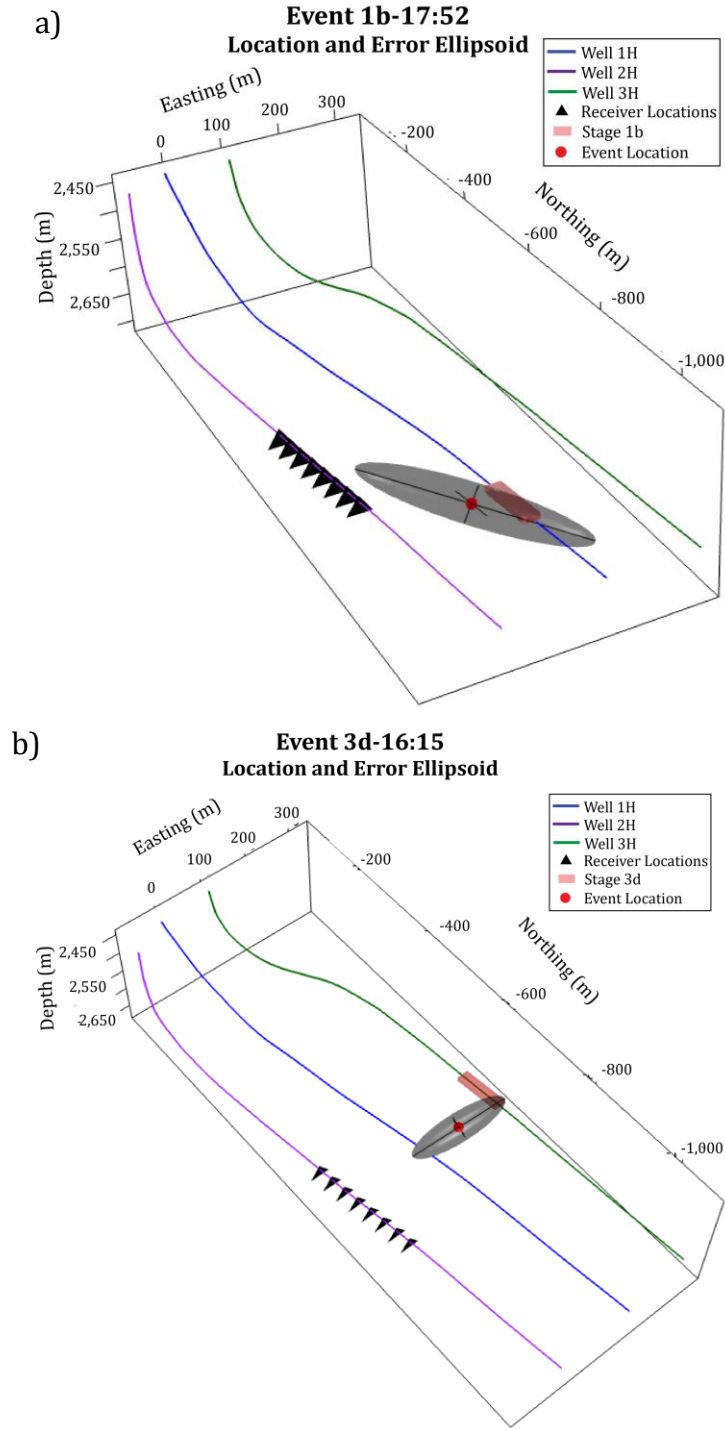


Figure 3.10: a) Error ellipsoid for event 1b-17:52 is oriented NW-SE. b) Error ellipsoid for event 3d-16:15 is oriented W-E. The error ellipsoids are orientated in the direction of the geophones (black triangles) relative to the stage (red rectangle) where the formation is being treated. The names of the microseismic events are the stage, hour, and minute of the event time in GMT (i.e. 1b-16:45 or 3d-14:00).

3.2.2 Event Magnitudes

Magnitudes from all 37 events range from -2.6 to -1.7 with an average of -2.16 ± 0.22 (Figure 3.11). Stage 1b has a slightly higher average magnitude of -2.10 ± 0.18 (Table 3.4) than stage 3d which has an average magnitude of -2.21 ± 0.25 (Table 3.5). The lowest magnitude events occur at the beginning of the treatment of stage 1b.

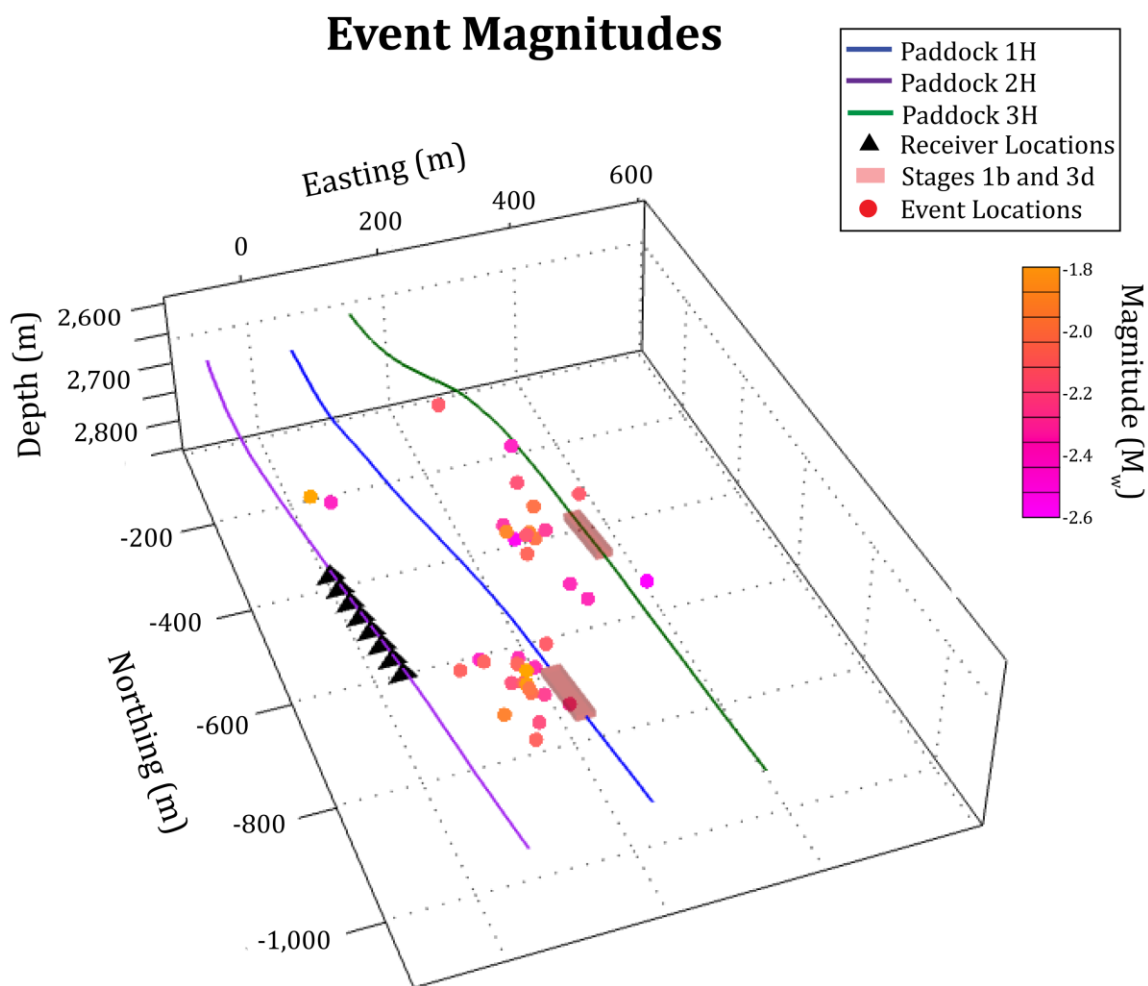


Figure 3.11: Oblique view of well paths and receiver locations (black triangles), and event locations (dots) colored by their event magnitude. Pink events are lower magnitude whereas orange events are higher magnitude. The origin 0,0,0 is the surface location of well 1H.

3.2.3 Event Frequency Content

Microseismic events from stage 1b contain lower frequencies (180 ± 34 Hz) and have longer P-wave durations (0.075 ± 0.009 s) (Table 3.4) than events from stage 3d (225 ± 33 Hz, 0.045 ± 0.003 s) (Figure 3.12, Table 3.5). The names of the selected microseismic events are the stage, hour, and minute of the event time in GMT (i.e. 1b-16:45 or 3d-14:00). Three events from stage 3d (3d-17:04, 3d-17:21, 3d-17:38) have characteristics more similar to those of stage 1b because of their lower frequencies, longer P-wave durations (Figure 3.12b), and higher magnitudes compared to the rest of stage 3d and are located along the estimated fault zone (Figures 3.9 and 3.1).

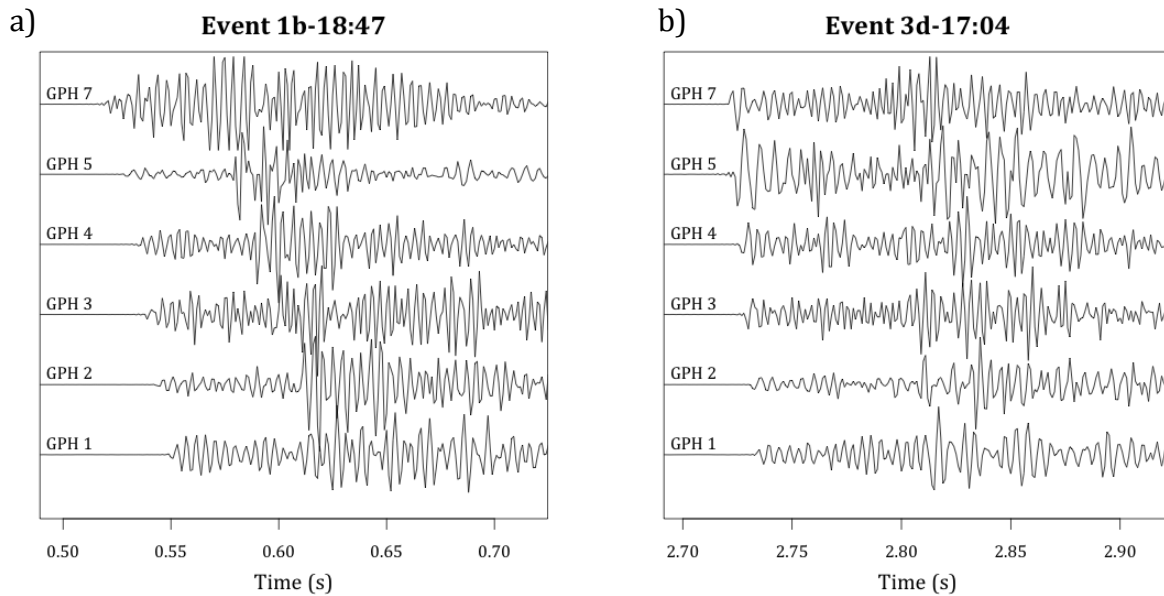


Figure 3.12: Seismograms from a) event 1b-18:47 and b) 3d-17:04. Event 3d-17:04 has a relatively long P-wave duration and lower frequency content, similar to events in stage 1b, compared to other events occurring in stage 3d.

Table 3.4: Summary of event characteristics for eighteen selected events occurring in stage 1b.

Event	Dominant Frequency (Hz)	P-wave Duration (s)	Magnitude
1b-16:45	103 ± 44	0.202 ± 0.009	-2.11 ± 0.36
1b-16:46	187 ± 11	0.072 ± 0.007	-2.07 ± 0.15
1b-16:54	175 ± 26	0.049 ± 0.006	-2.41 ± 0.22
1b-16:57	219 ± 52	0.049 ± 0.007	-2.17 ± 0.23
1b-17:00a	231 ± 61	0.191 ± 0.006	-2.36 ± 0.04
1b-17:00b	206 ± 57	0.048 ± 0.006	-2.35 ± 0.38
1b-17:04	60 ± 16	0.057 ± 0.010	-2.1 ± 0.17
1b-17:14	113 ± 17	0.058 ± 0.007	-2.07 ± 0.31
1b-17:21	110 ± 5	0.053 ± 0.007	-1.74 ± 0.17
1b-17:22	295 ± 23	0.069 ± 0.005	-2.05 ± 0.08
1b-17:46	277 ± 27	0.065 ± 0.010	-2.16 ± 0.12
1b-17:52	182 ± 67	0.060 ± 0.020	-1.79 ± 0.09
1b-17:55	169 ± 35	0.072 ± 0.011	-2.24 ± 0.08
1b-18:47	244 ± 27	0.083 ± 0.010	-2.06 ± 0.17
1b-18:48	112 ± 16	0.053 ± 0.012	-1.91 ± 0.21
1b-19:22	95 ± 21	0.058 ± 0.008	-2.01 ± 0.13
1b-19:23	149 ± 75	0.077 ± 0.025	-1.98 ± 0.13
1b-20:11	283 ± 21	0.067 ± 0.008	-2.27 ± 0.13

Table 3.5: Summary of event characteristics for nineteen selected events occurring in stage 3d.

Event	Dominant Frequency (Hz)	P-wave Duration (s)	Magnitude
3d-14:00	294 ± 35	0.054 ± 0.003	-2.37 ± 0.1
3d-15:08	182 ± 10	0.034 ± 0.003	-1.72 ± 0.2
3d-15:11	238 ± 13	0.056 ± 0.004	-1.99 ± 0.09
3d-15:30	304 ± 29	0.033 ± 0.003	-2.14 ± 0.16
3d-15:31	318 ± 20	0.044 ± 0.006	-2.44 ± 0.18
3d-15:34	219 ± 33	0.053 ± 0.002	-2.15 ± 0.06
3d-15:35	260 ± 10	0.046 ± 0.007	-2.05 ± 0.36
3d-16:15	161 ± 26	0.048 ± 0.002	-1.88 ± 0.29
3d-16:16	284 ± 30	0.041 ± 0.005	-2.13 ± 0.28
3d-16:37	182 ± 38	0.043 ± 0.003	-2.29 ± 0.1
3d-17:04	200 ± 44	0.078 ± 0.003	-1.71 ± 0.07
3d-17:13	198 ± 43	0.044 ± 0.004	-2.11 ± 0.19
3d-17:14	162 ± 16	0.037 ± 0.005	-1.85 ± 0.19
3d-17:21	188 ± 59	0.078 ± 0.002	-1.74 ± 0.11
3d-17:38	171 ± 47	0.079 ± 0.009	-2.3 ± 0.27
3d-17:54	301 ± 27	0.045 ± 0.004	-1.81 ± 0.24
3d-18:03	171 ± 18	0.037 ± 0.002	-1.94 ± 0.22
3d-19:08	226 ± 66	0.026 ± 0.004	-1.59 ± 0.05
3d-20:20	213 ± 57	0.020 ± 0.004	-2.37 ± 0.1

Chapter 4: Discussion

4.1 Receiver Angular Coverage of Source

The error in the resolved failure mechanism from moment tensor inversion of shear sources is related to the source-receiver distance and highlights the importance of the use of the full-wavefield in the moment tensor inversion. Previous studies of moment tensor inversion with only consideration of the far-field terms show that the pure shear source is the most accurate to retrieve from microseismic data from a single vertical array of receivers when applying a deviatoric constraint to the inversion (Vavryčuk, 2007; Warpinski & Du, 2010). When including the intermediate- and near-field terms and applying no source constraints, the calculated mechanism percentages are more accurate for pure shear sources located closer to a horizontal receiver array than sources located farther from the receiver array.

A preliminary understanding of the relationship between receiver angular coverage and the expected source radiation pattern should be considered when interpreting the results of moment tensor inversion. Sources that do not have receiver angular coverage of both sides of the shear failure plane will not be able to resolve the correct orientation fully. This is important for moment tensor inversion programs that apply a constraint on the source orientation to reduce the error in the results associated with lack of angular coverage (Song & Toksoz, 2011). Applying the source orientation constraint without receiver angular coverage of both sides of the failure plane could introduce greater error into the estimated source mechanism than the results without the constraint.

4.2 Deviatoric Constraint

The resolved strength of the shearing mechanism is greater for results of full-wavefield moment tensor inversion with the deviatoric constraint applied than the results for the unconstrained inversion for both shear and tensile sources. If the source is dominantly shear, the deviatoric constraint decreases the error in the source mechanism but increases the error in the source orientation. The introduction of these secondary errors indicates that, without prior knowledge of whether the source is dominantly shear or tensile, the deviatoric constraint should not be used to stabilize the inversion of sources with limited angular coverage. The results of unconstrained full-wavefield moment tensor inversion can be interpreted with an understanding of the errors associated with the lack of angular coverage rather than adding possible additional error with the use of the deviatoric constraint.

4.3 Neglect of Anisotropy in Moment Tensor Inversion

The effects of anisotropic velocities on moment tensor inversions that assume isotropic velocity models are well studied for shear sources but limited work is done for non-DC sources (Rößler et al., 2007; Sileny & Vavryčuk, 2002; Vavryčuk, 2005). A previous study shows that the CLVD mechanism can be overestimated by ~20% more than the ISO mechanism for pure shear sources when neglecting anisotropy in the moment tensor inversion (Sileny & Vavryčuk, 2002). Inversion of synthetic seismograms in ISOLA, which utilizes an isotropic velocity model, shows that the difference between the resolved source mechanism of sources generated in an isotropic medium and the resolved source mechanism of sources generated in a 5% VTI medium is ~40% greater for CLVD sources

than DC sources. If CLVD source mechanisms are expected, an understanding of both the errors that the neglect of anisotropy introduces into the results of moment tensor inversion and the errors associated with the lack of angular coverage should be considered in the interpretation of the results.

Previous studies suggest using only the P-wave amplitudes in the moment tensor inversion to mitigate the effect of anisotropy on S-wave splitting (Sileny & Vavryčuk, 2002). However, Vavryčuk (2007) shows that sufficient angular coverage of at least two non-parallel receiver arrays (i.e. one vertical and one horizontal) is required for moment tensor inversion using only the P-wave amplitudes and far-field terms of the wavefield. More work on full-wavefield moment tensor inversion with only use of the P-wave amplitudes is needed to determine if a single array of receivers located close (< 300 m) to the source can provide accurate source mechanisms.

Chapter 5: Conclusions

Based on my results of full-wavefield moment tensor inversion of synthetic seismograms using ISOLA, accurate source mechanisms and source orientations of pure DC and CLVD sources cannot be determined when using a single-horizontal array of receivers. Explosive (ISO) sources can be accurately determined however DC and CLVD sources associated with fracture growth are more likely to occur during hydraulic fracturing treatments. The tested locations and dominant frequencies of the synthetic seismograms used for analysis in ISOLA are similar to the estimated locations and dominant frequencies of the events in the provided microseismic data, indicating that full-wavefield moment tensor inversion cannot be used to retrieve accurate source mechanisms for these events.

I show several relationships between receiver angular coverage of the source and the full-wavefield moment tensor inversion results using synthetic seismograms. The first is the relationship with the resolvability of the source orientation. The strike of shear sources cannot be accurately resolved unless there is receiver angular coverage of both sides of the failure plane. The second relationship is with the error in source location such that sources with less angular coverage have greater error in source location. Moment tensor inversion results at all locations in the grid search show minimal variability between locations. This lack of variability indicates that the errors in the inversion results are mainly because of the lack of the angular coverage of the source rather than the source mislocation.

For moment tensor inversion of pure shear sources generated in a 5% VTI medium, I show that there is greater variability in the resolved source mechanism than the source orientation compared to the pure shear sources generated in an isotropic medium. The use of an isotropic velocity model for events occurring in an anisotropic medium can introduce a 25-50 m error into the estimation of the source location.

5.1 Recommendations

Future studies utilizing moment tensor inversion of microseismic data should consider the receiver angular coverage of the events being inverted to determine if the source mechanisms can be accurately resolved. Hydraulic fracturing treatments in complex geologic settings, such as the one presented here where the formation has natural fractures and a nearby fault, should consider what microseismic event characteristics are desired when designing the microseismic monitoring survey. With sufficient angular coverage, accurate source mechanisms can be retrieved to understand the interaction between the hydraulic fractures, fault, and natural fractures. To take advantage of the full-wavefield, receivers should be placed as close to the treatment area as possible and with more geophones and/or a wider spacing of geophones than the design of the horizontal array considered in this thesis.

5.2 Future Work

The presented analysis of the resolvability of source mechanisms from a single horizontal array of receivers assumes that the microseismic events result from vertical failure planes oriented in the direction of S_{HMAX} and that the types of failure are purely shear (100 % DC),

opening (100% CLVD), or explosive (100% ISO). Further work on understanding the relationships between angular coverage and results of full-wavefield moment tensor inversion should consider the resolvability of sources with combinations of the three mechanisms (i.e. 50% DC 50% CLVD) that could result from slippage induced by opening along a natural discontinuity. Source mechanisms with non-vertical failure planes not oriented in the direction of S_{HMAX} can also be studied to determine the resolvability of sources associated with horizontal bedding plane slip or opening and/or shearing along pre-existing natural fractures or faults.

As most rocks contain some kind of anisotropy, future studies on the use of an isotropic velocity model for moment tensor inversion of sources occurring in anisotropic media should include higher degrees of anisotropy and further analysis of the errors in the results of tensile sources. Also identifying the effects of attenuation on source mechanisms will lead to increased understanding of how the estimated formation properties affect the accuracy of moment tensor inversion and what kinds of errors are introduced if attenuation is neglected. Further understanding of how anisotropy and attenuation vary during the hydraulic fracturing treatment may be able to be incorporated into moment tensor inversion with more complex calculations in future studies.

References

- Adler, D., Murdock, D., & others. (2015). rgl: 3D Visualization Using OpenGL. Retrieved from <http://CRAN.R-project.org/package=rgl>
- Aki, K., & Richards, P. G. (2002). *Quantitative Seismology* (J. Ellis Ed.). Sausalito, CA: University Science Books.
- Baig, A., & Urbancic, T. (2010). Microseismic moment tensors: A path to understanding frac growth. *The Leading Edge*, 29(3), 320-324. doi:10.1190/1.3353729
- Boore, D. M., & Boatwright, J. (1984). Average Body-Wave Radiation Coefficients. *Bulletin of the Seismological Society of America*, 74(5), 1615-1621.
- Bormann, P., Wendt, S., & Giacomo, D. D. (2013). Seismic Sources and Source Parameters *New Manual of Seismological Observatory Practice*.
- Callahan, J., Casey, R., & Templeton, M. (2015). seismicRoll: Fast Rolling Functions for Seismology using Rcpp (R package version 1.0.1 ed.).
- Clarkson, C. R. (2011). Integration of Rate-Transient and Microseismic Analysis for Unconventional Gas Reservoirs: Where Reservoir Engineering Meets Geophysics. *CSEG Recorder*, 36(10), 44-61.
- Cosad, C. (1992). Choosing a Perforation Strategy. *Oilfield Review*, 54-69.
- Cronin, V. (2010). A Primer on Focal Mechanism Solutions for Geologists.
- Cuenot, N., Charlety, J., Dorbath, L., & Haessler, H. (2006). Faulting mechanisms and stress regime at the European HDR site of Soultz-sous-Forêts, France. *Geothermics*, 35(5-6), 561-575. doi:10.1016/j.geothermics.2006.11.007
- Dahm, T., & Krüger, F. (2014). Moment tensor inversion and moment tensor interpretation. In P. Bormann (Ed.), *New Manual of Seismological Observatory Practice 2 (NMSOP-2)* (pp. 1-37). Potsdam : Deutsches GeoForschungsZentrum GFZ.

- Das, I., & Zoback, M. D. (2011). Long-period, long-duration seismic events during hydraulic fracture stimulation of a shale gas reservoir. *The Leading Edge*, 30(7), 778-786. doi:10.1190/1.3609093
- Downie, R. C., Kronenberger, E., & Maxwell, S. C. (2010). *Using Microseismic Source Parameters to Evaluate the Influence of Faults on Fracture Treatments - A Geophysical Approach to Interpretation*. Paper presented at the Society of Petroleum Engineers Annual Technical Conference and Exhibition, Florence, Italy 19-22 September 2010.
- Drew, J., Primiero, P., Brook, K., Raymer, D., Probert, T., Kim, A., & Leslie, D. (2012). Microseismic monitoring field test using surface, shallow grid, and downhole arrays. 1-5. doi:10.1190/segam2012-0910.1
- Duncan, P., & Lakings, J. (2006). *Microseismic Monitoring with a Surface Array*. Paper presented at the European Association of Geoscientists and Engineers, Dubai, United Arab Emirates.
- Eaton, Baan, M. v. d., Tary, J.-B., Birkelo, B., Spriggs, N., Cutten, S., & Pike, K. (2013). Broadband microseismic observations from a Montney hydraulic fracture treatment, northeastern B.C., Canada. *CSEG Recorder*, 44-53.
- Eaton, & Forouhideh, F. (2011). Solid angles and the impact of receiver-array geometry on microseismic moment-tensor inversion. *Geophysics*, 76(6).
- Eisner, L., Fischer, T., & Calvez, J. H. L. (2006). Detection of repeated hydraulic fracturing (out-of-zone growth) by microseismic monitoring. *The Leading Edge*.
- Eisner, L., Hulsey, B. J., Duncan, P., Jurick, D., Werner, H., & Keller, W. (2010). Comparison of surface and borehole locations of induced seismicity. *Geophysical Prospecting*, 58(5), 809-820. doi:10.1111/j.1365-2478.2010.00867.x
- Forouhideh, F., & Eaton, D. W. (2009). Microseismic Monitoring: Insights from Moment Tensor Inversion. *CREWES Research Report*.
- Fox, J., Friendly, M., & Monette, G. (2016). heplots: Visualizing Tests in Multivariate Linear Models. Retrieved from <http://CRAN.R-project.org/package=heplots>

- Gale, J. F. W., Reed, R. M., & Holder, J. (2007). Natural fractures in the Barnett Shale and their importance for hydraulic fracture treatments. *AAPG Bulletin*, 91(4), 603-622. doi:10.1306/11010606061
- Gregorcic, G. (2001). The Singular Value Decomposition and the Psuedoinverse.
- Han, L., & Bancroft, J. C. (2010). Nearest approaches to multiple lines in n-dimensional space. *CREWES Research Report*, 22.
- Hardebeck, J. L., & Shearer, P. M. (2008). HASH: A FORTRAN Program for Computing Earthquake First-Motion Focal Mechanisms - v1.2 - January 31, 2008.
- Ichinose, G. A., Goldstein, P., & Rodgers, A. J. (2000). Relative Importance of Near-, Intermediate- and Far-Field Displacement Terms in Layered Earth Synthetic Seismograms. *Bulletin of the Seismological Society of America*, 90(2), 531-536.
- Ikelle, & Amundsen. (2005). *Introduction to Petroleum Seismology* (Vol. 12).
- Jechumtálová, Z., & Bulant, P. (2013). Effects of 1-D versus 3-D velocity models on moment tensor inversion in the Dobra Voda locality at the Little Carpathians region, Slovakia *Seismic Waves in Complex 3-D Structures* (Vol. 23, pp. 253-269). Dep. Geophys.: Charles Univ, Prague.
- Jones, J. R., & Britt, L. K. (2009). *Design and Appraisal of Hydraulic Fractures*. Richardson, TX: Society of Petroleum Engineers.
- Jost, M. L., & Hermann, R. B. (1989). A Student's Guide to and Review of Moment Tensors. *Seismological Research Letters*, 60(2), 37-57. doi:10.1785/gssrl.60.2.37
- Kikuchi, M., & Kanamori, H. (1991). Inversion of Complex Body Waves-III. *Bulletin of the Seismological Society of America*, 81(6), 2335-2350.
- Lees, J. M. (2015). RSEIS: Seismic Time Series Analysis in R. Retrieved from <http://CRAN.R-project.org/package=RSEIS>
- Maercklin, N. (2007). SUPOLAR and SUPOFILT: SU programs for polarization analysis and filtering of three-component data.

- Maxwell, S. (2014). *Microseismic Imaging of Hydraulic Fracturing: Improved Engineering of Unconventional Shale Reservoirs*. Tulsa, OK: Society of Exploration Geophysicists.
- Maxwell, S., & Norton, M. (2012). Enhancing shale gas reservoir characterization using hydraulic fracture microseismic data. *First Break*, 30(2), 95-101.
- Mirai Solutions GmbH. (2015). XLConnect: Excel Connector for R. Retrieved from <http://CRAN.R-project.org/package=XLConnect>
- Pollastro, R. M., Jarvie, D. M., Hill, R. J., & Adams, C. W. (2007). Geologic framework of the Mississippian Barnett Shale, Barnett-Paleozoic total petroleum system, Bend arch-Fort Worth Basin, Texas. *AAPG Bulletin*, 91(4), 405-436. doi:10.1306/10300606008
- RCoreTeam. (2015). R: A Language and Environment for Statistical Computing. Vienna, Austria: R Foundation for Statistical Computing.
- Rößler, D., Krüger, F., & Rumpker, G. (2007). Retrieval of moment tensors due to dislocation point sources in anisotropic media using standard techniques. *Geophysical Journal International*, 169(1), 136-148. doi:10.1111/j.1365-246X.2006.03243.x
- Ryan, H. (1994). Ricker, Ormsby, Klauder, Butterworth - A Choice of Wavelets. *CSEG Recorder*.
- Schlumberger. (2016). Schlumberger Oilfield Glossary. Retrieved from <http://www.glossary.oilfield.slb.com/>
- Sileny, J., & Vavryčuk, V. (2002). Can unbiased source be retrieved from anisotropic waveforms by using an isotropic model of the medium? *Tectonophysics*, 356(1-3), 125-138. doi:10.1016/S0040-1951(02)00380-3
- Sokos, & Zahradnik, J. (2008). ISOLA a Fortran code and a Matlab GUI to perform multiple-point source inversion of seismic data. *Computers & Geosciences*, 34(8), 967-977. doi:10.1016/j.cageo.2007.07.005
- Sokos, & Zahradnik, J. (2009). A Matlab GUI for use with ISOLA Fortran: User's Guide.

- Song, F., & Toksoz, M. N. (2011). Full-waveform based complete moment tensor inversion and source parameter estimation from downhole microseismic data for hydrofracture monitoring. *Geophysics*, 76(6), WC103-WC116.
- Song, F., Warpinski, N. R., & Toksoz, M. N. (2014). Full-waveform based microseismic source mechanism studies in the Barnett Shale: Linking microseismicity to reservoir geomechanics. *Geophysics*, 79(2), B109-B126. doi:10.1190/GEO2013-0094.1
- Stein, S., & Wysession, M. (2003). *An Introduction to Seismology, Earthquakes, and Earth Structure*. Malden, MA: Blackwell.
- Stockwell, J., John W., & Cohen, J. K. (2014). CWP/SU: Seismic Un*x Release No. 43: an open source software package for seismic research and processing.
- Stork, A. L., Verdon, J. P., & Kendall, J. M. (2014). The robustness of seismic moment and magnitudes estimated using spectral analysis. *Geophysical Prospecting*, 62(4), 862-878. doi:10.1111/1365-2478.12134
- Thomsen, L. (1986). Weak elastic anisotropy. *Geophysics*, 51(10), 1954-1966. doi:10.1190/1.1442051
- Urbancic, T., Morrish, T., & Shumila, V. (2009). *Understanding Hydraulic Fracture Growth by Mapping Source Failure Mechanisms*. Paper presented at the Frontiers + Innovation CSPG CSEG CWLS Convention, Alberta, Canada.
- van der Baan, M., Eaton, D., & Dusseault, M. (2013). Microseismic Monitoring Developments in Hydraulic Fracture Stimulation. doi:10.5772/56444
- Vavryčuk, V. (2001). Inversion for parameters of tensile earthquakes. *Journal of Geophysical Research*, 106(B8), 16339. doi:10.1029/2001jb000372
- Vavryčuk, V. (2005). Focal mechanisms in anisotropic media. *Geophysical Journal International*, 161(2), 334-346. doi:10.1111/j.1365-246X.2005.02585.x
- Vavryčuk, V. (2007). On the retrieval of moment tensors from borehole data. *Geophysical Prospecting*, 55(3), 381-391. doi:10.1111/j.1365-2478.2007.00624.x.

Vavryčuk, V. (2015). Moment Tensors: Decomposition and Visualization. 1-16.
doi:10.1007/978-3-642-36197-5_288-1

Warpinski, N. R., & Du, J. (2010). *Source-Mechanism Studies on Microseismicity Induced by Hydraulic Fracturing*. Paper presented at the Society of Petroleum Engineers Annual Technical Conference and Exhibition, Florence, Italy, 19-22 September 2010.

Warpinski, N. R., Waltman, C. K., Du, J., & Ma, Q. (2009). *Anisotropy Effects in Microseismic Monitoring*. Paper presented at the Society of Petroleum Engineers Annual Technical Conference and Exhibition, New Orleans, Louisiana, USA, 4-7 October, 2009.

Appendix A: Processing Workflows and Programs

Processing Workflow for Perforation Data

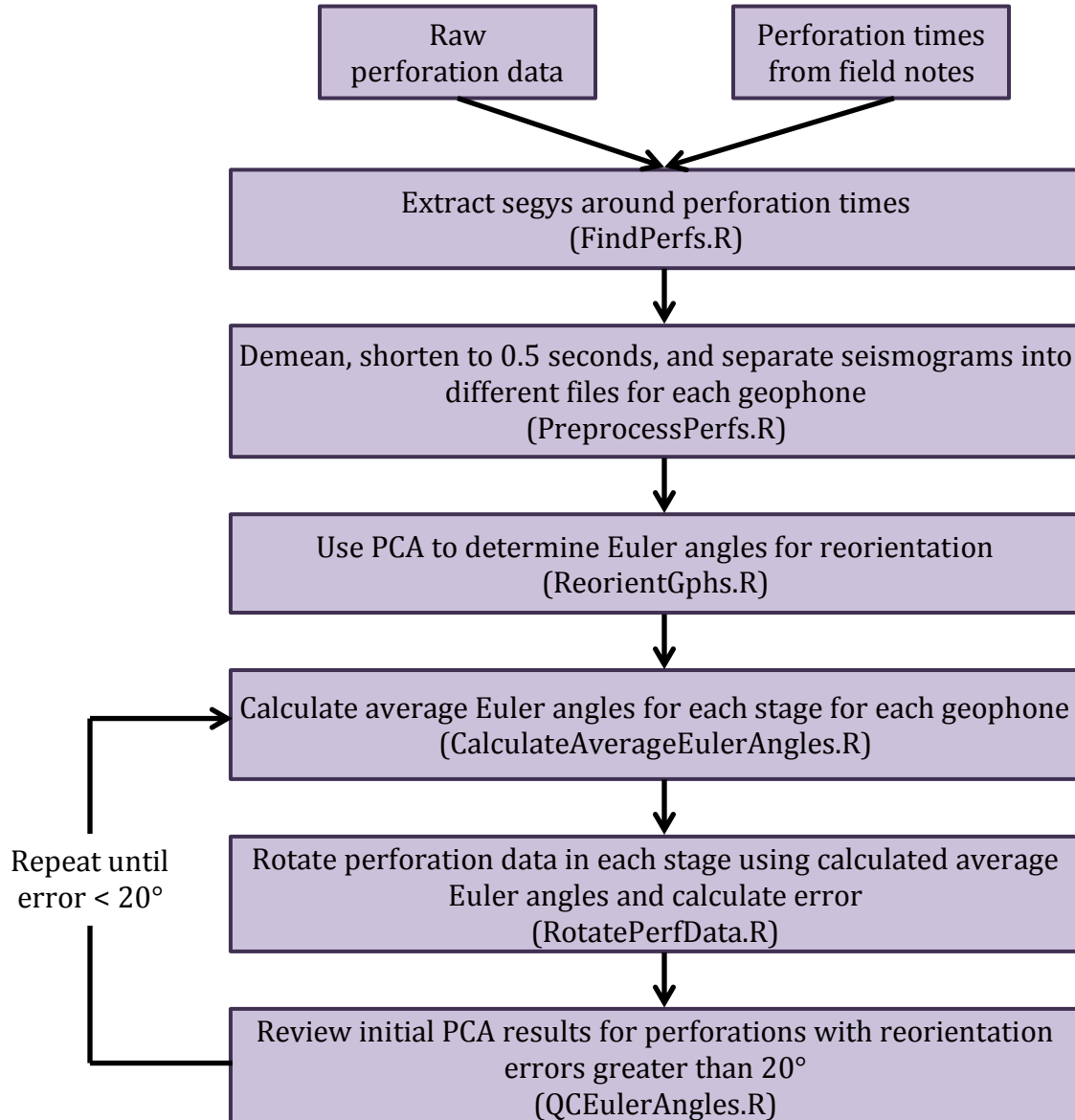


Figure A.1: I use the raw perforation data and perforation times from the provided field notes to extract the .sgy files containing the perforation events. I then preprocess the perforation seismograms and output them to .su files. The .su files are input into the program ReorientGphs.R to rotate the geophones into a common coordinate system (refer to section 2.3.1 for detailed description of method). I then calculate the average Euler angles for each geophone for each stage and use them to rotate the perforation data and determine the error in the reorientation. If the reorientation error is greater than 20°, I go back to the original PCA results for perforations with reorientation errors greater than 20° and search within a 20 ms window around the P-wave arrival for an azimuth and dip that can provide a lower error in the reorientation.

Processing Workflow for Treatment Data

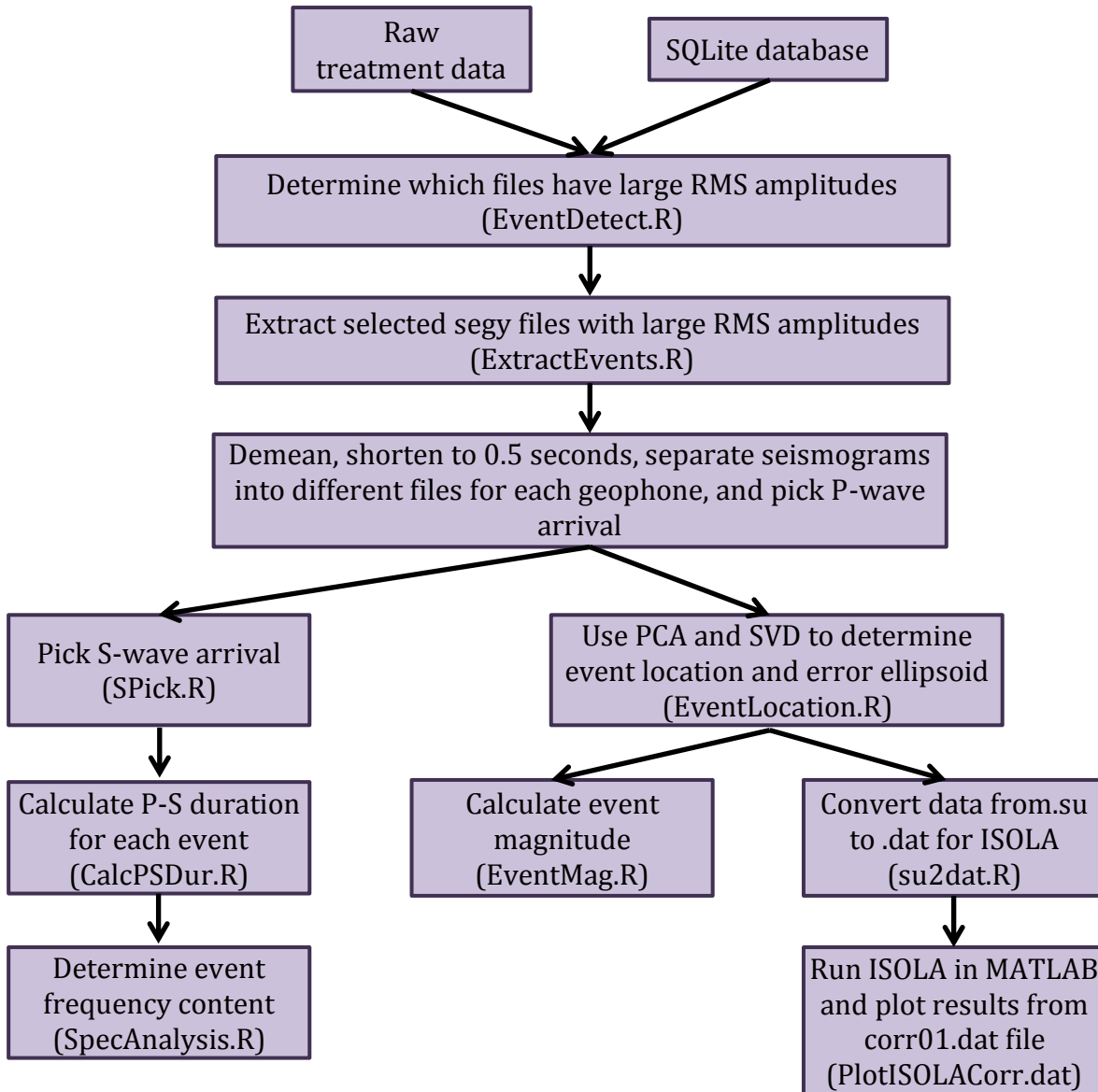


Figure A.2: The SQLite database for each stage contains a list of the .sgy files and the calculate rms amplitude in each file (provided by Dr. Juan Lorenzo). I use this database for input into EventDetect.R to determine which .sgy files contain events and extract them using ExtractEvents.R (refer to section 2.3.2). I then preprocess the seismograms, convert them to .su files, and pick the P-wave arrival. I determine the event frequency content using SpecAnalysis.R and calculate the P-S duration after picking the S-wave arrival. I use the PCA-SVD method to locate the events and calculate a 3D error ellipsoid (refer to section 2.3.3). With the event location determined, I then calculate the event magnitude using EventMag.R (refer to section 2.3.4). The next person to work with this dataset can then use su2dat.R to convert the .su files to .dat for input into ISOLA and plot the results of ISOLA using PlotISOLACorr.dat.

Programs (A=/home/trudyw/hydraulicfracturing/TLWFinal/Rfunctions)

cartmontens.m	74
Calculate synthetic seismograms using Eqn 4.29 from Aki & Richards, 2002	
Located in /home/trudyw/hydraulicfracturing/TLW	
srctfunc.m	130
Calculate source-time function for synthetic seismograms	
Located in /home/trudyw/hydraulicfracturing/TLW	
FindPerfs.R.....	132
Find perforation event data (segys) using times from provided field notes	
Located in A/PreprocessPerfs/	
PreprocessPerfs.R	138
Separate perforation data into su files by geophone, demean and cut seismograms to 0.5 seconds long	
Located in A/PreprocessPerfs/	
ReorientGphsExample.R.....	142
Call ReorientGphs function on input perforation data and perforation times	
Located in A/ReorientGphs/	
ReorientGphs.R.....	147
Run principal component analysis of perforation data and calculate Euler angles	
Located in A/ReorientGphs/	
CalculateAverageEulerAngles.R	154
Calculates average Euler angles for each geophone for each stage and outputs to excel file	
Located in A/ReorientGphs/	
RotatePerfData.R	158
Rotate perforation data using average Euler angles and calculate reorientation error	
Located in A/ReorientGphs/	
QCEulerAngles.R.....	165
Review PCA results for perforations with reorientation errors greater than 20°	
Located in A/ReorientGphs/	
EventDetectExample.R.....	172
Call EventDetect function for input database of treatment data and RMS amplitudes	
Located in A/EventDetect/	
EventDetect.R.....	173
Determine which treatment data files have large RMS amplitudes and output as list of files containing events	
Located in A/EventDetect/	

ExtractEvents.R	175
Extract segy files from treatment data containing events	
Located in A/EventDetect/	
PreprocessEvents.R	177
Separate treatment data into different files by geophone, demean and shorten	
seismograms to 0.5 seconds, pick P-wave arrival	
Located in A/PreprocessEvents/	
SPick.R	185
Pick S-wave arrival	
Located in A/FreqContent/	
CalcPSDur.R	189
Calculate P-S duration in seconds and write out to .csv file	
Located in A/FreqContent/	
SpecAnalysis.R	191
Determine event frequency content	
Located in A/FreqContent/	
EventLocationExample.R	195
Calls EventLocation function to interactively locate event	
Located in A/EventLocation/	
EventLocation.R	198
Interactively locate event using PCA-SVD	
Located in A/EventLocation/	
PCAEvent.R	201
Subfunction of EventLocation to run principal component analysis on treatment data	
Located in A/EventLocation/	
CalcAngMean.R	210
Subfunction of PCAEvent subfunction that calculates the mean of a list of angles	
Located in A/EventLocation/	
QCPCA.R	212
Subfunction of EventLocation function that reviews anomalous PCA results	
PlotAziLines.R	220
Subfunction of QCPCA subfunction that plots PCA results in map view to identify	
anomalies	
Located in A/EventLocation/	
SVDCalcMultDips.R	226
Calculate event location using PCA-SVD method	

Located in A/EventLocation/	
PlotSVDRes3D.R.....	234
Plot event location results and calculate error ellipsoid	
Located in A/EventLocation/	
PlotWells3DFunc.R.....	241
Subfunction of PlotSVDRes3D subfunction that plots well paths in 3D	
Located in A/EventLocation/	
EventMag.R.....	247
Calculate event magnitude using Brune's model	
Located in A/EventMagnitude/	
su2dat.R.....	253
Convert .su to .dat for input velocity seismograms in ISOLA	
Located in A/ISOLA/	
PlotISOLACorrExample.R.....	258
Calls PlotISOLACorr function to plot corr01.dat file containing outputted ISOLA results	
Located in A/ISOLA/	
PlotISOLACorr.R.....	259
Function to plot grid search results of moment tensor inversion outputted from ISOLA	
Located in A/ISOLA/	

cartmomtens.m

Calculate synthetic seismograms using Eqn 4.29 from Aki & Richards, 2002

Located in /home/trudyw/hydraulicfracturing/TLW

% Author: Trudy Watkins

% Adapted from Chennu Fan's dipoleDC9.m

% Date: March 6, 2015

% Program: cartmomtens.m

% MATLAB program calculates synthetic seismograms using Eqn 4.29 from

% Aki and Richards, 2002

% All available inputs to calculation are above marker at line 171

% Requires accompaniment of srctfunc.m

% Clear previous values, inputs, and figures

clear all

close all

tic

% If outputting for ISOLA, enter the name of the directory you want the

% data folder saved to, if directory already exists, data subfolder will be

% created in it

dirname = 'DirName';

% Options to display various plots or output data

% 0 = off, 1 = on

set(0,'Units','normalized');

aaa = 0; % Option to display source-receiver geometry

bbb = 0; % Option to display source-time functions for each term of displacement

ccc = 0; % Option to display source-time functions for each term of velocity

ddd = 0; % Option to plot frequency content of Ricker wavelet

eee = 0; % Option to plot radiation pattern

fff = 0; % Option to display overlapping displacement seismograms

f = 1; % Geophone number to display seismograms for

ggg = 0; % Option to display overlapping velocity seismograms

```

g = 1; % Geophone number to display seismograms for

iii = 0; % Option to output far field velocity data for ISOLA

jjj = 0; % Option to output all fields velocity data for ISOLA


% Formation Properties for sandstone from Mavko, 1998

% rho = 2370; % Density in kg/m3

% alpha0 = 4.09*1000; % Alpha = P wave velocity in m/s

% beta0 = 2.41*1000; % Beta = S wave velocity in m/s


% Formation properties for shale from Well sonic logs

alpha0 = 3850; % Alpha = P wave velocity in m/s

beta0 = 2370; % Beta = S wave velocity in m/s

rho = 2440; % Density in kg/m3


% Calculate Poisson's ratio, Young's modulus, lambda, and mu (Aki & Richards, 2002)

poissons = (((alpha0^2)/(beta0^2))-2)/(2*(((alpha0^2)/(beta0^2))-1));

youngs = 2*(1+poissons)*rho*(beta0^2);

lambda = (youngs*poissons)/((1+poissons)*(1-(2*poissons)));

mu = youngs/(2*(1+poissons));


% Noise level

% Input noise level in percent, i.e. 0.05 is 5 percent

nl = 0;

```

% Anisotropy parameters for VTI media

% Only edit percent anisotropy (perc_aniso)

perc_aniso = 0;

$C_{33} = \lambda + (2 * \mu);$

$C_{44} = \mu;$

$C_{11} = (1 + (\text{perc_aniso})/100) * C_{33};$

$C_{66} = (1 + (\text{perc_aniso})/100) * C_{44};$

$\epsilon = (C_{11} - C_{33}) / (2 * C_{33});$

$\gamma = (C_{66} - C_{44}) / (2 * C_{44});$

$\delta = 0;$

% Input event frequency

$f_0 = 125;$ % Frequency in Hz for Ricker wavelet

% Eqn 4 from Dahm and Kruger, 2014

% Strike ϕ , dip δ , rake γ , shear magnitude D_s , opening magnitude D_n

% Pure DC is $D_s=1$ and $D_n=0$

% Pure CLVD is $D_s=0$ and $D_n=1$

% N is 1st Lamé constant, ν is 2nd

% In NED coordinate system

$\text{str} = 66;$

$\text{dip} = 90;$

rake = 0;

Ds = 1;

Dn = 0;

N = lambda;

nu = mu;

m11 = -
Ds*N*(sind(2*str)*sind(dip)*cosd(rake)+sind(str)^2*sind(2*dip)*sind(rake))+(Dn*(nu+2*
N*(sind(str)^2)*sind(dip)^2));

m12 =
Ds*N*(cosd(2*str)*sind(dip)*cosd(rake)+(0.5*sind(2*str))*sind(2*dip)*sind(rake))-
Dn*N*sind(2*str)*sind(dip)^2;

m13 = -
Ds*N*(cosd(str)*cosd(dip)*cosd(rake)+(sind(str))*cosd(2*dip)*sind(rake))+Dn*N*sind(st
r)*sind(2*dip);

m22 = Ds*N*(sind(2*str)*sind(dip)*cosd(rake)-
(cosd(str)^2)*sind(2*dip)*sind(rake))+Dn*(nu+2*N*(cosd(str)^2)*sind(dip)^2);

m23 = -Ds*N*(sind(str)*cosd(dip)*cosd(rake)-(cosd(str))*cosd(2*dip)*sind(rake))-
Dn*N*cosd(str)*sind(2*dip);

m33 = Ds*N*(sind(2*dip)*sind(rake))+Dn*(nu+2*N*(cosd(dip)^2));

MT = [m11 m12 m13;

m12 m22 m23;

```

    m13 m23 m33];

MT = MT/(1e10);

% Uncomment next three lines if want pure ISO source
% MT = [1 0 0;
%      0 1 0;
%      0 0 1];

% Seismogram time in seconds
t1 = 0; % Start time
t2 = 8.5; % End time
deltat = 0.001; % Time step
numsamples = ((t2-t1)/deltat)+1; % Number of samples
t(:,1) = t1:deltat:t2; % Seismogram time matrix - one column of numsamples
numgph = 8; % number of geophones
% Note: Maximum number of geophones for outputting data is currently at 20
%      If using less than 20, ignore error on output

% Geophone coordinates (Cartesian) - horizontal array

srcloc = [0 0 0]; % Source location at origin

```



```
% Read in geophone locations

filename2 = ['/home/matlab/trudyw/hydraulicfracturing/well/data/' ...
'Denton_NewarkEast/Well2H/Well1H/Stage01/Perforation/Geo_XYZ.txt'];

format2 = '%f %f %f';

x = cell2mat(read_text(filename2,format2));
```

```
% 1b4 (1b)

% x(:,1) = x(:,1) - 2369827.65;

% x(:,2) = x(:,2) - 7125921.98;

% x(:,3) = x(:,3) - 8661.72;

% x = x*0.3048;
```

```
% 2344 (3d)

% x(:,1) = x(:,1) - 2370285.99;

% x(:,2) = x(:,2) - 7126896.84;

% x(:,3) = x(:,3) - 8729.014;

% x = x*0.3048;
```

```
% 3e4 (3e)

x(:,1) = x(:,1) - 2370255.75;

x(:,2) = x(:,2) - 7127295.63;

x(:,3) = x(:,3) - 8735.26;

x = x*0.3048;
```

```

% Four receivers on surface at 45 deg from source (90 from each other)

% distout = 100; % Horizontal distance of receivers from source

% XYdist = sqrt((distout^2)/2);

% x(:,1) = [-XYdist XYdist XYdist -XYdist];

% x(:,2) = [XYdist XYdist -XYdist -XYdist];

% x(:,3) = [760 760 760 760]; % Receivers on surface (source at 760m~2500ft depth)


% Geophone coordinates (Cartesian) - ring, full angular coverage

% Adapted from anaseis.m

% rad=100;          % radius of the ring (m)

% ang=[0:numgph-1]*2*pi/numgph; % angle in xy plane

% v1=rad*sin(ang);    % 1st coord in ring-plane

% v2=rad*cos(ang);    % 2nd coord in ring-plane

% v3=2660;          % the constant coordinate

% for j=1:numgph

%   x(j,1) = v1(j);

%   x(j,2) = v2(j);

%   x(j,3) = v3;

%   r(j) = sqrt((x(j,1)^2)+(x(j,2)^2)+(x(j,3)^2));

% end


% Calculate distance, azimuth, and dip between each geophone and source

```

```

for j=1:numgph

%   x(j,2) = 1000; % Geophones along line x = 1000 ft

%   x(j,1) = ((400-(500*j))); % Geophones spaced 100 ft apart going from 90 to -100

%   x(j,3) = 1500; % Geophones along line z = 20

    r(j)    =    sqrt(((x(j,1)-srcloc(1))^2)+((x(j,2)-srcloc(2))^2)+((x(j,3)-srcloc(3))^2));    %

Distance between each geophone and source

    r2(j) = sqrt(((x(j,1)-srcloc(1))^2)+((x(j,2)-srcloc(2))^2));

    dists(j,:) = x(j,:)-srcloc;

    azis(j) = atand(dists(j,1)/dists(j,2));

    dips(j) = atand((x(j,3)/(sqrt(x(j,1)^2+x(j,2)^2))))+90;

end

%-----%

% Preallocate large variables to increase speed

x = zeros(numgph,3);

r = zeros(numgph,1);

tp = zeros(numsamples,1);

ts = zeros(numsamples,1);

M0neardisp = zeros(numsamples,20);

M0intpdisp = zeros(numsamples,20);

M0intsdisp = zeros(numsamples,20);

M0farpdisp = zeros(numsamples,20);

M0farsdisp = zeros(numsamples,20);

```

```
M0nearvel = zeros(numsamples,20);
M0intpvel = zeros(numsamples,20);
M0intsvel = zeros(numsamples,20);
M0farpvel = zeros(numsamples,20);
M0farsvel = zeros(numsamples,20);
Afpd = zeros(numgph,3,numsamples);
Afsd = zeros(numgph,3,numsamples);
Aipd = zeros(numgph,3,numsamples);
Aisd = zeros(numgph,3,numsamples);
Annd = zeros(numgph,3,numsamples);
Afpv = zeros(numgph,3,numsamples);
Afsv = zeros(numgph,3,numsamples);
Aipv = zeros(numgph,3,numsamples);
Aisv = zeros(numgph,3,numsamples);
Annv = zeros(numgph,3,numsamples);
confp = zeros(numgph,1);
confs = zeros(numgph,1);
conip = zeros(numgph,1);
conis = zeros(numgph,1);
conn = zeros(numgph,1);
dispfar = zeros(numgph,3,numsamples);
dispint = zeros(numgph,3,numsamples);
dispnear = zeros(numgph,3,numsamples);
```

```
dispall = zeros(numgph,3,numsamples);  
velfar = zeros(numgph,3,numsamples);  
velint = zeros(numgph,3,numsamples);  
velnear = zeros(numgph,3,numsamples);  
velall = zeros(numgph,3,numsamples);  
reco1 = zeros(numsamples,4);  
reco2 = zeros(numsamples,4);  
reco3 = zeros(numsamples,4);  
reco4 = zeros(numsamples,4);  
reco5 = zeros(numsamples,4);  
reco6 = zeros(numsamples,4);  
reco7 = zeros(numsamples,4);  
reco8 = zeros(numsamples,4);  
reco9 = zeros(numsamples,4);  
reco10 = zeros(numsamples,4);  
reco11 = zeros(numsamples,4);  
reco12 = zeros(numsamples,4);  
reco13= zeros(numsamples,4);  
reco14 = zeros(numsamples,4);  
reco15 = zeros(numsamples,4);  
reco16 = zeros(numsamples,4);  
reco17 = zeros(numsamples,4);  
reco18 = zeros(numsamples,4);
```

```

reco19 = zeros(numsamples,4);
reco20 = zeros(numsamples,4);

%-----%
% Plot parameters for geophone-source geometry
if aaa==1
    Figure = figure;
    hold on
    scatter3(x(:,1),x(:,2),x(:,3),75,'^b');
    scatter3(srcloc(1),srcloc(2),srcloc(3),75,'*r');
    title('Geophone Array Relative to Source');
    legend('Geophones','Source')
    xlabel('x direction (m)');
    ylabel('y direction (m)');
    zlabel('z direction (m)');
    negxx = min(min(x(:,1),srcloc(1)));
    posxx = max(max(x(:,1),srcloc(1)));
    negyy = min(min(x(:,2),srcloc(2)));
    posyy = max(max(x(:,2),srcloc(2)));
    negzz = min(min(x(:,3),srcloc(3)));
    poszz = max(max(x(:,3),srcloc(3)));

```

```

%xlim([1.1*negxx,1.1*posxx]);
%ylim([1.1*negyy,1.1*posyy]);
%zlim([1.1*negzz,1.1*poszz]);
%xlim([722000,723000])
%ylim([2172000,2173000])
text(1.02*x(1,1),1.02*x(1,2),1.02*x(1,3),'1')

text(1.02*x(round(numgph/2),1),1.02*x(round(numgph/2),2),1.02*x(round(numgph/2),3
),num2str(round(numgph/2)))

text(1.02*x(round(numgph),1),1.02*x(round(numgph),2),1.02*x(round(numgph),3),num2
str(numgph))

hold off
end

%-----%
% Source parameters

T = 1/f0;

% A = 135000; % Area of fault in m^2 (Papazachos etal, 2004)

% A = 31.7212; % Area of fault in m^2 for event of magnitude -2.5 (average in Barnett,
Cabarcas & Davogustto, 2013)

A = 0.1;

for j=1:numgph

```

```

alpha = alpha0*(1+delta*sind(dips(j))^2*cosd(dips(j))^2+(epsilon*sind(dips(j))^4));
beta          =          beta0*(1+((alpha0^2)/(beta0^2))*(epsilon-
delta)*(sind(dips(j))^2)*(cosd(dips(j))^2));

cp = r(j)/alpha;
cs = r(j)/beta;

for i=1:length(t)

    tp(i) = t(i)-T-cp;
    ts(i) = t(i)-T-cs;
end

% Calculate source time function for displacement
M0neardisp(:,j) = A*mu*(srctfunc('intricker',t(:)-T,f0,r(j)/alpha)-srctfunc('intricker',t(:)-
T,f0,r(j)/beta)); % Ricker for near field

M0intpdisp(:,j) = A*mu*(srctfunc('ricker',tp,f0)); % Ricker for P - intermediate field
M0intsdisp(:,j) = A*mu*(srctfunc('ricker',ts,f0)); % Ricker for S - intermediate field
M0farpdisp(:,j) = A*mu*(srctfunc('dtricker',tp,f0)); % Derivative of Ricker for P - far field
M0farsdisp(:,j) = A*mu*(srctfunc('dtricker',ts,f0)); % Derivative of Ricker for S - far field

% Calculate source time function for velocity
M0nearvel(:,j)          =          A*mu*(srctfunc('dtintricker',t(:)-T,f0,r(j)/alpha)-
srctfunc('dtintricker',t(:)-T,f0,r(j)/beta)); % Ricker for near field

M0intpvel(:,j) = A*mu*(srctfunc('dtricker',tp,f0)); % Ricker for P - intermediate field
M0intsvel(:,j) = A*mu*(srctfunc('dtricker',ts,f0)); % Ricker for S - intermediate field
M0farpvel(:,j) = A*mu*(srctfunc('dttricker',tp,f0)); % Ricker for P - far field
M0farsvel(:,j) = A*mu*(srctfunc('dttricker',ts,f0)); % Ricker for S - far field

```


end

%-----%

% Plot parameters for source time functions for each term of displacement

if bbb==1

Figure = figure;

set(Figure,'Position',[50,50,1500,1000]);

set(gcf,'name','Source-Time Function for Each Term of Displacement at Geophone 1');

subplot('Position',[.05,.7,.4,.2])

hold on

plot(t,srctfunc('ricker',t,f0),'b');

title('Ricker Wavelet at Source');

xlabel('Time(s)')

ylabel('Amplitude')

hold off

subplot('Position',[.5,.7,.4,.2])

hold on

plot(t,M0neardisp(:,1),'b');

title('Source-Time Function for Near Displacement');

xlabel('Time(s)')

ylabel('Amplitude')

hold off

subplot('Position',[.05,4,4,2]);

hold on

plot(t,M0intpdisp(:,1),'b');

title('Source-Time Function for Intermediate Field P Wave Displacement');

xlabel('Time(s)')

ylabel('Amplitude')

hold off

subplot('Position',[.5,4,4,2]);

hold on

plot(t,M0intsdisp(:,1),'b');

title('Source-Time Function for Intermediate Field S Wave Displacement');

xlabel('Time(s)')

ylabel('Amplitude')

hold off

subplot('Position',[.05,1,4,2]);

hold on

plot(t,M0farpdisp(:,1),'b');

title('Source-Time Function for Far Field P Wave Displacement');

xlabel('Time(s)')

```

ylabel('Amplitude')

hold off

subplot('Position',[.5,.1,4,.2]);

hold on

plot(t,M0farsdisp(:,1),'b');

title('Source-Time Function for Far Field S Wave Displacement');

xlabel('Time(s)')

ylabel('Amplitude')

hold off

end

%-----%

% Plot parameters for source time functions for each term of velocity

if ccc==1

    Figure = figure;

    set(Figure,'Position',[50,50,1500,1000]);

    set(gcf,'name','Source-Time Function for Each Term of Velocity at Geophone 1');

    subplot('Position',[.05,.7,4,.2])

    hold on

    plot(t,srctfunc('ricker',t-T,f0),'b');

    title('Ricker Wavelet at Source');

```

```
xlabel('Time(s)')
```

```
ylabel('Amplitude')
```

```
hold off
```

```
subplot('Position',[.5,.7,4,2])
```

```
hold on
```

```
plot(t,M0nearvel(:,1),'b');
```

```
title('Source-Time Function for Near Velocity');
```

```
xlabel('Time(s)')
```

```
ylabel('Amplitude')
```

```
hold off
```

```
subplot('Position',[.05,4,4,2]);
```

```
hold on
```

```
plot(t,M0intpvel(:,1),'b');
```

```
title('Source-Time Function for Intermediate Field P Wave Velocity');
```

```
xlabel('Time(s)')
```

```
ylabel('Amplitude')
```

```
hold off
```

```
subplot('Position',[.5,4,4,2]);
```

```
hold on
```

```
plot(t,M0intsvel(:,1),'b');
```

```

title('Source-Time Function for Intermediate Field S Wave Velocity');

xlabel('Time(s)')

ylabel('Amplitude')

hold off


subplot('Position',[.05,.1,4,.2]);

hold on

plot(t,M0farpvel(:,1),'b');

title('Source-Time Function for Far Field P Wave Velocity');

xlabel('Time(s)')

ylabel('Amplitude')

hold off


subplot('Position',[.5,.1,4,.2]);

hold on

plot(t,M0farsvel(:,1),'b');

title('Source-Time Function for Far Field S Wave Velocity');

xlabel('Time(s)')

ylabel('Amplitude')

hold off

end

%-----%

```

```

% Plot parameters for frequency content of Ricker wavelet

if ddd==1

    Figure = figure;

    set(gcf,'name','Frequency Content of Ricker Wavelet')


    f2 = 0:0.01:(f0*5);

    F = zeros(length(f2),1);

    for i=1:length(f2)

        
$$F(i) = (2/\sqrt{\pi}) * ((f2(i)^2)/(f0^3)) * \exp(-(f2(i)^2)/(f0^2));$$


    end


    plot(f2,F,'b');

    hold on

    xlabel('Frequency (Hz)')

    title('Frequency Content of Ricker Wavelet')

end


% Calculate constants for each field

for j=1:numgph

    alpha = alpha0*(1+delta*sind(dips(j))^2*cosd(dips(j))^2+(epsilon*sind(dips(j))^4));

    beta = beta0*(1+((alpha0^2)/(beta0^2))*(epsilon-
delta)*(sind(dips(j))^2)*(cosd(dips(j))^2));

```

```

confp(j) = 1/(4*pi*rho*(alpha^3)*r(j)); % Far field P wave constant
confs(j) = 1/(4*pi*rho*(beta^3)*r(j)); % Far field S wave constant
conip(j) = 1/(4*pi*rho*(alpha^2)*(r(j)^2)); % Intermediate field P wave constant
conis(j) = 1/(4*pi*rho*(beta^2)*(r(j)^2)); % Intermediate field S wave constant
conn(j) = 1/(4*pi*rho*(r(j)^4)); % Near field constant

end

%-----%

% Calculate displacement at each geophone

for j=1:numgph
    for i=1:numsamples
        for p=1:3
            for q=1:3
                if MT(p,q) ~= 0
                    for n=1:3
                        gamn = abs(x(j,n))/r(j);
                        gamp = abs(x(j,p))/r(j);
                        gamq = abs(x(j,q))/r(j);
                        if p==n
                            kronp = 1;
                        else
                            kronp = 0;
                        end
                    end
                end
            end
        end
    end
end

```

```

if p==q
    kropq = 1;
else
    kropq = 0;
end

if n==q
    kronq = 1;
else
    kronq = 0;
end

% Far field P wave displacement term

Afpd(j,n,i) = Afpd(j,n,i) +
((gamn*gamp*gamq)*confp(j))*MT(p,q)*M0farpdisp(i,j);

% Far field S wave displacement term

Afsd(j,n,i) = Afsd(j,n,i) + (((gamn*gamp*gamq)-
(kronp*gamq))*confs(j))*MT(p,q)*M0farsdisp(i,j);

% Intermediate field P wave displacement term

Aipd(j,n,i) = Aipd(j,n,i) + (((6*gamn*gamp*gamq)-(gamn*kropq)-
(gamp*kronq)-(gamq*kronp))*(conip(j)))*MT(p,q)*M0intpdisp(i,j);

% Intermediate field S wave displacement term

Aisd(j,n,i) = Aisd(j,n,i) + (((6*gamn*gamp*gamq)-(gamn*kropq)-
(gamp*kronq)-(2*gamq*kronp))*(conis(j)))*MT(p,q)*M0intsdisp(i,j);

% Near field displacement term

```



```

Annd(j,n,i) = Annd(j,n,i) + (((15*gamn*gamp*gamq)-(3*gamn*kropq)-
(3*gamp*kronq)-(3*gamq*kronp))*conn(j))*MT(p,q)*M0neardisp(i,j);

```

```

% Far field P wave velocity term

```

```

Afpv(j,n,i) = Afpv(j,n,i) +
((gamn*gamp*gamq)*confp(j))*MT(p,q)*M0farpvel(i,j);

```

```

% Far field S wave velocity term

```

```

Afsv(j,n,i) = Afsv(j,n,i) + (((gamn*gamp*gamq)-
(kronp*gamq))*confs(j))*MT(p,q)*M0farsvel(i,j);

```

```

% Intermediate field P wave velocity term

```

```

Aipv(j,n,i) = Aipv(j,n,i) + (((6*gamn*gamp*gamq)-(gamn*kropq)-
(gamp*kronq)-(gamq*kronp))*(conip(j)))*MT(p,q)*M0intpvel(i,j);

```

```

% Intermediate field S wave velocity term

```

```

Aisv(j,n,i) = Aisv(j,n,i) + (((6*gamn*gamp*gamq)-(gamn*kropq)-
(gamp*kronq)-(2*gamq*kronp))*(conis(j)))*MT(p,q)*M0intsvel(i,j);

```

```

% Near field velocity term

```

```

Annv(j,n,i) = Annv(j,n,i) + (((15*gamn*gamp*gamq)-(3*gamn*kropq)-
(3*gamp*kronq)-(3*gamq*kronp))*conn(j))*MT(p,q)*M0nearvel(i,j);

```

```

end

```

```

end

```

```

end

```

```

end

```

```

end

```

```

end

```

```

%-----%

% Calculate radiation pattern in Cartesian coordinates

% Currently only works for DC sources, needs to be adapted for all input sources

% Suppose we have geophones in ring around source for complete angular
% coverage, need this to display radiation pattern properly

nr=80;          % number of receivers

rad=10;         % radius of the ring [km]

ang=[0:nr-1]*2*pi/nr; % angle in selected plane

v1=rad*sin(ang); % 1st coord in ring-plane

v2=rad*cos(ang); % 2nd coord in ring-plane

v3=zeros(1,nr); % the constant coordinate

xzring = [v1',v3',v2'];

xyring = [v1',v2',v3'];

yzring = [v3',v2',v1'];

radpatAfp1 = zeros(3,nr);

radpatAfs1 = zeros(3,nr);

radpatAip1 = zeros(3,nr);

radpatAis1 = zeros(3,nr);

radpatAnn1 = zeros(3,nr);

rr = zeros(nr,1);

rings = xyring; % Change this based on what plane DC is acting in

```

```

for j=1:50

    rr(j) = sqrt((rings(j,1)^2)+(rings(j,2)^2)+(rings(j,3)^2));

    for i=1:numsamples

        for p=1:3

            for q=1:3

                if MT(p,q) ~= 0

                    for n=1:3

                        gamn = abs(rings(j,n))/rr(j);

                        gamp = abs(rings(j,p))/rr(j);

                        gamq = abs(rings(j,q))/rr(j);

                        if p==n

                            kronp = 1;

                        else

                            kronp = 0;

                        end

                        if p==q

                            kropq = 1;

                        else

                            kropq = 0;

                        end

                        if n==q

                            kronq = 1;

                        else

```

```

        kronq = 0;

    end

    % Conditions to get best coverage of P wave, need

    % to change this to match what plane DC is acting

    if (rings(j,1)>=0 && rings(j,2)>=0)

        radpatAfp1(n,j) = radpatAfp1(n,j) + gamn*gamp*gamq;

        radpatAfs1(n,j) = radpatAfs1(n,j) + (gamn*gamp*gamq)-(kronp*gamq);

        radpatAip1(n,j) = radpatAip1(n,j) + (6*gamn*gamp*gamq)-(gamn*kropq)-
(gamp*kronq)-(gamq*kronp);

        radpatAis1(n,j) = radpatAis1(n,j) + (6*gamn*gamp*gamq)-(gamn*kropq)-
(gamp*kronq)-(2*gamq*kronp);

        radpatAnn1(n,j) = radpatAnn1(n,j) + (15*gamn*gamp*gamq)-
(3*gamn*kropq)-(3*gamp*kronq)-(3*gamq*kronp);

    end

end

end

end

end

end

end

end

%-----%

% Plot radiation pattern in Cartesian coordinates

```

```

if eee==1

    Figure = figure;

    set(gcf,'name','Radiation Pattern of Source in XY Plane')


    pp = max(max(abs(radpatAfp1(1,:))),max(abs(radpatAfp1(2,:))));
    ss = max(max(abs(radpatAfs1(1,:))),max(abs(radpatAfs1(2,:))));
    ps = 1.1*max(pp,ss);


    subplot('Position',[0.05,0.35,.4,.4])

    hold on

    title('P Wave Radiation Pattern')

    scatter(radpatAfp1(1,:),radpatAfp1(2:),'b','filled')
    scatter(-radpatAfp1(1:),-radpatAfp1(2:),'b','filled')
    scatter(radpatAfp1(1:),-radpatAfp1(2:),'b','filled')
    scatter(-radpatAfp1(1:),radpatAfp1(2:),'b','filled')

    xlim([-ps,ps])

    ylim([-ps,ps])

    xlabel('x-direction');

    ylabel('y-direction');

    hold off


    subplot('Position',[0.55,0.35,.4,.4])

    hold on

```

```

title('S Wave Radiation Pattern')

scatter(radpatAfs1(1,:),radpatAfs1(2,:),'r','filled')

scatter(-radpatAfs1(1,:),-radpatAfs1(2,:),'r','filled')

scatter(radpatAfs1(1,:),-radpatAfs1(2,:),'r','filled')

scatter(-radpatAfs1(1,:),radpatAfs1(2,:),'r','filled')

xlim([-ps,ps])

ylim([-ps,ps])

xlabel('x-direction');

ylabel('y-direction');

hold off

end

%-----%

% Calculate displacement

for j=1:numgph

    for i=1:numsamples

        for n=1:3

            dispfar(j,n,i) = Afpd(j,n,i)-Afsd(j,n,i);

            dispint(j,n,i) = Aipd(j,n,i)-Aisd(j,n,i);

            dispnear(j,n,i) = Annd(j,n,i);

            dispall(j,n,i) = dispfar(j,n,i)+dispint(j,n,i)+dispnear(j,n,i);

            velfar(j,n,i) = Afpv(j,n,i)-Afsv(j,n,i);

            velint(j,n,i) = Aipv(j,n,i)-Aisv(j,n,i);

```

```

        velnear(j,n,i) = Annv(j,n,i);

        velall(j,n,i) = velfar(j,n,i)+velint(j,n,i)+velnear(j,n,i);

    end

end

end

% Add noise

% Random noise Gaussian

z1 = randn(numgph, 3, length(t));

z1 = z1/(max(max(max(z1(:,:)))));

for g=1:numgph

    for c=1:3

        for tt=1:(length(t)-1)

            if mod(tt,2)==0

                z1(g,c,tt) = -z1(g,c,tt-1);

            end

        end

    end

end

end

maxvel = max(max(max(abs(velall(:,:)))));

maxdisp = max(max(max(dispsall(:,:)))));

velall = velall + z1*nl*maxvel;

```

```

dispall = dispall + z1*nl*maxdisp;

%-----%

% Plot parameters for overlapping displacement seismograms
if fff==1

    Figure = figure;

    set(gcf,'name',sprintf('Effect of Each Term on Total Velocity at Geophone %i',f))

    set(Figure,'Position',[50,50,1500,1000]);

    xx = max(max(max(abs(dispall(f,1,:)))));

    yy = max(max(max(abs(dispall(f,2,:)))));

    zz = max(max(max(abs(dispall(f,3,:)))));

    xyz = max([xx,yy,zz]);

    subplot(3,1,1)

    hold on

    dispnearx = dispnear(f,1,:); plot(t,dispnearx(:),'color',[0 0.5 0],'LineWidth',1.5)

    dispintx = dispint(f,1,:); plot(t,dispintx(:),'m','LineWidth',1.5)

    dispfarx = dispfar(f,1,:); plot(t,dispfarx(:),'b','LineWidth',1.5)

    dispallx = dispall(f,1,:); plot(t,dispallx(:),'r','LineWidth',1.5)

    title('x-direction')

    [legh,objh,outh,outm] = legend('Near','Intermediate','Far','Total');

    set(objh,'linewidth',2);

```



```

xlabel('Time(s)')

ylabel('Amplitude')

% ylim([-xyz,xyz])

hold off


subplot(3,1,2)

hold on

dispneary = dispnear(f,2,:); plot(t,dispneary(:),'color',[0 0.5 0])
dispinty = dispint(f,2,:); plot(t,dispinty(:),'m')
dispfary = dispfar(f,2,:); plot(t,dispfary(:),'b')
dispally = dispall(f,2,:); plot(t,dispally(:),'r')

title('y-direction')

legend('Near','Intermediate','Far','Total')

xlabel('Time(s)')

ylabel('Amplitude')

% ylim([-xyz,xyz])

hold off


subplot(3,1,3)

hold on

dispnearz = dispnear(f,3,:); plot(t,dispnearz(:),'color',[0 0.5 0])
dispintz = dispint(f,3,:); plot(t,dispintz(:),'m')
dispfarz = dispfar(f,3,:); plot(t,dispfarz(:),'b')

```

```

dispallz = dispall(f,3,:); plot(t,dispallz(:),'r')

title('z-direction')

legend('Near','Intermediate','Far','Total')

xlabel('Time(s)')

ylabel('Amplitude')

% ylim([-xyz,xyz])

hold off

end

%-----%

% Plot parameters for overlapping velocity seismograms
if ggg==1
    Figure = figure;
    set(gcf,'name',sprintf('Effect of Each Term on Total Velocity at Geophone %i',g))
    set(Figure,'Position',[50,50,1500,1000]);

    xx = max(max(max(abs(velall(g,1,:)))));
    yy = max(max(max(abs(velall(g,2,:)))));
    zz = max(max(max(abs(velall(g,3,:)))));
    xyz = max([xx,yy,zz]);

    subplot(3,1,1)

```

```

hold on

velnearx = velnear(g,1,:); plot(t,velnearx(:),'g')

velintx = velint(g,1,:); plot(t,velintx(:),'m')

velfarx = velfar(g,1,:); plot(t,velfarx(:),'b')

velallx = velall(g,1,:); plot(t,velallx(:),'r')

title('x-direction')

legend('Near','Intermediate','Far','Total')

xlabel('Time(s)')

ylabel('Amplitude')

hold off

```

```

subplot(3,1,2)

hold on

velneary = velnear(g,2,:); plot(t,velneary(:),'g')

velinty = velint(g,2,:); plot(t,velinty(:),'m')

velfary = velfar(g,2,:); plot(t,velfary(:),'b')

velally = velall(g,2,:); plot(t,velally(:),'r')

title('y-direction')

legend('Near','Intermediate','Far','Total')

xlabel('Time(s)')

ylabel('Amplitude')

hold off

```

```

subplot(3,1,3)

hold on

velnearz = velnear(g,3,:); plot(t,velnearz(:),'g')

velintz = velint(g,3,:); plot(t,velintz(:),'m')

velfarz = velfar(g,3,:); plot(t,velfarz(:),'b')

velallz = velall(g,3,:); plot(t,velallz(:),'r')

title('z-direction')

legend('Near','Intermediate','Far','Total')

xlabel('Time(s)')

ylabel('Amplitude')

hold off

end

%-----%

% Calculate percentage each component contributes to sum

% if hhh==1

%   sumnear = 0;

%   sumint = 0;

%   sumfar = 0;

%   sumall = 0;

%

%   for i=1:numsamples

%       sumnear = (dispnear(1,1,i)^2) + sumnear;

```

```

%    sumint = (dispint(1,1,i)^2) + sumint;
%    sumfar = (dispfar(1,1,i)^2) + sumfar;
%    sumall = sumnear+sumint+sumfar;
% end
%
% fprintf('Near field percentage of displacement: %.5f \n', (sumnear/sumall)*100)
% fprintf('Intermediate field percentage of displacement: %.5f \n', (sumint/sumall)*100)
% fprintf('Far field percentage of displacement: %.5f \n', (sumfar/sumall)*100)
% %fprintf('Average displacement: %.20f \n', (sumall/numsamples))
% b = sumall/numsamples
% sumnear = 0;
% sumint = 0;
% sumfar = 0;
% sumall = 0;
%
% for i=1:numsamples
%     sumnear = (velnear(10,3,i)^2) + sumnear;
%     sumint = (velint(10,3,i)^2) + sumint;
%     sumfar = (velfar(10,3,i)^2) + sumfar;
%     sumall = sumnear+sumint+sumfar;
% end
%
% fprintf('Near field percentage of velocity: %.5f \n', (sumnear/sumall)*100)

```

```

% fprintf('Intermediate field percentage of velocity: %.5f \n', (sumint/sumall)*100)

% fprintf('Far field percentage of velocity: %.5f \n', (sumfar/sumall)*100)

%

% end

%-----%

% Output far field velocity to max of 20 geophones

% Geophones 1-10 names are first three letters of 1-10 in english

% Geophones 11-20 names are first three letters of 1-10 in spanish

if iii==1

    mkdir(dirname);

    cd(dirname);

    mkdir invert;

    mkdir data;

    cd data;

    for i=1:numsamples

        reco1(i,1)=t(i,1);

        reco1(i,2)=velfar(1,2,i);

        reco1(i,3)=velfar(1,1,i);

        reco1(i,4)=velfar(1,3,i);

    end

```

```
fopen ('ONEunc.dat','w');  
save ONEunc.dat reco1 -ascii  
fclose ('all');
```

```
for i=1:numsamples  
    reco2(i,1)=t(i,1);  
    reco2(i,2)=velfar(2,2,i) ;  
    reco2(i,3)=velfar(2,1,i) ;  
    reco2(i,4)=velfar(2,3,i) ;  
end
```

```
fopen ('TWOunc.dat','w');  
save TWOunc.dat reco2 -ascii  
fclose ('all');
```

```
for i=1:numsamples  
    reco3(i,1)=t(i,1);  
    reco3(i,2)=velfar(3,2,i) ;  
    reco3(i,3)=velfar(3,1,i) ;  
    reco3(i,4)=velfar(3,3,i) ;  
end
```

```
fopen ('THRununc.dat','w');
```

```
save THRunc.dat reco3 -ascii
```

```
fclose ('all');
```

```
for i=1:numsamples
```

```
    reco4(i,1)=t(i,1);
```

```
    reco4(i,2)=velfar(4,2,i) ;
```

```
    reco4(i,3)=velfar(4,1,i) ;
```

```
    reco4(i,4)=velfar(4,3,i) ;
```

```
end
```

```
fopen ('FOUunc.dat','w');
```

```
save FOUunc.dat reco4 -ascii
```

```
fclose ('all');
```

```
for i=1:numsamples
```

```
    reco5(i,1)=t(i,1);
```

```
    reco5(i,2)=velfar(5,2,i) ;
```

```
    reco5(i,3)=velfar(5,1,i) ;
```

```
    reco5(i,4)=velfar(5,3,i) ;
```

```
end
```

```
fopen ('FIVunc.dat','w');
```

```
save FIVunc.dat reco5 -ascii
```



```
fclose ('all');
```

```
for i=1:numsamples
```

```
    reco6(i,1)=t(i,1);
```

```
    reco6(i,2)=velfar(6,2,i) ;
```

```
    reco6(i,3)=velfar(6,1,i) ;
```

```
    reco6(i,4)=velfar(6,3,i) ;
```

```
end
```

```
fopen ('SIXunc.dat','w');
```

```
save SIXunc.dat reco6 -ascii
```

```
fclose ('all');
```

```
for i=1:numsamples
```

```
    reco7(i,1)=t(i,1);
```

```
    reco7(i,2)=velfar(7,2,i) ;
```

```
    reco7(i,3)=velfar(7,1,i) ;
```

```
    reco7(i,4)=velfar(7,3,i) ;
```

```
end
```

```
fopen ('SEVunc.dat','w');
```

```
save SEVunc.dat reco7 -ascii
```

```
fclose ('all');
```

```

for i=1:numsamples
    reco8(i,1)=t(i,1);
    reco8(i,2)=velfar(8,2,i) ;
    reco8(i,3)=velfar(8,1,i) ;
    reco8(i,4)=velfar(8,3,i) ;
end

```

```

fopen ('ElGunc.dat','w');
save ElGunc.dat reco8 -ascii
fclose ('all');

```

```

for i=1:numsamples
    reco9(i,1)=t(i,1);
    reco9(i,2)=velfar(9,2,i) ;
    reco9(i,3)=velfar(9,1,i) ;
    reco9(i,4)=velfar(9,3,i) ;
end

```

```

fopen ('NINunc.dat','w');
save NINunc.dat reco9 -ascii
fclose ('all');

```

```

for i=1:numsamples
    reco10(i,1)=t(i,1);
    reco10(i,2)=velfar(10,2,i) ;
    reco10(i,3)=velfar(10,1,i) ;
    reco10(i,4)=velfar(10,3,i) ;
end

```

```

fopen ('TENunc.dat','w');
save TENunc.dat reco10 -ascii
fclose ('all');

```

```

for i=1:numsamples
    reco11(i,1)=t(i,1);
    reco11(i,2)=velfar(11,2,i) ;
    reco11(i,3)=velfar(11,1,i) ;
    reco11(i,4)=velfar(11,3,i) ;
end

```

```

fopen ('UNOunc.dat','w');
save UNOunc.dat reco11 -ascii
fclose ('all');

```

```

for i=1:numsamples

```

```

reco12(i,1)=t(i,1);
reco12(i,2)=velfar(12,2,i) ;
reco12(i,3)=velfar(12,1,i) ;
reco12(i,4)=velfar(12,3,i) ;
end

```

```

fopen ('DOSunc.dat','w');
save DOSunc.dat reco12 -ascii
fclose ('all');

```

```

for i=1:numsamples
    reco13(i,1)=t(i,1);
    reco13(i,2)=velfar(13,2,i) ;
    reco13(i,3)=velfar(13,1,i) ;
    reco13(i,4)=velfar(13,3,i) ;
end

```

```

fopen ('TREunc.dat','w');
save TREunc.dat reco13 -ascii
fclose ('all');

```

```

for i=1:numsamples
    reco14(i,1)=t(i,1);

```

```

    reco14(i,2)=velfar(14,2,i) ;
    reco14(i,3)=velfar(14,1,i) ;
    reco14(i,4)=velfar(14,3,i) ;
end

```

```

fopen ('CUAunc.dat','w');
save CUAunc.dat reco14 -ascii
fclose ('all');

```

```

for i=1:numsamples
    reco15(i,1)=t(i,1);
    reco15(i,2)=velfar(15,2,i) ;
    reco15(i,3)=velfar(15,1,i) ;
    reco15(i,4)=velfar(15,3,i) ;
end

```

```

fopen ('CINunc.dat','w');
save CINunc.dat reco15 -ascii
fclose ('all');

```

```

for i=1:numsamples
    reco16(i,1)=t(i,1);
    reco16(i,2)=velfar(16,2,i) ;

```

```
reco16(i,3)=velfar(16,1,i) ;  
reco16(i,4)=velfar(16,3,i) ;  
end
```

```
fopen ('SElunc.dat','w');  
save SElunc.dat reco16 -ascii  
fclose ('all');
```

```
for i=1:numsamples  
    reco17(i,1)=t(i,1);  
    reco17(i,2)=velfar(17,2,i) ;  
    reco17(i,3)=velfar(17,1,i) ;  
    reco17(i,4)=velfar(17,3,i) ;  
end
```

```
fopen ('SIEunc.dat','w');  
save SIEunc.dat reco17 -ascii  
fclose ('all');
```

```
for i=1:numsamples  
    reco18(i,1)=t(i,1);  
    reco18(i,2)=velfar(18,2,i) ;  
    reco18(i,3)=velfar(18,1,i) ;
```

```
    reco18(i,4)=velfar(18,3,i) ;  
end
```

```
    fopen ('OCHunc.dat','w');  
save OCHunc.dat reco18 -ascii  
    fclose ('all');
```

```
for i=1:numsamples  
    reco19(i,1)=t(i,1);  
    reco19(i,2)=velfar(19,2,i) ;  
    reco19(i,3)=velfar(19,1,i) ;  
    reco19(i,4)=velfar(19,3,i) ;  
end
```

```
fopen ('NUEunc.dat','w');  
save NUEunc.dat reco19 -ascii  
fclose ('all');
```

```
for i=1:numsamples  
    reco20(i,1)=t(i,1);  
    reco20(i,2)=velfar(20,2,i) ;  
    reco20(i,3)=velfar(20,1,i) ;  
    reco20(i,4)=velfar(20,3,i) ;
```

```

end

fopen ('DIEunc.dat','w');

save DIEunc.dat reco20 -ascii

fclose ('all');

cd ..

cd ..

end

%-----%

% Output all fields velocity to max of 20 geophones

% Geophones 1-10 names are first three letters of 1-10 in english

% Geophones 11-20 names are first three letters of 1-10 in spanish

if jjj==1

    mkdir(dirname);

    cd(dirname);

    mkdir data;

    cd data;


    velall(:,3,:) = -velall(:,3,:);

    for i=1:numsamples

        reco1(i,1)=t(i,1);

        reco1(i,2)=velall(1,2,i);

```



```
    reco1(i,3)=velall(1,1,i);  
    reco1(i,4)=velall(1,3,i);  
end
```

```
    fopen ('ONEunc.dat','w');  
save ONEunc.dat reco1 -ascii  
    fclose ('all');
```

```
for i=1:numsamples  
    reco2(i,1)=t(i,1);  
    reco2(i,2)=velall(2,2,i) ;  
    reco2(i,3)=velall(2,1,i) ;  
    reco2(i,4)=velall(2,3,i) ;  
end
```

```
    fopen ('TWOunc.dat','w');  
save TWOunc.dat reco2 -ascii  
    fclose ('all');
```

```
for i=1:numsamples  
    reco3(i,1)=t(i,1);  
    reco3(i,2)=velall(3,2,i) ;  
    reco3(i,3)=velall(3,1,i) ;
```

```

    reco3(i,4)=velall(3,3,i) ;
end

fopen ('THRuncl.dat','w');
save THRuncl.dat reco3 -ascii

fclose ('all');

```

```

for i=1:numsamples

    reco4(i,1)=t(i,1);

    reco4(i,2)=velall(4,2,i) ;

    reco4(i,3)=velall(4,1,i) ;

    reco4(i,4)=velall(4,3,i) ;

end

```

```

fopen ('FOUunc.dat','w');
save FOUunc.dat reco4 -ascii

fclose ('all');

```

```

for i=1:numsamples

    reco5(i,1)=t(i,1);

    reco5(i,2)=velall(5,2,i) ;

    reco5(i,3)=velall(5,1,i) ;

    reco5(i,4)=velall(5,3,i) ;

```

```
end
```

```
fopen ('FIVunc.dat','w');
```

```
save FIVunc.dat reco5 -ascii
```

```
fclose ('all');
```

```
for i=1:numsamples
```

```
    reco6(i,1)=t(i,1);
```

```
    reco6(i,2)=velall(6,2,i) ;
```

```
    reco6(i,3)=velall(6,1,i) ;
```

```
    reco6(i,4)=velall(6,3,i) ;
```

```
end
```

```
fopen ('SIXunc.dat','w');
```

```
save SIXunc.dat reco6 -ascii
```

```
fclose ('all');
```

```
for i=1:numsamples
```

```
    reco7(i,1)=t(i,1);
```

```
    reco7(i,2)=velall(7,2,i) ;
```

```
    reco7(i,3)=velall(7,1,i) ;
```

```
    reco7(i,4)=velall(7,3,i) ;
```

```
end
```

```
fopen ('SEVunc.dat','w');  
save SEVunc.dat reco7 -ascii  
fclose ('all');
```

```
for i=1:numsamples  
    reco8(i,1)=t(i,1);  
    reco8(i,2)=velall(8,2,i) ;  
    reco8(i,3)=velall(8,1,i) ;  
    reco8(i,4)=velall(8,3,i) ;  
end
```

```
fopen ('ElGunc.dat','w');  
save ElGunc.dat reco8 -ascii  
fclose ('all');
```

```
for i=1:numsamples  
    reco9(i,1)=t(i,1);  
    reco9(i,2)=velall(9,2,i) ;  
    reco9(i,3)=velall(9,1,i) ;  
    reco9(i,4)=velall(9,3,i) ;  
end
```

```
fopen ('NINunc.dat','w');  
save NINunc.dat reco9 -ascii  
fclose ('all');
```

```
for i=1:numsamples  
    reco10(i,1)=t(i,1);  
    reco10(i,2)=velall(10,2,i) ;  
    reco10(i,3)=velall(10,1,i) ;  
    reco10(i,4)=velall(10,3,i) ;  
end
```

```
fopen ('TENunc.dat','w');  
save TENunc.dat reco10 -ascii  
fclose ('all');
```

```
for i=1:numsamples  
    reco11(i,1)=t(i,1);  
    reco11(i,2)=velall(11,2,i) ;  
    reco11(i,3)=velall(11,1,i) ;  
    reco11(i,4)=velall(11,3,i) ;  
end
```

```
fopen ('UNOunc.dat','w');
```

```
save UNOunc.dat reco11 -ascii
```

```
fclose ('all');
```

```
for i=1:numsamples
```

```
    reco12(i,1)=t(i,1);
```

```
    reco12(i,2)=velall(12,2,i) ;
```

```
    reco12(i,3)=velall(12,1,i) ;
```

```
    reco12(i,4)=velall(12,3,i) ;
```

```
end
```

```
fopen ('DOSTLW.unc','w');
```

```
save DOSunc.dat reco12 -ascii
```

```
fclose ('all');
```

```
for i=1:numsamples
```

```
    reco13(i,1)=t(i,1);
```

```
    reco13(i,2)=velall(13,2,i) ;
```

```
    reco13(i,3)=velall(13,1,i) ;
```

```
    reco13(i,4)=velall(13,3,i) ;
```

```
end
```

```
fopen ('TREunc.dat','w');
```

```
save TREunc.dat reco13 -ascii
```

```
fclose ('all');
```

```
for i=1:numsamples
```

```
    reco14(i,1)=t(i,1);
```

```
    reco14(i,2)=velall(14,2,i) ;
```

```
    reco14(i,3)=velall(14,1,i) ;
```

```
    reco14(i,4)=velall(14,3,i) ;
```

```
end
```

```
fopen ('CUAunc.dat','w');
```

```
save CUAunc.dat reco14 -ascii
```

```
fclose ('all');
```

```
for i=1:numsamples
```

```
    reco15(i,1)=t(i,1);
```

```
    reco15(i,2)=velall(15,2,i) ;
```

```
    reco15(i,3)=velall(15,1,i) ;
```

```
    reco15(i,4)=velall(15,3,i) ;
```

```
end
```

```
fopen ('CINunc.dat','w');
```

```
save CINunc.dat reco15 -ascii
```

```
fclose ('all');
```

```

for i=1:numsamples
    reco16(i,1)=t(i,1);
    reco16(i,2)=velall(16,2,i) ;
    reco16(i,3)=velall(16,1,i) ;
    reco16(i,4)=velall(16,3,i) ;
end

```

```

fopen ('SElunc.dat','w');
save SElunc.dat reco16 -ascii
fclose ('all');

```

```

for i=1:numsamples
    reco17(i,1)=t(i,1);
    reco17(i,2)=velall(17,2,i) ;
    reco17(i,3)=velall(17,1,i) ;
    reco17(i,4)=velall(17,3,i) ;
end

```

```

fopen ('SIEunc.dat','w');
save SIEunc.dat reco17 -ascii
fclose ('all');

```



```

for i=1:numsamples
    reco18(i,1)=t(i,1);
    reco18(i,2)=velall(18,2,i) ;
    reco18(i,3)=velall(18,1,i) ;
    reco18(i,4)=velall(18,3,i) ;
end

```

```

fopen ('OCHunc.dat','w');
save OCHunc.dat reco18 -ascii
fclose ('all');

```

```

for i=1:numsamples
    reco19(i,1)=t(i,1);
    reco19(i,2)=velall(19,2,i) ;
    reco19(i,3)=velall(19,1,i) ;
    reco19(i,4)=velall(19,3,i) ;
end

```

```

fopen ('NUEunc.dat','w');
save NUEunc.dat reco19 -ascii
fclose ('all');

```

```

for i=1:numsamples

```

```

    reco20(i,1)=t(i,1);

    reco20(i,2)=velall(20,2,i) ;

    reco20(i,3)=velall(20,1,i) ;

    reco20(i,4)=velall(20,3,i) ;

end

fopen ('DIEunc.dat','w');

save DIEunc.dat reco20 -ascii

fclose ('all');

cd ..

% Write out table of geophone coordinates

stn_names = ['ONE','TWO','THR','FOU','FIV','SIX','SEV','EIG'];

fileID=fopen('GPH_LL.stn','w+');

for j=1:numgph

    fprintf(fileID,'%3s %f %f %f\r\n',stn_names((3*j-2):(j*3)),lat(j),long(j),x(j,3));

end

fclose(fileID);

cd ..

end

fprintf('Time taken to run: %.2f \n', toc)

```

srctfunc.m

Calculate source-time function for synthetic seismograms

Located in /home/trudyw/hydraulicfracturing/TLW

% srctfunc.m

% Trudy Watkins

% Adapated from Chennu Fan's srctfunc.m

% March 6, 2015

% Calculate source-time function for displacement calculation

% Use with cartmomtens.m

function [srctfunc] = srctfunc(type,t,f,tau)

a = strcmp(type,'ricker'); % Ricker wavelet

b = strcmp(type,'dtricker'); % Derivative of Ricker wavelet

c = strcmp(type,'intricker'); % Integral of Ricker wavelet

d = strcmp(type,'dttricker'); % Second derivative of Ricker wavelet

e = strcmp(type,'dtintricker'); % Derivative of integral of Ricker wavelet

for i=1:length(t)

if a==1

$$A(i) = (1-2*(\pi^2)*(f^2)*(t(i)^2))*\exp(-(\pi^2)*(f^2)*(t(i)^2));$$

```

end

if b==1
    A(i) = 2*(pi^2)*(f^2)*(t(i))*exp(-(pi^2)*(f^2)*((t(i)^2)))*(2*(pi^2)*(f^2)*(t(i)^2)-3);
end

if c==1
    A(i) = ((exp(-(f^2)*(pi^2)*(t(i)-tau)^2))*(2*(f^2)*(pi^2)*tau*(tau-
t(i))+1))/(2*(f^2)*(pi^2));
end

if d==1
    A(i) = exp(-(pi^2)*(f^2)*(t(i)^2))*((-
8*(pi^6)*(f^6)*(t(i)^4))+(24*(pi^4)*(f^4)*(t(i)^2))-6*(pi^2)*(f^2));
end

if e==1
    A(i) = (2*exp(-(f^2)*(pi^2)*(t(i)-tau)^2)*(f^2)*(pi^2)*(-t(i)/(2*(f^2)*(pi^2)))+((t(i)-
tau)^2)*tau));
end

srctfunc(i) = A(i);

```

end

end

FindPerfs.R

Find perforation event data (segys) using times from provided field notes

Located in A/PreprocessPerfs/

FindPerfs.R

Trudy Watkins

Updated December 12, 2016

Find perforation event data using times found in field notes

Sets directory as directory where this script is being sourced from

```
setwd(dirname(sys.frame(1)$ofile))
```

```
dirperf <- paste(dirname(dirname(getwd())),"/PerforationData",sep="")
```

Source required functions and/or packages

```
source(paste(dirname(getwd()),"/SUinRFuncs/readSu.R",sep=""))
```

```
source(paste(dirname(getwd()),"/SUinRFuncs/readSuTracehead.R",sep=""))
```

Set dir (directory) to where RAW_SLB_SEISMIC_DATA perforation data is located

```
dir_raw <- "/home/trudyw/hydraulicfracturing/seismics/data/RAW_SLB_SEISMIC_DATA"
```

```
setwd(dir_raw)
```

```

# Set stage name

stg <- "1a"


# Go to stage directory for perforation data

fls <- list.files()

fls <- fls[grepl("Perf",fls)]

twell <- substr(stg,1,1)

if (twell==2) {mw=3} else {mw=2}

fls <- fls[grepl(paste("TW_",twell,sep=""),fls)]

stglet <- substr(stg,2,2)

anlist <- c("a","b","c","d","e")

stgnum <- which(anlist==stglet)

fls <- fls[grepl(paste("Stage_0",stgnum,sep=""),fls)]

setwd(paste(dir_raw,"/",fls,sep=""))

dir_raw <- getwd()

sgys <- list.files()

sgys <- sgys[grepl("sgy",sgys)]

sgytms <- list()

for (i in 1:length(sgys)) {

  if (stg!="1a") {

    sgytms[[i]] <- as.POSIXct(substr(sgys[i],9,14),format="%H%M%S")

  } else {

```

```

sgytms[[i]] <- as.POSIXct(substr(sgys[i],52,59),format="%H%M%S")
}

}

# Read in perforation times

dir_out <- paste(dirperf,"/Pad",mw,"H/Pad",twell,"H/Stg",stgnum,"/su/",sep="")

ptims <- read.csv(paste(dir_out,"/PerfTimes",stg,".csv",sep=""),header=F)

# Get window of files around each perforation time

tdiff1 <- tdiff2 <- list()

for (i in 1:length(ptims$V1)) {

  possevs <- list()

  hrs <- as.POSIXct(ptims$V1[i],format="%H:%M:%S")

  if (stg!="1a") {

    con <- 10

  } else {con <- 30}

  hrs1 <- hrs-con

  hrs2 <- hrs+con

  for (j in 1:length(sgytms)) {

```

```

tdiff1[j] <- difftime(sgytms[[j]],hrs1,units="secs")
tdiff2[j] <- difftime(hrs2,sgytms[[j]],units="secs")
}
td1 <- which(tdiff1>0)
td2 <- which(tdiff2>0)
td12 <- intersect(td1,td2)

sgysp <- sgys[td12]

# Plot segys around perforation time and mark it if it has an event
# Note that perforations that are across two files (i.e. starts in one, ends in another)
# can be copied over together but must be concatenated, preprocessed, and renamed
manually

for (k in sgysp) {
  setwd(dir_out)
  system(paste("segypread tape=",dir_raw,"/",k," > temp.su ",sep=""))

  connection <- file("temp.su","rb")
  datalst <- list()
  for (m in 4:6) {
    data <- readSu(connection,3008)
    datalst[[m]] <- data$data[[1]]
  }
}

```



```

close(connection)

datalst <- unlist(datalst)-mean(unlist(datalst))

datalst <- datalst/max(unlist(datalst))

plot(datalst[1:3008]+1,type="l",col="red",ylim=c(0,4))

lines(datalst[3009:6017]+2,col="darkgreen")

lines(datalst[6018:9024]+3,col="blue")


ans <- readline("Is there an event? Enter y or n: ")


if (ans=="y") {
  possevs <- c(possevs,k)
}

}


if (length(possevs)>1) {
  print(paste("Perforation time is ",hrs,sep=""))
  print("SGY files are:")
  print(sgytms[which(sgys%in%possevs)])
  sgynum <- as.numeric(readline("Enter number of sgy file to use (if want both enter 0):
"))
  if (sgynum==0) {
    for (n in 1:2) {

```

```

    system(paste("cp ",dir_raw,"/",sgys[which(sgys%in%possevs)[n]],".",sep=""))
  }
} else {
  print(paste("Selected segy is at ",sgytms[which(sgys%in%possevs)][[sgynum]],sep=""))
  sgysel <- sgys[which(sgys%in%possevs)[sgynum]]
}
} else {
  sgysel <- sgys[which(sgys%in%possevs)[1]]
}

# Copy selected segy(s) to perforation data directory
if (sgynum!=0) {
  system(paste("cp ",dir_raw,"/",sgysel,".",sep=""))
}

if (length(possevs)==0) {
  print(paste("Sgy not found for perforation ",i,sep=""))
} else {
  print("Copied selected segy(s)")
}
}

```

PreprocessPerfs.R

Separate perforation data into su files by geophone, demean and cut seismograms to

0.5 seconds long

Located in A/PreprocessPerfs/

ProcessPerfs.R

Trudy Watkins

Updated December 15, 2016

Separate perfs in 8 files (1 for each gph, i.e. SPx_STNy.su)

Demean data and cut data around perf so that su is 0.5 seconds long

Sets directory as directory where this script is being sourced from

```
setwd(dirname(sys.frame(1)$ofile))
```

```
dirperf <- paste(dirname(dirname(getwd())),"/PerforationData",sep="")
```

Source required functions and/or packages

```
source(paste(dirname(getwd()),"/SUinRFuncs/readSu.R",sep=""))
```

```
source(paste(dirname(getwd()),"/SUinRFuncs/readSuTracehead.R",sep=""))
```

```
source(paste(dirname(getwd()),"/SUinRFuncs/writeSuBindata.R",sep=""))
```

Set directory for data

```
stg <- "3c"
```

```
twell <- substr(stg,1,1)
```

```
if (twell==2) {mw=3} else {mw=2}
```

```

anlist <- c("a","b","c","d","e")

stgnum <- which(anlist==substr(stg,2,2))

dir_dat <- paste(dirperf,"/Pad",mw,"H/Pad",twell,"H/Stg",stgnum,"/su/",sep="")

setwd(dir_dat)


# Get list of segys

fls <- list.files()

sgys <- fls[grepl(".sgy",fls)]


for (s in 1:length(sgys)) {


# Convert to su

system(paste("segysread tape=",sgys[s]," > temp.su ",sep=""))


# Read in su and demean

connection <- file("temp.su","rb")

datalst <- datalstplt <- list()

for (i in 1:24) {

data <- readSu(connection,3008)

datalst[[i]] <- data$data[[1]]-mean(data$data[[1]])


# Second data variable for plotting purposes

datalstplt[[i]] <- datalst[[i]]/max(datalst[[i]])

```

```

}

close(connection)

# Plot and set window of 0.5 seconds
tseq <- seq(from=0,to=3.007,by=0.001)

plot(tseq,datalstplt[[1]]+1,type="l",ylim=c(0,24),main=paste("SP",s,sep=""))

for (i in 2:24) {
  lines(tseq,datalstplt[[i]]+i)
}

# Select window and plot

winst <- as.numeric(readline("Enter window start in secs: "))

winend <- winst+0.501

plot(tseq,datalstplt[[1]]+1,type="l",ylim=c(0,24),xlim=c(winst,winend),main=paste("SP",s,sep=""))

for (i in 2:24) {
  lines(tseq,datalstplt[[i]]+i)
}

# Loop until ok with window

ans <- readline("Ok with window (y or n)? ")

```

```

while(ans=="n") {

  winst <- as.numeric(readline("Enter window start in secs: "))
  winend <- winst+0.501

  plot(tseq,datalstplt[[1]]+1,type="l",ylim=c(0,24),xlim=c(winst,winend))
  for (i in 2:24) {
    lines(tseq,datalstplt[[i]]+i)
  }

  ans <- readline("Ok with window (y or n)? ")
}

winst <- winst/0.001
winend <- winend/0.001

# Output data in ZYX order (for PCA) as bin and convert to su
for (i in 1:8) {
  end <- 3*i
  st <- end-2

  datout
  <-
  c(datalst[[end]][winst:winend],datalst[[st+1]][winst:winend],datalst[[st]][winst:winend])
}

```

```

outbound <- paste("SP",s,"_STN",i,".bin",sep="")
outbound_connection <- file(outbound,"wb")
writeSuBinData(datout,outbound_connection)
close(outbound_connection)

system(paste("suaddhead ns=",501," < SP",s,"_STN",i,".bin | sushw key=dt a=",1000," >
SP",s,"_STN",i,".su",sep=""))

system(paste("rm SP",s,"_STN",i,".bin",sep=""))

}

}

```

ReorientGphsExample.R

Call ReorientGphs function on input perforation data and perforation times

Located in A/ReorientGphs/

```

# ReorientGphsExample.R
# Trudy Watkins
# November 22, 2016
# Example script that runs ReorientGphs.R function

```

```

# Sets directory as directory where this script is being sourced from

```

```

setwd(dirname(sys.frame(1)$ofile))

```

```

dirperf <- paste(dirname(dirname(getwd())),"/PerforationData",sep="")

# Source required functions

# Note that when working with excel sheets in this manner, if a step is rerun,
# i.e. you recalculate the average Euler angles, you must clear the data and delete
# the cells in the spreadsheet before rerunning (only appends, does not overwrite)
source(paste(dirname(getwd()),"/SUinRFuncs/readSu.R",sep=""))
source(paste(dirname(getwd()),"/SUinRFuncs/readSuTracehead.R",sep=""))
source(paste(dirname(getwd()),"/SUinRFuncs/writeSuBindata.R",sep=""))
source("ReorientGphs.R")
require("seismicRoll")
require("XLConnect")

# Determine which MW, TW, Stg, SP, and GPH to look at

# Note that this step can be rewritten as a loop for faster analysis of data
Stg <- (readline("Enter stage name: "))
SP <- as.numeric(readline("Enter shot point number: "))
GPH <- as.numeric(readline("Enter geophone number: "))

# for (SP in 1:7) {
#   for (GPH in 1) {

TW <- substr(Stg,1,1)

```



```

if (TW==2) {MW=3} else {MW=2}

anlist <- c("a","b","c","d","e")

stgnum <- which(anlist==substr(stg,2,2))


# Read in data, data is demeaned and in ZYX

setwd(paste(dirperf,"/Pad",MW,"H/Pad",TW,"H/Stg",Stgn,"/su/",sep=""))

connection <- file(paste("SP",SP,"_STN",GPH,".su",sep=""),"rb")

data_in <- list()

for (i in 1:3) {

  dat <- readSu(connection,501)

  data_in[[i]] <- dat$data[[1]]

}

close(connection)


# Convert to XYZ for input to function

dat2 <- c(data_in[[3]],data_in[[2]],data_in[[1]])

data_test <- matrix(unlist(dat2),nrow=3,byrow=T)


# Use STA/LTA to find first break

fb_sec <- roll_stalta(data_in[[1]]^2,5,50)

fb_sec <- which.max(fb_sec)*0.001


# Check if ok with STA/LTA

```

```

layout(c(1,1))

par(cex.axis=0.75)

tseq <- seq(from=0,to=0.5,by=0.001)

plot(tseq,data_in[[1]],type="l",xlab="Time (s)",ylab="Amplitude")

lines(rep(fb_sec,2),c(-1e9,1e9),col="red",lwd=2)

ans <- readline("Ok with fb? ")

while (ans=="n") {

  print(paste("Current fb is ",fb_sec," seconds",sep=""))

  fb_sec <- as.numeric(readline("Enter new fb in seconds: "))

  plot(tseq,data_in[[1]],type="l",xlab="Time (s)",ylab="Amplitude")

  lines(rep(fb_sec,2),c(-1e9,1e9),col="red",lwd=2)

  ans <- readline("Ok with fb? ")

}

# Sample interval in seconds

samp_int <- 0.001

# Read in alpha and beta (SP relative to GPH)

fls <- list.files()

alpha_in <- fls[grepl("alpha",fls)]

beta_in <- fls[grepl("beta",fls)]

alpha_mat <- as.matrix(read.csv(alpha_in,header=F))

beta_mat <- as.matrix(read.csv(beta_in,header=F))

```

```

alpha <- unname(alpha_mat[GPH,SP])
beta <- unname(beta_mat[GPH,SP])

orout <- ReorientGphs(data_test,fb_sec,samp_int,alpha,beta)

# Write results to excel file

# Note excel file must have already been created (can be empty but needs to have sheet
names)

# Rating is your way of judging how good the result is (used for QCing later, must be
numeric)

rating <- as.numeric(readline("Rating: "))

setwd(dirperf)

file <- loadWorkbook(paste("EulerAnglesMW",MW,".xlsx",sep=""))

sheetname <- paste("GPH",GPH,sep="")

row_list1 <- c(GPH,MW,TW,Stgn,SP,orout$E1deg,orout$E2deg,orout$E3deg,orout$Az1,orout$Dip1,orout$Az4,orout$Dip4,alpha,beta,rating,orout$maxenloc,orout$a11,orout$a12,orout$a13,orout$a21,orout$a22,orout$a23,orout$a31,orout$a32,orout$a33)

row_list1 <- as.data.frame(t(row_list1))

appendWorksheet(file,row_list1,sheet=sheetname,header=FALSE)

saveWorkbook(file,paste("EulerAnglesMW",MW,".xlsx",sep=""))

```

```
# }
```

```
# }
```

ReorientGphs.R

Run principal component analysis of perforation data and calculate Euler angles

Located in A/ReorientGphs/

```
# ReorientGphs.R
```

```
# Trudy Watkins
```

```
# August 10, 2015
```

```
# Updated November 22, 2016
```

```
# Function to run polarization analysis on seismograms
```

```
# Uses supolar from SeismicUn*x (Stockwell and Cohen, 2014; Maercklin, 2007)
```

```
# Requires readSu, readSuTracehead, and writeSuBindata functions
```

```
# Outputs are a 3 x n matrix of the rotated data in XYZ and the three Euler angles (Ikelle  
and Amundsen, 2005)
```

```
# Inputs
```

```
# data_in must be a 3 x n matrix of demeaned data in ZYX order
```

```

# first_break_s is the time of the P-wave arrival in seconds relative to the start time of the
seismogram (0 sec)

# range_samples is the number of samples around the first break to search for time of
maximum energy

# sample_int is the sample interval in seconds

# alpha is the azimuth of the source relative to the receiver in degrees (N=0)

# beta is the angle from the vertical of the source relative to the receiver in degrees
(positive cc) (i.e. source and receiver at same depth have beta=90)


# References

# Maercklin, N. (2007). SUPOLAR and SUPOFILT: SU programs for polarization analysis and
filtering of three-component data.

# Stockwell, J., John W., & Cohen, J. K. (2014). CWP/SU: Seismic Un*x Release No. 43: an
open source software package for seismic research and processing.

# Ikelle, & Amundsen. (2005). Introduction to Petroleum Seismology (Vol. 12).


ReorientGphs <- function(data_in,first_break_s,sample_int,alpha,beta) {

  # Make new data matrix in XYZ for rotation

  data_mat <- data_in[c(3,2,1),]

  # Plot input seismogram

  datlen <- ncol(data_mat)

```

```

tlen <- datlen*sample_int

data_t <- seq(from=0,to=tlen-sample_int,by=sample_int)

winst <- first_break_s-35*sample_int

winend <- first_break_s+75*sample_int


# Write data_in to su and run polarization analysis (Stockwell and Cohen, 2014)

outbound_connection = file("temp.bin","wb")

datlst <- c(data_in[1,],data_in[2,],data_in[3,])

writeSuBinData(datlst,outbound_connection)

close(outbound_connection)

system(paste("suaddhead ns=",datlen," < temp.bin | sushw key=dt a=",1/sample_int," >
temp.su",sep=""))

system(paste("supolar < temp.su wl=0.01 win=boxcar file=polar angle=deg phi=3
theta=3 rl=1 dir=1 amp=1",sep=""))


# Read in energy of seismogram

inbound = paste("polar.er")

connection <- file(inbound,"rb")

energy = readSu(connection,501)

close(connection)

first_arrival = first_break_s / sample_int

range_samples <- 30

early_pos = first_arrival - range_samples/2

```

```

late_pos = first_arrival + range_samples/2

max_energy_site <- which.max(energy$data[[1]][early_pos:late_pos])

max_energy_loc <- early_pos + max_energy_site - 1


# Read in phi of seismogram

inbound = paste("polar.phi")

connection <- file(inbound,"rb")

azimuth <- readSu(connection,501)

close(connection)

azimuth_deg1 = azimuth$data[[1]][max_energy_loc]

# if (azimuth_deg1>180) {azimuth_deg1 <- azimuth_deg1-180}


# Read in theta of seismogram

inbound = paste("polar.theta")

connection <- file(inbound,"rb")

dip = readSu(connection,501)

close(connection)

dip_deg1 = dip$data[[1]][max_energy_loc]


# Calculate Euler angles (Ikelle and Amundsen, 2005)

E1 <- -azimuth_deg1*pi/180

E2 <- -(beta+dip_deg1)*pi/180

E3 <- alpha*pi/180

```

```

# Build rotation matrix

a11 <- cos(E3)*cos(E1)-cos(E2)*sin(E1)*sin(E3)
a12 <- cos(E3)*sin(E1)+cos(E2)*cos(E1)*sin(E3)
a13 <- sin(E3)*sin(E2)
a21 <- -sin(E3)*cos(E1)-cos(E2)*sin(E1)*cos(E3)
a22 <- -sin(E3)*sin(E1)+cos(E2)*cos(E1)*cos(E3)
a23 <- cos(E3)*sin(E2)
a31 <- sin(E2)*sin(E1)
a32 <- -sin(E2)*cos(E1)
a33 <- cos(E2)

# Rotate data

rotmat <- matrix(c(a11,a12,a13,a21,a22,a23,a31,a32,a33),ncol=3,byrow=TRUE)
rotated_data <- rotmat%*%data_mat

# Output rotated data as ZYX and rerun polarization analysis (Stockwell and Cohen,
2014)

system("rm temp.su")

rotated_data_sup <- c(rotated_data[3,],rotated_data[2,],rotated_data[1,])

outbound_connection = file("temp.bin","wb")

writeSuBinData(rotated_data_sup,outbound_connection)

close(outbound_connection)

```



```
system(paste("suaddhead ns=",datlen," < temp.bin | sushw key=dt a=",1/sample_int," >
temp.su",sep=""))
```

```
system(paste("supolar < temp.su wl=0.01 win=boxcar file=polar angle=deg phi=3
theta=3 rl=1 dir=1 amp=1",sep=""))
```

```
# Read in phi
```

```
inbound = paste("polar.phi")
```

```
connection <- file(inbound,"rb")
```

```
azimuth <- readSu(connection,501)
```

```
close(connection)
```

```
azimuth_deg4 = azimuth$data[[1]][max_energy_loc]
```

```
# Read in theta
```

```
inbound = paste("polar.theta")
```

```
connection <- file(inbound,"rb")
```

```
dip = readSu(connection,501)
```

```
close(connection)
```

```
dip_deg4 = dip$data[[1]][max_energy_loc]
```

```
# Plot rotated data with energy, phi, and theta
```

```
layout(matrix(c(1,2,3,4),nrow=4))
```

```
par(mar=c(3.5,4,2,2))
```

```
par(mgp=c(2.5,1,0))
```

```

plot(data_t,data_in[3,],type="l",
      xlab="Time (s)",ylab="Amplitude",main="X Component",xlim=c(winst,winend))

lines(rep(max_energy_loc*sample_int,2),c(1.5*min(rotated_data[1,]),1.5*max(rotated_data
[1,])),
      lwd=2,col="red")

points(winst+2*sample_int,max(rotated_data[1,]*0.8),pch=16,col="red",cex=1.5)
text(winst+10*sample_int,max(rotated_data[1,]*0.8),"Max Energy",col="red")

plot(data_t,energy$data[[1]],type="l",main="Average Energy",
      xlim=c(winst,winend),xlab="Time (s)",ylab="Energy")

points(max_energy_loc*sample_int,energy$data[[1]][max_energy_loc],pch=16,cex=1.5,col=
"red")

plot(data_t,azimuth$data[[1]],type="l",main="Azimuth (phi) (after reorientation)",
      xlim=c(winst,winend),xlab="Time (s)",ylab="Azimuth (deg)")

points(max_energy_loc*sample_int-0.001,alpha,pch=16,cex=1.5,col="red")

plot(data_t,dip$data[[1]],type="l",main="Dip (theta) (after reorientation)",
      xlim=c(winst,winend),xlab="Time (s)",ylab="Dip (deg)")

points(max_energy_loc*sample_int,dip$data[[1]][max_energy_loc],pch=16,cex=1.5,col="red
")

```

```

outdf <-
list(Rotated_Data_XYZ=rotated_data,E1deg=E1*180/pi,E2deg=E2*180/pi,E3deg=E3*180/
pi,

Az1=azimuth_deg1,Dip1=dip_deg1,a11=a11,a12=a12,a13=a13,a21=a21,a22=a22,a23=a23,

a31=a31,a32=a32,a33=a33,Az4=azimuth_deg4,Dip4=dip_deg4,maxenloc=max_energy_loc)

return(outdf)

}

```

CalculateAverageEulerAngles.R

Calculates average Euler angles for each geophone for each stage and outputs to excel file

Located in A/ReorientGphs/

```

# CalculateAvgEulerAngles.R

# Trudy Watkins

# Updated December 15, 2016

# Calculates average Euler angles at each geophone for each stage

# After this is completed, open RotationAngles excel file and check for large

# standard deviations for E1, go to stage in EulerAngles excel file

# and the large standard deviation will be a result of the 180 degree ambiguity

```

```
# in PCA, adjust E1s within stage (add or subtract 180) and rerun this to get low  
# standard deviation
```

```
# Sets directory as directory where this script is being sourced from  
setwd(dirname(sys.frame(1)$ofile))  
dirperf <- paste(dirname(dirname(getwd())),"/PerforationData",sep="")
```

```
# Source required functions and/or packages  
# Note that when working with excel sheets in this manner, if a step is rerun,  
# i.e. you recalculate the average Euler angles, you must clear the data and delete  
# the cells in the spreadsheet before rerunning (only appends, does not overwrite)  
require("XLConnect")
```

```
# Set working directory to perforation data  
setwd(dirperf)
```

```
# Read in euler angle results in excel file  
MWin <- "2"  
file <- loadWorkbook(paste("EulerAnglesMW",MWin,".xlsx",sep=""))
```

```
for (GPH in 1:8) {  
  sheetname <- paste("GPH",GPH,sep="")  
  data <- readWorksheet(file,sheetname,header=TRUE)
```

```

Az1 <- as.numeric(data$Az1)
Dip1 <- as.numeric(data$Dip1)
TW <- as.numeric(data$TW)
MW <- as.numeric(data$MW)
Stage <- as.numeric(data$Stage)
E1 <- as.numeric(data$E1)
E2 <- as.numeric(data$E2)
E3 <- as.numeric(data$E3)

if (MWin=="2") {
  MWs <- rep(2,6)
  TWs <- c(1,1,3,3,3,3)
  Stgs <- c(1,2,2,3,4,5)
} else {
  MWs <- rep(3,3)
  TWs <- c(2,2,2)
  Stgs <- c(1,2,4)
}

for (m in 1:length(MWs)) {
  mrows <- which(data$MW==MWs[m])
  data2 <- data[mrows,]
  trows <- which(data2$TW==TWs[m])

```

```

data3 <- data2[trows,]

srows <- which(data3$Stage==Stgs[m])

data4 <- data3[srows,]


# Calculate averages and sds of Euler Angles

E1m <- mean(data4$E1)

E1sd <- sd(data4$E1)

E2m <- mean(data4$E2)

E2sd <- sd(data4$E2)

E3m <- mean(data4$E3)

E3sd <- sd(data4$E3)


# Write to excel file

# Note excel file must have already been created (can be empty)

file <- loadWorkbook(paste("RotationAnglesMW",MW,".xlsx",sep=""))

datlst <- (c(MWs[m],TWs[m],Stgs[m],GPH,E1m,E1sd,E2m,E2sd,E3m,E3sd))

datlst <- as.data.frame(t(datlst))

appendWorksheet(file,datlst,sheet=sheetname,header=F)

saveWorkbook(file,paste("RotationAnglesMW",MW,".xlsx",sep=""))

}

}

```

RotatePerfData.R

Rotate perforation data using average Euler angles and calculate reorientation error

Located in A/ReorientGphs/

```
# RotatePerfData.R

# Trudy Watkins

# Updated December 16, 2016

# Rotate perforation using Euler angles and calculate error in reorientation


# Sets directory as directory where this script is being sourced from
setwd(dirname(sys.frame(1)$ofile))

dirperf <- paste(dirname(dirname(getwd())),"/PerforationData",sep="")


# Source required functions and/or packages

# Note that when working with excel sheets in this manner, if a step is rerun,
# i.e. you recalculate the average Euler angles, you must clear the data and delete
# the cells in the spreadsheet before rerunning (only appends, does not overwrite)

require("XLConnect")

source(paste(dirname(getwd()),"/SUinRFuncs/readSu.R",sep=""))
source(paste(dirname(getwd()),"/SUinRFuncs/readSuTracehead.R",sep=""))
source(paste(dirname(getwd()),"/SUinRFuncs/writeSuBindata.R",sep=""))


# Set stage

Stg <- "3c"
```

```

TW <- as.numeric(substr(Stg,1,1))

if (TW==2) {MW=3} else {MW=2}

stgs <- c("a","b","c","d","e")

Stage <- which(substr(Stg,2,2)==stgs)


for (gph_num in 1:8) {

  # Sample interval

  sample_int = 0.001


  # Read in max energy loc and Euler angles

  setwd(dir_perf)

  file <- loadWorkbook(paste("RotationAnglesMW",MW,".xlsx",sep=""))

  sheet <- paste("GPH",gph_num,sep="")

  input_rot <- as.list(readWorksheet(wkbook,sheet,header=TRUE))

  for (k in 1:length(input_rot$MW)) {

    if (input_rot$MW[k]==MW && input_rot$TW[k]==TW && input_rot$Stage[k]==Stage) {

      E1 <- input_rot$E1Avg[k]*pi/180

      E2 <- input_rot$E2Avg[k]*pi/180

      E3 <- input_rot$E3Avg[k]*pi/180

    }

  }

}

```



```

wkbk <- loadWorkbook(paste("EulerAnglesMW",MW,".xlsx",sep=""))
input <- as.list(readWorksheet(wkbk,sheet,header=TRUE))

a = 1

OrigRating <- list()

FBs <-list()

for (i in 1:length(input$MW)) {
  if (input$MW[i]==MW) {
    if (input$TW[i]==TW) {
      if (input$Stage[i]==Stage) {
        FBs[a] <- input$FirstBreak[i]
        OrigRating[a] <- input$Rating[i]
        a = a + 1
      }
    }
  }
}

FBs <- unlist(FBs)

OrigRating <- unlist(OrigRating)

for (sp_num in 1:7) {

  max_energy_loc <- FBs[sp_num]

```

```

# Set directory for data, data is demeaned and in ZYX

setwd(paste(dirperf,"/Pad",mw,"H/Pad",twell,"H/Stg",stgnum,"/su/",sep=""))

file_in <- paste("SP",sp_num,"_STN",gph_num,".su",sep="")

connection      <- file(file_in,"rb")

data_in         = readSu(connection,80000)

close(connection)


# Extract amplitudes as XYZ

data_list <- list()

data_list                                              <-

c(data_in$data[[1]][1123:1623],data_in$data[[1]][562:1062],data_in$data[[1]][1:501])

data_list <- unlist(data_list)

data_mat <- matrix(data_list,nrow=3,byrow=TRUE)


# Read in alpha and beta (SP relative to GPH)

fls <- list.files()

alpha_file <- fls[grepl("alpha",fls)]

alpha_mat <- data.matrix(read.csv(alpha_file,header=FALSE))

beta_file <- fls[grepl("beta",fls)]

beta_mat <- data.matrix(read.csv(beta_file,header=FALSE))


# Isolate alpha and beta for particular SP-GPH pair

alpha <- alpha_mat[[gph_num,sp_num]]

```

```

beta <- beta_mat[[gph_num,sp_num]]

if (alpha<0) {
  alpha2 <- alpha+360
} else {
  alpha2 <- alpha
}

if (beta<0) {
  beta2 <- -1*beta
} else {
  beta2 <- beta
}

# Rotation matrix

a11 <- cos(E3)*cos(E1)-cos(E2)*sin(E1)*sin(E3)
a12 <- cos(E3)*sin(E1)+cos(E2)*cos(E1)*sin(E3)
a13 <- sin(E3)*sin(E2)
a21 <- -sin(E3)*cos(E1)-cos(E2)*sin(E1)*cos(E3)
a22 <- -sin(E3)*sin(E1)+cos(E2)*cos(E1)*cos(E3)
a23 <- cos(E3)*sin(E2)
a31 <- sin(E2)*sin(E1)
a32 <- -sin(E2)*cos(E1)
a33 <- cos(E2)

```

```

rotmat <- matrix(c(a11,a12,a13,a21,a22,a23,a31,a32,a33),ncol=3,byrow=TRUE)

rotated_data <- rotmat%%data_mat

# Output rotated data

rotated_data_sup    <- c(rotated_data[3,],rotated_data[2,],rotated_data[1,])

outbound_bin        = paste("SP",sp_num,"_STN",gph_num,"_rot.bin",sep="")

outbound_connection  = file(outbound_bin,"wb")

writeSuBinData(rotated_data_sup,outbound_connection)

close(outbound_connection)

system(paste("suaddhead ns=",501," < SP",sp_num,"_STN",gph_num,"_rot.bin | sushw
key=dt a=",1000," > SP",sp_num,"_STN",gph_num,"_rot.su",sep=""))

# Run final polarization analysis to confirm correct rotation

system(paste("supolar < SP",sp_num,"_STN",gph_num,"_rot.su wl=0.01 win=boxcar
file=polar angle=deg phi=3 theta=2 rl=1 dir=1 amp=1",sep=""))

i=1

# Read in phi again

inbound             = paste("polar.phi")

connection          <- file(inbound,"rb")

azimuth            <- readSu(connection,501)

close(connection)

```

```

azimuth_deg4      = azimuth$data[[1]][max_energy_loc]

# Read in theta again

inbound           = paste("polar.theta")
connection         <- file(inbound,"rb")
dip               = readSu(connection,501)
close(connection)
dip_deg4          = dip$data[[1]][max_energy_loc]

file_in <- paste("SP",sp_num,"_STN",gph_num,"_rot.su",sep="")
connection        <- file(file_in,"rb")
data_in_2         = readSu(connection,80000)
close(connection)

data_list_2 <- list()

data_list_2                                              <-
c(data_in_2$data[[1]][1123:1623],data_in_2$data[[1]][562:1062],data_in_2$data[[1]][1:50
1])
data_list_2 <- unlist(data_list_2)

if (azimuth_deg4>180) {azimuth_deg4 <- azimuth_deg4-180}

azdiff <- abs(alpha2-azimuth_deg4)

dipdiff <- abs(beta2-dip_deg4)

```

```

azdiff <- abs(alpha2-azimuth_deg4)

if (azdiff>20 || dipdiff>15) {
  rate <- 1
} else {rate <- 0}

# Save results to excel file
file <- loadWorkbook(paste(dirperf,"/RotatedEulerAnglesMW",MW,".xlsx",sep=""))
sheetname <- paste("GPH",gph_num,sep="")
row_list1 <- c(gph_num,MW,TW,Stage,sp_num,azimuth_deg4,dip_deg4,alpha2,beta2,azdiff,dipdiff,rate)
row_list1 <- as.data.frame(t(row_list1))
appendWorksheet(file,row_list1,sheet=sheetname,header=FALSE)
saveWorkbook(file,paste(dirperf,"/RotatedEulerAnglesMW",MW,".xlsx",sep=""))
}
}

```

QCEulerAngles.R

Review PCA results for perforations with reorientation errors greater than 20°

Located in A/ReorientGphs/

QCEulerAngles.R

Trudy Watkins

```

# Updated December 17, 2016

# Review initial PCA results for perforations with reorientation errors

# greater than 20 degrees in azimuth and/or greater than 15 degrees in dip


# Sets directory as directory where this script is being sourced from

setwd(dirname(sys.frame(1)$ofile))

dirperf <- paste(dirname(dirname(getwd())),"/PerforationData",sep="")


# Source required functions and/or packages

# Note that when working with excel sheets in this manner, if a step is rerun,
# i.e. you recalculate the average Euler angles, you must clear the data and delete
# the cells in the spreadsheet before rerunning (only appends, does not overwrite)

require("XLConnect")

source(paste(dirname(getwd()),"/SUinRFuncs/readSu.R",sep=""))

source(paste(dirname(getwd()),"/SUinRFuncs/readSuTracehead.R",sep=""))

source(paste(dirname(getwd()),"/SUinRFuncs/writeSuBindata.R",sep=""))


# Select stage

Stg <- "3c"

TW <- as.numeric(substr(Stg,1,1))

if (TW==2) {MW=3} else {TW=2}

stgs <- c("a","b","c","d","e")

Stage <- which(substr(Stg,2,2)==stgs)

```

```

gph_lst <- c(1,3,4,5,7)
for (gph_num in gph_lst[1]) {

  file <- loadWorkbook(paste(dirperf,"/RotatedEulerAnglesMW",MW,".xlsx",sep=""))
  sheetname <- paste("GPH",gph_num,sep="")

  resin <- as.data.frame(readWorksheet(file,sheetname,header=TRUE))

  file <- loadWorkbook(paste(dirperf,"/RotationAnglesMW",MW,".xlsx",sep=""))
  RAsin <- as.data.frame(readWorksheet(file,sheetname,header=TRUE))

  file <- loadWorkbook(paste(dirperf,"/EulerAnglesMW",MW,".xlsx",sep=""))
  EAsin <- as.data.frame(readWorksheet(file,sheetname,header=TRUE))

  rowm <- which(RAsin$MW==MW)
  RAsin <- RAsin[rowm,]
  rowm <- which(EAsin$MW==MW)
  EAsin <- EAsin[rowm,]

  rowt <- which(RAsin$TW==TW)
  RAsin <- RAsin[rowt,]
  rowt <- which(EAsin$TW==TW)
  EAsin <- EAsin[rowt,]

```



```

rows <- which(RAsin$Stage==Stage)

RAsin <- RAsin[rows,]

rows <- which(EAsin$Stage==Stage)

EAsin <- EAsin[rows,]


for (sp in 1:length(resin$Rate)) {

  if (resin$Rate[sp]==1) {

    rowsp <- which(EAsin$SP==sp)

    EAsin <- EAsin[rowsp,]

    max_energy_loc <- EAsin$FirstBreak[sp]


    setwd(paste(dirperf,"/Pad",resin$MW[sp],"H/Pad",resin$TW[sp],"H/Stg",resin$Stage[sp],"
/su/",sep=""))

    sufl <- paste("SP",resin$SP[sp],"_STN",resin$GPH[sp],".su",sep="")

    connection <- file(sufl,"rb")

    data_in <- list()

    for (i in 1:3) {

      dat <- readSu(connection,501)

      data_in[[i]] <- dat$data[[1]]

    }

```

```

close(connection)

system(paste("supolar < ",sufl," wl=0.01 win=boxcar file=polar angle=deg phi=3 theta=3
rl=1 dir=1 amp=1",sep=""))

# Read in energy of seismogram
inbound = paste("polar.er")
connection <- file(inbound,"rb")
energy <- readSu(connection,501)
close(connection)

# Read in phi of seismogram
inbound = paste("polar.phi")
connection <- file(inbound,"rb")
azimuth <- readSu(connection,501)
close(connection)
azimuth_deg1 = azimuth$data[[1]][max_energy_loc]

# Read in theta of seismogram
inbound = paste("polar.theta")
connection <- file(inbound,"rb")
dip = readSu(connection,501)
close(connection)

```

```

dip_deg1 = dip$data[[1]][max_energy_loc]

print(paste("E1 should be ~",-round(RAsin$E1Avg,1),sep=""))

E1est <- -round(RAsin$E1Avg,1)

# Plot

data_t <- seq(from=0,to=500,by=1)

par(cex.axis=1)

winst <- (max_energy_loc-30)
winend <- (max_energy_loc+50)

layout(matrix(c(1,2,3),nrow=3))

par(mar=c(3.5,4,2,2))

par(mgp=c(2.5,1,0))

plot(data_t,energy$data[[1]],type="l",main="Average Energy",
      xlim=c(winst,winend),xlab="Time (s)",ylab="Energy")

points(max_energy_loc,energy$data[[1]][max_energy_loc],pch=16,cex=1.5,col="red")

plot(data_t,azimuth$data[[1]],type="l",main="Azimuth (phi) (after reorientation)",
      xlim=c(winst,winend),xlab="Time (s)",ylab="Azimuth (deg)")

points(max_energy_loc,azimuth$data[[1]][max_energy_loc],pch=16,cex=1.5,col="red")

plot(data_t,dip$data[[1]],type="l",main="Dip (theta) (after reorientation)",
      xlim=c(winst,winend),xlab="Time (s)",ylab="Dip (deg)")

points(max_energy_loc,dip$data[[1]][max_energy_loc],pch=16,cex=1.5,col="red")

```

```

winst <- max_energy_loc-20

winend <- max_energy_loc+20

azis <- azimuth$data[[1]][winst:winend]

for (i in 1:length(azis)) {

  if (azis[i]>180) {azis[i] <- azis[i]-180}

}

azisest1 <- which(azis>(E1est-10))

azisest2 <- which(azis<(E1est+10))

azisestw <- intersect(azisest1,azisest2)

azisest <- azis[azisestw]

azis <- data.frame(Loc=azisestw+max_energy_loc-20,Azi=azisest)

print(paste("Current loc is ",max_energy_loc),sep="")

print(azis)


max_energy_loc <- as.numeric(readline("Enter new Loc: "))


E1out <- azimuth$data[[1]][max_energy_loc]

if (E1out>180) {E1out <- E1out-180}

EAsin$E1 <- -E1out

EAsin$FirstBreak <- max_energy_loc


appendWorksheet(file,EAsin,sheet=sheetname,header=FALSE)

```

```

    setwd(dirperf)

    saveWorkbook(file,paste("EulerAnglesMW",MW,".xlsx",sep=""))

  }

}

}

```

EventDetectExample.R

Call EventDetect function for input database of treatment data and RMS amplitudes

Located in A/EventDetect/

```

# EventDetectExample.R

# Trudy Watkins

# November 27, 2016

# Example script that runs EventDetect.R


# Sets directory as directory where this script is being sourced from
setwd(dirname(sys.frame(1)$ofile))


# Source required functions

source("EventDetect.R")


# Read in database

# Database and rms amplitudes provided by Dr. Juan M Lorenzo

DB <- read.csv("TLWdb1.csv")

```

```
DB2 <- data.frame(File=DB$filename,RMSAmp=DB$rm)
```

```
testout <- EventDetect(DB2)
```

```
# Write out list of files
```

```
write.csv(testout$File,"Events3dFiles.csv")
```

EventDetect.R

Determine which treatment data files have large RMS amplitudes and output as list of files containing events

Located in A/EventDetect/

```
# EventDetect.R
```

```
# Trudy Watkins
```

```
# Created: September 4, 2015
```

```
# Updated: November 27, 2016
```

```
# Function to read in event database and detect
```

```
# events with largest amplitudes with plot included
```

```
# Input DB is a data frame with two columns
```

```
# First column is named File and has list of su files
```

```
# Second column is named RMSAmp and is the calculated rms amplitude
```

```
# of the microseismic data in each su file
```

```
# Returns input data frame with only rows with largest rms amplitudes
```

```
EventDetect <- function(DB) {
```

```
  # Calculate mean and standard deviation of rms amplitudes
```

```
  avg <- mean(DB$RMSAmp[DB$RMSAmp!=0])
```

```
  std <- sd(DB$RMSAmp[DB$RMSAmp!=0])
```

```
  # Determine which files have largest rms amplitudes
```

```
  rms_large <- DB$RMSAmp[DB$RMSAmp>mean(avg+2*std)]
```

```
  id_large <- which(DB$RMSAmp>mean(avg+2*std))
```

```
  fns_large <- DB$File[id_large]
```

```
  # Plot rms amplitude for each file and highlight ones with greatest RMS amplitudes
```

```
  layout(matrix(c(1)))
```

```
  par(mar=c(5,4,4,2))
```

```
  plot(DB$RMSAmp,col="black",xlab="File Number",ylab="RMS Amplitude",
```

```
       ylim=c(50000,5e+05),pch=20,xaxt="n",yaxt="n")
```

```
  title("RMS Amplitudes",line=1.5)
```

```
  points(id_large,rms_large,col="red",pch=20,cex=1.5)
```

```
  axis(side=1,at=axTicks(1),labels=formatC(axTicks(1),format="d",big.mark=","))
```

```

axis(side=2,at=axTicks(2),labels=formatC(axTicks(2),format="d",big.mark=","))
legend("topright",legend=c("Files with greatest","RMS amplitudes"),pch=c(20,20),
      pt.cex=c(1.5),col=c("red","white"),cex=0.9)

return(DB[id_large,])
}

```

ExtractEvents.R

Extract segy files from treatment data containing events

Located in A/EventDetect/

ExtractEvents.R

Trudy Watkins

Updated December 16, 2016

Sets directory as directory where this script is being sourced from

```
setwd(dirname(sys.frame(1)$ofile))
```

```
dirtreat <- paste(dirname(dirname(getwd())),"/TreatmentData",sep="")
```

Read in csv containing list of files to extract

```
evs <- (read.csv("Events3dFiles.csv"))
```

```
evs <- evs$x
```

Set dir (directory) to where RAW_SLB_SEISMIC_DATA treatment data is located


```

dir_raw <- "/home/trudyw/hydraulicfracturing/seismics/data/RAW_SLB_SEISMIC_DATA"

setwd(dir_raw)


# Set stage name

stg <- "3d"


# Go to stage directory for perforation data

fls <- list.files()

fls <- fls[grept("Treat",fls)]

twell <- substr(stg,1,1)

fls <- fls[grept(paste("TW_",twell,sep=""),fls)]

stglet <- substr(stg,2,2)

anlist <- c("a","b","c","d","e")

stgnum <- which(anlist==stglet)

fls <- fls[grept(paste("Stage_0",stgnum,sep=""),fls)]

setwd(paste(dir_raw,"/",fls,sep=""))

dir_raw <- getwd()

sgys <- list.files()

sgys <- sgys[grept("sgy",sgys)]


# Set directory to where files will by copied to

dir_to <- paste(dirtreat,"/RawData/Events",stg,sep="")

```

```
# Make and copy files in event list to event directory

for (f in evs) {

  f <- paste(substr(f,1,16),".sgy",sep="")

  system(paste("mkdir ",dir_to,"/",substr(f,9,16),sep=""))

  system(paste("cp ",dir_raw,"/",f," ",dir_to,"/",substr(f,9,16),sep=""))

}
```

PreprocessEvents.R

Separate treatment data into different files by geophone, demean and shorten seismograms to 0.5 seconds, pick P-wave arrival

Located in A/PreprocessEvents/

```
# PreprocessEvents.R

# Trudy Watkins

# Updated December 16, 2016

# Demean, shorten to 0.5 seconds, separate seismograms into different

# SU files by geophone, and pick P-wave arrival


# Sets directory as directory where this script is being sourced from

setwd(dirname(sys.frame(1)$ofile))

dirtreat <- paste(dirname(dirname(getwd())),"/TreatmentData",sep="")

dirperf <- paste(dirname(dirname(getwd())),"/PerforationData",sep="")
```

```

# Source required functions and/or packages

source(paste(dirname(getwd()),"/SUinRFuncs/readSu.R",sep=""))

source(paste(dirname(getwd()),"/SUinRFuncs/readSuTracehead.R",sep=""))

source(paste(dirname(getwd()),"/SUinRFuncs/writeSuBindata.R",sep=""))


# Set stage

stg <- "3d"

MW <- "2"

TW <- as.numeric(substr(stg,1,1))

stgs <- c("a","b","c","d","e")

Stage <- which(stgs==substr(stg,2,2))


# Go to raw data directory

setwd(paste(dirtreat,"/RawData/Events",stg,sep=""))


# Get list of event directories

evs <- list.files()


# Make list of geophones to output

gphlst <- c(1,3,4,5,7)

fbs_out <- data.frame(GPH=gphlst,FB=rep(0,length(gphlst)))


for (ev in evs) {

```

```

# Go to event directory

setwd(paste(dirtreat,"/RawData/Events",Stg,"/",ev,sep=""))

fls <- list.files()

fls <- fls[grep(".sgy",fls)]

# Convert sgy to su

system(paste("segypread tape=",fls," > ",ev,".su ",sep=""))

# Read in su and demean

connection <- file(paste(ev,".su",sep=""),"rb")

datalst <- datalstplt <- list()

for (i in 1:24) {

  data <- readSu(connection,3008)

  datalst[[i]] <- data$data[[1]]-mean(data$data[[1]])

  datalstplt[[i]] <- datalst[[i]]/max(datalst[[i]])

}

close(connection)

# Plot and set window of 0.5 seconds

tseq <- seq(from=0,to=3.007,by=0.001)

plot(tseq,datalstplt[[1]]+1,type="l",ylim=c(0,24),main=ev)

for (i in 2:24) {

```

```

    lines(tseq,datalstplt[[i]]+i)
}

```

```

winst <- as.numeric(readline("Enter window start in secs: "))
winend <- winst+0.5

```

```

plot(tseq,datalstplt[[1]]+1,type="l",ylim=c(0,24),xlim=c(winst,winend),main=ev)
for (i in 2:24) {
    lines(tseq,datalstplt[[i]]+i)
}

```

```

ans <- readline("Ok with window (y or n)? ")

```

```

while(ans=="n") {

```

```

    winst <- as.numeric(readline("Enter window start in secs: "))
    winend <- winst+0.5

```

```

    plot(tseq,datalstplt[[1]]+1,type="l",ylim=c(0,24),xlim=c(winst,winend),main=ev)
    for (i in 2:24) {
        lines(tseq,datalstplt[[i]]+i)
    }
}

```

```

ans <- readline("Ok with window (y or n)? ")
}

winst <- winst/0.001
winend <- winend/0.001

# Rotate data
for (gph_num in gphlst) {
  gphrow <- which(fbs_out$GPH==gph_num)
  end <- gph_num*3

  # Read in rotation angles
  wkbk <- loadWorkbook(paste(dirperf,"/RotationAnglesMW2.xlsx",sep=""))
  sheet <- paste("GPH",gph_num,sep="")
  angledat <- as.list(readWorksheet(wkbk,sheet,header=TRUE))
  for (k in 1:length(angledat$MW)) {
    if (angledat$MW[k]==MW && angledat$TW[k]==TW && angledat$Stage[k]==Stage) {
      E1 <- angledat$E1Avg[k]*pi/180
      E2 <- angledat$E2Avg[k]*pi/180
      E3 <- angledat$E3Avg[k]*pi/180
    }
  }
}

```

```

# Rotation matrix

a11 <- cos(E3)*cos(E1)-cos(E2)*sin(E1)*sin(E3)
a12 <- cos(E3)*sin(E1)+cos(E2)*cos(E1)*sin(E3)
a13 <- sin(E3)*sin(E2)
a21 <- -sin(E3)*cos(E1)-cos(E2)*sin(E1)*cos(E3)
a22 <- -sin(E3)*sin(E1)+cos(E2)*cos(E1)*cos(E3)
a23 <- cos(E3)*sin(E2)
a31 <- sin(E2)*sin(E1)
a32 <- -sin(E2)*cos(E1)
a33 <- cos(E2)

rotmat <- matrix(c(a11,a12,a13,a21,a22,a23,a31,a32,a33),ncol=3,byrow=TRUE)

# Set up data matrix

data_mat <- matrix(c(data1st[end-2][[1]][winst:winend],data1st[end-
1][[1]][winst:winend],data1st[end][[1]][winst:winend]),byrow=T,nrow=3)

# Apply rotation

rotated_data <- rotmat%*%data_mat

rotatdatplt <- rotated_data/max(unlist(rotated_data))

# Determine first break

# Use STA/LTA to find first guess for first break

```

```

fb_sec <- roll_stalta(rotated_data[2,]^2,5,50)

fb_sec <- which.max(fb_sec)*0.001


# Plot to check if ok with first break
layout(c(1,1))

par(cex.axis=0.75)

tseq <- seq(from=0,to=0.5,by=0.001)

plot(tseq,rotatplt[1,]+3,type="l",xlab="Time (s)",ylab="Amplitude",ylim=c(0,4))

lines(tseq,rotatplt[2,]+2)

lines(tseq,rotatplt[3,]+1)

lines(rep(fb_sec,2),c(-1e9,1e9),col="red",lwd=2)

ans <- readline("Ok with fb? ")

while (ans=="n") {

  print(paste("Current fb is ",fb_sec," seconds",sep=""))

  fb_sec <- as.numeric(readline("Enter new fb in seconds: "))

  plot(tseq,rotatplt[1,]+3,type="l",xlab="Time (s)",ylab="Amplitude",ylim=c(0,4))

  lines(tseq,rotatplt[2,]+2)

  lines(tseq,rotatplt[3,]+1)

  lines(rep(fb_sec,2),c(-1e9,1e9),col="red",lwd=2)

  ans <- readline("Ok with fb? ")

}

fbs_out$FB[gphrow] <- fb_sec

```



```

# Write out data to su

datlst <- unlist(as.list(rotated_data))

outbound <- paste(ev,"GPH",gph_num,".bin",sep="")

outbound_connection <- file(outbound,"wb")

writeSuBinData(datlst,outbound_connection)

close(outbound_connection)

system(paste("suaddhead ns=",501," < ",ev,"GPH",gph_num,".bin | sushw key=dt
a=",1000," > ",ev,"GPH",gph_num,".su",sep=""))

system(paste("rm *.bin",sep=""))

}

# Write out first break picks file

write.csv(fbs_out,paste(ev,"FBS.csv",sep=""))

# Write out unprocessed data

gphseq <- seq(from=1,to=8,by=1)

gphsbad <- gphseq[-gphlst]

for (gph_num in gphsbad) {

  end <- 3*gph_num

```

```

datlst          <-          c(datalst[end-2][[1]][winst:winend],datalst[end-
1][[1]][winst:winend],datalst[end][[1]][winst:winend])

outbound <- paste(ev,"GPH",gph_num,".bin",sep="")
outbound_connection <- file(outbound,"wb")
writeSuBinData(datlst,outbound_connection)
close(outbound_connection)

system(paste("suaddhead ns=",501," < ",ev,"GPH",gph_num,".bin | sushw key=dt
a=",1000," > ",ev,"GPH",gph_num,".su",sep=""))

system(paste("rm *.bin",sep=""))

}

}

```

SPick.R

Pick S-wave arrival

Located in A/FreqContent/

SPick.R

Trudy Watkins

Updated December 17, 2016

Pick S-wave arrival

Sets directory as directory where this script is being sourced from

```
setwd(dirname(sys.frame(1)$ofile))
```

```

dirtreat <- paste(dirname(dirname(getwd())),"/TreatmentData",sep="")

# Source required functions and/or packages
source(paste(dirname(getwd()),"/SUinRFuncs/readSu.R",sep=""))
source(paste(dirname(getwd()),"/SUinRFuncs/readSuTracehead.R",sep=""))

# Set stage name
stgname <- "3d"

# Go to stage directory
setwd(paste(dirtreat,"/MyData/Events",stgname,sep=""))

# Get list of events
evs <- list.files()

for (ev in evs[1]) {

# Go to event directory
setwd(paste(dirtreat,"/CleanData/Events",stgname,"/",ev,sep=""))

# Read in P-picks
fbs <- read.csv(paste(ev,"FBs.csv",sep=""))

fbs$FB <- fbs$FB*0.001

```

```

gph_lst <- c(1,3,4,5,7)

spick <- list()

for (g in gph_lst) {

  gphrow <- which(g==fbs$GPH)

  # Read in data

  su_in <- paste(ev,"GPH",g,".su",sep="")

  connection <- file(su_in,"rb")

  data_in <- datainplt <- list()

  for (i in 1:3) {

    dat <- readSu(connection,501)

    data_in[[i]] <- dat$data[[1]]

    datainplt[[i]] <- data_in[[i]]/max(data_in[[i]])

  }

  close(connection)

  # Plot data with p-pick

  tseq <- seq(from=0,to=0.5,by=0.001)

  plot(tseq,datainplt[[1]]+3,type='l',ylim=c(0,4),

       ylab="Component (ZYX)",xlab="Time (s)",

       xlim=c(fbs$FB[[gphrow]]-0.05,fbs$FB[[gphrow]]+0.2))

```

```

lines(tseq,datainplt[[2]]+2)

lines(tseq,datainplt[[3]]+1)

lines(rep(fbs$FB[[gphrow]],2),c(-1,5),col="red",lwd=2)


# Make s pick

if (g==1) {

  spick[gphrow] <- as.numeric(readline("Enter S pick in secs: "))

} else {

  diff <- spick[[1]]-fbs$FB[1]

  spick[gphrow] <- fbs$FB[gphrow]+diff

}


# Plot s pick

lines(rep(spick[gphrow],2),c(-1,5),col="red",lwd=2)


# Loop until ok with S-pick

ans <- readline("Ok with S-pick (y or n)? ")

while (ans=="n") {

  print(paste("Current S-pick is ",spick[gphrow]))

  spick[gphrow] <- as.numeric(readline("Enter S pick in secs: "))

}

plot(tseq,datainplt[[1]]+3,type='l',ylim=c(0,4),

```

```

      ylab="Component (ZYX)",xlab="Time (s)",
      xlim=c(fbs$FB[[gphrow]]-0.05,fbs$FB[[gphrow]]+0.2))
    lines(tseq,datainplt[[2]]+2)
    lines(tseq,datainplt[[3]]+1)
    lines(rep(fbs$FB[[gphrow]],2),c(-1,5),col="red",lwd=2)
    lines(rep(spick[gphrow],2),c(-1,5),col="red",lwd=2)

    ans <- readline("Ok with S-pick (y or n)? ")
  }
}

psout <- data.frame(GPH=gph_lst,PPick=fbs$FB,SPick=unlist(spick))

write.csv(psout,paste(ev,"PSPicks.csv"))

}

```

CalcPSDur.R

Calculate P-S duration in seconds and write out to .csv file

Located in A/FreqContent/

CalcPSDur.R

Trudy Watkins

Updated December 17, 2016

```
# Calculate P-S duration
```

```
# Sets directory as directory where this script is being sourced from
```

```
setwd(dirname(sys.frame(1)$ofile))
```

```
dirtreat <- paste(dirname(dirname(getwd())),"/TreatmentData",sep="")
```

```
# Set stage name
```

```
stgname <- "1b"
```

```
# Go to stage directory
```

```
setwd(paste(dirtreat,"/MyData/Events",stgname,sep=""))
```

```
# Get list of events
```

```
evs <- list.files()
```

```
for (ev in evs) {
```

```
  # Go to event directory
```

```
  setwd(paste(dirtreat,"/MyData/Events",stgname,"/",ev,sep=""))
```

```
  # Read in pick file
```

```
  picks <- read.csv(paste(ev,"PSPicks.csv",sep=""))
```

```

# Calculate P-S duration

picks$PSDur <- picks$SPick-picks$PPick


# Write out P-S duration

write.csv(picks,paste(ev,"PSPicksDur.csv",sep=""))


# Write out average and sd P-S duration for event

meanPSD <- mean(picks$PSDur)

sdPSD <- sd(picks$PSDur)


PSDout <- data.frame(meanPSDur=meanPSD,sdPSDur=sdPSD)


write.csv(PSDout,paste(ev,"EventPSDur.csv",sep=""))

}

```

SpecAnalysis.R

Determine event frequency content

Located in A/FreqContent/

```

# SpecAnalysis.R

# Trudy Watkins

# Updated December 16, 2016

# Determine event frequency content

```



```

# Sets directory as directory where this script is being sourced from
setwd(dirname(sys.frame(1)$ofile))

dirtreat <- paste(dirname(dirname(getwd())),"/TreatmentData",sep="")

# Source required functions and packages
source(paste(dirname(getwd()),"/SUinRFuncs/readSu.R",sep=""))
source(paste(dirname(getwd()),"/SUinRFuncs/readSuTracehead.R",sep=""))
require("RSEIS")

# Set stage name
stgname <- "3d"

setwd(paste(dirtreat,"/MyData/Events",stgname,sep=""))

evs <- list.files()

gph_lst <- c(1,3,4,5,7)

mfreqs <- list()

sdfreqs <- list()

mfreq <- list()

sdfreq <- list()

j = 0

# Loop over events
for (ev in evs) {

```

```

freqs <- list()

print(ev)

evhr <- substr(ev,1,2)

evmin <- substr(ev,3,4)

j = j + 1

k = 0


# Move to event directory

setwd(paste(dirtreat,"/MyData/Events",stgname,"/",ev,sep=""))


# Loop over each geophone

for (gph in gph_lst) {

# Read in data

su_in <- paste(ev,"GPH",gph,".su",sep="")

connection <- file(su_in,"rb")

data_in <- list()

for (i in 1:3) {

  dat <- readSu(connection,501)

  data_in[[i]] <- dat$data[[1]]

}

close(connection)

```

```

for (i in 1) {

  k = k + 1

  startT <- 0.0*1000

  endT <- 0.5*1000

  sig <- data_in[[i]][startT:endT]


  # Get spectrogram

  spec <- evolfft(sig,dt=0.001,Ns=26,Nov=23)

  dspec <- spec$DSPEC


  # Get maximum amplitude

  maxamp <- max(unlist(dspec))

  maxamp90 <- 0.95*maxamp


  # Get indices of maximum 90% amplitudes

  locs <- which(dspec[1:256,]>maxamp90,arr.ind=T)

  flocs <- locs[,1]

  freqs <- c(freqs,spec$freqs[flocs])


  mfreq[k] <- mean(unlist(freqs))

  sdfreq[k] <- sd(unlist(freqs))

```

```

    }

}

mfreqs[j] <- mean(unlist(mfreq))
sdfreqs[j] <- mean(unlist(sdfreq))

# Write out mean and sd freq
fout <- data.frame(MeanF=mfreqs[[j]],SDF=sdfreqs[[j]])
write.csv(fout,paste(ev,"Freq.csv",sep=""))

}

```

EventLocationExample.R

Calls EventLocation function to interactively locate event

Located in A/EventLocation/

```

# EventLocationExample.R
# Trudy Watkins
# Updated December 18, 2016
# Run interactive event location

```

```

# Sets directory as directory where this script is being sourced from
setwd(dirname(sys.frame(1)$ofile))

dirtreat <- paste(dirname(dirname(getwd())),"/TreatmentData",sep="")

# Source required functions

source(paste(dirname(getwd()),"/SUinRFuncs/readSu.R",sep=""))
source(paste(dirname(getwd()),"/SUinRFuncs/readSuTracehead.R",sep=""))
source("EventLocation.R")
source("PCAEvent.R")
source("QCPCA.R")
source("PlotAziLines.R")
source("SVDCalcMultDips.R")
source("PlotWells3DFunc.R")
source("PlotSVDRes3D.R")
source("CalcAngMean.R")
require("rgl")
require("heplots")

# Select stage and event

stgname <- "1b"

setwd(paste(dirtreat,"/MyData/Events",stgname,sep=""))

fls <- list.files()

```

```

evs <- fls

for (ev in evs[11:18]) {

  setwd(paste(dirtreat,"/MyData/Events",stgname,sep=""))

  setwd(paste(getwd(),"/",ev,sep=""))

  fls <- list.files()

  sus <- fls[grep(".su",fls)]

  sus <- sus[grep("GPH",sus)]


  datamat <- matrix(nrow=24,ncol=501)

  for (su in 1:length(sus)) {

    connection <- file(sus[su],"rb")

    data_in <- list()

    for (i in 1:3) {

      dat <- readSu(connection,501)

      datamat[3*su-1-i,] <- dat$data[[1]]

    }

    close(connection)

  }


  fbsfl <- fls[grep("FBs.csv",fls)]

  fbs <- read.csv(fbsfl)

  fbs <- fbs$FB

```

```
EventLocation(ev,datamat,c(1,3,4,5,7),fbs,stg="1b",plterrell=T,pltlocs=F)

}
```

EventLocation.R

Interactively locate event using PCA-SVD

Located in A/EventLocation/

```
# EventLocation.R
# Trudy Watkins
# July 3, 2016
# Script to interactively locate event using PCA-SVD
```

```
EventLocation <- function(ev,data,gphlst,fbs,stg,plterrell,pltlocs) {

  # Check if initial PCA has already been done

  # If not, then do it

  pcafl <- grep("PCARes.csv",fls)

  if (length(pcafl)==0) {

    PCAres <- PCAEvent(data,gphlst,fbs,ev,single=F,PCARes=NULL,gphrow=NULL)
```

```

} else {

  PCAres <- read.csv(paste(ev,"PCARes.csv",sep=""))

}

# Check if QC standard deviations of PCA windows has already been done

# If not, then do it

pcafl <- grep("PCARes_QCSD.csv",fls)

if (length(pcafl)==0) {

  print(PCARes)

  ans <- readline("Fix anything? ")

  while (ans=="y") {

    gph <- as.numeric(readline("Enter gph number to change: "))

    gphrow <- which(PCARes$GPH==gph)

    PCAres <- PCAEvent(data,gph,PCARes$FB,ev,single=T,PCARes,gphrow)

    print(PCARes)

    ans <- readline("Fix anything? ")

  }

  # Write out updated PCARes

  write.csv(PCARes,paste(ev,"PCARes_QCSD.csv",sep=""))

} else {

  PCAres <- read.csv(paste(ev,"PCARes_QCSD.csv",sep=""))

}

```



```

# Check if QC PCA results using expected azimuth and dip has already been done

# If not, then do it

pcafl <- grep("PCARes_QCMap.csv",fls)

if (length(pcafl)==0) {

  PCAres <- QCPCA(ev,PCARes,stg)

  # Write out final PCA results after QCing azimuths in map view

  write.csv(PCARes,paste(ev,"PCARes_QCMap.csv",sep=""),row.names=F)

} else {

  PCAres <- read.csv(paste(ev,"PCARes_QCMap.csv",sep=""))

}

```

```

# Check if Calculation of location using SVD has already been done

# If not, then do it

pcafl <- grep("UsedGphs",fls)

if (length(pcafl)==0) {

  SVDCalcMultDips(ev,PCARes,stg)

}

```

```

if(!plterrell && !pltlocs) {

```

```

    PlotSVDRes3D(ev,stg,plterrell,pltlocs,justfinal=T)
  } else {
    PlotSVDRes3D(ev,stg,plterrell,pltlocs,justfinal=F)
  }
#
# }
}

```

PCAEvent.R

Subfunction of EventLocation to run principal component analysis on treatment data

Located in A/EventLocation/

```

# PCAEvent.R
# Trudy Watkins
# May 9, 2016
# Run supolar on event and output results

PCAEvent <- function(data,gphlst,fbs,ev,single,PCARES,gphrow) {

  # Set plotting parameters
  par(mar=c(2,4,2,2))

  # Preassign lists
  azi_out <- list()

```

```

dip_out <- list()
fb_out <- list()
azi_mean <- list()
dip_mean <- list()
azi_sd <- list()
dip_sd <- list()
win_st <- list()
win_st2 <- list()
win_end2 <- list()
win_end <- list()

for (gph in gphlst) {
  fb_all <- list()
  if (!single) {
    gphrow <- which(gph==gphlst)
  }

  # Print first break
  fb <- fbs[gphrow]

  # Run polarization analysis

```

```

system(paste("supolar  <  ",paste(ev,"GPH",gph,".su",sep=""),"  wl=0.01  win=boxcar
file=polar angle=deg phi=3 theta=3 rl=1 dir=1 amp=1",sep=""))

```

```

# Read in energy

```

```

connection      <- file("polar.er","rb")

```

```

energy          = readSu(connection,501)

```

```

close(connection)

```

```

# Read in phi

```

```

connection      <- file("polar.phi","rb")

```

```

azis            <- readSu(connection,501)

```

```

close(connection)

```

```

# Read in theta

```

```

connection      <- file("polar.theta","rb")

```

```

dips            = readSu(connection,501)

```

```

close(connection)

```

```

# Get first break and set plot window size

```

```

win_start <- fb-50

```

```

win_end <- fb+50

```

```

if (win_start<0) {win_start=0}

```

```

if (win_end>501) {win_end=501}

```

```

ws_en <- fb-15

we_en <- fb+15

max_er <- which.max(energy$data[[1]][ws_en:we_en])

if (!single) {
  fb <- max_er+ws_en
}

# Set initial guess for pca window

pca_win_st <- fb-7

pca_win_end <- fb+7

# Plot results

plot.new()

par(mfrow=c(4,1))

par(mfg=c(1,1))

plot(data[3*gphrow-2,],type="l",main=paste(ev,"
GPH",gph,sep=""),xlim=c(win_start,win_end))

points(fb,data[3*gphrow-2,][fb],col="red",pch=1,cex=1.5)

lines(rep(pca_win_st,2),c(-1e10,1e10),col="red",lwd=2)

lines(rep(pca_win_end,2),c(-1e10,1e10),col="red",lwd=2)

par(mfg=c(2,1))

```

<pre> plot(energy\$data[[1]],type="l",main=paste(ev," GPH",gph,sep=""),xlim=c(win_start,win_end)) points(fb,energy\$data[[1]][fb],col="red",pch=1,cex=1.5) lines(rep(pca_win_st,2),c(-1e10,1e10),col="red",lwd=2) lines(rep(pca_win_end,2),c(-1e10,1e10),col="red",lwd=2) par(mfg=c(3,1)) </pre>	Average	Energy
<pre> plot(azis\$data[[1]],type="l",main=paste(ev," GPH",gph,sep=""),xlim=c(win_start,win_end)) points(fb,azis\$data[[1]][fb],col="red",pch=1,cex=1.5) lines(rep(pca_win_st,2),c(-1e10,1e10),col="red",lwd=2) lines(rep(pca_win_end,2),c(-1e10,1e10),col="red",lwd=2) par(mfg=c(4,1)) </pre>	Azimuth	(phi)
<pre> plot(dips\$data[[1]],type="l",main=paste(ev," GPH",gph,sep=""),xlim=c(win_start,win_end)) points(fb,dips\$data[[1]][fb],col="red",pch=1,cex=1.5) lines(rep(pca_win_st,2),c(-1e10,1e10),col="red",lwd=2) lines(rep(pca_win_end,2),c(-1e10,1e10),col="red",lwd=2) </pre>	Dip	(theta)

```

# Check if ok with auto fb, if not then loop for manual input

ans_fb <- readline("Ok with fb and pca wins? ")

while (ans_fb=="n") {

  ans <- readline("Edit fb or pca wins? Enter f for fb, ps or pca window start, or pe for pca
window end")

```

```

if (ans=="f") {

  print(paste("Current first break is ",fb,sep=""))

  fb <- as.numeric(readline("Enter new first break: "))

}

if (ans=="ps") {

  print(paste("Current pca win start is ",pca_win_st,sep=""))

  pca_win_st <- as.numeric(readline("Enter new pca win start: "))

}

if (ans=="pe") {

  print(paste("Current pca win end is ",pca_win_end,sep=""))

  pca_win_end <- as.numeric(readline("Enter new pca win end: "))

}


# Plot results

plot.new()

par(mfrow=c(4,1))

par(mfg=c(1,1))

plot(data[3*gphrow-2,],type="l",main=paste(ev,"
GPH",gph,sep=""),xlim=c(win_start,win_end))

points(fb,data[3*gphrow-2,][fb],col="red",pch=1,cex=1.5)

lines(rep(pca_win_st,2),c(-1e10,1e10),col="red",lwd=2)

```

```

lines(rep(pca_win_end,2),c(-1e10,1e10),col="red",lwd=2)

par(mfg=c(2,1))

plot(energy$data[[1]],type="l",main=paste(ev,"          Average          Energy
GPH",gph,sep=""),xlim=c(win_start,win_end))

points(fb,energy$data[[1]][fb],col="red",pch=1,cex=1.5)

lines(rep(pca_win_st,2),c(-1e10,1e10),col="red",lwd=2)

lines(rep(pca_win_end,2),c(-1e10,1e10),col="red",lwd=2)

par(mfg=c(3,1))

plot(azis$data[[1]],type="l",main=paste(ev,"          Azimuth          (phi)
GPH",gph,sep=""),xlim=c(win_start,win_end))

points(fb,azis$data[[1]][fb],col="red",pch=1,cex=1.5)

lines(rep(pca_win_st,2),c(-1e10,1e10),col="red",lwd=2)

lines(rep(pca_win_end,2),c(-1e10,1e10),col="red",lwd=2)

par(mfg=c(4,1))

plot(dips$data[[1]],type="l",main=paste(ev,"          Dip          (theta)
GPH",gph,sep=""),xlim=c(win_start,win_end))

points(fb,dips$data[[1]][fb],col="red",pch=1,cex=1.5)

lines(rep(pca_win_st,2),c(-1e10,1e10),col="red",lwd=2)

lines(rep(pca_win_end,2),c(-1e10,1e10),col="red",lwd=2)

ans_fb <- readline("Ok with fb and pca wins ? ")

dev.copy(png,paste(ev,"GPH",gph,"PCA.png",sep=""))

dev.off()

```



```

}

# Organize final PCA results

azi_out[gphrow] <- azis$data[[1]][fb]
dip_out[gphrow] <- dips$data[[1]][fb]
fb_out[gphrow] <- fb
win_st2[gphrow] <- pca_win_st
win_end2[gphrow] <- pca_win_end
msd_azi <- CalcAngMean(azis$data[[1]][pca_win_st:pca_win_end])
msd_dip <- CalcAngMean(dips$data[[1]][pca_win_st:pca_win_end])
azi_mean[gphrow] <- msd_azi[1]
azi_sd[gphrow] <- msd_azi[2]
dip_mean[gphrow] <- msd_dip[1]
dip_sd[gphrow] <- msd_dip[2]
}

```

```

if (!single) {
  pca_out <- data.frame(GPH=gphlst,AziFB=unlist(azi_out),
    DipFB=unlist(dip_out),FB=unlist(fb_out),
    WinSt=unlist(win_st2),WinEnd=unlist(win_end2),
    AziMean=unlist(azi_mean),AziSD=unlist(azi_sd),

```

```

        DipMean=unlist(dip_mean),DipSD=unlist(dip_sd))

# Write out final PCA results

write.csv(pca_out,paste(ev,"PCARes.csv",sep=""),row.names=F)

} else {

  datlst <- c(gphlst,unlist(azi_out),

             unlist(dip_out),unlist(fb_out),

             unlist(win_st2),unlist(win_end2),

             unlist(azi_mean),unlist(azi_sd),

             unlist(dip_mean),unlist(dip_sd))

  pca_out <- PCARes[-gphrow,]

  pca_out <- rbind(pca_out,datlst)

  pca_out <- pca_out[order(pca_out$GPH),]

}

```

```
return(pca_out)

}
```

CalcAngMean.R

Subfunction of PCAEvent subfunction that calculates the mean of a list of angles

Located in A/EventLocation/

```
# CalcAngMean.R
# Trudy Watkins
# May 9, 2016
# Calculate angular mean of input list of angles
```

```
CalcAngMean <- function(angs) {
```

```
  cos_angs <- cos(angs*pi/180)
```

```
  sin_angs <- sin(angs*pi/180)
```

```
  cos_sum <- sum(cos_angs)
```

```
  sin_sum <- sum(sin_angs)
```

```
  YY <- sin_sum/length(angs)
```

```
  XX <- cos_sum/length(angs)
```

```
  RR <- sqrt(XX^2+YY^2)
```

```

sin_mean <- YY/RR

cos_mean <- XX/RR

sign_sin <- sign(sin_mean)

sign_cos <- sign(cos_mean)

theta <- abs(atan(sin_mean/cos_mean)*180/pi)

if (sign_sin==1 && sign_cos==1) {
  ang_mean <- theta
} else if (sign_sin==1 && sign_cos== -1) {
  ang_mean <- 180-theta
} else if (sign_sin== -1 && sign_cos== -1) {
  ang_mean <- 180+theta
} else if (sign_sin== -1 && sign_cos==1) {
  ang_mean <- 360-theta
}

ang_sd <- sqrt(-2*log(RR))*180/pi

mean_sd <- c(ang_mean,ang_sd)

```

```
    return(mean_sd)
}
```

QCPCA.R

Subfunction of EventLocation function that reviews anomalous PCA results

```
# QCPCA.R
# Trudy Watkins
# May 6, 2016
# QC PCA based on expected azimuth and dip range
```

```
QCPCA <- function(ev,pca_in,stg) {

  # Plot azimuths in map view for QCing
  PlotAziLines(pca_in,stg)
  Sys.sleep(2)

  # Recalc azimuths to be less than 180 to
  # account for 180 ambiguity in PCA
  for (i in 1:length(pca_in$GPH)) {
    if (pca_in$AziFB[i]>180) {
      pca_in$AziFB[i] <- pca_in$AziFB[i]-180
    }
    if (pca_in$AziMean[i]>180) {
```

```

    pca_in$AziMean[i] <- pca_in$AziMean[i]-180
  }
}

print(pca_in)

ans1 <- readline("Ok with pca_in? ")

# Loop until okay with azimuths
while (ans1!="n") {
  gph <- as.numeric(readline("Enter gph number to edit: "))
  gphrow <- which(pca_in$GPH==gph)

  su_use <- paste(ev,"GPH",gph,".su",sep="")

  # Read in data
  su_in <- paste(ev,"GPH",gph,".su",sep="")
  connection <- file(su_in,"rb")
  data_in <- list()
  for (i in 1:3) {
    dat <- readSu(connection,501)
    data_in[[i]] <- dat$data[[1]]
  }
}

```

```

close(connection)

# Run polarization analysis

system(paste("supolar < ",su_use," wl=0.01 win=boxcar file=polar angle=deg phi=3
theta=3 rl=1 dir=1 amp=1",sep=""))

# Read in energy

connection      <- file("polar.er","rb")

energy          = readSu(connection,501)

close(connection)

# Read in phi

connection      <- file("polar.phi","rb")

azis           <- readSu(connection,501)

close(connection)

# Read in theta

connection      <- file("polar.theta","rb")

dips           = readSu(connection,501)

close(connection)

# Get windows

fb <- pca_in$FB[gphrow]

```

```

win_start <- fb-15

win_end <- fb+15


# Plot current results

plot.new()

par(mfrow=c(4,1))

par(mfg=c(1,1))

plot(data_in[[1]],type="l",main=paste(ev,"          GPH",gph,sep=""),xlim=c(win_start-
50,win_end+50))

points(fb,data_in[[1]][fb],col="red",pch=1)

lines(rep(win_start,2),c(-1e20,1e20),col="red",lwd=2)

lines(rep(win_end,2),c(-1e20,1e20),col="red",lwd=2)

par(mfg=c(2,1))

plot(energy$data[[1]],type="l",main=paste(ev,"          Average          Energy
GPH",gph,sep=""),xlim=c(win_start-50,win_end+50))

points(fb,energy$data[[1]][fb],col="red",pch=1)

lines(rep(win_start,2),c(-1e20,1e20),col="red",lwd=2)

lines(rep(win_end,2),c(-1e20,1e20),col="red",lwd=2)

par(mfg=c(3,1))

plot(azis$data[[1]],type="l",main=paste(ev,"          Azimuth          (phi)
GPH",gph,sep=""),xlim=c(win_start-50,win_end+50))

points(fb,azis$data[[1]][fb],col="red",pch=1)

lines(rep(win_start,2),c(-1e20,1e20),col="red",lwd=2)

```



```

lines(rep(win_end,2),c(-1e20,1e20),col="red",lwd=2)

par(mfg=c(4,1))

plot(dips$data[[1]],type="l",main=paste(ev,"          Dip          (theta)
GPH",gph,sep=""),xlim=c(win_start-50,win_end+50))

points(fb,dips$data[[1]][fb],col="red",pch=1)

lines(rep(win_start,2),c(-1e20,1e20),col="red",lwd=2)

lines(rep(win_end,2),c(-1e20,1e20),col="red",lwd=2)


# Input possible azimuth and dip find closest values
# in PCA results

possaz <- as.numeric(readline("Possible Azimuth: "))
possdip <- as.numeric(readline("Possible Dip: "))

azlist <- azis$data[[1]][win_start:win_end]
diplist <- dips$data[[1]][win_start:win_end]

for (i in 1:length(azlist)) {
  if (azlist[i]>180) {
    azlist[i] <- azlist[i]-180
  }
}

az_diff <- abs(azlist-possaz)
dip_diff <- abs(diplist-possdip)
diff_locs_az <- which(az_diff<15)
diff_locs_dip <- which(dip_diff<15)

```

```

diff_locs <- unique(diff_locs_az,diff_locs_dip)
if (length(diff_locs)<3) {
  diff_locs <- unique(c(diff_locs_az,diff_locs_dip))
  print("Warning: No az and dip range match")
}

az_df <- data.frame(Locs=diff_locs+win_start-
1,Azis=azlist[diff_locs],Dips=diplist[diff_locs])
if (length(diff_locs)<1) {
  diff_locs <- seq(from=win_start,to=win_end,by=1)
  az_df <-
data.frame(Locs=diff_locs,Azis=azis$data[[1]][diff_locs],Dips=dips$data[[1]][diff_locs])
}

# Select new fb
print(paste("Current fb is ",fb,sep=""))
print(az_df)

fb_loc <- as.numeric(readline("Location: "))
pca_in$FB[gphrow] <- (diff_locs[fb_loc]+win_start-1)
pca_in$AziFB[gphrow] <- az_df$Azis[fb_loc]
pca_in$DipFB[gphrow] <- az_df$Dips[fb_loc]

print(pca_in)

```

```

# Update windows

fb <- pca_in$FB[gphrow]

win_start <- fb-15

win_end <- fb+15


# Plot updated fb

plot.new()

par(mfrow=c(4,1))

par(mfg=c(1,1))

plot(data_in[[1]],type="l",main=paste(ev,"          GPH",gph,sep=""),xlim=c(win_start-
50,win_end+50))

points(fb,data_in[[1]][fb],col="red",pch=1)

lines(rep(win_start,2),c(-1e20,1e20),col="red",lwd=2)

lines(rep(win_end,2),c(-1e20,1e20),col="red",lwd=2)

par(mfg=c(2,1))

plot(energy$data[[1]],type="l",main=paste(ev,"          Average          Energy
GPH",gph,sep=""),xlim=c(win_start-50,win_end+50))

points(fb,energy$data[[1]][fb],col="red",pch=1)

lines(rep(win_start,2),c(-1e20,1e20),col="red",lwd=2)

lines(rep(win_end,2),c(-1e20,1e20),col="red",lwd=2)

par(mfg=c(3,1))

```

<pre> plot(azis\$data[[1]],type="l",main=paste(ev," GPH",gph,sep=""),xlim=c(win_start-50,win_end+50)) points(fb,azis\$data[[1]][fb],col="red",pch=1) lines(rep(win_start,2),c(-1e20,1e20),col="red",lwd=2) lines(rep(win_end,2),c(-1e20,1e20),col="red",lwd=2) par(mfg=c(4,1)) plot(dips\$data[[1]],type="l",main=paste(ev," GPH",gph,sep=""),xlim=c(win_start-50,win_end+50)) points(fb,dips\$data[[1]][fb],col="red",pch=1) lines(rep(win_start,2),c(-1e20,1e20),col="red",lwd=2) lines(rep(win_end,2),c(-1e20,1e20),col="red",lwd=2) # Replot azimuths in map view and check if okay PlotAziLines(pca_in,stg) Sys.sleep(2) dev.copy(png,paste(ev,"AziMap.png",sep="")) dev.off() ans1 <- readline("Ok with pca_in? ") } return(pca_in) </pre>	<p>Azimuth</p> <p>Dip</p>	<p>(phi)</p> <p>(theta)</p>
---	---------------------------	-----------------------------

```
}
```

PlotAziLines.R

Subfunction of QCPCA subfunction that plots PCA results in map view to identify anomalies

Located in A/EventLocation/

```
# PlotAziLines.R
```

```
# Trudy Watkins
```

```
# May 5, 2016
```

```
# Plot azimuth lines from PCA for QCing
```

```
PlotAziLines <- function(pca_res,stg) {
```

```
  # Initiate plot and set plotting parameters
```

```
  plot.new()
```

```
  par(mfrow=c(1,1))
```

```
  # Read in geophone locations
```

```
  dirpltfils <-
```

```
  paste(dirname(dirname(dirname(getwd()))),"/TreatmentData/MyData/PlottingFiles",sep  
  ="" )
```

```

gph_locs <-
read.table(paste(dirpltfls,"/GPH_XYZ_MW2.txt",sep=""),col.names=c("X","Y","Z"))

# Read in well paths

cols_1H <-
c("MD","Inc","Az","TVD","TVD2","NS","NSC","EW","EWC","NSXY","NSXYC","EWXY","EWXYC",
,"A","B")

cols_2H <- c("MD","Inc","Az","TVD","NS","EW","VertSec","A","B","C")
cols_3H <- c("MD","Inc","Az","TVD","NS","EW","VertSec","A","B","C")

data_1H <- read.table(paste(dirpltfls,"/Paddock_1H_Surveys-
Final.txt",sep=""),col.names=cols_1H)

data_2H <- read.table(paste(dirpltfls,"/Teleo-
Paddock_2H_Final_Surveys.txt",sep=""),col.names=cols_2H)

data_3H <- (read.table(paste(dirpltfls,"/Teleo-Paddock_3H-
Final_Surveys.txt",sep=""),col.names=cols_3H))

data_3H$MD <- as.numeric(gsub(",","",as.character(data_3H$MD)))
data_3H$TVD <- as.numeric(gsub(",","",as.character(data_3H$TVD)))
data_3H$NS <- as.numeric(gsub(",","",as.character(data_3H$NS)))
data_3H$EW <- as.numeric(gsub(",","",as.character(data_3H$EW)))
data_3H$VertSec <- as.numeric(gsub(",","",as.character(data_3H$VertSec)))

```

```
welllocs <- read.csv(paste(dirpltfils,"/WellLocs.csv",sep=""),header=T)
```

```
Y01 = welllocs$Y01
```

```
X01 = welllocs$X01
```

```
Y02 = welllocs$Y02
```

```
X02 = welllocs$X02
```

```
Y03 = welllocs$Y03
```

```
X03 = welllocs$X03
```

```
for(j in 1:length(data_1H$TVD)) {
```

```
  if (data_1H$NSC[j]=="S") {
```

```
    data_1H$NS[j] = data_1H$NS[j]*-1
```

```
  }
```

```
  if (data_1H$EWC[j]=="W") {
```

```
    data_1H$EW[j] = data_1H$EW[j]*-1
```

```
  }
```

```
}
```

```
xs1H <- (data_1H$EW[which(data_1H$TVD>6500)]+X01)
```

```
ys1H <- (data_1H$NS[which(data_1H$TVD>6500)]+Y01)
```

```
zs1H <- -data_1H$TVD[data_1H$TVD>6500]
```

```
xs2H <- (data_2H$EW[which(data_2H$TVD>6500)]+X02)
```

```
ys2H <- (data_2H$NS[which(data_2H$TVD>6500)]+Y02)
```

```
zs2H <- -data_2H$TVD[data_2H$TVD>6500]
```

```
xs3H <- (data_3H$EW[which(data_3H$TVD>6500)]+X03)
```

```
ys3H <- (data_3H$NS[which(data_3H$TVD>6500)]+Y03)
```

```
zs3H <- -data_3H$TVD[data_3H$TVD>6500]
```

```
# Read in perforation locations and plot
```

```
if (stg=="1b") {stgn <- "12"; ylims=c(7125500,7127100)}
```

```
if (stg=="3d") {stgn <- "34"; ylims=c(7126300,7127400)}
```

```
fl <- paste("PerfLocs",stg,".csv",sep="")
```

```
perf_locs <- read.csv(paste(dirpltfils,"/",fl,sep=""),col.names=c("Y","X","Z"))
```

```
# Plot well paths and geophone locations
```

```
par(xaxs="i", yaxs="i")
```

```
plot(xs1H,ys1H,type="l",lwd=3,col="blue",
```

```
  xlab="Easting (m)",ylab="Northing (m)",
```

```
  main=ev,
```

```
  xlim=c(2369000,2370500),ylim=ylims, # for stage 212
```

```
  lty=2)
```



```

lines(xs2H,ys2H,lwd=3,col="blue",lty=2)
lines(xs3H,ys3H,lwd=3,col="blue",lty=2)
points(perf_locs$X,perf_locs$Y,pch=16,col="red",cex=1.5)
points(gph_locs$X,gph_locs$Y,pch=17,cex=1.5)

```

```

X01 = X01*0.3048

```

```

Y01 = Y01*0.3048

```

```

azi_lists <- list()
dip_lists <- list()
for (i in 1:length(pca_res$GPH)) {
  azi_lists[[i]] <- c(pca_res$AziFB[i],pca_res$AziMean[i]-
pca_res$AziSD[i],pca_res$AziMean[i]+pca_res$AziSD[i])*pi/180
  dip_lists[[i]] <- c(pca_res$DipFB[i],pca_res$DipMean[i]-
pca_res$DipSD[i],pca_res$DipMean[i]+pca_res$DipSD[i])*pi/180
}
azi_lists <- matrix(unlist(azi_lists),ncol=3,byrow=T)
dip_lists <- matrix(unlist(dip_lists),ncol=3,byrow=T)

```

```

# Plot azimuth lines

print("Purple is first break azimuth, green is window of SDs around original FB")

for (gphrow in 1:length(pca_res$GPH)) {

  cols <- c("purple","green","green")

  px <- list()

  py <- list()

  for (i in 1:3) {

    gphnum <- pca_res$GPH[gphrow]

    dirx <- cos(dip_lists[gphrow,i])*sin(azi_lists[gphrow,i])

    diry <- cos(dip_lists[gphrow,i])*cos(azi_lists[gphrow,i])

    dirz <- -sin(dip_lists[gphrow,i])

    d <- 1e6

    px[[i]] <- c(gph_locs$X[gphnum]-d*dirx,gph_locs$X[gphnum]+d*dirx)

    py[[i]] <- c(gph_locs$Y[gphnum]-d*diry,gph_locs$Y[gphnum]+d*diry)

    lines(px[[i]],py[[i]],col=cols[i],lwd=2)

  }

  polyx1 <- c(px[[2]][1],gph_locs$X[gphnum],px[[3]][1])

  polyy1 <- c(py[[2]][1],gph_locs$Y[gphnum],py[[3]][1])

  polygon(polyx1,polyy1,density=NA,col=rgb(0,1,0,0.3))

  polyx2 <- c(px[[2]][2],gph_locs$X[gphnum],px[[3]][2])

  polyy2 <- c(py[[2]][2],gph_locs$Y[gphnum],py[[3]][2])

```

```

    polygon(polyx2,poly2,density=NA,col=rgb(0,1,0,0.3))
  }

}

```

SVDCalcMultDips.R

Calculate event location using PCA-SVD method

Located in A/EventLocation/

```
# SVDCalcMultDips.R
```

```
# Trudy Watkins
```

```
# May 4, 2016
```

```
# Determine event location using PCA-SVD
```

```
SVDCalcMultDips <- function(ev,pca_res,stg) {
```

```
  # Read in geophone locations
```

```
  dir <- dirname(dirname(dirname(dirname(getwd()))))
```

```
  gph_locs <-
```

```
  read.table(paste(dir,"/TreatmentData/MyData/PlottingFiles/GPH_XYZ_MW2.txt",sep=""),c
```

```
  ol.names=c("V1","V2","V3"))
```

```
  # Correct dip
```

```
  pca_res$DipFB <- 90-pca_res$DipFB
```

```
pca_res$DipMean <- 90-pca_res$DipMean
```

```
if (stg=="1b") {
```

```
  for (k in 1:length(pca_res$DipFB)) {
```

```
    if (pca_res$DipFB[k]>45) {pca_res$DipFB[k] <- 90-pca_res$DipFB[k]}
```

```
    if (pca_res$DipMean[k]>45) {pca_res$DipMean[k] <- 90-pca_res$DipMean[k]}
```

```
  }
```

```
}
```

```
azis_test <- data.frame(FB=pca_res$AziFB,Mean=pca_res$AziMean,Min=pca_res$AziMean-  
pca_res$AziSD,Max=pca_res$AziMean+pca_res$AziSD)*pi/180
```

```
dips_test <-
```

```
data.frame(FB=pca_res$DipFB,Mean=pca_res$DipMean,Min=pca_res$DipMean-  
pca_res$DipSD,Max=pca_res$DipMean+pca_res$DipSD)*pi/180
```

```
# Set up direction cosines
```

```
dirx <- data.frame(FB=cos(dips_test$FB)*sin(azis_test$FB),
```

```
  Mean=cos(dips_test$Mean)*sin(azis_test$Mean),
```

```
  Min=cos(dips_test$Min)*sin(azis_test$Min),
```

```
  Max=cos(dips_test$Max)*sin(azis_test$Max))
```

```
diry <- data.frame(FB=cos(dips_test$FB)*cos(azis_test$FB),
```

```

Mean=cos(dips_test$Mean)*cos(azis_test$Mean),

Min=cos(dips_test$Min)*cos(azis_test$Min),

Max=cos(dips_test$Max)*cos(azis_test$Max))

dirz <- data.frame(FB=-sin(dips_test$FB),

Mean=-sin(dips_test$Mean),

Min=-sin(dips_test$Min),

Max=-sin(dips_test)$Max)

# Build combination list

combs <- list()

s = 1

for (n in 2:length(pca_res$GPH)) {

  combs_new <- combn(pca_res$GPH,n)

  for (i in 1:ncol(combs_new)) {

    combs[[s]] <- combs_new[,i]

    s = s + 1

  }

}

# Preallocate lists

dirx_test <- list()

diry_test <- list()

```

```

dirz_test <- list()

dirxlst <- list()

dirylst <- list()

dirzlst <- list()


# Build SVD matrices and get possible locations

s = 1

loc <- list()

gphs_used <- list()

for (a in 1:length(combs)) {

  gphstemp <- combs[[a]]

  gphrows <- which(pca_res$GPH %in% gphstemp)

  b = 1

  for (row in gphrows) {

    dirxlst[[b]] <- unname(unlist(dirx[row,]))

    dirylst[[b]] <- unname(unlist(diry[row,]))

    dirzlst[[b]] <- unname(unlist(dirz[row,]))

    b = b + 1

  }

  dirx_test <- as.matrix(expand.grid(dirxlst))

  diry_test <- as.matrix(expand.grid(dirylst))

  dirz_test <- as.matrix(expand.grid(dirzlst))

  n = length(gphstemp)

```

```

Gmat <- matrix(rep(0,3*n*n+9*n),nrow=n*3,ncol=n+3)

dmat <- matrix(nrow=3*n,ncol=1)

for (b in 1:nrow(dirx_test)) {
  for (i in 1:n) {
    k <- which(gphstemp==gphstemp[i])
    k2 <- gphstemp[i]
    Gmat[3*i-2,1] <- 1
    Gmat[3*i-1,2] <- 1
    Gmat[3*i,3] <- 1
    Gmat[3*i-2,i+3] <- -dirx_test[b,k]
    Gmat[3*i-1,i+3] <- -diry_test[b,k]
    Gmat[3*i,i+3] <- -dirz_test[b,k]
    dmat[3*i-2,1] <- gph_locs$V1[k2]
    dmat[3*i-1,1] <- gph_locs$V2[k2]
    dmat[3*i,1] <- gph_locs$V3[k2]
  }
  GSVD <- svd(Gmat,nu=n*3,nv=n+3)
  Sp_inv <- diag(1/GSVD$d,ncol=n*3,nrow=n+3)
  mSVD <- GSVD$v%*%Sp_inv%*%t(GSVD$u)%*%dmat
  loc[[s]] <- round(mSVD[1:3,1])
  gphs_used[[s]] <- gphstemp
  s = s + 1
}

```

```

}

# Remove duplicate locations

loc_mat <- matrix(unlist(loc),ncol=3,byrow=T)

unik <- !duplicated(loc_mat)

unik_ind <- which(unik==T)

loc_mat <- loc_mat[unik_ind,]

gphs_used <- gphs_used[unik_ind]


# Cut locs that are outside expected area


# Cuts for stage 234

if (stg=="3d") {

  ptA <- c(2369631+82,7127634)

  ptB <- c(2369950+82,7125567)


  loc_mat_cut <- loc_mat

  gphs_used_cut <- gphs_used


  pos <- list()

  for (i in 1:nrow(loc_mat_cut)) {

    pos[i] <- sign((ptB[1]-ptA[1])*(loc_mat_cut[i,2]-ptA[2])-(ptB[2]-
ptA[2])*(loc_mat_cut[i,1]-ptA[1]))

```



```

}

locs_keep <- which(pos==1)

loc_mat_cut <- loc_mat_cut[locs_keep,]
gphs_used_cut <- gphs_used[locs_keep]
xcut <- which(loc_mat_cut[,1]<2371000)
loc_mat_cut <- loc_mat_cut[xcut,]
gphs_used_cut <- gphs_used_cut[xcut]
}

if (stg=="1b") {
  # Cuts for stage 212
  ptA <- c(2369032+164,7128480)
  ptB <- c(2369422+164,7125287)

  pos <- list()
  for (i in 1:nrow(loc_mat)) {
    pos[i] <- sign((ptB[1]-ptA[1])*(loc_mat[i,2]-ptA[2])-(ptB[2]-ptA[2])*(loc_mat[i,1]-
ptA[1]))
  }

  locs_keep <- which(pos==1)

```

```

loc_mat_cut <- loc_mat[locs_keep,]
gphs_used_cut <- gphs_used[locs_keep]

zcut1 <- which(loc_mat_cut[,3]>7500)
zcut2 <- which(loc_mat_cut[,3]<9500)
zcut <- intersect(zcut1,zcut2)
loc_mat_cut <- loc_mat_cut[zcut,]
gphs_used_cut <- gphs_used_cut[zcut]
xcut <- which(loc_mat_cut[,1]<2370600)
loc_mat_cut <- loc_mat_cut[xcut,]
gphs_used_cut <- gphs_used_cut[xcut]
ycut <- which(loc_mat_cut[,2]<7127700)
loc_mat_cut <- loc_mat_cut[ycut,]
gphs_used_cut <- gphs_used_cut[ycut]
}

# Output
write.csv(loc_mat_cut,paste(ev,"LocsCut.csv",sep=""),row.names=F)
write.csv(loc_mat,paste(ev,"AllLocs.csv",sep=""),row.names=F)
saveRDS(gphs_used_cut,file=paste(ev,"UsedGPHsCut.rds",sep=""))
saveRDS(gphs_used,file=paste(ev,"UsedGPHs.rds",sep=""))
}

```

PlotSVDRes3D.R

Plot event location results and calculate error ellipsoid

Located in A/EventLocation/

PlotSVDRes3D.R

Trudy Watkins

July 4, 2016

Function to plot results of PCA-SVD in 3D

and calculate final location with error ellipse

```
PlotSVDRes3D <- function(ev,stg,plterrell,pltlocs,justfinal) {
```

```
  dirpltfls <- paste(dirname(dirname(dirname(getwd()))),"/MyData/PlottingFiles",sep="")
```

```
  welllocs <- read.csv(paste(dirpltfls,"/WellLocs.csv",sep=""),header=T)
```

```
  Y01 = welllocs$Y01
```

```
  X01 = welllocs$X01
```

```
  Y02 = welllocs$Y02
```

```
  X02 = welllocs$X02
```

```
  Y03 = welllocs$Y03
```

```
X03 = welllocs$X03
```

```
# Read in PCA-SVD results
```

```
all_locs <- read.csv(paste(ev,"LocsCut.csv",sep=""),col.names=c("X","Y","Z"))*0.3048
```

```
# Readin used GPHs
```

```
gphs_used <- readRDS(paste(paste(ev,"UsedGPHsCut.rds",sep="")))
```

```
# Read in geophone locations
```

```
gph_locs <- read.table(paste(dirpltfils,"/GPH_XYZ_MW2.txt",sep=""),header=F)*0.3048
```

```
gphlocs <- list()
```

```
# Read in perforation locations and plot
```

```
X01 <- X01*0.3048
```

```
Y01 <- Y01*0.3048
```

```
if (stg=="1b") {stgn <- "12"}
```

```
if (stg=="3d") {stgn <- "34"}
```

```
fl <- paste("PerfLocs",stg,".csv",sep="")
```

```
perf_locs <- read.csv(paste(dirpltfils,"/",fl,sep=""),col.names=c("Y","X","Z"))*0.3048
```

```
perf_locs$X <- perf_locs$X-X01
```

```
perf_locs$Y <- perf_locs$Y-Y01
```

```
perf_locs$Z <- -perf_locs$Z
```

```

# Plot geophone locations

gphlocs$X <- (gph_locs$V1-X01)
gphlocs$Y <- (gph_locs$V2-Y01)
gphlocs$Z <- -(gph_locs$V3)

ptsy <- list()
ptsx <- list()
ptsz <- list()
for (i in 1:8) {
  ptsx[3*i-2] <- gphlocs$X[i]-20
  ptsx[3*i-1] <- gphlocs$X[i]+20
  ptsx[3*i] <- gphlocs$X[i]
  ptsy[3*i-2] <- gphlocs$Y[i]
  ptsy[3*i-1] <- gphlocs$Y[i]
  ptsy[3*i] <- gphlocs$Y[i]
  ptsz[3*i-2] <- gphlocs$Z[i]-20
  ptsz[3*i-1] <- gphlocs$Z[i]-20
  ptsz[3*i] <- gphlocs$Z[i]+10
}

ptsx <- unlist(ptsx)
ptsy <- unlist(ptsy)
ptsz <- unlist(ptsz)

```

```
cols <- c("magenta","orange","green","lightblue","magenta")
```

```
if (!justfinal) {
```

```
  PlotWells3D()
```

```
  points3d(perf_locs$X,perf_locs$Y,perf_locs$Z,col="red",size=5,add=T)
```

```
  for (i in 1:8) {
```

```
    start <- 3*i-2
```

```
    end <- 3*i
```

```
    triangles3d(ptsx[start:end],ptsy[start:end],ptsz[start:end],add=T)
```

```
  }
```

```
if (pltlocs) {
```

```
  for (i in 1:length(all_locs$X)) {
```

```
    j <- length(gphs_used[[i]])
```

```
    points3d(all_locs$X[i]-X01,all_locs$Y[i]-Y01,-all_locs$Z[i],col=cols[j],size=5,add=T)
```

```
  }
```

```
}
```

```
}
```

```
all_locs$X <- all_locs$X-X01
```

```

all_locs$Y <- all_locs$Y-Y01
all_locs$Z <- -all_locs$Z

xmean <- mean(all_locs$X)
ymean <- mean(all_locs$Y)
zmean <- mean(all_locs$Z)

# Covariance matrix
locs_mat <- data.matrix(all_locs,rownames.force=F)
sdx <- sd(locs_mat[,1])
sdy <- sd(locs_mat[,2])
sdz <- sd(locs_mat[,3])
maxsd <- max(c(sdx,sdy,sdz))
sdx <- sdx/maxsd
sdy <- sdy/maxsd
sdz <- sdz/maxsd
cov_mat <- cov(locs_mat)
ell <- ellipse3d(cov_mat,add=T,centre=c(xmean,ymean,zmean),level=0.9)
if (plterrell) {
  plot3d(ell,add=T,alpha=0.3)
  points3d(xmean,ymean,zmean,col="red",size=10)
}

```

```

ell_ax <- ellipse3d.axes(cov_mat,centre=c(xmean,ymean,zmean),add=T,level=0.9)
} else {

# From ellipse3d.axes function but with plotting taken out

eig <- eigen(cov_mat)

axes <- matrix(c(-1, 0, 0, 1, 0, 0, 0, -1, 0, 0, 1, 0, 0,
               0, -1, 0, 0, 1), 6, 3, byrow = TRUE)

rownames(axes) <- apply(expand.grid(c("min", "max"), c("X",
               "Y", "Z"))[, 2:1], 1, paste, collapse = "")

axes <- axes %*% sqrt(diag(eig$values)) %*% t(eig$vectors)

t = sqrt(qchisq(0.9, 3))

result <- rgl::scale3d(axes, t, t, t)


scale <- rep(c(xmean,ymean,zmean), length.out = 3)

ell_ax <- rgl::translate3d(result, xmean, ymean,
               zmean)

}

# Calculate error ellipse and plot

```



```

#ell_ax <- ellipse3d.axes(cov_mat,centre=c(xmean,ymean,zmean),add=T,level=0.9)

ell_ax[,1] <- ell_ax[,1]-xmean
ell_ax[,2] <- ell_ax[,2]-ymean
ell_ax[,3] <- ell_ax[,3]-zmean

xdiff <- max(ell_ax[,1])
ydiff <- max(ell_ax[,2])
zdiff <- max(ell_ax[,3])

# Output final event location with xyz errors

final_loc <- c(xmean+X01,ymean+Y01,zmean)

dat_out <- data.frame(LocX=final_loc[1],
                     LocY=final_loc[2],
                     LocZ=final_loc[3],
                     ErrX=xdiff,
                     ErrY=ydiff,
                     ErrZ=zdiff)

dat_out2 <- dat_out

dat_out2$LocX <- (dat_out2$LocX-X01)
dat_out2$LocY <- (dat_out2$LocY-Y01)

```

```

print(dat_out2)

write.csv(dat_out,paste(ev,"FinalLoc.csv",sep=""))

}

```

PlotWells3DFunc.R

Subfunction of PlotSVDRes3D subfunction that plots well paths in 3D

Located in A/EventLocation/

```
# PlotWells3DFunc.R
```

```
# Trudy Watkins
```

```
# July 9, 2016
```

```
# Plot wells in 3D
```

```
PlotWells3D <- function() {
```

```
  dirpltfils <- paste(dirname(dirname(dirname(getwd()))),"/MyData/PlottingFiles",sep="")
```

```
  cols_1H <-
```

```
  c("MD","Inc","Az","TVD","TVD2","NS","NSC","EW","EWC","NSXY","NSXYC","EWXY","EWXYC",
    "A","B")
```

```
  cols_2H <- c("MD","Inc","Az","TVD","NS","EW","VertSec","A","B","C")
```

```
  cols_3H <- c("MD","Inc","Az","TVD","NS","EW","VertSec","A","B","C")
```

```
data_1H <- read.table(paste(dirpltfls,"/Paddock_1H_Surveys-  
Final.txt",sep=""),col.names=cols_1H)
```

```
data_2H <- read.table(paste(dirpltfls,"/Teleo-  
Paddock_2H_Final_Surveys.txt",sep=""),col.names=cols_2H)
```

```
data_3H <- (read.table(paste(dirpltfls,"/Teleo-Paddock_3H-  
Final_Surveys.txt",sep=""),col.names=cols_3H))
```

```
data_3H$MD <- as.numeric(gsub(",","",as.character(data_3H$MD)))
```

```
data_3H$TVD <- as.numeric(gsub(",","",as.character(data_3H$TVD)))
```

```
data_3H$NS <- as.numeric(gsub(",","",as.character(data_3H$NS)))
```

```
data_3H$EW <- as.numeric(gsub(",","",as.character(data_3H$EW)))
```

```
data_3H$VertSec <- as.numeric(gsub(",","",as.character(data_3H$VertSec)))
```

```
welllocs <- read.csv(paste(dirpltfls,"/WellLocs.csv",sep=""),header=T)
```

```
Y01 = welllocs$Y01
```

```
X01 = welllocs$X01
```

```
Y02 = welllocs$Y02
```

```
X02 = welllocs$X02
```

```
Y03 = welllocs$Y03
```

```
X03 = welllocs$X03
```

```

for(j in 1:length(data_1H$TVD)) {
  if (data_1H$NSC[j]=="S") {
    data_1H$NS[j] = data_1H$NS[j]*-1
  }
  if (data_1H$EWC[j]=="W") {
    data_1H$EW[j] = data_1H$EW[j]*-1
  }
}

xs1H <- (data_1H$EW[which(data_1H$TVD>8500)]+X01)-X01
ys1H <- (data_1H$NS[which(data_1H$TVD>8500)]+Y01)-Y01
zs1H <- -data_1H$TVD[data_1H$TVD>8500]

xs2H <- (data_2H$EW[which(data_2H$TVD>8500)]+X02)-X01
ys2H <- (data_2H$NS[which(data_2H$TVD>8500)]+Y02)-Y01
zs2H <- -data_2H$TVD[data_2H$TVD>8500]

xs3H <- (data_3H$EW[which(data_3H$TVD>8500)]+X03)-X01
ys3H <- (data_3H$NS[which(data_3H$TVD>8500)]+Y03)-Y01
zs3H <- -data_3H$TVD[data_3H$TVD>8500]

xs1H <- 0.3048*xs1H

```

```
ys1H <- 0.3048*ys1H
```

```
zs1H <- 0.3048*zs1H
```

```
xs2H <- 0.3048*xs2H
```

```
ys2H <- 0.3048*ys2H
```

```
zs2H <- 0.3048*zs2H
```

```
xs3H <- 0.3048*xs3H
```

```
ys3H <- 0.3048*ys3H
```

```
zs3H <- 0.3048*zs3H
```

```
maxx <- max(unlist(c(xs1H,xs2H,xs3H)))+100
```

```
minx <- min(unlist(c(xs1H,xs2H,xs3H)))-100
```

```
maxy <- max(unlist(c(ys1H,ys2H,ys3H)))+100
```

```
miny <- min(unlist(c(ys1H,ys2H,ys3H)))-100
```

```
maxz <- max(unlist(c(zs1H,zs2H,zs3H)))+100
```

```
minz <- min(unlist(c(zs1H,zs2H,zs3H)))-100
```

```
xrange <- c(-100,600)
```

```
yrange <- c(-30,-1100)
```

```
zrange <- c(-2600,-2800)
```

```
xseq <- seq(from=xrange[1],to=xrange[2],by=20)
```

```

yseq <- seq(from=yrange[1],to=yrange[2],by=-20)
zseq <- seq(from=zrange[1],to=zrange[2],by=-20)

xlines <- c(0,200,400,600)
ylines <- c(-200,-400,-600,-800,-1000)
zlines <- c(-2600,-2800)

# Plot "back wall 1", constant y, xlines, zseq
for (i in 1:length(xlines)) {
  const1 <- rep(xlines[i],length(zseq))
  const2 <- rep(max(yrange),length(zseq))
  points3d(const1,const2,zseq,col="black",size=0.25,alpha=0.75)
}

# Plot "bottom1", constant z, xlines, yseq
for (i in 1:length(xlines)) {
  const1 <- rep(xlines[i],length(yseq))
  const2 <- rep(min(zrange),length(yseq))
  points3d(const1,yseq,const2,col="black",size=0.25,alpha=0.75)
}

# Plot "right wall 1", constant x, ylines, zseq
for (i in 1:length(ylines)) {

```

```

const1 <- rep(ylines[i],length(zseq))
const2 <- rep(max(xrange),length(zseq))
points3d(const2,const1,zseq,col="black",size=0.25,alpha=0.75)
}

```

```

# Plot "bottom2", constant z, ylines, xseq
for (i in 1:length(ylines)) {
  const1 <- rep(ylines[i],length(xseq))
  const2 <- rep(min(zrange),length(xseq))
  points3d(xseq,const1,const2,col="black",size=0.25,alpha=0.75)
}

```

```

# Plot "right wall 2", constant x, zlines, yseq
for (i in 1:length(zlines)) {
  const1 <- rep(zlines[i],length(yseq))
  const2 <- rep(max(xrange),length(yseq))
  points3d(const2,yseq,const1,col="black",size=0.25,alpha=0.75)
}

```

```

# Plot "back wall 2", constant y, zlines, xseq
for (i in 1:length(zlines)) {
  const1 <- rep(zlines[i],length(xseq))
  const2 <- rep(max(yrange),length(xseq))

```

```

points3d(xseq,const2,const1,col="black",size=0.25,alpha=0.75)
}

plot3d(xs1H,ys1H,zs1H,type="l",col="blue",lwd=2,add=T,xlim=c(-100,400))
plot3d(xs2H,ys2H,zs2H,type="l",add=T,col="purple",lwd=2)
plot3d(xs3H,ys3H,zs3H,type="l",add=T,col="darkgreen",lwd=2)
#box3d()
}

```

EventMag.R

Calculate event magnitude using Brune's model

Located in A/EventMagnitude/

```

# EventMag.R
# Trudy Watkins
# Updated December 16, 2016
# Calculate event magnitude using Brune's model
# for low-frequency asymptote (Stork, 2014)

# Sets directory as directory where this script is being sourced from
setwd(dirname(sys.frame(1)$ofile))

dirtreat <- paste(dirname(dirname(getwd())),"/TreatmentData",sep="")

```



```
# Source required functions
```

```
source(paste(dirname(getwd()),"/SUinRFuncs/readSu.R",sep=""))
```

```
source(paste(dirname(getwd()),"/SUinRFuncs/readSuTracehead.R",sep=""))
```

```
# Set stage
```

```
stg <- "3d"
```

```
# Go to events directory
```

```
setwd(paste(dirtreat,"/MyData/Events",stgname,sep=""))
```

```
# Get list of event directories
```

```
evs <- list.files()
```

```
# Read in geophone locations
```

```
gphlocs <-
```

```
read.table(paste(dirtreat,"/MyData/PlottingFiles/GPH_XYZ_MW2.txt",sep=""),col.names=c(
```

```
"X","Y","Z"))*0.3048
```

```
gphlocs$Z <- -gphlocs$Z
```

```
for (ev in evs) {
```

```
  k = 0
```

```

# Move to event directory

setwd(paste(dirtreat,"/MyData/Events",stgname,"/",ev,sep=""))

# Read in event location

evloc <- read.csv(paste(ev,"FinalLoc.csv",sep=""))

# Read in first breaks

fbs <- read.csv(paste(ev,"FBs.csv",sep=""))

# Loop over geophones

gph_lst <- c(1,3,4,5,7)

Mw <- list()

for (g in gph_lst) {

  gphrow <- which(gph_lst==g)

  # Read in data

  su_in <- paste(ev,"GPH",g,".su",sep="")

  connection <- file(su_in,"rb")

  data_in <- list()

  for (i in 1:3) {

    dat <- readSu(connection,501)

    data_in[[i]] <- dat$data[[1]]
  }
}

```

```
}
```

```
# Plot data and get first pick using STA/LTA
```

```
tseq <- seq(from=0,to=0.5,by=0.001)
```

```
fb_sec <- fbs$FB[gphrow]*0.001
```

```
plot(tseq,data_in[[1]],type="l")
```

```
lines(rep(fb_sec,2),c(-1e9,1e9),col="red",lwd=2)
```

```
ans <- readline("Ok with fb (y or n)? ")
```

```
while (ans=="n") {
```

```
  print(paste("Current fb is ",fb_sec,sep=""))
```

```
  fb_sec <- as.numeric(readline("Enter new fb: "))
```

```
  plot(tseq,data_in[[1]],type="l")
```

```
  lines(rep(fb_sec,2),c(-1e9,1e9),col="red",lwd=2)
```

```
  ans <- readline("Ok with fb (y or n)? ")
```

```
}
```

```
# Set window for P-wave for Brune fitting
```

```

winst <- (fb_sec/0.001)-20
winend <- (fb_sec/0.001)+40

dataX <- data_in[[1]]
tseq <- seq(from=0,to=0.5,by=0.001)

# Demean data and convert to displacement
amp <- (dataX-mean(dataX))
val <- list()
for (i in 1:(length(amp))) {
  b <- i+1
  val[i] <- integ1(tseq[i:b],amp[i:b])
}
val <- unlist(val)
val2 <- list()
for (i in 1:(length(val))) {
  b <- i + 1
  val2[i] <- integ1(tseq[i:b],val[i:b])
}

amp <- unlist(val2)*(1e-9)
amp <- amp[1:(length(amp)-2)]
amp <- amp[winst:winend]

```

```

# Find model fit to get low frequency asymptote

jmod <- brune.doom(amp,0.001,f1=1,f2=500,PLOTB=F)

# Calculate source-receiver difference

srd      <-      sqrt((gphlocs$X[gphrow]-evloc$LocX)^2+(gphlocs$Y[gphrow]-
evloc$LocY)^2+(gphlocs$Z[gphrow]-evloc$LocZ)^2)

# Calculate M0 and Mw

M0 <- (4*pi*2440*(3850^3)*(srd)*jmod$omega0)/0.52

Mw[g] <- (2/3)*log10(M0)-6

}

meanMw <- mean(unlist(Mw))

sdMw <- sd(unlist(Mw))

mwout <- data.frame(meanMw=meanMw,sdMw=sdMw)

write.csv(mwout,paste(ev,"Mw.csv",sep=""))

}

```

su2dat.R

Convert .su to .dat for input velocity seismograms in ISOLA

Located in A/ISOLA/

```
# su2dat.R
```

```
# Trudy Watkins
```

```
# Updated December 16, 2016
```

```
# Sets directory as directory where this script is being sourced from
```

```
setwd(dirname(sys.frame(1)$ofile))
```

```
dirtreat <- paste(dirname(dirname(getwd())),"/TreatmentData",sep="")
```

```
# Source required functions and/or packages
```

```
source(paste(dirname(getwd()),"/SUinRFuncs/readSu.R",sep=""))
```

```
source(paste(dirname(getwd()),"/SUinRFuncs/readSuTracehead.R",sep=""))
```

```
# Set stage name
```

```
stgname <- "3d"
```

```
# Set directory as events directory and get list of events
```

```
setwd(paste(dirtreat,"/MyData/Events",stgname,sep=""))
```

```
evs <- list.files()
```

```
# Select event number
```

```

evno <- 1

# Set directory to specific event directory
setwd(paste(dirtreat,"/MyData/Events",stgname,"/",evs[evno],sep=""))

# Loop over geophones
gph_lst <- c(1,3,4,5,7)
tseq <- seq(from=0,to=0.5,by=0.001)
for (g in gph_lst) {
  ev <- evs[evno]
  tseq <- seq(from=0,to=0.5,by=0.001)

  # Read in data
  su_in <- paste(ev,"GPH",g,".su",sep="")
  connection <- file(su_in,"rb")
  data_in <- datainplt <- list()
  for (i in 1:3) {
    dat <- readSu(connection,501)
    data_in[[i]] <- dat$data[[1]]
  }
  close(connection)

  for (i in 1:3) {

```

```

    datainplt[[i]] <- data_in[[i]]/max(unlist(data_in))
  }

# Read in first break

fbs <- read.csv(paste(ev,"FBs.csv",sep=""))

fbs$FB <- fbs$FB*0.001

fbs$FB <- fbs$FB-0.005

gphrow <- which(fbs$GPH==g)

# Plot data

plot(tseq,datainplt[[1]]+3,type="l",ylim=c(0,4),main=paste(ev,"GPH",g),
     ylab="Component",xlab="Time (s)",
     xlim=c(fbs$FB[gphrow]-0.1,fbs$FB[gphrow]+0.1))

lines(tseq,datainplt[[2]]+2)

lines(tseq,datainplt[[3]]+1)

# Plot first break

lines(rep(fbs$FB[gphrow],2),c(-1,5),col="red",lwd=2)

ans <- readline("Ok with start? ")

while (ans=="n") {

  print(paste("Current start is ",fbs$FB[gphrow]," seconds",sep=""))

  fbs$FB[gphrow] <- as.numeric(readline("Enter new start: "))
}

```



```

plot(tseq,datainplt[[1]]+3,type="l",ylim=c(0,4),main=paste(ev,"GPH",g),
     ylab="Component",xlab="Time (s)",
     xlim=c(fbs$FB[gphrow]-0.1,fbs$FB[gphrow]+0.1))
lines(tseq,datainplt[[2]]+2)
lines(tseq,datainplt[[3]]+1)
lines(rep(fbs$FB[gphrow],2),c(-1,5),col="red",lwd=2)
ans <- readline("Ok with start? ")
}

```

```

# Convert to velocity

amps <- list()
for (j in 1:3) {
  amp <- (data_in[[j]]-mean(data_in[[j]]))
  val <- list()
  for (i in 1:(length(amp))) {
    b <- i+1
    val[i] <- integ1(tseq[i:b],amp[i:b])
  }
  val <- unlist(val)

  amp <- val*(1e-9)
  amps[[j]] <- amp[1:(length(amp)-2)]
}

```

```

}

# Cut front of data to start and pad with zeroes to fill 8.192 seconds

data_out <- list()

for (i in 1:3) {

  st <- fbs$FB[gphrow]/0.001

  data_out[[i]] <- amps[[i]][st:length(amps[[i]])]

  len <- 8192-length(data_out[[i]])

  data_out[[i]] <- c(data_out[[i]],rep(0,len))

}

tseq <- seq(from=0,to=8.191,by=0.001)

# Plot to confirm output

plot(tseq,data_out[[1]],type="l",ylab="Amplitude",xlab="Time (s)",
     main=paste(ev," GPH ",g,sep=""))

# Make ISOLA directory and output to data

if (g==1) {

  system(paste("mkdir ",ev,"4ISOLA",sep=""))

  setwd(paste(getwd(),"/",ev,"4ISOLA",sep=""))

  system("mkdir data")

  setwd(dirname(getwd()))

}

```

```

matout <- cbind(tseq,data_out[[1]],data_out[[2]],data_out[[3]])

write.table(matout,paste(getwd(),"/",ev,"4ISOLA/data/",ev,"GPH",g,"unc.dat",sep=""),
            row.names=F,col.names=F)

}

```

PlotISOLACorrExample.R

Calls PlotISOLACorr function to plot corr01.dat file containing outputted ISOLA results

Located in A/ISOLA/

```

# PlotISOLACorrExample.R

# Trudy Watkins

# December 8, 2016

# Example for PlotISOLACorr function


# Sets directory as directory where this script is being sourced from
setwd(dirname(sys.frame(1)$ofile))


# Source required functions and packages

require("akima")

require("RFOC")

source("justfocXYTLW.R")

```

```
source("PlotISOLACorr.R")
```

```
corrfl <- "235CLVD125Fullcorr.dat"
```

```
dist <- 25
```

```
PlotISOLACorr(corrfl,dist,pltttitle="235 CLVD 125 Full",pngout=F,pngfl=NULL)
```

PlotISOLACorr.R

Function to plot grid search results of moment tensor inversion outputted from ISOLA

Located in A/ISOLA/

```
# PlotISOLACorr.R
```

```
# Trudy Watkins
```

```
# Created September 16, 2016
```

```
# Modified December 8, 2-016
```

```
# Function to plot grid search results of ISOLA
```

```
PlotISOLACorr <- function(corrfl,dist,pltttitle,pngout,pngfl) {
```

```
  if (pngout) {
```

```
    png(pngfl)
```

```
}
```

```
layout(matrix(c(1,2),1,2),widths=c(5,1.5))
```

```
corrcols
```

```
<-
```

```
c("LocNum","DeltaT","Corr","Str1","Dip1","Rake1","Str2","Dip2","Rake2","DC","ISO","X","XX")
```

```
corr <- read.table(corrfl,skip=2,col.names=corrcols)
```

```
corr <- corr[,1:11]
```

```
par(pty="s")
```

```
par(mar=c(4,4,3,1))
```

```
par(mgp=c(2.5,1,0))
```

```
par(omd=rep(0,4))
```

```
par(omi=rep(0,4))
```

```
quartzFonts(Cambria=c("Cambria","Cambria Bold","Cambria Italic","Cambria Bold Italic"))
```

```
par(family="Cambria")
```

```
par(cex.axis=1.25)
```

```
par(oma=c(0,0,0,0))
```

```
numPos <- max(corr$LocNum)
```

```
numT <- length(corr$LocNum)/numPos
```

```
gridsize <- sqrt(numPos)
```

```

xpts <- seq(from=1,to=gridsize,by=1)
xpts <- rep(xpts,gridsize)
xpts <- sort(xpts)
ypts <- seq(from=1,to=gridsize,by=1)
ypts <- rep(ypts,gridsize)

# Get best correlation locations in data frame
corrs <- list()
bestcorr <- list()
DC <- list()
for (n in 1:numPos) {
  testPos <- which(corr$LocNum==n)
  bestcorr[n] <- which.max(corr$Corr[testPos])+min(testPos)-1
  corrs[n] <- corrs$Corr[bestcorr[[n]]]
  DC[n] <- corrs$DC[bestcorr[[n]]]
  if (round(DC[[n]])==0) {DC[[n]]=1}
}

# Make finer grid for contouring
corrs <- unlist(corrs)
corrsinter <- akima::interp(x=xpts,y=ypts,z=corrs,
  xo=seq(from=1,to=gridsize,by=0.01),

```

```

yo=seq(from=1,to=gridsize,by=0.01),duplicate="mean")

# Plot correlation contours

cols <- colorRampPalette(c("cyan","magenta3"))

maxcorr <- round(max(corrs),2)

mincorr <- round(min(corrs),2)

maxcon <- ceiling(maxcorr*10)/10

maxcon <- maxcorr+0.05

bks <- seq(from=mincorr,to=maxcon,by=0.05)

image(corrsinter$x,corrsinter$y,corrsinter$z,col=cols(length(bks)-1),
      xlim=c(0.5,gridsize+0.5),ylim=c(0.5,gridsize+0.5),
      xlab="East of Source Location (m)",ylab="North of Source Location (m)",cex.lab=1.25,
      breaks=bks,axes=F,bty="o")

box()

# Add guiding lines

for (i in 1:gridsize) {

  lines(c(i,i),c(0.5,gridsize+0.5))

  lines(c(0.5,gridsize+0.5),c(i,i))

}

# Locate maximum correlation

locmax <- which.max(corrs)

```

```

# Plot beach balls

cols <- colorRampPalette(c("yellow","black"))

cols <- cols(100)

for (n in 1:numPos) {

  mec <- SDRfoc(corr$Str1[bestcorr[[n]]],corr$Dip1[bestcorr[[n]]],

    corr$Rake1[bestcorr[[n]]],PLOT=F)

  if (n==13) {

justfocXYTLW(mec,x=xpts[n],y=ypts[n],size=c(0.25,0.25),fcol=cols[round(DC[[n]])],circol=
"black",linew=2)

  }

  if (n==locmax) {

    justfocXYTLW(mec,x=xpts[n],y=ypts[n],size=c(0.25,0.25),fcol=cols[round(DC[[n]])],

      linew=2,fcolback="red")

  } else {

    justfocXYTLW(mec,x=xpts[n],y=ypts[n],size=c(0.25,0.25),fcol=cols[round(DC[[n]])])

  }

}

sqdist <- (gridsize-1)/2

labs <- seq(from=-dist*sqdist,to=dist*sqdist,by=dist)

```



```

axis(1,at=seq(from=1,to=gridsize,by=1),labels=labs)
axis(2,at=seq(from=1,to=gridsize,by=1),labels=labs)
title(pltttitle,cex=1.5,line=1.5)
#title(paste("Loc      ",stgstr,"          Source:      ",src,"          Inversion:
",invtype,sep=""),line=1.5,cex.main=1.5)
#title(paste("f=",freq,"Hz  ",casestrplt,sep=""),line=0.4,cex=0.5)

cols <- colorRampPalette(c("cyan","magenta3"))

par(pty="m")
par(mgp=c(0,0,0))
par(oma=c(0,0,0,0))
par(mar=rep(0,4))
par(mai=rep(0,4))
par(cex.axis=0.5)

# Correlation scale
rect(0,0.7*gridsize,1,gridsize+0.5)
nboxes <- length(bks)-1
cols <- colorRampPalette(c("cyan","magenta3"))
cols <- cols(nboxes)
lenbx <- gridsize+0.5-0.7*gridsize
boxwidth <- (lenbx)/nboxes

```

```

for (i in 1:nboxes) {
  rect(0,0.7*gridsize+boxwidth*(i-1),1,0.7*gridsize+boxwidth*(i),col=cols[i])
}

nboxes <- nboxes/2

bks <- bks[c(TRUE,FALSE)]

boxwidth <- boxwidth*2

for (i in 1:nboxes) {
  lines(c(0,1.5),rep(0.7*gridsize+boxwidth*(i-1),2))
  text(1.3,(0.7*gridsize+boxwidth*(i-1)),bks[i],pos=4,cex=0.9)
}

lines(c(0,1.5),rep(gridsize+0.5,2))
text(1.3,gridsize+0.5,bks[nboxes+1],pos=4,cex=0.9)

#text(1.3,5.5,"0.3",pos=4,cex=0.9)

text(gridsize,gridsize*0.9+0.05,"Correlation",srt=-90,cex=1.3)


# DC Scale

rect(0,0.5,1,0.5+lenbx)

ys <- seq(from=0.5,to=lenbx+0.5,len=11)

perc <- seq(from=0,to=100,by=10)

cols <- colorRampPalette(c("yellow","black"))

cols <- cols(10)

for (i in 1:10) {
  rect(0,ys[i],1,ys[i+1],col=cols[i])
}

```

```

}

for (i in c(1,3,5,7,9)) {

  lines(c(0,1.5),rep(ys[i],2))

  text(1.3,ys[i],perc[i],pos=4,cex=0.9)

}

text(1.3,0.5+lenbx,"100",pos=4,cex=0.9)

lines(c(0,1.5),rep(0.5+lenbx,2))

text(gridsize,gridsize*0.4+0.05,"DC Percent",srt=-90,cex=1.3)


if (pngout) {

  dev.off()

}

}

```

Appendix B: Data Tables and Plots

Table B.1: Summary of geophone reorientation.	267
Table B.2: Combinations of geophones for event location.	270
Table B.3: Event locations for stage 1b.....	271
Table B.4: Event locations for stage 3d.....	272
Figure B.1: 3D error ellipsoids and event locations for events in stage 1b.....	273
Figure B.2: 3D error ellipsoids and event locations for events in stage 3d.	276

Table B.1: Summary of geophone reorientation. E1, E2, and E3 are the three Euler angles used for rotated the microseismic data and the number of calibration points are the number of perforations used to average the values of the Euler angles (see section 2.3 for detailed description of the geophone reorientation).

Stage	Geophone Number	E1(°)	E2(°)	E3(°)	Azimuth Error(°)	Dip Error(°)	Number of Calibration Points
1a	1	-36.554	62.555	154.869	2.644	0.912	7
1a	2	-	-	-	-	-	0
1a	3	-251.677	7.395	153.105	5.481	12.065	6
1a	4	-322.256	75.058	150.849	2.218	3.237	7
1a	5	-348.546	66.656	149.143	1.637	1.775	7
1a	6	-	-	-	-	-	0
1a	7	-197.712	8.612	143.394	8.567	4.007	5
1a	8	-	-	-	-	-	0
1b	1	-123.51	3.043	149.044	0.891	0.707	7
1b	2	-	-	-	-	-	0
1b	3	-263.515	10.006	144.545	1.803	4.072	8
1b	4	-290.337	73.519	140.257	1.855	1.845	6
1b	5	-349.522	0.354	138.43	3.701	1.628	8
1b	6	-	-	-	-	-	0
1b	7	-196.059	15.808	129.236	4.323	3.408	7
1b	8	-232.76	1.321	124.213	9.145	6.927	7
3b	1	-18.174	34.602	129.94	2.625	2.033	8

Stage	Geophone Number	E1(°)	E2(°)	E3(°)	Azimuth Error(°)	Dip Error(°)	Number of Calibration Points
3b	2	-	-	-	-	-	0
3b	3	-257.672	5.586	124.208	8.498	4.251	6
3b	4	-344.934	61.679	120.966	1.758	1.574	8
3b	5	-334.59	14.777	117.383	1.662	1.12	8
3b	6	-	-	-	-	-	0
3b	7	-195.693	12.843	109.108	2.895	0.799	8
3b	8	-	-	-	-	-	0
3c	1	-22.974	24.624	117.357	6.451	2.225	7
3c	2	-	-	-	-	-	0
3c	3	-300.555	25.436	109.261	3.835	1.849	7
3c	4	-315.634	41.691	104.764	1.964	6.72	7
3c	5	-328.53	8.216	99.987	3.818	2.24	7
3c	6	-	-	-	-	-	0
3c	7	-232.995	3.248	89.513	7.821	0.629	6
3c	8	-256.319	8.429	84.035	5.755	6.025	5
3d	1	-37.188	13.336	98.719	8.028	3.178	8
3d	2	-	-	-	-	-	0
3d	3	-303.596	13.272	88.428	5.962	2.159	8
3d	4	-303.128	12.477	83.099	4.958	3.975	8
3d	5	-320.215	5.791	77.693	3.148	10.773	8
3d	6	-	-	-	-	-	0
3d	7	-240.479	3.383	67.27	5.829	0.477	8
3d	8	-254.011	27.828	62.377	2.519	1.7	8
3e	1	-38.794	6.535	77.263	2.675	10.209	7
3e	2	-	-	-	-	-	0
3e	3	-293.741	-176.894	67.142	6.522	4.524	6
3e	4	-	-	-	-	-	6
3e	5	-	-	-	-	-	7
3e	6	-	-	-	-	-	0
3e	7	-219.479	-167.394	50.001	5.532	2.315	8
3e	8	-244.747	-146.163	46.028	6.634	3.604	7
2a	1	-18.55	-131.084	266.879	3.098	6.401	7
2a	2	-	-	-	-	-	0

Stage	Geophone Number	E1(°)	E2(°)	E3(°)	Azimuth Error(°)	Dip Error(°)	Number of Calibration Points
2a	3	-	-	-	-	-	0
2a	4	-	-	-	-	-	0
2a	5	-	-	-	-	-	0
2a	6	-11.371	-163.191	265.636	3.732	4.562	8
2a	7	-	-	-	-	-	0
2a	8	-249.204	-161.04	265.163	3.57	3.488	8
2b	1	-21.295	-128.851	265.453	1.888	3.194	8
2b	2	-	-	-	-	-	0
2b	3	-	-	-	-	-	0
2b	4	-105.88	-145.286	264.3	5.306	4.333	3
2b	5	-	-	-	-	-	0
2b	6	-17.478	-151.58	264.04	1.77	10.672	6
2b	7	-	-	-	-	-	0
2b	8	-249.437	-152.437	263.498	2.18	4.486	8
2d	1	-32.718	-95.859	251.088	1.16	3.693	6
2d	2	-211.098	-126.881	250.533	1.615	2.533	6
2d	3	-	-	-	-	-	0
2d	4	-114.239	-121.991	249.375	1.338	3.671	6
2d	5	-301.933	-123.699	247.63	4.715	4.899	4
2d	6	-34.717	-117.995	248.275	0.5	3.06	6
2d	7	-	-	-	-	-	0
2d	8	-274.144	-128.401	247.019	1.126	2.428	6

Table B.2: Combinations of geophones for event location. There are ten combinations of two geophones, ten combinations of three geophones, five combinations of four geophones, and one combination of five geophones (see section 2.3.3 for description of use of these combinations)

Combination Number	Number of Geophones Used	Geophones Used
1	2	1, 3
2	2	1, 4
3	2	1, 5
4	2	1, 7
5	2	3, 4
6	2	3, 5
7	2	3, 7
8	2	4, 5
9	2	4, 7
10	2	5, 7
11	3	1, 3, 4
12	3	1, 3, 5
13	3	1, 3, 7
14	3	1, 4, 5
15	3	1, 4, 7
16	3	1, 5, 7
17	3	3, 4, 5
18	3	3, 4, 7
19	3	3, 5, 7
20	3	4, 5, 7
21	4	1, 3, 4, 5
22	4	1, 3, 4, 7
23	4	1, 3, 5, 7
24	4	1, 4, 5, 7
25	4	3, 4, 5, 7
26	5	1, 3, 4, 5, 7

Table B.3: Event locations for stage 1b. The X, Y, and Z locations are with respect to the surface location of well 1H (see section 2.3.3 for method and section 3.2.1 for results and figures).

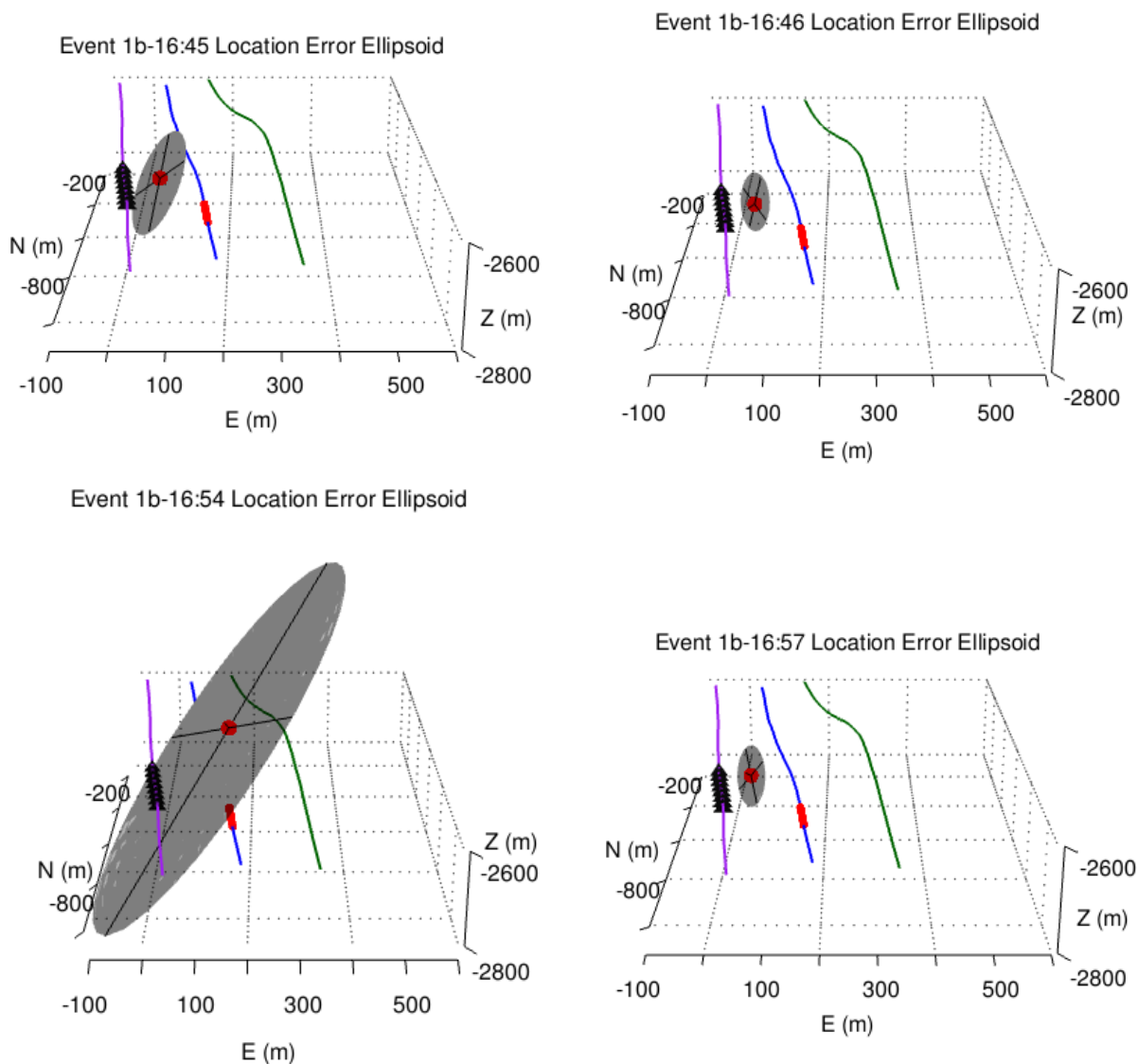
Event	X-Location (m E)	Y-Location (m N)	Z-Location (m)
1b-16:45	130 ± 152	-791 ± 102	-2653 ± 66
1b-16:46	128 ± 93	-840 ± 199	-2652 ± 125
1b-16:54	65 ± 23	-766 ± 47	-2664 ± 1
1b-16:57	85 ± 120	-808 ± 325	-2663 ± 1
1b-17:00a	94 ± 76	-755 ± 28	-2664 ± 1
1b-17:00b	174 ± 76	-773 ± 41	-2649 ± 61
1b-17:04	173 ± 78	-856 ± 263	-2677 ± 83
1b-17:14	96 ± 111	-765 ± 117	-2660 ± 29
1b-17:21	152 ± 70	-793 ± 83	-2664 ± 1
1b-17:22	95 ± 101	-841 ± 154	-2681 ± 80
1b-17:46	120 ± 79	-796 ± 163	-2676 ± 55
1b-17:52	134 ± 101	-813 ± 156	-2668 ± 45
1b-17:55	136 ± 63	-806 ± 110	-2654 ± 119
1b-18:47	133 ± 107	-804 ± 148	-2674 ± 40
1b-18:48	113 ± 124	-903 ± 392	-2675 ± 92
1b-18:57	147 ± 134	-840 ± 161	-2667 ± 16
1b-19:22	129 ± 78	-842 ± 223	-2657 ± 51
1b-19:23	122 ± 48	-887 ± 67	-2663 ± 1
1b-20:11	138 ± 65	-771 ± 64	-2663 ± 1

Table B.4: Event locations for stage 3d. The X, Y, and Z locations are with respect to the surface location of well 1H (see section 2.3.3 for method and section 3.2.1 for results and figures).

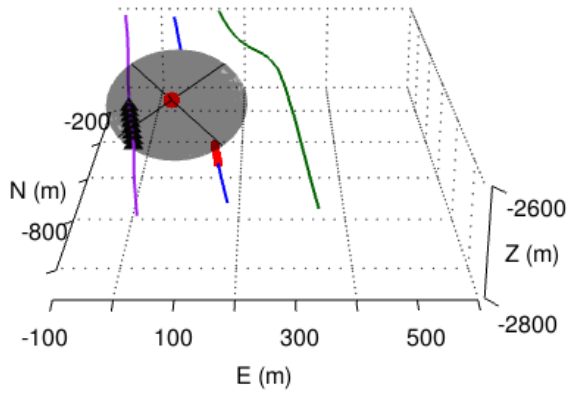
Event	X-Location (m E)	Y-Location (m N)	Z-Location (m)
3d-14:00	198 ± 99	-595 ± 46	-2625 ± 21
3d-15:08	211 ± 95	-612 ± 33	-2605 ± 48
3d-15:11	205 ± 148	-586 ± 35	-2543 ± 74
3d-15:30	187 ± 42	-581 ± 26	-2610 ± 75
3d-15:31	209 ± 110	-607 ± 25	-2612 ± 17
3d-15:34	231 ± 96	-705 ± 69	-2623 ± 25
3d-15:35	232 ± 226	-614 ± 56	-2606 ± 40
3d-16:15	201 ± 90	-632 ± 27	-2623 ± 29
3d-16:16	239 ± 171	-470 ± 114	-2576 ± 87
3d-16:37	318 ± 196	-741 ± 92	-2617 ± 27
3d-17:04	198 ± 66	-286 ± 447	-2621 ± 33
3d-17:13	248 ± 128	-722 ± 81	-2640 ± 21
3d-17:14	236 ± 190	-560 ± 44	-2608 ± 26
3d-17:21	-6 ± 65	-355 ± 347	-2674 ± 232
3d-17:38	5 ± 37	-420 ± 98	-2639 ± 24
3d-17:54	219 ± 127	-611 ± 37	-2619 ± 18
3d-18:08	206 ± 95	-617 ± 36	-2604 ± 54
3d-19:08	183 ± 26	-607 ± 18	-2601 ± 57
3d-20:20	276 ± 235	-619 ± 37	-2557 ± 182

Error Ellipsoids for Event Locations

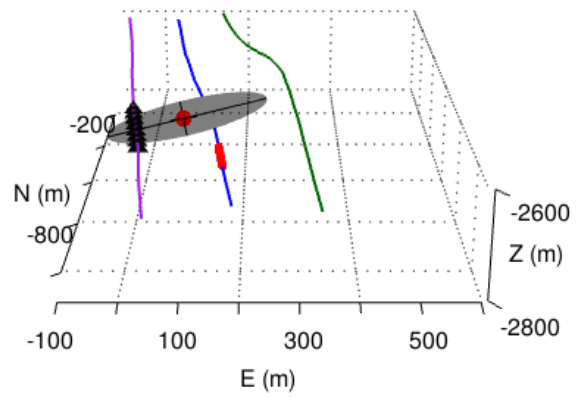
Figure B.1: 3D error ellipsoids and event locations for events in stage 1b. The error ellipsoids are shaded in gray with the axes outlined in black and the event locations are in the center of the ellipsoids noted by the red dot. The X, Y, and Z coordinates are with respect to the surface location of well 1H (see section 2.3.3 for method and section 3.2.1 for results and figures). The well paths for wells 1H, 2H, and 3H are outlined in blue, purple, and green, respectively. The black triangles represent the geophones and the red dots along the 1H well path (blue) are the locations of the perforations for stage 1b. Refer to Table B.3 for numerical coordinates and X, Y, Z errors.



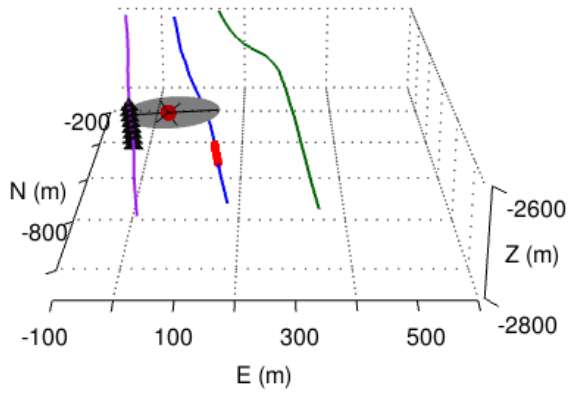
Event 1b-17:00a Location Error Ellipsoid



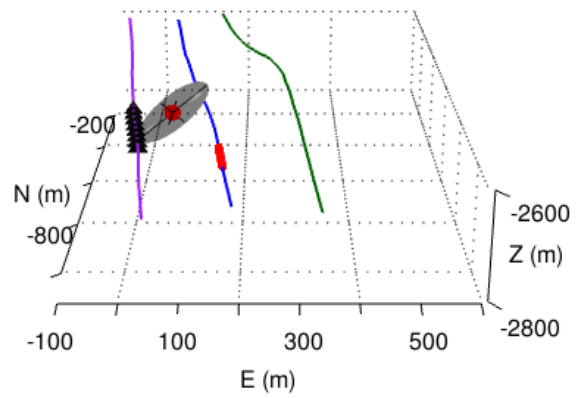
Event 1b-17:00b Location Error Ellipsoid



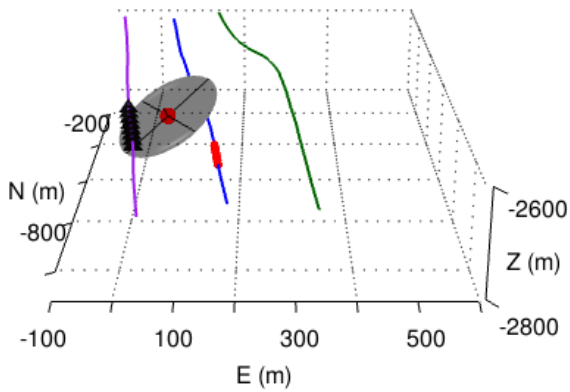
Event 1b-17:04 Location Error Ellipsoid



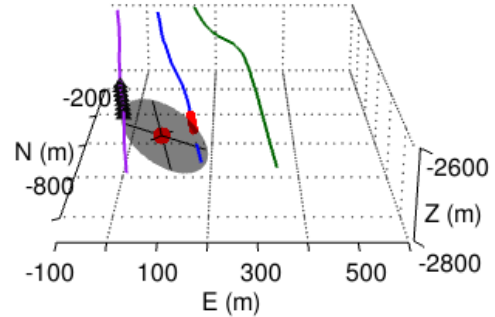
Event 1b-17:14 Location Error Ellipsoid



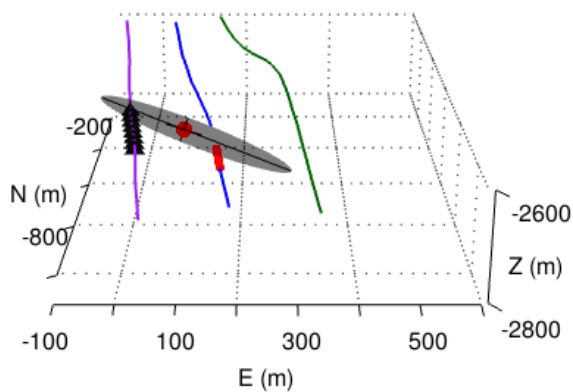
Event 1b-17:21 Location Error Ellipsoid



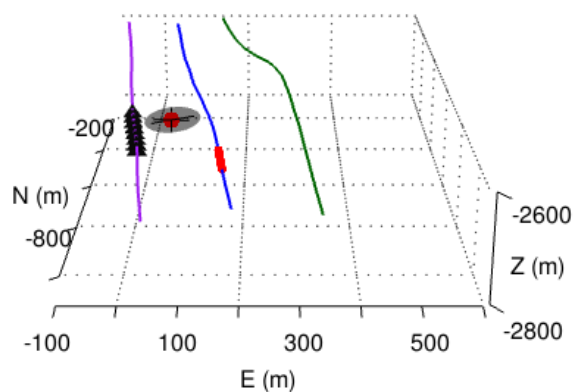
Event 1b-17:22 Location Error Ellipsoid



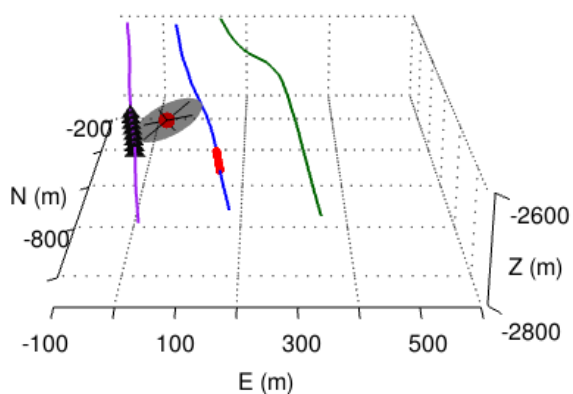
Event 1b-17:46 Location Error Ellipsoid



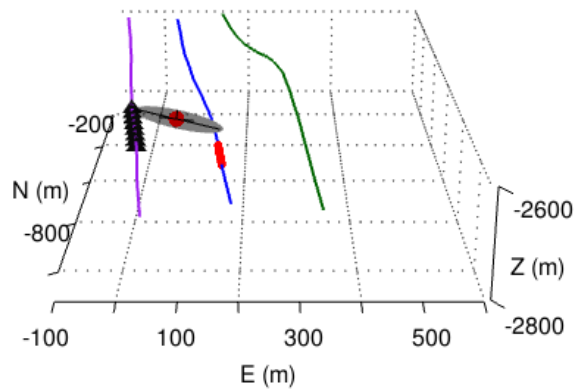
Event 1b-17:52 Location Error Ellipsoid



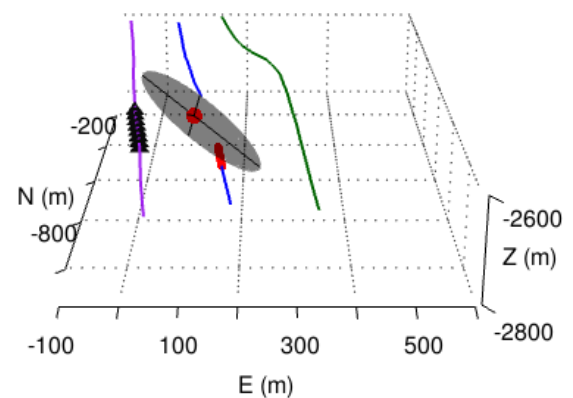
Event 1b-17:55 Location Error Ellipsoid



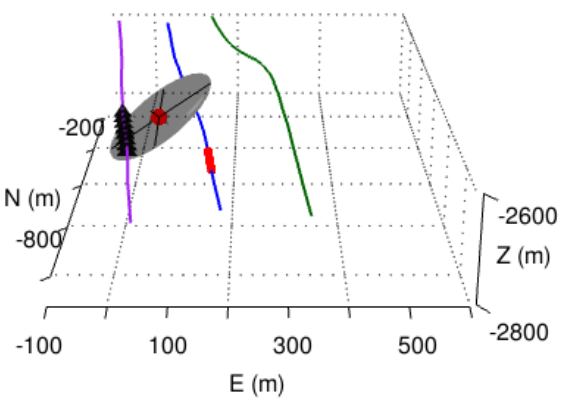
Event 1b-18:47 Location Error Ellipsoid



Event 1b-18:48 Location Error Ellipsoid



Event 1b-19:22 Location Error Ellipsoid



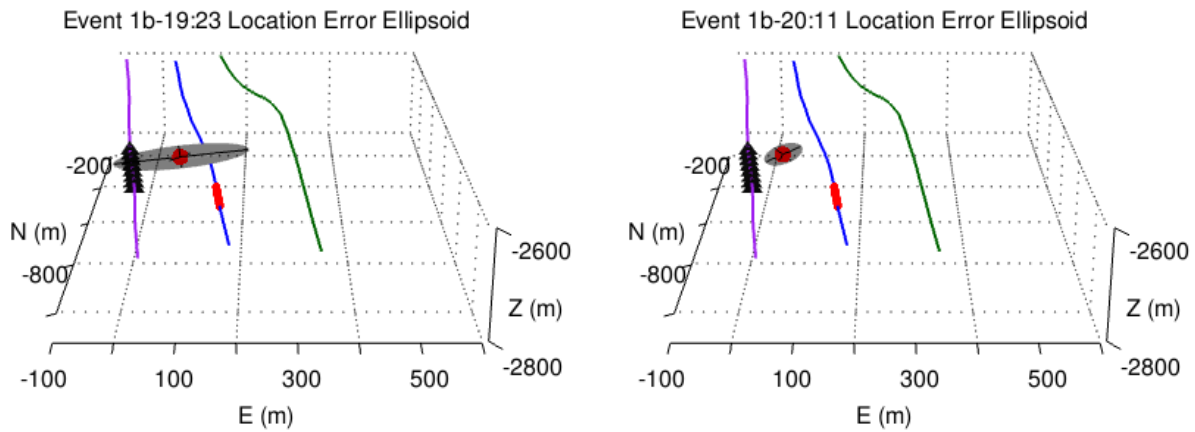
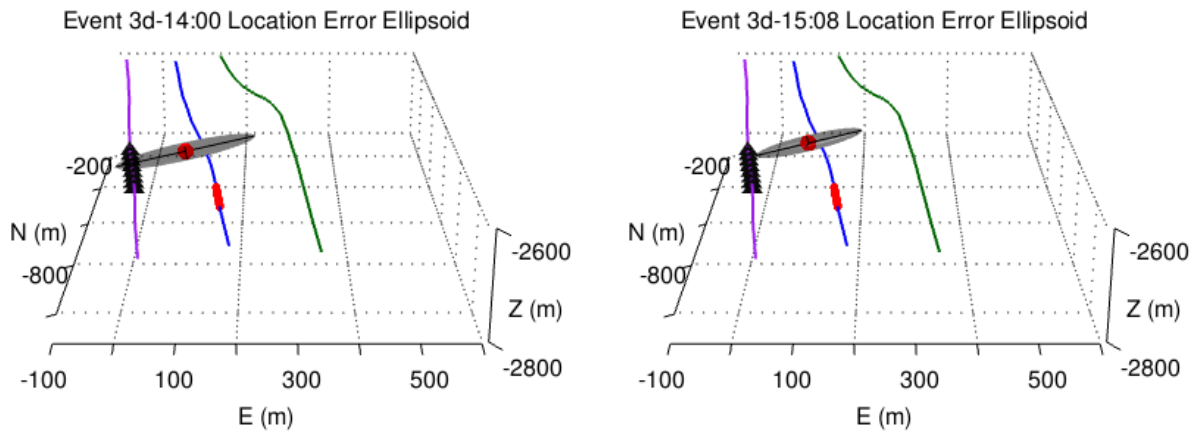
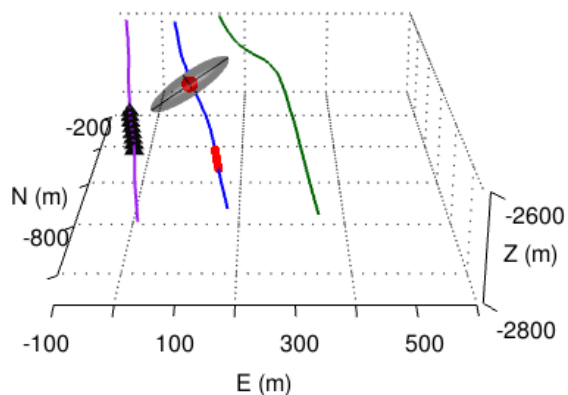


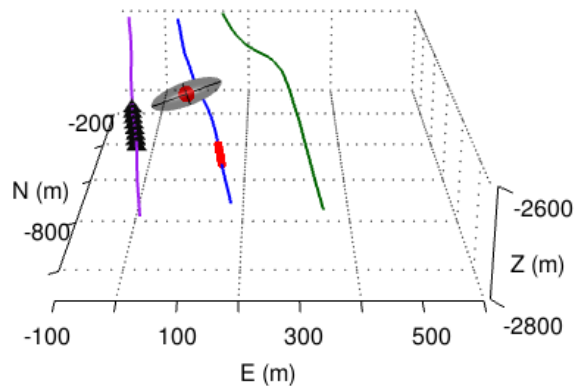
Figure B.2: 3D error ellipsoids and event locations for events in stage 3d. The error ellipsoids are shaded in gray with the axes outlined in black and the event locations are in the center of the ellipsoids noted by the red dot. The X, Y, and Z coordinates are with respect to the surface location of well 1H (see section 2.3.3 for method and section 3.2.1 for results and figures). The well paths for wells 1H, 2H, and 3H are outlined in blue, purple, and green, respectively. The black triangles represent the geophones and the red dots along the 3H well path (green) are the locations of the perforations for stage 3d. Refer to Table B.4 for numerical coordinates and X, Y, Z errors.



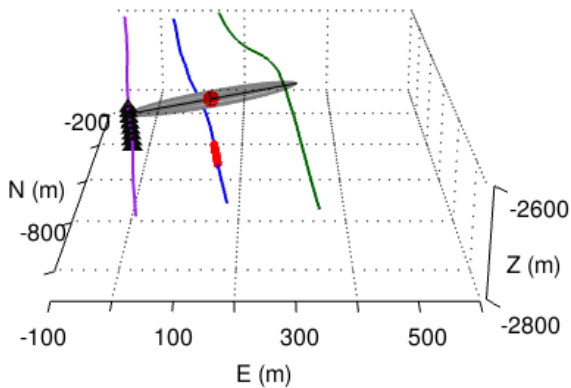
Event 3d-15:11 Location Error Ellipsoid



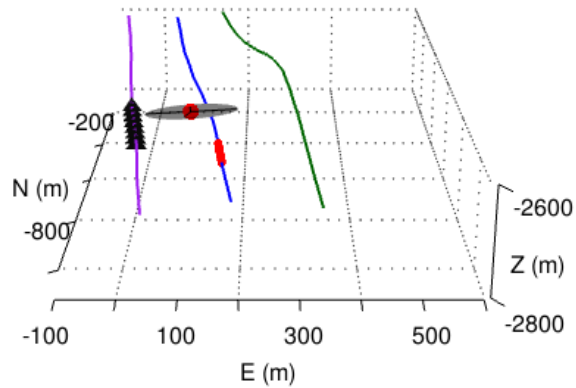
Event 3d-15:30 Location Error Ellipsoid



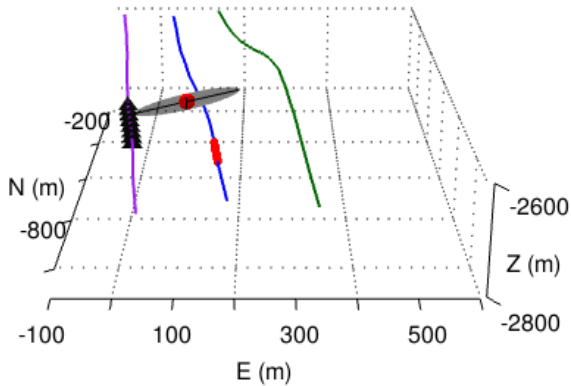
Event 3d-15:31 Location Error Ellipsoid



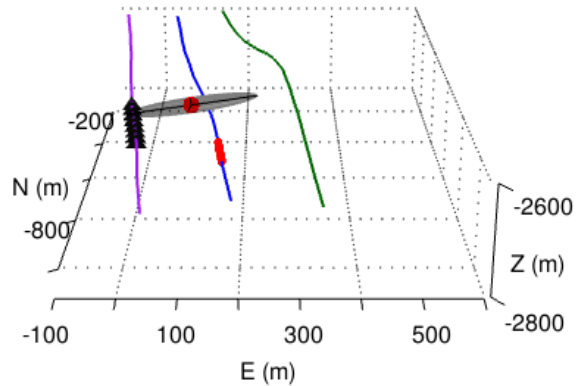
Event 3d-15:34 Location Error Ellipsoid



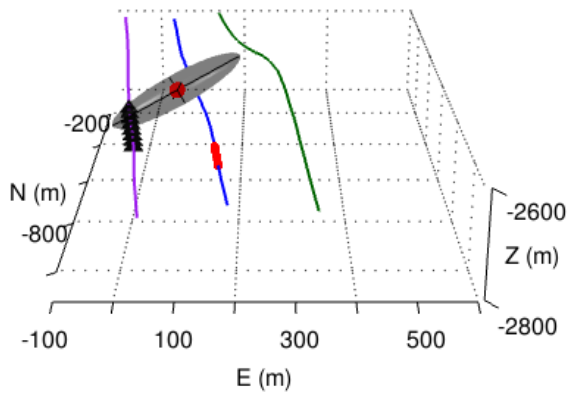
Event 3d-15:35 Location Error Ellipsoid



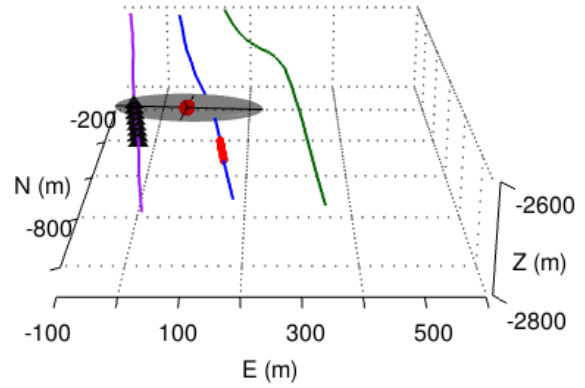
Event 3d-16:15 Location Error Ellipsoid



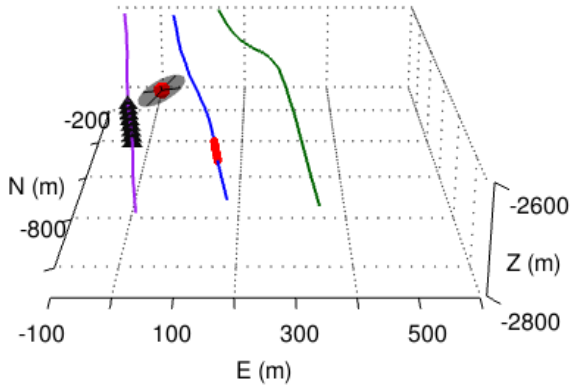
Event 3d-16:16 Location Error Ellipsoid



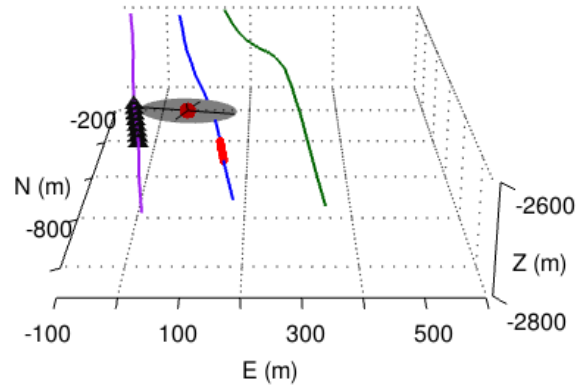
Event 3d-16:37 Location Error Ellipsoid



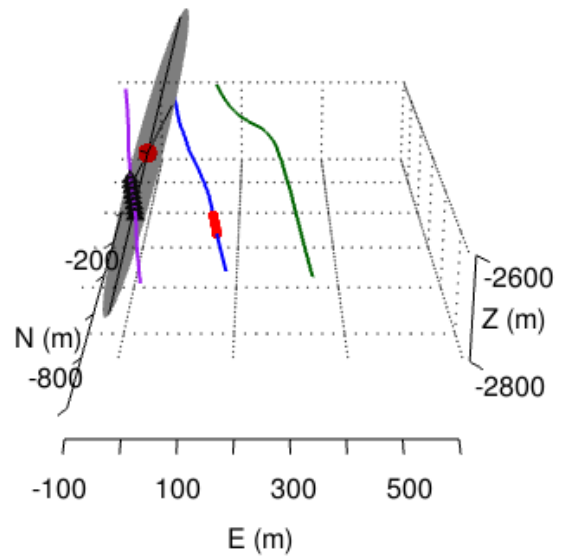
Event 3d-17:04 Location Error Ellipsoid



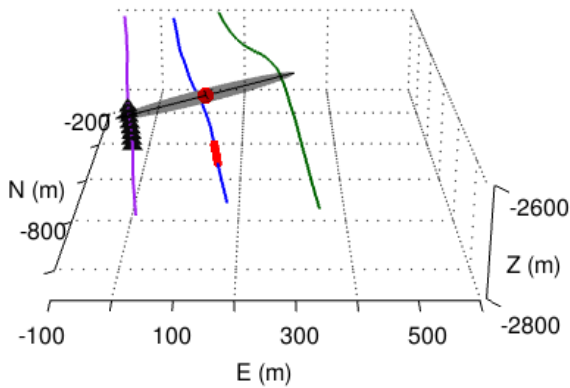
Event 3d-17:13 Location Error Ellipsoid

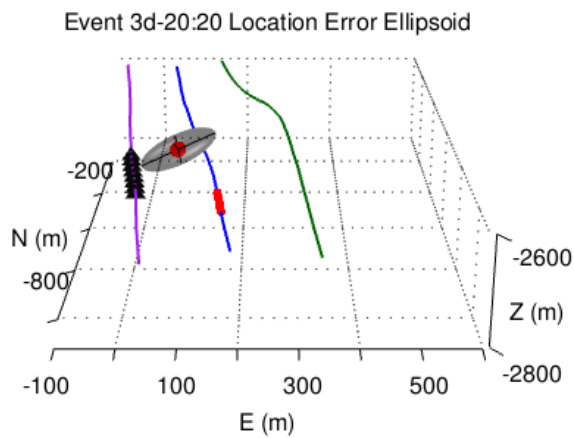
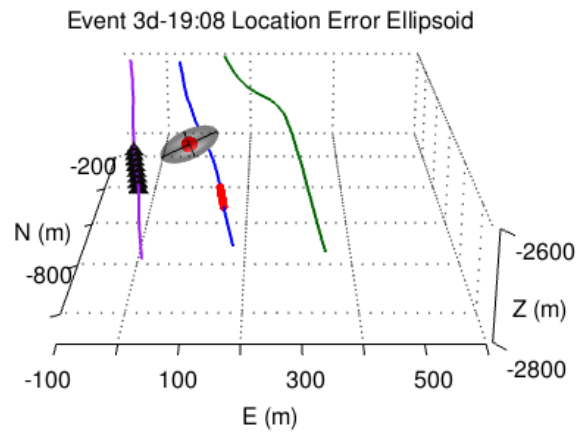
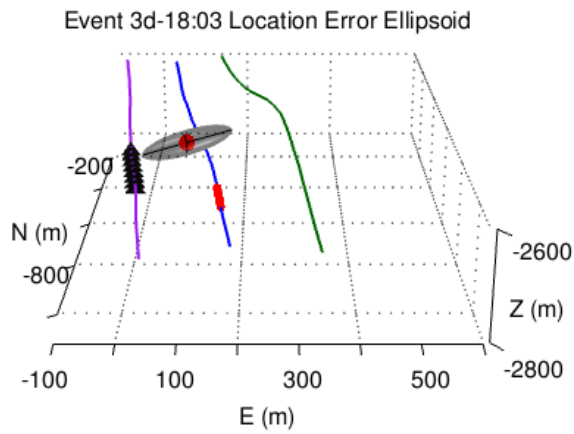
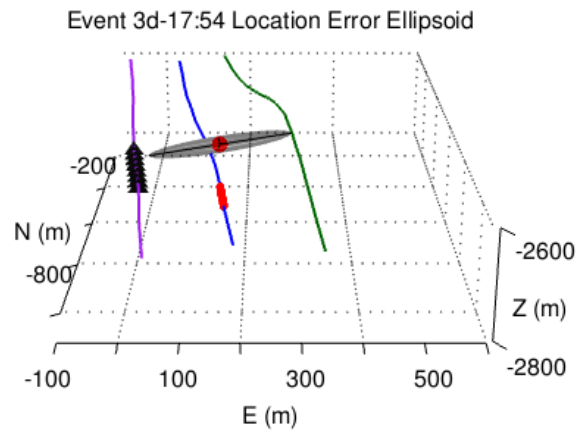
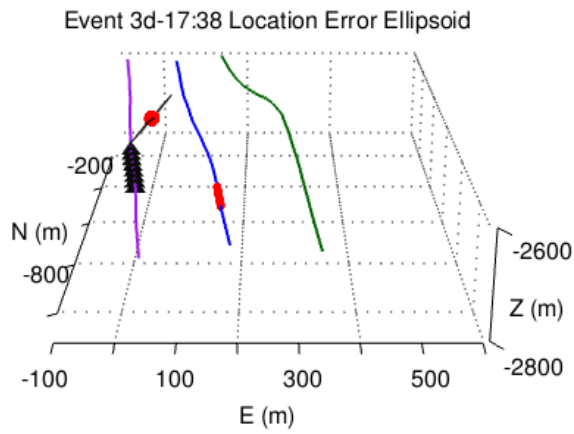


Event 3d-17:21 Location Error Ellipsoid



Event 3d-17:14 Location Error Ellipsoid





Appendix C: Full-Wavefield Moment Tensor Inversion Results

Table C.1: Full-wavefield moment tensor inversion results for location 1b, DC input mechanism, isotropic medium, and dominant source frequency of 125 Hz with no constraints applied to the inversion.	293
Table C.2: Full-wavefield moment tensor inversion results for location 1b, DC input mechanism, isotropic medium, and dominant source frequency of 125 Hz with a deviatoric constraint applied to the inversion.	294
Table C.3: Full-wavefield moment tensor inversion results for location 1b, DC input mechanism, isotropic medium, and dominant source frequency of 125 Hz with a DC constraint applied to the inversion.	295
Table C.4: Full-wavefield moment tensor inversion results for location 3d, DC input mechanism, isotropic medium, and dominant source frequency of 125 Hz with no constraints applied to the inversion.	296
Table C.5: Full-wavefield moment tensor inversion results for location 3d, DC input mechanism, isotropic medium, and dominant source frequency of 125 Hz with a deviatoric constraint applied to the inversion.	297
Table C.6: Full-wavefield moment tensor inversion results for location 3d, DC input mechanism, isotropic medium, and dominant source frequency of 125 Hz with a DC constraint applied to the inversion.	298
Table C.7: Full-wavefield moment tensor inversion results for location 3e, DC input mechanism, isotropic medium, and dominant source frequency of 125 Hz with no constraints applied to the inversion.	299
Table C.8: Full-wavefield moment tensor inversion results for location 3e, DC input mechanism, isotropic medium, and dominant source frequency of 125 Hz with a deviatoric constraint applied to the inversion.	300
Table C.9: Full-wavefield moment tensor inversion results for location 3e, DC input mechanism, isotropic medium, and dominant source frequency of 125 Hz with a DC constraint applied to the inversion.	301
Figure C.1: Full-wavefield moment tensor inversion results for a DC source mechanism in an isotropic medium and source frequency of 125 Hz.....	302
Table C.10: Full-wavefield moment tensor inversion results for location 1b, CLVD input mechanism, isotropic medium, and dominant source frequency of 125 Hz with no constraints applied to the inversion.	303

Table C.11: Full-wavefield moment tensor inversion results for location 1b, CLVD input mechanism, isotropic medium, and dominant source frequency of 125 Hz with a deviatoric constraint applied to the inversion.	304
Table C.12: Full-wavefield moment tensor inversion results for location 1b, CLVD input mechanism, isotropic medium, and dominant source frequency of 125 Hz with a DC constraint applied to the inversion.	305
Table C.13: Full-wavefield moment tensor inversion results for location 3d, CLVD input mechanism, isotropic medium, and dominant source frequency of 125 Hz with no constraints applied to the inversion.	306
Table C.14: Full-wavefield moment tensor inversion results for location 3d, CLVD input mechanism, isotropic medium, and dominant source frequency of 125 Hz with a deviatoric constraint applied to the inversion.	307
Table C.15: Full-wavefield moment tensor inversion results for location 3d, CLVD input mechanism, isotropic medium, and dominant source frequency of 125 Hz with a DC constraint applied to the inversion.	308
Table C.16: Full-wavefield moment tensor inversion results for location 3e, CLVD input mechanism, isotropic medium, and dominant source frequency of 125 Hz with no constraints applied to the inversion.	309
Table C.17: Full-wavefield moment tensor inversion results for location 3e, CLVD input mechanism, isotropic medium, and dominant source frequency of 125 Hz with a deviatoric constraint applied to the inversion.	310
Table C.18: Full-wavefield moment tensor inversion results for location 3e, CLVD input mechanism, isotropic medium, and dominant source frequency of 125 Hz with a DC constraint applied to the inversion.	311
Figure C.2: Full-wavefield moment tensor inversion results for a CLVD source mechanism in an isotropic medium and source frequency of 125 Hz.....	312
Table C.19: Full-wavefield moment tensor inversion results for location 1b, ISO input mechanism, isotropic medium, and dominant source frequency of 125 Hz with no constraints applied to the inversion.	313
Table C.20: Full-wavefield moment tensor inversion results for location 1b, ISO input mechanism, isotropic medium, and dominant source frequency of 125 Hz with a deviatoric constraint applied to the inversion.	314
Table C.21: Full-wavefield moment tensor inversion results for location 1b, ISO input mechanism, isotropic medium, and dominant source frequency of 125 Hz with a DC constraint applied to the inversion.	315

Table C.22: Full-wavefield moment tensor inversion results for location 3d, ISO input mechanism, isotropic medium, and dominant source frequency of 125 Hz with no constraints applied to the inversion.	316
Table C.23: Full-wavefield moment tensor inversion results for location 3d, ISO input mechanism, isotropic medium, and dominant source frequency of 125 Hz with a deviatoric constraint applied to the inversion.	317
Table C.24: Full-wavefield moment tensor inversion results for location 3d, ISO input mechanism, isotropic medium, and dominant source frequency of 125 Hz with a DC constraint applied to the inversion.	318
Table C.25: Full-wavefield moment tensor inversion results for location 3e, ISO input mechanism, isotropic medium, and dominant source frequency of 125 Hz with no constraints applied to the inversion.	319
Table C.26: Full-wavefield moment tensor inversion results for location 3e, ISO input mechanism, isotropic medium, and dominant source frequency of 125 Hz with a deviatoric constraint applied to the inversion.	320
Table C.27: Full-wavefield moment tensor inversion results for location 3e, ISO input mechanism, isotropic medium, and dominant source frequency of 125 Hz with a DC constraint applied to the inversion.	321
Figure C.3: Full-wavefield moment tensor inversion results for an ISO source mechanism in an isotropic medium and source frequency of 125 Hz.....	322
Table C.28: Full-wavefield moment tensor inversion results for location 1b, DC input mechanism, 5% anisotropic medium, and dominant source frequency of 125 Hz with no constraints applied to the inversion.	324
Table C.29: Full-wavefield moment tensor inversion results for location 1b, DC input mechanism, 5% anisotropic medium, and dominant source frequency of 125 Hz with a deviatoric constraint applied to the inversion.	325
Table C.30: Full-wavefield moment tensor inversion results for location 1b, DC input mechanism, 5% anisotropic medium, and dominant source frequency of 125 Hz with a DC constraint applied to the inversion.	326
Table C.31: Full-wavefield moment tensor inversion results for location 3d, DC input mechanism, 5% anisotropic medium, and dominant source frequency of 125 Hz with no constraints applied to the inversion.	327
Table C.32: Full-wavefield moment tensor inversion results for location 3d, DC input mechanism, 5% anisotropic medium, and dominant source frequency of 125 Hz with a deviatoric constraint applied to the inversion.	328

Table C.33: Full-wavefield moment tensor inversion results for location 3d, DC input mechanism, 5% anisotropic medium, and dominant source frequency of 125 Hz with a DC constraint applied to the inversion.	329
Table C.34: Full-wavefield moment tensor inversion results for location 3e, DC input mechanism, 5% anisotropic medium, and dominant source frequency of 125 Hz with no constraints applied to the inversion.	330
Table C.35: Full-wavefield moment tensor inversion results for location 3e, DC input mechanism, 5% anisotropic medium, and dominant source frequency of 125 Hz with a deviatoric constraint applied to the inversion.	331
Table C.36: Full-wavefield moment tensor inversion results for location 3e, DC input mechanism, 5% anisotropic medium, and dominant source frequency of 125 Hz with a DC constraint applied to the inversion.	332
Figure C.4: Full-wavefield moment tensor inversion results for a DC source mechanism in a 5% anisotropic medium and source frequency of 125 Hz.....	333
Table C.37: Full-wavefield moment tensor inversion results for location 1b, CLVD input mechanism, 5% anisotropic medium, and dominant source frequency of 125 Hz with no constraints applied to the inversion.	334
Table C.38: Full-wavefield moment tensor inversion results for location 1b, CLVD input mechanism, 5% anisotropic medium, and dominant source frequency of 125 Hz with a deviatoric constraint applied to the inversion.	335
Table C.39: Full-wavefield moment tensor inversion results for location 1b, CLVD input mechanism, 5% anisotropic medium, and dominant source frequency of 125 Hz with a DC constraint applied to the inversion.	336
Table C.40: Full-wavefield moment tensor inversion results for location 3d, CLVD input mechanism, 5% anisotropic medium, and dominant source frequency of 125 Hz with no constraints applied to the inversion.	337
Table C.41: Full-wavefield moment tensor inversion results for location 3d, CLVD input mechanism, 5% anisotropic medium, and dominant source frequency of 125 Hz with a deviatoric constraint applied to the inversion.	338
Table C.42: Full-wavefield moment tensor inversion results for location 3d, CLVD input mechanism, 5% anisotropic medium, and dominant source frequency of 125 Hz with a DC constraint applied to the inversion.	339
Table C.43: Full-wavefield moment tensor inversion results for location 3e, CLVD input mechanism, 5% anisotropic medium, and dominant source frequency of 125 Hz with no constraints applied to the inversion.	340

Table C.44: Full-wavefield moment tensor inversion results for location 3e, CLVD input mechanism, 5% anisotropic medium, and dominant source frequency of 125 Hz with a deviatoric constraint applied to the inversion.	341
Table C.45: Full-wavefield moment tensor inversion results for location 3e, CLVD input mechanism, 5% anisotropic medium, and dominant source frequency of 125 Hz with a DC constraint applied to the inversion.	342
Figure C.5: Full-wavefield moment tensor inversion results for a CLVD source mechanism in a 5% anisotropic medium and source frequency of 125 Hz	343
Table C.46: Full-wavefield moment tensor inversion results for location 1b, ISO input mechanism, 5% anisotropic medium, and dominant source frequency of 125 Hz with no constraints applied to the inversion.	344
Table C.47: Full-wavefield moment tensor inversion results for location 1b, ISO input mechanism, 5% anisotropic medium, and dominant source frequency of 125 Hz with a deviatoric constraint applied to the inversion.	345
Table C.48: Full-wavefield moment tensor inversion results for location 1b, ISO input mechanism, 5% anisotropic medium, and dominant source frequency of 125 Hz with a DC constraint applied to the inversion.	346
Table C.49: Full-wavefield moment tensor inversion results for location 3d, ISO input mechanism, 5% anisotropic medium, and dominant source frequency of 125 Hz with no constraints applied to the inversion.	347
Table C.50: Full-wavefield moment tensor inversion results for location 3d, ISO input mechanism, 5% anisotropic medium, and dominant source frequency of 125 Hz with a deviatoric constraint applied to the inversion.	348
Table C.51: Full-wavefield moment tensor inversion results for location 3d, ISO input mechanism, 5% anisotropic medium, and dominant source frequency of 125 Hz with a DC constraint applied to the inversion.	349
Table C.52: Full-wavefield moment tensor inversion results for location 3e, ISO input mechanism, 5% anisotropic medium, and dominant source frequency of 125 Hz with no constraints applied to the inversion.	350
Table C.53: Full-wavefield moment tensor inversion results for location 3e, ISO input mechanism, 5% anisotropic medium, and dominant source frequency of 125 Hz with a deviatoric constraint applied to the inversion.	351
Table C.54: Full-wavefield moment tensor inversion results for location 3e, ISO input mechanism, 5% anisotropic medium, and dominant source frequency of 125 Hz with a DC constraint applied to the inversion.	352

Figure C.6: Full-wavefield moment tensor inversion results for an ISO source mechanism in a 5% anisotropic medium and source frequency of 125 Hz	353
Table C.55: Full-wavefield moment tensor inversion results for location 1b, DC input mechanism, isotropic medium, dominant source frequency of 125 Hz, and 5% noise with no constraints applied to the inversion.	354
Table C.56: Full-wavefield moment tensor inversion results for location 1b, DC input mechanism, isotropic medium, dominant source frequency of 125 Hz, and 5% noise with a deviatoric constraint applied to the inversion.	355
Table C.57: Full-wavefield moment tensor inversion results for location 1b, DC input mechanism, isotropic medium, dominant source frequency of 125 Hz, and 5% noise with a DC constraint applied to the inversion.	356
Table C.58: Full-wavefield moment tensor inversion results for location 3d, DC input mechanism, isotropic medium, dominant source frequency of 125 Hz, and 5% noise with no constraints applied to the inversion.	357
Table C.59: Full-wavefield moment tensor inversion results for location 3d, DC input mechanism, isotropic medium, dominant source frequency of 125 Hz, and 5% noise with a deviatoric constraint applied to the inversion.	358
Table C.60: Full-wavefield moment tensor inversion results for location 3d, DC input mechanism, isotropic medium, dominant source frequency of 125 Hz, and 5% noise with a DC constraint applied to the inversion.	359
Table C.61: Full-wavefield moment tensor inversion results for location 3e, DC input mechanism, isotropic medium, dominant source frequency of 125 Hz, and 5% noise with no constraints applied to the inversion.	360
Table C.62: Full-wavefield moment tensor inversion results for location 3e, DC input mechanism, isotropic medium, dominant source frequency of 125 Hz, and 5% noise with a deviatoric constraint applied to the inversion.	361
Table C.63: Full-wavefield moment tensor inversion results for location 3e, DC input mechanism, isotropic medium, dominant source frequency of 125 Hz, and 5% noise with a DC constraint applied to the inversion.	362
Figure C.7: Full-wavefield moment tensor inversion results for a DC source mechanism in an isotropic medium, 5% noise, and source frequency of 125 Hz.....	363
Table C.64: Full-wavefield moment tensor inversion results for location 1b, CLVD input mechanism, isotropic medium, dominant source frequency of 125 Hz, and 5% noise with no constraints applied to the inversion.	364

Table C.65: Full-wavefield moment tensor inversion results for location 1b, CLVD input mechanism, isotropic medium, dominant source frequency of 125 Hz, and 5% noise with a deviatoric constraint applied to the inversion.	365
Table C.66: Full-wavefield moment tensor inversion results for location 1b, CLVD input mechanism, isotropic medium, dominant source frequency of 125 Hz, and 5% noise with a DC constraint applied to the inversion.	366
Table C.67: Full-wavefield moment tensor inversion results for location 3d, CLVD input mechanism, isotropic medium, dominant source frequency of 125 Hz, and 5% noise with no constraints applied to the inversion.	367
Table C.68: Full-wavefield moment tensor inversion results for location 3d, CLVD input mechanism, isotropic medium, dominant source frequency of 125 Hz, and 5% noise with a deviatoric constraint applied to the inversion.	368
Table C.69: Full-wavefield moment tensor inversion results for location 3d, CLVD input mechanism, isotropic medium, dominant source frequency of 125 Hz, and 5% noise a DC constraint applied to the inversion.	369
Table C.70: Full-wavefield moment tensor inversion results for location 3e, CLVD input mechanism, isotropic medium, dominant source frequency of 125 Hz, and 5% noise with no constraints applied to the inversion.	370
Table C.71: Full-wavefield moment tensor inversion results for location 3e, CLVD input mechanism, isotropic medium, dominant source frequency of 125 Hz, and 5% noise with a deviatoric constraint applied to the inversion.	371
Table C.72: Full-wavefield moment tensor inversion results for location 3e, CLVD input mechanism, isotropic medium, dominant source frequency of 125 Hz, and 5% noise with a DC constraint applied to the inversion.	372
Figure C.8: Full-wavefield moment tensor inversion results for a CLVD source mechanism in an isotropic medium, 5% noise, and source frequency of 125 Hz.....	373
Table C.73: Full-wavefield moment tensor inversion results for location 1b, ISO input mechanism, isotropic medium, dominant source frequency of 125 Hz, and 5% noise with no constraints applied to the inversion.	374
Table C.74: Full-wavefield moment tensor inversion results for location 1b, ISO input mechanism, isotropic medium, dominant source frequency of 125 Hz, and 5% noise with a deviatoric constraint applied to the inversion.	375
Table C.75: Full-wavefield moment tensor inversion results for location 1b, ISO input mechanism, isotropic medium, dominant source frequency of 125 Hz, and 5% noise with a DC constraint applied to the inversion.	376

Table C.76: Full-wavefield moment tensor inversion results for location 3d, ISO input mechanism, isotropic medium, dominant source frequency of 125 Hz, and 5% noise with no constraints applied to the inversion.	377
Table C.77: Full-wavefield moment tensor inversion results for location 3d, ISO input mechanism, isotropic medium, dominant source frequency of 125 Hz, and 5% noise with a deviatoric constraint applied to the inversion.	378
Table C.78: Full-wavefield moment tensor inversion results for location 3d, ISO input mechanism, isotropic medium, dominant source frequency of 125 Hz, and 5% noise with a DC constraint applied to the inversion.	379
Table C.79: Full-wavefield moment tensor inversion results for location 3e, ISO input mechanism, isotropic medium, dominant source frequency of 125 Hz, and 5% noise with no constraints applied to the inversion.	380
Table C.80: Full-wavefield moment tensor inversion results for location 3e, ISO input mechanism, isotropic medium, dominant source frequency of 125 Hz, and 5% noise with a deviatoric constraint applied to the inversion.	381
Table C.81: Full-wavefield moment tensor inversion results for location 3e, ISO input mechanism, isotropic medium, dominant source frequency of 125 Hz, and 5% noise with a DC constraint applied to the inversion.	382
Figure C.9: Full-wavefield moment tensor inversion results for an ISO source mechanism in an isotropic medium, 5% noise, and source frequency of 125 Hz.....	383
Table C.82: Full-wavefield moment tensor inversion results for location 1b, DC input mechanism, isotropic medium, and dominant source frequency of 50 Hz with no constraints applied to the inversion.	384
Table C.83: Full-wavefield moment tensor inversion results for location 1b, DC input mechanism, isotropic medium, and dominant source frequency of 50 Hz with a deviatoric constraint applied to the inversion.	385
Table C.84: Full-wavefield moment tensor inversion results for location 1b, DC input mechanism, isotropic medium, and dominant source frequency of 50 Hz with a DC constraint applied to the inversion.	386
Table C.85: Full-wavefield moment tensor inversion results for location 3d, DC input mechanism, isotropic medium, and dominant source frequency of 50 Hz with no constraints applied to the inversion.	387
Table C.86: Full-wavefield moment tensor inversion results for location 3d, DC input mechanism, isotropic medium, and dominant source frequency of 50 Hz with a deviatoric constraint applied to the inversion.	388

Table C.87: Full-wavefield moment tensor inversion results for location 3d, DC input mechanism, isotropic medium, and dominant source frequency of 50 Hz with a DC constraint applied to the inversion.	389
Table C.88: Full-wavefield moment tensor inversion results for location 3e, DC input mechanism, isotropic medium, and dominant source frequency of 50 Hz with no constraints applied to the inversion.	390
Table C.89: Full-wavefield moment tensor inversion results for location 3e, DC input mechanism, isotropic medium, and dominant source frequency of 50 Hz with a deviatoric constraint applied to the inversion.	391
Table C.90: Full-wavefield moment tensor inversion results for location 3e, DC input mechanism, isotropic medium, and dominant source frequency of 50 Hz with a DC constraint applied to the inversion.	392
Figure C.10: Full-wavefield moment tensor inversion results for a DC source mechanism in an isotropic medium and source frequency of 50 Hz	393
Table C.91: Full-wavefield moment tensor inversion results for location 1b, CLVD input mechanism, isotropic medium, and dominant source frequency of 50 Hz with no constraints applied to the inversion.	394
Table C.92: Full-wavefield moment tensor inversion results for location 1b, CLVD input mechanism, isotropic medium, and dominant source frequency of 50 Hz with a deviatoric constraint applied to the inversion.	395
Table C.93: Full-wavefield moment tensor inversion results for location 1b, CLVD input mechanism, isotropic medium, and dominant source frequency of 50 Hz with a DC constraint applied to the inversion.	396
Table C.94: Full-wavefield moment tensor inversion results for location 3d, CLVD input mechanism, isotropic medium, and dominant source frequency of 50 Hz with no constraints applied to the inversion.	397
Table C.95: Full-wavefield moment tensor inversion results for location 3d, CLVD input mechanism, isotropic medium, and dominant source frequency of 50 Hz with a deviatoric constraint applied to the inversion.	398
Table C.96: Full-wavefield moment tensor inversion results for location 3d, CLVD input mechanism, isotropic medium, and dominant source frequency of 50 Hz with a DC constraint applied to the inversion.	399
Table C.97: Full-wavefield moment tensor inversion results for location 3e, CLVD input mechanism, isotropic medium, and dominant source frequency of 50 Hz with no constraints applied to the inversion.	400

Table C.98: Full-wavefield moment tensor inversion results for location 3e, CLVD input mechanism, isotropic medium, and dominant source frequency of 50 Hz with a deviatoric constraint applied to the inversion.	401
Table C.99: Full-wavefield moment tensor inversion results for location 3e, CLVD input mechanism, isotropic medium, and dominant source frequency of 50 Hz with a DC constraint applied to the inversion.	402
Figure C.11: Full-wavefield moment tensor inversion results for a CLVD source mechanism in an isotropic medium and source frequency of 50 Hz	403
Table C.100: Full-wavefield moment tensor inversion results for location 1b, ISO input mechanism, isotropic medium, and dominant source frequency of 50 Hz with no constraints applied to the inversion.	404
Table C.101: Full-wavefield moment tensor inversion results for location 1b, ISO input mechanism, isotropic medium, and dominant source frequency of 50 Hz with a deviatoric constraint applied to the inversion.	405
Table C.102: Full-wavefield moment tensor inversion results for location 1b, ISO input mechanism, isotropic medium, and dominant source frequency of 50 Hz with a DC constraint applied to the inversion.	406
Table C.103: Full-wavefield moment tensor inversion results for location 3d, ISO input mechanism, isotropic medium, and dominant source frequency of 50 Hz with no constraints applied to the inversion.	407
Table C.104: Full-wavefield moment tensor inversion results for location 3d, ISO input mechanism, isotropic medium, and dominant source frequency of 50 Hz with a deviatoric constraint applied to the inversion.	408
Table C.105: Full-wavefield moment tensor inversion results for location 3d, ISO input mechanism, isotropic medium, and dominant source frequency of 50 Hz with a DC constraint applied to the inversion.	409
Table C.106: Full-wavefield moment tensor inversion results for location 3e, ISO input mechanism, isotropic medium, and dominant source frequency of 50 Hz with no constraints applied to the inversion.	410
Table C.107: Full-wavefield moment tensor inversion results for location 3e, ISO input mechanism, isotropic medium, and dominant source frequency of 50 Hz with a deviatoric constraint applied to the inversion.	411
Table C.108: Full-wavefield moment tensor inversion results for location 3e, ISO input mechanism, isotropic medium, and dominant source frequency of 50 Hz with a DC constraint applied to the inversion.	412

Figure C.12: Full-wavefield moment tensor inversion results for an ISO source mechanism in an isotropic medium and source frequency of 50 Hz	413
Table C.109: Full-wavefield moment tensor inversion results for location 1b, DC input mechanism, isotropic medium, and dominant source frequency of 175 Hz with no constraints applied to the inversion.	414
Table C.110: Full-wavefield moment tensor inversion results for location 1b, DC input mechanism, isotropic medium, and dominant source frequency of 175 Hz with a deviatoric constraint applied to the inversion.	415
Table C.111: Full-wavefield moment tensor inversion results for location 1b, DC input mechanism, isotropic medium, and dominant source frequency of 175 Hz with a DC constraint applied to the inversion.	416
Table C.112: Full-wavefield moment tensor inversion results for location 3d, DC input mechanism, isotropic medium, and dominant source frequency of 175 Hz with no constraints applied to the inversion.	417
Table C.113: Full-wavefield moment tensor inversion results for location 3d, DC input mechanism, isotropic medium, and dominant source frequency of 175 Hz with a deviatoric constraint applied to the inversion.	418
Table C.114: Full-wavefield moment tensor inversion results for location 3d, DC input mechanism, isotropic medium, and dominant source frequency of 175 Hz with a DC constraint applied to the inversion.	419
Table C.115: Full-wavefield moment tensor inversion results for location 3e, DC input mechanism, isotropic medium, and dominant source frequency of 175 Hz with no constraints applied to the inversion.	420
Table C.116: Full-wavefield moment tensor inversion results for location 3e, DC input mechanism, isotropic medium, and dominant source frequency of 175 Hz with a deviatoric constraint applied to the inversion.	421
Table C.117: Full-wavefield moment tensor inversion results for location 3e, DC input mechanism, isotropic medium, and dominant source frequency of 175 Hz with a DC constraint applied to the inversion.	422
Figure C.13: Full-wavefield moment tensor inversion results for a DC source mechanism in an isotropic medium and source frequency of 175 Hz.....	423
Table C.118: Full-wavefield moment tensor inversion results for location 1b, CLVD input mechanism, isotropic medium, and dominant source frequency of 175 Hz with no constraints applied to the inversion.	424

Table C.119: Full-wavefield moment tensor inversion results for location 1b, CLVD input mechanism, isotropic medium, and dominant source frequency of 175 Hz with a deviatoric constraint applied to the inversion.	425
Table C.120: Full-wavefield moment tensor inversion results for location 1b, CLVD input mechanism, isotropic medium, and dominant source frequency of 175 Hz with a DC constraint applied to the inversion.	426
Table C.121: Full-wavefield moment tensor inversion results for location 3d, CLVD input mechanism, isotropic medium, and dominant source frequency of 175 Hz with no constraints applied to the inversion.	427
Table C.122: Full-wavefield moment tensor inversion results for location 3d, CLVD input mechanism, isotropic medium, and dominant source frequency of 175 Hz with a deviatoric constraint applied to the inversion.	428
Table C.123: Full-wavefield moment tensor inversion results for location 3d, CLVD input mechanism, isotropic medium, and dominant source frequency of 175 Hz with a DC constraint applied to the inversion.	429
Table C.124: Full-wavefield moment tensor inversion results for location 3e, CLVD input mechanism, isotropic medium, and dominant source frequency of 175 Hz with no constraints applied to the inversion.	430
Table C.125: Full-wavefield moment tensor inversion results for location 3e, CLVD input mechanism, isotropic medium, and dominant source frequency of 175 Hz with a deviatoric constraint applied to the inversion.	431
Table C.126: Full-wavefield moment tensor inversion results for location 3e, CLVD input mechanism, isotropic medium, and dominant source frequency of 175 Hz with a DC constraint applied to the inversion.	432
Figure C.14: Full-wavefield moment tensor inversion results for a CLVD source mechanism in an isotropic medium and source frequency of 175 Hz.....	433
Table C.127: Full-wavefield moment tensor inversion results for location 1b, ISO input mechanism, isotropic medium, and dominant source frequency of 175 Hz with no constraints applied to the inversion.	434
Table C.128: Full-wavefield moment tensor inversion results for location 1b, ISO input mechanism, isotropic medium, and dominant source frequency of 175 Hz with a deviatoric constraint applied to the inversion.	435
Table C.129: Full-wavefield moment tensor inversion results for location 1b, ISO input mechanism, isotropic medium, and dominant source frequency of 175 Hz with a DC constraint applied to the inversion.	436

Table C.130: Full-wavefield moment tensor inversion results for location 3d, ISO input mechanism, isotropic medium, and dominant source frequency of 175 Hz with no constraints applied to the inversion.	437
Table C.131: Full-wavefield moment tensor inversion results for location 3d, ISO input mechanism, isotropic medium, and dominant source frequency of 175 Hz with a deviatoric constraint applied to the inversion.	438
Table C.132: Full-wavefield moment tensor inversion results for location 3d, ISO input mechanism, isotropic medium, and dominant source frequency of 175 Hz with a DC constraint applied to the inversion.	439
Table C.133: Full-wavefield moment tensor inversion results for location 3e, ISO input mechanism, isotropic medium, and dominant source frequency of 175 Hz with no constraints applied to the inversion.	440
Table C.134: Full-wavefield moment tensor inversion results for location 3e, ISO input mechanism, isotropic medium, and dominant source frequency of 175 Hz with a deviatoric constraint applied to the inversion.	441
Table C.135: Full-wavefield moment tensor inversion results for location 3e, ISO input mechanism, isotropic medium, and dominant source frequency of 175 Hz with a DC constraint applied to the inversion.	442
Figure C.15: Full-wavefield moment tensor inversion results for an ISO source mechanism in an isotropic medium and source frequency of 175 Hz.....	443

Table C.1: Full-wavefield moment tensor inversion results for location 1b, DC input mechanism, isotropic medium, and dominant source frequency of 125 Hz with no constraints applied to the inversion. The bolded row is the location with the highest correlation in the grid search and thus the final ouputted result. Refer to Figure C.1a for visual.

Location Number	X Coord (m)	Y Coord (m)	Correlation	Strike 1 (°)	Dip 1 (°)	Rake 1 (°)	Strike 2 (°)	Dip 2 (°)	Rake 2 (°)	DC %	CLVD %	ISO %
1	-50	-50	0.1707	328	45	-97	158	46	-83	60.14	25.51	14.35
2	-50	-25	0.2087	323	45	-98	155	46	-82	64.95	19.34	15.71
3	-50	0	0.25	314	46	-100	148	45	-80	83	12.12	4.88
4	-50	25	0.2453	307	46	-103	146	45	-76	65.32	22.76	11.92
5	-50	50	0.2474	146	44	105	305	48	76	41.83	33.94	-24.23
6	-25	-50	0.2204	321	46	-97	151	45	-83	67.78	21.53	10.69
7	-25	-25	0.2802	312	47	-98	143	43	-82	62.11	21.72	16.17
8	-25	0	0.2552	311	47	-99	144	44	-80	49.27	31.41	19.32
9	-25	25	0.1945	308	49	80	142	42	101	25.32	44.32	-30.36
10	-25	50	0.1517	308	47	80	142	44	100	51.57	28.37	-20.06
11	0	-50	0.0703	197	77	168	289	78	13	1.49	18.41	-80.1
12	0	-25	0.2256	314	47	-97	144	43	-82	34.49	37.22	28.29
13	0	0	0.1488	141	42	99	309	49	82	24.01	49.42	-26.57
14	0	25	0.114	142	44	98	310	47	82	46.7	31.26	-22.04
15	0	50	0.0973	136	43	-80	302	48	-99	55.7	27.11	17.19
16	25	-50	0.0825	193	79	171	285	81	11	1.75	17.5	-80.75
17	25	-25	0.1191	314	47	-96	143	43	-83	33.11	39.38	27.51
18	25	0	0.1032	78	48	128	208	54	55	3.88	4.28	91.84
19	25	25	0.0959	67	43	110	220	50	72	6.46	5.61	87.93
20	25	50	0.1191	224	49	-101	60	42	-78	14.34	1.13	-84.53
21	50	-50	0.0921	308	50	-113	161	45	-65	1.95	12.99	85.06
22	50	-25	0.1057	98	88	177	188	87	2	6.3	6.07	87.63
23	50	0	0.1151	187	87	-174	97	84	-3	8.16	2.58	-89.26
24	50	25	0.1153	212	51	66	68	45	117	3.58	4.67	91.75
25	50	50	0.111	221	49	82	54	42	100	11.47	3.61	84.92

Table C.2: Full-wavefield moment tensor inversion results for location 1b, DC input mechanism, isotropic medium, and dominant source frequency of 125 Hz with a deviatoric constraint applied to the inversion. The bolded row is the location with the highest correlation in the grid search and thus the final ouputted result. Refer to Figure C.1b for visual.

Location Number	X Coord (m)	Y Coord (m)	Correlation	Strike 1 (°)	Dip 1 (°)	Rake 1 (°)	Strike 2 (°)	Dip 2 (°)	Rake 2 (°)	DC %	CLVD %	ISO %
1	-50	-50	0.1676	327	45	-98	158	46	-83	82.5	17.5	0
2	-50	-25	0.2049	323	45	-98	155	46	-82	90.77	9.23	0
3	-50	0	0.2498	313	46	-100	148	45	-80	90.85	9.15	0
4	-50	25	0.2444	306	46	-103	145	46	-77	83.43	16.57	0
5	-50	50	0.2423	305	47	76	144	45	104	77.25	22.75	0
6	-25	-50	0.219	320	46	-97	151	45	-83	84.74	15.26	0
7	-25	-25	0.278	311	47	-98	142	44	-82	87.44	12.56	0
8	-25	0	0.2515	310	47	-99	143	44	-81	77.82	22.18	0
9	-25	25	0.1876	140	43	100	306	48	81	68.33	31.67	0
10	-25	50	0.1488	141	44	100	307	47	80	82.73	17.27	0
11	0	-50	0.0542	139	42	95	312	48	85	57.27	42.73	0
12	0	-25	0.2148	312	47	-97	142	44	-83	76.36	23.64	0
13	0	0	0.1444	140	43	98	308	48	82	59.76	40.24	0
14	0	25	0.1105	141	44	98	310	46	82	80.55	19.45	0
15	0	50	0.0962	135	43	-80	302	47	-99	82.56	17.44	0
16	25	-50	0.0459	57	41	97	227	50	84	76.28	23.72	0
17	25	-25	0.1117	313	46	-96	142	44	-83	74.13	25.87	0
18	25	0	0.0828	141	44	97	312	46	84	73.53	26.47	0
19	25	25	0.0844	135	43	-82	304	47	-97	78.92	21.08	0
20	25	50	0.0582	197	52	88	21	38	93	19.46	80.54	0
21	50	-50	0.0543	57	41	-83	228	49	-96	86.46	13.54	0
22	50	-25	0.0596	51	41	-84	223	50	-95	75.08	24.92	0
23	50	0	0.0727	135	43	-83	306	47	-96	77.15	22.85	0
24	50	25	0.0616	40	40	-85	214	50	-94	41.43	58.57	0
25	50	50	0.0588	313	44	-95	141	46	-85	68.74	31.26	0

Table C.3: Full-wavefield moment tensor inversion results for location 1b, DC input mechanism, isotropic medium, and dominant source frequency of 125 Hz with a DC constraint applied to the inversion. The bolded row is the location with the highest correlation in the grid search and thus the final ouputted result. Refer to Figure C.1c for visual.

Location Number	X Coord (m)	Y Coord (m)	Correlation	Strike 1 (°)	Dip 1 (°)	Rake 1 (°)	Strike 2 (°)	Dip 2 (°)	Rake 2 (°)	DC %	CLVD %	ISO %
1	-50	-50	0.1588	327	44	-98	157	46	-83	96.12	3.88	0
2	-50	-25	0.2009	322	44	-99	154	46	-82	95.72	4.28	0
3	-50	0	0.2476	313	45	-100	148	45	-80	97.37	2.63	0
4	-50	25	0.2405	307	45	-103	145	46	-77	99.39	0.61	0
5	-50	50	0.2341	305	46	76	144	46	104	99.08	0.92	0
6	-25	-50	0.2142	320	45	-97	150	45	-83	98.01	1.99	0
7	-25	-25	0.2754	311	47	-98	142	44	-82	97.24	2.76	0
8	-25	0	0.243	310	46	-99	143	45	-81	97.23	2.77	0
9	-25	25	0.1793	140	44	100	306	47	80	97.73	2.27	0
10	-25	50	0.1463	141	45	100	307	46	80	96.66	3.34	0
11	0	-50	0.0518	139	43	96	312	48	85	97.08	2.92	0
12	0	-25	0.2067	312	46	-97	142	44	-83	97.01	2.99	0
13	0	0	0.1346	139	44	98	308	47	82	97.81	2.19	0
14	0	25	0.1079	141	45	98	310	46	82	97.42	2.58	0
15	0	50	0.0928	135	44	-80	302	47	-99	95.06	4.94	0
16	25	-50	0.0459	59	41	99	227	50	82	91.2	8.8	0
17	25	-25	0.1063	312	46	-96	141	44	-83	99.67	0.33	0
18	25	0	0.0786	141	44	97	311	46	83	99.1	0.9	0
19	25	25	0.0809	135	44	-82	304	47	-98	95.96	4.04	0
20	25	50	0.0555	215	51	91	34	39	89	95.45	4.55	0
21	50	-50	0.0543	56	41	-84	228	49	-95	98.15	1.85	0
22	50	-25	0.0596	52	41	-83	223	50	-96	94.34	5.66	0
23	50	0	0.0689	135	44	-83	305	47	-96	94.34	5.66	0
24	50	25	0.0609	44	40	-83	215	50	-96	95.14	4.86	0
25	50	50	0.0554	313	43	-96	141	47	-85	97.05	2.95	0

Table C.4: Full-wavefield moment tensor inversion results for location 3d, DC input mechanism, isotropic medium, and dominant source frequency of 125 Hz with no constraints applied to the inversion. The bolded row is the location with the highest correlation in the grid search and thus the final ouputted result. Refer to Figure C.1d for visual.

Location Number	X Coord (m)	Y Coord (m)	Correlation	Strike 1 (°)	Dip 1 (°)	Rake 1 (°)	Strike 2 (°)	Dip 2 (°)	Rake 2 (°)	DC %	CLVD %	ISO %
1	-50	-50	0.1848	88	45	-90	268	45	-90	33.36	42.59	24.05
2	-50	-25	0.378	254	45	90	74	45	90	34.88	44.66	-20.46
3	-50	0	0.1883	71	45	-91	252	45	-89	31.26	45.89	22.85
4	-50	25	0.0497	240	46	92	58	44	88	20.59	58.02	-21.39
5	-50	50	0.0812	54	44	-92	236	46	-88	30.33	51.24	18.43
6	-25	-50	0.3052	76	44	-93	260	46	-87	25.63	50.41	23.96
7	-25	-25	0.3238	259	45	90	78	45	90	36.05	41.68	-22.27
8	-25	0	0.1571	73	45	-91	255	45	-89	31.01	44.73	24.26
9	-25	25	0.0434	243	47	101	48	44	79	13.15	67.88	18.97
10	-25	50	0.1068	51	44	-94	237	46	-86	17.29	51.76	30.95
11	0	-50	0.4447	68	44	-98	258	47	-83	15.18	51.61	33.21
12	0	-25	0.2363	264	45	90	84	45	90	41.77	45.26	-12.97
13	0	0	0.1212	75	45	-91	257	45	-89	29.35	44.66	25.99
14	0	25	0.0473	267	46	92	84	45	88	40.12	54.96	4.92
15	0	50	0.0965	42	44	-103	240	47	-77	11.81	52.47	-35.72
16	25	-50	0.5556	57	45	-108	262	48	-73	9.05	39.8	-51.15
17	25	-25	0.2098	93	46	91	271	44	89	19.8	28.25	-51.95
18	25	0	0.0874	77	45	-91	258	45	-89	24.16	38.62	37.22
19	25	25	0.0466	70	44	-92	252	46	-88	22.45	47.89	29.66
20	25	50	0.0684	4	74	-167	270	78	-17	6.29	50.09	43.62
21	50	-50	0.0656	265	46	86	90	44	94	6.87	18	-75.13
22	50	-25	0.1085	256	46	92	73	44	88	12.52	35.36	-52.12
23	50	0	0.051	80	46	-94	265	45	-86	22.03	50.02	-27.95
24	50	25	0.0632	72	45	-92	255	45	-88	18.88	48.34	32.78
25	50	50	0.0259	248	46	94	63	44	86	27.53	42.88	29.59

Table C.5: Full-wavefield moment tensor inversion results for location 3d, DC input mechanism, isotropic medium, and dominant source frequency of 125 Hz with a deviatoric constraint applied to the inversion. The bolded row is the location with the highest correlation in the grid search and thus the final ouputted result. Refer to Figure C.1e for visual.

Location Number	X Coord (m)	Y Coord (m)	Correlation	Strike 1 (°)	Dip 1 (°)	Rake 1 (°)	Strike 2 (°)	Dip 2 (°)	Rake 2 (°)	DC %	CLVD %	ISO %
1	-50	-50	0.1813	89	45	-90	268	45	-90	68.38	31.62	0
2	-50	-25	0.3745	254	45	90	74	45	90	63.83	36.17	0
3	-50	0	0.1857	71	45	-90	251	45	-90	63.56	36.44	0
4	-50	25	0.0493	239	46	91	58	44	89	47.33	52.67	0
5	-50	50	0.0807	54	44	-91	235	46	-89	54.3	45.7	0
6	-25	-50	0.3009	76	44	-91	258	46	-89	57.55	42.45	0
7	-25	-25	0.3185	258	45	90	78	45	90	68.09	31.91	0
8	-25	0	0.154	73	45	-90	254	45	-90	65.37	34.63	0
9	-25	25	0.0433	262	54	128	29	51	50	5.08	94.92	0
10	-25	50	0.1047	51	44	-92	234	46	-88	57.03	42.97	0
11	0	-50	0.4324	70	44	-93	254	46	-87	58.31	41.69	0
12	0	-25	0.2349	264	45	90	84	45	90	59.34	40.66	0
13	0	0	0.1176	75	45	-91	256	45	-89	65.95	34.05	0
14	0	25	0.0472	267	46	92	84	45	88	38.59	61.41	0
15	0	50	0.0957	9	76	-168	276	78	-15	9.3	90.7	0
16	25	-50	0.5392	27	83	-177	297	87	-7	32.09	67.91	0
17	25	-25	0.1587	94	46	90	274	44	90	85.2	14.8	0
18	25	0	0.0789	77	45	-90	257	45	-90	81.08	18.92	0
19	25	25	0.0446	69	44	-91	251	46	-89	62.43	37.57	0
20	25	50	0.066	37	43	-99	229	47	-82	40.18	59.82	0
21	50	-50	0.0326	259	45	90	79	45	90	19.79	80.21	0
22	50	-25	0.0891	251	46	91	70	44	89	97.89	2.11	0
23	50	0	0.0502	77	46	-98	268	45	-82	12.96	87.04	0
24	50	25	0.0589	72	45	-91	253	45	-89	61.95	38.05	0
25	50	50	0.0256	253	46	96	65	45	84	18.22	81.78	0

Table C.6: Full-wavefield moment tensor inversion results for location 3d, DC input mechanism, isotropic medium, and dominant source frequency of 125 Hz with a DC constraint applied to the inversion. The bolded row is the location with the highest correlation in the grid search and thus the final ouputted result. Refer to Figure C.1f for visual.

Location Number	X Coord (m)	Y Coord (m)	Correlation	Strike 1 (°)	Dip 1 (°)	Rake 1 (°)	Strike 2 (°)	Dip 2 (°)	Rake 2 (°)	DC %	CLVD %	ISO %
1	-50	-50	0.1709	89	45	-90	268	45	-90	93.95	6.05	0
2	-50	-25	0.3607	253	45	90	74	45	90	99.91	0.09	0
3	-50	0	0.1781	72	45	-90	252	45	-90	99.32	0.68	0
4	-50	25	0.0473	240	46	90	60	44	90	96.18	3.82	0
5	-50	50	0.0773	56	44	-91	236	46	-89	98.97	1.03	0
6	-25	-50	0.2805	77	44	-91	258	46	-89	91.13	8.87	0
7	-25	-25	0.3115	258	45	90	78	45	90	94.19	5.81	0
8	-25	0	0.1467	74	45	-90	254	45	-90	96.89	3.11	0
9	-25	25	0.0362	16	31	29	260	75	118	97.49	2.51	0
10	-25	50	0.1006	54	44	-91	235	46	-89	94.68	5.32	0
11	0	-50	0.4089	73	44	-91	255	46	-89	90.52	9.48	0
12	0	-25	0.2206	264	45	90	84	45	90	98.95	1.05	0
13	0	0	0.111	75	45	-90	256	45	-90	95.43	4.57	0
14	0	25	0.0431	266	45	91	85	45	89	94.7	5.3	0
15	0	50	0.0944	4	85	179	94	89	5	95.83	4.17	0
16	25	-50	0.5347	25	85	180	115	90	5	90.4	9.6	0
17	25	-25	0.1548	94	46	90	274	44	90	92.44	7.56	0
18	25	0	0.0774	77	45	-90	257	45	-90	98.08	1.92	0
19	25	25	0.0424	70	44	-91	250	46	-89	98.31	1.69	0
20	25	50	0.0632	173	88	-180	83	90	-2	96.41	3.59	0
21	50	-50	0.0326	259	45	90	79	45	90	19.79	80.21	0
22	50	-25	0.0891	251	46	91	69	44	89	96	4	0
23	50	0	0.0356	307	89	1	217	89	179	90.56	9.44	0
24	50	25	0.0552	72	45	-91	253	45	-89	96.12	3.88	0
25	50	50	0.0255	251	46	96	62	44	83	19.62	80.38	0

Table C.7: Full-wavefield moment tensor inversion results for location 3e, DC input mechanism, isotropic medium, and dominant source frequency of 125 Hz with no constraints applied to the inversion. The bolded row is the location with the highest correlation in the grid search and thus the final ouputted result. Refer to Figure C.1g for visual.

Location Number	X Coord (m)	Y Coord (m)	Correlation	Strike 1 (°)	Dip 1 (°)	Rake 1 (°)	Strike 2 (°)	Dip 2 (°)	Rake 2 (°)	DC %	CLVD %	ISO %
1	-50	-50	0.2561	77	46	-90	258	44	-90	40.84	38.87	20.29
2	-50	-25	0.4882	253	44	91	72	46	89	41.59	37.94	-20.47
3	-50	0	0.2239	63	45	-90	242	45	-90	34.58	32.86	32.56
4	-50	25	0.1719	245	44	91	64	46	89	41.13	38.91	-19.96
5	-50	50	0.0737	239	44	90	59	46	90	32.56	38.82	-28.62
6	-25	-50	0.2272	81	46	-91	263	44	-89	35.12	43.74	21.14
7	-25	-25	0.3624	78	46	-92	260	44	-88	32.9	45.34	21.76
8	-25	0	0.4922	255	44	91	73	46	89	19.56	31.02	-49.42
9	-25	25	0.191	61	45	-90	240	45	-90	28.31	35.84	35.85
10	-25	50	0.0869	49	44	-90	229	46	-90	26.65	36.96	36.39
11	0	-50	0.1358	255	45	90	74	45	90	40.79	45.4	-13.81
12	0	-25	0.2138	83	48	-101	279	43	-78	14.58	52.35	33.07
13	0	0	0.5412	70	46	-92	252	44	-88	35.03	42.45	-22.52
14	0	25	0.1599	234	46	91	53	44	89	45.81	51.45	2.74
15	0	50	0.0948	50	44	-92	233	46	-88	24.42	46.31	-29.27
16	25	-50	0.1068	78	46	-90	258	44	-90	28.47	39.29	32.24
17	25	-25	0.2096	250	45	90	70	45	90	31.2	37.56	-31.24
18	25	0	0.139	254	44	90	74	46	90	16.52	27.02	-56.46
19	25	25	0.0428	60	45	-86	234	45	-94	11.59	1.99	86.42
20	25	50	0.0132	61	45	-84	233	45	-96	9.92	7.25	82.83
21	50	-50	0.1516	79	46	-91	261	44	-89	29.84	48.7	21.46
22	50	-25	0.0183	301	83	175	32	85	7	5.04	11.53	83.43
23	50	0	0.006	235	46	87	60	44	94	13.25	7.99	-78.76
24	50	25	0.0074	60	45	-86	234	46	-94	14.18	4.88	80.94
1	50	50	0.2561	77	46	-90	258	44	-90	40.84	38.87	20.29

Table C.8: Full-wavefield moment tensor inversion results for location 3e, DC input mechanism, isotropic medium, and dominant source frequency of 125 Hz with a deviatoric constraint applied to the inversion. The bolded row is the location with the highest correlation in the grid search and thus the final ouputted result. Refer to Figure C.1h for visual.

Location Number	X Coord (m)	Y Coord (m)	Correlation	Strike 1 (°)	Dip 1 (°)	Rake 1 (°)	Strike 2 (°)	Dip 2 (°)	Rake 2 (°)	DC %	CLVD %	ISO %
1	-50	-50	0.2529	78	45	-90	258	45	-90	71.93	28.07	0
2	-50	-25	0.4809	253	44	90	73	46	90	72.84	27.16	0
3	-50	0	0.2079	63	45	-90	242	45	-90	88.28	11.72	0
4	-50	25	0.1691	246	44	90	65	46	90	70.98	29.02	0
5	-50	50	0.0698	240	44	90	60	46	90	76.61	23.39	0
6	-25	-50	0.2244	82	46	-91	263	44	-89	65.98	34.02	0
7	-25	-25	0.3578	79	46	-91	261	44	-89	63.82	36.18	0
8	-25	0	0.4174	257	44	90	76	46	90	91.37	8.63	0
9	-25	25	0.1695	61	45	-90	241	45	-90	87.08	12.92	0
10	-25	50	0.0785	48	44	-90	228	46	-90	85.44	14.56	0
11	0	-50	0.1348	255	45	90	75	45	90	60.1	39.9	0
12	0	-25	0.2095	90	47	-94	276	43	-86	57.09	42.91	0
13	0	0	0.5356	69	46	-93	252	44	-87	28.3	71.7	0
14	0	25	0.1598	234	46	91	53	44	89	45.06	54.94	0
15	0	50	0.0932	48	44	-95	236	46	-85	13.59	86.41	0
16	25	-50	0.0995	78	46	-90	259	44	-90	78.47	21.53	0
17	25	-25	0.1928	251	45	90	71	45	90	80.42	19.58	0
18	25	0	0.0993	259	44	90	79	46	90	72.27	27.73	0
19	25	25	0.027	335	45	-90	156	45	-90	48.57	51.43	0
20	25	50	0.0075	333	45	-90	153	45	-90	40.01	59.99	0
21	50	-50	0.1482	80	46	-91	261	44	-89	58.94	41.06	0
22	50	-25	0.0144	300	78	-169	208	79	-12	8.06	91.94	0
23	50	0	0.0035	179	46	91	358	44	89	27	73	0
24	50	25	0.0043	342	45	-91	163	45	-89	39.59	60.41	0
25	50	50	0.006	338	44	-91	160	46	-89	52.93	47.07	0

Table C.9: Full-wavefield moment tensor inversion results for location 3e, DC input mechanism, isotropic medium, and dominant source frequency of 125 Hz with a DC constraint applied to the inversion. The bolded row is the location with the highest correlation in the grid search and thus the final ouputted result. Refer to Figure C.1i for visual.

Location Number	X Coord (m)	Y Coord (m)	Correlation	Strike 1 (°)	Dip 1 (°)	Rake 1 (°)	Strike 2 (°)	Dip 2 (°)	Rake 2 (°)	DC %	CLVD %	ISO %
1	-50	-50	0.2416	78	45	-90	258	45	-90	93.18	6.82	0
2	-50	-25	0.4718	253	45	90	73	45	90	95.83	4.17	0
3	-50	0	0.2045	63	45	-90	242	45	-90	94.91	5.09	0
4	-50	25	0.1663	245	44	90	65	46	90	91.95	8.05	0
5	-50	50	0.0685	240	44	90	60	46	90	96.94	3.06	0
6	-25	-50	0.2161	82	46	-90	263	44	-90	96.78	3.22	0
7	-25	-25	0.3463	79	46	-91	260	44	-89	99.77	0.23	0
8	-25	0	0.4161	256	44	90	76	46	90	99.31	0.69	0
9	-25	25	0.1665	61	45	-90	241	45	-90	95.71	4.29	0
10	-25	50	0.0775	48	44	-90	228	46	-90	97.97	2.03	0
11	0	-50	0.1263	255	45	90	75	45	90	99.87	0.13	0
12	0	-25	0.2027	88	47	-92	272	43	-88	91.83	8.17	0
13	0	0	0.4434	71	46	-91	251	44	-89	95.45	4.55	0
14	0	25	0.1461	233	46	90	53	44	90	98.33	1.67	0
15	0	50	0.0705	97	90	0	7	90	180	93.53	6.47	0
16	25	-50	0.0962	79	46	-90	259	44	-90	93.9	6.1	0
17	25	-25	0.1919	251	45	90	71	45	90	90.09	9.91	0
18	25	0	0.0951	258	44	90	77	46	90	99.44	0.56	0
19	25	25	0.0266	334	44	-91	155	46	-89	97.85	2.15	0
20	25	50	0.0074	331	45	-91	152	45	-89	96.6	3.4	0
21	50	-50	0.1385	80	46	-90	261	44	-90	98.17	1.83	0
22	50	-25	0.0141	298	87	-179	208	89	-3	91.26	8.74	0
23	50	0	0.0034	169	46	93	345	44	87	90.14	9.86	0
24	50	25	0.0043	338	44	-91	160	46	-89	97.13	2.87	0
25	50	50	0.0059	336	44	-92	158	46	-88	94.24	5.76	0

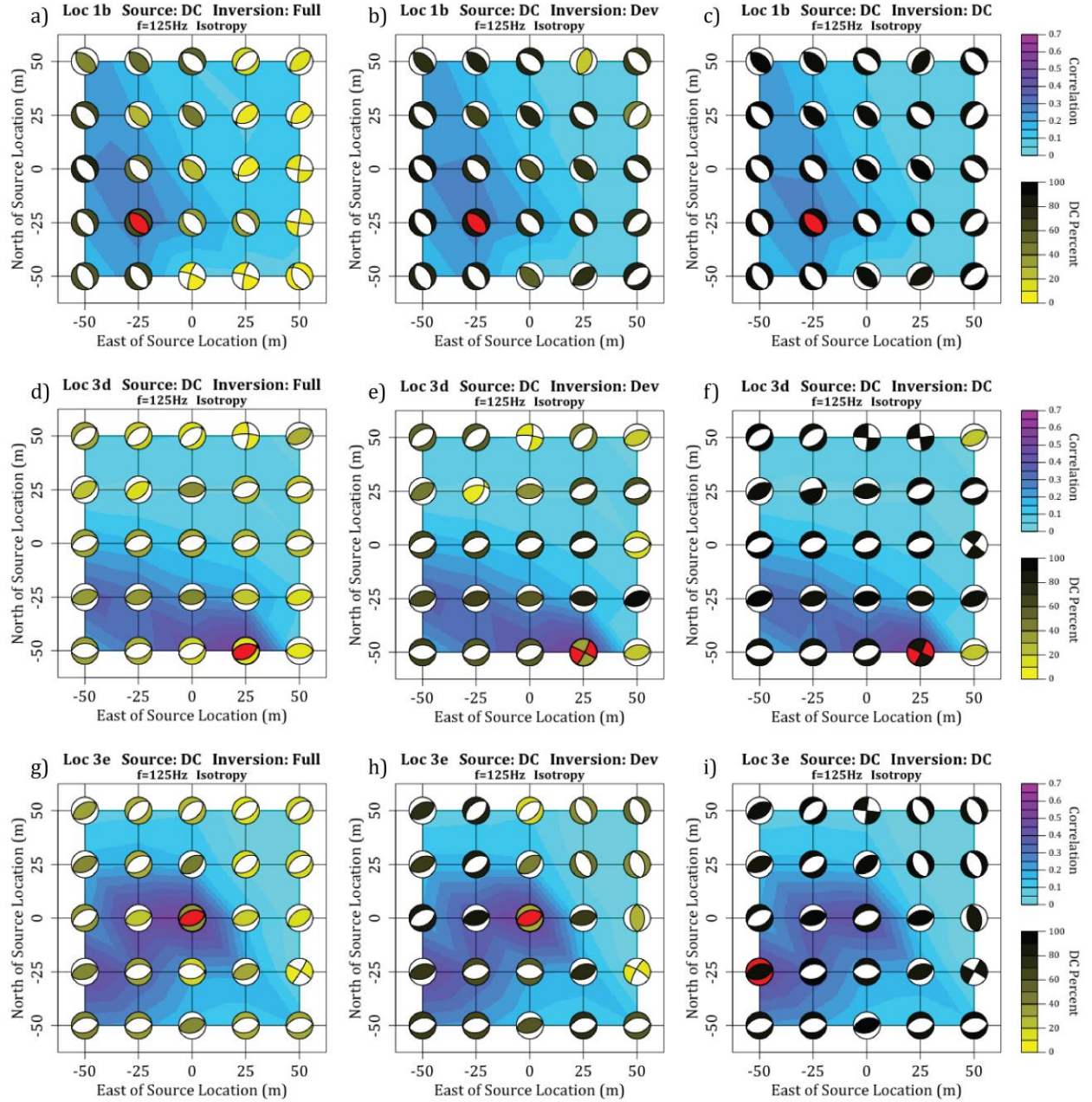


Figure C.1: Full-wavefield moment tensor inversion results for a DC source mechanism in an isotropic medium and source frequency of 125 Hz for a) location 1b with no constraints on the inversion, b) location 1b with a deviatoric constraint, c) location 1b with a DC constraint, d) location 3d with no constraints, e) location 3d with a deviatoric constraint, f) location 3d with a DC constraint, g) location 3e with no constraints, h) location 3e with a deviatoric constraint, and i) location 3e with a DC constraint. The red beach-ball is the location and source mechanism with the highest correlation to the input seismograms. Refer to Tables C.1-C.9 for numerical values of results.

Table C.10: Full-wavefield moment tensor inversion results for location 1b, CLVD input mechanism, isotropic medium, and dominant source frequency of 125 Hz with no constraints applied to the inversion. The bolded row is the location with the highest correlation in the grid search and thus the final ouputted result. Refer to Figure C.2a for visual.

Location Number	X Coord (m)	Y Coord (m)	Correlation	Strike 1 (°)	Dip 1 (°)	Rake 1 (°)	Strike 2 (°)	Dip 2 (°)	Rake 2 (°)	DC %	CLVD %	ISO %
1	-50	-50	0.1078	324	48	-97	154	42	-83	18.42	26.6	54.98
2	-50	-25	0.1381	117	41	-79	282	50	-100	21.94	2.2	-75.86
3	-50	0	0.1271	192	85	-168	101	78	-5	18.11	1.29	-80.6
4	-50	25	0.1291	150	56	122	281	45	52	77.5	17.09	-5.41
5	-50	50	0.1318	326	43	-98	157	47	-82	61.18	24.41	14.41
6	-25	-50	0.1236	154	45	95	326	45	85	39.1	13	47.9
7	-25	-25	0.1487	141	44	104	303	48	77	38.03	13.6	-48.37
8	-25	0	0.1223	209	62	-140	98	56	-35	3.84	7.58	-88.58
9	-25	25	0.1073	172	84	35	78	55	173	30.52	19.47	50.01
10	-25	50	0.0727	214	53	78	53	38	105	13.11	8.62	78.27
11	0	-50	0.1123	290	77	-165	196	75	-14	1.38	18.13	80.49
12	0	-25	0.1406	181	73	169	274	80	17	1.75	34.59	-63.66
13	0	0	0.1314	95	57	147	204	63	38	2.65	7.71	89.64
14	0	25	0.0951	225	50	-106	69	42	-72	13.34	2.33	-84.33
15	0	50	0.0725	315	35	-101	147	56	-83	39.95	40.62	19.43
16	25	-50	0.1261	286	78	-166	193	76	-13	1.48	17.56	80.96
17	25	-25	0.1369	192	88	-176	102	86	-2	11.68	2.47	-85.85
18	25	0	0.1375	191	85	-172	100	82	-5	6.03	4.19	-89.78
19	25	25	0.141	220	50	-108	67	43	-70	6.56	5.53	-87.91
20	25	50	0.162	224	49	79	60	42	102	14.57	0.6	84.83
21	50	-50	0.0974	311	48	-113	162	47	-67	2.43	17.41	80.16
22	50	-25	0.149	279	90	-177	189	87	0	5.26	9.8	84.94
23	50	0	0.1583	97	85	177	187	87	5	8.9	2.01	89.09
24	50	25	0.1299	71	46	-59	210	51	-118	2.83	4.98	-92.19
25	50	50	0.1403	219	49	77	59	43	104	5.48	4.92	89.6

Table C.11: Full-wavefield moment tensor inversion results for location 1b, CLVD input mechanism, isotropic medium, and dominant source frequency of 125 Hz with a deviatoric constraint applied to the inversion. The bolded row is the location with the highest correlation in the grid search and thus the final ouputted result. Refer to Figure C.2b for visual.

Location Number	X Coord (m)	Y Coord (m)	Correlation	Strike 1 (°)	Dip 1 (°)	Rake 1 (°)	Strike 2 (°)	Dip 2 (°)	Rake 2 (°)	DC %	CLVD %	ISO %
1	-50	-50	0.0805	137	43	-83	308	47	-97	68.33	31.67	0
2	-50	-25	0.104	95	81	177	185	87	9	36.92	63.08	0
3	-50	0	0.1142	240	87	-168	149	78	-3	71.36	28.64	0
4	-50	25	0.1291	149	56	121	282	45	53	85	15	0
5	-50	50	0.1307	326	43	-98	157	48	-82	83.15	16.85	0
6	-25	-50	0.0921	155	44	95	329	47	86	56.44	43.56	0
7	-25	-25	0.1393	74	89	172	164	82	1	85.07	14.93	0
8	-25	0	0.1139	292	47	66	146	48	114	56.37	43.63	0
9	-25	25	0.1008	326	68	-60	89	37	-141	33.34	66.66	0
10	-25	50	0.0608	153	64	87	339	26	96	79.87	20.13	0
11	0	-50	0.0628	230	50	-98	62	40	-81	84.66	15.34	0
12	0	-25	0.0945	131	43	99	300	47	82	80.26	19.74	0
13	0	0	0.0873	177	84	35	83	56	173	62.8	37.2	0
14	0	25	0.0575	150	51	96	321	39	83	64.02	35.98	0
15	0	50	0.0715	315	35	-100	147	55	-83	68.07	31.93	0
16	25	-50	0.0708	227	50	-96	57	41	-83	78.29	21.71	0
17	25	-25	0.0716	52	40	97	223	50	85	54.81	45.19	0
18	25	0	0.0706	217	51	85	45	40	96	37.44	62.56	0
19	25	25	0.0685	207	51	86	33	39	94	24.58	75.42	0
20	25	50	0.0797	20	38	-87	196	52	-92	19.21	80.79	0
21	50	-50	0.0543	52	41	-84	224	50	-95	71.58	28.42	0
22	50	-25	0.0822	48	40	-85	221	50	-95	57	43	0
23	50	0	0.0845	42	40	-85	215	50	-94	41.2	58.8	0
24	50	25	0.0697	213	50	86	40	40	95	39.95	60.05	0
25	50	50	0.0912	141	51	96	311	40	83	64.73	35.27	0

Table C.12: Full-wavefield moment tensor inversion results for location 1b, CLVD input mechanism, isotropic medium, and dominant source frequency of 125 Hz with a DC constraint applied to the inversion. The bolded row is the location with the highest correlation in the grid search and thus the final ouputed result. Refer to Figure C.2c for visual.

Location Number	X Coord (m)	Y Coord (m)	Correlation	Strike 1 (°)	Dip 1 (°)	Rake 1 (°)	Strike 2 (°)	Dip 2 (°)	Rake 2 (°)	DC %	CLVD %	ISO %
1	-50	-50	0.0793	129	42	-84	300	49	-96	94.62	5.38	0
2	-50	-25	0.1036	91	81	176	182	86	9	90.28	9.72	0
3	-50	0	0.1142	242	86	-166	151	76	-4	96.9	3.1	0
4	-50	25	0.1287	149	59	121	280	42	50	97.49	2.51	0
5	-50	50	0.1266	325	42	-99	157	49	-82	99.14	0.86	0
6	-25	-50	0.0847	351	41	-87	168	49	-92	97.44	2.56	0
7	-25	-25	0.1393	75	90	172	165	82	0	97.47	2.53	0
8	-25	0	0.1095	145	53	110	293	42	66	98.59	1.41	0
9	-25	25	0.0948	48	25	160	156	82	66	99.17	0.83	0
10	-25	50	0.06	153	64	88	336	26	93	99.21	0.79	0
11	0	-50	0.0628	230	50	-98	63	40	-80	97.14	2.86	0
12	0	-25	0.0927	129	42	99	297	49	82	91.91	8.09	0
13	0	0	0.0869	178	79	31	82	59	168	91.51	8.49	0
14	0	25	0.0489	150	51	95	321	39	83	99.37	0.63	0
15	0	50	0.0669	315	36	-100	147	55	-83	98.44	1.56	0
16	25	-50	0.0708	227	50	-97	58	41	-81	99.59	0.41	0
17	25	-25	0.0711	225	50	85	54	40	96	93.13	6.87	0
18	25	0	0.0696	51	40	99	219	51	82	93.54	6.46	0
19	25	25	0.0665	213	51	82	46	39	100	90.83	9.17	0
20	25	50	0.0797	20	38	-87	196	52	-92	19.21	80.79	0
21	50	-50	0.0542	53	41	-83	224	50	-96	91.81	8.19	0
22	50	-25	0.0819	51	41	-83	221	50	-96	93.55	6.45	0
23	50	0	0.0838	46	40	-83	217	50	-96	90.36	9.64	0
24	50	25	0.0686	215	50	84	45	40	97	91.68	8.32	0
25	50	50	0.0862	141	50	96	311	40	83	99.03	0.97	0

Table C.13: Full-wavefield moment tensor inversion results for location 3d, CLVD input mechanism, isotropic medium, and dominant source frequency of 125 Hz with no constraints applied to the inversion. The bolded row is the location with the highest correlation in the grid search and thus the final ouputted result. Refer to Figure C.2d for visual.

Location Number	X Coord (m)	Y Coord (m)	Correlation	Strike 1 (°)	Dip 1 (°)	Rake 1 (°)	Strike 2 (°)	Dip 2 (°)	Rake 2 (°)	DC %	CLVD %	ISO %
1	-50	-50	0.1483	190	45	90	9	45	90	4.67	13.81	81.52
2	-50	-25	0.2313	258	46	90	78	44	90	38.53	40.66	-20.81
3	-50	0	0.1431	71	44	-90	252	46	-90	32.17	45.28	22.55
4	-50	25	0.0465	251	46	90	72	44	90	43.65	36.49	-19.86
5	-50	50	0.069	83	45	-91	264	45	-89	35.33	41.37	23.3
6	-25	-50	0.307	2	46	-90	183	44	-90	8.17	2.47	-89.36
7	-25	-25	0.2004	262	46	90	82	44	90	37.27	39.86	-22.87
8	-25	0	0.1367	73	44	-91	254	46	-89	31.54	44.59	23.87
9	-25	25	0.0402	347	76	167	80	77	14	2.41	9.7	87.89
10	-25	50	0.0588	89	46	-94	274	44	-86	27.41	54.22	18.37
11	0	-50	0.3699	6	83	-179	276	89	-7	41.63	24.44	-33.93
12	0	-25	0.2205	95	45	-91	276	45	-89	34.89	41.5	23.61
13	0	0	0.1203	74	44	-91	255	46	-89	29.82	45.13	25.05
14	0	25	0.0745	84	45	-91	265	45	-89	37.89	50.76	11.35
15	0	50	0.0612	249	46	90	68	44	90	29.43	40.85	-29.72
16	25	-50	0.557	8	84	179	98	89	6	18.66	11.48	69.86
17	25	-25	0.2456	92	45	-92	275	45	-88	30.07	52.77	17.16
18	25	0	0.0941	75	44	-92	258	46	-88	36.3	61.2	2.5
19	25	25	0.0355	67	44	-94	252	46	-86	17.17	64.94	17.89
20	25	50	0.0562	249	46	91	67	44	89	36.97	52.5	-10.53
21	50	-50	0.0754	106	47	-87	282	43	-93	3.65	23.65	72.7
22	50	-25	0.0903	266	47	101	70	44	78	4.94	15.71	79.35
23	50	0	0.0929	77	44	-90	256	46	-90	19.32	27.75	52.93
24	50	25	0.0617	71	44	-91	253	46	-89	22.62	43.88	33.5
25	50	50	0.0321	248	46	90	68	44	90	20.21	31.8	-47.99

Table C.14: Full-wavefield moment tensor inversion results for location 3d, CLVD input mechanism, isotropic medium, and dominant source frequency of 125 Hz with a deviatoric constraint applied to the inversion. The bolded row is the location with the highest correlation in the grid search and thus the final ouputted result. Refer to Figure C.2e for visual.

Location Number	X Coord (m)	Y Coord (m)	Correlation	Strike 1 (°)	Dip 1 (°)	Rake 1 (°)	Strike 2 (°)	Dip 2 (°)	Rake 2 (°)	DC %	CLVD %	ISO %
1	-50	-50	0.0911	86	63	-147	340	61	-31	6.02	93.98	0
2	-50	-25	0.2286	257	46	90	78	44	90	68.89	31.11	0
3	-50	0	0.1412	71	44	-90	251	46	-90	64.15	35.85	0
4	-50	25	0.0459	251	46	90	71	44	90	73.01	26.99	0
5	-50	50	0.068	84	45	-90	265	45	-90	68.62	31.38	0
6	-25	-50	0.2183	11	82	-176	281	86	-8	23.81	76.19	0
7	-25	-25	0.1964	261	46	90	81	44	90	70.75	29.25	0
8	-25	0	0.1341	73	44	-90	253	46	-90	65.32	34.68	0
9	-25	25	0.0329	249	46	90	68	44	90	63.33	36.67	0
10	-25	50	0.0584	90	46	-92	273	44	-88	49.96	50.04	0
11	0	-50	0.3678	7	84	179	97	89	6	98.04	1.96	0
12	0	-25	0.2161	96	45	-90	276	45	-90	68.54	31.46	0
13	0	0	0.1173	74	44	-91	255	46	-89	64.79	35.21	0
14	0	25	0.0742	84	45	-91	265	45	-89	52.45	47.55	0
15	0	50	0.0582	249	46	90	68	44	90	72.55	27.45	0
16	25	-50	0.4844	38	43	-96	227	47	-84	60.27	39.73	0
17	25	-25	0.2431	93	45	-91	275	45	-89	51.51	48.49	0
18	25	0	0.0941	75	44	-92	258	46	-88	39.13	60.87	0
19	25	25	0.0352	68	44	-92	251	46	-88	36.89	63.11	0
20	25	50	0.056	249	46	91	67	44	89	49.79	50.21	0
21	50	-50	0.0457	120	46	-91	301	44	-89	48.53	51.47	0
22	50	-25	0.0705	126	89	-178	36	88	-1	62.37	37.63	0
23	50	0	0.0676	73	44	-90	254	46	-90	83.02	16.98	0
24	50	25	0.0574	70	44	-91	252	46	-89	68.86	31.14	0
25	50	50	0.0262	246	46	91	64	44	89	85.46	14.54	0

Table C.15: Full-wavefield moment tensor inversion results for location 3d, CLVD input mechanism, isotropic medium, and dominant source frequency of 125 Hz with a DC constraint applied to the inversion. The bolded row is the location with the highest correlation in the grid search and thus the final ouputted result. Refer to Figure C.2f for visual.

Location Number	X Coord (m)	Y Coord (m)	Correlation	Strike 1 (°)	Dip 1 (°)	Rake 1 (°)	Strike 2 (°)	Dip 2 (°)	Rake 2 (°)	DC %	CLVD %	ISO %
1	-50	-50	0.0899	82	89	-177	352	87	-1	98.06	1.94	0
2	-50	-25	0.2239	257	46	90	78	44	90	94.35	5.65	0
3	-50	0	0.1353	72	44	-90	252	46	-90	98.76	1.24	0
4	-50	25	0.0449	251	46	90	72	44	90	97.12	2.88	0
5	-50	50	0.0657	84	45	-90	264	45	-90	97.35	2.65	0
6	-25	-50	0.2168	7	86	179	97	89	4	94.65	5.35	0
7	-25	-25	0.1914	261	46	90	82	44	90	96.74	3.26	0
8	-25	0	0.1279	73	44	-90	253	46	-90	96.92	3.08	0
9	-25	25	0.0317	248	46	90	68	44	90	96.83	3.17	0
10	-25	50	0.0555	90	46	-91	271	44	-89	96.53	3.47	0
11	0	-50	0.3678	7	84	179	97	89	6	98.04	1.96	0
12	0	-25	0.2049	96	45	-90	276	45	-90	92.38	7.62	0
13	0	0	0.1112	74	44	-90	255	46	-90	96.54	3.46	0
14	0	25	0.068	85	45	-90	265	45	-90	98.1	1.9	0
15	0	50	0.0568	248	46	90	68	44	90	97.14	2.86	0
16	25	-50	0.4791	45	43	-95	232	47	-86	92.25	7.75	0
17	25	-25	0.2201	94	45	-90	274	45	-90	94.53	5.47	0
18	25	0	0.0803	76	44	-90	257	46	-90	92.85	7.15	0
19	25	25	0.0311	69	44	-91	250	46	-89	96.95	3.05	0
20	25	50	0.0521	247	46	90	67	44	90	93.69	6.31	0
21	50	-50	0.0426	127	46	-92	309	44	-88	97.57	2.43	0
22	50	-25	0.0703	127	89	-178	36	88	-1	95	5	0
23	50	0	0.0672	73	44	-90	254	46	-90	92.77	7.23	0
24	50	25	0.0553	71	44	-90	252	46	-90	99.25	0.75	0
25	50	50	0.0261	245	46	91	64	44	89	95.22	4.78	0

Table C.16: Full-wavefield moment tensor inversion results for location 3e, CLVD input mechanism, isotropic medium, and dominant source frequency of 125 Hz with no constraints applied to the inversion. The bolded row is the location with the highest correlation in the grid search and thus the final ouputted result. Refer to Figure C.2g for visual.

Location Number	X Coord (m)	Y Coord (m)	Correlation	Strike 1 (°)	Dip 1 (°)	Rake 1 (°)	Strike 2 (°)	Dip 2 (°)	Rake 2 (°)	DC %	CLVD %	ISO %
1	-50	-50	0.166	77	46	-90	258	44	-90	41.57	38.49	19.94
2	-50	-25	0.5018	65	89	-174	335	84	-1	89.96	8.42	-1.62
3	-50	0	0.3031	52	44	-90	233	46	-90	37.42	40.98	21.6
4	-50	25	0.0848	117	44	87	301	46	93	7.34	0.79	91.87
5	-50	50	0.0629	48	45	-90	229	45	-90	35.28	40.84	23.88
6	-25	-50	0.1422	260	44	91	79	46	89	37.46	40.98	-21.56
7	-25	-25	0.3036	230	48	101	34	43	78	12.75	62.03	-25.22
8	-25	0	0.3889	73	46	-90	253	44	-90	16.28	26.67	57.05
9	-25	25	0.0646	230	46	91	49	44	89	31.55	43.79	-24.66
10	-25	50	0.0698	51	45	-91	232	46	-89	41.83	56.45	-1.72
11	0	-50	0.0964	244	46	90	64	44	90	23.46	36.52	-40.02
12	0	-25	0.188	259	44	91	77	46	89	28.47	37.57	-33.96
13	0	0	0.5794	342	81	-179	252	89	-9	21.57	15.1	63.33
14	0	25	0.1338	254	43	92	70	47	88	13.88	36.62	-49.5
15	0	50	0.1008	53	45	-89	232	45	-91	22.2	27.24	50.56
16	25	-50	0.0412	257	44	90	77	46	90	25.17	32.42	-42.41
17	25	-25	0.0643	62	44	-89	241	46	-91	22.14	21.19	56.67
18	25	0	0.111	78	47	-91	259	43	-89	9.93	23.13	66.94
19	25	25	0.0487	235	45	86	61	45	94	13.29	1.33	-85.38
20	25	50	0.0162	52	44	-87	227	46	-93	16.97	0.23	82.8
21	50	-50	0.0619	260	44	91	78	46	89	31.72	52.65	-15.63
22	50	-25	0.0185	164	48	89	345	42	91	4.62	4.58	-90.8
23	50	0	0.0017	285	86	175	16	85	4	7.64	18.6	73.76
24	50	25	0.0032	223	47	88	46	43	92	15.83	1.61	-82.56
25	50	50	0.0205	59	45	-86	233	45	-94	10.93	3.74	85.33

Table C.17: Full-wavefield moment tensor inversion results for location 3e, CLVD input mechanism, isotropic medium, and dominant source frequency of 125 Hz with a deviatoric constraint applied to the inversion. The bolded row is the location with the highest correlation in the grid search and thus the final ouputted result. Refer to Figure C.2h for visual.

Location Number	X Coord (m)	Y Coord (m)	Correlation	Strike 1 (°)	Dip 1 (°)	Rake 1 (°)	Strike 2 (°)	Dip 2 (°)	Rake 2 (°)	DC %	CLVD %	ISO %
1	-50	-50	0.164	78	46	-90	258	44	-90	72.16	27.84	0
2	-50	-25	0.5018	65	90	-174	335	84	0	93.17	6.83	0
3	-50	0	0.298	52	44	-90	232	46	-90	69.43	30.57	0
4	-50	25	0.0804	64	46	-90	244	44	-90	73.98	26.02	0
5	-50	50	0.0609	48	44	-90	228	46	-90	70.73	29.27	0
6	-25	-50	0.14	260	44	90	80	46	90	69.75	30.25	0
7	-25	-25	0.3011	224	47	95	38	43	85	42.78	57.22	0
8	-25	0	0.3652	49	44	-91	231	46	-89	55.67	44.33	0
9	-25	25	0.0631	229	46	91	48	44	89	67.04	32.96	0
10	-25	50	0.0698	51	45	-91	232	45	-89	41.24	58.76	0
11	0	-50	0.0865	243	46	90	63	44	90	89.47	10.53	0
12	0	-25	0.1778	260	44	91	79	46	89	81.8	18.2	0
13	0	0	0.5337	10	43	-102	207	48	-79	47.85	52.15	0
14	0	25	0.1117	256	44	91	75	46	89	98.81	1.19	0
15	0	50	0.072	51	44	-90	231	46	-90	79.38	20.62	0
16	25	-50	0.0346	258	45	90	78	45	90	99.15	0.85	0
17	25	-25	0.0458	58	44	-90	238	46	-90	63.21	36.79	0
18	25	0	0.0743	90	46	-91	271	44	-89	51.74	48.26	0
19	25	25	0.0305	156	45	90	335	45	90	44.26	55.74	0
20	25	50	0.0102	336	45	-91	158	45	-89	48.31	51.69	0
21	50	-50	0.0613	260	44	91	79	46	89	51.87	48.13	0
22	50	-25	0.0131	162	46	91	341	44	89	87.43	12.57	0
23	50	0	0.0014	108	90	-178	18	88	0	59.41	40.59	0
24	50	25	0.0021	167	46	92	344	44	88	60.57	39.43	0
25	50	50	0.013	332	45	-91	154	45	-89	74.84	25.16	0

Table C.18: Full-wavefield moment tensor inversion results for location 3e, CLVD input mechanism, isotropic medium, and dominant source frequency of 125 Hz with a DC constraint applied to the inversion. The bolded row is the location with the highest correlation in the grid search and thus the final ouputted result. Refer to Figure C.2i for visual.

Location Number	X Coord (m)	Y Coord (m)	Correlation	Strike 1 (°)	Dip 1 (°)	Rake 1 (°)	Strike 2 (°)	Dip 2 (°)	Rake 2 (°)	DC %	CLVD %	ISO %
1	-50	-50	0.1566	78	45	-90	258	45	-90	92.97	7.03	0
2	-50	-25	0.5018	66	90	-174	336	84	0	97.38	2.62	0
3	-50	0	0.2866	52	44	-90	232	46	-90	97.35	2.65	0
4	-50	25	0.0769	64	46	-90	244	44	-90	94.85	5.15	0
5	-50	50	0.0583	48	45	-90	228	45	-90	98.67	1.33	0
6	-25	-50	0.1373	260	44	90	80	46	90	94.86	5.14	0
7	-25	-25	0.2916	78	90	-175	348	85	0	92.05	7.95	0
8	-25	0	0.3465	50	44	-90	231	46	-90	98.14	1.86	0
9	-25	25	0.0612	228	46	90	47	44	90	97.54	2.46	0
10	-25	50	0.0596	51	45	-90	231	45	-90	97.01	2.99	0
11	0	-50	0.0862	243	46	90	63	44	90	99.09	0.91	0
12	0	-25	0.1774	260	44	91	79	46	89	91.03	8.97	0
13	0	0	0.5258	21	42	-98	211	49	-83	93.99	6.01	0
14	0	25	0.1117	256	44	91	75	46	89	98.81	1.19	0
15	0	50	0.0707	50	44	-90	231	46	-90	95.33	4.67	0
16	25	-50	0.0346	258	45	90	78	45	90	99.15	0.85	0
17	25	-25	0.044	218	88	176	308	86	2	90.58	9.42	0
18	25	0	0.0689	100	46	-92	282	44	-88	98.32	1.68	0
19	25	25	0.03	155	46	91	334	44	89	96.96	3.04	0
20	25	50	0.0101	334	44	-91	156	46	-89	97.17	2.83	0
21	50	-50	0.0573	260	44	90	79	46	90	94.88	5.12	0
22	50	-25	0.0131	162	46	91	341	44	89	98.48	1.52	0
23	50	0	0.0014	18	89	0	288	90	179	97.39	2.61	0
24	50	25	0.0021	165	46	93	341	44	87	96.78	3.22	0
25	50	50	0.0129	332	44	-91	153	46	-89	97.04	2.96	0

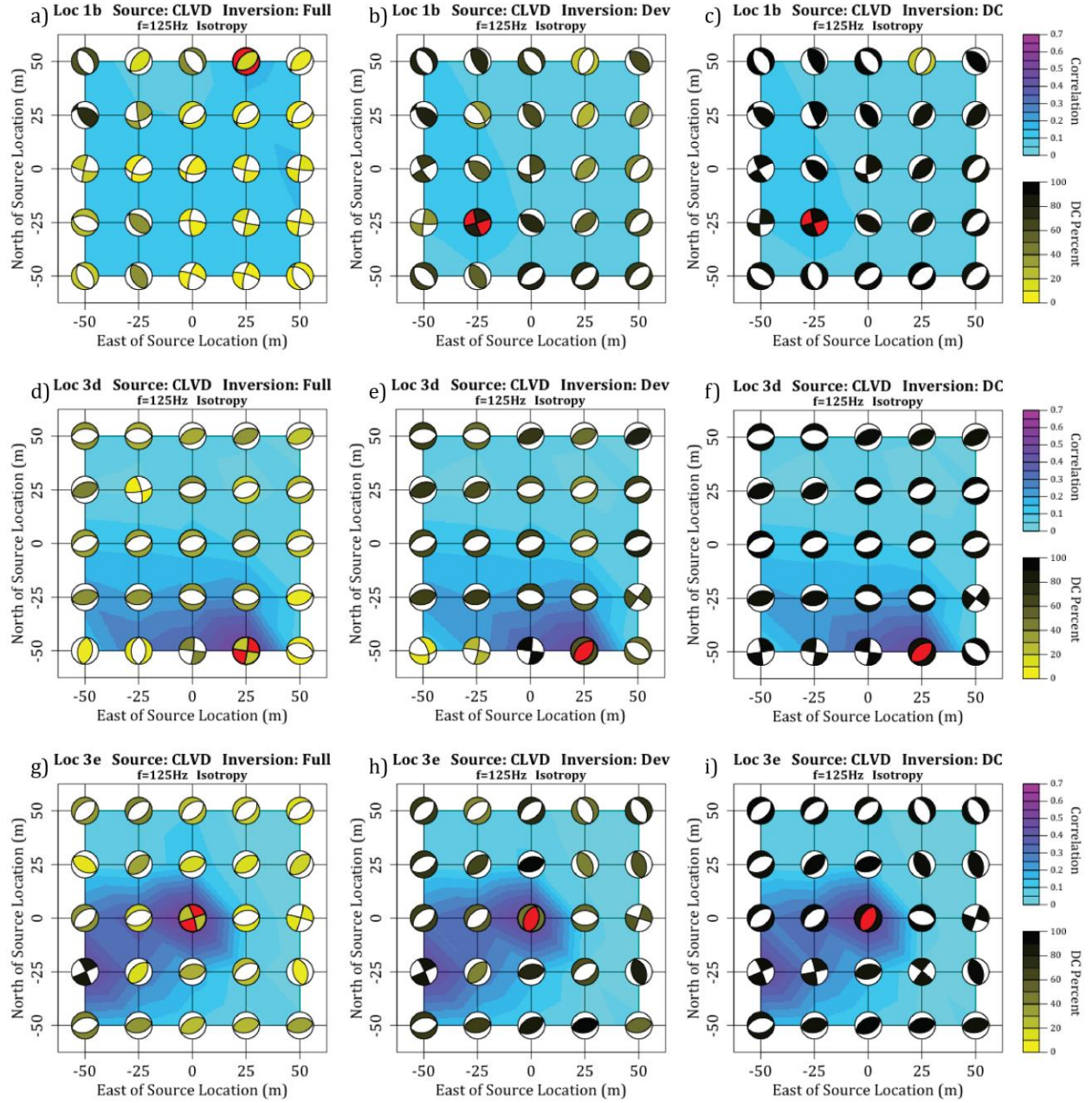


Figure C.2: Full-wavefield moment tensor inversion results for a CLVD source mechanism in an isotropic medium and source frequency of 125 Hz for a) location 1b with no constraints on the inversion, b) location 1b with a deviatoric constraint, c) location 1b with a DC constraint, d) location 3d with no constraints, e) location 3d with a deviatoric constraint, f) location 3d with a DC constraint, g) location 3e with no constraints, h) location 3e with a deviatoric constraint, and i) location 3e with a DC constraint. The red beach-ball is the location and source mechanism with the highest correlation to the input seismograms. Refer to Tables C.10-C.18 for numerical values of results.

Table C.19: Full-wavefield moment tensor inversion results for location 1b, ISO input mechanism, isotropic medium, and dominant source frequency of 125 Hz with no constraints applied to the inversion. The bolded row is the location with the highest correlation in the grid search and thus the final ouputted result. Refer to Figure C.3a for visual.

Location Number	X Coord (m)	Y Coord (m)	Correlation	Strike 1 (°)	Dip 1 (°)	Rake 1 (°)	Strike 2 (°)	Dip 2 (°)	Rake 2 (°)	DC %	CLVD %	ISO %
1	-50	-50	0.1627	203	90	-175	113	85	0	4.41	17.09	-78.5
2	-50	-25	0.1911	201	86	-169	110	79	-4	14.46	1.58	-83.96
3	-50	0	0.2037	212	61	-134	96	51	-38	6.92	6.31	-86.77
4	-50	25	0.1783	222	54	-109	72	40	-66	14.78	4.16	-81.06
5	-50	50	0.1975	326	43	-98	157	47	-82	60.84	24.55	14.61
6	-25	-50	0.1878	108	84	179	198	89	6	6.28	12.74	80.98
7	-25	-25	0.1983	104	78	174	196	85	12	11.53	1.92	86.55
8	-25	0	0.1892	83	47	131	211	57	55	6.26	5.41	88.33
9	-25	25	0.1554	58	39	107	217	53	77	13.27	6.19	80.54
10	-25	50	0.1254	214	53	78	53	38	105	13.35	8.19	78.46
11	0	-50	0.1758	194	85	179	285	89	5	1.19	16.26	-82.55
12	0	-25	0.1646	191	85	-170	100	80	-5	11.22	0.42	-88.36
13	0	0	0.1323	210	54	-117	70	44	-59	6.58	4.98	-88.44
14	0	25	0.1023	56	40	-70	210	53	-106	11.52	1.81	-86.67
15	0	50	0.069	44	39	-77	207	53	-100	14.93	2.95	-82.12
16	25	-50	0.0321	318	48	-102	156	43	-76	2.87	12.62	84.51
17	25	-25	0.1039	93	75	170	185	80	15	5.74	3.65	90.61
18	25	0	0.0892	89	71	166	184	77	20	4.39	5.06	90.55
19	25	25	0.0445	46	40	-77	210	51	-100	9.95	3.93	-86.12
20	25	50	0.0433	221	50	-103	60	42	-75	14.21	1.4	-84.39
21	50	-50	0.0049	313	48	-98	145	43	-81	4.26	13.53	82.21
22	50	-25	0.0716	180	88	-174	90	84	-2	4.97	7.22	-87.81
23	50	0	0.056	176	86	-170	85	80	-4	10.05	0.83	-89.12
24	50	25	0.041	172	82	-164	80	75	-8	4.94	4.79	-90.27
25	50	50	0.0443	59	43	-73	217	50	-105	5.52	5.85	-88.63

Table C.20: Full-wavefield moment tensor inversion results for location 1b, ISO input mechanism, isotropic medium, and dominant source frequency of 125 Hz with a deviatoric constraint applied to the inversion. The bolded row is the location with the highest correlation in the grid search and thus the final ouputted result. Refer to Figure C.3b for visual.

Location Number	X Coord (m)	Y Coord (m)	Correlation	Strike 1 (°)	Dip 1 (°)	Rake 1 (°)	Strike 2 (°)	Dip 2 (°)	Rake 2 (°)	DC %	CLVD %	ISO %
1	-50	-50	0.087	81	41	107	239	51	76	59.39	40.61	0
2	-50	-25	0.0953	77	41	104	239	51	79	92.76	7.24	0
3	-50	0	0.0939	76	40	104	238	51	79	56.86	43.14	0
4	-50	25	0.0759	81	41	105	241	51	77	39.95	60.05	0
5	-50	50	0.1957	326	43	-98	157	48	-82	83.1	16.9	0
6	-25	-50	0.1006	239	50	-100	74	41	-79	83.19	16.81	0
7	-25	-25	0.1004	238	50	-99	72	41	-79	80.69	19.31	0
8	-25	0	0.0906	238	50	-100	72	41	-79	59.36	40.64	0
9	-25	25	0.0704	241	50	-101	78	41	-77	48.17	51.83	0
10	-25	50	0.0737	154	47	96	325	44	83	75.72	24.28	0
11	0	-50	0.1007	67	41	99	235	50	82	94.34	5.66	0
12	0	-25	0.0897	66	41	99	234	50	82	82.51	17.49	0
13	0	0	0.0682	67	41	99	235	50	82	59.05	40.95	0
14	0	25	0.0503	73	41	100	240	49	81	34.19	65.81	0
15	0	50	0.0323	93	44	101	258	47	80	23.81	76.19	0
16	25	-50	0.0198	62	41	-82	231	49	-97	90.08	9.92	0
17	25	-25	0.0573	233	50	-97	63	41	-82	97.17	2.83	0
18	25	0	0.0454	234	49	-96	63	41	-83	44.17	55.83	0
19	25	25	0.0242	59	41	98	228	50	83	57.96	42.04	0
20	25	50	0.0216	70	42	99	239	49	82	29.53	70.47	0
21	50	-50	0.0029	61	41	-84	233	49	-95	90.45	9.55	0
22	50	-25	0.0413	231	49	85	58	41	96	78.74	21.26	0
23	50	0	0.0306	233	49	85	61	41	96	45.23	54.77	0
24	50	25	0.0215	71	42	97	242	48	84	25.44	74.56	0
25	50	50	0.0218	186	51	90	6	39	90	16.67	83.33	0

Table C.21: Full-wavefield moment tensor inversion results for location 1b, ISO input mechanism, isotropic medium, and dominant source frequency of 125 Hz with a DC constraint applied to the inversion. The bolded row is the location with the highest correlation in the grid search and thus the final ouputted result. Refer to Figure C.3c for visual.

Location Number	X Coord (m)	Y Coord (m)	Correlation	Strike 1 (°)	Dip 1 (°)	Rake 1 (°)	Strike 2 (°)	Dip 2 (°)	Rake 2 (°)	DC %	CLVD %	ISO %
1	-50	-50	0.0869	78	41	103	241	50	79	96.21	3.79	0
2	-50	-25	0.0953	77	41	104	239	51	78	99.08	0.92	0
3	-50	0	0.0935	74	40	102	238	51	80	91.74	8.26	0
4	-50	25	0.0752	79	41	109	234	52	74	92.27	7.73	0
5	-50	50	0.1897	325	42	-99	157	49	-82	99.19	0.81	0
6	-25	-50	0.1006	240	50	-99	73	41	-80	99.51	0.49	0
7	-25	-25	0.1004	237	50	-99	72	41	-79	92.04	7.96	0
8	-25	0	0.0904	235	51	-101	72	41	-77	93.6	6.4	0
9	-25	25	0.07	236	51	-102	74	41	-76	92.76	7.24	0
10	-25	50	0.0715	154	47	96	324	43	83	97.9	2.1	0
11	0	-50	0.1007	67	41	99	235	50	82	94.34	5.66	0
12	0	-25	0.0896	66	41	100	233	50	82	93.63	6.37	0
13	0	0	0.0679	67	41	101	232	50	81	95.9	4.1	0
14	0	25	0.0494	64	40	99	233	50	83	94.1	5.9	0
15	0	50	0.0323	93	44	101	258	47	80	23.81	76.19	0
16	25	-50	0.0198	61	41	-83	232	49	-96	97.41	2.59	0
17	25	-25	0.0573	233	50	-97	63	41	-82	97.17	2.83	0
18	25	0	0.045	230	50	-97	61	41	-82	94.37	5.63	0
19	25	25	0.0241	58	41	99	226	50	82	95.09	4.91	0
20	25	50	0.0211	60	41	100	227	50	82	99.29	0.71	0
21	50	-50	0.0029	61	41	-84	233	49	-95	92.97	7.03	0
22	50	-25	0.0413	230	49	84	58	41	97	91.31	8.69	0
23	50	0	0.0303	230	49	85	57	41	96	96.14	3.86	0
24	50	25	0.0208	229	49	83	59	41	98	97.15	2.85	0
25	50	50	0.0206	209	51	89	31	39	91	93.05	6.95	0

Table C.22: Full-wavefield moment tensor inversion results for location 3d, ISO input mechanism, isotropic medium, and dominant source frequency of 125 Hz with no constraints applied to the inversion. The bolded row is the location with the highest correlation in the grid search and thus the final ouputted result. Refer to Figure C.3d for visual.

Location Number	X Coord (m)	Y Coord (m)	Correlation	Strike 1 (°)	Dip 1 (°)	Rake 1 (°)	Strike 2 (°)	Dip 2 (°)	Rake 2 (°)	DC %	CLVD %	ISO %
1	-50	-50	0.2499	192	45	90	12	45	90	4.7	13.91	81.39
2	-50	-25	0.2578	152	45	89	333	45	91	9.58	6.6	83.82
3	-50	0	0.0666	123	45	89	305	45	91	5.28	9.19	85.53
4	-50	25	0.0415	20	83	-8	111	82	-172	0.33	8.93	-90.74
5	-50	50	0.0367	345	48	-68	135	47	-112	0.11	7.61	-92.28
6	-25	-50	0.5219	4	46	-90	184	44	-90	8.67	1.73	-89.6
7	-25	-25	0.1658	318	45	-88	136	45	-92	9.94	6.4	-83.66
8	-25	0	0.1251	136	48	61	355	50	118	0.57	6.13	93.3
9	-25	25	0.0526	13	87	174	104	84	3	2.24	3.54	94.22
10	-25	50	0.0254	105	86	177	195	87	4	5.17	5.22	-89.61
11	0	-50	0.1208	178	43	88	1	47	92	0.57	4.25	95.18
12	0	-25	0.0892	121	84	178	211	88	6	5.61	0.04	-94.35
13	0	0	0.0803	323	84	-172	233	82	-6	3.56	3.75	-92.69
14	0	25	0.0698	202	89	-177	112	87	-1	7.71	5.07	87.22
15	0	50	0.0607	199	80	-168	107	78	-11	1.91	12.06	86.03
16	25	-50	0.5532	117	52	-52	245	52	-128	1.71	7.09	91.2
17	25	-25	0.2725	115	56	-41	231	57	-138	1.56	5.08	93.36
18	25	0	0.0454	245	47	81	77	44	99	5.91	6.39	-87.7
19	25	25	0.0414	108	62	150	213	64	31	1.08	17.05	-81.87
20	25	50	0.0248	235	47	74	78	45	106	2.84	15.27	-81.89
21	50	-50	0.1161	239	63	-151	134	65	-31	1.4	10.87	87.73
22	50	-25	0.1244	79	43	-78	242	48	-101	3.46	11.29	85.25
23	50	0	0.0819	71	44	-85	244	47	-95	10.34	4.45	85.21
24	50	25	0.0297	247	46	86	72	44	94	14.82	2.71	-82.47
25	50	50	0.0254	244	46	87	68	45	93	17.62	0.96	-81.42

Table C.23: Full-wavefield moment tensor inversion results for location 3d, ISO input mechanism, isotropic medium, and dominant source frequency of 125 Hz with a deviatoric constraint applied to the inversion. The bolded row is the location with the highest correlation in the grid search and thus the final ouputted result. Refer to Figure C.3e for visual.

Location Number	X Coord (m)	Y Coord (m)	Correlation	Strike 1 (°)	Dip 1 (°)	Rake 1 (°)	Strike 2 (°)	Dip 2 (°)	Rake 2 (°)	DC %	CLVD %	ISO %
1	-50	-50	0.1205	353	44	-90	173	46	-90	25.74	74.26	0
2	-50	-25	0.1322	22	44	-90	202	46	-90	26.94	73.06	0
3	-50	0	0.0388	2	44	-90	182	46	-90	41.58	58.42	0
4	-50	25	0.0202	234	46	90	55	44	90	36.81	63.19	0
5	-50	50	0.0183	220	46	90	41	44	90	24.92	75.08	0
6	-25	-50	0.2659	176	46	90	356	44	90	21.18	78.82	0
7	-25	-25	0.0902	195	46	91	14	44	89	59.47	40.53	0
8	-25	0	0.067	30	44	-90	210	46	-90	23.43	76.57	0
9	-25	25	0.0302	11	44	-90	191	46	-90	26.24	73.76	0
10	-25	50	0.0144	196	46	90	16	44	90	19.16	80.84	0
11	0	-50	0.0626	2	45	-90	182	45	-90	23.94	76.06	0
12	0	-25	0.0586	324	44	-86	139	46	-94	76.2	23.8	0
13	0	0	0.0439	148	46	90	328	44	90	29.33	70.67	0
14	0	25	0.0376	29	44	-90	209	46	-90	21.16	78.84	0
15	0	50	0.0338	17	44	-90	197	46	-90	20.6	79.4	0
16	25	-50	0.3129	360	45	-90	180	45	-90	31.35	68.65	0
17	25	-25	0.1578	359	45	-90	179	45	-90	40.61	59.39	0
18	25	0	0.027	187	45	90	6	45	90	29.66	70.34	0
19	25	25	0.022	216	46	90	35	44	90	18.54	81.46	0
20	25	50	0.0134	201	46	90	20	44	90	19.19	80.81	0
21	50	-50	0.0603	351	45	-90	171	45	-90	34.22	65.78	0
22	50	-25	0.0712	17	44	-91	198	46	-89	42.15	57.85	0
23	50	0	0.0492	7	44	-91	188	46	-89	42.92	57.08	0
24	50	25	0.0178	183	45	91	2	45	89	32.67	67.33	0
25	50	50	0.0155	179	45	91	358	45	89	34.82	65.18	0

Table C.24: Full-wavefield moment tensor inversion results for location 3d, ISO input mechanism, isotropic medium, and dominant source frequency of 125 Hz with a DC constraint applied to the inversion. The bolded row is the location with the highest correlation in the grid search and thus the final ouputted result. Refer to Figure C.3f for visual.

Location Number	X Coord (m)	Y Coord (m)	Correlation	Strike 1 (°)	Dip 1 (°)	Rake 1 (°)	Strike 2 (°)	Dip 2 (°)	Rake 2 (°)	DC %	CLVD %	ISO %
1	-50	-50	0.1205	353	44	-90	173	46	-90	25.74	74.26	0
2	-50	-25	0.1322	22	44	-90	202	46	-90	26.94	73.06	0
3	-50	0	0.038	358	44	-90	179	46	-90	97.08	2.92	0
4	-50	25	0.0202	234	46	90	55	44	90	36.81	63.19	0
5	-50	50	0.016	188	46	89	10	44	91	99.62	0.38	0
6	-25	-50	0.2659	176	46	90	356	44	90	21.18	78.82	0
7	-25	-25	0.0893	191	46	91	10	44	89	97.83	2.17	0
8	-25	0	0.067	30	44	-90	210	46	-90	23.43	76.57	0
9	-25	25	0.0289	359	44	-91	180	46	-89	91.57	8.43	0
10	-25	50	0.0132	174	46	89	355	44	91	99.12	0.88	0
11	0	-50	0.0626	2	45	-90	182	45	-90	23.94	76.06	0
12	0	-25	0.0584	320	44	-87	136	46	-93	96.4	3.6	0
13	0	0	0.0439	148	46	90	328	44	90	29.33	70.67	0
14	0	25	0.0376	29	44	-90	209	46	-90	21.16	78.84	0
15	0	50	0.0338	17	44	-90	197	46	-90	20.6	79.4	0
16	25	-50	0.3129	360	45	-90	180	45	-90	31.35	68.65	0
17	25	-25	0.1549	358	44	-90	178	46	-90	93.33	6.67	0
18	25	0	0.0259	180	46	91	359	44	89	92.33	7.67	0
19	25	25	0.0181	179	45	85	6	45	95	98.48	1.52	0
20	25	50	0.0122	174	45	88	357	45	92	96.62	3.38	0
21	50	-50	0.0585	356	45	-89	175	46	-90	98.98	1.02	0
22	50	-25	0.0696	9	44	-92	191	46	-89	99.23	0.77	0
23	50	0	0.0484	2	44	-91	184	46	-89	94.69	5.31	0
24	50	25	0.0172	177	46	91	355	44	89	91.43	8.57	0
25	50	50	0.0151	173	45	91	352	45	89	99.54	0.46	0

Table C.25: Full-wavefield moment tensor inversion results for location 3e, ISO input mechanism, isotropic medium, and dominant source frequency of 125 Hz with no constraints applied to the inversion. The bolded row is the location with the highest correlation in the grid search and thus the final ouputted result. Refer to Figure C.3g for visual.

Location Number	X Coord (m)	Y Coord (m)	Correlation	Strike 1 (°)	Dip 1 (°)	Rake 1 (°)	Strike 2 (°)	Dip 2 (°)	Rake 2 (°)	DC %	CLVD %	ISO %
1	-50	-50	0.1048	5	44	-96	193	46	-84	13.23	5.01	-81.76
2	-50	-25	0.3194	333	46	-93	157	44	-87	4.57	2.87	-92.56
3	-50	0	0.0962	62	87	-170	332	80	-4	4.4	8.74	86.86
4	-50	25	0.1343	90	87	0	180	90	-177	5.89	2.35	91.76
5	-50	50	0.0448	182	87	4	92	86	177	4.29	14.5	-81.21
6	-25	-50	0.0862	98	86	-178	8	88	-4	8.91	1.34	-89.75
7	-25	-25	0.4598	327	48	-103	166	44	-76	0.98	3.71	-95.31
8	-25	0	0.4933	200	83	-176	109	86	-7	3.68	2.78	93.54
9	-25	25	0.0607	200	83	177	291	87	7	4.24	2.21	93.55
10	-25	50	0.0426	223	46	84	52	45	96	8.03	5.76	-86.21
11	0	-50	0.05	251	44	71	97	49	108	1.83	7.82	-90.35
12	0	-25	0.1818	340	50	-122	204	49	-58	1.89	4.25	-93.86
13	0	0	0.5196	87	51	-58	222	49	-123	1.61	7.82	90.57
14	0	25	0.0963	236	45	85	62	46	95	10.51	0.87	-88.62
15	0	50	0.0983	48	44	-84	220	46	-95	8.94	4.42	86.64
16	25	-50	0.0432	65	44	-88	242	46	-92	16.36	10.62	73.02
17	25	-25	0.0512	348	54	-142	233	60	-43	4.75	26.45	68.8
18	25	0	0.1999	81	48	-79	245	43	-102	3.93	8.62	87.45
19	25	25	0.0899	237	45	86	62	45	94	13.9	1.06	-85.04
20	25	50	0.0066	229	46	87	54	45	93	17.24	1.48	-81.28
21	50	-50	0.0276	261	44	86	86	47	93	13.18	3.56	-83.26
22	50	-25	0.0392	258	44	87	82	46	93	7.19	5.99	-86.82
23	50	0	0.0031	253	44	87	77	46	93	17.79	0.02	-82.19
24	50	25	7.00E-04	67	45	-86	241	45	-94	16.64	0.08	83.28
25	50	50	4.00E-04	234	45	87	58	45	93	21.01	0.25	-78.74

Table C.26: Full-wavefield moment tensor inversion results for location 3e, ISO input mechanism, isotropic medium, and dominant source frequency of 125 Hz with a deviatoric constraint applied to the inversion. The bolded row is the location with the highest correlation in the grid search and thus the final ouputted result. Refer to Figure C.3h for visual.

Location Number	X Coord (m)	Y Coord (m)	Correlation	Strike 1 (°)	Dip 1 (°)	Rake 1 (°)	Strike 2 (°)	Dip 2 (°)	Rake 2 (°)	DC %	CLVD %	ISO %
1	-50	-50	0.0642	116	46	89	297	44	91	69.53	30.47	0
2	-50	-25	0.1775	154	45	90	334	45	90	14.14	85.86	0
3	-50	0	0.0712	126	46	-91	308	44	-89	57.99	42.01	0
4	-50	25	0.0762	349	44	-91	170	46	-89	23.83	76.17	0
5	-50	50	0.0238	204	46	90	24	44	90	19.45	80.55	0
6	-25	-50	0.0511	203	46	90	22	44	90	24.61	75.39	0
7	-25	-25	0.2559	156	45	90	336	45	90	24.85	75.15	0
8	-25	0	0.2902	331	45	-90	151	45	-90	27.74	72.26	0
9	-25	25	0.0404	183	48	111	333	46	68	24.71	75.29	0
10	-25	50	0.0262	156	45	91	335	45	89	32.03	67.97	0
11	0	-50	0.0303	147	45	90	327	45	90	24.17	75.83	0
12	0	-25	0.1038	142	46	89	324	44	91	51.29	48.71	0
13	0	0	0.3034	334	45	-90	154	45	-90	31.89	68.11	0
14	0	25	0.0609	152	45	90	332	45	90	41.7	58.3	0
15	0	50	0.0614	337	44	-91	158	46	-89	50.32	49.68	0
16	25	-50	0.0271	47	44	-90	227	46	-90	24.05	75.95	0
17	25	-25	0.0452	5	44	-96	193	47	-84	85.64	14.36	0
18	25	0	0.1153	328	45	-90	147	45	-90	37.42	62.58	0
19	25	25	0.056	155	45	90	335	45	90	42.52	57.48	0
20	25	50	0.0041	159	45	91	337	45	89	40.86	59.14	0
21	50	-50	0.0177	337	44	-89	156	46	-91	66.8	33.2	0
22	50	-25	0.0259	156	45	90	337	45	90	50.44	49.56	0
23	50	0	0.0019	149	45	90	330	45	90	38.29	61.71	0
24	50	25	4.00E-04	334	45	-90	154	45	-90	49.17	50.83	0
25	50	50	2.00E-04	157	45	91	336	45	89	43.1	56.9	0

Table C.27: Full-wavefield moment tensor inversion results for location 3e, ISO input mechanism, isotropic medium, and dominant source frequency of 125 Hz with a DC constraint applied to the inversion. The bolded row is the location with the highest correlation in the grid search and thus the final ouputted result. Refer to Figure C.3i for visual.

Location Number	X Coord (m)	Y Coord (m)	Correlation	Strike 1 (°)	Dip 1 (°)	Rake 1 (°)	Strike 2 (°)	Dip 2 (°)	Rake 2 (°)	DC %	CLVD %	ISO %
1	-50	-50	0.0635	122	46	89	304	44	91	90.81	9.19	0
2	-50	-25	0.1775	154	45	90	334	45	90	14.14	85.86	0
3	-50	0	0.0707	131	46	-91	313	44	-89	96.18	3.82	0
4	-50	25	0.0733	337	44	-91	158	46	-89	90.19	9.81	0
5	-50	50	0.0187	180	47	94	355	44	86	96.84	3.16	0
6	-25	-50	0.0473	176	45	89	358	45	91	96.59	3.41	0
7	-25	-25	0.2445	157	46	90	336	44	90	91.53	8.47	0
8	-25	0	0.2902	331	45	-90	151	45	-90	27.74	72.26	0
9	-25	25	0.0399	184	49	104	343	43	74	99.06	0.94	0
10	-25	50	0.0255	151	46	91	330	44	89	99.08	0.92	0
11	0	-50	0.0289	154	46	89	335	44	91	94.1	5.9	0
12	0	-25	0.1023	147	46	89	328	44	91	95.67	4.33	0
13	0	0	0.3034	334	45	-90	154	45	-90	31.89	68.11	0
14	0	25	0.0598	152	46	90	331	44	90	99.18	0.82	0
15	0	50	0.0608	334	44	-92	156	46	-88	97.45	2.55	0
16	25	-50	0.0271	47	44	-90	227	46	-90	24.05	75.95	0
17	25	-25	0.0451	8	43	-95	195	47	-85	94.43	5.57	0
18	25	0	0.1132	331	44	-90	150	46	-90	90.72	9.28	0
19	25	25	0.0546	154	46	90	334	44	90	90.1	9.9	0
20	25	50	0.004	155	46	91	334	44	89	98.89	1.11	0
21	50	-50	0.0177	338	44	-89	157	46	-91	94.66	5.34	0
22	50	-25	0.0253	158	46	90	338	44	90	96.71	3.29	0
23	50	0	0.0019	152	45	90	333	45	90	97.94	2.06	0
24	50	25	4.00E-04	333	45	-91	154	45	-89	91.06	8.94	0
25	50	50	2.00E-04	155	45	91	334	45	89	90.94	9.06	0

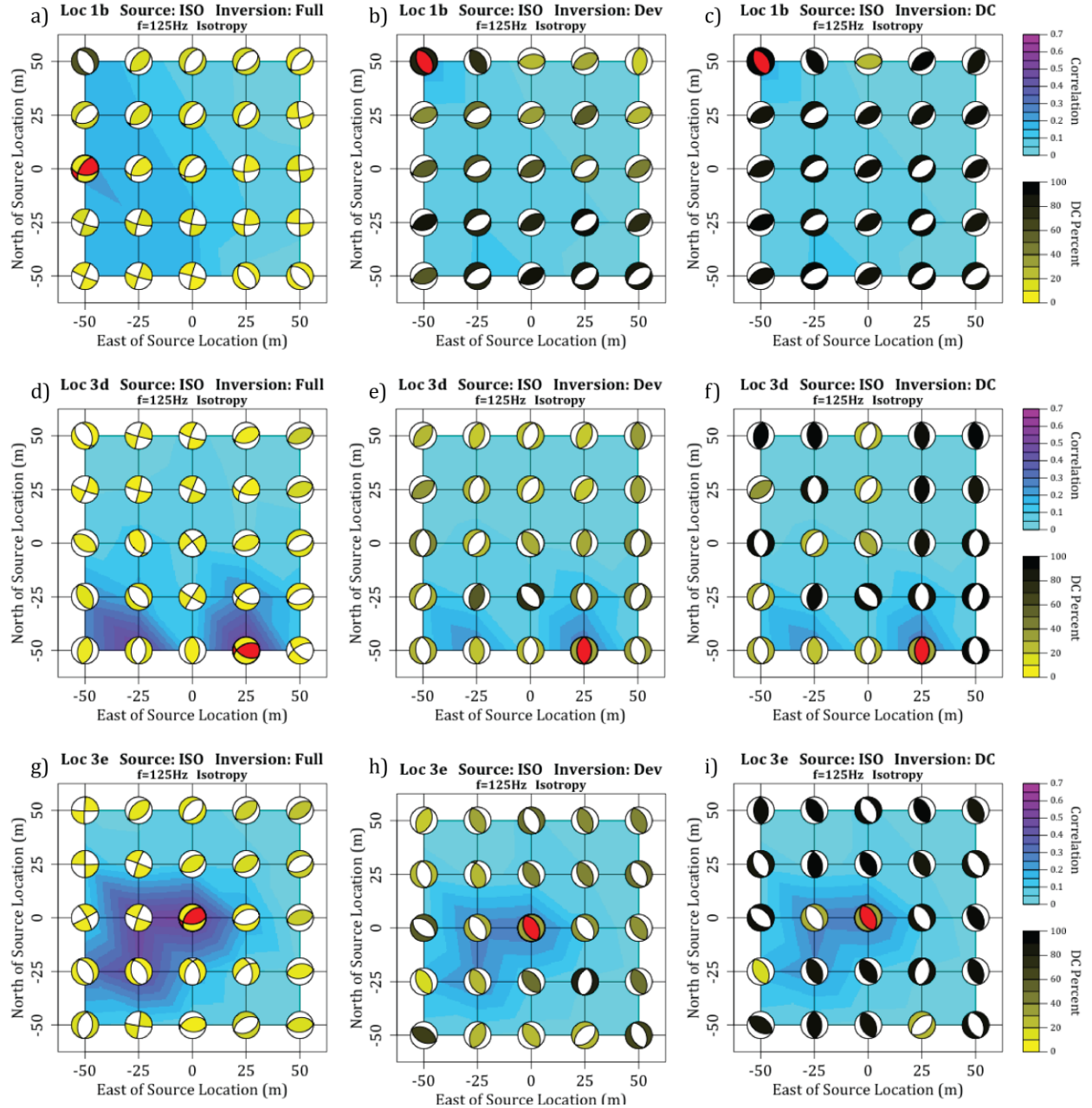


Figure C.3: Full-wavefield moment tensor inversion results for an ISO source mechanism in an isotropic medium and source frequency of 125 Hz for a) location 1b with no constraints on the inversion, b) location 1b with a deviatoric constraint, c) location 1b with a DC constraint, d) location 3d with no constraints, e) location 3d with a deviatoric constraint, f) location 3d with a DC constraint, g) location 3e with no constraints, h) location 3e with a deviatoric constraint, and i) location 3e with a DC constraint. The red beach-ball is the location and source mechanism with the highest correlation to the input seismograms. Refer to Tables C.19-C.27 for numerical values of results.

Table C.28: Full-wavefield moment tensor inversion results for location 1b, DC input mechanism, 5% anisotropic medium, and dominant source frequency of 125 Hz with no constraints applied to the inversion. The bolded row is the location with the highest correlation in the grid search and thus the final ouputted result. Refer to Figure C.4a for visual.

Location Number	X Coord (m)	Y Coord (m)	Correlation	Strike 1 (°)	Dip 1 (°)	Rake 1 (°)	Strike 2 (°)	Dip 2 (°)	Rake 2 (°)	DC %	CLVD %	ISO %
1	-50	-50	0.0947	331	45	-97	160	46	-83	53.66	27.55	18.79
2	-50	-25	0.1249	328	45	-98	159	46	-83	55.5	23.11	21.39
3	-50	0	0.1611	323	45	-99	155	46	-82	75.56	14.01	10.43
4	-50	25	0.2169	310	46	-101	146	46	-79	93.2	1.38	-5.42
5	-50	50	0.232	145	46	-74	303	46	-105	67.55	20.79	11.66
6	-25	-50	0.0634	159	46	97	328	44	83	43.02	29.2	-27.78
7	-25	-25	0.2118	146	43	98	315	47	82	45.06	30.75	-24.19
8	-25	0	0.2455	309	47	-99	142	44	-81	86.53	11.42	2.05
9	-25	25	0.2326	142	43	-79	307	48	-100	48.67	30.99	20.34
10	-25	50	0.1896	137	41	100	303	50	81	39.77	36.4	-23.83
11	0	-50	0.0505	197	89	1	107	89	179	6.91	13.13	79.96
12	0	-25	0.2445	139	43	-83	309	48	-97	67.35	26.68	5.97
13	0	0	0.2043	310	48	-98	142	43	-81	36.94	37.83	25.23
14	0	25	0.1598	138	42	99	307	48	82	38.23	37.03	-24.74
15	0	50	0.1263	135	42	-80	301	48	-99	55.47	27.52	17.01
16	25	-50	0.0637	190	87	-176	100	86	-3	4.59	10.18	-85.23
17	25	-25	0.0945	192	88	-177	102	87	-2	8.78	5.42	-85.8
18	25	0	0.1321	140	43	97	311	48	84	32.27	37.3	-30.43
19	25	25	0.1117	135	43	-82	304	48	-97	45.57	33.31	21.12
20	25	50	0.1207	224	49	-100	59	42	-78	14.01	2.21	-83.78
21	50	-50	0.0803	306	51	-114	161	45	-64	1.51	13.21	85.28
22	50	-25	0.0972	97	86	-4	188	86	-176	7.37	3.67	-88.96
23	50	0	0.1116	96	78	171	187	81	12	4	4.5	91.5
24	50	25	0.1172	215	50	69	65	44	113	4.61	4.51	90.88
25	50	50	0.1134	53	42	-80	221	49	-98	9.57	5.24	-85.19

Table C.29: Full-wavefield moment tensor inversion results for location 1b, DC input mechanism, 5% anisotropic medium, and dominant source frequency of 125 Hz with a deviatoric constraint applied to the inversion. The bolded row is the location with the highest correlation in the grid search and thus the final ouputted result. Refer to Figure C.4b for visual.

Location Number	X Coord (m)	Y Coord (m)	Correlation	Strike 1 (°)	Dip 1 (°)	Rake 1 (°)	Strike 2 (°)	Dip 2 (°)	Rake 2 (°)	DC %	CLVD %	ISO %
1	-50	-50	0.0902	330	44	-97	160	46	-83	83.27	16.73	0
2	-50	-25	0.1173	327	44	-98	158	46	-83	90.99	9.01	0
3	-50	0	0.1597	323	44	-99	155	46	-82	92.91	7.09	0
4	-50	25	0.2166	310	46	-101	146	45	-79	97.53	2.47	0
5	-50	50	0.2312	144	46	-75	303	46	-105	85.37	14.63	0
6	-25	-50	0.055	158	47	97	328	43	83	89.35	10.65	0
7	-25	-25	0.2063	144	44	98	313	47	82	81.98	18.02	0
8	-25	0	0.2454	309	47	-99	142	44	-81	89.79	10.21	0
9	-25	25	0.2289	141	44	-79	307	47	-100	79.63	20.37	0
10	-25	50	0.1862	136	42	100	302	49	81	74.96	25.04	0
11	0	-50	0.0252	229	50	-97	61	40	-81	77.02	22.98	0
12	0	-25	0.2442	138	43	-83	309	48	-97	76.01	23.99	0
13	0	0	0.1977	140	44	-82	309	47	-98	74.67	25.33	0
14	0	25	0.1552	138	43	98	306	48	82	74.7	25.3	0
15	0	50	0.125	134	43	-80	301	48	-99	81.95	18.05	0
16	25	-50	0.0363	233	49	83	63	41	98	80.57	19.43	0
17	25	-25	0.0518	52	40	97	224	50	85	56.58	43.42	0
18	25	0	0.1224	139	44	97	310	47	83	78.6	21.4	0
19	25	25	0.1092	135	43	-82	304	47	-97	78.01	21.99	0
20	25	50	0.0603	132	43	-81	301	48	-98	76.52	23.48	0
21	50	-50	0.0473	58	41	-84	229	49	-96	84.3	15.7	0
22	50	-25	0.055	224	50	85	52	41	96	84.83	15.17	0
23	50	0	0.089	135	43	-83	306	47	-96	75.48	24.52	0
24	50	25	0.0612	40	40	-85	214	50	-94	41.4	58.6	0
25	50	50	0.059	211	51	86	37	40	95	39.01	60.99	0

Table C.30: Full-wavefield moment tensor inversion results for location 1b, DC input mechanism, 5% anisotropic medium, and dominant source frequency of 125 Hz with a DC constraint applied to the inversion. The bolded row is the location with the highest correlation in the grid search and thus the final ouputted result. Refer to Figure C.4c for visual.

Location Number	X Coord (m)	Y Coord (m)	Correlation	Strike 1 (°)	Dip 1 (°)	Rake 1 (°)	Strike 2 (°)	Dip 2 (°)	Rake 2 (°)	DC %	CLVD %	ISO %
1	-50	-50	0.0837	330	44	-97	159	46	-83	95.03	4.97	0
2	-50	-25	0.1156	327	44	-98	158	47	-83	99.96	0.04	0
3	-50	0	0.1581	323	44	-99	155	47	-82	99.21	0.79	0
4	-50	25	0.2165	310	46	-101	146	46	-79	99.88	0.12	0
5	-50	50	0.2275	144	47	-75	303	45	-105	99.59	0.41	0
6	-25	-50	0.0547	158	47	97	328	43	83	94.85	5.15	0
7	-25	-25	0.204	144	44	98	313	46	82	97.32	2.68	0
8	-25	0	0.2428	309	46	-99	142	45	-81	95.78	4.22	0
9	-25	25	0.2228	141	45	-79	307	46	-100	99.67	0.33	0
10	-25	50	0.1801	136	43	101	302	48	80	99.14	0.86	0
11	0	-50	0.0251	229	50	-98	62	40	-80	98.84	1.16	0
12	0	-25	0.238	138	43	-83	309	47	-97	97.56	2.44	0
13	0	0	0.1884	140	44	-82	309	46	-98	97.3	2.7	0
14	0	25	0.1508	138	44	98	306	47	82	96.51	3.49	0
15	0	50	0.1209	134	44	-80	301	47	-99	95.65	4.35	0
16	25	-50	0.0363	233	49	84	63	41	97	92.83	7.17	0
17	25	-25	0.0515	225	50	85	54	40	96	92.46	7.54	0
18	25	0	0.1191	139	44	97	309	46	83	98.22	1.78	0
19	25	25	0.1049	135	44	-82	304	47	-98	96.86	3.14	0
20	25	50	0.0578	133	44	98	301	47	82	97.68	2.32	0
21	50	-50	0.0473	57	41	-84	230	49	-95	99.35	0.65	0
22	50	-25	0.055	224	50	84	53	41	97	91.75	8.25	0
23	50	0	0.0845	135	44	-83	305	47	-96	95.98	4.02	0
24	50	25	0.0605	44	40	-83	215	50	-96	95.09	4.91	0
25	50	50	0.0579	212	51	84	41	40	97	90.26	9.74	0

Table C.31: Full-wavefield moment tensor inversion results for location 3d, DC input mechanism, 5% anisotropic medium, and dominant source frequency of 125 Hz with no constraints applied to the inversion. The bolded row is the location with the highest correlation in the grid search and thus the final ouputted result. Refer to Figure C.4d for visual.

Location Number	X Coord (m)	Y Coord (m)	Correlation	Strike 1 (°)	Dip 1 (°)	Rake 1 (°)	Strike 2 (°)	Dip 2 (°)	Rake 2 (°)	DC %	CLVD %	ISO %
1	-50	-50	0.298	262	50	117	44	47	61	12.47	73.18	-14.35
2	-50	-25	0.3223	72	45	-91	253	45	-89	30.68	48.33	20.99
3	-50	0	0.064	250	45	91	69	45	89	29.61	47.99	-22.4
4	-50	25	0.0528	102	47	-92	284	44	-88	21.48	10.72	-67.8
5	-50	50	0.1346	266	78	166	359	76	12	9.23	84.99	-5.78
6	-25	-50	0.3377	261	50	114	46	46	64	16.73	81.16	-2.11
7	-25	-25	0.2272	76	45	-91	256	45	-89	32.3	45.01	22.69
8	-25	0	0.0944	48	45	-109	254	48	-72	5.77	68.59	25.64
9	-25	25	0.0473	265	46	91	84	44	89	40.57	30.51	28.92
10	-25	50	0.1225	270	85	172	1	82	5	11.09	44.31	-44.6
11	0	-50	0.3307	278	59	137	34	54	39	3.86	36.97	-59.17
12	0	-25	0.3008	253	46	101	57	45	79	1.99	47.65	-50.36
13	0	0	0.1237	68	44	-92	251	46	-88	16.41	48.49	35.1
14	0	25	0.0362	255	45	91	73	45	89	47.03	49.16	3.81
15	0	50	0.072	263	86	172	353	82	4	25.17	30.35	44.48
16	25	-50	0.2767	36	47	58	258	52	119	5.42	9.35	85.23
17	25	-25	0.2966	252	46	92	69	44	88	21	47.85	31.15
18	25	0	0.1264	72	44	-93	256	46	-87	30.2	62.56	-7.24
19	25	25	0.0326	252	46	93	67	44	87	28.98	65.94	-5.08
20	25	50	0.0341	53	43	-99	246	47	-81	11.97	61.98	26.05
21	50	-50	0.056	257	46	83	88	44	97	9.26	0.41	-90.33
22	50	-25	0.0356	87	45	-85	261	45	-95	7.87	3.22	88.91
23	50	0	0.0254	256	46	91	74	44	89	13.81	41.04	-45.15
24	50	25	0.0539	251	46	90	71	44	90	15.94	31.23	-52.83
25	50	50	0.0355	247	46	89	68	44	91	15.23	23.02	-61.75

Table C.32: Full-wavefield moment tensor inversion results for location 3d, DC input mechanism, 5% anisotropic medium, and dominant source frequency of 125 Hz with a deviatoric constraint applied to the inversion. The bolded row is the location with the highest correlation in the grid search and thus the final ouputted result. Refer to Figure C.4e for visual.

Location Number	X Coord (m)	Y Coord (m)	Correlation	Strike 1 (°)	Dip 1 (°)	Rake 1 (°)	Strike 2 (°)	Dip 2 (°)	Rake 2 (°)	DC %	CLVD %	ISO %
1	-50	-50	0.2975	253	48	104	53	44	76	26.55	73.45	0
2	-50	-25	0.3195	71	45	-90	252	45	-90	59.62	40.38	0
3	-50	0	0.0633	249	45	90	69	45	90	60.7	39.3	0
4	-50	25	0.0454	256	45	90	76	45	90	73.11	26.89	0
5	-50	50	0.1346	263	69	155	2	66	23	6.4	93.6	0
6	-25	-50	0.3377	259	49	112	47	45	66	18.47	81.53	0
7	-25	-25	0.2239	75	45	-90	256	45	-90	64.1	35.9	0
8	-25	0	0.0935	58	44	-94	243	47	-86	34.3	65.7	0
9	-25	25	0.0464	266	46	92	83	44	88	31.5	68.5	0
10	-25	50	0.1185	227	47	96	38	44	83	38.25	61.75	0
11	0	-50	0.2896	244	47	94	59	43	86	93.37	6.63	0
12	0	-25	0.2777	242	46	91	61	44	89	73.18	26.82	0
13	0	0	0.1183	68	44	-91	249	46	-89	64.95	35.05	0
14	0	25	0.0361	255	45	91	73	45	89	46.08	53.92	0
15	0	50	0.0711	86	90	-174	356	84	0	93.53	6.47	0
16	25	-50	0.2007	355	44	-72	151	48	-106	34.69	65.31	0
17	25	-25	0.2936	257	46	98	65	45	82	8.6	91.4	0
18	25	0	0.1263	72	44	-93	256	46	-87	27.54	72.46	0
19	25	25	0.0326	251	46	93	67	44	87	34.46	65.54	0
20	25	50	0.0335	55	43	-94	241	47	-86	40.4	59.6	0
21	50	-50	0.0333	184	45	90	4	45	90	52.01	47.99	0
22	50	-25	0.0219	358	45	-90	178	45	-90	48.74	51.26	0
23	50	0	0.0217	253	46	91	72	44	89	81.59	18.41	0
24	50	25	0.0406	248	46	91	67	44	89	89.93	10.07	0
25	50	50	0.0228	240	46	90	60	44	90	59.23	40.77	0

Table C.33: Full-wavefield moment tensor inversion results for location 3d, DC input mechanism, 5% anisotropic medium, and dominant source frequency of 125 Hz with a DC constraint applied to the inversion. The bolded row is the location with the highest correlation in the grid search and thus the final ouputted result. Refer to Figure C.4f for visual.

Location Number	X Coord (m)	Y Coord (m)	Correlation	Strike 1 (°)	Dip 1 (°)	Rake 1 (°)	Strike 2 (°)	Dip 2 (°)	Rake 2 (°)	DC %	CLVD %	ISO %
1	-50	-50	0.2826	285	89	-173	195	83	-1	92.13	7.87	0
2	-50	-25	0.2989	73	45	-90	253	45	-90	90.74	9.26	0
3	-50	0	0.0619	351	84	179	81	89	6	96.56	3.44	0
4	-50	25	0.0443	256	45	90	77	45	90	97.1	2.9	0
5	-50	50	0.1331	263	90	176	353	86	0	94.2	5.8	0
6	-25	-50	0.3169	287	88	-164	196	74	-2	93.02	6.98	0
7	-25	-25	0.214	76	45	-90	256	45	-90	97.1	2.9	0
8	-25	0	0.0896	9	88	-180	279	90	-2	96.94	3.06	0
9	-25	25	0.0446	254	45	90	73	45	90	95.4	4.6	0
10	-25	50	0.1134	83	90	178	173	88	0	97.25	2.75	0
11	0	-50	0.2896	245	47	94	59	43	86	96.55	3.45	0
12	0	-25	0.2759	242	46	90	61	44	90	94.11	5.89	0
13	0	0	0.1138	68	44	-91	249	46	-90	96.24	3.76	0
14	0	25	0.0333	254	45	91	74	45	89	94.67	5.33	0
15	0	50	0.0711	86	90	-174	356	84	0	93.53	6.47	0
16	25	-50	0.1984	347	43	-76	149	49	-102	99.41	0.59	0
17	25	-25	0.2747	296	89	-178	206	88	-1	94.29	5.71	0
18	25	0	0.1081	73	44	-91	254	46	-89	96.38	3.62	0
19	25	25	0.0299	250	46	91	68	44	89	93.16	6.84	0
20	25	50	0.0311	57	43	-92	240	47	-88	95.71	4.29	0
21	50	-50	0.0326	183	45	90	3	45	90	93.9	6.1	0
22	50	-25	0.0216	357	45	-90	178	45	-90	97.71	2.29	0
23	50	0	0.0216	253	46	91	72	44	89	91.96	8.04	0
24	50	25	0.0405	248	46	91	67	44	89	99.98	0.02	0
25	50	50	0.0204	244	46	91	63	44	89	98.79	1.21	0

Table C.34: Full-wavefield moment tensor inversion results for location 3e, DC input mechanism, 5% anisotropic medium, and dominant source frequency of 125 Hz with no constraints applied to the inversion. The bolded row is the location with the highest correlation in the grid search and thus the final ouputted result. Refer to Figure C.4g for visual.

Location Number	X Coord (m)	Y Coord (m)	Correlation	Strike 1 (°)	Dip 1 (°)	Rake 1 (°)	Strike 2 (°)	Dip 2 (°)	Rake 2 (°)	DC %	CLVD %	ISO %
1	-50	-50	0.4753	81	46	-91	262	44	-89	38.45	41.99	19.56
2	-50	-25	0.3242	250	45	90	69	45	90	53.04	40.68	-6.28
3	-50	0	0.1324	38	44	-92	221	46	-88	19.79	5.78	-74.43
4	-50	25	0.1611	244	44	90	63	46	90	47.45	42.15	-10.4
5	-50	50	0.0901	46	44	-90	227	46	-90	31.94	38.18	29.88
6	-25	-50	0.1391	67	45	-90	247	45	-90	44.27	26.37	-29.36
7	-25	-25	0.473	77	46	-92	259	44	-88	31.32	41.71	26.97
8	-25	0	0.2802	254	44	92	72	46	88	26.3	18.72	54.98
9	-25	25	0.1266	230	46	90	50	44	90	28.09	34.56	-37.35
10	-25	50	0.0874	47	44	-92	229	46	-88	32.59	40.02	-27.39
11	0	-50	0.2113	257	44	90	77	46	90	28.91	37.43	-33.66
12	0	-25	0.3013	251	44	89	72	46	91	22.55	29.07	-48.38
13	0	0	0.4619	72	46	-90	252	44	-90	18.89	30.76	50.35
14	0	25	0.1388	37	44	-105	238	48	-76	3.54	12.22	-84.24
15	0	50	0.0248	231	46	91	50	44	89	18.03	41.79	-40.18
16	25	-50	0.1964	78	46	-91	260	44	-89	35.01	46.77	18.22
17	25	-25	0.1083	70	45	-92	253	45	-88	21.53	31.23	-47.24
18	25	0	0.0553	69	46	-85	242	44	-95	11.58	0.5	87.92
19	25	25	0.0063	230	46	89	52	44	92	25.38	1.81	-72.81
20	25	50	0.0234	233	45	85	59	45	95	12.55	4.48	-82.97
21	50	-50	0.0488	261	44	91	80	46	89	24.42	41.24	-34.34
22	50	-25	0.0074	240	46	87	63	44	93	17.4	4.71	-77.89
23	50	0	0.0079	237	46	88	60	44	92	20.24	5.72	-74.04
24	50	25	0.0153	233	46	87	58	44	93	18.6	1.72	-79.68
25	50	50	0.012	60	45	-86	235	45	-94	17.29	2.2	80.51

Table C.35: Full-wavefield moment tensor inversion results for location 3e, DC input mechanism, 5% anisotropic medium, and dominant source frequency of 125 Hz with a deviatoric constraint applied to the inversion. The bolded row is the location with the highest correlation in the grid search and thus the final ouputted result. Refer to Figure C.4h for visual.

Location Number	X Coord (m)	Y Coord (m)	Correlation	Strike 1 (°)	Dip 1 (°)	Rake 1 (°)	Strike 2 (°)	Dip 2 (°)	Rake 2 (°)	DC %	CLVD %	ISO %
1	-50	-50	0.4708	81	46	-91	262	44	-89	67.62	32.38	0
2	-50	-25	0.3238	250	45	90	69	45	90	62.1	37.9	0
3	-50	0	0.1084	235	45	90	55	45	90	69.96	30.04	0
4	-50	25	0.1605	244	44	90	63	46	90	62.24	37.76	0
5	-50	50	0.0856	45	44	-90	226	46	-90	78.25	21.75	0
6	-25	-50	0.1355	66	45	-91	247	45	-89	33.19	66.81	0
7	-25	-25	0.4615	78	46	-91	260	44	-89	71.45	28.55	0
8	-25	0	0.2499	296	87	179	26	89	3	28.59	71.41	0
9	-25	25	0.1159	229	46	90	49	44	90	89.63	10.37	0
10	-25	50	0.0861	46	44	-93	230	46	-87	23.47	76.53	0
11	0	-50	0.1968	258	44	90	78	46	90	82.44	17.56	0
12	0	-25	0.2347	253	45	90	73	45	90	87.92	12.08	0
13	0	0	0.3625	74	46	-90	254	44	-90	88.14	11.86	0
14	0	25	0.1054	8	78	169	100	79	12	9.15	90.85	0
15	0	50	0.0217	229	46	91	48	44	89	80.68	19.32	0
16	25	-50	0.1936	79	46	-91	260	44	-89	60.15	39.85	0
17	25	-25	0.1009	296	86	-3	26	87	-176	10.79	89.21	0
18	25	0	0.0345	335	45	-90	156	45	-90	42.18	57.82	0
19	25	25	0.0042	190	46	91	9	44	89	22.51	77.49	0
20	25	50	0.0138	154	45	91	333	45	89	42.74	57.26	0
21	50	-50	0.045	262	44	91	81	46	89	76.86	23.14	0
22	50	-25	0.0045	184	46	91	3	44	89	20.41	79.59	0
23	50	0	0.0048	192	46	91	11	44	89	18.85	81.15	0
24	50	25	0.0094	165	46	91	344	45	89	38.46	61.54	0
25	50	50	0.0071	334	45	-91	155	45	-89	48.8	51.2	0

Table C.36: Full-wavefield moment tensor inversion results for location 3e, DC input mechanism, 5% anisotropic medium, and dominant source frequency of 125 Hz with a DC constraint applied to the inversion. The bolded row is the location with the highest correlation in the grid search and thus the final ouputted result. Refer to Figure C.4i for visual.

Location Number	X Coord (m)	Y Coord (m)	Correlation	Strike 1 (°)	Dip 1 (°)	Rake 1 (°)	Strike 2 (°)	Dip 2 (°)	Rake 2 (°)	DC %	CLVD %	ISO %
1	-50	-50	0.4545	81	46	-90	261	44	-90	96.97	3.03	0
2	-50	-25	0.3092	250	45	90	70	45	90	96.47	3.53	0
3	-50	0	0.1063	235	45	90	55	45	90	92.26	7.74	0
4	-50	25	0.1543	244	44	90	63	46	90	93.68	6.32	0
5	-50	50	0.0821	45	44	-90	225	46	-90	91.61	8.39	0
6	-25	-50	0.114	67	45	-90	247	45	-90	96.31	3.69	0
7	-25	-25	0.4443	78	46	-90	259	44	-90	92.74	7.26	0
8	-25	0	0.2476	297	88	-180	207	90	-2	94.22	5.78	0
9	-25	25	0.1156	229	46	90	49	44	90	97.73	2.27	0
10	-25	50	0.064	94	90	1	4	89	180	90.14	9.86	0
11	0	-50	0.1961	258	45	90	78	45	90	92.05	7.95	0
12	0	-25	0.229	253	45	90	73	45	90	91.21	8.79	0
13	0	0	0.3613	74	46	-90	254	44	-90	96.68	3.32	0
14	0	25	0.1042	10	87	178	100	88	3	92.85	7.15	0
15	0	50	0.0216	229	46	90	48	44	90	91.73	8.27	0
16	25	-50	0.182	79	46	-90	260	44	-90	98.45	1.55	0
17	25	-25	0.0979	296	89	0	26	90	-179	91.68	8.32	0
18	25	0	0.034	335	45	-90	156	45	-90	91.09	8.91	0
19	25	25	0.0037	160	45	85	347	45	95	97.99	2.01	0
20	25	50	0.0136	152	45	90	331	45	90	99.86	0.14	0
21	50	-50	0.0447	262	44	90	82	46	90	90.77	9.23	0
22	50	-25	0.0045	184	46	91	3	44	89	20.41	79.59	0
23	50	0	0.0048	192	46	91	11	44	89	18.85	81.15	0
24	50	25	0.0091	160	46	91	339	44	89	91.31	8.69	0
25	50	50	0.0071	333	45	-91	154	46	-89	95.06	4.94	0

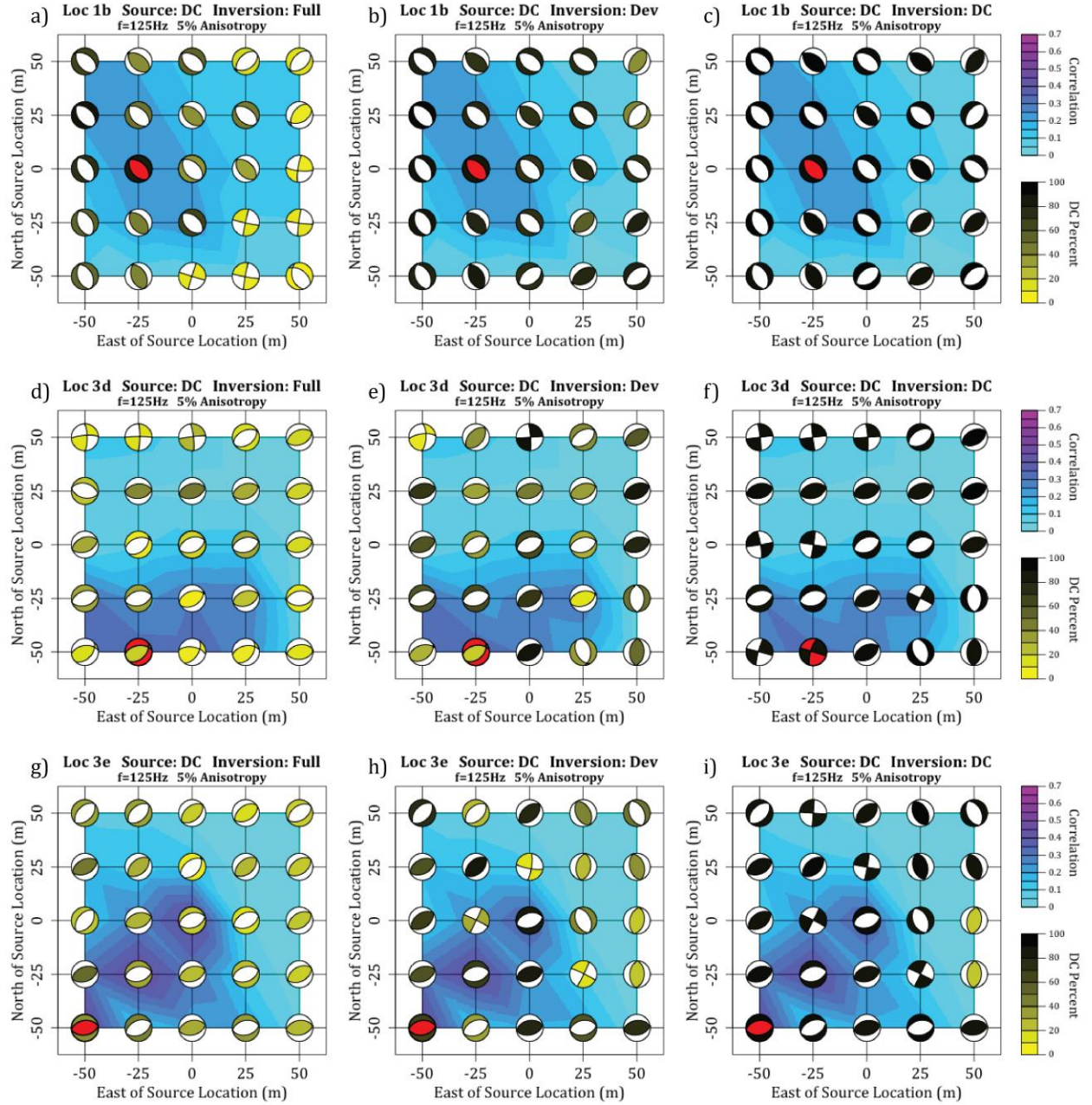


Figure C.4: Full-wavefield moment tensor inversion results for a DC source mechanism in a 5% anisotropic medium and source frequency of 125 Hz for a) location 1b with no constraints on the inversion, b) location 1b with a deviatoric constraint, c) location 1b with a DC constraint, d) location 3d with no constraints, e) location 3d with a deviatoric constraint, f) location 3d with a DC constraint, g) location 3e with no constraints, h) location 3e with a deviatoric constraint, and i) location 3e with a DC constraint. The red beach-ball is the location and source mechanism with the highest correlation to the input seismograms. Refer to Tables C.28-C.36 for numerical values of results.

Table C.37: Full-wavefield moment tensor inversion results for location 1b, CLVD input mechanism, 5% anisotropic medium, and dominant source frequency of 125 Hz with no constraints applied to the inversion. The bolded row is the location with the highest correlation in the grid search and thus the final ouputted result. Refer to Figure C.5a for visual.

Location Number	X Coord (m)	Y Coord (m)	Correlation	Strike 1 (°)	Dip 1 (°)	Rake 1 (°)	Strike 2 (°)	Dip 2 (°)	Rake 2 (°)	DC %	CLVD %	ISO %
1	-50	-50	0.1166	115	88	-2	205	88	-178	5.2	17.07	-77.73
2	-50	-25	0.134	203	87	-172	113	82	-3	16.24	0.52	-83.24
3	-50	0	0.0889	344	39	-95	171	51	-86	5.61	26.12	-68.27
4	-50	25	0.107	275	51	-135	153	57	-49	54.23	30.23	15.54
5	-50	50	0.1352	326	43	-98	157	47	-82	60.43	24.76	14.81
6	-25	-50	0.0856	204	90	-173	114	83	0	18.15	2.27	-79.58
7	-25	-25	0.1419	315	48	-98	148	42	-81	21.34	24.63	54.03
8	-25	0	0.1285	271	55	-141	156	59	-42	29.05	29.86	-41.09
9	-25	25	0.1044	148	44	115	294	51	67	21.44	48.09	-30.47
10	-25	50	0.0887	321	68	-68	94	31	-133	32.16	38.63	29.21
11	0	-50	0.0896	294	67	-154	193	66	-25	1.09	19.54	79.37
12	0	-25	0.1338	196	88	-175	106	85	-2	11.56	2.87	-85.57
13	0	0	0.1135	82	80	171	174	81	10	13.84	11.85	74.31
14	0	25	0.1464	72	43	112	223	51	71	8.35	4.42	87.23
15	0	50	0.1094	227	50	-101	64	41	-77	13.88	4.52	-81.6
16	25	-50	0.0945	287	74	-162	192	73	-16	1.31	18.86	79.83
17	25	-25	0.1365	192	88	2	102	88	178	8.16	6.08	85.76
18	25	0	0.1428	191	84	-171	100	81	-6	5.43	4.73	-89.84
19	25	25	0.1474	70	44	114	218	51	68	4.39	5.78	89.83
20	25	50	0.1675	60	42	102	224	49	80	14.28	1.6	84.12
21	50	-50	0.1087	157	46	106	315	47	74	4.13	15.04	-80.83
22	50	-25	0.1149	189	88	0	99	90	178	5.8	9.94	84.26
23	50	0	0.1316	97	85	177	187	87	5	8.65	2.52	88.83
24	50	25	0.1364	67	45	-65	213	50	-113	3.83	4.85	-91.32
25	50	50	0.1568	220	49	79	57	42	103	7.15	4.17	88.68

Table C.38: Full-wavefield moment tensor inversion results for location 1b, CLVD input mechanism, 5% anisotropic medium, and dominant source frequency of 125 Hz with a deviatoric constraint applied to the inversion. The bolded row is the location with the highest correlation in the grid search and thus the final ouputted result. Refer to Figure C.5b for visual.

Location Number	X Coord (m)	Y Coord (m)	Correlation	Strike 1 (°)	Dip 1 (°)	Rake 1 (°)	Strike 2 (°)	Dip 2 (°)	Rake 2 (°)	DC %	CLVD %	ISO %
1	-50	-50	0.0606	79	41	108	235	52	75	70.65	29.35	0
2	-50	-25	0.0634	72	40	105	233	52	78	80.26	19.74	0
3	-50	0	0.0784	159	44	95	332	46	85	90.77	9.23	0
4	-50	25	0.1068	277	49	-131	149	55	-53	72.61	27.39	0
5	-50	50	0.1339	326	43	-98	157	48	-82	82.98	17.02	0
6	-25	-50	0.0586	338	46	-93	162	44	-87	75.37	24.63	0
7	-25	-25	0.1104	138	44	-82	307	47	-98	71.31	28.69	0
8	-25	0	0.1267	265	68	-161	167	72	-23	46.63	53.37	0
9	-25	25	0.102	297	49	74	141	44	107	61.69	38.31	0
10	-25	50	0.0873	311	62	-78	107	30	-111	64.31	35.69	0
11	0	-50	0.0498	229	50	-97	61	40	-81	74.4	25.6	0
12	0	-25	0.112	280	53	-128	153	51	-50	28.79	71.21	0
13	0	0	0.085	276	51	-119	138	47	-59	51.93	48.07	0
14	0	25	0.0731	154	53	94	327	37	85	67.73	32.27	0
15	0	50	0.0711	316	34	-100	148	56	-84	53.19	46.81	0
16	25	-50	0.0524	226	50	-96	55	40	-83	68.74	31.26	0
17	25	-25	0.0755	224	50	-96	52	40	-83	56.68	43.32	0
18	25	0	0.0724	217	51	85	44	40	96	37.17	62.83	0
19	25	25	0.0767	36	39	-85	209	51	-94	26.66	73.34	0
20	25	50	0.0808	21	38	-87	197	52	-92	19.6	80.4	0
21	50	-50	0.0627	225	49	85	53	41	96	77.72	22.28	0
22	50	-25	0.0623	47	40	-85	220	50	-94	52.14	47.86	0
23	50	0	0.0706	219	50	85	46	40	95	53.49	46.51	0
24	50	25	0.0716	213	50	86	40	40	95	40.07	59.93	0
25	50	50	0.0831	140	50	96	311	40	83	73.76	26.24	0

Table C.39: Full-wavefield moment tensor inversion results for location 1b, CLVD input mechanism, 5% anisotropic medium, and dominant source frequency of 125 Hz with a DC constraint applied to the inversion. The bolded row is the location with the highest correlation in the grid search and thus the final ouputted result. Refer to Figure C.5c for visual.

Location Number	X Coord (m)	Y Coord (m)	Correlation	Strike 1 (°)	Dip 1 (°)	Rake 1 (°)	Strike 2 (°)	Dip 2 (°)	Rake 2 (°)	DC %	CLVD %	ISO %
1	-50	-50	0.0605	76	40	106	236	51	77	94.47	5.53	0
2	-50	-25	0.0633	74	40	106	233	52	77	94.61	5.39	0
3	-50	0	0.0776	159	44	95	332	46	85	98.68	1.32	0
4	-50	25	0.1056	272	42	-139	150	64	-55	98.71	1.29	0
5	-50	50	0.1298	325	42	-99	157	48	-82	99.32	0.68	0
6	-25	-50	0.0549	338	45	-93	162	45	-87	98.2	1.8	0
7	-25	-25	0.1066	136	43	-82	305	48	-97	98.59	1.41	0
8	-25	0	0.1261	258	72	-176	166	86	-18	91.34	8.66	0
9	-25	25	0.0971	141	47	105	299	45	74	99.89	0.11	0
10	-25	50	0.0838	311	65	-81	110	27	-109	99.68	0.32	0
11	0	-50	0.0498	229	50	-98	62	40	-80	95.95	4.05	0
12	0	-25	0.1059	258	62	6	165	85	152	96.34	3.66	0
13	0	0	0.0826	279	42	-121	138	55	-65	98.86	1.14	0
14	0	25	0.0674	50	39	-80	217	52	-98	97.93	2.07	0
15	0	50	0.0659	145	52	97	314	38	81	99.73	0.27	0
16	25	-50	0.0523	226	50	-97	58	41	-81	97.74	2.26	0
17	25	-25	0.0752	224	50	-97	55	40	-81	93.15	6.85	0
18	25	0	0.0713	51	40	99	219	51	82	94.21	5.79	0
19	25	25	0.0751	45	39	-82	215	51	-97	92.37	7.63	0
20	25	50	0.0808	21	38	-87	197	52	-92	19.6	80.4	0
21	50	-50	0.0626	225	50	83	55	41	98	90.08	9.92	0
22	50	-25	0.0619	50	40	-83	221	50	-96	99.56	0.44	0
23	50	0	0.07	220	50	85	48	40	96	91.62	8.38	0
24	50	25	0.0704	215	50	84	45	40	97	91.45	8.55	0
25	50	50	0.0809	140	50	96	311	40	83	96.59	3.41	0

Table C.40: Full-wavefield moment tensor inversion results for location 3d, CLVD input mechanism, 5% anisotropic medium, and dominant source frequency of 125 Hz with no constraints applied to the inversion. The bolded row is the location with the highest correlation in the grid search and thus the final ouputted result. Refer to Figure C.5d for visual.

Location Number	X Coord (m)	Y Coord (m)	Correlation	Strike 1 (°)	Dip 1 (°)	Rake 1 (°)	Strike 2 (°)	Dip 2 (°)	Rake 2 (°)	DC %	CLVD %	ISO %
1	-50	-50	0.3935	106	47	-100	301	44	-80	11.81	69.54	18.65
2	-50	-25	0.211	75	44	-90	256	46	-90	36.28	42.98	20.74
3	-50	0	0.0825	90	45	-90	270	45	-90	45.15	19.29	-35.56
4	-50	25	0.0648	315	89	0	225	90	179	6.65	18.17	75.18
5	-50	50	0.0937	65	44	-90	245	46	-90	35.29	42.15	22.56
6	-25	-50	0.4485	103	47	-106	306	45	-74	11.18	79.54	9.28
7	-25	-25	0.1625	79	44	-90	259	46	-90	36.13	41.31	22.56
8	-25	0	0.0572	217	79	11	125	79	168	0.74	31.14	-68.12
9	-25	25	0.0725	83	45	-91	264	45	-89	50.49	45.04	-4.47
10	-25	50	0.089	65	44	-90	246	46	-90	32.95	42.99	24.06
11	0	-50	0.4878	75	63	-146	328	60	-31	1.64	42.87	55.49
12	0	-25	0.2499	267	45	91	86	45	89	33.1	26.82	40.08
13	0	0	0.0495	68	44	-94	253	46	-87	19.4	47.7	-32.9
14	0	25	0.0627	251	46	90	71	44	90	23.91	35.69	-40.4
15	0	50	0.0574	66	44	-91	247	46	-89	30.41	44.44	25.15
16	25	-50	0.4376	101	47	-101	298	44	-78	7.69	23.62	-68.69
17	25	-25	0.3246	267	45	89	88	45	91	18.55	33.38	-48.07
18	25	0	0.118	73	44	-90	253	46	-90	11.7	33.03	55.27
19	25	25	0.0517	256	46	92	73	44	88	25.78	37.86	36.36
20	25	50	0.0195	67	44	-93	251	46	-87	20.73	31.7	-47.57
21	50	-50	0.0677	96	45	95	268	45	85	11.83	0.33	-87.84
22	50	-25	0.0529	257	46	86	83	45	94	12.19	1.36	-86.45
23	50	0	0.0146	257	46	91	75	44	88	44.61	47.48	7.91
24	50	25	0.0426	258	46	99	66	44	81	7.19	25.32	67.49
25	50	50	0.0338	293	85	172	24	82	5	6.17	2.99	90.84

Table C.41: Full-wavefield moment tensor inversion results for location 3d, CLVD input mechanism, 5% anisotropic medium, and dominant source frequency of 125 Hz with a deviatoric constraint applied to the inversion. The bolded row is the location with the highest correlation in the grid search and thus the final ouputted result. Refer to Figure C.5e for visual.

Location Number	X Coord (m)	Y Coord (m)	Correlation	Strike 1 (°)	Dip 1 (°)	Rake 1 (°)	Strike 2 (°)	Dip 2 (°)	Rake 2 (°)	DC %	CLVD %	ISO %
1	-50	-50	0.392	111	46	-94	297	44	-86	33.04	66.96	0
2	-50	-25	0.2088	75	44	-90	255	46	-90	66.01	33.99	0
3	-50	0	0.0795	89	45	-91	270	45	-89	30.19	69.81	0
4	-50	25	0.0505	249	46	90	69	44	90	67.43	32.57	0
5	-50	50	0.0921	64	44	-90	245	46	-90	67.52	32.48	0
6	-25	-50	0.4482	108	47	-99	301	44	-80	20.1	79.9	0
7	-25	-25	0.1597	79	44	-90	259	46	-90	68.73	31.27	0
8	-25	0	0.052	88	45	-90	268	45	-90	79.72	20.28	0
9	-25	25	0.0725	83	45	-91	264	45	-89	49.53	50.47	0
10	-25	50	0.0871	65	44	-90	246	46	-90	66.7	33.3	0
11	0	-50	0.4337	114	46	-92	296	44	-88	82.49	17.51	0
12	0	-25	0.2374	269	45	94	84	45	86	12.79	87.21	0
13	0	0	0.0489	52	47	-117	269	50	-64	3.92	96.08	0
14	0	25	0.0563	250	46	90	70	44	90	88.76	11.24	0
15	0	50	0.0558	66	44	-91	247	46	-89	65.09	34.91	0
16	25	-50	0.3898	240	90	177	330	87	0	89.82	10.18	0
17	25	-25	0.2528	268	45	90	88	45	90	98.72	1.28	0
18	25	0	0.0902	70	44	-90	250	46	-90	89.93	10.07	0
19	25	25	0.0501	260	46	97	69	45	83	10.27	89.73	0
20	25	50	0.0183	25	83	-175	295	85	-7	7.58	92.42	0
21	50	-50	0.0404	179	45	90	359	45	90	41.69	58.31	0
22	50	-25	0.032	182	45	90	1	45	90	39.43	60.57	0
23	50	0	0.0146	257	46	92	75	44	88	43.35	56.65	0
24	50	25	0.0371	299	90	178	29	88	0	64.61	35.39	0
25	50	50	0.0237	344	44	-88	162	46	-92	32.03	67.97	0

Table C.42: Full-wavefield moment tensor inversion results for location 3d, CLVD input mechanism, 5% anisotropic medium, and dominant source frequency of 125 Hz with a DC constraint applied to the inversion. The bolded row is the location with the highest correlation in the grid search and thus the final ouputted result. Refer to Figure C.5f for visual.

Location Number	X Coord (m)	Y Coord (m)	Correlation	Strike 1 (°)	Dip 1 (°)	Rake 1 (°)	Strike 2 (°)	Dip 2 (°)	Rake 2 (°)	DC %	CLVD %	ISO %
1	-50	-50	0.3757	345	89	-1	75	89	-179	95.02	4.98	0
2	-50	-25	0.1998	76	44	-90	255	46	-90	96.15	3.85	0
3	-50	0	0.0646	315	89	0	45	90	-179	98.18	1.82	0
4	-50	25	0.0495	249	46	90	69	44	90	91.72	8.28	0
5	-50	50	0.0882	65	44	-90	245	46	-90	98.26	1.74	0
6	-25	-50	0.4253	72	89	176	162	86	1	96.6	3.4	0
7	-25	-25	0.1511	79	44	-90	259	46	-90	92.91	7.09	0
8	-25	0	0.0506	88	45	-90	268	45	-90	95.14	4.86	0
9	-25	25	0.0653	84	45	-90	264	45	-90	95.83	4.17	0
10	-25	50	0.0832	65	44	-90	245	46	-90	97.7	2.3	0
11	0	-50	0.4304	113	46	-91	295	44	-89	95.54	4.46	0
12	0	-25	0.2374	269	45	94	84	45	86	12.79	87.21	0
13	0	0	0.0434	267	45	90	87	45	90	98.49	1.51	0
14	0	25	0.0561	250	46	90	70	44	90	97.86	2.14	0
15	0	50	0.0531	66	44	-90	246	46	-90	98.22	1.78	0
16	25	-50	0.3898	240	90	177	330	87	0	99.76	0.24	0
17	25	-25	0.2528	268	45	90	88	45	90	99.49	0.51	0
18	25	0	0.0898	70	44	-90	250	46	-90	99.71	0.29	0
19	25	25	0.0417	210	90	0	120	90	180	95.09	4.91	0
20	25	50	0.0177	294	90	-1	24	89	-180	98.55	1.45	0
21	50	-50	0.0393	180	45	90	360	45	90	94.04	5.96	0
22	50	-25	0.0311	180	46	90	359	44	90	93.22	6.78	0
23	50	0	0.0134	255	46	91	74	44	89	92.28	7.72	0
24	50	25	0.037	119	90	-178	29	88	0	91.39	8.61	0
25	50	50	0.0234	343	45	-89	162	45	-91	94.98	5.02	0

Table C.43: Full-wavefield moment tensor inversion results for location 3e, CLVD input mechanism, 5% anisotropic medium, and dominant source frequency of 125 Hz with no constraints applied to the inversion. The bolded row is the location with the highest correlation in the grid search and thus the final ouputted result. Refer to Figure C.5g for visual.

Location Number	X Coord (m)	Y Coord (m)	Correlation	Strike 1 (°)	Dip 1 (°)	Rake 1 (°)	Strike 2 (°)	Dip 2 (°)	Rake 2 (°)	DC %	CLVD %	ISO %
1	-50	-50	0.3067	261	44	91	80	46	89	39.68	40.63	-19.69
2	-50	-25	0.3411	343	83	-178	253	88	-7	43.8	46.33	9.87
3	-50	0	0.159	63	45	-88	240	45	-92	7.49	25.51	67
4	-50	25	0.0801	232	45	90	53	45	90	33.54	33.3	-33.16
5	-50	50	0.0885	47	44	-90	228	46	-90	42.52	44.04	13.44
6	-25	-50	0.0784	79	46	-81	246	45	-99	1.76	27.44	70.8
7	-25	-25	0.4341	301	50	130	69	54	53	6.26	66.39	-27.35
8	-25	0	0.2843	285	44	111	76	49	71	14.12	74.2	-11.68
9	-25	25	0.1244	236	45	91	55	45	89	37.63	49.58	-12.79
10	-25	50	0.1242	49	44	-90	229	46	-90	22.53	31.83	45.64
11	0	-50	0.0852	76	46	-90	256	44	-90	21.78	32.77	45.45
12	0	-25	0.2466	59	44	-89	238	46	-91	14.54	26.85	58.61
13	0	0	0.3757	278	43	108	74	49	74	3.32	29.59	-67.09
14	0	25	0.1517	65	46	-88	242	44	-93	13.86	14.41	71.73
15	0	50	0.0206	232	46	91	50	44	89	37.32	32.11	30.57
16	25	-50	0.078	258	44	91	77	46	89	42.54	51.7	-5.76
17	25	-25	0.0807	242	47	98	50	44	81	6.61	13.39	80
18	25	0	0.0606	244	44	85	71	46	95	11.39	0.53	-88.08
19	25	25	0.0097	130	53	-90	309	37	-91	0.37	2.18	97.45
20	25	50	0.024	227	46	87	52	44	93	18.15	0.08	-81.77
21	50	-50	0.0251	80	46	-91	261	44	-89	19.87	37.76	42.37
22	50	-25	0.008	240	46	86	65	44	94	13.9	5.01	-81.09
23	50	0	0.0045	239	46	87	63	44	93	15.88	11.04	-73.08
24	50	25	0.002	235	46	92	53	44	88	37.19	46.88	-15.93
25	50	50	0.0133	231	45	86	56	45	94	10.22	4.67	-85.11

Table C.44: Full-wavefield moment tensor inversion results for location 3e, CLVD input mechanism, 5% anisotropic medium, and dominant source frequency of 125 Hz with a deviatoric constraint applied to the inversion. The bolded row is the location with the highest correlation in the grid search and thus the final ouputted result. Refer to Figure C.5h for visual.

Location Number	X Coord (m)	Y Coord (m)	Correlation	Strike 1 (°)	Dip 1 (°)	Rake 1 (°)	Strike 2 (°)	Dip 2 (°)	Rake 2 (°)	DC %	CLVD %	ISO %
1	-50	-50	0.3036	261	44	90	80	46	90	69.35	30.65	0
2	-50	-25	0.341	343	82	-177	252	87	-8	38.28	61.72	0
3	-50	0	0.1164	326	79	174	57	84	11	31	69	0
4	-50	25	0.0741	232	45	90	52	45	90	88.35	11.65	0
5	-50	50	0.0879	47	44	-90	228	46	-90	61.28	38.72	0
6	-25	-50	0.059	340	83	177	70	87	7	60.04	39.96	0
7	-25	-25	0.4305	90	47	82	282	43	99	34.3	65.7	0
8	-25	0	0.284	280	43	103	82	48	78	25.33	74.67	0
9	-25	25	0.1235	235	45	90	55	45	89	54.75	45.25	0
10	-25	50	0.1014	47	44	-90	227	46	-90	95.52	4.48	0
11	0	-50	0.0732	246	45	90	66	45	90	74.06	25.94	0
12	0	-25	0.2094	242	45	90	62	45	90	80.6	19.4	0
13	0	0	0.2942	96	47	88	278	44	92	73.12	26.88	0
14	0	25	0.0854	69	45	-90	249	45	-90	21.14	78.86	0
15	0	50	0.0201	233	46	92	50	44	88	28.23	71.77	0
16	25	-50	0.0779	258	44	91	77	46	89	49.97	50.03	0
17	25	-25	0.0624	107	86	-175	16	85	-4	27.52	72.48	0
18	25	0	0.0378	155	45	90	335	45	90	42.81	57.19	0
19	25	25	0.0062	332	45	-90	152	45	-90	99.06	0.94	0
20	25	50	0.0152	159	46	91	338	45	89	45.23	54.77	0
21	50	-50	0.0216	82	46	-90	263	44	-89	89.86	10.14	0
22	50	-25	0.0048	174	45	91	354	45	89	25.84	74.16	0
23	50	0	0.0026	207	46	90	27	44	90	15.14	84.86	0
24	50	25	0.002	235	46	91	52	44	88	57.81	42.19	0
25	50	50	0.0085	155	45	91	333	45	89	75.02	24.98	0

Table C.45: Full-wavefield moment tensor inversion results for location 3e, CLVD input mechanism, 5% anisotropic medium, and dominant source frequency of 125 Hz with a DC constraint applied to the inversion. The bolded row is the location with the highest correlation in the grid search and thus the final ouputted result. Refer to Figure C.5i for visual.

Location Number	X Coord (m)	Y Coord (m)	Correlation	Strike 1 (°)	Dip 1 (°)	Rake 1 (°)	Strike 2 (°)	Dip 2 (°)	Rake 2 (°)	DC %	CLVD %	ISO %
1	-50	-50	0.2988	260	44	90	80	46	90	93.29	6.71	0
2	-50	-25	0.3398	340	84	179	70	89	6	94.17	5.83	0
3	-50	0	0.1161	329	83	179	59	89	7	92.74	7.26	0
4	-50	25	0.0739	232	45	90	52	45	90	95.9	4.1	0
5	-50	50	0.082	47	44	-90	227	46	-90	98.32	1.68	0
6	-25	-50	0.0589	342	84	179	72	89	6	95.76	4.24	0
7	-25	-25	0.4206	328	84	180	58	90	6	95.89	4.11	0
8	-25	0	0.2755	139	87	180	229	90	3	91.5	8.5	0
9	-25	25	0.114	235	45	90	55	45	90	98.34	1.66	0
10	-25	50	0.1014	47	44	-90	227	46	-90	97.67	2.33	0
11	0	-50	0.071	245	45	90	65	45	90	99.91	0.09	0
12	0	-25	0.206	242	45	90	62	45	90	99.24	0.76	0
13	0	0	0.2901	99	47	87	283	43	93	94.22	5.78	0
14	0	25	0.0854	69	45	-90	249	45	-90	21.14	78.86	0
15	0	50	0.0175	231	46	91	51	44	89	93.73	6.27	0
16	25	-50	0.0734	258	44	90	78	46	90	91.59	8.41	0
17	25	-25	0.0619	107	89	-177	17	87	-1	95.53	4.47	0
18	25	0	0.0369	155	46	90	335	44	90	93.47	6.53	0
19	25	25	0.0062	332	45	-90	152	45	-90	99.06	0.94	0
20	25	50	0.015	156	46	91	334	44	89	96.87	3.13	0
21	50	-50	0.0215	83	46	-90	263	44	-90	99.76	0.24	0
22	50	-25	0.0046	167	46	91	345	44	89	95.69	4.31	0
23	50	0	0.0023	163	45	83	352	45	97	99.06	0.94	0
24	50	25	0.0019	234	46	91	53	44	89	97.31	2.69	0
25	50	50	0.0085	154	46	91	333	44	89	90.5	9.5	0

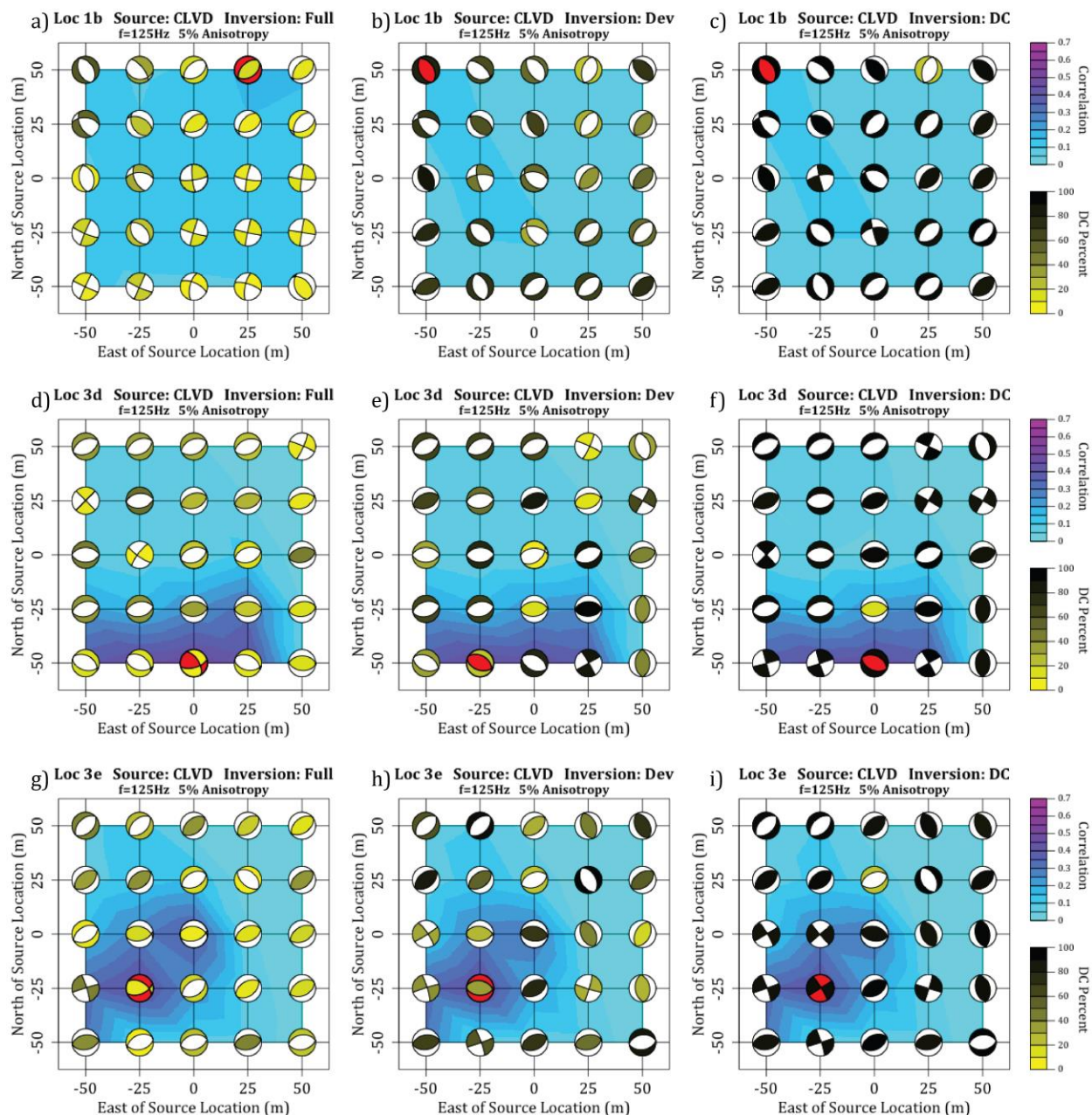


Figure C.5: Full-wavefield moment tensor inversion results for a CLVD source mechanism in a 5% anisotropic medium and source frequency of 125 Hz for a) location 1b with no constraints on the inversion, b) location 1b with a deviatoric constraint, c) location 1b with a DC constraint, d) location 3d with no constraints, e) location 3d with a deviatoric constraint, f) location 3d with a DC constraint, g) location 3e with no constraints, h) location 3e with a deviatoric constraint, and i) location 3e with a DC constraint. The red beach-ball is the location and source mechanism with the highest correlation to the input seismograms. Refer to Tables C.37-C.45 for numerical values of results.

Table C.46: Full-wavefield moment tensor inversion results for location 1b, ISO input mechanism, 5% anisotropic medium, and dominant source frequency of 125 Hz with no constraints applied to the inversion. The bolded row is the location with the highest correlation in the grid search and thus the final ouputted result. Refer to Figure C.6a for visual.

Location Number	X Coord (m)	Y Coord (m)	Correlation	Strike 1 (°)	Dip 1 (°)	Rake 1 (°)	Strike 2 (°)	Dip 2 (°)	Rake 2 (°)	DC %	CLVD %	ISO %
1	-50	-50	0.1129	112	83	-179	22	89	-7	4.59	17.63	77.78
2	-50	-25	0.1278	201	86	-169	110	79	-4	13.47	2.63	-83.9
3	-50	0	0.1606	210	63	-138	98	53	-34	6.77	6.28	-86.95
4	-50	25	0.1627	223	54	-110	75	41	-65	15.07	3.53	-81.4
5	-50	50	0.211	326	43	-98	157	47	-82	60.08	24.9	15.02
6	-25	-50	0.1436	199	89	-175	109	85	-1	6.34	12.65	-81.01
7	-25	-25	0.176	104	78	175	195	85	12	12.89	1.05	86.06
8	-25	0	0.1866	87	49	138	207	59	49	5.41	5.92	88.67
9	-25	25	0.1607	59	39	107	217	53	76	13.54	5.78	80.68
10	-25	50	0.1439	214	53	79	52	38	104	12.07	10.06	77.87
11	0	-50	0.0463	286	83	-169	194	79	-7	0.67	17.4	81.93
12	0	-25	0.1796	191	87	-171	100	81	-3	10.48	2.15	-87.37
13	0	0	0.1485	209	54	-118	72	44	-57	6.2	5.29	-88.51
14	0	25	0.114	56	40	-70	211	52	-106	12.09	1.5	-86.41
15	0	50	0.0938	211	52	80	46	39	102	11.95	8.1	79.95
16	25	-50	0.016	279	90	-175	189	85	0	1.25	15.55	83.2
17	25	-25	0.0889	184	87	-171	94	81	-3	12.23	0.46	-87.31
18	25	0	0.1202	89	69	164	184	75	22	3.81	5.2	90.99
19	25	25	0.0757	51	41	-73	209	51	-104	11.16	1.37	-87.47
20	25	50	0.0593	40	39	-77	203	52	-101	14.59	0.35	-85.06
21	50	-50	2.00E-04	320	47	-94	146	43	-85	10.65	21.85	67.5
22	50	-25	0.0174	90	85	179	180	89	5	3.13	10.82	86.05
23	50	0	0.0685	88	75	170	180	81	15	5.28	4.15	90.57
24	50	25	0.042	188	72	-156	90	67	-20	2.24	6.57	-91.19
25	50	50	0.0362	59	43	-74	218	49	-104	4.65	5.74	-89.61

Table C.47: Full-wavefield moment tensor inversion results for location 1b, ISO input mechanism, 5% anisotropic medium, and dominant source frequency of 125 Hz with a deviatoric constraint applied to the inversion. The bolded row is the location with the highest correlation in the grid search and thus the final ouputted result. Refer to Figure C.6b for visual.

Location Number	X Coord (m)	Y Coord (m)	Correlation	Strike 1 (°)	Dip 1 (°)	Rake 1 (°)	Strike 2 (°)	Dip 2 (°)	Rake 2 (°)	DC %	CLVD %	ISO %
1	-50	-50	0.0592	242	50	-103	82	42	-75	67.6	32.4	0
2	-50	-25	0.065	76	41	103	239	51	79	92.42	7.58	0
3	-50	0	0.0749	74	40	103	238	51	79	53.7	46.3	0
4	-50	25	0.0693	77	41	104	239	51	78	35.43	64.57	0
5	-50	50	0.2089	326	43	-98	157	48	-82	82.95	17.05	0
6	-25	-50	0.0768	72	41	101	237	50	81	83.24	16.76	0
7	-25	-25	0.089	239	50	-99	72	41	-80	75.65	24.35	0
8	-25	0	0.089	238	50	-99	72	41	-79	52.75	47.25	0
9	-25	25	0.0725	241	50	-101	78	41	-77	46.08	53.92	0
10	-25	50	0.0594	255	48	-103	93	44	-76	21.67	78.33	0
11	0	-50	0.0264	235	50	-97	66	41	-82	99.2	0.8	0
12	0	-25	0.097	66	41	98	235	50	83	73.67	26.33	0
13	0	0	0.076	67	41	99	236	50	82	56.49	43.51	0
14	0	25	0.0556	73	41	100	239	49	81	34.35	65.65	0
15	0	50	0.0417	245	49	-99	78	42	-80	21.58	78.42	0
16	25	-50	0.0093	63	41	-83	234	49	-96	99.57	0.43	0
17	25	-25	0.0475	236	49	84	65	41	97	68.64	31.36	0
18	25	0	0.0618	233	49	-96	63	41	-83	47.61	52.39	0
19	25	25	0.0397	62	41	98	232	50	83	41.55	58.45	0
20	25	50	0.0297	77	42	99	245	48	82	24.7	75.3	0
21	50	-50	1.00E-04	314	45	-95	142	46	-85	9.23	90.77	0
22	50	-25	0.01	59	41	-85	232	49	-95	67.03	32.97	0
23	50	0	0.0362	56	41	-85	229	49	-95	49.87	50.13	0
24	50	25	0.0208	207	50	88	31	40	93	21.3	78.7	0
25	50	50	0.0185	191	51	89	12	39	91	17.79	82.21	0

Table C.48: Full-wavefield moment tensor inversion results for location 1b, ISO input mechanism, 5% anisotropic medium, and dominant source frequency of 125 Hz with a DC constraint applied to the inversion. The bolded row is the location with the highest correlation in the grid search and thus the final ouputted result. Refer to Figure C.6c for visual.

Location Number	X Coord (m)	Y Coord (m)	Correlation	Strike 1 (°)	Dip 1 (°)	Rake 1 (°)	Strike 2 (°)	Dip 2 (°)	Rake 2 (°)	DC %	CLVD %	ISO %
1	-50	-50	0.0592	244	50	-101	80	41	-78	95.77	4.23	0
2	-50	-25	0.065	77	41	103	239	51	79	99.4	0.6	0
3	-50	0	0.0746	73	40	102	238	51	80	93.41	6.59	0
4	-50	25	0.0687	76	41	108	233	52	75	96.71	3.29	0
5	-50	50	0.2024	325	42	-99	156	48	-82	99.35	0.65	0
6	-25	-50	0.0768	71	41	100	238	50	81	96.75	3.25	0
7	-25	-25	0.0889	238	50	-100	72	41	-79	96.18	3.82	0
8	-25	0	0.0886	235	51	-101	71	41	-77	98.02	1.98	0
9	-25	25	0.072	235	51	-102	74	41	-76	96.47	3.53	0
10	-25	50	0.0578	72	41	106	231	51	77	97.05	2.95	0
11	0	-50	0.0264	235	50	-97	66	41	-82	99.2	0.8	0
12	0	-25	0.0969	66	41	100	233	50	82	96.38	3.62	0
13	0	0	0.0756	67	41	101	232	50	80	91.44	8.56	0
14	0	25	0.0546	64	40	99	233	50	83	94.45	5.55	0
15	0	50	0.0417	245	49	-99	78	42	-80	21.58	78.42	0
16	25	-50	0.0093	63	41	-83	234	49	-96	99.57	0.43	0
17	25	-25	0.0474	234	49	83	64	41	98	91.39	8.61	0
18	25	0	0.0614	230	50	-97	61	41	-82	90.84	9.16	0
19	25	25	0.0392	58	41	98	228	50	83	98.33	1.67	0
20	25	50	0.0285	231	50	86	56	40	94	95.2	4.8	0
21	50	-50	1.00E-04	314	45	-95	142	46	-85	9.23	90.77	0
22	50	-25	0.01	59	41	-84	231	49	-95	93.4	6.6	0
23	50	0	0.036	55	41	-84	227	49	-95	94.55	5.45	0
24	50	25	0.0201	215	50	87	41	40	94	96.52	3.48	0
25	50	50	0.0176	211	51	91	30	40	89	97.55	2.45	0

Table C.49: Full-wavefield moment tensor inversion results for location 3d, ISO input mechanism, 5% anisotropic medium, and dominant source frequency of 125 Hz with no constraints applied to the inversion. The bolded row is the location with the highest correlation in the grid search and thus the final ouputted result. Refer to Figure C.6d for visual.

Location Number	X Coord (m)	Y Coord (m)	Correlation	Strike 1 (°)	Dip 1 (°)	Rake 1 (°)	Strike 2 (°)	Dip 2 (°)	Rake 2 (°)	DC %	CLVD %	ISO %
1	-50	-50	0.2389	25	45	-90	206	45	-90	4.2	18.07	-77.73
2	-50	-25	0.1702	323	45	-89	141	45	-91	14.29	5.48	-80.23
3	-50	0	0.0796	154	45	88	336	45	92	9.06	4.46	86.48
4	-50	25	0.0906	149	44	88	332	46	92	3.74	5.37	90.89
5	-50	50	0.0406	220	85	-5	311	85	-175	4.91	4.84	-90.25
6	-25	-50	0.451	179	43	89	0	47	91	2.86	2.85	94.29
7	-25	-25	0.1418	219	44	95	32	46	85	5.24	2.69	92.07
8	-25	0	0.0792	24	88	-3	114	87	-178	3.59	6.58	-89.83
9	-25	25	0.0439	316	84	-173	226	83	-6	2.96	5.11	-91.93
10	-25	50	0.0574	106	88	-1	196	89	-178	10.65	0.59	88.76
11	0	-50	0.3653	203	45	116	348	51	66	0.26	3.85	95.89
12	0	-25	0.2543	125	57	36	13	60	141	0.51	4.21	95.28
13	0	0	0.0486	98	45	72	303	47	107	2.79	1.83	95.38
14	0	25	0.0345	319	77	-165	225	75	-13	1.5	4.91	-93.59
15	0	50	0.0329	110	86	177	200	87	4	5.21	10.65	-84.14
16	25	-50	0.5491	227	77	14	134	77	166	2.28	5.96	-91.76
17	25	-25	0.2486	125	83	178	215	88	7	3.44	1.41	-95.15
18	25	0	0.1107	213	64	-148	108	61	-30	1.09	12.59	86.32
19	25	25	0.0506	73	44	-79	238	47	-101	4.74	8	87.26
20	25	50	0.0239	240	46	84	69	44	96	8.19	7.77	-84.04
21	50	-50	0.123	96	45	95	268	45	85	12.7	0.28	-87.02
22	50	-25	0.0911	258	45	86	85	45	94	11.1	1.84	-87.06
23	50	0	0.0133	118	88	1	28	89	178	10.85	17.66	71.49
24	50	25	0.0647	74	44	-84	246	46	-96	9.03	10.09	80.88
25	50	50	0.0607	70	44	-85	244	46	-95	12.13	7.34	80.53

Table C.50: Full-wavefield moment tensor inversion results for location 3d, ISO input mechanism, 5% anisotropic medium, and dominant source frequency of 125 Hz with a deviatoric constraint applied to the inversion. The bolded row is the location with the highest correlation in the grid search and thus the final ouputted result. Refer to Figure C.6e for visual.

Location Number	X Coord (m)	Y Coord (m)	Correlation	Strike 1 (°)	Dip 1 (°)	Rake 1 (°)	Strike 2 (°)	Dip 2 (°)	Rake 2 (°)	DC %	CLVD %	ISO %
1	-50	-50	0.1078	169	46	90	349	44	90	39.48	60.52	0
2	-50	-25	0.0908	209	46	90	29	44	90	55.27	44.73	0
3	-50	0	0.0396	45	44	-90	225	46	-90	30.22	69.78	0
4	-50	25	0.0479	31	44	-90	211	46	-90	22.28	77.72	0
5	-50	50	0.0218	106	45	90	286	45	90	25.39	74.61	0
6	-25	-50	0.247	1	44	-90	181	46	-90	17.41	82.59	0
7	-25	-25	0.0853	347	44	-90	167	46	-90	41.24	58.76	0
8	-25	0	0.0406	230	46	90	51	44	90	28.95	71.05	0
9	-25	25	0.0231	126	45	90	306	45	90	21.76	78.24	0
10	-25	50	0.0304	30	44	-90	210	46	-90	20.6	79.4	0
11	0	-50	0.195	356	45	-90	176	45	-90	26.82	73.18	0
12	0	-25	0.1407	11	44	-90	192	46	-90	32.86	67.14	0
13	0	0	0.0312	358	44	-91	179	46	-89	68.36	31.64	0
14	0	25	0.0184	187	46	90	7	44	90	25.33	74.67	0
15	0	50	0.0172	215	46	90	35	44	90	20.36	79.64	0
16	25	-50	0.3026	180	45	90	0	45	90	31.54	68.46	0
17	25	-25	0.1368	181	45	90	0	45	90	44.81	55.19	0
18	25	0	0.0624	18	44	-91	199	46	-89	26.73	73.27	0
19	25	25	0.0301	4	44	-91	185	46	-89	33.11	66.89	0
20	25	50	0.0141	184	46	91	3	44	89	26.84	73.16	0
21	50	-50	0.0731	179	45	90	359	45	90	38.3	61.7	0
22	50	-25	0.0553	180	45	90	360	45	90	41.39	58.61	0
23	50	0	0.0073	63	44	-91	244	46	-89	76.73	23.27	0
24	50	25	0.0362	13	44	-91	194	46	-89	25.63	74.37	0
25	50	50	0.0349	4	44	-91	185	46	-89	28.74	71.26	0

Table C.51: Full-wavefield moment tensor inversion results for location 3d, ISO input mechanism, 5% anisotropic medium, and dominant source frequency of 125 Hz with a DC constraint applied to the inversion. The bolded row is the location with the highest correlation in the grid search and thus the final ouputted result. Refer to Figure C.6f for visual.

Location Number	X Coord (m)	Y Coord (m)	Correlation	Strike 1 (°)	Dip 1 (°)	Rake 1 (°)	Strike 2 (°)	Dip 2 (°)	Rake 2 (°)	DC %	CLVD %	ISO %
1	-50	-50	0.1049	173	46	90	354	44	90	95.61	4.39	0
2	-50	-25	0.0891	202	46	91	21	44	89	92.27	7.73	0
3	-50	0	0.0358	20	44	-90	200	46	-90	95.56	4.44	0
4	-50	25	0.0434	10	44	-91	191	46	-89	97.48	2.52	0
5	-50	50	0.0218	106	45	90	286	45	90	25.39	74.61	0
6	-25	-50	0.247	1	44	-90	181	46	-90	17.41	82.59	0
7	-25	-25	0.0836	350	44	-90	170	46	-90	95.61	4.39	0
8	-25	0	0.0328	205	45	87	29	45	93	99.4	0.6	0
9	-25	25	0.0212	152	46	90	331	44	90	99.67	0.33	0
10	-25	50	0.0277	0	44	-90	181	46	-90	96.39	3.61	0
11	0	-50	0.195	356	45	-90	176	45	-90	26.82	73.18	0
12	0	-25	0.1407	11	44	-90	192	46	-90	32.86	67.14	0
13	0	0	0.0311	357	44	-91	178	46	-89	94.21	5.79	0
14	0	25	0.0184	187	46	90	7	44	90	25.33	74.67	0
15	0	50	0.0172	215	46	90	35	44	90	20.36	79.64	0
16	25	-50	0.2914	180	46	90	0	44	90	93.63	6.37	0
17	25	-25	0.134	180	46	90	359	44	90	93.4	6.6	0
18	25	0	0.0624	18	44	-91	199	46	-89	26.73	73.27	0
19	25	25	0.0301	4	44	-91	185	46	-89	33.11	66.89	0
20	25	50	0.0141	184	46	91	3	44	89	26.84	73.16	0
21	50	-50	0.0709	180	45	90	360	45	90	94.6	5.4	0
22	50	-25	0.0537	179	45	90	359	45	90	93.36	6.64	0
23	50	0	0.0072	61	44	-91	243	46	-89	96.01	3.99	0
24	50	25	0.0362	13	44	-91	194	46	-89	25.63	74.37	0
25	50	50	0.0349	4	44	-91	185	46	-89	28.74	71.26	0

Table C.52: Full-wavefield moment tensor inversion results for location 3e, ISO input mechanism, 5% anisotropic medium, and dominant source frequency of 125 Hz with no constraints applied to the inversion. The bolded row is the location with the highest correlation in the grid search and thus the final ouputted result. Refer to Figure C.6g for visual.

Location Number	X Coord (m)	Y Coord (m)	Correlation	Strike 1 (°)	Dip 1 (°)	Rake 1 (°)	Strike 2 (°)	Dip 2 (°)	Rake 2 (°)	DC %	CLVD %	ISO %
1	-50	-50	0.3051	180	45	93	356	45	87	9.13	4.62	86.25
2	-50	-25	0.1293	334	46	-92	157	44	-88	7.12	0.63	-92.25
3	-50	0	0.2301	133	44	86	318	46	94	3.03	4.13	92.84
4	-50	25	0.0706	298	84	-173	207	83	-6	6.21	2.18	-91.61
5	-50	50	0.0624	183	67	-153	81	66	-26	1.07	9.15	89.78
6	-25	-50	0.1787	195	47	116	339	49	65	1.43	5.33	93.24
7	-25	-25	0.3507	104	84	-6	195	84	-174	3.38	2.81	93.81
8	-25	0	0.441	289	89	-174	199	84	-1	2.71	2.44	-94.85
9	-25	25	0.1116	242	43	73	85	49	106	1.15	12.13	-86.72
10	-25	50	0.0928	59	46	-72	214	47	-108	2.34	13.35	84.31
11	0	-50	0.106	220	86	180	310	90	4	5.43	6.8	87.77
12	0	-25	0.3446	209	68	-160	111	71	-23	1.38	4.85	93.77
13	0	0	0.5148	108	83	171	199	81	7	2.99	5.61	-91.4
14	0	25	0.2665	60	45	-80	226	46	-100	5.58	4.35	90.07
15	0	50	0.0149	94	88	1	4	89	178	10.99	17.92	71.09
16	25	-50	0.0614	95	49	-73	250	44	-109	1.46	16.03	82.51
17	25	-25	0.1849	91	48	-80	256	42	-101	3.63	6.16	90.21
18	25	0	0.1282	245	44	85	71	46	94	12.86	0.25	-86.89
19	25	25	0.0057	233	45	86	59	45	94	15.04	1.36	-83.6
20	25	50	2.00E-04	220	46	87	45	44	93	13.6	1.92	-84.48
21	50	-50	0.0284	88	47	-81	256	44	-99	3.19	19.06	77.75
22	50	-25	0.0147	257	44	87	82	47	93	15.26	2.32	-82.42
23	50	0	5.00E-04	235	46	87	60	44	93	15.4	2.76	-81.84
24	50	25	7.00E-04	66	45	-86	240	45	-94	16.63	0.17	83.2
25	50	50	3.00E-04	242	44	87	66	46	92	21.97	0.23	-77.8

Table C.53: Full-wavefield moment tensor inversion results for location 3e, ISO input mechanism, 5% anisotropic medium, and dominant source frequency of 125 Hz with a deviatoric constraint applied to the inversion. The bolded row is the location with the highest correlation in the grid search and thus the final ouputted result. Refer to Figure C.6h for visual.

Location Number	X Coord (m)	Y Coord (m)	Correlation	Strike 1 (°)	Dip 1 (°)	Rake 1 (°)	Strike 2 (°)	Dip 2 (°)	Rake 2 (°)	DC %	CLVD %	ISO %
1	-50	-50	0.167	319	45	-90	139	45	-90	23.97	76.03	0
2	-50	-25	0.0738	154	45	90	334	45	90	20	80	0
3	-50	0	0.1278	348	44	-90	169	46	-90	26.44	73.56	0
4	-50	25	0.0405	123	46	90	304	44	90	27.26	72.74	0
5	-50	50	0.0377	336	44	-91	157	46	-89	32.38	67.62	0
6	-25	-50	0.1004	132	46	-90	313	44	-90	23.92	76.08	0
7	-25	-25	0.2101	342	45	-90	163	45	-90	22.59	77.41	0
8	-25	0	0.2499	151	45	90	331	45	90	29.03	70.97	0
9	-25	25	0.0674	126	46	90	307	44	90	28.66	71.34	0
10	-25	50	0.0536	346	44	-91	167	46	-89	24.39	75.61	0
11	0	-50	0.0603	126	46	-90	307	44	-90	21.56	78.44	0
12	0	-25	0.2055	336	45	-90	156	45	-90	34.97	65.03	0
13	0	0	0.2908	155	45	90	335	45	90	32.4	67.6	0
14	0	25	0.1616	335	45	-91	156	45	-89	44.85	55.15	0
15	0	50	0.008	38	44	-91	218	46	-89	66.71	33.29	0
16	25	-50	0.0349	122	46	-90	302	44	-90	20.49	79.51	0
17	25	-25	0.1124	330	45	-89	149	45	-91	43.36	56.64	0
18	25	0	0.0795	154	45	90	334	45	90	38.41	61.59	0
19	25	25	0.0035	159	45	91	339	45	89	37.32	62.68	0
20	25	50	1.00E-04	161	45	91	339	45	89	60.79	39.21	0
21	50	-50	0.0156	112	46	-90	292	44	-90	22.4	77.6	0
22	50	-25	0.009	148	45	90	329	45	90	32.51	67.49	0
23	50	0	3.00E-04	169	45	91	347	45	89	37.33	62.67	0
24	50	25	4.00E-04	334	45	-90	155	45	-90	48.84	51.16	0
25	50	50	2.00E-04	147	45	90	327	45	90	38.69	61.31	0

Table C.54: Full-wavefield moment tensor inversion results for location 3e, ISO input mechanism, 5% anisotropic medium, and dominant source frequency of 125 Hz with a DC constraint applied to the inversion. The bolded row is the location with the highest correlation in the grid search and thus the final ouputted result. Refer to Figure C.6i for visual.

Location Number	X Coord (m)	Y Coord (m)	Correlation	Strike 1 (°)	Dip 1 (°)	Rake 1 (°)	Strike 2 (°)	Dip 2 (°)	Rake 2 (°)	DC %	CLVD %	ISO %
1	-50	-50	0.167	319	45	-90	139	45	-90	23.97	76.03	0
2	-50	-25	0.0738	154	45	90	334	45	90	20	80	0
3	-50	0	0.1278	348	44	-90	169	46	-90	26.44	73.56	0
4	-50	25	0.0389	136	46	90	317	44	90	96.43	3.57	0
5	-50	50	0.0377	336	44	-91	157	46	-89	32.38	67.62	0
6	-25	-50	0.1004	132	46	-90	313	44	-90	23.92	76.08	0
7	-25	-25	0.2101	342	45	-90	163	45	-90	22.59	77.41	0
8	-25	0	0.2416	152	46	90	332	44	90	97.06	2.94	0
9	-25	25	0.0674	126	46	90	307	44	90	28.66	71.34	0
10	-25	50	0.0536	346	44	-91	167	46	-89	24.39	75.61	0
11	0	-50	0.0603	126	46	-90	307	44	-90	21.56	78.44	0
12	0	-25	0.2004	337	44	-90	157	46	-90	99.77	0.23	0
13	0	0	0.2813	155	46	90	334	44	90	91.22	8.78	0
14	0	25	0.1598	334	44	-91	155	46	-89	91.21	8.79	0
15	0	50	0.0078	34	43	-91	216	47	-89	93.13	6.87	0
16	25	-50	0.0349	122	46	-90	302	44	-90	20.49	79.51	0
17	25	-25	0.1109	333	44	-89	152	46	-91	90.45	9.55	0
18	25	0	0.0774	155	46	90	335	44	90	94.05	5.95	0
19	25	25	0.0034	157	46	91	335	44	89	94.77	5.23	0
20	25	50	1.00E-04	159	46	92	336	45	88	98.71	1.29	0
21	50	-50	0.0142	326	45	-90	146	45	-90	98.78	1.22	0
22	50	-25	0.0088	154	46	90	335	44	90	99.87	0.13	0
23	50	0	3.00E-04	163	45	91	342	45	89	95.31	4.69	0
24	50	25	4.00E-04	334	45	-91	155	45	-89	90.59	9.41	0
25	50	50	1.00E-04	149	45	90	329	45	90	92.01	7.99	0

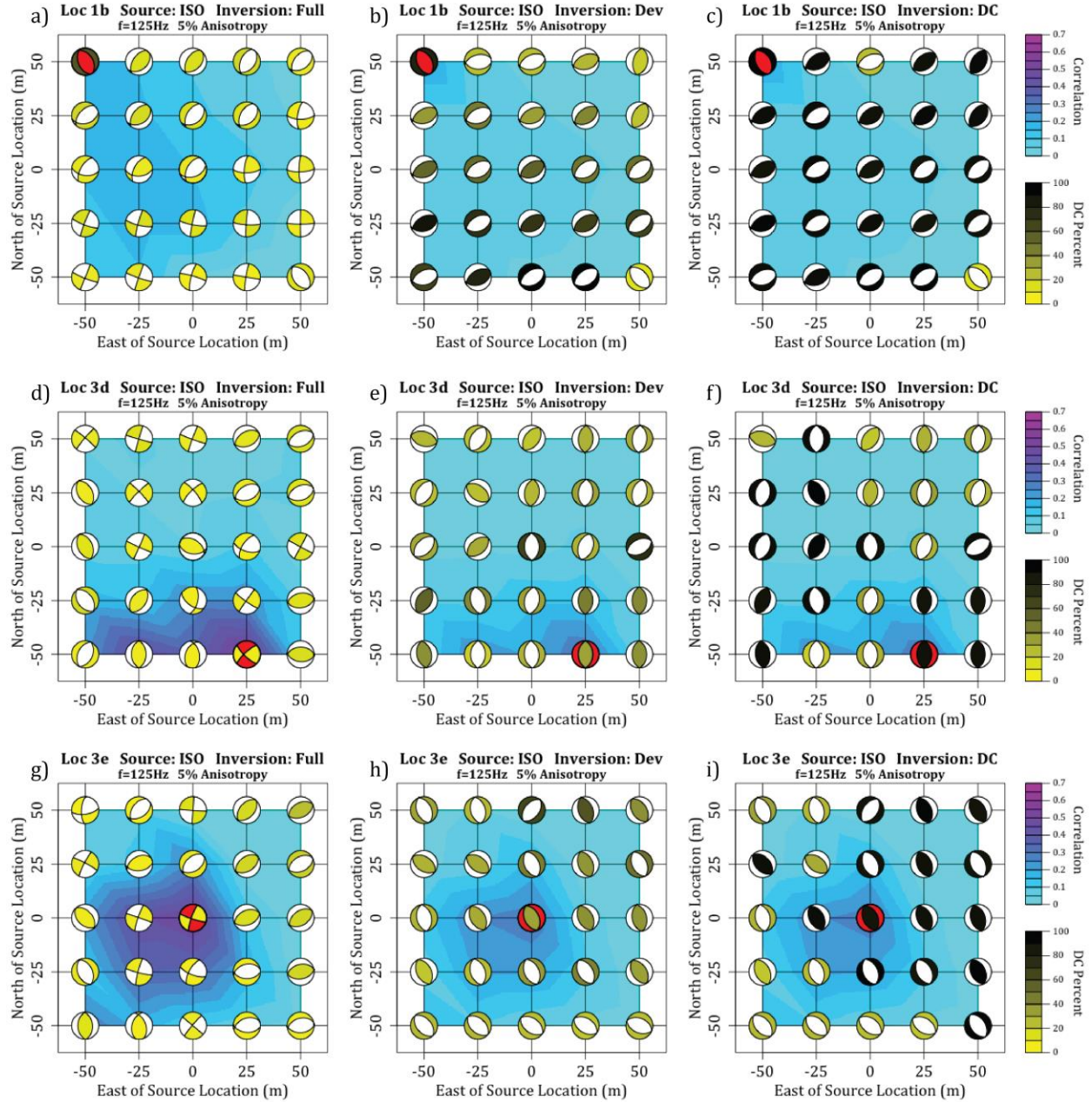


Figure C.6: Full-wavefield moment tensor inversion results for an ISO source mechanism in a 5% anisotropic medium and source frequency of 125 Hz for a) location 1b with no constraints on the inversion, b) location 1b with a deviatoric constraint, c) location 1b with a DC constraint, d) location 3d with no constraints, e) location 3d with a deviatoric constraint, f) location 3d with a DC constraint, g) location 3e with no constraints, h) location 3e with a deviatoric constraint, and i) location 3e with a DC constraint. The red beach-ball is the location and source mechanism with the highest correlation to the input seismograms. Refer to Tables C.46-C.54 for numerical values of results.

Table C.55: Full-wavefield moment tensor inversion results for location 1b, DC input mechanism, isotropic medium, dominant source frequency of 125 Hz, and 5% noise with no constraints applied to the inversion. The bolded row is the location with the highest correlation in the grid search and thus the final ouputted result. Refer to Figure C.7a for visual.

Location Number	X Coord (m)	Y Coord (m)	Correlation	Strike 1 (°)	Dip 1 (°)	Rake 1 (°)	Strike 2 (°)	Dip 2 (°)	Rake 2 (°)	DC %	CLVD %	ISO %
1	-50	-50	0.1497	327	45	-98	159	46	-82	58.34	26.67	14.99
2	-50	-25	0.1829	323	45	-99	156	46	-81	64.25	20.04	15.71
3	-50	0	0.2188	313	46	-101	148	45	-79	83.27	12.5	4.23
4	-50	25	0.214	307	47	-103	146	45	-77	64.53	23.22	12.25
5	-50	50	0.2153	145	43	104	306	48	77	42.07	33.51	-24.42
6	-25	-50	0.1951	321	46	-98	152	45	-82	66.04	22.24	11.72
7	-25	-25	0.2454	312	47	-98	144	43	-82	61.06	22.33	16.61
8	-25	0	0.2244	312	47	-99	144	43	-81	49.9	31.74	18.36
9	-25	25	0.1697	309	50	82	141	41	99	24.65	43.76	-31.59
10	-25	50	0.1323	307	48	80	141	43	100	51.49	28.43	-20.08
11	0	-50	0.0621	287	87	178	17	88	3	6.67	13.75	79.58
12	0	-25	0.1999	314	47	-97	144	43	-83	34.33	37.32	28.35
13	0	0	0.1299	309	48	82	141	42	98	25.39	49.07	-25.54
14	0	25	0.1007	142	43	98	310	47	82	45.8	30.59	-23.61
15	0	50	0.0855	136	43	-80	302	48	-100	57.09	27.02	15.89
16	25	-50	0.0725	186	57	149	294	65	37	1.45	17.79	-80.76
17	25	-25	0.1044	313	47	-97	143	44	-82	32.31	39.56	28.13
18	25	0	0.0907	73	46	120	212	51	62	7.16	2.63	90.21
19	25	25	0.0842	62	42	104	224	49	78	15.65	0.57	83.78
20	25	50	0.1046	59	42	-80	225	49	-99	14.49	0.43	-85.08
21	50	-50	0.0812	293	67	41	184	53	150	1.81	11.69	-86.5
22	50	-25	0.094	188	89	-1	278	89	-179	8.23	3.32	88.45
23	50	0	0.0996	187	86	-173	96	83	-4	10.24	1.93	-87.83
24	50	25	0.1023	70	46	123	207	53	61	4.18	4.71	91.11
25	50	50	0.0978	221	49	80	55	42	101	9.81	6.65	83.54

Table C.56: Full-wavefield moment tensor inversion results for location 1b, DC input mechanism, isotropic medium, dominant source frequency of 125 Hz, and 5% noise with a deviatoric constraint applied to the inversion. The bolded row is the location with the highest correlation in the grid search and thus the final outpitted result. Refer to Figure C.7b for visual.

Location Number	X Coord (m)	Y Coord (m)	Correlation	Strike 1 (°)	Dip 1 (°)	Rake 1 (°)	Strike 2 (°)	Dip 2 (°)	Rake 2 (°)	DC %	CLVD %	ISO %
1	-50	-50	0.1467	327	44	-98	158	46	-82	81.49	18.51	0
2	-50	-25	0.1795	323	45	-99	155	46	-81	89.93	10.07	0
3	-50	0	0.2187	313	46	-101	148	45	-79	90.04	9.96	0
4	-50	25	0.2131	307	46	-103	145	45	-77	83.13	16.87	0
5	-50	50	0.2106	305	47	77	144	44	103	77.91	22.09	0
6	-25	-50	0.1936	320	46	-98	151	45	-82	84.62	15.38	0
7	-25	-25	0.2433	311	47	-98	142	44	-82	87.05	12.95	0
8	-25	0	0.2214	311	47	-99	143	44	-81	76.88	23.12	0
9	-25	25	0.1628	140	43	99	307	48	81	69.82	30.18	0
10	-25	50	0.1298	141	44	100	307	47	80	82.67	17.33	0
11	0	-50	0.0435	140	42	96	312	48	85	56.92	43.08	0
12	0	-25	0.1902	312	47	-97	142	44	-83	76.25	23.75	0
13	0	0	0.1265	139	43	98	308	48	82	59.74	40.26	0
14	0	25	0.097	141	44	98	310	47	82	82.46	17.54	0
15	0	50	0.0847	135	43	-80	302	47	-99	81.83	18.17	0
16	25	-50	0.0411	232	50	88	54	40	92	79.23	20.77	0
17	25	-25	0.0976	312	46	-97	142	44	-83	74.28	25.72	0
18	25	0	0.0736	141	44	97	312	46	83	73.82	26.18	0
19	25	25	0.0743	135	44	-82	304	47	-98	76.23	23.77	0
20	25	50	0.0514	192	52	88	16	38	93	19.15	80.85	0
21	50	-50	0.0482	232	49	91	51	41	89	69.88	30.12	0
22	50	-25	0.0524	222	50	-98	54	40	-81	78.8	21.2	0
23	50	0	0.0644	135	44	-84	306	47	-96	76.02	23.98	0
24	50	25	0.0532	41	40	-86	216	50	-93	38.15	61.85	0
25	50	50	0.0525	314	44	-95	140	46	-86	66.1	33.9	0

Table C.57: Full-wavefield moment tensor inversion results for location 1b, DC input mechanism, isotropic medium, dominant source frequency of 125 Hz, and 5% noise with a DC constraint applied to the inversion. The bolded row is the location with the highest correlation in the grid search and thus the final ouputted result. Refer to Figure C.7c for visual.

Location Number	X Coord (m)	Y Coord (m)	Correlation	Strike 1 (°)	Dip 1 (°)	Rake 1 (°)	Strike 2 (°)	Dip 2 (°)	Rake 2 (°)	DC %	CLVD %	ISO %
1	-50	-50	0.1392	326	44	-98	157	47	-82	97.16	2.84	0
2	-50	-25	0.176	322	45	-99	155	46	-81	96.55	3.45	0
3	-50	0	0.2168	313	45	-101	148	46	-80	98.15	1.85	0
4	-50	25	0.2097	307	45	-103	145	46	-77	99.71	0.29	0
5	-50	50	0.2034	305	46	77	144	45	103	99.73	0.27	0
6	-25	-50	0.1893	320	45	-98	151	45	-82	98.13	1.87	0
7	-25	-25	0.241	311	47	-98	143	44	-82	97.63	2.37	0
8	-25	0	0.2139	311	46	-99	143	45	-81	98.14	1.86	0
9	-25	25	0.1554	140	44	100	307	47	81	99.16	0.84	0
10	-25	50	0.1277	141	45	100	307	46	80	96.59	3.41	0
11	0	-50	0.0416	140	43	96	311	47	84	96.77	3.23	0
12	0	-25	0.183	312	46	-97	142	44	-83	97.11	2.89	0
13	0	0	0.118	139	44	98	308	47	82	97.78	2.22	0
14	0	25	0.0947	141	44	98	310	46	82	99.35	0.65	0
15	0	50	0.0817	135	44	-80	301	47	-99	95.75	4.25	0
16	25	-50	0.0411	232	50	88	55	40	92	95.14	4.86	0
17	25	-25	0.0929	312	46	-97	142	45	-83	99.52	0.48	0
18	25	0	0.0714	141	44	97	312	46	83	93.43	6.57	0
19	25	25	0.0713	135	44	-82	304	46	-98	98.59	1.41	0
20	25	50	0.0492	212	51	89	34	39	92	95.97	4.03	0
21	50	-50	0.0482	231	49	91	50	41	89	91.22	8.78	0
22	50	-25	0.0524	221	50	-99	55	41	-80	98.08	1.92	0
23	50	0	0.0611	134	44	-84	306	46	-96	95.45	4.55	0
24	50	25	0.0525	44	40	-84	217	50	-95	96.49	3.51	0
25	50	50	0.0496	313	43	-95	140	47	-85	99.66	0.34	0

Table C.58: Full-wavefield moment tensor inversion results for location 3d, DC input mechanism, isotropic medium, dominant source frequency of 125 Hz, and 5% noise with no constraints applied to the inversion. The bolded row is the location with the highest correlation in the grid search and thus the final ouputted result. Refer to Figure C.7d for visual.

Location Number	X Coord (m)	Y Coord (m)	Correlation	Strike 1 (°)	Dip 1 (°)	Rake 1 (°)	Strike 2 (°)	Dip 2 (°)	Rake 2 (°)	DC %	CLVD %	ISO %
1	-50	-50	0.1407	89	44	-90	268	46	-90	37.21	40.34	22.45
2	-50	-25	0.2808	254	45	90	74	45	90	32.71	46.17	-21.12
3	-50	0	0.1411	71	45	-91	252	46	-89	32.3	44.53	23.17
4	-50	25	0.0352	238	46	89	60	44	91	15.16	64.56	-20.28
5	-50	50	0.0587	53	44	-94	238	46	-86	34.19	47.17	18.64
6	-25	-50	0.2305	76	44	-93	260	46	-87	27.78	49.27	22.95
7	-25	-25	0.2404	258	45	90	79	45	90	34.12	42.39	-23.49
8	-25	0	0.1189	73	44	-92	256	46	-88	36.23	40.63	23.14
9	-25	25	0.0319	94	67	149	197	62	27	6.16	91.28	2.56
10	-25	50	0.0789	51	44	-92	235	46	-88	21.47	49.94	28.59
11	0	-50	0.3337	69	44	-97	258	47	-84	17.92	49.85	32.23
12	0	-25	0.175	264	45	90	84	45	90	38.57	47.17	-14.26
13	0	0	0.0912	74	45	-93	258	45	-87	33.22	42.26	24.52
14	0	25	0.036	270	42	97	82	49	84	26.6	55.87	17.53
15	0	50	0.0717	51	46	-88	228	44	-92	9.55	59.16	-31.29
16	25	-50	0.416	58	44	-107	261	48	-74	11.14	39.18	-49.68
17	25	-25	0.1568	92	46	90	272	44	90	16.82	30.33	-52.85
18	25	0	0.068	76	46	-92	259	45	-87	28.47	34.54	36.99
19	25	25	0.0374	71	48	-90	251	42	-90	33.19	39.23	27.58
20	25	50	0.0517	50	45	-85	223	45	-95	12.7	49.37	37.93
21	50	-50	0.0489	128	81	165	220	75	9	6.08	14.43	-79.49
22	50	-25	0.0794	246	46	78	83	45	102	5.6	40.4	-54
23	50	0	0.0409	77	45	-95	264	45	-85	37.83	35.89	-26.28
24	50	25	0.0499	72	45	-92	255	45	-88	31.77	40.74	27.49
25	50	50	0.0189	289	78	168	21	78	12	25.39	67.17	7.44

Table C.59: Full-wavefield moment tensor inversion results for location 3d, DC input mechanism, isotropic medium, dominant source frequency of 125 Hz, and 5% noise with a deviatoric constraint applied to the inversion. The bolded row is the location with the highest correlation in the grid search and thus the final ouputted result. Refer to Figure C.7e for visual.

Location Number	X Coord (m)	Y Coord (m)	Correlation	Strike 1 (°)	Dip 1 (°)	Rake 1 (°)	Strike 2 (°)	Dip 2 (°)	Rake 2 (°)	DC %	CLVD %	ISO %
1	-50	-50	0.1384	88	44	-90	268	46	-90	70.22	29.78	0
2	-50	-25	0.2781	253	45	90	73	45	90	62.34	37.66	0
3	-50	0	0.1391	71	45	-90	252	45	-90	65.37	34.63	0
4	-50	25	0.035	238	46	89	59	44	91	39.21	60.79	0
5	-50	50	0.0583	53	44	-93	237	46	-87	59.14	40.86	0
6	-25	-50	0.2276	76	44	-92	258	46	-88	58.55	41.45	0
7	-25	-25	0.236	258	45	90	78	45	90	67.87	32.13	0
8	-25	0	0.1167	73	44	-91	255	46	-89	69.86	30.14	0
9	-25	25	0.0319	97	72	156	195	67	20	7.11	92.89	0
10	-25	50	0.0776	51	44	-91	233	46	-89	58.43	41.57	0
11	0	-50	0.3249	70	44	-93	254	46	-87	60.41	39.59	0
12	0	-25	0.1738	264	45	90	84	45	90	57.68	42.32	0
13	0	0	0.0889	74	45	-92	257	45	-88	68.21	31.79	0
14	0	25	0.0359	273	42	100	79	49	81	20.72	79.28	0
15	0	50	0.0714	96	87	-4	186	86	-177	5.59	94.41	0
16	25	-50	0.4039	28	81	-176	297	86	-9	27.24	72.76	0
17	25	-25	0.1172	94	46	90	274	44	90	87.48	12.52	0
18	25	0	0.0615	75	45	-91	257	45	-89	87.04	12.96	0
19	25	25	0.0361	70	48	-90	250	42	-90	73.15	26.85	0
20	25	50	0.0504	44	45	-89	222	45	-91	56.59	43.41	0
21	50	-50	0.022	242	44	87	66	46	93	23.25	76.75	0
22	50	-25	0.0644	249	45	89	71	45	91	89.15	10.85	0
23	50	0	0.0401	75	46	-98	267	45	-82	32.63	67.37	0
24	50	25	0.0476	72	45	-92	254	45	-88	70.19	29.81	0
25	50	50	0.0189	289	80	170	21	80	10	31.29	68.71	0

Table C.60: Full-wavefield moment tensor inversion results for location 3d, DC input mechanism, isotropic medium, dominant source frequency of 125 Hz, and 5% noise with a DC constraint applied to the inversion. The bolded row is the location with the highest correlation in the grid search and thus the final ouputted result. Refer to Figure C.7f for visual.

Location Number	X Coord (m)	Y Coord (m)	Correlation	Strike 1 (°)	Dip 1 (°)	Rake 1 (°)	Strike 2 (°)	Dip 2 (°)	Rake 2 (°)	DC %	CLVD %	ISO %
1	-50	-50	0.1304	89	45	-89	268	45	-91	92.26	7.74	0
2	-50	-25	0.2684	253	45	90	73	45	90	97.67	2.33	0
3	-50	0	0.1332	72	45	-90	252	45	-90	97.62	2.38	0
4	-50	25	0.0332	239	46	89	60	44	91	95.94	4.06	0
5	-50	50	0.0557	55	44	-92	237	46	-89	94.82	5.18	0
6	-25	-50	0.2119	77	44	-91	258	46	-89	90.3	9.7	0
7	-25	-25	0.2308	258	45	90	78	45	90	93.97	6.03	0
8	-25	0	0.1108	73	44	-91	255	46	-89	92.78	7.22	0
9	-25	25	0.0314	277	87	-166	187	76	-3	93.54	6.46	0
10	-25	50	0.0746	53	44	-91	234	46	-89	93.16	6.84	0
11	0	-50	0.3149	72	44	-92	254	46	-88	98.72	1.28	0
12	0	-25	0.1635	264	45	90	84	45	90	97.31	2.69	0
13	0	0	0.0838	75	45	-91	256	45	-89	93.39	6.61	0
14	0	25	0.0296	220	87	-3	310	87	-177	93.45	6.55	0
15	0	50	0.0705	272	89	1	182	89	179	99.55	0.45	0
16	25	-50	0.3998	25	86	180	115	90	4	91.92	8.08	0
17	25	-25	0.1157	93	46	90	274	44	90	96.63	3.37	0
18	25	0	0.0603	76	45	-91	257	45	-89	92.4	7.6	0
19	25	25	0.0348	70	47	-90	250	43	-90	96.4	3.6	0
20	25	50	0.0496	47	45	-89	226	45	-91	98.89	1.11	0
21	50	-50	0.0175	219	49	96	30	41	83	99.72	0.28	0
22	50	-25	0.0643	249	45	89	71	45	91	99.71	0.29	0
23	50	0	0.0331	79	45	-93	263	45	-87	96.01	3.99	0
24	50	25	0.0456	73	45	-91	254	45	-89	98.05	1.95	0
25	50	50	0.0188	288	86	175	19	85	4	91.63	8.37	0

Table C.61: Full-wavefield moment tensor inversion results for location 3e, DC input mechanism, isotropic medium, dominant source frequency of 125 Hz, and 5% noise with no constraints applied to the inversion. The bolded row is the location with the highest correlation in the grid search and thus the final ouputted result. Refer to Figure C.7g for visual.

Location Number	X Coord (m)	Y Coord (m)	Correlation	Strike 1 (°)	Dip 1 (°)	Rake 1 (°)	Strike 2 (°)	Dip 2 (°)	Rake 2 (°)	DC %	CLVD %	ISO %
1	-50	-50	0.2243	77	45	-91	258	45	-89	40.82	38.75	20.43
2	-50	-25	0.4258	253	44	91	72	46	89	41.39	38.01	-20.6
3	-50	0	0.1953	62	45	-90	242	45	-90	35.6	32.32	32.08
4	-50	25	0.1521	245	44	91	64	46	89	39.86	38.84	-21.3
5	-50	50	0.0646	239	44	90	59	46	90	31.77	40.15	-28.08
6	-25	-50	0.2007	81	46	-92	263	44	-88	35.57	43.35	21.08
7	-25	-25	0.317	78	46	-92	261	44	-88	33.63	45.07	21.3
8	-25	0	0.4282	254	44	91	73	46	89	19.8	30.96	-49.24
9	-25	25	0.167	60	45	-90	241	45	-90	28.78	35.93	35.29
10	-25	50	0.0761	48	44	-91	229	46	-89	31.09	34.73	34.18
11	0	-50	0.1177	255	44	90	74	46	90	40.45	45.96	-13.59
12	0	-25	0.1888	83	47	-100	278	43	-79	15.32	52.62	32.06
13	0	0	0.4719	69	46	-92	252	44	-88	35.16	42.73	-22.11
14	0	25	0.1381	233	46	90	53	44	90	45.5	53.06	1.44
15	0	50	0.0835	50	44	-92	233	46	-88	26.32	45.17	-28.51
16	25	-50	0.0936	77	46	-91	259	44	-89	31.97	38.52	29.51
17	25	-25	0.1839	250	45	90	71	45	90	31.44	37.69	-30.87
18	25	0	0.1205	254	44	90	74	46	90	15.8	27.7	-56.5
19	25	25	0.0372	55	46	-86	230	45	-94	9.97	3.47	86.56
20	25	50	0.0132	59	65	-83	223	26	-104	2.39	5.09	92.52
21	50	-50	0.1327	79	46	-92	261	44	-88	30.93	48.59	20.48
22	50	-25	0.0154	131	73	-160	35	71	-18	16.45	7.13	76.42
23	50	0	0.0065	56	60	78	259	32	110	8.4	32.41	-59.19
24	50	25	0.0093	44	62	-64	178	37	-129	5.61	14.21	80.18
25	50	50	0.0096	4	46	-94	190	44	-85	5.43	15.29	79.28

Table C.62: Full-wavefield moment tensor inversion results for location 3e, DC input mechanism, isotropic medium, dominant source frequency of 125 Hz, and 5% noise with a deviatoric constraint applied to the inversion. The bolded row is the location with the highest correlation in the grid search and thus the final ouputted result. Refer to Figure C.7h for visual.

Location Number	X Coord (m)	Y Coord (m)	Correlation	Strike 1 (°)	Dip 1 (°)	Rake 1 (°)	Strike 2 (°)	Dip 2 (°)	Rake 2 (°)	DC %	CLVD %	ISO %
1	-50	-50	0.2214	78	45	-90	258	45	-90	72.16	27.84	0
2	-50	-25	0.4193	253	45	90	72	45	90	72.84	27.16	0
3	-50	0	0.1818	63	45	-90	243	45	-90	88.57	11.43	0
4	-50	25	0.1491	245	44	90	65	46	90	71.89	28.11	0
5	-50	50	0.0615	240	44	90	60	46	90	74.42	25.58	0
6	-25	-50	0.1983	82	46	-91	264	44	-89	66.43	33.57	0
7	-25	-25	0.3131	79	46	-91	261	44	-89	63.89	36.11	0
8	-25	0	0.3632	256	44	90	76	46	90	91.47	8.53	0
9	-25	25	0.1489	61	45	-90	241	45	-90	86.42	13.58	0
10	-25	50	0.0699	47	44	-91	228	46	-89	86.65	13.35	0
11	0	-50	0.1168	255	44	90	75	46	90	59.36	40.64	0
12	0	-25	0.1853	90	47	-94	275	43	-86	56.36	43.64	0
13	0	0	0.4673	68	46	-93	253	44	-87	28.66	71.34	0
14	0	25	0.138	233	46	90	53	44	90	45.08	54.92	0
15	0	50	0.0821	49	44	-94	235	46	-86	16.26	83.74	0
16	25	-50	0.0886	78	46	-91	259	44	-89	77.44	22.56	0
17	25	-25	0.1697	251	45	90	71	45	90	79.93	20.07	0
18	25	0	0.0861	259	44	90	79	46	90	73.33	26.67	0
19	25	25	0.0239	337	45	-90	157	45	-90	51.55	48.45	0
20	25	50	0.0087	338	45	-79	143	46	-101	97.49	2.51	0
21	50	-50	0.1301	79	46	-91	261	44	-89	58.63	41.37	0
22	50	-25	0.013	18	53	-45	139	55	-133	50.86	49.14	0
23	50	0	0.0037	246	34	93	62	56	88	72.39	27.61	0
24	50	25	0.0072	0	46	-65	147	49	-113	71.12	28.88	0
25	50	50	0.0075	335	46	-93	159	44	-87	78.48	21.52	0

Table C.63: Full-wavefield moment tensor inversion results for location 3e, DC input mechanism, isotropic medium, dominant source frequency of 125 Hz, and 5% noise with a DC constraint applied to the inversion. The bolded row is the location with the highest correlation in the grid search and thus the final ouputted result. Refer to Figure C.7i for visual.

Location Number	X Coord (m)	Y Coord (m)	Correlation	Strike 1 (°)	Dip 1 (°)	Rake 1 (°)	Strike 2 (°)	Dip 2 (°)	Rake 2 (°)	DC %	CLVD %	ISO %
1	-50	-50	0.2114	78	45	-90	258	45	-90	92.98	7.02	0
2	-50	-25	0.4113	253	45	90	73	45	90	95.83	4.17	0
3	-50	0	0.1789	63	45	-90	242	45	-90	94.63	5.37	0
4	-50	25	0.1466	245	44	90	65	46	90	92.86	7.14	0
5	-50	50	0.0603	240	44	90	60	46	90	94.75	5.25	0
6	-25	-50	0.1909	82	46	-90	263	44	-89	96.39	3.61	0
7	-25	-25	0.3031	79	46	-90	260	44	-89	99.69	0.31	0
8	-25	0	0.362	256	44	90	76	46	90	99.2	0.8	0
9	-25	25	0.1464	61	45	-90	241	45	-90	96.35	3.65	0
10	-25	50	0.0691	47	44	-90	228	46	-90	96.8	3.2	0
11	0	-50	0.1096	255	45	90	75	45	90	99.14	0.86	0
12	0	-25	0.1793	88	47	-92	272	43	-88	92.4	7.6	0
13	0	0	0.3868	70	46	-91	252	44	-89	95.22	4.78	0
14	0	25	0.1262	232	45	90	53	45	90	98.38	1.62	0
15	0	50	0.0612	97	90	1	7	89	180	94.71	5.29	0
16	25	-50	0.0857	79	46	-90	259	44	-90	94.89	5.11	0
17	25	-25	0.1677	251	45	90	71	45	90	94.58	5.42	0
18	25	0	0.0825	257	44	90	77	46	90	98.76	1.24	0
19	25	25	0.0238	336	45	-90	156	45	-90	91.07	8.93	0
20	25	50	0.0087	338	45	-79	143	46	-101	97.49	2.51	0
21	50	-50	0.1216	80	46	-91	261	44	-89	98.5	1.5	0
22	50	-25	0.0128	17	53	-50	142	52	-131	92.26	7.74	0
23	50	0	0.0035	62	59	-91	244	31	-89	92.95	7.05	0
24	50	25	0.0072	1	46	-62	144	50	-116	95.63	4.37	0
25	50	50	0.0075	334	46	-93	158	44	-87	90.43	9.57	0

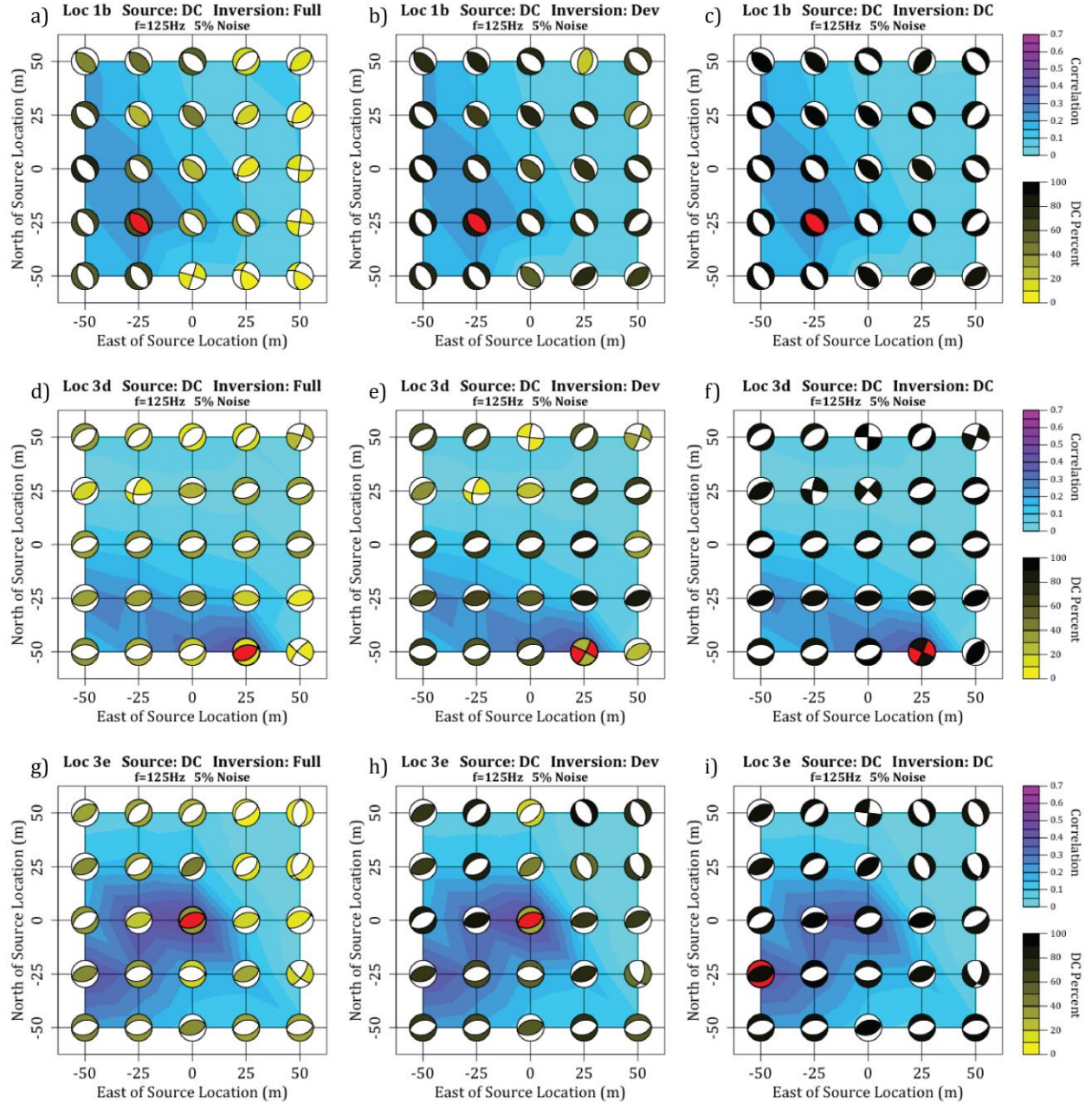


Figure C.7: Full-wavefield moment tensor inversion results for a DC source mechanism in an isotropic medium, 5% noise, and source frequency of 125 Hz for a) location 1b with no constraints on the inversion, b) location 1b with a deviatoric constraint, c) location 1b with a DC constraint, d) location 3d with no constraints, e) location 3d with a deviatoric constraint, f) location 3d with a DC constraint, g) location 3e with no constraints, h) location 3e with a deviatoric constraint, and i) location 3e with a DC constraint. The red beach-ball is the location and source mechanism with the highest correlation to the input seismograms. Refer to Tables C.55-C.63 for numerical values of results.

Table C.64: Full-wavefield moment tensor inversion results for location 1b, CLVD input mechanism, isotropic medium, dominant source frequency of 125 Hz, and 5% noise with no constraints applied to the inversion. The bolded row is the location with the highest correlation in the grid search and thus the final ouputted result. Refer to Figure C.8a for visual.

Location Number	X Coord (m)	Y Coord (m)	Correlation	Strike 1 (°)	Dip 1 (°)	Rake 1 (°)	Strike 2 (°)	Dip 2 (°)	Rake 2 (°)	DC %	CLVD %	ISO %
1	-50	-50	0.0909	324	47	-96	153	43	-83	16.66	28.59	54.75
2	-50	-25	0.1155	118	41	-81	286	50	-98	22.42	2.38	-75.2
3	-50	0	0.1039	192	86	-167	101	77	-5	15.72	4.41	-79.87
4	-50	25	0.1057	149	57	123	280	46	50	81.71	14.94	-3.35
5	-50	50	0.1079	84	83	170	176	80	7	14.72	37.92	47.36
6	-25	-50	0.1025	154	43	95	326	47	85	36	14.97	49.03
7	-25	-25	0.122	301	48	77	141	43	105	35.64	13.72	-50.64
8	-25	0	0.1019	199	82	-166	106	76	-9	4	7.33	-88.67
9	-25	25	0.0914	172	86	36	79	54	175	25.99	25.07	48.94
10	-25	50	0.0592	60	39	115	209	55	71	12.78	9.95	77.27
11	0	-50	0.0932	197	86	-178	106	88	-4	5.61	14.71	-79.68
12	0	-25	0.1135	181	82	178	271	88	8	5.35	28.07	-66.58
13	0	0	0.1074	98	63	154	201	67	29	4.88	6.91	88.21
14	0	25	0.0776	59	41	-86	234	49	-93	10.13	3.99	-85.88
15	0	50	0.0608	313	36	-102	148	55	-81	36.38	43.05	20.57
16	25	-50	0.1026	290	63	-153	187	66	-30	0.42	18.4	81.18
17	25	-25	0.1124	192	88	-175	102	85	-2	11.25	3.75	-85
18	25	0	0.1127	190	88	-173	100	83	-2	6.44	3.62	-89.94
19	25	25	0.1146	61	41	-79	227	50	-100	6.56	5.12	-88.32
20	25	50	0.1314	226	50	82	59	41	99	14.83	0.77	84.4
21	50	-50	0.0787	319	47	-101	154	44	-79	3.9	16.87	79.23
22	50	-25	0.1221	279	85	-172	188	82	-5	3.81	11.94	84.25
23	50	0	0.1304	188	82	8	97	82	172	5.77	3.79	90.44
24	50	25	0.1068	203	56	-131	80	51	-46	2.6	5.14	-92.26
25	50	50	0.1154	223	49	80	57	42	101	9.85	2.34	87.81

Table C.65: Full-wavefield moment tensor inversion results for location 1b, CLVD input mechanism, isotropic medium, dominant source frequency of 125 Hz, and 5% noise with a deviatoric constraint applied to the inversion. The bolded row is the location with the highest correlation in the grid search and thus the final ouputed result. Refer to Figure C.8b for visual.

Location Number	X Coord (m)	Y Coord (m)	Correlation	Strike 1 (°)	Dip 1 (°)	Rake 1 (°)	Strike 2 (°)	Dip 2 (°)	Rake 2 (°)	DC %	CLVD %	ISO %
1	-50	-50	0.0681	138	44	-82	308	46	-97	73.42	26.58	0
2	-50	-25	0.0886	95	80	178	185	88	10	34.12	65.88	0
3	-50	0	0.0941	240	89	-168	150	78	-1	68.56	31.44	0
4	-50	25	0.1057	149	57	123	280	45	51	86.34	13.66	0
5	-50	50	0.1061	325	43	-99	157	48	-82	82.97	17.03	0
6	-25	-50	0.0765	352	46	-87	168	44	-93	42	58	0
7	-25	-25	0.1143	74	88	172	164	82	2	83.85	16.15	0
8	-25	0	0.0921	147	49	117	289	47	62	55.49	44.51	0
9	-25	25	0.0855	323	66	-67	96	33	-132	36.39	63.61	0
10	-25	50	0.0515	312	45	-99	144	46	-82	86.04	13.96	0
11	0	-50	0.0523	231	50	-98	63	40	-81	95.09	4.91	0
12	0	-25	0.0755	128	44	100	295	47	80	78.52	21.48	0
13	0	0	0.0743	176	87	35	84	55	177	47.5	52.5	0
14	0	25	0.0488	149	52	95	320	39	83	63.78	36.22	0
15	0	50	0.0599	315	36	-101	148	55	-82	65.74	34.26	0
16	25	-50	0.0588	224	50	-101	60	41	-78	78.14	21.86	0
17	25	-25	0.0581	224	50	86	50	40	95	49.2	50.8	0
18	25	0	0.0589	218	51	84	47	40	97	37.97	62.03	0
19	25	25	0.0574	208	51	84	37	39	97	28.3	71.7	0
20	25	50	0.0638	18	38	-86	194	52	-93	19.94	80.06	0
21	50	-50	0.0443	50	41	-86	224	49	-94	65.53	34.47	0
22	50	-25	0.0681	48	40	-85	222	50	-94	53.15	46.85	0
23	50	0	0.0701	43	40	-85	217	51	-94	49.08	50.92	0
24	50	25	0.0574	212	50	87	37	40	94	37.74	62.26	0
25	50	50	0.0761	141	50	96	311	40	82	67.1	32.9	0

Table C.66: Full-wavefield moment tensor inversion results for location 1b, CLVD input mechanism, isotropic medium, dominant source frequency of 125 Hz, and 5% noise with a DC constraint applied to the inversion. The bolded row is the location with the highest correlation in the grid search and thus the final ouputted result. Refer to Figure C.8c for visual.

Location Number	X Coord (m)	Y Coord (m)	Correlation	Strike 1 (°)	Dip 1 (°)	Rake 1 (°)	Strike 2 (°)	Dip 2 (°)	Rake 2 (°)	DC %	CLVD %	ISO %
1	-50	-50	0.0675	133	44	-82	303	47	-97	91.32	8.68	0
2	-50	-25	0.0883	92	80	176	182	86	10	93.77	6.23	0
3	-50	0	0.0941	242	88	-167	152	77	-2	94.43	5.57	0
4	-50	25	0.1053	149	60	122	278	43	48	99.33	0.67	0
5	-50	50	0.1028	325	42	-99	157	48	-82	99.34	0.66	0
6	-25	-50	0.0706	349	43	-90	169	47	-90	99.19	0.81	0
7	-25	-25	0.1143	75	89	171	165	81	1	96.2	3.8	0
8	-25	0	0.0884	146	56	113	289	41	60	99.99	0.01	0
9	-25	25	0.0787	328	88	-69	65	21	-173	99.99	0.01	0
10	-25	50	0.0504	312	44	-99	144	46	-81	99.93	0.07	0
11	0	-50	0.0523	231	50	-98	62	40	-81	96.83	3.17	0
12	0	-25	0.0748	291	48	81	125	42	100	99.87	0.13	0
13	0	0	0.0737	178	82	27	84	63	171	95.37	4.63	0
14	0	25	0.0413	149	52	95	321	39	84	99.77	0.23	0
15	0	50	0.0552	315	37	-100	147	54	-82	97.31	2.69	0
16	25	-50	0.0587	224	50	-102	62	41	-76	98.68	1.32	0
17	25	-25	0.0577	226	50	85	53	40	96	96.03	3.97	0
18	25	0	0.058	53	40	101	219	51	81	91.23	8.77	0
19	25	25	0.0561	215	51	84	45	40	98	95.96	4.04	0
20	25	50	0.0638	18	38	-86	194	52	-93	19.94	80.06	0
21	50	-50	0.0443	52	41	-85	225	49	-95	93.72	6.28	0
22	50	-25	0.0677	51	40	-84	222	50	-95	94.23	5.77	0
23	50	0	0.0697	46	40	-84	218	51	-95	93.24	6.76	0
24	50	25	0.0565	215	50	85	43	40	96	97.57	2.43	0
25	50	50	0.0729	140	50	96	311	40	82	96.63	3.37	0

Table C.67: Full-wavefield moment tensor inversion results for location 3d, CLVD input mechanism, isotropic medium, dominant source frequency of 125 Hz, and 5% noise with no constraints applied to the inversion. The bolded row is the location with the highest correlation in the grid search and thus the final ouputted result. Refer to Figure C.8d for visual.

Location Number	X Coord (m)	Y Coord (m)	Correlation	Strike 1 (°)	Dip 1 (°)	Rake 1 (°)	Strike 2 (°)	Dip 2 (°)	Rake 2 (°)	DC %	CLVD %	ISO %
1	-50	-50	0.1332	191	45	90	11	45	90	4.71	13.35	81.94
2	-50	-25	0.2035	257	46	90	77	44	90	36.3	42.48	-21.22
3	-50	0	0.1252	71	44	-90	251	46	-90	35.77	43.46	20.77
4	-50	25	0.0406	253	46	92	70	44	88	33.33	42.85	-23.82
5	-50	50	0.0615	83	46	-91	264	44	-89	38.33	38.97	22.7
6	-25	-50	0.2675	0	46	-92	184	44	-88	8.25	2.77	-88.98
7	-25	-25	0.1755	262	46	90	81	45	90	36.17	40.83	-23
8	-25	0	0.1207	73	44	-90	253	46	-90	33.69	42.47	23.84
9	-25	25	0.0368	353	85	-179	263	89	-5	12.45	2.42	85.13
10	-25	50	0.0508	93	45	-87	269	45	-93	32.18	50.65	17.17
11	0	-50	0.3259	6	82	-178	275	88	-8	42.07	23.39	-34.54
12	0	-25	0.1944	95	45	-91	276	45	-89	35.18	40.47	24.35
13	0	0	0.1063	75	44	-89	254	46	-91	31.04	43.86	25.1
14	0	25	0.0658	83	45	-93	267	45	-87	43.64	47.61	8.75
15	0	50	0.0536	250	46	91	68	44	89	26.59	42.93	-30.48
16	25	-50	0.4899	8	82	180	98	90	8	18.11	12.25	69.64
17	25	-25	0.2161	92	46	-92	275	44	-88	31.28	51.89	16.83
18	25	0	0.0837	76	43	-90	257	47	-90	40.99	56.81	2.2
19	25	25	0.0307	68	40	-92	251	50	-88	30.67	55.23	14.1
20	25	50	0.0495	248	45	90	68	45	90	28.26	55.22	-16.52
21	50	-50	0.0672	111	46	-80	277	45	-100	7.3	20.67	72.03
22	50	-25	0.0788	278	48	118	59	50	63	2.97	15.38	81.65
23	50	0	0.083	77	44	-88	255	46	-92	21.38	26.48	52.14
24	50	25	0.0542	72	44	-90	252	46	-90	25.7	41.99	32.31
25	50	50	0.0277	242	41	81	74	49	98	19.21	32.68	-48.11

Table C.68: Full-wavefield moment tensor inversion results for location 3d, CLVD input mechanism, isotropic medium, dominant source frequency of 125 Hz, and 5% noise with a deviatoric constraint applied to the inversion. The bolded row is the location with the highest correlation in the grid search and thus the final ouputed result. Refer to Figure C.8e for visual.

Location Number	X Coord (m)	Y Coord (m)	Correlation	Strike 1 (°)	Dip 1 (°)	Rake 1 (°)	Strike 2 (°)	Dip 2 (°)	Rake 2 (°)	DC %	CLVD %	ISO %
1	-50	-50	0.0808	110	47	-107	315	46	-73	11.42	88.58	0
2	-50	-25	0.201	257	46	90	77	44	90	66.94	33.06	0
3	-50	0	0.1238	71	44	-90	251	46	-90	65.44	34.56	0
4	-50	25	0.0398	252	46	91	70	44	89	67.46	32.54	0
5	-50	50	0.0606	84	45	-91	265	45	-89	71.27	28.73	0
6	-25	-50	0.1928	11	78	-172	280	82	-12	22.92	77.08	0
7	-25	-25	0.172	261	45	90	81	45	90	69.63	30.37	0
8	-25	0	0.1184	73	44	-90	253	46	-90	67.93	32.07	0
9	-25	25	0.0288	250	46	94	65	44	86	54.87	45.13	0
10	-25	50	0.0506	93	45	-88	270	45	-92	53.85	46.15	0
11	0	-50	0.324	7	82	179	97	89	8	95.79	4.21	0
12	0	-25	0.1901	95	45	-91	276	45	-89	70.26	29.74	0
13	0	0	0.1036	74	44	-90	254	46	-90	66.43	33.57	0
14	0	25	0.0657	83	45	-92	267	45	-88	55.04	44.96	0
15	0	50	0.0509	249	46	91	68	44	89	70.14	29.86	0
16	25	-50	0.4265	37	43	-97	227	47	-83	61.4	38.6	0
17	25	-25	0.2139	93	46	-91	275	45	-88	52.46	47.54	0
18	25	0	0.0837	76	43	-90	257	47	-90	43.58	56.42	0
19	25	25	0.0305	68	40	-92	251	50	-88	47.65	52.35	0
20	25	50	0.049	248	45	90	67	45	90	48.1	51.9	0
21	50	-50	0.0415	122	45	-89	301	45	-91	45.61	54.39	0
22	50	-25	0.0614	306	87	-179	216	89	-3	46.9	53.1	0
23	50	0	0.0615	73	44	-90	253	46	-90	82.14	17.86	0
24	50	25	0.0507	71	44	-90	251	46	-90	71	29	0
25	50	50	0.0231	246	47	92	63	43	88	78.26	21.74	0

Table C.69: Full-wavefield moment tensor inversion results for location 3d, CLVD input mechanism, isotropic medium, dominant source frequency of 125 Hz, and 5% noise a DC constraint applied to the inversion. The bolded row is the location with the highest correlation in the grid search and thus the final ouputted result. Refer to Figure C.8f for visual.

Location Number	X Coord (m)	Y Coord (m)	Correlation	Strike 1 (°)	Dip 1 (°)	Rake 1 (°)	Strike 2 (°)	Dip 2 (°)	Rake 2 (°)	DC %	CLVD %	ISO %
1	-50	-50	0.0793	83	88	-179	353	89	-2	98.13	1.87	0
2	-50	-25	0.197	257	46	90	78	44	90	92.45	7.55	0
3	-50	0	0.1186	72	44	-90	251	46	-90	97.51	2.49	0
4	-50	25	0.039	252	46	91	71	44	89	91.57	8.43	0
5	-50	50	0.0584	84	45	-90	264	45	-90	94.91	5.09	0
6	-25	-50	0.1915	7	84	180	97	90	6	97.31	2.69	0
7	-25	-25	0.1677	261	45	90	81	45	90	95.63	4.37	0
8	-25	0	0.1128	73	44	-90	253	46	-90	94.47	5.53	0
9	-25	25	0.0277	250	46	92	66	44	88	91.81	8.19	0
10	-25	50	0.0485	92	45	-88	269	45	-92	98.47	1.53	0
11	0	-50	0.324	7	82	179	97	89	8	95.79	4.21	0
12	0	-25	0.1799	96	45	-90	276	45	-90	90.84	9.16	0
13	0	0	0.0982	75	44	-89	254	46	-91	94.96	5.04	0
14	0	25	0.0602	84	45	-91	266	45	-89	95.79	4.21	0
15	0	50	0.0496	249	46	90	68	44	90	94.72	5.28	0
16	25	-50	0.4218	45	43	-95	232	48	-85	91.44	8.56	0
17	25	-25	0.1933	94	45	-91	274	45	-89	93.67	6.33	0
18	25	0	0.074	76	43	-90	256	47	-90	96.1	3.9	0
19	25	25	0.0274	69	41	-91	250	49	-89	94.21	5.79	0
20	25	50	0.0453	247	45	90	68	45	90	97.52	2.48	0
21	50	-50	0.0386	130	46	-89	309	44	-91	93.2	6.8	0
22	50	-25	0.0611	307	87	-180	217	90	-3	96.15	3.85	0
23	50	0	0.0612	74	44	-90	253	46	-90	91.8	8.2	0
24	50	25	0.0487	71	44	-90	251	46	-90	96.79	3.21	0
25	50	50	0.023	245	47	91	63	43	89	91.32	8.68	0

Table C.70: Full-wavefield moment tensor inversion results for location 3e, CLVD input mechanism, isotropic medium, dominant source frequency of 125 Hz, and 5% noise with no constraints applied to the inversion. The bolded row is the location with the highest correlation in the grid search and thus the final ouputted result. Refer to Figure C.8g for visual.

Location Number	X Coord (m)	Y Coord (m)	Correlation	Strike 1 (°)	Dip 1 (°)	Rake 1 (°)	Strike 2 (°)	Dip 2 (°)	Rake 2 (°)	DC %	CLVD %	ISO %
1	-50	-50	0.1389	77	46	-90	258	44	-90	41.36	39.42	19.22
2	-50	-25	0.4207	65	89	-173	335	83	-1	88.38	8.84	-2.78
3	-50	0	0.2544	52	44	-91	232	46	-89	38.32	40.83	20.85
4	-50	25	0.0728	131	44	95	304	47	85	3.25	3.47	93.28
5	-50	50	0.0511	50	45	-87	225	45	-93	30.48	43.26	26.26
6	-25	-50	0.1197	260	44	91	79	46	89	36.69	40.83	-22.48
7	-25	-25	0.2553	233	49	105	31	43	74	13.49	61.08	-25.43
8	-25	0	0.3267	72	46	-90	253	44	-90	16.56	26.42	57.02
9	-25	25	0.0544	232	46	92	48	44	88	32.86	39.72	-27.42
10	-25	50	0.0578	51	46	-89	230	44	-91	46.58	51.72	-1.7
11	0	-50	0.0812	246	46	93	62	44	87	24.79	35.79	-39.42
12	0	-25	0.1569	259	44	90	78	46	90	26.61	38.25	-35.14
13	0	0	0.4884	342	82	-179	252	89	-8	21.46	14.98	63.56
14	0	25	0.1115	252	44	90	72	46	90	13.91	35.96	-50.13
15	0	50	0.0844	53	45	-89	232	45	-91	20.74	27.98	51.28
16	25	-50	0.0319	252	45	85	79	45	95	18.5	38.37	-43.13
17	25	-25	0.0531	62	46	-90	241	44	-90	21.94	21.46	56.6
18	25	0	0.0953	81	47	-87	256	44	-94	9.28	23.87	66.85
19	25	25	0.0408	243	49	93	59	41	87	21.61	0.59	-77.8
20	25	50	0.0116	52	23	-90	232	67	-90	11.79	13.86	74.35
21	50	-50	0.0529	259	45	91	78	45	89	33.94	50.56	-15.5
22	50	-25	0.0175	118	38	94	294	52	87	7.74	9.53	-82.73
23	50	0	0.0045	12	56	-39	126	58	-139	18.04	19.05	-62.91
24	50	25	0.0042	253	36	90	74	54	90	61.76	2.64	-35.6
25	50	50	0.0171	114	69	-145	10	58	-25	10.43	1.48	88.09

Table C.71: Full-wavefield moment tensor inversion results for location 3e, CLVD input mechanism, isotropic medium, dominant source frequency of 125 Hz, and 5% noise with a deviatoric constraint applied to the inversion. The bolded row is the location with the highest correlation in the grid search and thus the final ouputed result. Refer to Figure C.8h for visual.

Location Number	X Coord (m)	Y Coord (m)	Correlation	Strike 1 (°)	Dip 1 (°)	Rake 1 (°)	Strike 2 (°)	Dip 2 (°)	Rake 2 (°)	DC %	CLVD %	ISO %
1	-50	-50	0.1373	77	46	-90	258	44	-90	70.62	29.38	0
2	-50	-25	0.4206	65	90	-173	335	83	0	93.89	6.11	0
3	-50	0	0.2505	51	44	-90	232	46	-90	69.17	30.83	0
4	-50	25	0.0686	63	46	-91	244	44	-89	71.51	28.49	0
5	-50	50	0.0491	49	45	-88	226	45	-92	68.97	31.03	0
6	-25	-50	0.1176	260	44	91	80	46	89	70.49	29.51	0
7	-25	-25	0.2532	225	48	96	37	43	83	43.73	56.27	0
8	-25	0	0.3069	49	44	-91	231	46	-89	55.92	44.08	0
9	-25	25	0.0525	230	46	91	48	44	89	74.1	25.9	0
10	-25	50	0.0578	51	46	-89	230	44	-91	46.08	53.92	0
11	0	-50	0.0731	244	46	91	62	44	89	89.95	10.05	0
12	0	-25	0.1477	260	44	90	80	46	90	81.79	18.21	0
13	0	0	0.4492	10	43	-102	206	48	-79	48.34	51.66	0
14	0	25	0.0922	255	44	90	75	46	90	99	1	0
15	0	50	0.0599	50	45	-90	230	45	-90	79.54	20.46	0
16	25	-50	0.0265	255	45	88	78	45	92	90.07	9.93	0
17	25	-25	0.0392	37	80	-171	305	81	-10	15.4	84.6	0
18	25	0	0.0638	90	46	-90	270	44	-90	52.97	47.03	0
19	25	25	0.0257	158	44	94	333	46	86	18.36	81.64	0
20	25	50	0.0086	317	45	-114	170	50	-68	34.15	65.85	0
21	50	-50	0.0523	259	45	91	78	45	89	54.3	45.7	0
22	50	-25	0.0131	155	43	95	328	47	85	61.94	38.06	0
23	50	0	0.0042	90	25	84	276	66	93	71.71	28.29	0
24	50	25	0.0038	257	37	91	76	53	89	62.34	37.66	0
25	50	50	0.0124	349	47	-64	134	49	-115	33.33	66.67	0

Table C.72: Full-wavefield moment tensor inversion results for location 3e, CLVD input mechanism, isotropic medium, dominant source frequency of 125 Hz, and 5% noise with a DC constraint applied to the inversion. The bolded row is the location with the highest correlation in the grid search and thus the final outputted result. Refer to Figure C.8i for visual.

Location Number	X Coord (m)	Y Coord (m)	Correlation	Strike 1 (°)	Dip 1 (°)	Rake 1 (°)	Strike 2 (°)	Dip 2 (°)	Rake 2 (°)	DC %	CLVD %	ISO %
1	-50	-50	0.1312	77	46	-90	257	44	-90	94.38	5.62	0
2	-50	-25	0.4206	66	90	-173	336	83	0	96.69	3.31	0
3	-50	0	0.2411	52	44	-90	232	46	-90	97.59	2.41	0
4	-50	25	0.0656	63	46	-90	244	44	-90	97.2	2.8	0
5	-50	50	0.0456	48	45	-88	226	45	-92	91.1	8.9	0
6	-25	-50	0.1153	260	44	90	80	46	90	95.58	4.42	0
7	-25	-25	0.2448	78	90	-174	348	84	0	95.57	4.43	0
8	-25	0	0.291	50	44	-91	231	46	-90	97.92	2.08	0
9	-25	25	0.0517	230	46	91	48	44	89	96.63	3.37	0
10	-25	50	0.051	51	46	-89	230	44	-91	98.6	1.4	0
11	0	-50	0.0728	244	46	91	63	44	89	99.55	0.45	0
12	0	-25	0.1473	260	44	90	80	46	90	91.03	8.97	0
13	0	0	0.4426	21	42	-97	211	49	-83	93.3	6.7	0
14	0	25	0.0922	255	44	90	75	46	90	99.5	0.5	0
15	0	50	0.0589	50	45	-90	230	45	-90	95.49	4.51	0
16	25	-50	0.0264	256	45	88	78	45	92	98.87	1.13	0
17	25	-25	0.0385	38	87	-179	308	89	-3	90.66	9.34	0
18	25	0	0.0594	99	46	-90	280	44	-90	98.56	1.44	0
19	25	25	0.0243	159	44	98	328	46	82	91.03	8.97	0
20	25	50	0.0085	312	46	-119	170	51	-63	90.94	9.06	0
21	50	-50	0.0487	259	45	90	79	45	90	97.34	2.66	0
22	50	-25	0.013	158	43	97	328	48	83	92.85	7.15	0
23	50	0	0.0042	277	71	91	94	19	87	98.56	1.44	0
24	50	25	0.0037	22	27	-113	228	65	-79	90.44	9.56	0
25	50	50	0.0123	339	45	-78	143	47	-101	94.05	5.95	0

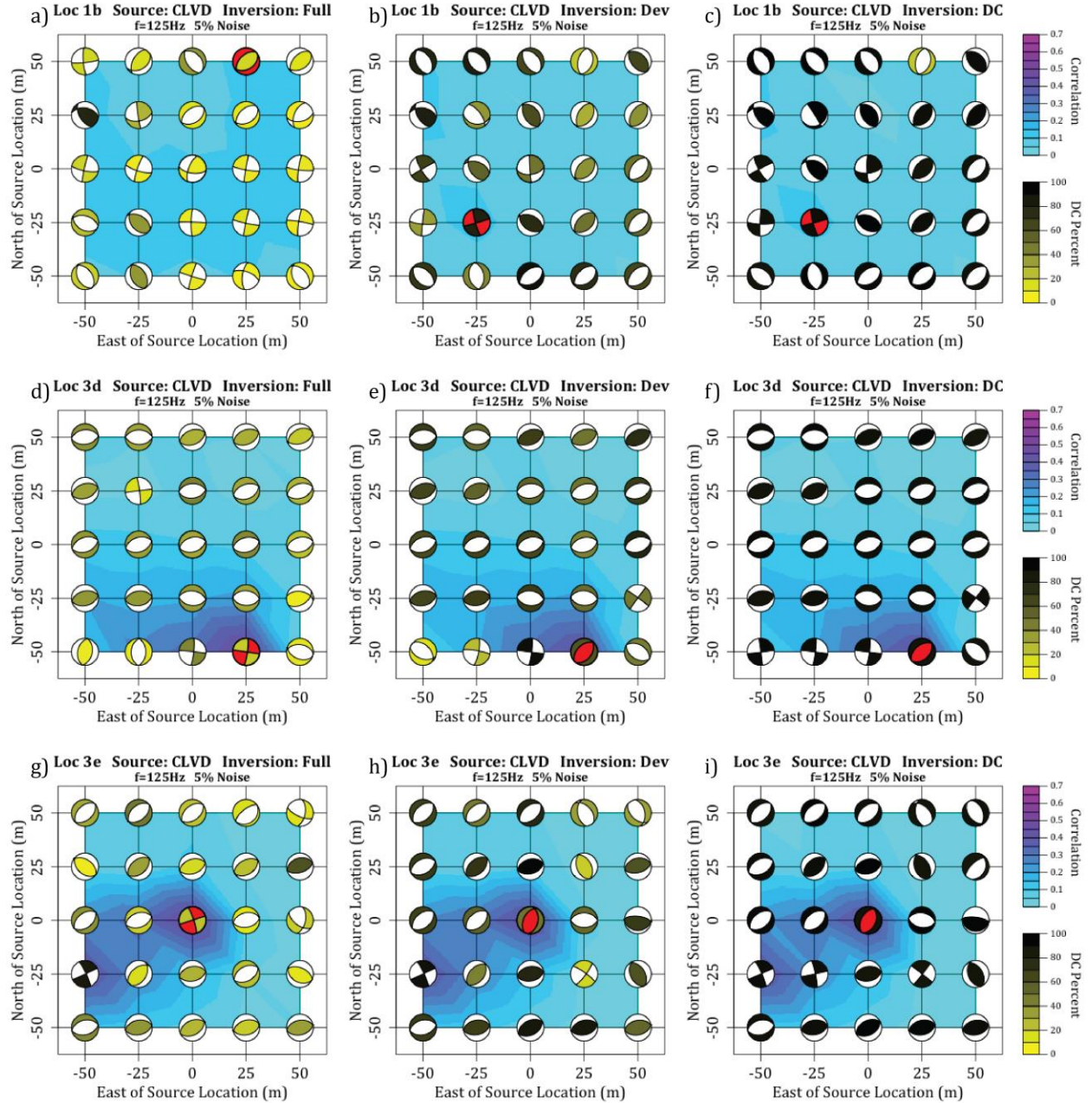


Figure C.8: Full-wavefield moment tensor inversion results for a CLVD source mechanism in an isotropic medium, 5% noise, and source frequency of 125 Hz for a) location 1b with no constraints on the inversion, b) location 1b with a deviatoric constraint, c) location 1b with a DC constraint, d) location 3d with no constraints, e) location 3d with a deviatoric constraint, f) location 3d with a DC constraint, g) location 3e with no constraints, h) location 3e with a deviatoric constraint, and i) location 3e with a DC constraint. The red beach-ball is the location and source mechanism with the highest correlation to the input seismograms. Refer to Tables C.64-C.72 for numerical values of results.

Table C.73: Full-wavefield moment tensor inversion results for location 1b, ISO input mechanism, isotropic medium, dominant source frequency of 125 Hz, and 5% noise with no constraints applied to the inversion. The bolded row is the location with the highest correlation in the grid search and thus the final ouputted result. Refer to Figure C.9a for visual.

Location Number	X Coord (m)	Y Coord (m)	Correlation	Strike 1 (°)	Dip 1 (°)	Rake 1 (°)	Strike 2 (°)	Dip 2 (°)	Rake 2 (°)	DC %	CLVD %	ISO %
1	-50	-50	0.1366	203	89	-173	113	83	-1	2.79	19.8	-77.41
2	-50	-25	0.1589	202	83	-165	110	75	-7	14.86	0.16	-84.98
3	-50	0	0.1675	210	63	-138	97	53	-34	7.7	5.66	-86.64
4	-50	25	0.1474	225	53	-107	72	40	-69	17.16	0.09	-82.75
5	-50	50	0.1623	326	43	-98	157	48	-82	63.79	23.6	12.61
6	-25	-50	0.1575	108	83	179	198	89	7	4.56	15.95	79.49
7	-25	-25	0.166	105	82	178	195	88	8	12.6	1.38	86.02
8	-25	0	0.1568	84	48	132	211	57	54	4.66	6.4	88.94
9	-25	25	0.1273	56	39	106	216	53	77	12.58	7.66	79.76
10	-25	50	0.1037	212	54	78	52	38	106	13.32	8.44	78.24
11	0	-50	0.1455	285	88	3	194	87	178	1.37	16.24	-82.39
12	0	-25	0.1363	191	84	-166	100	76	-7	10.89	0.13	-88.98
13	0	0	0.1137	209	54	-118	71	44	-57	7.52	4.47	-88.01
14	0	25	0.0844	52	41	-75	213	51	-102	9.5	2.79	-87.71
15	0	50	0.0565	42	38	-77	205	53	-100	15.53	1.52	-82.95
16	25	-50	0.0273	316	58	-112	174	38	-58	6.98	11.9	81.12
17	25	-25	0.0857	94	79	172	185	83	12	9.81	3.85	86.34
18	25	0	0.0732	78	52	140	195	60	46	1.5	6.44	92.06
19	25	25	0.0357	57	40	98	227	50	83	9.91	9.58	80.51
20	25	50	0.0373	181	66	-146	76	60	-28	1.4	7.37	-91.23
21	50	-50	0.0041	315	87	75	212	15	167	41.65	6.09	52.26
22	50	-25	0.0589	1	78	174	92	84	12	3.7	9.39	-86.91
23	50	0	0.0459	179	86	-173	88	83	-4	8.69	1.72	-89.59
24	50	25	0.0354	179	70	-156	80	68	-21	8.89	1.78	-89.33
25	50	50	0.036	205	55	-124	75	47	-51	8.7	4.59	-86.71

Table C.74: Full-wavefield moment tensor inversion results for location 1b, ISO input mechanism, isotropic medium, dominant source frequency of 125 Hz, and 5% noise with a deviatoric constraint applied to the inversion. The bolded row is the location with the highest correlation in the grid search and thus the final ouputted result. Refer to Figure C.9b for visual.

Location Number	X Coord (m)	Y Coord (m)	Correlation	Strike 1 (°)	Dip 1 (°)	Rake 1 (°)	Strike 2 (°)	Dip 2 (°)	Rake 2 (°)	DC %	CLVD %	ISO %
1	-50	-50	0.0733	245	50	85	73	41	96	69.54	30.46	0
2	-50	-25	0.0804	75	41	102	240	50	80	85.49	14.51	0
3	-50	0	0.0788	75	40	101	240	51	80	56.6	43.4	0
4	-50	25	0.0627	84	42	109	239	51	74	25.09	74.91	0
5	-50	50	0.1612	326	43	-98	157	48	-82	82.99	17.01	0
6	-25	-50	0.0841	69	41	-85	243	49	-94	98.65	1.35	0
7	-25	-25	0.083	236	50	-101	73	41	-77	69.98	30.02	0
8	-25	0	0.074	236	51	-101	73	41	-77	52.5	47.5	0
9	-25	25	0.0575	241	50	-101	78	42	-77	55.72	44.28	0
10	-25	50	0.0641	155	48	96	325	43	83	73.8	26.2	0
11	0	-50	0.0829	69	41	103	232	50	79	99.01	0.99	0
12	0	-25	0.0755	235	49	83	65	41	98	90.71	9.29	0
13	0	0	0.0585	67	41	98	236	50	83	60.58	39.42	0
14	0	25	0.0428	75	42	102	239	50	79	34.42	65.58	0
15	0	50	0.0275	94	44	101	259	47	80	26.81	73.19	0
16	25	-50	0.017	237	50	-82	45	40	-99	90.75	9.25	0
17	25	-25	0.0465	61	40	-88	238	50	-92	65.84	34.16	0
18	25	0	0.037	231	49	-99	65	41	-80	55.28	44.72	0
19	25	25	0.0197	64	40	95	238	50	86	26.69	73.31	0
20	25	50	0.0191	278	44	79	113	47	100	14.17	85.83	0
21	50	-50	0.004	132	50	77	331	42	105	94.2	5.8	0
22	50	-25	0.0342	62	43	102	227	48	80	69.16	30.84	0
23	50	0	0.026	228	49	85	55	41	96	46.82	53.18	0
24	50	25	0.0188	234	50	88	57	40	92	24.34	75.66	0
25	50	50	0.0174	180	48	94	355	42	86	18.91	81.09	0

Table C.75: Full-wavefield moment tensor inversion results for location 1b, ISO input mechanism, isotropic medium, dominant source frequency of 125 Hz, and 5% noise with a DC constraint applied to the inversion. The bolded row is the location with the highest correlation in the grid search and thus the final ouputted result. Refer to Figure C.9c for visual.

Location Number	X Coord (m)	Y Coord (m)	Correlation	Strike 1 (°)	Dip 1 (°)	Rake 1 (°)	Strike 2 (°)	Dip 2 (°)	Rake 2 (°)	DC %	CLVD %	ISO %
1	-50	-50	0.0733	245	50	86	72	41	95	95.51	4.49	0
2	-50	-25	0.0804	75	41	101	241	50	81	98.47	1.53	0
3	-50	0	0.0785	73	40	100	239	51	81	92	8	0
4	-50	25	0.0618	76	40	107	235	52	77	96.5	3.5	0
5	-50	50	0.1562	325	42	-99	156	49	-82	99.31	0.69	0
6	-25	-50	0.0841	69	41	-85	243	49	-94	92.63	7.37	0
7	-25	-25	0.0829	234	51	-103	74	41	-75	98.06	1.94	0
8	-25	0	0.0737	233	51	-103	72	41	-75	97.38	2.62	0
9	-25	25	0.0573	237	50	-102	75	41	-76	95.07	4.93	0
10	-25	50	0.0617	154	48	96	324	42	83	99.13	0.87	0
11	0	-50	0.0829	69	41	103	232	50	79	99.01	0.99	0
12	0	-25	0.0755	234	50	83	65	41	98	97.45	2.55	0
13	0	0	0.0583	65	40	98	235	50	83	99.32	0.68	0
14	0	25	0.042	66	40	101	232	51	81	93.37	6.63	0
15	0	50	0.0264	238	50	85	66	41	96	95.96	4.04	0
16	25	-50	0.017	237	50	-82	45	40	-100	93.3	6.7	0
17	25	-25	0.0464	60	40	-88	237	50	-92	92.36	7.64	0
18	25	0	0.0368	228	50	-100	64	41	-78	99.66	0.34	0
19	25	25	0.0193	230	51	87	55	39	94	97.62	2.38	0
20	25	50	0.0157	218	51	99	23	40	79	98.48	1.52	0
21	50	-50	0.004	131	50	76	332	42	106	95.51	4.49	0
22	50	-25	0.0341	63	43	104	224	49	77	91.72	8.28	0
23	50	0	0.0257	226	50	85	54	41	96	95.86	4.14	0
24	50	25	0.0182	227	51	89	49	39	91	96.8	3.2	0
25	50	50	0.0163	205	49	87	30	41	93	96.42	3.58	0

Table C.76: Full-wavefield moment tensor inversion results for location 3d, ISO input mechanism, isotropic medium, dominant source frequency of 125 Hz, and 5% noise with no constraints applied to the inversion. The bolded row is the location with the highest correlation in the grid search and thus the final ouputted result. Refer to Figure C.9d for visual.

Location Number	X Coord (m)	Y Coord (m)	Correlation	Strike 1 (°)	Dip 1 (°)	Rake 1 (°)	Strike 2 (°)	Dip 2 (°)	Rake 2 (°)	DC %	CLVD %	ISO %
1	-50	-50	0.2034	191	44	89	13	46	91	4.99	12.74	82.27
2	-50	-25	0.2092	153	45	88	335	45	92	10.24	4.69	85.07
3	-50	0	0.0552	116	42	89	297	48	91	6.37	4.87	88.76
4	-50	25	0.033	330	43	-92	153	47	-88	10.77	6.13	-83.1
5	-50	50	0.0284	320	45	-104	159	46	-76	16.05	2.34	-81.61
6	-25	-50	0.4206	3	46	-91	185	44	-88	8.2	2.89	-88.91
7	-25	-25	0.1323	131	45	-94	316	45	-86	8.9	9.37	-81.73
8	-25	0	0.1012	21	81	174	112	84	9	3.37	4.43	92.2
9	-25	25	0.0448	5	75	170	97	80	15	3.45	3.77	92.78
10	-25	50	0.0225	16	55	-8	111	83	-145	10.57	6.7	-82.73
11	0	-50	0.1017	225	80	176	316	86	10	1.98	3.54	94.48
12	0	-25	0.0732	336	48	-104	176	44	-75	4.11	2.68	-93.21
13	0	0	0.0674	34	53	-53	162	50	-129	0.91	5.02	-94.07
14	0	25	0.0581	60	41	-105	260	50	-77	5.94	12.32	81.74
15	0	50	0.0498	74	48	-79	237	43	-102	12.17	7.16	80.67
16	25	-50	0.4494	113	50	-57	248	50	-123	2.14	6.99	90.87
17	25	-25	0.2209	241	54	-121	107	46	-55	1.87	5.08	93.05
18	25	0	0.0364	8	42	6	273	86	132	3.79	3.68	-92.53
19	25	25	0.0306	289	86	-162	198	72	-4	8.07	3.53	-88.4
20	25	50	0.0183	73	49	-81	239	42	-101	11.12	10.41	78.47
21	50	-50	0.0955	114	50	-65	258	46	-117	2.76	9.99	87.25
22	50	-25	0.1023	80	47	-74	237	46	-107	5.75	8.14	86.11
23	50	0	0.0672	76	46	-84	248	44	-96	16.64	2.88	80.48
24	50	25	0.0225	45	25	53	265	70	106	3.99	11.3	-84.71
25	50	50	0.0176	6	25	19	259	82	113	1.99	11.19	-86.82

Table C.77: Full-wavefield moment tensor inversion results for location 3d, ISO input mechanism, isotropic medium, dominant source frequency of 125 Hz, and 5% noise with a deviatoric constraint applied to the inversion. The bolded row is the location with the highest correlation in the grid search and thus the final ouputted result. Refer to Figure C.9e for visual.

Location Number	X Coord (m)	Y Coord (m)	Correlation	Strike 1 (°)	Dip 1 (°)	Rake 1 (°)	Strike 2 (°)	Dip 2 (°)	Rake 2 (°)	DC %	CLVD %	ISO %
1	-50	-50	0.0999	351	44	-91	173	46	-89	23.99	76.01	0
2	-50	-25	0.1092	24	44	-90	205	46	-90	24.75	75.25	0
3	-50	0	0.0345	3	44	-89	181	46	-91	41.92	58.08	0
4	-50	25	0.0149	230	45	93	46	45	87	51.11	48.89	0
5	-50	50	0.0116	208	42	87	32	48	92	28.73	71.27	0
6	-25	-50	0.2127	176	45	90	357	45	90	22.73	77.27	0
7	-25	-25	0.0703	193	46	92	11	44	88	67.04	32.96	0
8	-25	0	0.0562	31	44	-91	213	46	-89	21.02	78.98	0
9	-25	25	0.0279	5	44	-93	189	46	-87	31.08	68.92	0
10	-25	50	0.0118	312	45	-99	145	46	-81	31.29	68.71	0
11	0	-50	0.0535	1	44	-89	180	46	-91	19.86	80.14	0
12	0	-25	0.0494	321	45	-89	140	45	-91	85.92	14.08	0
13	0	0	0.036	154	45	92	332	45	88	33.25	66.75	0
14	0	25	0.034	43	44	-93	226	46	-88	13.81	86.19	0
15	0	50	0.0303	30	45	-88	206	45	-92	13.07	86.93	0
16	25	-50	0.2547	1	45	-90	181	45	-90	30.36	69.64	0
17	25	-25	0.1287	358	45	-91	179	45	-89	40.07	59.93	0
18	25	0	0.022	188	46	98	356	45	81	57.74	42.26	0
19	25	25	0.0158	195	45	84	23	45	96	41.56	58.44	0
20	25	50	0.0107	30	46	-87	206	44	-93	17.88	82.12	0
21	50	-50	0.0508	353	44	-89	172	46	-91	33.49	66.51	0
22	50	-25	0.0603	15	45	-89	194	45	-91	46.67	53.33	0
23	50	0	0.0406	14	45	-89	192	45	-91	25.6	74.4	0
24	50	25	0.012	191	47	106	348	45	73	38.1	61.9	0
25	50	50	0.0099	190	50	110	341	44	68	71.55	28.45	0

Table C.78: Full-wavefield moment tensor inversion results for location 3d, ISO input mechanism, isotropic medium, dominant source frequency of 125 Hz, and 5% noise with a DC constraint applied to the inversion. The bolded row is the location with the highest correlation in the grid search and thus the final ouputted result. Refer to Figure C.9f for visual.

Location Number	X Coord (m)	Y Coord (m)	Correlation	Strike 1 (°)	Dip 1 (°)	Rake 1 (°)	Strike 2 (°)	Dip 2 (°)	Rake 2 (°)	DC %	CLVD %	ISO %
1	-50	-50	0.0999	351	44	-91	173	46	-89	23.99	76.01	0
2	-50	-25	0.103	11	44	-91	192	46	-89	96.52	3.48	0
3	-50	0	0.0338	359	44	-89	178	46	-91	97.76	2.24	0
4	-50	25	0.0137	220	42	90	40	48	90	98.79	1.21	0
5	-50	50	0.0105	190	44	98	360	47	83	99.36	0.64	0
6	-25	-50	0.2127	176	45	90	357	45	90	22.73	77.27	0
7	-25	-25	0.0699	191	46	92	8	44	88	99.62	0.38	0
8	-25	0	0.0562	31	44	-91	213	46	-89	21.02	78.98	0
9	-25	25	0.0279	5	44	-93	189	46	-87	31.08	68.92	0
10	-25	50	0.0116	46	38	80	238	53	97	22.35	77.65	0
11	0	-50	0.0535	1	44	-89	180	46	-91	19.86	80.14	0
12	0	-25	0.0493	319	45	-89	138	45	-91	97.87	2.13	0
13	0	0	0.0347	163	45	92	339	45	88	95.72	4.28	0
14	0	25	0.034	43	44	-93	226	46	-88	13.81	86.19	0
15	0	50	0.0275	356	44	-87	173	47	-92	97.56	2.44	0
16	25	-50	0.2547	1	45	-90	181	45	-90	30.36	69.64	0
17	25	-25	0.1264	357	44	-91	179	46	-89	92.48	7.52	0
18	25	0	0.0217	183	45	96	355	45	84	93.68	6.32	0
19	25	25	0.0154	184	47	85	11	43	95	99.54	0.46	0
20	25	50	0.0099	360	44	-87	175	46	-93	95.4	4.6	0
21	50	-50	0.0493	357	44	-89	175	46	-91	98.23	1.77	0
22	50	-25	0.0595	10	44	-89	189	46	-91	91.47	8.53	0
23	50	0	0.0406	14	45	-89	192	45	-91	25.6	74.4	0
24	50	25	0.0117	185	46	104	345	46	76	97.16	2.84	0
25	50	50	0.0099	191	51	113	337	45	64	92.06	7.94	0

Table C.79: Full-wavefield moment tensor inversion results for location 3e, ISO input mechanism, isotropic medium, dominant source frequency of 125 Hz, and 5% noise with no constraints applied to the inversion. The bolded row is the location with the highest correlation in the grid search and thus the final ouputted result. Refer to Figure C.9g for visual.

Location Number	X Coord (m)	Y Coord (m)	Correlation	Strike 1 (°)	Dip 1 (°)	Rake 1 (°)	Strike 2 (°)	Dip 2 (°)	Rake 2 (°)	DC %	CLVD %	ISO %
1	-50	-50	0.0849	3	44	-100	197	47	-80	14.81	3.79	-81.4
2	-50	-25	0.2643	323	48	-105	164	44	-75	4.05	2.98	-92.97
3	-50	0	0.0838	238	89	-169	148	79	-1	9.22	2.38	88.4
4	-50	25	0.1109	353	64	152	96	65	29	3.04	4.33	92.63
5	-50	50	0.0323	234	49	103	36	43	76	10.59	15.11	-74.3
6	-25	-50	0.0707	7	87	-3	97	87	-177	7.7	4.46	-87.84
7	-25	-25	0.382	298	66	-150	195	63	-27	0.73	3.6	-95.67
8	-25	0	0.4116	200	84	-176	110	86	-6	4.67	1.54	93.79
9	-25	25	0.0506	137	50	50	10	54	128	6.12	2.54	91.34
10	-25	50	0.036	52	61	95	222	29	81	15.54	4.23	-80.23
11	0	-50	0.0412	262	43	94	77	48	86	13.07	2.36	-84.57
12	0	-25	0.1516	134	85	177	225	87	5	1.65	3.95	-94.4
13	0	0	0.4326	99	60	-38	210	58	-144	1.26	8	90.74
14	0	25	0.078	223	46	90	44	44	90	3.83	5.52	-90.65
15	0	50	0.0829	57	49	-69	207	45	-112	5.97	5.8	88.23
16	25	-50	0.036	59	39	-96	246	51	-85	8.09	18.31	73.6
17	25	-25	0.0436	70	85	5	339	85	175	7.62	19.18	73.2
18	25	0	0.1675	88	48	-69	239	46	-111	2.42	9	88.58
19	25	25	0.0753	235	46	88	59	44	93	16.24	1.28	-82.48
20	25	50	0.0056	10	81	-168	278	78	-9	24.1	27.82	48.08
21	50	-50	0.0255	255	38	89	77	52	91	6.62	11.87	-81.51
22	50	-25	0.0302	161	49	102	322	42	76	4.64	4.7	-90.66
23	50	0	0.0051	23	78	-168	291	78	-12	49.09	20.85	30.06
24	50	25	0.0058	114	62	74	325	32	117	38.88	17.69	43.43
25	50	50	0.006	66	70	77	280	24	122	50.23	27.92	21.85

Table C.80: Full-wavefield moment tensor inversion results for location 3e, ISO input mechanism, isotropic medium, dominant source frequency of 125 Hz, and 5% noise with a deviatoric constraint applied to the inversion. The bolded row is the location with the highest correlation in the grid search and thus the final ouputted result. Refer to Figure C.9h for visual.

Location Number	X Coord (m)	Y Coord (m)	Correlation	Strike 1 (°)	Dip 1 (°)	Rake 1 (°)	Strike 2 (°)	Dip 2 (°)	Rake 2 (°)	DC %	CLVD %	ISO %
1	-50	-50	0.0518	116	47	88	299	43	92	68.81	31.19	0
2	-50	-25	0.1484	157	45	89	338	45	91	14.16	85.84	0
3	-50	0	0.0599	127	44	-87	303	46	-93	56.63	43.37	0
4	-50	25	0.0614	343	44	-93	168	46	-87	27.68	72.32	0
5	-50	50	0.0199	213	47	93	29	43	87	25.72	74.28	0
6	-25	-50	0.0436	205	46	91	24	44	89	25.94	74.06	0
7	-25	-25	0.2147	157	45	90	337	45	90	23.49	76.51	0
8	-25	0	0.2402	330	45	-90	151	45	-90	27.9	72.1	0
9	-25	25	0.0342	188	51	118	329	47	60	45.77	54.23	0
10	-25	50	0.0245	147	45	78	343	46	101	24.96	75.04	0
11	0	-50	0.0263	140	45	89	322	45	91	12.88	87.12	0
12	0	-25	0.0878	143	46	92	321	44	88	44.91	55.09	0
13	0	0	0.2503	334	45	-90	154	45	-90	31.84	68.16	0
14	0	25	0.0526	155	45	91	333	45	89	54.35	45.65	0
15	0	50	0.051	338	44	-89	157	46	-91	56.45	43.55	0
16	25	-50	0.0222	149	47	86	334	44	94	10.04	89.96	0
17	25	-25	0.0373	8	42	-93	192	48	-87	80.52	19.48	0
18	25	0	0.0959	328	45	-90	148	45	-90	40.9	59.1	0
19	25	25	0.0474	159	45	92	337	45	88	34.84	65.16	0
20	25	50	0.0049	169	55	113	313	41	61	72.47	27.53	0
21	50	-50	0.0182	159	45	85	346	45	95	33.61	66.39	0
22	50	-25	0.0212	162	46	94	336	44	86	89.12	10.88	0
23	50	0	0.005	24	75	-164	290	75	-16	88.3	11.7	0
24	50	25	0.0054	102	68	80	307	24	113	80.14	19.86	0
25	50	50	0.0059	63	71	77	279	23	124	82.62	17.38	0

Table C.81: Full-wavefield moment tensor inversion results for location 3e, ISO input mechanism, isotropic medium, dominant source frequency of 125 Hz, and 5% noise with a DC constraint applied to the inversion. The bolded row is the location with the highest correlation in the grid search and thus the final ouputted result. Refer to Figure C.9i for visual.

Location Number	X Coord (m)	Y Coord (m)	Correlation	Strike 1 (°)	Dip 1 (°)	Rake 1 (°)	Strike 2 (°)	Dip 2 (°)	Rake 2 (°)	DC %	CLVD %	ISO %
1	-50	-50	0.0513	123	47	87	307	43	93	90.7	9.3	0
2	-50	-25	0.1484	157	45	89	338	45	91	14.16	85.84	0
3	-50	0	0.0595	133	45	-86	308	46	-94	93.34	6.66	0
4	-50	25	0.0614	343	44	-93	168	46	-87	27.68	72.32	0
5	-50	50	0.0199	213	47	93	29	43	87	25.72	74.28	0
6	-25	-50	0.0404	178	45	89	359	45	91	97.21	2.79	0
7	-25	-25	0.2049	156	45	90	337	45	90	93.94	6.06	0
8	-25	0	0.2402	330	45	-90	151	45	-90	27.9	72.1	0
9	-25	25	0.034	188	50	111	337	44	67	95.45	4.55	0
10	-25	50	0.0245	147	45	78	343	46	101	24.96	75.04	0
11	0	-50	0.0263	140	45	89	322	45	91	12.88	87.12	0
12	0	-25	0.0862	149	46	91	327	44	89	96.73	3.27	0
13	0	0	0.2503	334	45	-90	154	45	-90	31.84	68.16	0
14	0	25	0.0519	154	45	91	333	45	89	95.27	4.73	0
15	0	50	0.0507	336	44	-89	154	46	-91	93.76	6.24	0
16	25	-50	0.0222	149	47	86	334	44	94	10.04	89.96	0
17	25	-25	0.0372	11	43	-92	194	48	-88	99.57	0.43	0
18	25	0	0.0943	331	45	-90	151	45	-90	96.48	3.52	0
19	25	25	0.0459	156	45	91	334	45	89	90.75	9.25	0
20	25	50	0.0049	168	54	111	315	41	64	98.28	1.72	0
21	50	-50	0.0176	161	45	87	345	45	93	97.32	2.68	0
22	50	-25	0.0212	162	46	95	335	44	85	97.33	2.67	0
23	50	0	0.005	24	74	-163	289	74	-17	99.24	0.76	0
24	50	25	0.0054	104	70	76	320	24	124	95.01	4.99	0
25	50	50	0.0058	61	72	75	281	23	129	95.07	4.93	0

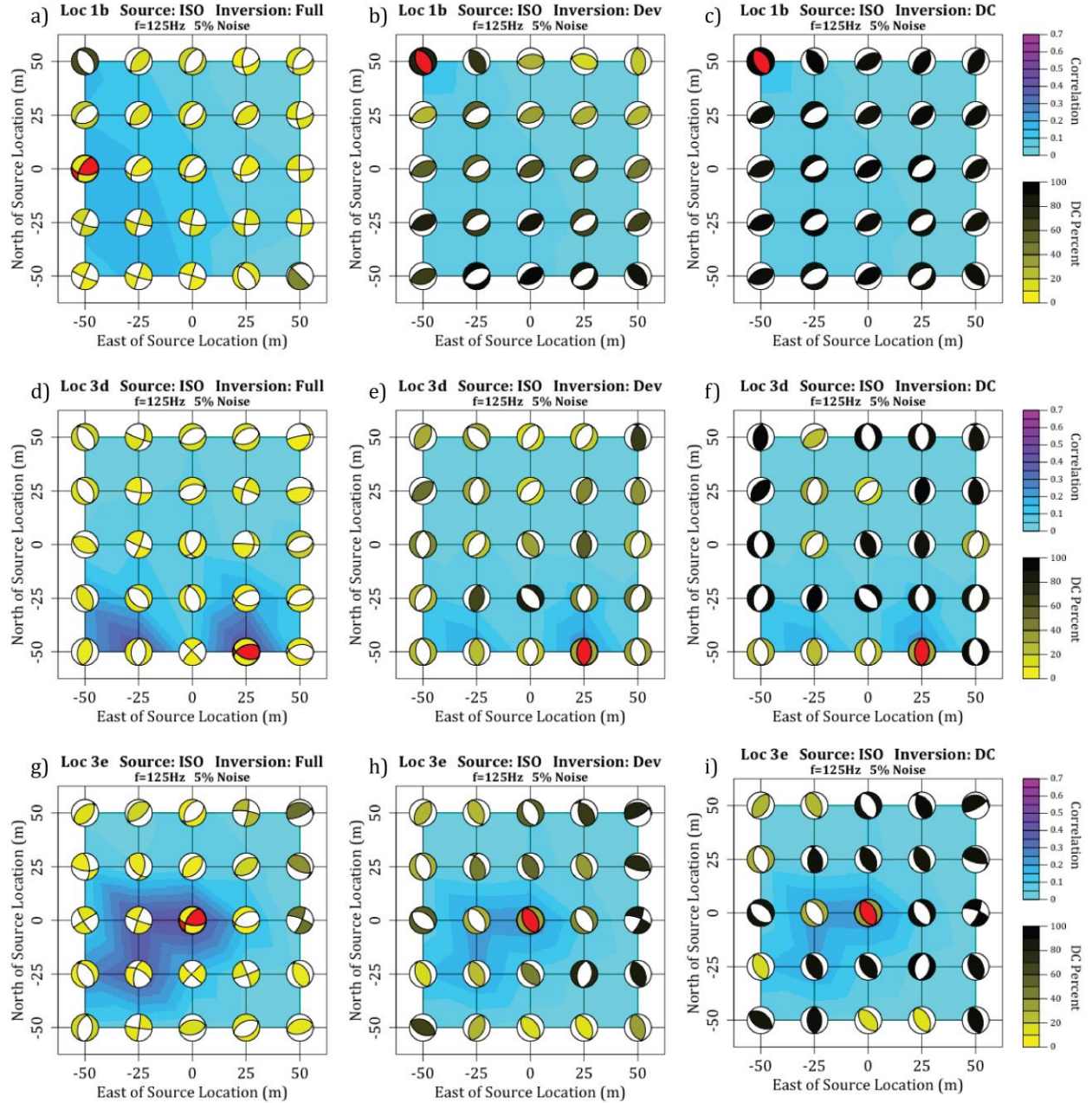


Figure C.9: Full-wavefield moment tensor inversion results for an ISO source mechanism in an isotropic medium, 5% noise, and source frequency of 125 Hz for a) location 1b with no constraints on the inversion, b) location 1b with a deviatoric constraint, c) location 1b with a DC constraint, d) location 3d with no constraints, e) location 3d with a deviatoric constraint, f) location 3d with a DC constraint, g) location 3e with no constraints, h) location 3e with a deviatoric constraint, and i) location 3e with a DC constraint. The red beach-ball is the location and source mechanism with the highest correlation to the input seismograms. Refer to Tables C.73-C.81 for numerical values of results.

Table C.82: Full-wavefield moment tensor inversion results for location 1b, DC input mechanism, isotropic medium, and dominant source frequency of 50 Hz with no constraints applied to the inversion. The bolded row is the location with the highest correlation in the grid search and thus the final ouputted result. Refer to Figure C.10a for visual.

Location Number	X Coord (m)	Y Coord (m)	Correlation	Strike 1 (°)	Dip 1 (°)	Rake 1 (°)	Strike 2 (°)	Dip 2 (°)	Rake 2 (°)	DC %	CLVD %	ISO %
1	-50	-50	0.2749	139	42	-84	311	48	-95	75.7	20.18	-4.12
2	-50	-25	0.2881	139	42	-82	309	48	-97	72.45	21.05	6.5
3	-50	0	0.2856	139	43	-80	305	48	-99	78.27	16.01	-5.72
4	-50	25	0.2612	143	45	-77	306	47	-102	72.23	18.99	8.78
5	-50	50	0.1512	303	45	74	146	47	106	69.97	18.14	-11.89
6	-25	-50	0.278	129	41	-87	305	49	-93	62.58	18.34	-19.08
7	-25	-25	0.2738	135	41	-84	307	49	-95	60.26	25.84	13.9
8	-25	0	0.2473	140	43	-81	308	48	-98	54.83	26.78	18.39
9	-25	25	0.2357	145	43	102	308	48	79	26.39	40.79	-32.82
10	-25	50	0.2138	137	37	97	308	53	85	4.47	49.14	-46.39
11	0	-50	0.2513	129	40	-88	306	50	-91	61.71	29.91	-8.38
12	0	-25	0.2353	144	42	96	316	49	85	7.93	47.98	-44.09
13	0	0	0.2296	143	42	99	310	49	82	10.3	46.83	-42.87
14	0	25	0.1896	135	39	94	310	51	87	2.84	54.07	-43.09
15	0	50	0.1529	133	41	-81	301	50	-98	37.81	35.33	26.86
16	25	-50	0.2109	141	42	91	319	48	89	5.45	53.88	-40.67
17	25	-25	0.21	141	42	96	313	49	85	7	51.13	-41.87
18	25	0	0.1741	87	85	-2	178	88	-175	1.7	50.22	-48.08
19	25	25	0.1374	347	82	161	80	71	8	3.08	51.79	-45.13
20	25	50	0.1132	129	41	-82	298	50	-97	39.84	35.11	25.05
21	50	-50	0.1584	134	41	-87	309	49	-93	37.62	40.87	21.51
22	50	-25	0.1517	87	89	-5	177	85	-179	1.87	56.34	-41.79
23	50	0	0.1277	351	88	170	82	80	2	1.12	51.29	-47.59
24	50	25	0.1082	130	41	-83	301	49	-96	28.03	38.85	33.12
25	50	50	0.0828	125	40	-83	296	50	-96	39.09	35.73	25.18

Table C.83: Full-wavefield moment tensor inversion results for location 1b, DC input mechanism, isotropic medium, and dominant source frequency of 50 Hz with a deviatoric constraint applied to the inversion. The bolded row is the location with the highest correlation in the grid search and thus the final ouputted result. Refer to Figure C.10b for visual.

Location Number	X Coord (m)	Y Coord (m)	Correlation	Strike 1 (°)	Dip 1 (°)	Rake 1 (°)	Strike 2 (°)	Dip 2 (°)	Rake 2 (°)	DC %	CLVD %	ISO %
1	-50	-50	0.2748	311	48	-95	139	42	-84	77.5	22.5	0
2	-50	-25	0.288	138	42	-82	308	48	-97	80.32	19.68	0
3	-50	0	0.2854	140	43	-80	306	48	-99	80.33	19.67	0
4	-50	25	0.2607	143	45	-77	305	46	-102	84.84	15.16	0
5	-50	50	0.1506	303	45	74	145	47	105	87.6	12.4	0
6	-25	-50	0.2769	132	41	-87	307	49	-93	69.82	30.18	0
7	-25	-25	0.273	133	42	-84	305	49	-95	77.74	22.26	0
8	-25	0	0.2449	139	43	-81	307	48	-98	79.44	20.56	0
9	-25	25	0.2229	308	47	80	142	44	101	66.72	33.28	0
10	-25	50	0.1908	137	41	100	304	50	82	61.79	38.21	0
11	0	-50	0.2511	129	40	-88	307	50	-91	64.36	35.64	0
12	0	-25	0.2216	136	42	-84	308	48	-95	74.99	25.01	0
13	0	0	0.2005	139	43	98	309	48	83	61.42	38.58	0
14	0	25	0.1755	135	43	-81	303	48	-98	76.13	23.87	0
15	0	50	0.1485	132	42	-81	300	49	-98	74.12	25.88	0
16	25	-50	0.1998	135	42	-87	310	48	-93	62.14	37.86	0
17	25	-25	0.1826	138	42	95	310	48	85	50.69	49.31	0
18	25	0	0.157	134	42	-83	305	48	-96	72.05	27.95	0
19	25	25	0.1297	132	42	-83	302	48	-96	70.75	29.25	0
20	25	50	0.1105	127	41	-82	297	49	-97	73.09	26.91	0
21	50	-50	0.1556	132	42	-87	308	49	-93	61.34	38.66	0
22	50	-25	0.1416	133	42	-85	306	48	-95	61.06	38.94	0
23	50	0	0.1108	126	40	95	300	50	86	46.38	53.62	0
24	50	25	0.1016	128	42	-84	300	49	-96	71.58	28.42	0
25	50	50	0.0807	124	41	-83	295	49	-96	72.33	27.67	0

Table C.84: Full-wavefield moment tensor inversion results for location 1b, DC input mechanism, isotropic medium, and dominant source frequency of 50 Hz with a DC constraint applied to the inversion. The bolded row is the location with the highest correlation in the grid search and thus the final ouputted result. Refer to Figure C.10c for visual.

Location Number	X Coord (m)	Y Coord (m)	Correlation	Strike 1 (°)	Dip 1 (°)	Rake 1 (°)	Strike 2 (°)	Dip 2 (°)	Rake 2 (°)	DC %	CLVD %	ISO %
1	-50	-50	0.2708	315	47	-96	143	43	-84	99.41	0.59	0
2	-50	-25	0.2844	311	47	-97	142	43	-82	99.23	0.77	0
3	-50	0	0.2805	309	47	-100	143	44	-80	99.64	0.36	0
4	-50	25	0.2546	307	45	-103	144	46	-77	98.63	1.37	0
5	-50	50	0.1474	145	48	105	303	44	74	99.79	0.21	0
6	-25	-50	0.2708	137	41	-86	312	49	-94	99.6	0.4	0
7	-25	-25	0.2682	137	42	-84	309	48	-96	99.11	0.89	0
8	-25	0	0.2383	140	44	-81	308	47	-98	99.67	0.33	0
9	-25	25	0.2019	142	45	100	308	46	80	98.3	1.7	0
10	-25	50	0.1683	304	49	81	137	42	100	97.92	2.08	0
11	0	-50	0.2419	134	41	-87	310	49	-93	98.46	1.54	0
12	0	-25	0.2136	137	43	-84	309	48	-95	98.38	1.62	0
13	0	0	0.1787	135	43	-82	305	47	-97	99.1	0.9	0
14	0	25	0.1669	135	43	-81	304	47	-98	99.51	0.49	0
15	0	50	0.1393	132	43	-81	300	48	-98	99.69	0.31	0
16	25	-50	0.1849	135	42	-86	310	48	-94	98.49	1.51	0
17	25	-25	0.1582	134	42	-85	306	48	-95	98.71	1.29	0
18	25	0	0.1473	134	43	-83	304	47	-96	97.58	2.42	0
19	25	25	0.1197	132	43	-83	302	48	-97	97.93	2.07	0
20	25	50	0.1036	128	42	-82	297	48	-97	98.06	1.94	0
21	50	-50	0.1453	132	42	-86	307	48	-93	99.91	0.09	0
22	50	-25	0.1266	133	43	-85	306	47	-95	96.87	3.13	0
23	50	0	0.1039	129	42	-84	300	48	-95	97.36	2.64	0
24	50	25	0.0951	128	42	-84	299	48	-96	98.2	1.8	0
25	50	50	0.0765	124	42	-83	295	49	-96	99.65	0.35	0

Table C.85: Full-wavefield moment tensor inversion results for location 3d, DC input mechanism, isotropic medium, and dominant source frequency of 50 Hz with no constraints applied to the inversion. The bolded row is the location with the highest correlation in the grid search and thus the final ouputted result. Refer to Figure C.10d for visual.

Location Number	X Coord (m)	Y Coord (m)	Correlation	Strike 1 (°)	Dip 1 (°)	Rake 1 (°)	Strike 2 (°)	Dip 2 (°)	Rake 2 (°)	DC %	CLVD %	ISO %
1	-50	-50	0.2695	254	49	109	46	45	69	17.17	46.19	36.64
2	-50	-25	0.4263	247	46	98	56	44	82	22.01	77.32	-0.67
3	-50	0	0.2927	247	46	92	64	45	88	30.14	52.43	-17.43
4	-50	25	0.1631	248	46	92	66	44	88	27.45	45.17	-27.38
5	-50	50	0.0899	245	46	91	63	44	89	19.82	43.86	-36.32
6	-25	-50	0.4681	60	44	-106	262	48	-75	11.48	52.7	35.82
7	-25	-25	0.4267	253	47	102	56	45	77	7.45	54.52	-38.03
8	-25	0	0.3199	249	46	92	66	44	88	15.8	43.96	-40.24
9	-25	25	0.2044	67	44	-92	250	46	-88	24.32	43.25	32.43
10	-25	50	0.1508	62	44	-93	246	46	-87	22.51	43.35	34.14
11	0	-50	0.4578	62	44	-104	260	48	-77	17.46	56.52	26.02
12	0	-25	0.4382	251	46	94	66	44	86	8.08	37.04	-54.88
13	0	0	0.3241	250	45	90	70	45	90	16.02	35.85	-48.13
14	0	25	0.1907	253	45	91	71	45	89	23.5	35.43	-41.07
15	0	50	0.145	65	44	-92	248	46	-88	22.39	41.23	36.38
16	25	-50	0.4647	57	45	-109	262	48	-72	14.42	40.09	-45.49
17	25	-25	0.4635	47	46	-115	261	50	-67	10.87	46.68	-42.45
18	25	0	0.2858	12	71	-163	276	74	-20	7.94	38.26	-53.8
19	25	25	0.1769	257	45	91	75	45	89	29.24	36.04	-34.72
20	25	50	0.1229	66	45	-93	251	45	-87	27.77	46.6	25.63
21	50	-50	0.3972	57	45	-114	269	50	-67	13.24	70.96	15.8
22	50	-25	0.4498	45	48	-123	269	52	-59	10.16	78.42	11.42
23	50	0	0.3193	16	72	-165	282	76	-19	12.17	71.38	-16.45
24	50	25	0.1801	65	81	-167	333	77	-9	5.47	36.98	57.55
25	50	50	0.1098	67	45	-95	254	45	-85	31.13	63.72	5.15

Table C.86: Full-wavefield moment tensor inversion results for location 3d, DC input mechanism, isotropic medium, and dominant source frequency of 50 Hz with a deviatoric constraint applied to the inversion. The bolded row is the location with the highest correlation in the grid search and thus the final ouputted result. Refer to Figure C.10e for visual.

Location Number	X Coord (m)	Y Coord (m)	Correlation	Strike 1 (°)	Dip 1 (°)	Rake 1 (°)	Strike 2 (°)	Dip 2 (°)	Rake 2 (°)	DC %	CLVD %	ISO %
1	-50	-50	0.2671	26	57	36	275	61	141	13.25	86.75	0
2	-50	-25	0.4263	247	46	98	56	44	82	22.56	77.44	0
3	-50	0	0.291	247	45	92	64	45	88	49.05	50.95	0
4	-50	25	0.159	247	46	91	65	44	89	60.02	39.98	0
5	-50	50	0.0842	244	46	91	63	44	89	64.47	35.53	0
6	-25	-50	0.4529	65	44	-97	254	47	-84	48.21	51.79	0
7	-25	-25	0.4139	52	44	-102	248	47	-79	30.84	69.16	0
8	-25	0	0.2997	247	46	92	65	45	88	63.76	36.24	0
9	-25	25	0.1951	66	44	-92	249	46	-88	63.03	36.97	0
10	-25	50	0.1424	62	44	-92	245	46	-88	63.31	36.69	0
11	0	-50	0.4512	64	44	-99	256	47	-82	41.31	58.69	0
12	0	-25	0.4314	55	44	-102	251	47	-79	30.76	69.24	0
13	0	0	0.2771	248	45	91	66	45	89	80.17	19.83	0
14	0	25	0.1715	67	44	-92	250	46	-88	66.88	33.12	0
15	0	50	0.1329	64	44	-92	247	46	-88	66.1	33.9	0
16	25	-50	0.4529	36	59	-147	287	62	-36	9.85	90.15	0
17	25	-25	0.456	26	65	-156	286	69	-27	10.14	89.86	0
18	25	0	0.2785	13	82	-177	282	87	-8	39.74	60.26	0
19	25	25	0.1595	256	45	92	74	45	88	73.54	26.46	0
20	25	50	0.1187	66	45	-93	250	45	-87	54.92	45.08	0
21	50	-50	0.3954	60	44	-108	264	48	-73	23.03	76.97	0
22	50	-25	0.449	50	46	-115	264	50	-67	15.75	84.25	0
23	50	0	0.3188	16	76	-170	284	80	-14	17.99	82.01	0
24	50	25	0.1749	12	77	-172	280	82	-13	19.55	80.45	0
25	50	50	0.1097	67	45	-95	254	45	-85	35.32	64.68	0

Table C.87: Full-wavefield moment tensor inversion results for location 3d, DC input mechanism, isotropic medium, and dominant source frequency of 50 Hz with a DC constraint applied to the inversion. The bolded row is the location with the highest correlation in the grid search and thus the final ouputted result. Refer to Figure C.10f for visual.

Location Number	X Coord (m)	Y Coord (m)	Correlation	Strike 1 (°)	Dip 1 (°)	Rake 1 (°)	Strike 2 (°)	Dip 2 (°)	Rake 2 (°)	DC %	CLVD %	ISO %
1	-50	-50	0.2537	278	86	139	12	49	6	98.05	1.95	0
2	-50	-25	0.3849	282	89	-172	192	82	-1	98.57	1.43	0
3	-50	0	0.2708	248	46	91	66	44	89	95.7	4.3	0
4	-50	25	0.1478	248	46	91	66	44	89	98.91	1.09	0
5	-50	50	0.0795	245	46	91	63	44	89	96.87	3.13	0
6	-25	-50	0.4174	69	42	-95	256	48	-85	96.03	3.97	0
7	-25	-25	0.3892	248	47	93	64	43	87	98.6	1.4	0
8	-25	0	0.2891	248	46	91	66	44	89	96.56	3.44	0
9	-25	25	0.1799	67	44	-92	249	46	-89	96.14	3.86	0
10	-25	50	0.1318	62	44	-92	245	46	-88	97.3	2.7	0
11	0	-50	0.4082	68	42	-96	257	48	-84	95.34	4.66	0
12	0	-25	0.4085	189	84	175	280	85	6	98.99	1.01	0
13	0	0	0.2737	248	45	91	67	45	89	98.16	1.84	0
14	0	25	0.1632	252	45	91	70	45	89	95.41	4.59	0
15	0	50	0.1234	64	44	-92	246	46	-88	96.46	3.54	0
16	25	-50	0.4529	36	59	-147	287	62	-36	9.85	90.15	0
17	25	-25	0.4445	16	78	177	107	87	12	95.45	4.55	0
18	25	0	0.2768	10	84	179	100	89	6	96.01	3.99	0
19	25	25	0.1563	256	45	91	74	45	89	91.75	8.25	0
20	25	50	0.1064	66	44	-92	249	46	-88	99.03	0.97	0
21	50	-50	0.3352	261	52	-80	64	39	-103	94.95	5.05	0
22	50	-25	0.3757	259	57	-75	53	36	-112	95.92	4.08	0
23	50	0	0.3143	11	85	180	101	90	5	94.1	5.9	0
24	50	25	0.1725	7	85	180	97	90	5	93.42	6.58	0
25	50	50	0.0872	68	44	-93	252	46	-87	97.24	2.76	0

Table C.88: Full-wavefield moment tensor inversion results for location 3e, DC input mechanism, isotropic medium, and dominant source frequency of 50 Hz with no constraints applied to the inversion. The bolded row is the location with the highest correlation in the grid search and thus the final ouputted result. Refer to Figure C.10g for visual.

Location Number	X Coord (m)	Y Coord (m)	Correlation	Strike 1 (°)	Dip 1 (°)	Rake 1 (°)	Strike 2 (°)	Dip 2 (°)	Rake 2 (°)	DC %	CLVD %	ISO %
1	-50	-50	0.4027	274	44	97	84	47	84	23.77	52.29	-23.94
2	-50	-25	0.5481	252	44	91	71	46	89	23.63	33.79	-42.58
3	-50	0	0.4079	74	47	-93	258	44	-87	34.55	41.35	24.1
4	-50	25	0.3602	252	44	93	68	46	88	45.6	22	32.4
5	-50	50	0.2656	59	46	-91	240	44	-89	32.46	37.05	30.49
6	-25	-50	0.4084	82	46	-93	266	44	-87	29.02	41.34	29.64
7	-25	-25	0.4423	253	44	91	72	46	89	27.36	31.01	-41.63
8	-25	0	0.47	253	44	92	70	46	88	60.02	38.74	1.24
9	-25	25	0.4199	74	48	-102	272	43	-77	18.61	41.04	-40.35
10	-25	50	0.3311	248	43	93	64	47	87	30.56	39.78	-29.66
11	0	-50	0.3586	83	47	-94	269	43	-86	28.57	42.68	28.75
12	0	-25	0.4308	78	47	-93	263	44	-87	39.15	46.18	14.67
13	0	0	0.4385	70	46	-93	254	44	-87	42.25	35.63	-22.12
14	0	25	0.4314	255	43	94	69	47	86	32	46.04	-21.96
15	0	50	0.4556	70	48	-97	260	42	-82	12.24	36.52	51.24
16	25	-50	0.3009	261	44	91	80	46	89	31.66	33.43	-34.91
17	25	-25	0.3994	80	47	-98	272	43	-81	20.83	35.27	-43.9
18	25	0	0.48	71	46	-93	256	44	-87	30.52	47.78	21.7
19	25	25	0.5108	67	46	-91	249	44	-89	20.17	34.78	45.05
20	25	50	0.3247	68	47	-91	249	43	-89	13.42	27.56	59.02
21	50	-50	0.2602	264	44	93	80	46	87	44.33	44.57	11.1
22	50	-25	0.389	72	55	55	303	48	129	8.97	43.71	47.32
23	50	0	0.4538	74	46	-91	255	44	-89	17.89	30.47	51.64
24	50	25	0.2704	246	44	87	70	46	93	15.57	18.04	-66.39
25	50	50	0.1987	242	44	88	65	46	92	21.82	13.82	-64.36

Table C.89: Full-wavefield moment tensor inversion results for location 3e, DC input mechanism, isotropic medium, and dominant source frequency of 50 Hz with a deviatoric constraint applied to the inversion. The bolded row is the location with the highest correlation in the grid search and thus the final ouputted result. Refer to Figure C.10h for visual.

Location Number	X Coord (m)	Y Coord (m)	Correlation	Strike 1 (°)	Dip 1 (°)	Rake 1 (°)	Strike 2 (°)	Dip 2 (°)	Rake 2 (°)	DC %	CLVD %	ISO %
1	-50	-50	0.3986	273	44	94	87	47	86	50.47	49.53	0
2	-50	-25	0.4806	253	44	91	72	46	89	86.8	13.2	0
3	-50	0	0.4014	75	46	-92	259	44	-88	64.68	35.32	0
4	-50	25	0.35	251	44	93	67	46	87	43.18	56.82	0
5	-50	50	0.2486	60	46	-91	241	44	-89	72.98	27.02	0
6	-25	-50	0.3964	83	46	-92	266	44	-88	66.19	33.81	0
7	-25	-25	0.3842	255	44	91	73	46	89	90.07	9.93	0
8	-25	0	0.47	253	44	92	70	46	88	60.03	39.97	0
9	-25	25	0.4131	57	54	-125	286	48	-52	10.72	89.28	0
10	-25	50	0.316	249	44	92	66	46	88	67.55	32.45	0
11	0	-50	0.349	85	46	-93	269	44	-87	62.95	37.05	0
12	0	-25	0.4284	79	46	-93	263	44	-87	55.74	44.26	0
13	0	0	0.4335	69	46	-93	253	44	-87	41.55	58.45	0
14	0	25	0.4236	255	43	93	71	47	87	56.85	43.15	0
15	0	50	0.3942	79	47	-94	265	43	-85	78.03	21.97	0
16	25	-50	0.2762	263	44	91	81	46	89	79.92	20.08	0
17	25	-25	0.3866	67	50	-114	282	46	-64	10.84	89.16	0
18	25	0	0.4696	73	46	-93	256	44	-87	54.6	45.4	0
19	25	25	0.3972	69	46	-91	251	44	-89	85.95	14.05	0
20	25	50	0.2046	76	47	-92	258	43	-88	80.81	19.19	0
21	50	-50	0.2595	264	44	93	80	46	87	44.45	55.55	0
22	50	-25	0.3817	317	71	167	51	78	19	16.95	83.05	0
23	50	0	0.3177	77	46	-91	259	44	-89	98.62	1.38	0
24	50	25	0.1311	259	44	90	79	46	90	33.13	66.87	0
25	50	50	0.1017	253	45	90	73	45	90	25.7	74.3	0

Table C.90: Full-wavefield moment tensor inversion results for location 3e, DC input mechanism, isotropic medium, and dominant source frequency of 50 Hz with a DC constraint applied to the inversion. The bolded row is the location with the highest correlation in the grid search and thus the final ouputted result. Refer to Figure C.10i for visual.

Location Number	X Coord (m)	Y Coord (m)	Correlation	Strike 1 (°)	Dip 1 (°)	Rake 1 (°)	Strike 2 (°)	Dip 2 (°)	Rake 2 (°)	DC %	CLVD %	ISO %
1	-50	-50	0.3774	269	43	93	85	47	87	98.26	1.74	0
2	-50	-25	0.4791	253	44	91	72	46	89	93.73	6.27	0
3	-50	0	0.3821	75	46	-92	257	44	-88	98.36	1.64	0
4	-50	25	0.3076	250	44	92	67	46	88	99.4	0.6	0
5	-50	50	0.2359	60	46	-91	241	44	-89	99.5	0.5	0
6	-25	-50	0.3753	83	46	-91	265	44	-89	95.91	4.09	0
7	-25	-25	0.3835	255	44	91	73	46	89	95.74	4.26	0
8	-25	0	0.4331	252	44	91	71	46	89	99.48	0.52	0
9	-25	25	0.348	303	32	-27	56	76	-119	99.51	0.49	0
10	-25	50	0.304	248	44	92	66	46	88	96.71	3.29	0
11	0	-50	0.3307	85	46	-92	268	44	-88	96.48	3.52	0
12	0	-25	0.3989	79	46	-92	262	44	-88	99.98	0.02	0
13	0	0	0.352	70	46	-92	253	44	-88	95.34	4.66	0
14	0	25	0.3952	254	44	92	72	47	88	98.83	1.17	0
15	0	50	0.3889	78	47	-93	263	43	-86	96.2	3.8	0
16	25	-50	0.271	263	44	91	81	46	89	99.37	0.63	0
17	25	-25	0.3202	70	68	63	304	34	139	94.65	5.35	0
18	25	0	0.4229	74	46	-91	256	44	-88	98.73	1.27	0
19	25	25	0.3894	70	46	-91	251	44	-89	96.06	3.94	0
20	25	50	0.202	76	47	-92	259	43	-88	98.18	1.82	0
21	50	-50	0.2306	263	44	92	81	46	88	97.5	2.5	0
22	50	-25	0.3774	323	82	-179	233	89	-8	99.7	0.3	0
23	50	0	0.3176	77	46	-91	259	44	-89	97.39	2.61	0
24	50	25	0.1311	259	44	90	79	46	90	33.13	66.87	0
25	50	50	0.1017	253	45	90	73	45	90	25.7	74.3	0

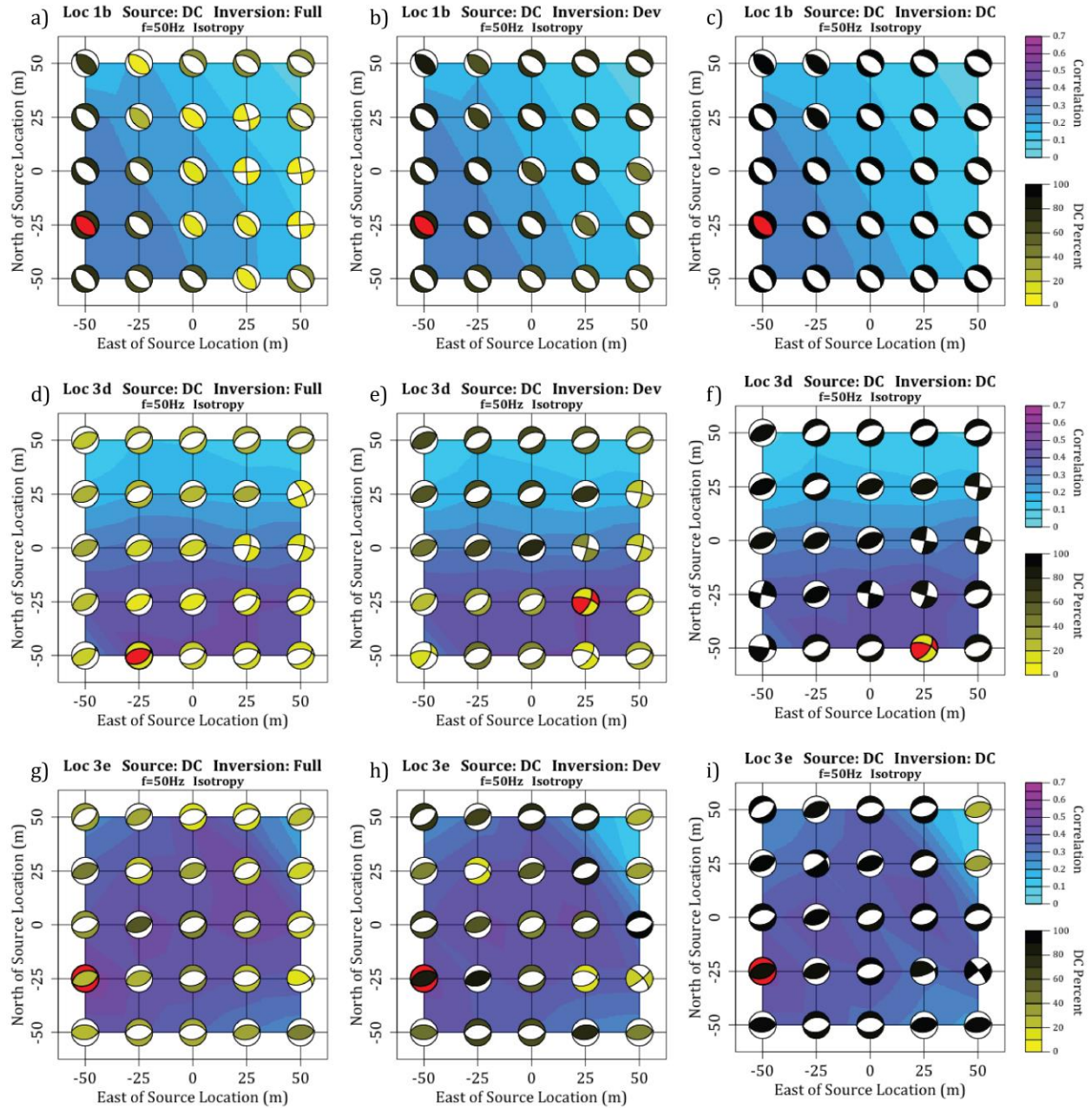


Figure C.10: Full-wavefield moment tensor inversion results for a DC source mechanism in an isotropic medium and source frequency of 50 Hz for a) location 1b with no constraints on the inversion, b) location 1b with a deviatoric constraint, c) location 1b with a DC constraint, d) location 3d with no constraints, e) location 3d with a deviatoric constraint, f) location 3d with a DC constraint, g) location 3e with no constraints, h) location 3e with a deviatoric constraint, and i) location 3e with a DC constraint. The red beach-ball is the location and source mechanism with the highest correlation to the input seismograms. Refer to Tables C.82-C.91 for numerical values of results.

Table C.91: Full-wavefield moment tensor inversion results for location 1b, CLVD input mechanism, isotropic medium, and dominant source frequency of 50 Hz with no constraints applied to the inversion. The bolded row is the location with the highest correlation in the grid search and thus the final ouputted result. Refer to Figure C.11a for visual.

Location Number	X Coord (m)	Y Coord (m)	Correlation	Strike 1 (°)	Dip 1 (°)	Rake 1 (°)	Strike 2 (°)	Dip 2 (°)	Rake 2 (°)	DC %	CLVD %	ISO %
1	-50	-50	0.2139	94	85	175	184	85	6	2.71	31.87	65.42
2	-50	-25	0.1781	81	82	173	171	83	8	26.18	22.55	51.27
3	-50	0	0.1934	245	73	-155	148	66	-19	13.17	12.19	-74.64
4	-50	25	0.1602	266	87	-175	176	85	-3	37.25	0.52	62.23
5	-50	50	0.1804	330	42	-96	158	48	-85	50.67	29.62	19.71
6	-25	-50	0.2102	87	68	162	184	73	23	10.36	10.76	78.88
7	-25	-25	0.2066	177	83	8	86	82	173	28.23	1.3	70.47
8	-25	0	0.1588	260	88	-172	170	82	-2	43.07	21.93	-35
9	-25	25	0.1755	330	43	-95	156	47	-86	50.25	28.96	20.79
10	-25	50	0.2027	328	43	-94	154	47	-86	47.41	33.79	18.8
11	0	-50	0.1608	94	80	175	185	85	10	24.45	2.78	72.77
12	0	-25	0.2013	90	81	175	181	85	9	26.56	2.07	71.37
13	0	0	0.1598	84	77	171	176	81	13	25.33	6.54	68.13
14	0	25	0.118	62	43	165	163	80	47	71.38	10.22	-18.4
15	0	50	0.2363	325	44	-93	149	46	-87	42.04	36.33	21.63
16	25	-50	0.1372	103	88	-2	193	88	-178	9.9	10.41	-79.69
17	25	-25	0.147	84	76	172	176	82	14	30.33	2.23	67.44
18	25	0	0.1536	183	59	53	59	47	135	18.26	8.24	73.5
19	25	25	0.1257	168	57	80	6	34	105	32.98	11.6	55.42
20	25	50	0.1093	148	51	93	323	39	86	28.09	21.64	50.27
21	50	-50	0.1307	190	86	178	280	88	4	4.79	15.2	-80.01
22	50	-25	0.1226	98	88	-2	188	88	-178	11.95	4.93	-83.12
23	50	0	0.1146	186	87	-175	96	85	-3	9.35	4.14	-86.51
24	50	25	0.1106	151	52	90	330	38	89	51.37	5.89	42.74
25	50	50	0.1046	144	51	93	320	39	87	46.73	6.57	46.7

Table C.92: Full-wavefield moment tensor inversion results for location 1b, CLVD input mechanism, isotropic medium, and dominant source frequency of 50 Hz with a deviatoric constraint applied to the inversion. The bolded row is the location with the highest correlation in the grid search and thus the final ouputted result. Refer to Figure C.11b for visual.

Location Number	X Coord (m)	Y Coord (m)	Correlation	Strike 1 (°)	Dip 1 (°)	Rake 1 (°)	Strike 2 (°)	Dip 2 (°)	Rake 2 (°)	DC %	CLVD %	ISO %
1	-50	-50	0.1753	139	86	-169	48	79	-4	76.1	23.9	0
2	-50	-25	0.1718	71	84	172	162	82	6	40.11	59.89	0
3	-50	0	0.173	78	89	171	168	81	1	99.06	0.94	0
4	-50	25	0.1469	333	41	-96	161	49	-85	82.98	17.02	0
5	-50	50	0.1778	330	41	-96	159	49	-85	78.42	21.58	0
6	-25	-50	0.1638	65	81	176	155	86	9	18.86	81.14	0
7	-25	-25	0.1645	247	85	-165	156	75	-5	33.63	66.37	0
8	-25	0	0.1579	82	89	174	172	84	1	82.3	17.7	0
9	-25	25	0.1719	330	43	-95	156	48	-86	78.38	21.62	0
10	-25	50	0.2005	328	43	-95	154	47	-86	72.55	27.45	0
11	0	-50	0.1469	161	83	7	70	83	173	58.81	41.19	0
12	0	-25	0.1274	257	79	-159	163	69	-12	8.31	91.69	0
13	0	0	0.1269	75	88	171	165	81	2	27.49	72.51	0
14	0	25	0.1178	62	44	162	166	78	48	88.6	11.4	0
15	0	50	0.2328	325	44	-94	150	47	-86	70.58	29.42	0
16	25	-50	0.1152	82	80	177	173	87	10	47.55	52.45	0
17	25	-25	0.1106	72	74	179	162	89	16	39.97	60.03	0
18	25	0	0.1059	147	77	36	48	55	165	70.16	29.84	0
19	25	25	0.1048	153	59	78	356	33	110	66.68	33.32	0
20	25	50	0.1026	147	53	92	323	37	87	85.21	14.79	0
21	50	-50	0.0802	177	88	-169	87	79	-3	62.64	37.36	0
22	50	-25	0.0996	166	66	50	50	46	145	66.51	33.49	0
23	50	0	0.0963	155	58	77	358	34	110	62.32	37.68	0
24	50	25	0.0994	147	52	90	326	38	90	65.41	34.59	0
25	50	50	0.094	139	49	94	314	41	86	73.2	26.8	0

Table C.93: Full-wavefield moment tensor inversion results for location 1b, CLVD input mechanism, isotropic medium, and dominant source frequency of 50 Hz with a DC constraint applied to the inversion. The bolded row is the location with the highest correlation in the grid search and thus the final ouputted result. Refer to Figure C.11c for visual.

Location Number	X Coord (m)	Y Coord (m)	Correlation	Strike 1 (°)	Dip 1 (°)	Rake 1 (°)	Strike 2 (°)	Dip 2 (°)	Rake 2 (°)	DC %	CLVD %	ISO %
1	-50	-50	0.1753	137	85	-169	47	79	-5	98.28	1.72	0
2	-50	-25	0.1715	65	83	171	156	82	7	95.39	4.61	0
3	-50	0	0.173	77	89	171	167	81	1	94.49	5.51	0
4	-50	25	0.1427	161	83	-32	255	58	-172	90.84	9.16	0
5	-50	50	0.1659	329	41	-96	157	50	-85	98.84	1.16	0
6	-25	-50	0.1631	57	79	173	149	83	11	95.47	4.53	0
7	-25	-25	0.164	241	88	-170	150	80	-2	94.79	5.21	0
8	-25	0	0.1579	81	88	174	171	84	2	91.39	8.61	0
9	-25	25	0.1625	329	42	-95	156	48	-86	99.33	0.67	0
10	-25	50	0.1866	326	42	-95	152	48	-86	99.3	0.7	0
11	0	-50	0.1467	67	82	171	158	82	8	92.47	7.53	0
12	0	-25	0.1263	65	84	172	156	82	6	96.88	3.12	0
13	0	0	0.1263	70	85	173	160	83	5	97.79	2.21	0
14	0	25	0.1178	61	44	159	167	75	48	97.64	2.36	0
15	0	50	0.2162	323	43	-94	149	48	-86	98.31	1.69	0
16	25	-50	0.1148	79	80	175	170	85	10	91.16	8.84	0
17	25	-25	0.1101	67	76	173	159	84	14	92.03	7.97	0
18	25	0	0.1058	146	83	33	52	57	171	94.7	5.3	0
19	25	25	0.1025	151	62	80	351	29	108	99.93	0.07	0
20	25	50	0.1015	146	53	92	322	37	87	98.6	1.4	0
21	50	-50	0.0801	176	86	-169	85	79	-4	98.59	1.41	0
22	50	-25	0.0993	164	71	51	52	43	151	98.87	1.13	0
23	50	0	0.0941	153	61	80	352	31	107	98.84	1.16	0
24	50	25	0.0945	146	52	91	325	38	89	97	3	0
25	50	50	0.0891	139	50	94	313	41	85	98.93	1.07	0

Table C.94: Full-wavefield moment tensor inversion results for location 3d, CLVD input mechanism, isotropic medium, and dominant source frequency of 50 Hz with no constraints applied to the inversion. The bolded row is the location with the highest correlation in the grid search and thus the final ouputted result. Refer to Figure C.11d for visual.

Location Number	X Coord (m)	Y Coord (m)	Correlation	Strike 1 (°)	Dip 1 (°)	Rake 1 (°)	Strike 2 (°)	Dip 2 (°)	Rake 2 (°)	DC %	CLVD %	ISO %
1	-50	-50	0.3347	79	75	-162	344	72	-16	8.1	55.72	-36.18
2	-50	-25	0.3608	258	46	90	78	44	90	27.32	35.6	-37.08
3	-50	0	0.2069	258	46	90	78	44	90	28.59	34.02	-37.39
4	-50	25	0.1159	85	45	-91	267	45	-89	59.25	32.43	-8.32
5	-50	50	0.0754	191	90	-177	101	87	0	1.88	7.34	90.78
6	-25	-50	0.4706	352	83	178	82	88	7	34.48	28.16	-37.36
7	-25	-25	0.3759	98	46	-92	280	44	-88	10.58	32.97	56.45
8	-25	0	0.232	263	45	91	81	45	89	56.36	33.44	10.2
9	-25	25	0.1515	68	44	-92	251	46	-88	36.46	43.1	20.44
10	-25	50	0.1151	62	44	-93	246	46	-87	35.58	45.49	18.93
11	0	-50	0.4694	353	81	176	84	86	9	37.09	45.25	-17.66
12	0	-25	0.3807	263	46	93	79	44	87	34.46	19.7	45.84
13	0	0	0.2927	265	45	93	82	45	87	39.37	30.61	30.02
14	0	25	0.1441	69	44	-93	253	46	-87	40.09	49.87	10.04
15	0	50	0.1183	64	44	-93	248	46	-87	36.36	51.37	12.27
16	25	-50	0.5222	359	80	175	90	85	10	20.85	10.91	68.24
17	25	-25	0.4351	14	83	-179	284	89	-7	7.71	26.79	65.5
18	25	0	0.2936	265	45	92	82	45	88	25.81	42.46	-31.73
19	25	25	0.1512	263	45	89	84	45	91	14.38	32.53	-53.09
20	25	50	0.1257	65	44	-93	249	46	-87	21.99	43.75	34.26
21	50	-50	0.4461	354	81	178	85	88	9	47.6	11.76	40.64
22	50	-25	0.4253	266	45	89	87	45	91	17.44	27.42	-55.14
23	50	0	0.3925	266	45	90	86	45	90	18.08	31.56	-50.36
24	50	25	0.181	266	44	91	85	46	89	20.13	32.53	-47.34
25	50	50	0.1486	68	44	-91	249	46	-89	17.26	33.11	49.63

Table C.95: Full-wavefield moment tensor inversion results for location 3d, CLVD input mechanism, isotropic medium, and dominant source frequency of 50 Hz with a deviatoric constraint applied to the inversion. The bolded row is the location with the highest correlation in the grid search and thus the final ouputted result. Refer to Figure C.11e for visual.

Location Number	X Coord (m)	Y Coord (m)	Correlation	Strike 1 (°)	Dip 1 (°)	Rake 1 (°)	Strike 2 (°)	Dip 2 (°)	Rake 2 (°)	DC %	CLVD %	ISO %
1	-50	-50	0.3329	76	85	-172	345	82	-5	31.29	68.71	0
2	-50	-25	0.3377	258	46	91	77	44	89	78.02	21.98	0
3	-50	0	0.1908	258	46	90	77	44	90	80.73	19.27	0
4	-50	25	0.1157	85	45	-91	267	45	-89	60.11	39.89	0
5	-50	50	0.0568	75	45	-92	257	45	-88	45.89	54.11	0
6	-25	-50	0.4642	354	77	171	86	81	13	24.17	75.83	0
7	-25	-25	0.3269	5	84	-180	275	90	-6	69.44	30.56	0
8	-25	0	0.2315	263	45	91	81	45	89	57.35	42.65	0
9	-25	25	0.1493	67	44	-92	250	46	-88	60.4	39.6	0
10	-25	50	0.1138	62	44	-92	245	46	-88	57.03	42.97	0
11	0	-50	0.4684	354	79	173	85	84	11	35.71	64.29	0
12	0	-25	0.3504	265	46	95	78	44	85	25.5	74.5	0
13	0	0	0.2853	265	45	93	81	45	87	37.84	62.16	0
14	0	25	0.1437	69	44	-93	252	46	-87	50.61	49.39	0
15	0	50	0.1177	64	44	-93	248	46	-87	48.88	51.12	0
16	25	-50	0.4743	350	81	-177	260	87	-9	65.89	34.11	0
17	25	-25	0.3595	41	43	-100	234	48	-81	49.57	50.43	0
18	25	0	0.2728	265	45	92	82	45	88	62.47	37.53	0
19	25	25	0.132	69	44	-93	253	46	-87	57.07	42.93	0
20	25	50	0.1164	64	44	-93	248	46	-87	60.13	39.87	0
21	50	-50	0.4405	351	82	-180	261	90	-8	97.56	2.44	0
22	50	-25	0.3575	103	47	-97	294	43	-82	44.48	55.52	0
23	50	0	0.2685	268	45	91	86	45	89	92.44	7.56	0
24	50	25	0.1372	269	45	92	86	45	88	86.84	13.16	0
25	50	50	0.11	64	44	-92	246	46	-88	86.66	13.34	0

Table C.96: Full-wavefield moment tensor inversion results for location 3d, CLVD input mechanism, isotropic medium, and dominant source frequency of 50 Hz with a DC constraint applied to the inversion. The bolded row is the location with the highest correlation in the grid search and thus the final ouputted result. Refer to Figure C.11f for visual.

Location Number	X Coord (m)	Y Coord (m)	Correlation	Strike 1 (°)	Dip 1 (°)	Rake 1 (°)	Strike 2 (°)	Dip 2 (°)	Rake 2 (°)	DC %	CLVD %	ISO %
1	-50	-50	0.3297	79	90	-173	349	83	0	92.03	7.97	0
2	-50	-25	0.3333	258	46	90	77	44	90	93.64	6.36	0
3	-50	0	0.1879	258	46	90	77	44	90	95.96	4.04	0
4	-50	25	0.105	85	45	-91	266	45	-89	97.31	2.69	0
5	-50	50	0.0492	82	46	-91	264	44	-89	95.85	4.15	0
6	-25	-50	0.4607	359	83	179	89	89	7	94.03	5.97	0
7	-25	-25	0.3263	3	84	179	93	89	6	90.87	9.13	0
8	-25	0	0.2087	263	45	91	81	45	89	98.6	1.4	0
9	-25	25	0.1372	68	44	-91	250	46	-89	98.9	1.1	0
10	-25	50	0.1035	63	44	-92	245	46	-88	98.98	1.02	0
11	0	-50	0.4662	358	82	179	88	89	8	95.18	4.82	0
12	0	-25	0.3469	2	84	179	92	89	6	92.48	7.52	0
13	0	0	0.2354	265	45	92	82	45	88	98.15	1.85	0
14	0	25	0.1232	70	44	-92	252	46	-88	95.33	4.67	0
15	0	50	0.1028	64	44	-92	247	46	-88	98.72	1.28	0
16	25	-50	0.4735	348	81	-180	258	90	-9	92.84	7.16	0
17	25	-25	0.3496	50	41	-98	240	49	-83	95.47	4.53	0
18	25	0	0.2514	265	45	91	83	45	89	98.84	1.16	0
19	25	25	0.1177	70	44	-92	252	46	-88	95.83	4.17	0
20	25	50	0.1076	65	44	-92	247	46	-88	99.35	0.65	0
21	50	-50	0.4405	351	82	-180	261	90	-8	97.56	2.44	0
22	50	-25	0.333	103	48	-95	290	42	-84	97.05	2.95	0
23	50	0	0.2676	268	45	91	86	45	89	99.76	0.24	0
24	50	25	0.1368	269	45	92	86	45	89	93.87	6.13	0
25	50	50	0.1089	64	44	-92	246	46	-88	98.42	1.58	0

Table C.97: Full-wavefield moment tensor inversion results for location 3e, CLVD input mechanism, isotropic medium, and dominant source frequency of 50 Hz with no constraints applied to the inversion. The bolded row is the location with the highest correlation in the grid search and thus the final ouputted result. Refer to Figure C.11g for visual.

Location Number	X Coord (m)	Y Coord (m)	Correlation	Strike 1 (°)	Dip 1 (°)	Rake 1 (°)	Strike 2 (°)	Dip 2 (°)	Rake 2 (°)	DC %	CLVD %	ISO %
1	-50	-50	0.3603	83	47	-94	269	44	-86	28.1	50.58	21.32
2	-50	-25	0.5456	244	85	170	335	80	5	20.67	20.34	58.99
3	-50	0	0.4595	239	80	165	332	75	11	9.18	16.6	74.22
4	-50	25	0.2937	45	44	-92	228	46	-88	46.2	44.67	9.13
5	-50	50	0.1834	235	45	92	53	45	88	44.63	23	32.37
6	-25	-50	0.3416	81	47	-94	266	43	-86	5.97	34.23	59.8
7	-25	-25	0.4982	250	85	168	341	78	5	19.79	20.81	59.4
8	-25	0	0.4681	63	81	-165	331	76	-9	17.51	28.14	-54.35
9	-25	25	0.3687	42	43	-94	228	47	-86	18.25	42.92	38.83
10	-25	50	0.2676	44	43	-91	225	47	-89	15.27	31.73	53
11	0	-50	0.3238	245	46	90	65	44	90	16.61	31.49	-51.9
12	0	-25	0.4774	269	85	170	360	80	5	5.87	33.28	-60.85
13	0	0	0.4997	344	81	180	75	90	9	25.12	11.42	63.46
14	0	25	0.4879	22	44	-114	234	51	-69	4.19	38.39	57.42
15	0	50	0.4122	237	45	90	57	45	90	23.33	31.2	-45.47
16	25	-50	0.2519	245	46	91	63	44	89	31.75	36.12	-32.13
17	25	-25	0.3769	235	48	98	43	43	81	13.37	42.87	-43.76
18	25	0	0.4892	336	78	-180	246	90	-12	55.97	7.09	36.94
19	25	25	0.5315	333	76	-176	242	86	-14	30.16	11.08	-58.76
20	25	50	0.4024	322	77	179	52	89	13	18.94	12.65	-68.41
21	50	-50	0.1773	68	44	-92	251	46	-88	47.12	40.48	-12.4
22	50	-25	0.3507	67	45	-92	250	45	-88	44.24	50.77	-4.99
23	50	0	0.4968	333	77	-179	243	89	-13	27.62	5.79	-66.59
24	50	25	0.2751	87	50	-85	260	40	-96	4.48	13.47	82.05
25	50	50	0.2237	66	80	-157	331	67	-11	4.36	12.07	83.57

Table C.98: Full-wavefield moment tensor inversion results for location 3e, CLVD input mechanism, isotropic medium, and dominant source frequency of 50 Hz with a deviatoric constraint applied to the inversion. The bolded row is the location with the highest correlation in the grid search and thus the final ouputted result. Refer to Figure C.11h for visual.

Location Number	X Coord (m)	Y Coord (m)	Correlation	Strike 1 (°)	Dip 1 (°)	Rake 1 (°)	Strike 2 (°)	Dip 2 (°)	Rake 2 (°)	DC %	CLVD %	ISO %
1	-50	-50	0.3571	85	46	-93	269	44	-87	52.51	47.49	0
2	-50	-25	0.5251	69	88	-172	339	82	-2	70.36	29.64	0
3	-50	0	0.4086	71	82	-168	339	78	-8	38.59	61.41	0
4	-50	25	0.2931	45	44	-92	228	46	-88	56.96	43.04	0
5	-50	50	0.1778	41	44	-92	224	46	-88	64.5	35.5	0
6	-25	-50	0.2625	87	46	-91	269	44	-89	98.95	1.05	0
7	-25	-25	0.4792	76	88	-171	345	81	-2	82.26	17.74	0
8	-25	0	0.4565	58	89	-170	327	80	-1	82.37	17.63	0
9	-25	25	0.3592	241	45	92	59	45	88	49.93	50.07	0
10	-25	50	0.2486	236	45	91	55	45	89	67.9	32.1	0
11	0	-50	0.2432	243	46	91	62	44	89	98.43	1.57	0
12	0	-25	0.4079	221	48	96	32	43	84	63.43	36.57	0
13	0	0	0.4538	347	53	-141	230	60	-44	19.7	80.3	0
14	0	25	0.4222	25	42	-96	214	48	-84	71.84	28.16	0
15	0	50	0.2951	237	45	91	57	45	89	94.58	5.42	0
16	25	-50	0.2358	244	46	91	62	44	89	74.36	25.64	0
17	25	-25	0.3621	65	45	-92	247	45	-88	53.53	46.47	0
18	25	0	0.4843	333	77	-176	242	86	-13	68.88	31.12	0
19	25	25	0.5076	341	78	177	72	87	12	87.86	12.14	0
20	25	50	0.3501	334	63	157	75	69	29	28.65	71.35	0
21	50	-50	0.1766	68	45	-92	251	46	-88	47.64	52.36	0
22	50	-25	0.3504	67	45	-92	250	45	-88	43.97	56.03	0
23	50	0	0.4474	345	71	168	79	78	19	41.26	58.74	0
24	50	25	0.1638	320	44	-84	131	46	-96	84.22	15.78	0
25	50	50	0.1629	95	72	-158	358	69	-20	19.93	80.07	0

Table C.99: Full-wavefield moment tensor inversion results for location 3e, CLVD input mechanism, isotropic medium, and dominant source frequency of 50 Hz with a DC constraint applied to the inversion. The bolded row is the location with the highest correlation in the grid search and thus the final ouputted result. Refer to Figure C.11i for visual.

Location Number	X Coord (m)	Y Coord (m)	Correlation	Strike 1 (°)	Dip 1 (°)	Rake 1 (°)	Strike 2 (°)	Dip 2 (°)	Rake 2 (°)	DC %	CLVD %	ISO %
1	-50	-50	0.3304	83	47	-92	266	43	-88	96.92	3.08	0
2	-50	-25	0.5246	71	89	-172	341	82	-1	94.7	5.3	0
3	-50	0	0.4071	74	88	-171	343	81	-2	99.17	0.83	0
4	-50	25	0.2661	46	44	-91	228	46	-89	98.14	1.86	0
5	-50	50	0.1669	42	44	-91	224	46	-89	99.46	0.54	0
6	-25	-50	0.2625	87	46	-91	269	44	-89	99.96	0.04	0
7	-25	-25	0.479	77	89	-171	347	81	-1	94.95	5.05	0
8	-25	0	0.4564	238	89	170	329	80	1	97.29	2.71	0
9	-25	25	0.3315	42	43	-92	225	47	-88	98.81	1.19	0
10	-25	50	0.232	236	45	91	55	45	89	97.51	2.49	0
11	0	-50	0.2432	243	46	91	62	44	89	97.3	2.7	0
12	0	-25	0.4025	223	48	94	37	42	85	97.17	2.83	0
13	0	0	0.4377	338	43	-162	235	78	-49	94.53	5.47	0
14	0	25	0.4171	30	42	-95	216	48	-86	96.85	3.15	0
15	0	50	0.2951	237	45	91	57	45	89	93.55	6.45	0
16	25	-50	0.2316	244	46	91	62	44	89	93.77	6.23	0
17	25	-25	0.3461	229	48	94	44	43	86	93.63	6.37	0
18	25	0	0.4839	331	78	-179	241	89	-12	99.42	0.58	0
19	25	25	0.5075	342	78	178	72	88	12	99.53	0.47	0
20	25	50	0.3478	75	81	25	341	65	170	92.26	7.74	0
21	50	-50	0.1497	69	45	-91	250	45	-89	98.61	1.39	0
22	50	-25	0.2825	68	45	-91	249	45	-89	96.94	3.06	0
23	50	0	0.4459	350	76	176	81	86	14	98.35	1.65	0
24	50	25	0.1636	130	46	-95	317	44	-84	90.55	9.45	0
25	50	50	0.1607	95	80	-163	2	73	-10	93.76	6.24	0

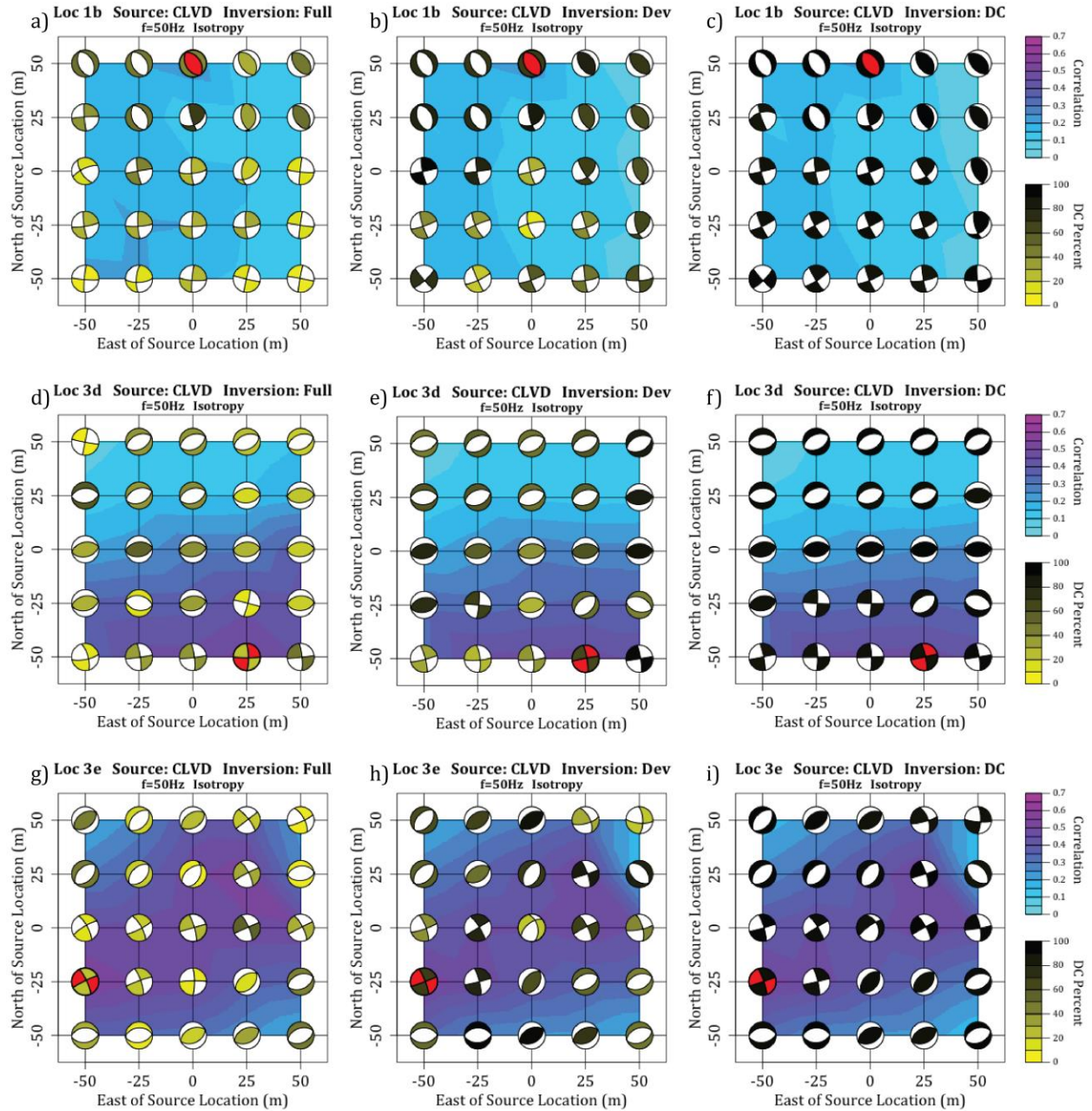


Figure C.11: Full-wavefield moment tensor inversion results for a CLVD source mechanism in an isotropic medium and source frequency of 50 Hz for a) location 1b with no constraints on the inversion, b) location 1b with a deviatoric constraint, c) location 1b with a DC constraint, d) location 3d with no constraints, e) location 3d with a deviatoric constraint, f) location 3d with a DC constraint, g) location 3e with no constraints, h) location 3e with a deviatoric constraint, and i) location 3e with a DC constraint. The red beach-ball is the location and source mechanism with the highest correlation to the input seismograms. Refer to Tables C.91-C.99 for numerical values of results.

Table C.100: Full-wavefield moment tensor inversion results for location 1b, ISO input mechanism, isotropic medium, and dominant source frequency of 50 Hz with no constraints applied to the inversion. The bolded row is the location with the highest correlation in the grid search and thus the final ouputted result. Refer to Figure C.12a for visual.

Location Number	X Coord (m)	Y Coord (m)	Correlation	Strike 1 (°)	Dip 1 (°)	Rake 1 (°)	Strike 2 (°)	Dip 2 (°)	Rake 2 (°)	DC %	CLVD %	ISO %
1	-50	-50	0.2496	204	89	-177	114	87	-1	4.99	18.11	-76.9
2	-50	-25	0.24	201	88	-173	111	83	-2	11.88	7.17	-80.95
3	-50	0	0.2194	201	76	-158	106	69	-15	8.47	5.98	-85.55
4	-50	25	0.2307	332	42	-96	160	48	-85	51.21	27.2	21.59
5	-50	50	0.2779	330	42	-96	158	48	-85	48.47	30.7	20.83
6	-25	-50	0.2207	108	85	179	198	89	5	10.86	10.5	78.64
7	-25	-25	0.2041	104	79	174	195	84	11	14	2.65	83.35
8	-25	0	0.1823	91	56	147	201	64	39	5.56	7.46	86.98
9	-25	25	0.2704	330	43	-94	156	47	-86	48.81	29.71	21.48
10	-25	50	0.3154	328	43	-94	154	47	-86	45.22	34.97	19.81
11	0	-50	0.198	103	86	178	193	88	4	8.32	10.92	80.76
12	0	-25	0.1682	191	86	-172	101	82	-4	12.44	2.42	-85.14
13	0	0	0.1365	199	60	-136	83	53	-38	4.54	7.17	-88.29
14	0	25	0.1158	209	52	73	55	41	111	14.32	2.61	83.07
15	0	50	0.3705	325	44	-93	149	46	-87	40.15	37.43	22.42
16	25	-50	0.1511	190	88	-176	99	86	-2	9.44	8.93	-81.63
17	25	-25	0.1275	93	78	172	185	82	12	9.22	3.9	86.88
18	25	0	0.1149	191	60	44	76	53	141	4.1	6.66	89.24
19	25	25	0.1189	202	52	66	58	44	118	7.3	5.73	86.97
20	25	50	0.1255	147	46	85	334	44	95	23.15	52.42	-24.43
21	50	-50	0.1243	183	86	4	93	86	176	6.65	10.54	82.81
22	50	-25	0.1069	89	82	175	179	85	8	14.31	0	85.69
23	50	0	0.1	87	79	173	178	83	11	9.23	4.11	86.66
24	50	25	0.1139	191	57	49	69	51	135	3.34	7.37	89.29
25	50	50	0.104	206	49	75	48	43	107	9.08	4.05	86.87

Table C.101: Full-wavefield moment tensor inversion results for location 1b, ISO input mechanism, isotropic medium, and dominant source frequency of 50 Hz with a deviatoric constraint applied to the inversion. The bolded row is the location with the highest correlation in the grid search and thus the final ouputted result. Refer to Figure C.12b for visual.

Location Number	X Coord (m)	Y Coord (m)	Correlation	Strike 1 (°)	Dip 1 (°)	Rake 1 (°)	Strike 2 (°)	Dip 2 (°)	Rake 2 (°)	DC %	CLVD %	ISO %
1	-50	-50	0.1036	93	46	125	228	54	59	27.73	72.27	0
2	-50	-25	0.0921	81	42	110	235	51	73	65.78	34.22	0
3	-50	0	0.1899	337	41	-95	163	49	-86	82.06	17.94	0
4	-50	25	0.2246	333	41	-96	161	49	-85	82.48	17.52	0
5	-50	50	0.2734	330	41	-96	159	49	-85	77.64	22.36	0
6	-25	-50	0.0893	80	43	111	232	51	71	37.31	62.69	0
7	-25	-25	0.076	237	50	-104	78	42	-74	58.1	41.9	0
8	-25	0	0.0774	161	48	93	337	42	87	76.89	23.11	0
9	-25	25	0.2644	330	43	-95	156	48	-86	77.73	22.27	0
10	-25	50	0.3117	328	43	-95	154	48	-86	71.52	28.48	0
11	0	-50	0.0865	71	42	105	232	50	77	48.09	51.91	0
12	0	-25	0.0719	69	42	102	233	50	79	68.17	31.83	0
13	0	0	0.056	71	42	102	235	50	79	76.57	23.43	0
14	0	25	0.0912	154	47	93	330	43	87	71.09	28.91	0
15	0	50	0.3647	325	43	-94	151	47	-87	69.49	30.51	0
16	25	-50	0.0685	232	49	79	69	42	103	38.59	61.41	0
17	25	-25	0.0551	71	42	-76	233	50	-102	31.84	68.16	0
18	25	0	0.0492	234	50	-101	71	41	-77	46.94	53.06	0
19	25	25	0.0468	237	49	-98	70	41	-80	84.39	15.61	0
20	25	50	0.124	151	47	89	332	43	91	49.3	50.7	0
21	50	-50	0.0595	229	49	79	65	42	102	32.84	67.16	0
22	50	-25	0.0494	230	49	81	63	42	100	45	55	0
23	50	0	0.0454	64	41	-79	230	50	-99	53.56	46.44	0
24	50	25	0.0457	231	49	-96	60	41	-83	65.2	34.8	0
25	50	50	0.0405	225	50	-96	53	41	-83	45.94	54.06	0

Table C.102: Full-wavefield moment tensor inversion results for location 1b, ISO input mechanism, isotropic medium, and dominant source frequency of 50 Hz with a DC constraint applied to the inversion. The bolded row is the location with the highest correlation in the grid search and thus the final ouputted result. Refer to Figure C.12c for visual.

Location Number	X Coord (m)	Y Coord (m)	Correlation	Strike 1 (°)	Dip 1 (°)	Rake 1 (°)	Strike 2 (°)	Dip 2 (°)	Rake 2 (°)	DC %	CLVD %	ISO %
1	-50	-50	0.1031	83	42	110	237	51	73	99.28	0.72	0
2	-50	-25	0.092	80	42	108	236	51	74	91.98	8.02	0
3	-50	0	0.1794	337	41	-95	163	49	-86	98.84	1.16	0
4	-50	25	0.2126	332	41	-96	160	49	-85	99.51	0.49	0
5	-50	50	0.2554	329	40	-96	157	50	-85	99.57	0.43	0
6	-25	-50	0.089	76	42	104	237	50	78	94.12	5.88	0
7	-25	-25	0.0759	241	50	-100	77	42	-78	92.97	7.03	0
8	-25	0	0.0743	160	49	93	336	41	87	98.13	1.87	0
9	-25	25	0.2502	329	42	-95	156	48	-86	99.99	0.01	0
10	-25	50	0.2873	326	41	-95	152	49	-86	98.34	1.66	0
11	0	-50	0.0863	68	42	100	235	49	81	95.53	4.47	0
12	0	-25	0.0719	69	41	101	234	49	80	94.03	5.97	0
13	0	0	0.056	71	42	101	236	49	80	99.11	0.89	0
14	0	25	0.086	153	48	93	329	42	87	99.47	0.53	0
15	0	50	0.3394	324	42	-94	149	48	-87	99.31	0.69	0
16	25	-50	0.0683	235	49	83	67	42	98	93.64	6.36	0
17	25	-25	0.0548	238	49	-99	71	42	-80	98.53	1.47	0
18	25	0	0.049	239	49	-100	74	42	-79	90.86	9.14	0
19	25	25	0.0468	237	49	-99	70	41	-80	91.71	8.29	0
20	25	50	0.1151	147	49	90	328	41	90	96.71	3.29	0
21	50	-50	0.0593	233	49	84	62	42	97	91.82	8.18	0
22	50	-25	0.0493	233	49	84	63	42	97	97.25	2.75	0
23	50	0	0.0452	64	41	-82	233	49	-97	98.87	1.13	0
24	50	25	0.0456	58	41	-83	229	50	-96	93.95	6.05	0
25	50	50	0.0403	51	40	-83	222	50	-96	90.09	9.91	0

Table C.103: Full-wavefield moment tensor inversion results for location 3d, ISO input mechanism, isotropic medium, and dominant source frequency of 50 Hz with no constraints applied to the inversion. The bolded row is the location with the highest correlation in the grid search and thus the final ouputted result. Refer to Figure C.12d for visual.

Location Number	X Coord (m)	Y Coord (m)	Correlation	Strike 1 (°)	Dip 1 (°)	Rake 1 (°)	Strike 2 (°)	Dip 2 (°)	Rake 2 (°)	DC %	CLVD %	ISO %
1	-50	-50	0.4512	1	46	-90	181	44	-90	11.87	3.2	-84.93
2	-50	-25	0.402	357	46	-91	178	44	-89	11.62	3.83	-84.55
3	-50	0	0.2174	154	44	89	335	46	91	14.5	0.61	84.89
4	-50	25	0.1558	149	44	89	331	46	91	7.93	4.31	87.76
5	-50	50	0.113	147	43	88	329	47	91	2.12	6.97	90.91
6	-25	-50	0.5091	1	47	-90	182	43	-90	7.67	3.37	-88.96
7	-25	-25	0.4327	354	47	-90	174	43	-90	8.23	3.03	-88.74
8	-25	0	0.1979	190	42	101	355	49	80	3.39	3.17	93.44
9	-25	25	0.1233	17	81	168	109	78	9	1.22	7.54	91.24
10	-25	50	0.107	196	89	-176	106	86	-1	5.76	5.13	89.11
11	0	-50	0.5089	136	86	-4	226	86	-176	5.63	2.29	92.08
12	0	-25	0.4566	221	85	-176	131	86	-5	6.14	1.83	92.03
13	0	0	0.276	214	85	-176	123	86	-5	4.59	2.42	92.99
14	0	25	0.126	200	89	-170	110	80	-1	2.61	2.9	94.49
15	0	50	0.0971	310	89	-173	220	83	-1	10	1.33	-88.67
16	25	-50	0.4567	227	80	-171	135	81	-10	5.37	5.85	88.78
17	25	-25	0.4095	220	80	-169	128	79	-10	4.88	6.7	88.42
18	25	0	0.2931	130	81	169	222	80	9	5.27	5.99	-88.74
19	25	25	0.1537	204	80	-166	111	77	-10	4.02	8.66	87.32
20	25	50	0.1053	128	83	168	219	78	7	4.43	8.31	-87.26
21	50	-50	0.4843	248	50	57	113	50	123	3.12	11.53	-85.35
22	50	-25	0.4636	244	50	56	111	51	124	3.02	11.68	-85.3
23	50	0	0.3189	228	59	37	117	59	143	2.44	11.47	-86.09
24	50	25	0.1553	260	44	77	98	48	102	6.34	11.04	-82.62
25	50	50	0.1063	227	57	36	116	61	141	2.45	10.59	-86.96

Table C.104: Full-wavefield moment tensor inversion results for location 3d, ISO input mechanism, isotropic medium, and dominant source frequency of 50 Hz with a deviatoric constraint applied to the inversion. The bolded row is the location with the highest correlation in the grid search and thus the final ouputted result. Refer to Figure C.12e for visual.

Location Number	X Coord (m)	Y Coord (m)	Correlation	Strike 1 (°)	Dip 1 (°)	Rake 1 (°)	Strike 2 (°)	Dip 2 (°)	Rake 2 (°)	DC %	CLVD %	ISO %
1	-50	-50	0.1713	180	45	90	360	45	90	24.56	75.44	0
2	-50	-25	0.1504	171	45	90	351	45	90	29.09	70.91	0
3	-50	0	0.0879	19	44	-91	201	46	-89	56.23	43.77	0
4	-50	25	0.0668	17	44	-92	200	46	-88	54.18	45.82	0
5	-50	50	0.0498	14	44	-92	196	46	-88	48.21	51.79	0
6	-25	-50	0.1955	178	45	90	358	45	90	35.64	64.36	0
7	-25	-25	0.1671	348	45	-90	168	45	-90	34.25	65.75	0
8	-25	0	0.0989	344	45	-90	164	45	-90	60.67	39.33	0
9	-25	25	0.0523	24	44	-92	206	46	-88	55.64	44.36	0
10	-25	50	0.0459	20	44	-92	202	46	-88	45.97	54.03	0
11	0	-50	0.2319	0	45	-90	180	45	-90	42.64	57.36	0
12	0	-25	0.2081	356	45	-90	176	45	-90	44.83	55.17	0
13	0	0	0.1291	355	45	-91	176	45	-89	59.1	40.9	0
14	0	25	0.064	354	45	-92	177	45	-88	93.81	6.19	0
15	0	50	0.0442	144	45	89	326	45	91	66.28	33.72	0
16	25	-50	0.2051	360	45	-90	179	45	-90	53.98	46.02	0
17	25	-25	0.1837	360	45	-90	181	45	-90	54.24	45.76	0
18	25	0	0.1312	167	45	90	347	45	90	64.04	35.96	0
19	25	25	0.0742	2	45	-92	185	46	-88	74.33	25.67	0
20	25	50	0.0504	360	44	-93	183	46	-87	71.9	28.1	0
21	50	-50	0.2239	180	45	90	1	45	90	65.77	34.23	0
22	50	-25	0.2126	175	45	90	355	45	90	66.42	33.58	0
23	50	0	0.1428	174	45	90	354	45	90	79.48	20.52	0
24	50	25	0.0789	154	45	88	336	45	92	72.46	27.54	0
25	50	50	0.0502	159	45	89	341	45	91	76.48	23.52	0

Table C.105: Full-wavefield moment tensor inversion results for location 3d, ISO input mechanism, isotropic medium, and dominant source frequency of 50 Hz with a DC constraint applied to the inversion. The bolded row is the location with the highest correlation in the grid search and thus the final ouputted result. Refer to Figure C.12f for visual.

Location Number	X Coord (m)	Y Coord (m)	Correlation	Strike 1 (°)	Dip 1 (°)	Rake 1 (°)	Strike 2 (°)	Dip 2 (°)	Rake 2 (°)	DC %	CLVD %	ISO %
1	-50	-50	0.1659	180	46	90	0	44	90	98.54	1.46	0
2	-50	-25	0.1465	174	46	90	354	44	90	99.83	0.17	0
3	-50	0	0.0873	13	44	-92	195	46	-89	91.39	8.61	0
4	-50	25	0.0662	10	44	-92	192	46	-88	90.85	9.15	0
5	-50	50	0.0491	4	44	-92	187	46	-88	94.67	5.33	0
6	-25	-50	0.1914	179	45	90	359	45	90	95.55	4.45	0
7	-25	-25	0.1639	352	45	-90	171	45	-90	96.21	3.79	0
8	-25	0	0.0984	346	45	-90	165	45	-90	95.13	4.87	0
9	-25	25	0.0518	15	44	-92	198	46	-88	92.54	7.46	0
10	-25	50	0.0452	9	44	-92	192	46	-88	90.48	9.52	0
11	0	-50	0.2294	0	45	-90	180	45	-90	90.72	9.28	0
12	0	-25	0.2059	356	45	-90	176	45	-90	93.76	6.24	0
13	0	0	0.1286	355	45	-91	175	45	-89	90.93	9.07	0
14	0	25	0.064	354	45	-92	177	45	-88	93.81	6.19	0
15	0	50	0.0439	148	45	89	330	45	91	91.85	8.15	0
16	25	-50	0.2035	360	45	-90	180	45	-90	99.44	0.56	0
17	25	-25	0.1823	359	45	-90	180	45	-90	99.54	0.46	0
18	25	0	0.1304	168	45	90	348	45	90	96.1	3.9	0
19	25	25	0.074	0	45	-92	183	46	-88	96.82	3.18	0
20	25	50	0.0504	358	44	-93	182	46	-87	91.9	8.1	0
21	50	-50	0.2229	180	45	90	1	45	90	95.92	4.08	0
22	50	-25	0.2116	176	45	90	356	45	90	95.21	4.79	0
23	50	0	0.1425	174	45	90	353	45	90	91.65	8.35	0
24	50	25	0.0786	156	45	88	339	45	92	92.47	7.53	0
25	50	50	0.0501	159	45	89	340	45	91	94.24	5.76	0

Table C.106: Full-wavefield moment tensor inversion results for location 3e, ISO input mechanism, isotropic medium, and dominant source frequency of 50 Hz with no constraints applied to the inversion. The bolded row is the location with the highest correlation in the grid search and thus the final ouputted result. Refer to Figure C.12g for visual.

Location Number	X Coord (m)	Y Coord (m)	Correlation	Strike 1 (°)	Dip 1 (°)	Rake 1 (°)	Strike 2 (°)	Dip 2 (°)	Rake 2 (°)	DC %	CLVD %	ISO %
1	-50	-50	0.4519	161	44	92	338	47	88	11.77	0.66	87.57
2	-50	-25	0.5033	333	46	-93	158	44	-87	8.96	2.83	-88.21
3	-50	0	0.4802	156	43	97	326	47	83	3.74	5.06	91.2
4	-50	25	0.3207	322	47	-94	148	43	-86	4.77	5.21	-90.02
5	-50	50	0.2105	92	87	-3	182	87	-177	4.3	3.87	91.83
6	-25	-50	0.3922	169	43	97	339	47	84	4.26	4.13	91.61
7	-25	-25	0.528	331	48	-99	163	43	-81	2.08	5.9	-92.02
8	-25	0	0.5031	197	83	177	288	87	7	2.17	5.21	92.62
9	-25	25	0.4	283	89	-175	193	85	-1	2.99	5.4	-91.61
10	-25	50	0.2884	103	88	174	193	84	2	9.3	1.11	-89.59
11	0	-50	0.3042	212	79	173	304	83	11	2.07	4.62	93.31
12	0	-25	0.4618	294	88	-173	204	83	-2	3.22	4.88	-91.9
13	0	0	0.4387	200	85	-177	110	87	-5	8.96	1.69	89.35
14	0	25	0.4737	201	69	-160	103	71	-22	2.3	10.3	87.4
15	0	50	0.3759	102	79	167	195	77	11	3.47	10.2	-86.33
16	25	-50	0.2679	117	87	175	207	85	3	5.11	2.62	-92.27
17	25	-25	0.424	210	64	-152	107	65	-29	2.07	9.73	88.2
18	25	0	0.4881	108	74	162	203	73	17	2.62	10.84	-86.54
19	25	25	0.529	78	48	-68	227	46	-113	3.79	11.39	84.82
20	25	50	0.4491	221	47	64	78	49	116	3.34	13.01	-83.65
21	50	-50	0.1773	126	90	172	216	82	0	8.38	0.5	-91.12
22	50	-25	0.3611	85	48	-71	238	46	-109	4.66	9.37	85.97
23	50	0	0.4988	228	48	63	85	49	116	3.39	12.25	-84.36
24	50	25	0.5088	72	46	-79	236	45	-101	8.08	9.4	82.52
25	50	50	0.4184	67	46	-84	239	44	-96	15.26	3.44	81.3

Table C.107: Full-wavefield moment tensor inversion results for location 3e, ISO input mechanism, isotropic medium, and dominant source frequency of 50 Hz with a deviatoric constraint applied to the inversion. The bolded row is the location with the highest correlation in the grid search and thus the final ouputted result. Refer to Figure C.12h for visual.

Location Number	X Coord (m)	Y Coord (m)	Correlation	Strike 1 (°)	Dip 1 (°)	Rake 1 (°)	Strike 2 (°)	Dip 2 (°)	Rake 2 (°)	DC %	CLVD %	ISO %
1	-50	-50	0.2012	336	45	-90	156	45	-90	28.71	71.29	0
2	-50	-25	0.2099	153	45	90	332	45	90	27.68	72.32	0
3	-50	0	0.2179	330	45	-90	151	45	-90	37.2	62.8	0
4	-50	25	0.1334	151	45	91	330	45	89	58.53	41.47	0
5	-50	50	0.1008	331	44	-92	153	46	-88	69.85	30.15	0
6	-25	-50	0.1778	334	45	-90	154	45	-90	39.97	60.03	0
7	-25	-25	0.224	155	45	90	335	45	90	36.41	63.59	0
8	-25	0	0.23	333	45	-90	153	45	-90	42.1	57.9	0
9	-25	25	0.1868	324	45	-90	144	45	-90	55.54	44.46	0
10	-25	50	0.1339	143	45	90	323	45	90	73.85	26.15	0
11	0	-50	0.1412	332	45	-89	152	45	-91	50.77	49.23	0
12	0	-25	0.2132	340	45	-90	161	45	-90	46.78	53.22	0
13	0	0	0.2025	333	45	-90	153	45	-90	49.29	50.71	0
14	0	25	0.2422	329	45	-90	149	45	-90	59.11	40.89	0
15	0	50	0.1794	146	45	90	326	45	90	74.54	25.46	0
16	25	-50	0.1225	162	45	90	342	45	90	68.5	31.5	0
17	25	-25	0.2154	339	45	-90	159	45	-90	57.38	42.62	0
18	25	0	0.236	156	45	90	336	45	90	59.07	40.93	0
19	25	25	0.2712	332	45	-90	152	45	-90	66.62	33.38	0
20	25	50	0.2186	149	45	90	329	45	90	78.94	21.06	0
21	50	-50	0.0925	350	44	-93	174	46	-87	96.89	3.11	0
22	50	-25	0.1851	338	45	-90	158	45	-90	70.16	29.84	0
23	50	0	0.2427	157	45	90	337	45	90	70.13	29.87	0
24	50	25	0.262	333	45	-90	154	45	-90	75.43	24.57	0
25	50	50	0.2357	329	45	-90	149	45	-90	89.15	10.85	0

Table C.108: Full-wavefield moment tensor inversion results for location 3e, ISO input mechanism, isotropic medium, and dominant source frequency of 50 Hz with a DC constraint applied to the inversion. The bolded row is the location with the highest correlation in the grid search and thus the final ouputted result. Refer to Figure C.12i for visual.

Location Number	X Coord (m)	Y Coord (m)	Correlation	Strike 1 (°)	Dip 1 (°)	Rake 1 (°)	Strike 2 (°)	Dip 2 (°)	Rake 2 (°)	DC %	CLVD %	ISO %
1	-50	-50	0.1966	338	44	-90	158	46	-90	99.05	0.95	0
2	-50	-25	0.2048	154	46	90	334	44	90	98.53	1.47	0
3	-50	0	0.215	330	44	-90	151	46	-90	94.94	5.06	0
4	-50	25	0.1328	150	46	91	329	44	89	99.39	0.61	0
5	-50	50	0.1007	329	44	-92	152	46	-88	91.75	8.25	0
6	-25	-50	0.1755	337	45	-90	156	45	-90	95.59	4.41	0
7	-25	-25	0.2203	156	45	90	335	45	90	98.92	1.08	0
8	-25	0	0.2277	332	45	-90	153	45	-90	92.23	7.77	0
9	-25	25	0.1859	325	45	-90	145	45	-90	93.77	6.23	0
10	-25	50	0.1337	144	45	90	324	45	90	99.16	0.84	0
11	0	-50	0.1401	335	44	-89	154	46	-91	96.51	3.49	0
12	0	-25	0.2115	339	44	-91	160	46	-89	92.37	7.63	0
13	0	0	0.201	333	45	-90	154	45	-90	95.55	4.45	0
14	0	25	0.2412	330	45	-90	150	45	-90	95.59	4.41	0
15	0	50	0.179	147	45	90	326	45	90	96.84	3.16	0
16	25	-50	0.122	162	45	90	342	45	90	95.36	4.64	0
17	25	-25	0.2143	339	45	-90	159	45	-90	96.38	3.62	0
18	25	0	0.2341	156	46	90	336	44	90	94.19	5.81	0
19	25	25	0.2706	332	45	-90	152	45	-90	93.7	6.3	0
20	25	50	0.2182	149	46	90	329	44	90	90.18	9.82	0
21	50	-50	0.0925	350	44	-93	174	46	-87	96.89	3.11	0
22	50	-25	0.1848	338	45	-90	158	45	-90	90.78	9.22	0
23	50	0	0.2421	157	45	90	337	45	90	98.58	1.42	0
24	50	25	0.2616	333	45	-90	154	45	-90	96.24	3.76	0
25	50	50	0.2357	329	45	-90	149	45	-90	91.63	8.37	0

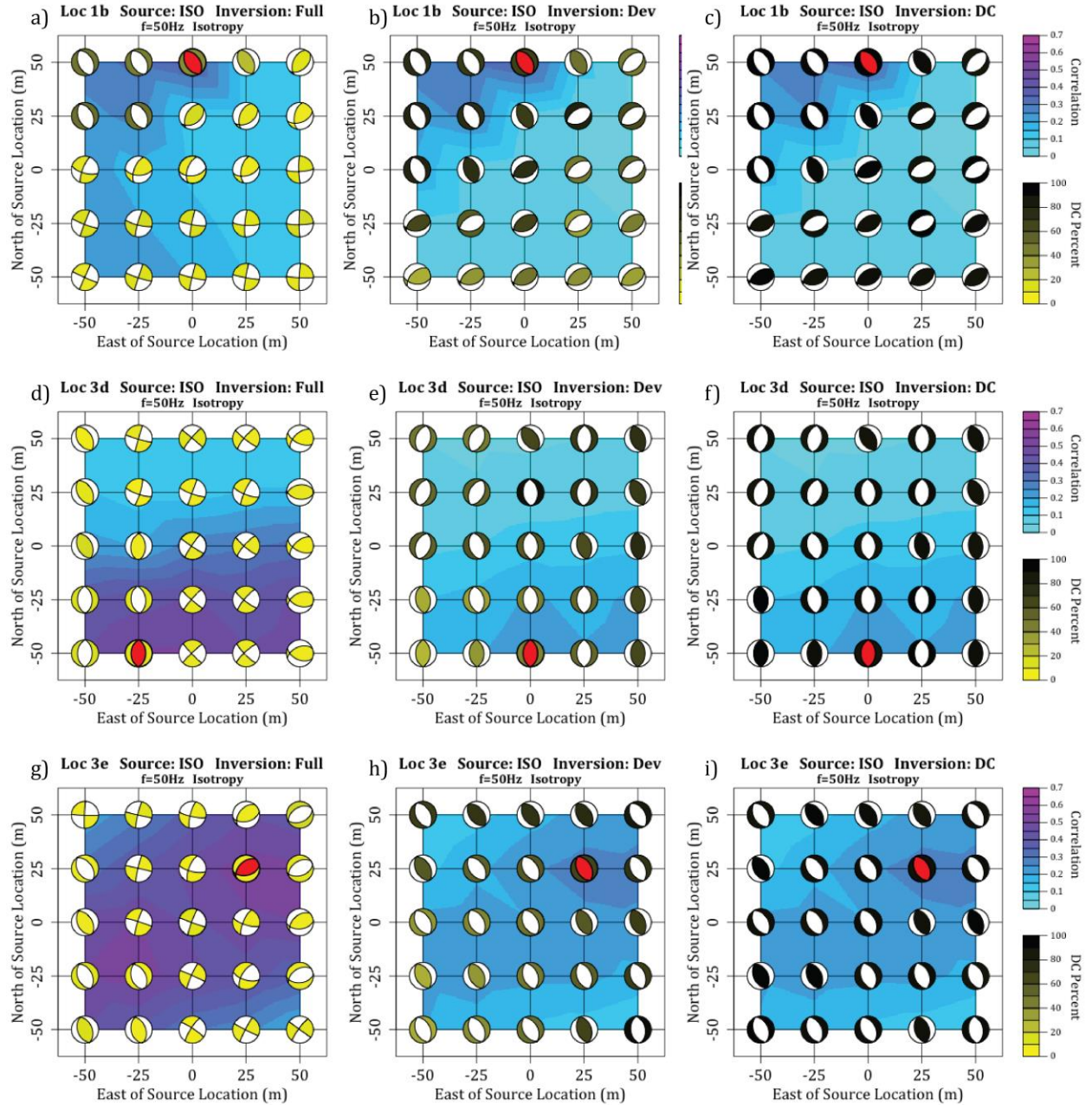


Figure C.12: Full-wavefield moment tensor inversion results for an ISO source mechanism in an isotropic medium and source frequency of 50 Hz for a) location 1b with no constraints on the inversion, b) location 1b with a deviatoric constraint, c) location 1b with a DC constraint, d) location 3d with no constraints, e) location 3d with a deviatoric constraint, f) location 3d with a DC constraint, g) location 3e with no constraints, h) location 3e with a deviatoric constraint, and i) location 3e with a DC constraint. The red beach-ball is the location and source mechanism with the highest correlation to the input seismograms. Refer to Tables C.100-C.108 for numerical values of results.

Table C.109: Full-wavefield moment tensor inversion results for location 1b, DC input mechanism, isotropic medium, and dominant source frequency of 175 Hz with no constraints applied to the inversion. The bolded row is the location with the highest correlation in the grid search and thus the final ouputted result. Refer to Figure C.13a for visual.

Location Number	X Coord (m)	Y Coord (m)	Correlation	Strike 1 (°)	Dip 1 (°)	Rake 1 (°)	Strike 2 (°)	Dip 2 (°)	Rake 2 (°)	DC %	CLVD %	ISO %
1	-50	-50	0.0834	114	85	178	204	88	5	6.4	12.7	80.9
2	-50	-25	0.1122	204	83	-167	112	77	-7	11.03	3.51	-85.46
3	-50	0	0.1226	286	50	-104	127	42	-74	38.2	37.19	-24.61
4	-50	25	0.1076	149	46	101	313	45	79	97.05	2.01	0.94
5	-50	50	0.2034	143	45	-76	303	47	-104	76.38	17.14	6.48
6	-25	-50	0.0641	199	87	-174	108	84	-3	5.09	9.53	-85.38
7	-25	-25	0.2088	310	48	-97	141	42	-82	50.13	35.24	14.63
8	-25	0	0.1184	214	58	-132	94	51	-43	4.08	5.88	-90.04
9	-25	25	0.1312	138	40	99	307	51	82	22.8	48.2	-29
10	-25	50	0.1287	140	44	-79	305	47	-100	64.88	23.07	12.05
11	0	-50	0.097	197	81	174	288	84	9	1.81	15.84	-82.35
12	0	-25	0.1135	318	47	-97	148	44	-82	27.44	41.07	31.49
13	0	0	0.1027	222	51	-111	73	43	-66	10.33	1.56	-88.11
14	0	25	0.0918	139	43	-81	307	47	-98	54.7	28.55	16.75
15	0	50	0.0808	137	43	-80	303	48	-99	53.45	28.71	17.84
16	25	-50	0.1059	311	51	-113	165	45	-64	1.63	12.18	86.19
17	25	-25	0.1204	192	88	-176	102	86	-2	9.41	3.18	-87.41
18	25	0	0.1031	72	45	119	213	52	64	5.55	2.6	91.85
19	25	25	0.1048	220	50	-110	70	44	-67	5.67	4.89	-89.44
20	25	50	0.0701	62	42	-78	226	49	-100	12.78	0.91	-86.31
21	50	-50	0.1042	307	50	-113	161	45	-65	1.76	11.93	86.31
22	50	-25	0.1124	279	86	-172	189	82	-4	2.42	8.91	88.67
23	50	0	0.0949	95	73	166	189	76	17	2.55	4.25	93.2
24	50	25	0.0926	56	42	105	216	50	77	8.28	1.8	89.92
25	50	50	0.0969	56	42	-80	223	49	-98	8.26	6.5	-85.24

Table C.110: Full-wavefield moment tensor inversion results for location 1b, DC input mechanism, isotropic medium, and dominant source frequency of 175 Hz with a deviatoric constraint applied to the inversion. The bolded row is the location with the highest correlation in the grid search and thus the final ouputted result. Refer to Figure C.13b for visual.

Location Number	X Coord (m)	Y Coord (m)	Correlation	Strike 1 (°)	Dip 1 (°)	Rake 1 (°)	Strike 2 (°)	Dip 2 (°)	Rake 2 (°)	DC %	CLVD %	ISO %
1	-50	-50	0.0689	325	45	-98	156	45	-82	78.02	21.98	0
2	-50	-25	0.095	320	45	-99	153	46	-81	87.36	12.64	0
3	-50	0	0.1222	288	51	-104	130	41	-73	36.05	63.95	0
4	-50	25	0.1076	149	46	101	313	45	79	97.25	2.75	0
5	-50	50	0.2032	143	45	-76	303	47	-104	86.92	13.08	0
6	-25	-50	0.061	155	46	98	324	44	82	85.68	14.32	0
7	-25	-25	0.2079	140	43	-82	309	48	-97	71.72	28.28	0
8	-25	0	0.0851	316	46	-98	148	45	-81	68.47	31.53	0
9	-25	25	0.1281	138	42	100	305	49	81	66.44	33.56	0
10	-25	50	0.1281	139	44	-79	304	47	-100	84.29	15.71	0
11	0	-50	0.0572	62	40	98	232	50	83	75.44	24.56	0
12	0	-25	0.1021	317	46	-97	147	45	-83	78.58	21.42	0
13	0	0	0.0816	310	48	83	141	43	98	65.11	34.89	0
14	0	25	0.0906	139	44	-81	307	47	-99	81.99	18.01	0
15	0	50	0.0798	136	44	-80	303	47	-99	83.3	16.7	0
16	25	-50	0.066	60	41	-83	231	50	-96	94.9	5.1	0
17	25	-25	0.0717	53	40	96	224	50	85	48.53	51.47	0
18	25	0	0.0752	139	44	-83	308	47	-97	78.42	21.58	0
19	25	25	0.0627	136	44	-82	305	47	-98	79.22	20.78	0
20	25	50	0.0372	197	52	88	20	38	93	15.66	84.34	0
21	50	-50	0.0658	56	41	-84	229	49	-95	91.3	8.7	0
22	50	-25	0.0688	51	41	-85	224	50	-94	60.16	39.84	0
23	50	0	0.057	46	40	-85	220	50	-94	46.37	53.63	0
24	50	25	0.0549	220	50	85	47	40	95	45.38	54.62	0
25	50	50	0.0556	210	51	86	36	40	94	29.69	70.31	0

Table C.111: Full-wavefield moment tensor inversion results for location 1b, DC input mechanism, isotropic medium, and dominant source frequency of 175 Hz with a DC constraint applied to the inversion. The bolded row is the location with the highest correlation in the grid search and thus the final ouputted result. Refer to Figure C.13c for visual.

Location Number	X Coord (m)	Y Coord (m)	Correlation	Strike 1 (°)	Dip 1 (°)	Rake 1 (°)	Strike 2 (°)	Dip 2 (°)	Rake 2 (°)	DC %	CLVD %	ISO %
1	-50	-50	0.0663	324	45	-98	155	46	-82	99.34	0.66	0
2	-50	-25	0.0937	320	45	-99	153	46	-81	98.43	1.57	0
3	-50	0	0.1205	61	69	175	153	85	21	98.58	1.42	0
4	-50	25	0.1076	149	46	101	313	45	79	96.72	3.28	0
5	-50	50	0.2011	143	46	-76	303	46	-104	99.63	0.37	0
6	-25	-50	0.06	155	47	98	324	44	82	98.2	1.8	0
7	-25	-25	0.2036	310	47	-98	141	43	-82	98.5	1.5	0
8	-25	0	0.0789	316	45	-99	148	45	-81	98.72	1.28	0
9	-25	25	0.1232	138	43	100	305	48	81	99.71	0.29	0
10	-25	50	0.1256	139	45	-79	304	46	-101	97.56	2.44	0
11	0	-50	0.0571	64	41	100	231	50	81	90.56	9.44	0
12	0	-25	0.0965	317	45	-97	147	45	-83	95.34	4.66	0
13	0	0	0.0778	309	47	82	140	44	98	97.84	2.16	0
14	0	25	0.0886	139	44	-81	306	46	-99	98.21	1.79	0
15	0	50	0.0778	136	44	-80	303	46	-99	97.23	2.77	0
16	25	-50	0.066	60	41	-83	231	50	-96	94.9	5.1	0
17	25	-25	0.0711	226	50	85	54	40	96	98.79	1.21	0
18	25	0	0.0732	138	44	-83	308	46	-97	99.42	0.58	0
19	25	25	0.0609	136	44	-82	305	46	-98	99.08	0.92	0
20	25	50	0.0347	217	51	92	34	39	88	95.84	4.16	0
21	50	-50	0.0658	56	41	-84	229	49	-95	91.3	8.7	0
22	50	-25	0.0685	52	41	-83	224	50	-96	98.36	1.64	0
23	50	0	0.0565	49	40	-83	220	50	-95	90.65	9.35	0
24	50	25	0.0543	219	50	85	47	40	96	99.59	0.41	0
25	50	50	0.054	214	50	87	39	40	94	95.8	4.2	0

Table C.112: Full-wavefield moment tensor inversion results for location 3d, DC input mechanism, isotropic medium, and dominant source frequency of 175 Hz with no constraints applied to the inversion. The bolded row is the location with the highest correlation in the grid search and thus the final ouputted result. Refer to Figure C.13d for visual.

Location Number	X Coord (m)	Y Coord (m)	Correlation	Strike 1 (°)	Dip 1 (°)	Rake 1 (°)	Strike 2 (°)	Dip 2 (°)	Rake 2 (°)	DC %	CLVD %	ISO %
1	-50	-50	0.0953	226	45	90	46	45	90	4.47	19.52	76.01
2	-50	-25	0.3701	70	45	-91	251	45	-89	26.49	54.42	19.09
3	-50	0	0.0636	255	45	90	74	45	90	35.06	43.22	-21.72
4	-50	25	0.1104	38	45	-108	243	48	-72	6.11	78.11	15.78
5	-50	50	0.1323	237	46	92	55	44	88	26.01	53.76	-20.23
6	-25	-50	0.2329	7	46	-91	189	44	-89	6.41	3.36	-90.23
7	-25	-25	0.3304	74	45	-91	255	45	-89	28.99	49.4	21.61
8	-25	0	0.052	262	44	90	81	46	90	37.72	40.47	-21.81
9	-25	25	0.0652	71	45	-90	251	45	-90	33.82	43.86	22.32
10	-25	50	0.1715	239	46	92	56	44	88	24.44	53.47	-22.09
11	0	-50	0.2478	259	46	93	75	44	87	23.11	58.62	-18.27
12	0	-25	0.2459	77	45	-91	258	45	-89	28.37	47.77	23.86
13	0	0	0.0458	263	44	91	82	46	89	37.4	42.3	-20.3
14	0	25	0.0736	248	46	91	66	44	88	31.11	54.46	-14.43
15	0	50	0.1197	241	46	94	56	44	86	23.01	60.95	-16.04
16	25	-50	0.4557	259	47	101	63	44	78	9.37	36.68	53.95
17	25	-25	0.1592	80	45	-90	261	45	-90	24.8	40.52	34.68
18	25	0	0.0502	259	45	90	80	45	90	18.99	24.95	-56.06
19	25	25	0.0664	15	62	-151	271	65	-31	5.79	82.73	11.48
20	25	50	0.1456	251	50	117	33	47	62	6.54	70.48	-22.98
21	50	-50	0.0119	82	43	-83	253	47	-96	5.12	8.64	86.24
22	50	-25	0.0115	66	44	-87	243	46	-92	13.51	2.92	83.57
23	50	0	0.0144	290	60	144	40	59	35	1.46	32.08	66.46
24	50	25	0.0368	252	45	90	72	45	90	18.16	33.66	-48.18
25	50	50	0.0269	29	87	-175	299	85	-3	8.25	1.87	-89.88

Table C.113: Full-wavefield moment tensor inversion results for location 3d, DC input mechanism, isotropic medium, and dominant source frequency of 175 Hz with a deviatoric constraint applied to the inversion. The bolded row is the location with the highest correlation in the grid search and thus the final ouputted result. Refer to Figure C.13e for visual.

Location Number	X Coord (m)	Y Coord (m)	Correlation	Strike 1 (°)	Dip 1 (°)	Rake 1 (°)	Strike 2 (°)	Dip 2 (°)	Rake 2 (°)	DC %	CLVD %	ISO %
1	-50	-50	0.0825	95	46	91	274	44	89	71.42	28.58	0
2	-50	-25	0.3679	70	45	-90	251	45	-90	53.85	46.15	0
3	-50	0	0.0628	254	45	90	74	45	90	68.82	31.18	0
4	-50	25	0.1102	47	44	-95	234	46	-85	24.37	75.63	0
5	-50	50	0.1314	236	46	91	55	44	89	54.98	45.02	0
6	-25	-50	0.1363	175	46	90	355	44	90	17.8	82.2	0
7	-25	-25	0.3268	74	45	-90	254	45	-90	60.75	39.25	0
8	-25	0	0.051	262	45	90	82	45	90	71.57	28.43	0
9	-25	25	0.0641	71	45	-90	251	45	-90	68.01	31.99	0
10	-25	50	0.1698	238	46	91	56	44	89	55.4	44.6	0
11	0	-50	0.2462	257	46	91	75	45	89	47.59	52.41	0
12	0	-25	0.2414	77	45	-90	257	45	-90	63.89	36.11	0
13	0	0	0.045	263	45	90	82	45	90	68.52	31.48	0
14	0	25	0.0732	248	46	91	66	44	89	50.95	49.05	0
15	0	50	0.1191	240	46	92	57	44	88	43.8	56.2	0
16	25	-50	0.4387	298	89	176	28	86	1	49.94	50.06	0
17	25	-25	0.1482	80	45	-90	260	45	-90	81.15	18.85	0
18	25	0	0.0353	259	45	90	79	45	90	68.13	31.87	0
19	25	25	0.0664	36	46	-114	249	49	-67	11.39	88.61	0
20	25	50	0.1446	236	47	97	46	43	82	30.58	69.42	0
21	50	-50	0.007	18	45	-90	199	45	-90	27.82	72.18	0
22	50	-25	0.0076	17	44	-90	198	46	-90	34.82	65.18	0
23	50	0	0.0132	32	89	1	302	89	179	95.46	4.54	0
24	50	25	0.0296	250	45	90	70	45	90	94.29	5.71	0
25	50	50	0.0191	166	46	92	344	44	88	70.14	29.86	0

Table C.114: Full-wavefield moment tensor inversion results for location 3d, DC input mechanism, isotropic medium, and dominant source frequency of 175 Hz with a DC constraint applied to the inversion. The bolded row is the location with the highest correlation in the grid search and thus the final ouputted result. Refer to Figure C.13f for visual.

Location Number	X Coord (m)	Y Coord (m)	Correlation	Strike 1 (°)	Dip 1 (°)	Rake 1 (°)	Strike 2 (°)	Dip 2 (°)	Rake 2 (°)	DC %	CLVD %	ISO %
1	-50	-50	0.0812	96	46	91	274	44	89	92.66	7.34	0
2	-50	-25	0.3539	71	45	-90	251	45	-90	99.34	0.66	0
3	-50	0	0.0612	254	45	90	75	45	90	98.52	1.48	0
4	-50	25	0.1058	272	89	1	182	89	179	92.87	7.13	0
5	-50	50	0.1278	236	46	90	56	44	90	95.68	4.32	0
6	-25	-50	0.1363	175	46	90	355	44	90	17.8	82.2	0
7	-25	-25	0.3118	74	45	-90	254	45	-90	93.92	6.08	0
8	-25	0	0.0501	262	45	90	82	45	90	93.58	6.42	0
9	-25	25	0.0604	71	45	-90	251	45	-90	90.13	9.87	0
10	-25	50	0.165	238	46	90	57	44	90	96.92	3.08	0
11	0	-50	0.2371	257	46	90	76	44	89	94.53	5.47	0
12	0	-25	0.2277	77	45	-90	257	45	-90	91.21	8.79	0
13	0	0	0.0435	263	45	90	83	45	90	98.76	1.24	0
14	0	25	0.0703	247	46	90	67	44	90	94.3	5.7	0
15	0	50	0.1139	239	46	91	58	44	89	96.92	3.08	0
16	25	-50	0.4376	297	90	177	27	87	0	93.62	6.38	0
17	25	-25	0.1452	80	45	-90	260	45	-90	95.28	4.72	0
18	25	0	0.0318	259	45	90	79	45	90	97.58	2.42	0
19	25	25	0.0629	187	74	176	278	86	16	93.55	6.45	0
20	25	50	0.1409	269	90	176	359	86	0	99.88	0.12	0
21	50	-50	0.007	18	45	-90	199	45	-90	27.82	72.18	0
22	50	-25	0.0074	9	44	-91	190	46	-89	90.5	9.5	0
23	50	0	0.0132	32	89	1	302	89	179	95.46	4.54	0
24	50	25	0.0296	250	45	90	70	45	90	97.2	2.8	0
25	50	50	0.0191	166	46	92	344	44	88	91.44	8.56	0

Table C.115: Full-wavefield moment tensor inversion results for location 3e, DC input mechanism, isotropic medium, and dominant source frequency of 175 Hz with no constraints applied to the inversion. The bolded row is the location with the highest correlation in the grid search and thus the final ouputted result. Refer to Figure C.13g for visual.

Location Number	X Coord (m)	Y Coord (m)	Correlation	Strike 1 (°)	Dip 1 (°)	Rake 1 (°)	Strike 2 (°)	Dip 2 (°)	Rake 2 (°)	DC %	CLVD %	ISO %
1	-50	-50	0.2356	253	45	90	74	45	90	42.59	37.72	-19.69
2	-50	-25	0.4655	72	46	-90	253	44	-90	41	39.36	19.64
3	-50	0	0.1782	246	44	90	66	46	90	29.34	36.29	-34.37
4	-50	25	0.1191	50	44	-90	230	46	-90	35.07	42.63	22.3
5	-50	50	0.083	228	46	90	47	44	90	33.46	43.2	-23.34
6	-25	-50	0.0762	260	44	90	79	46	90	35.57	43.56	-20.87
7	-25	-25	0.3992	260	44	91	78	46	89	32.8	46.72	-20.48
8	-25	0	0.3378	78	47	-94	264	43	-86	18.69	45.6	35.71
9	-25	25	0.1544	245	44	91	65	46	89	37.31	47.38	-15.31
10	-25	50	0.0843	231	45	90	51	45	90	24.15	37.28	-38.57
11	0	-50	0.1821	78	46	-90	258	44	-90	33.62	43.46	22.92
12	0	-25	0.1359	324	78	173	55	83	12	6.11	26.71	-67.18
13	0	0	0.5936	252	44	92	70	46	88	29.77	43.63	26.6
14	0	25	0.1302	52	44	-92	235	46	-88	21.06	36.87	-42.07
15	0	50	0.0181	246	48	111	36	46	68	1.91	21.18	76.91
16	25	-50	0.0576	257	44	90	77	46	90	24.17	39.89	-35.94
17	25	-25	0.1963	75	46	-91	256	44	-89	33.31	54.15	12.54
18	25	0	0.0092	321	41	-87	137	49	-93	4.49	1.51	94
19	25	25	0.0068	62	45	-86	236	45	-94	10.37	7.82	81.81
20	25	50	0.0174	229	45	87	53	45	93	14.07	2.28	-83.65
21	50	-50	0.059	261	44	91	80	46	89	25.89	44.39	-29.72
22	50	-25	0.0033	60	44	-85	234	46	-94	8.86	6.43	84.71
23	50	0	0.0017	65	45	-75	224	47	-105	3.29	8.15	88.56
24	50	25	0.0026	236	46	89	57	44	91	34.1	5.28	-60.62
25	50	50	0.0123	236	45	87	60	45	93	16.96	2.11	-80.93

Table C.116: Full-wavefield moment tensor inversion results for location 3e, DC input mechanism, isotropic medium, and dominant source frequency of 175 Hz with a deviatoric constraint applied to the inversion. The bolded row is the location with the highest correlation in the grid search and thus the final ouputted result. Refer to Figure C.13h for visual.

Location Number	X Coord (m)	Y Coord (m)	Correlation	Strike 1 (°)	Dip 1 (°)	Rake 1 (°)	Strike 2 (°)	Dip 2 (°)	Rake 2 (°)	DC %	CLVD %	ISO %
1	-50	-50	0.2324	254	45	90	74	45	90	75.66	24.34	0
2	-50	-25	0.4595	72	45	-90	253	45	-90	72.75	27.25	0
3	-50	0	0.1702	228	46	90	47	44	90	61.61	38.39	0
4	-50	25	0.1167	50	44	-90	230	46	-90	70.72	29.28	0
5	-50	50	0.0809	227	46	90	47	44	90	70.44	29.56	0
6	-25	-50	0.0752	260	45	90	80	45	90	69.06	30.94	0
7	-25	-25	0.3949	260	44	91	79	46	89	64.7	35.3	0
8	-25	0	0.3273	82	46	-91	264	44	-89	76.18	23.82	0
9	-25	25	0.153	245	44	90	65	46	90	60.4	39.6	0
10	-25	50	0.0742	230	45	90	50	45	90	93.46	6.54	0
11	0	-50	0.1781	78	46	-90	259	44	-90	70.38	29.62	0
12	0	-25	0.1186	107	46	88	290	44	92	87.55	12.45	0
13	0	0	0.5854	253	44	94	67	46	86	16.6	83.4	0
14	0	25	0.1251	279	87	-4	9	86	-177	11.61	88.39	0
15	0	50	0.0154	98	89	-178	8	88	-1	44.58	55.42	0
16	25	-50	0.0523	257	44	90	77	46	90	86.63	13.37	0
17	25	-25	0.1952	75	46	-91	256	44	-89	51.02	48.98	0
18	25	0	0.0064	333	45	-90	153	45	-90	72.19	27.81	0
19	25	25	0.0042	340	45	-91	161	45	-89	18.61	81.39	0
20	25	50	0.0116	156	45	91	335	45	89	40.86	59.14	0
21	50	-50	0.0561	262	44	90	81	46	90	72.85	27.15	0
22	50	-25	0.0021	355	45	-91	175	45	-89	32.22	67.78	0
23	50	0	0.0011	346	45	-90	166	45	-90	47.62	52.38	0
24	50	25	0.0018	225	46	90	45	44	90	28.9	71.1	0
25	50	50	0.008	154	45	90	333	45	90	42.15	57.85	0

Table C.117: Full-wavefield moment tensor inversion results for location 3e, DC input mechanism, isotropic medium, and dominant source frequency of 175 Hz with a DC constraint applied to the inversion. The bolded row is the location with the highest correlation in the grid search and thus the final ouputted result. Refer to Figure C.13i for visual.

Location Number	X Coord (m)	Y Coord (m)	Correlation	Strike 1 (°)	Dip 1 (°)	Rake 1 (°)	Strike 2 (°)	Dip 2 (°)	Rake 2 (°)	DC %	CLVD %	ISO %
1	-50	-50	0.229	254	45	90	74	45	90	95.38	4.62	0
2	-50	-25	0.4408	72	45	-90	252	45	-90	93.24	6.76	0
3	-50	0	0.1656	247	45	90	67	45	90	98.87	1.13	0
4	-50	25	0.1117	50	45	-90	229	45	-90	94.07	5.93	0
5	-50	50	0.0794	227	45	90	47	45	90	93.43	6.57	0
6	-25	-50	0.0736	260	45	90	80	45	90	97.25	2.75	0
7	-25	-25	0.3889	259	44	90	79	46	90	91.79	8.21	0
8	-25	0	0.3239	82	46	-91	263	44	-89	97.84	2.16	0
9	-25	25	0.1458	245	44	90	65	46	90	97.26	2.74	0
10	-25	50	0.0742	230	45	90	50	45	90	91.97	8.03	0
11	0	-50	0.1692	78	45	-90	258	45	-90	92.96	7.04	0
12	0	-25	0.1184	109	46	87	293	44	93	96.17	3.83	0
13	0	0	0.508	205	90	-1	295	89	-180	96.76	3.24	0
14	0	25	0.1222	8	88	179	98	89	2	91.48	8.52	0
15	0	50	0.0153	9	88	0	99	90	-178	98.72	1.28	0
16	25	-50	0.052	257	44	90	77	46	90	97.39	2.61	0
17	25	-25	0.176	76	46	-90	256	44	-90	92.87	7.13	0
18	25	0	0.0064	333	45	-90	153	45	-90	93.21	6.79	0
19	25	25	0.0042	340	45	-91	161	45	-89	18.61	81.39	0
20	25	50	0.0113	153	46	91	332	45	89	90.57	9.43	0
21	50	-50	0.055	262	44	90	82	46	90	96.37	3.63	0
22	50	-25	0.002	348	44	-91	169	46	-89	96.46	3.54	0
23	50	0	0.001	343	45	-91	164	46	-89	97.02	2.98	0
24	50	25	0.0018	225	46	90	45	44	90	28.9	71.1	0
25	50	50	0.0078	153	45	90	332	45	90	97.07	2.93	0

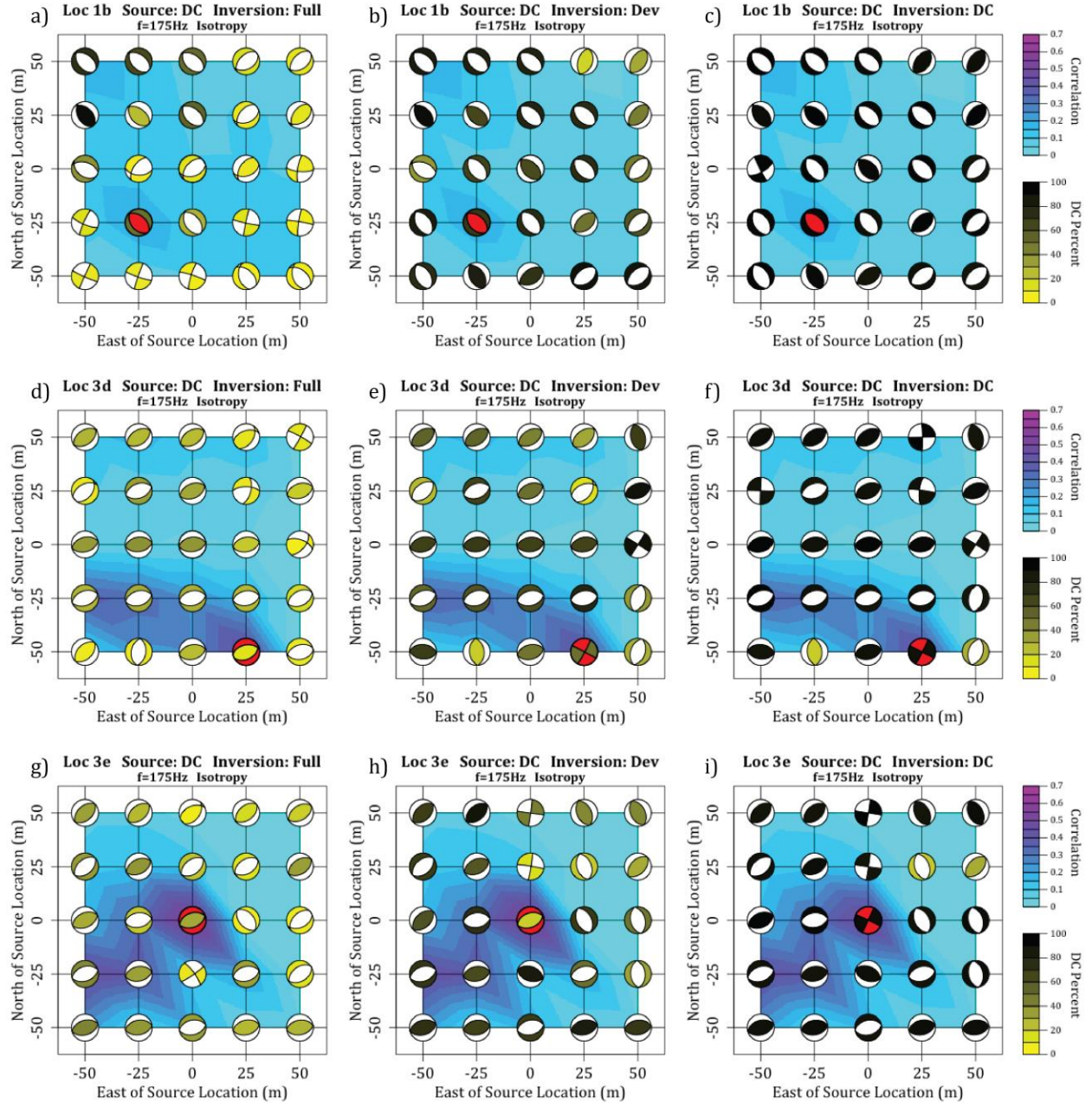


Figure C.13: Full-wavefield moment tensor inversion results for a DC source mechanism in an isotropic medium and source frequency of 175 Hz for a) location 1b with no constraints on the inversion, b) location 1b with a deviatoric constraint, c) location 1b with a DC constraint, d) location 3d with no constraints, e) location 3d with a deviatoric constraint, f) location 3d with a DC constraint, g) location 3e with no constraints, h) location 3e with a deviatoric constraint, and i) location 3e with a DC constraint. The red beach-ball is the location and source mechanism with the highest correlation to the input seismograms. Refer to Tables C.109-C.117 for numerical values of results.

Table C.118: Full-wavefield moment tensor inversion results for location 1b, CLVD input mechanism, isotropic medium, and dominant source frequency of 175 Hz with no constraints applied to the inversion. The bolded row is the location with the highest correlation in the grid search and thus the final ouputted result. Refer to Figure C.14a for visual.

Location Number	X Coord (m)	Y Coord (m)	Correlation	Strike 1 (°)	Dip 1 (°)	Rake 1 (°)	Strike 2 (°)	Dip 2 (°)	Rake 2 (°)	DC %	CLVD %	ISO %
1	-50	-50	0.093	296	84	-170	205	80	-6	1.65	18.06	80.29
2	-50	-25	0.1564	113	78	173	204	83	12	11.34	3.21	85.45
3	-50	0	0.0873	281	50	73	126	43	109	65.49	0.53	33.98
4	-50	25	0.0508	164	47	97	334	43	83	17.28	47.64	35.08
5	-50	50	0.107	168	90	34	77	56	179	19.68	37.26	43.06
6	-25	-50	0.0804	201	89	-176	111	86	-1	10.16	9.13	-80.71
7	-25	-25	0.1468	245	83	-167	154	77	-8	22.72	4.53	-72.75
8	-25	0	0.1612	97	54	142	211	60	42	3.73	6.01	90.26
9	-25	25	0.0846	57	39	105	218	53	78	12.08	9.1	78.82
10	-25	50	0.0577	43	37	-78	208	54	-99	9.73	9.65	-80.62
11	0	-50	0.1374	289	80	-167	197	77	-10	1.36	16.45	82.19
12	0	-25	0.1134	196	87	3	106	87	177	6.9	5.79	87.31
13	0	0	0.1055	221	52	-114	76	44	-63	7.91	3.54	-88.55
14	0	25	0.1158	70	42	107	227	50	75	14.09	0.16	85.75
15	0	50	0.0738	314	34	-102	148	56	-82	34.52	42.88	22.6
16	25	-50	0.122	311	49	-117	168	47	-62	1.78	15.6	82.62
17	25	-25	0.1664	102	86	178	192	88	4	9.1	3.64	87.26
18	25	0	0.1423	102	85	177	192	87	5	9.43	0.09	90.48
19	25	25	0.148	70	44	112	220	50	70	5.61	4.9	89.49
20	25	50	0.0999	225	49	79	62	42	103	12.97	0.51	86.52
21	50	-50	0.0867	160	45	113	309	50	69	1.96	11.83	-86.21
22	50	-25	0.1241	189	81	175	279	85	9	2.12	9.44	-88.44
23	50	0	0.1049	188	79	-165	96	76	-11	3	4.04	-92.96
24	50	25	0.0932	67	45	-66	215	50	-112	4.4	3.15	-92.45
25	50	50	0.1154	222	49	80	57	42	101	9.51	2.67	87.82

Table C.119: Full-wavefield moment tensor inversion results for location 1b, CLVD input mechanism, isotropic medium, and dominant source frequency of 175 Hz with a deviatoric constraint applied to the inversion. The bolded row is the location with the highest correlation in the grid search and thus the final ouputted result. . Refer to Figure C.14b for visual.

Location Number	X Coord (m)	Y Coord (m)	Correlation	Strike 1 (°)	Dip 1 (°)	Rake 1 (°)	Strike 2 (°)	Dip 2 (°)	Rake 2 (°)	DC %	CLVD %	ISO %
1	-50	-50	0.0573	237	51	-104	79	41	-73	75.85	24.15	0
2	-50	-25	0.0862	235	52	-101	73	40	-76	74.09	25.91	0
3	-50	0	0.0859	285	50	71	133	43	111	72.03	27.97	0
4	-50	25	0.0422	356	61	-111	214	35	-58	68.56	31.44	0
5	-50	50	0.1035	309	60	-83	116	31	-101	31.93	68.07	0
6	-25	-50	0.0587	335	47	-91	157	43	-89	36.6	63.4	0
7	-25	-25	0.1349	73	64	151	177	64	30	14.11	85.89	0
8	-25	0	0.0858	225	52	-98	57	39	-80	34.59	65.41	0
9	-25	25	0.0774	326	75	-64	83	29	-149	65.84	34.16	0
10	-25	50	0.0425	139	43	100	305	48	81	79.79	20.21	0
11	0	-50	0.0814	232	50	-97	62	40	-82	74.54	25.46	0
12	0	-25	0.069	228	51	-97	58	40	-82	51.54	48.46	0
13	0	0	0.0573	56	40	98	225	51	83	44.86	55.14	0
14	0	25	0.06	42	38	-83	214	52	-95	22.49	77.51	0
15	0	50	0.0725	315	35	-100	148	56	-83	70.06	29.94	0
16	25	-50	0.0733	229	50	-96	57	41	-83	70.62	29.38	0
17	25	-25	0.0992	224	50	-95	52	40	-84	47.93	52.07	0
18	25	0	0.0847	45	40	-84	218	51	-95	31.67	68.33	0
19	25	25	0.0838	34	39	-85	208	51	-94	19.98	80.02	0
20	25	50	0.0531	19	38	-88	196	52	-92	15.11	84.89	0
21	50	-50	0.0548	229	49	85	56	41	96	90.68	9.32	0
22	50	-25	0.076	224	50	86	51	41	95	59.22	40.78	0
23	50	0	0.063	220	50	86	46	40	95	45.12	54.88	0
24	50	25	0.0548	215	50	86	41	40	95	35.65	64.35	0
25	50	50	0.0719	141	52	97	310	39	81	40.42	59.58	0

Table C.120: Full-wavefield moment tensor inversion results for location 1b, CLVD input mechanism, isotropic medium, and dominant source frequency of 175 Hz with a DC constraint applied to the inversion. The bolded row is the location with the highest correlation in the grid search and thus the final ouputted result. . Refer to Figure C.14c for visual.

Location Number	X Coord (m)	Y Coord (m)	Correlation	Strike 1 (°)	Dip 1 (°)	Rake 1 (°)	Strike 2 (°)	Dip 2 (°)	Rake 2 (°)	DC %	CLVD %	ISO %
1	-50	-50	0.0572	238	51	-102	76	40	-76	99.04	0.96	0
2	-50	-25	0.0861	234	52	-103	74	40	-74	95.57	4.43	0
3	-50	0	0.0856	137	46	110	290	47	71	98.79	1.21	0
4	-50	25	0.042	352	60	-106	202	34	-65	98.19	1.81	0
5	-50	50	0.0945	75	86	174	165	84	4	96.31	3.69	0
6	-25	-50	0.0587	335	47	-91	157	43	-89	36.6	63.4	0
7	-25	-25	0.1344	84	79	170	175	80	11	93.46	6.54	0
8	-25	0	0.0849	226	52	-100	63	39	-77	93.72	6.28	0
9	-25	25	0.0761	330	88	-64	63	26	-176	99.99	0.01	0
10	-25	50	0.0418	139	44	100	305	47	80	98.02	1.98	0
11	0	-50	0.0813	231	50	-98	64	41	-81	96.41	3.59	0
12	0	-25	0.0686	228	51	-99	61	40	-80	99.54	0.46	0
13	0	0	0.0568	58	40	99	226	51	83	98.47	1.53	0
14	0	25	0.0583	219	52	-98	52	39	-80	99.69	0.31	0
15	0	50	0.0693	315	36	-100	147	55	-83	99.85	0.15	0
16	25	-50	0.0732	229	50	-96	58	41	-83	91.31	8.69	0
17	25	-25	0.0986	225	50	-97	55	40	-82	94.43	5.57	0
18	25	0	0.0834	221	51	-97	51	40	-82	91.23	8.77	0
19	25	25	0.0812	46	39	-82	216	51	-96	92.69	7.31	0
20	25	50	0.0531	19	38	-88	196	52	-92	15.11	84.89	0
21	50	-50	0.0548	228	49	85	57	41	96	96.78	3.22	0
22	50	-25	0.0755	225	50	86	51	41	95	94.7	5.3	0
23	50	0	0.0623	221	50	85	48	40	96	99.8	0.2	0
24	50	25	0.0536	216	50	83	46	40	98	90.23	9.77	0
25	50	50	0.0644	18	39	-88	195	51	-92	16.47	83.53	0

Table C.121: Full-wavefield moment tensor inversion results for location 3d, CLVD input mechanism, isotropic medium, and dominant source frequency of 175 Hz with no constraints applied to the inversion. The bolded row is the location with the highest correlation in the grid search and thus the final ouputted result. . Refer to Figure C.14d for visual.

Location Number	X Coord (m)	Y Coord (m)	Correlation	Strike 1 (°)	Dip 1 (°)	Rake 1 (°)	Strike 2 (°)	Dip 2 (°)	Rake 2 (°)	DC %	CLVD %	ISO %
1	-50	-50	0.1137	54	45	-90	234	45	-90	4.3	20.57	-75.13
2	-50	-25	0.2362	73	44	-90	253	46	-90	30.97	49.92	19.11
3	-50	0	0.0617	250	46	90	70	44	90	32.2	48.23	-19.57
4	-50	25	0.0844	70	44	-90	250	46	-90	36.24	42.6	21.16
5	-50	50	0.1139	263	45	90	83	45	90	47.33	39.4	13.27
6	-25	-50	0.2961	184	44	90	4	46	90	6.07	3.9	90.03
7	-25	-25	0.2199	76	44	-90	257	46	-90	31.57	46.5	21.93
8	-25	0	0.0689	254	46	90	74	44	90	34.01	44.63	-21.36
9	-25	25	0.0749	70	44	-90	250	46	-90	33.99	43.91	22.1
10	-25	50	0.1013	270	44	92	87	46	88	23.23	47.55	-29.22
11	0	-50	0.194	257	46	91	76	44	89	24.08	43.44	-32.48
12	0	-25	0.1814	78	44	-90	259	46	-90	29.79	46.65	23.56
13	0	0	0.0698	255	46	90	75	44	90	29.97	43.86	-26.17
14	0	25	0.0559	91	46	88	274	44	92	24.85	50.84	-24.31
15	0	50	0.1077	66	44	-91	247	46	-89	27.84	46.93	25.23
16	25	-50	0.4447	252	47	94	66	43	85	3.96	29.61	-66.43
17	25	-25	0.147	91	45	91	271	45	89	17.67	33.81	-48.52
18	25	0	0.0634	259	46	92	77	44	88	22.91	31.19	45.9
19	25	25	0.0347	48	43	-103	246	48	-78	8.44	63.81	27.75
20	25	50	0.0718	248	50	113	34	45	65	5.34	64.35	-30.31
21	50	-50	0.0063	263	46	88	86	44	92	18.36	5.93	-75.71
22	50	-25	0.0163	247	46	87	71	44	93	11.67	1.41	-86.92
23	50	0	0.0223	252	46	89	74	44	91	19.54	17.12	-63.34
24	50	25	0.0295	256	46	95	69	44	85	10.37	42.43	47.2
25	50	50	0.0374	68	44	-89	246	46	-91	20.19	13.11	66.7

Table C.122: Full-wavefield moment tensor inversion results for location 3d, CLVD input mechanism, isotropic medium, and dominant source frequency of 175 Hz with a deviatoric constraint applied to the inversion. The bolded row is the location with the highest correlation in the grid search and thus the final ouputted result. . Refer to Figure C.14e for visual.

Location Number	X Coord (m)	Y Coord (m)	Correlation	Strike 1 (°)	Dip 1 (°)	Rake 1 (°)	Strike 2 (°)	Dip 2 (°)	Rake 2 (°)	DC %	CLVD %	ISO %
1	-50	-50	0.0707	96	45	90	276	45	90	70.62	29.38	0
2	-50	-25	0.2345	73	44	-90	253	46	-90	59.18	40.82	0
3	-50	0	0.0612	250	46	90	70	44	90	61.48	38.52	0
4	-50	25	0.0833	70	44	-90	249	46	-90	69.06	30.94	0
5	-50	50	0.1136	263	45	91	82	45	89	43.68	56.32	0
6	-25	-50	0.173	358	44	-90	178	46	-90	17.97	82.03	0
7	-25	-25	0.2171	76	44	-90	256	46	-90	64.51	35.49	0
8	-25	0	0.0679	254	46	90	74	44	90	66.17	33.83	0
9	-25	25	0.0737	70	44	-90	250	46	-90	67.79	32.21	0
10	-25	50	0.0998	238	46	91	57	44	89	54.8	45.2	0
11	0	-50	0.1878	256	46	90	75	44	90	74.62	25.38	0
12	0	-25	0.1779	78	44	-90	258	46	-90	65.17	34.83	0
13	0	0	0.068	255	46	90	75	44	90	70.33	29.67	0
14	0	25	0.055	92	46	89	274	44	91	59.8	40.2	0
15	0	50	0.105	66	44	-90	246	46	-90	65.76	34.24	0
16	25	-50	0.3548	240	46	91	60	44	89	69.34	30.66	0
17	25	-25	0.1371	80	44	-91	261	46	-89	35.05	64.95	0
18	25	0	0.0598	33	87	2	303	88	177	14.03	85.97	0
19	25	25	0.0342	53	43	-94	238	47	-87	41.77	58.23	0
20	25	50	0.0707	233	47	95	46	43	85	40.1	59.9	0
21	50	-50	0.0038	239	45	90	60	45	90	10.77	89.23	0
22	50	-25	0.0106	188	45	90	7	45	90	35.44	64.56	0
23	50	0	0.0154	245	46	90	65	44	90	46.05	53.95	0
24	50	25	0.0283	298	89	177	28	87	1	25.2	74.8	0
25	50	50	0.0237	56	44	-90	236	46	-90	33.27	66.73	0

Table C.123: Full-wavefield moment tensor inversion results for location 3d, CLVD input mechanism, isotropic medium, and dominant source frequency of 175 Hz with a DC constraint applied to the inversion. The bolded row is the location with the highest correlation in the grid search and thus the final ouputted result. . Refer to Figure C.14f for visual.

Location Number	X Coord (m)	Y Coord (m)	Correlation	Strike 1 (°)	Dip 1 (°)	Rake 1 (°)	Strike 2 (°)	Dip 2 (°)	Rake 2 (°)	DC %	CLVD %	ISO %
1	-50	-50	0.0687	97	45	90	276	45	90	99.1	0.9	0
2	-50	-25	0.224	74	44	-90	253	46	-90	94.95	5.05	0
3	-50	0	0.06	250	46	90	70	44	90	91.7	8.3	0
4	-50	25	0.0798	70	44	-89	250	46	-91	95.18	4.82	0
5	-50	50	0.1075	262	45	90	82	45	90	94.46	5.54	0
6	-25	-50	0.173	358	44	-90	178	46	-90	17.97	82.03	0
7	-25	-25	0.2054	77	44	-90	256	46	-90	90.72	9.28	0
8	-25	0	0.0662	254	45	90	74	45	90	96.87	3.13	0
9	-25	25	0.0695	70	44	-90	250	46	-90	90.32	9.68	0
10	-25	50	0.0978	270	45	90	89	45	90	94.55	5.45	0
11	0	-50	0.1869	256	46	90	76	44	90	90.05	9.95	0
12	0	-25	0.167	78	44	-90	258	46	-90	90.08	9.92	0
13	0	0	0.0661	254	46	90	74	44	90	99.21	0.79	0
14	0	25	0.0538	93	46	90	274	44	90	93.25	6.75	0
15	0	50	0.0995	66	44	-90	246	46	-90	93.71	6.29	0
16	25	-50	0.3466	237	46	91	55	44	88	91.91	8.09	0
17	25	-25	0.1207	80	44	-90	260	46	-90	96.66	3.34	0
18	25	0	0.0587	33	89	0	303	90	179	92.48	7.52	0
19	25	25	0.033	56	43	-92	239	47	-88	98.46	1.54	0
20	25	50	0.0642	67	44	-90	247	46	-90	97.92	2.08	0
21	50	-50	0.0038	239	45	90	60	45	90	10.77	89.23	0
22	50	-25	0.0102	183	46	91	2	44	89	95.22	4.78	0
23	50	0	0.0128	248	46	90	67	44	90	97.92	2.08	0
24	50	25	0.028	117	90	-178	27	88	0	92.14	7.86	0
25	50	50	0.0188	53	44	-91	235	46	-89	90.27	9.73	0

Table C.124: Full-wavefield moment tensor inversion results for location 3e, CLVD input mechanism, isotropic medium, and dominant source frequency of 175 Hz with no constraints applied to the inversion. The bolded row is the location with the highest correlation in the grid search and thus the final ouputted result. . Refer to Figure C.14g for visual.

Location Number	X Coord (m)	Y Coord (m)	Correlation	Strike 1 (°)	Dip 1 (°)	Rake 1 (°)	Strike 2 (°)	Dip 2 (°)	Rake 2 (°)	DC %	CLVD %	ISO %
1	-50	-50	0.0891	301	82	9	210	81	172	1.2	6.9	91.9
2	-50	-25	0.4644	335	84	179	65	89	6	86.63	10.67	2.7
3	-50	0	0.2096	235	45	90	55	45	90	37.98	40.29	-21.73
4	-50	25	0.1158	51	45	-90	231	45	-90	36.56	41.23	22.21
5	-50	50	0.083	227	46	90	47	44	90	33.44	43.12	-23.44
6	-25	-50	0.0574	71	45	-88	249	45	-92	8.45	28.77	62.78
7	-25	-25	0.2971	66	45	-90	246	45	-90	37.75	40.28	21.97
8	-25	0	0.4127	238	45	90	58	45	90	30.4	37.56	-32.04
9	-25	25	0.1106	54	45	-90	234	45	-90	34.79	44.43	20.78
10	-25	50	0.0552	233	45	91	52	45	89	30.11	36.58	33.31
11	0	-50	0.0744	258	44	90	77	46	90	33.93	43.29	-22.78
12	0	-25	0.1304	69	45	-89	248	45	-91	21.81	28.82	49.37
13	0	0	0.6321	252	88	171	342	81	2	16.73	19.66	-63.61
14	0	25	0.1498	57	45	-89	236	45	-91	19.44	28.01	52.55
15	0	50	0.0237	230	46	89	52	44	91	21.41	16.83	-61.76
16	25	-50	0.0223	77	46	-89	256	44	-91	15.78	31.48	52.74
17	25	-25	0.0872	255	44	91	73	46	89	35.81	57.64	6.55
18	25	0	0.0096	238	45	87	62	45	93	15.81	4	-80.19
19	25	25	0.0013	43	44	-90	222	46	-90	27.71	9.46	62.83
20	25	50	0.0025	223	47	92	40	43	88	43.38	5.71	50.91
21	50	-50	0.0278	80	46	-91	261	44	-89	23.18	41.21	35.61
22	50	-25	0.002	68	44	-87	244	46	-93	14.3	1.54	84.16
23	50	0	0.0013	182	48	92	0	42	88	2.75	6.49	-90.76
24	50	25	0.0039	328	42	-85	141	48	-95	7.46	1.68	90.86
25	50	50	0.0158	229	45	88	52	45	92	12.55	5.96	-81.49

Table C.125: Full-wavefield moment tensor inversion results for location 3e, CLVD input mechanism, isotropic medium, and dominant source frequency of 175 Hz with a deviatoric constraint applied to the inversion. The bolded row is the location with the highest correlation in the grid search and thus the final ouputted result. . Refer to Figure C.14h for visual.

Location Number	X Coord (m)	Y Coord (m)	Correlation	Strike 1 (°)	Dip 1 (°)	Rake 1 (°)	Strike 2 (°)	Dip 2 (°)	Rake 2 (°)	DC %	CLVD %	ISO %
1	-50	-50	0.0804	66	45	-90	246	45	-90	74.99	25.01	0
2	-50	-25	0.4644	335	84	180	65	90	6	92.39	7.61	0
3	-50	0	0.2055	235	45	90	55	45	90	73.5	26.5	0
4	-50	25	0.1133	51	45	-90	231	45	-90	72.41	27.59	0
5	-50	50	0.0808	227	46	90	47	44	90	70.59	29.41	0
6	-25	-50	0.0389	71	45	-90	250	45	-90	61.72	38.28	0
7	-25	-25	0.2902	66	45	-90	246	45	-90	73.97	26.03	0
8	-25	0	0.3872	237	45	90	58	45	90	86.01	13.99	0
9	-25	25	0.1083	54	45	-90	234	45	-90	67.42	32.58	0
10	-25	50	0.0535	235	45	94	50	45	86	10.8	89.2	0
11	0	-50	0.0728	258	44	90	78	46	90	70.49	29.51	0
12	0	-25	0.1001	69	45	-90	248	45	-90	80.04	19.96	0
13	0	0	0.5811	203	47	96	14	43	83	72.18	27.82	0
14	0	25	0.1084	55	45	-90	235	45	-90	72.34	27.66	0
15	0	50	0.016	224	46	90	45	44	90	40.64	59.36	0
16	25	-50	0.0165	78	45	-90	258	45	-90	78.06	21.94	0
17	25	-25	0.0871	255	44	91	73	46	89	32.62	67.38	0
18	25	0	0.0061	174	45	90	354	45	90	13.21	86.79	0
19	25	25	0.001	25	44	-90	206	46	-90	45.13	54.87	0
20	25	50	0.0022	239	48	107	34	45	71	7.43	92.57	0
21	50	-50	0.0255	82	46	-90	262	44	-90	82.55	17.45	0
22	50	-25	0.0013	344	45	-91	165	45	-89	28.66	71.34	0
23	50	0	9.00E-04	160	45	91	338	45	89	71.28	28.72	0
24	50	25	0.0028	332	45	-90	152	45	-90	92.75	7.25	0
25	50	50	0.0107	157	45	91	337	45	89	49.19	50.81	0

Table C.126: Full-wavefield moment tensor inversion results for location 3e, CLVD input mechanism, isotropic medium, and dominant source frequency of 175 Hz with a DC constraint applied to the inversion. The bolded row is the location with the highest correlation in the grid search and thus the final ouputted result. . Refer to Figure C.14i for visual.

Location Number	X Coord (m)	Y Coord (m)	Correlation	Strike 1 (°)	Dip 1 (°)	Rake 1 (°)	Strike 2 (°)	Dip 2 (°)	Rake 2 (°)	DC %	CLVD %	ISO %
1	-50	-50	0.0782	67	45	-90	246	45	-90	98.15	1.85	0
2	-50	-25	0.4644	335	84	180	65	90	6	92.39	7.61	0
3	-50	0	0.2009	235	45	90	55	45	90	98.47	1.53	0
4	-50	25	0.1078	51	45	-90	231	45	-90	92.5	7.5	0
5	-50	50	0.0793	227	46	90	47	44	90	93.57	6.43	0
6	-25	-50	0.0378	76	45	-90	256	45	-90	99.28	0.72	0
7	-25	-25	0.2814	66	45	-90	246	45	-90	99.24	0.76	0
8	-25	0	0.3859	237	45	90	58	45	90	95.26	4.74	0
9	-25	25	0.1026	54	45	-90	234	45	-90	95.86	4.14	0
10	-25	50	0.0535	235	45	94	50	45	86	10.8	89.2	0
11	0	-50	0.0708	258	44	90	78	46	90	99.55	0.45	0
12	0	-25	0.0984	69	45	-90	248	45	-90	94.94	5.06	0
13	0	0	0.5796	205	47	95	18	43	85	98.26	1.74	0
14	0	25	0.1038	55	45	-90	235	45	-90	97.21	2.79	0
15	0	50	0.012	225	46	90	45	44	90	96.93	3.07	0
16	25	-50	0.0162	78	46	-90	258	44	-90	93.56	6.44	0
17	25	-25	0.0772	254	44	90	74	46	90	97.09	2.91	0
18	25	0	0.0061	174	45	90	354	45	90	13.21	86.79	0
19	25	25	0.001	7	44	-92	189	46	-88	98.32	1.68	0
20	25	50	0.002	273	89	-176	183	86	-1	96.34	3.66	0
21	50	-50	0.025	82	46	-90	262	44	-90	93.5	6.5	0
22	50	-25	0.0012	341	45	-91	163	46	-89	96.24	3.76	0
23	50	0	9.00E-04	160	46	92	338	45	88	94.28	5.72	0
24	50	25	0.0028	332	45	-90	152	45	-90	98.95	1.05	0
25	50	50	0.0105	155	45	90	335	45	90	96.22	3.78	0

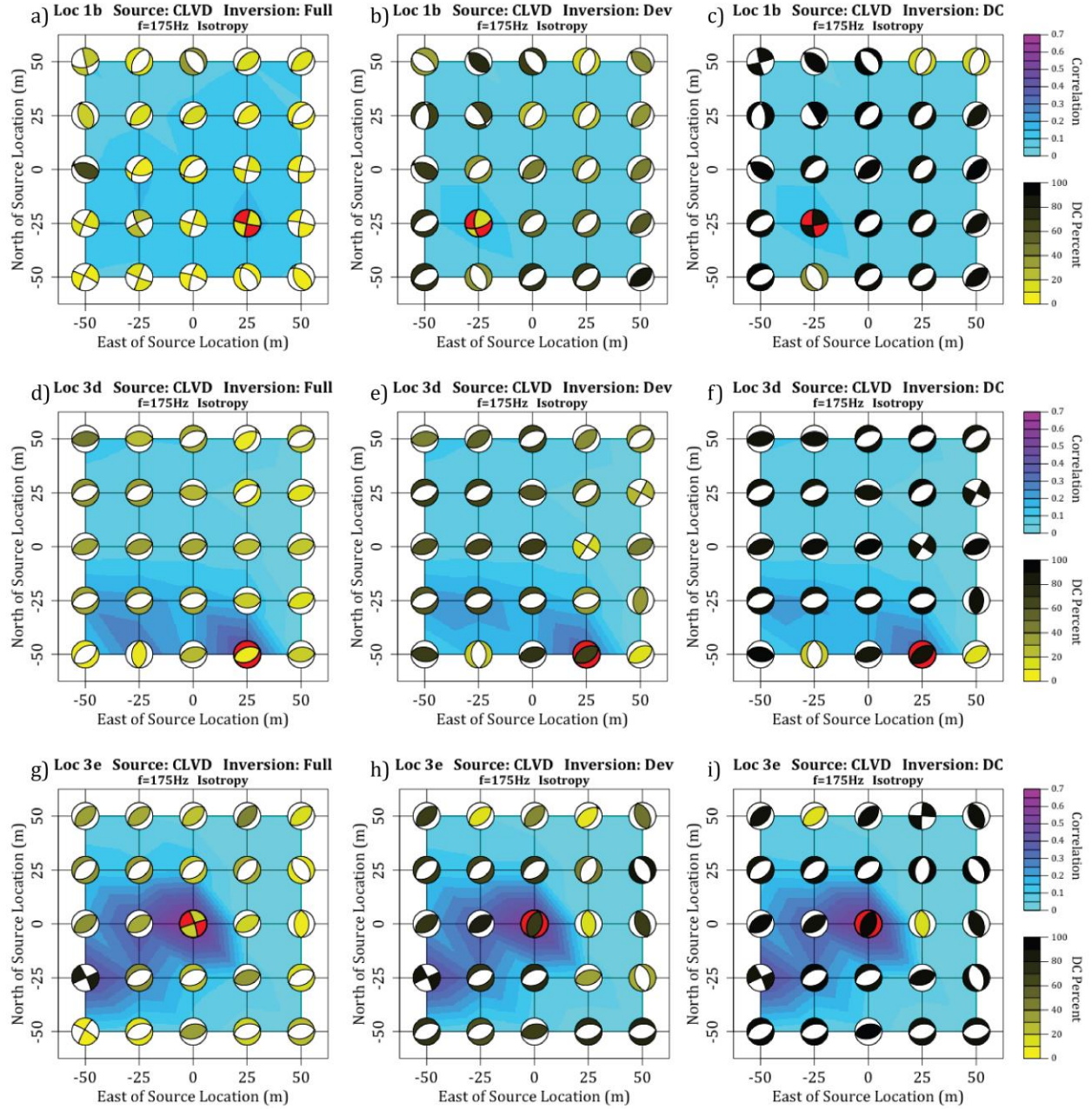


Figure C.14: Full-wavefield moment tensor inversion results for a CLVD source mechanism in an isotropic medium and source frequency of 175 Hz for a) location 1b with no constraints on the inversion, b) location 1b with a deviatoric constraint, c) location 1b with a DC constraint, d) location 3d with no constraints, e) location 3d with a deviatoric constraint, f) location 3d with a DC constraint, g) location 3e with no constraints, h) location 3e with a deviatoric constraint, and i) location 3e with a DC constraint. The red beach-ball is the location and source mechanism with the highest correlation to the input seismograms. Refer to Tables C.118-C.126 for numerical values of results.

Table C.127: Full-wavefield moment tensor inversion results for location 1b, ISO input mechanism, isotropic medium, and dominant source frequency of 175 Hz with no constraints applied to the inversion. The bolded row is the location with the highest correlation in the grid search and thus the final ouputted result. Refer to Figure C.15a for visual.

Location Number	X Coord (m)	Y Coord (m)	Correlation	Strike 1 (°)	Dip 1 (°)	Rake 1 (°)	Strike 2 (°)	Dip 2 (°)	Rake 2 (°)	DC %	CLVD %	ISO %
1	-50	-50	0.0873	111	82	-177	21	87	-8	2.6	18.88	78.52
2	-50	-25	0.0776	206	77	-160	111	70	-14	8.51	5.46	-86.03
3	-50	0	0.0669	220	56	-126	92	48	-49	8.93	3.8	-87.27
4	-50	25	0.0745	74	40	117	221	55	69	15.45	1.54	83.01
5	-50	50	0.0886	207	56	82	42	35	102	5.19	21.23	73.58
6	-25	-50	0.1044	149	42	86	334	48	93	1.15	17.37	-81.48
7	-25	-25	0.1581	104	77	174	196	84	13	10.82	1.37	87.81
8	-25	0	0.1764	208	59	-130	86	49	-43	4.93	4.31	-90.76
9	-25	25	0.1435	56	39	105	218	53	78	12.16	8.96	78.88
10	-25	50	0.1014	43	37	-78	209	54	-99	9.9	9.23	-80.87
11	0	-50	0.057	323	48	-99	155	43	-80	3.53	13.41	83.06
12	0	-25	0.1398	189	84	-167	98	77	-6	9.31	1.63	-89.06
13	0	0	0.0858	193	66	-142	85	56	-30	3.61	5.91	-90.48
14	0	25	0.0498	67	44	-53	201	56	-120	4.63	6.07	-89.3
15	0	50	0.0261	49	39	-72	206	53	-104	12.39	4.24	-83.37
16	25	-50	8.00E-04	321	47	-96	150	43	-84	11.67	19.2	69.13
17	25	-25	0.0414	217	51	-119	79	48	-59	5.33	0.34	-94.33
18	25	0	0.0417	66	45	-54	200	55	-121	4.35	2.15	-93.5
19	25	25	0.0397	47	40	-73	205	52	-104	10.8	1.37	-87.83
20	25	50	0.0384	62	42	-77	225	49	-101	12.07	1.2	-86.73
21	50	-50	4.00E-04	334	44	-89	154	46	-90	20.86	34.4	44.74
22	50	-25	0.0181	311	48	-97	141	43	-83	5.08	9.88	85.04
23	50	0	0.0358	175	90	-172	85	82	0	9.84	3.29	-86.87
24	50	25	0.0175	170	89	-171	80	81	-1	11.93	0.56	-87.51
25	50	50	0.0439	59	42	-75	219	49	-103	6.85	4.8	-88.35

Table C.128: Full-wavefield moment tensor inversion results for location 1b, ISO input mechanism, isotropic medium, and dominant source frequency of 175 Hz with a deviatoric constraint applied to the inversion. The bolded row is the location with the highest correlation in the grid search and thus the final ouputted result. Refer to Figure C.15b for visual.

Location Number	X Coord (m)	Y Coord (m)	Correlation	Strike 1 (°)	Dip 1 (°)	Rake 1 (°)	Strike 2 (°)	Dip 2 (°)	Rake 2 (°)	DC %	CLVD %	ISO %
1	-50	-50	0.0515	243	50	-102	81	41	-76	90.47	9.53	0
2	-50	-25	0.0413	73	40	103	236	51	79	88.21	11.79	0
3	-50	0	0.0331	71	39	103	234	52	79	55.84	44.16	0
4	-50	25	0.0376	245	50	-103	84	42	-75	20.16	79.84	0
5	-50	50	0.0861	139	84	-164	48	74	-6	56.69	43.31	0
6	-25	-50	0.0659	73	41	100	240	50	82	90.68	9.32	0
7	-25	-25	0.0923	70	41	100	237	50	82	59.44	40.56	0
8	-25	0	0.0989	70	40	101	235	50	81	44.67	55.33	0
9	-25	25	0.0734	75	41	102	239	50	79	32.21	67.79	0
10	-25	50	0.0511	91	44	104	252	48	77	20.55	79.45	0
11	0	-50	0.0358	236	50	-97	66	41	-82	82.08	17.92	0
12	0	-25	0.0812	67	41	98	237	50	83	60.5	39.5	0
13	0	0	0.0475	73	41	99	241	49	82	32.84	67.16	0
14	0	25	0.0268	224	51	-98	56	39	-81	45.88	54.12	0
15	0	50	0.0131	283	44	79	118	47	100	26.69	73.31	0
16	25	-50	4.00E-04	273	48	-95	100	43	-85	3.51	96.49	0
17	25	-25	0.0274	59	41	99	227	50	82	88.47	11.53	0
18	25	0	0.0257	59	41	97	230	50	84	59.58	40.42	0
19	25	25	0.0228	66	41	98	235	49	83	30.36	69.64	0
20	25	50	0.0206	91	44	99	259	47	81	15.53	84.47	0
21	50	-50	4.00E-04	157	46	93	334	44	87	85.68	14.32	0
22	50	-25	0.0114	57	41	-85	231	49	-94	46.85	53.15	0
23	50	0	0.0208	68	42	96	240	49	85	24.06	75.94	0
24	50	25	0.0099	89	43	98	259	47	83	17.01	82.99	0
25	50	50	0.0241	186	51	90	6	39	90	14.29	85.71	0

Table C.129: Full-wavefield moment tensor inversion results for location 1b, ISO input mechanism, isotropic medium, and dominant source frequency of 175 Hz with a DC constraint applied to the inversion. The bolded row is the location with the highest correlation in the grid search and thus the final ouputted result. Refer to Figure C.15c for visual.

Location Number	X Coord (m)	Y Coord (m)	Correlation	Strike 1 (°)	Dip 1 (°)	Rake 1 (°)	Strike 2 (°)	Dip 2 (°)	Rake 2 (°)	DC %	CLVD %	ISO %
1	-50	-50	0.0515	244	50	-101	80	41	-77	94.73	5.27	0
2	-50	-25	0.0413	74	40	104	236	51	78	98.87	1.13	0
3	-50	0	0.0329	71	39	102	235	52	80	94.01	5.99	0
4	-50	25	0.037	235	51	-103	76	40	-74	90.62	9.38	0
5	-50	50	0.086	141	87	-166	51	76	-3	96.67	3.33	0
6	-25	-50	0.0658	74	41	101	240	50	81	95.27	4.73	0
7	-25	-25	0.092	71	41	102	236	50	80	99.74	0.26	0
8	-25	0	0.0981	68	40	101	234	51	81	98.98	1.02	0
9	-25	25	0.0723	68	40	101	234	51	81	99.97	0.03	0
10	-25	50	0.0486	73	41	107	232	51	76	90.54	9.46	0
11	0	-50	0.0358	236	50	-97	67	41	-82	94.56	5.44	0
12	0	-25	0.0808	236	50	84	66	41	97	94.74	5.26	0
13	0	0	0.0467	69	41	102	233	50	80	96.42	3.58	0
14	0	25	0.0266	223	51	-99	57	40	-79	92.93	7.07	0
15	0	50	0.0115	172	52	93	347	38	86	9.89	90.11	0
16	25	-50	4.00E-04	273	48	-95	100	43	-85	3.51	96.49	0
17	25	-25	0.0274	59	41	99	227	50	83	99.79	0.21	0
18	25	0	0.0255	229	50	84	58	40	97	90.35	9.65	0
19	25	25	0.0222	229	50	84	58	40	97	91.54	8.46	0
20	25	50	0.0206	91	44	99	259	47	81	15.53	84.47	0
21	50	-50	4.00E-04	158	46	93	334	44	87	93.3	6.7	0
22	50	-25	0.0114	57	41	-84	229	49	-95	93.3	6.7	0
23	50	0	0.0202	230	49	86	57	41	95	99.83	0.17	0
24	50	25	0.0091	233	50	90	53	40	90	97.08	2.92	0
25	50	50	0.0226	210	51	89	32	39	91	99.4	0.6	0

Table C.130: Full-wavefield moment tensor inversion results for location 3d, ISO input mechanism, isotropic medium, and dominant source frequency of 175 Hz with no constraints applied to the inversion. The bolded row is the location with the highest correlation in the grid search and thus the final ouputted result. Refer to Figure C.15d for visual.

Location Number	X Coord (m)	Y Coord (m)	Correlation	Strike 1 (°)	Dip 1 (°)	Rake 1 (°)	Strike 2 (°)	Dip 2 (°)	Rake 2 (°)	DC %	CLVD %	ISO %
1	-50	-50	0.1897	49	45	-90	229	45	-90	4.56	20.04	-75.4
2	-50	-25	0.1736	329	45	-89	148	45	-91	11.01	4.48	-84.51
3	-50	0	0.0184	320	89	1	230	89	179	7.56	8.31	84.13
4	-50	25	0.0715	149	45	88	332	45	92	2.67	5.85	91.48
5	-50	50	0.0477	186	45	92	3	45	88	3.1	11.09	85.81
6	-25	-50	0.5071	187	44	91	6	46	89	6.7	2.99	90.31
7	-25	-25	0.1043	93	45	87	277	45	93	5.04	3.04	91.92
8	-25	0	0.063	22	90	-2	112	88	-180	7.85	1.66	-90.49
9	-25	25	0.023	321	70	-158	224	69	-21	0.82	5.62	-93.56
10	-25	50	0.0411	221	86	0	311	90	-176	4.49	7.74	-87.77
11	0	-50	0.092	198	44	92	16	46	88	8.91	0.05	91.04
12	0	-25	0.1322	22	88	176	113	86	2	6.18	2.06	91.76
13	0	0	0.0338	236	62	-151	131	64	-31	0.64	13.48	85.88
14	0	25	0.033	202	88	3	112	87	178	5.73	8.95	-85.32
15	0	50	0.0208	231	47	76	72	45	105	2.73	10.83	-86.44
16	25	-50	0.4963	253	47	69	102	47	111	2.36	5.19	-92.45
17	25	-25	0.1009	111	45	-96	299	46	-85	4.97	2.52	-92.51
18	25	0	0.0725	79	44	-78	243	47	-101	3.01	12.31	84.68
19	25	25	0.0324	66	44	-86	241	46	-94	11.22	3.23	85.55
20	25	50	0.0153	234	47	72	79	46	108	1.92	17.33	-80.75
21	50	-50	0.011	101	46	93	277	44	87	11.13	2.87	-86
22	50	-25	0.0262	252	46	87	76	44	93	15.47	0.18	-84.35
23	50	0	0.0287	248	46	87	71	44	93	11.24	3.79	-84.97
24	50	25	0.0339	72	44	-87	248	46	-93	12.7	7.4	79.9
25	50	50	0.0562	68	44	-87	244	46	-93	17.72	2.1	80.18

Table C.131: Full-wavefield moment tensor inversion results for location 3d, ISO input mechanism, isotropic medium, and dominant source frequency of 175 Hz with a deviatoric constraint applied to the inversion. The bolded row is the location with the highest correlation in the grid search and thus the final ouputted result. Refer to Figure C.15e for visual.

Location Number	X Coord (m)	Y Coord (m)	Correlation	Strike 1 (°)	Dip 1 (°)	Rake 1 (°)	Strike 2 (°)	Dip 2 (°)	Rake 2 (°)	DC %	CLVD %	ISO %
1	-50	-50	0.0979	168	46	90	348	44	90	39.71	60.29	0
2	-50	-25	0.098	210	46	90	30	44	90	24.2	75.8	0
3	-50	0	0.0117	103	45	-89	282	45	-91	31.67	68.33	0
4	-50	25	0.0409	38	44	-90	218	46	-90	18.48	81.52	0
5	-50	50	0.0277	336	44	-90	157	46	-90	28.89	71.11	0
6	-25	-50	0.2959	356	44	-90	176	46	-90	16.89	83.11	0
7	-25	-25	0.0672	358	44	-90	178	46	-90	40.31	59.69	0
8	-25	0	0.0364	222	46	90	43	44	90	18.95	81.05	0
9	-25	25	0.0129	128	45	90	308	45	90	17.29	82.71	0
10	-25	50	0.0245	116	45	90	295	45	90	16.4	83.6	0
11	0	-50	0.0508	349	44	-90	169	46	-90	27.76	72.24	0
12	0	-25	0.0787	28	44	-90	209	46	-90	22.94	77.06	0
13	0	0	0.0204	125	45	-90	304	45	-90	15.28	84.72	0
14	0	25	0.0191	223	46	90	43	44	90	18.93	81.07	0
15	0	50	0.0129	195	46	90	14	44	90	16.69	83.31	0
16	25	-50	0.3014	182	45	90	2	45	90	25.87	74.13	0
17	25	-25	0.0624	181	46	90	1	44	90	65.93	34.07	0
18	25	0	0.0434	27	44	-90	207	46	-90	17.31	82.69	0
19	25	25	0.0208	8	44	-90	188	46	-90	23.86	76.14	0
20	25	50	0.0086	217	46	90	37	44	90	17.31	82.69	0
21	50	-50	0.0069	174	45	90	354	45	90	28.52	71.48	0
22	50	-25	0.0167	191	45	90	10	45	90	26.7	73.3	0
23	50	0	0.019	183	45	90	2	45	90	31.42	68.58	0
24	50	25	0.0202	18	44	-90	198	46	-90	17.92	82.08	0
25	50	50	0.0348	4	44	-91	185	46	-89	22.89	77.11	0

Table C.132: Full-wavefield moment tensor inversion results for location 3d, ISO input mechanism, isotropic medium, and dominant source frequency of 175 Hz with a DC constraint applied to the inversion. The bolded row is the location with the highest correlation in the grid search and thus the final ouputted result. Refer to Figure C.15f for visual.

Location Number	X Coord (m)	Y Coord (m)	Correlation	Strike 1 (°)	Dip 1 (°)	Rake 1 (°)	Strike 2 (°)	Dip 2 (°)	Rake 2 (°)	DC %	CLVD %	ISO %
1	-50	-50	0.0948	172	46	90	353	44	90	92.52	7.48	0
2	-50	-25	0.098	210	46	90	30	44	90	24.2	75.8	0
3	-50	0	0.009	109	46	-90	289	44	-90	93.5	6.5	0
4	-50	25	0.0358	5	44	-90	185	46	-90	96.96	3.04	0
5	-50	50	0.0277	336	44	-90	157	46	-90	28.89	71.11	0
6	-25	-50	0.2959	356	44	-90	176	46	-90	16.89	83.11	0
7	-25	-25	0.0657	357	44	-90	178	46	-90	95.69	4.31	0
8	-25	0	0.0287	188	45	86	13	45	94	99.35	0.65	0
9	-25	25	0.0129	128	45	90	308	45	90	17.29	82.71	0
10	-25	50	0.0245	116	45	90	295	45	90	16.4	83.6	0
11	0	-50	0.0508	349	44	-90	169	46	-90	27.76	72.24	0
12	0	-25	0.0787	28	44	-90	209	46	-90	22.94	77.06	0
13	0	0	0.018	338	44	-91	159	46	-89	99.22	0.78	0
14	0	25	0.0153	200	46	92	17	44	88	91.11	8.89	0
15	0	50	0.0129	195	46	90	14	44	90	16.69	83.31	0
16	25	-50	0.2853	181	46	90	1	44	90	91.28	8.72	0
17	25	-25	0.0619	180	46	91	360	44	89	90.86	9.14	0
18	25	0	0.0434	27	44	-90	207	46	-90	17.31	82.69	0
19	25	25	0.0208	8	44	-90	188	46	-90	23.86	76.14	0
20	25	50	0.0075	178	45	87	2	45	93	97.2	2.8	0
21	50	-50	0.0066	177	46	90	358	44	90	93.25	6.75	0
22	50	-25	0.0159	184	46	91	2	44	89	95.96	4.04	0
23	50	0	0.0183	178	46	90	358	44	90	96.97	3.03	0
24	50	25	0.0202	18	44	-90	198	46	-90	17.92	82.08	0
25	50	50	0.0348	4	44	-91	185	46	-89	22.89	77.11	0

Table C.133: Full-wavefield moment tensor inversion results for location 3e, ISO input mechanism, isotropic medium, and dominant source frequency of 175 Hz with no constraints applied to the inversion. The bolded row is the location with the highest correlation in the grid search and thus the final ouputted result. Refer to Figure C.15g for visual.

Location Number	X Coord (m)	Y Coord (m)	Correlation	Strike 1 (°)	Dip 1 (°)	Rake 1 (°)	Strike 2 (°)	Dip 2 (°)	Rake 2 (°)	DC %	CLVD %	ISO %
1	-50	-50	0.2099	181	45	93	357	45	87	11.85	1.13	87.02
2	-50	-25	0.0733	36	45	-90	216	45	-90	3.68	25.86	-70.46
3	-50	0	0.0902	313	79	-169	221	79	-11	2.55	4.16	-93.29
4	-50	25	0.0648	205	86	-1	295	89	-176	4.35	7.14	-88.51
5	-50	50	0.0502	47	45	-83	218	46	-96	5.26	7.68	87.06
6	-25	-50	0.1148	311	84	7	220	83	174	3.31	4.42	92.27
7	-25	-25	0.3087	144	42	88	328	48	92	0.23	2.55	97.22
8	-25	0	0.319	297	89	-174	206	84	-1	5.53	0.06	-94.41
9	-25	25	0.0676	250	43	88	73	47	92	6.95	10.97	-82.08
10	-25	50	0.052	59	46	-73	215	47	-106	1.91	15.07	83.02
11	0	-50	0.0703	218	86	-179	128	89	-4	3.38	10.21	86.41
12	0	-25	0.1655	228	71	-171	135	81	-19	0.8	3.35	95.85
13	0	0	0.5925	239	44	83	70	46	97	5.78	3.63	-90.59
14	0	25	0.1518	54	44	-79	218	47	-101	3.31	8.29	88.4
15	0	50	0.0341	227	45	87	51	45	93	12.34	2.05	-85.61
16	25	-50	0.0385	92	48	-76	252	44	-105	1.63	16.2	82.17
17	25	-25	0.0872	90	48	-87	266	42	-93	7	4.97	88.03
18	25	0	0.0214	253	44	87	77	47	93	13.58	0.34	-86.08
19	25	25	0.0018	77	47	-87	253	43	-93	13.72	0.62	85.66
20	25	50	6.00E-04	61	46	-88	238	44	-92	18.72	1.11	80.17
21	50	-50	0.0162	84	46	-86	259	44	-94	7.04	14.62	78.34
22	50	-25	0.0024	258	44	87	81	46	93	13.91	1.54	-84.55
23	50	0	0.0018	244	45	87	68	45	93	14.92	1.22	-83.86
24	50	25	0.0018	245	45	87	69	46	93	12.25	4.04	-83.71
25	50	50	1.00E-04	58	41	-87	234	49	-93	19.17	6.46	74.37

Table C.134: Full-wavefield moment tensor inversion results for location 3e, ISO input mechanism, isotropic medium, and dominant source frequency of 175 Hz with a deviatoric constraint applied to the inversion. The bolded row is the location with the highest correlation in the grid search and thus the final ouputted result. Refer to Figure C.15h for visual.

Location Number	X Coord (m)	Y Coord (m)	Correlation	Strike 1 (°)	Dip 1 (°)	Rake 1 (°)	Strike 2 (°)	Dip 2 (°)	Rake 2 (°)	DC %	CLVD %	ISO %
1	-50	-50	0.1251	128	45	-90	308	45	-90	17.85	82.15	0
2	-50	-25	0.0333	148	45	90	328	45	90	85.21	14.79	0
3	-50	0	0.0582	123	46	90	303	44	90	27.31	72.69	0
4	-50	25	0.04	114	45	90	294	45	90	15.93	84.07	0
5	-50	50	0.0323	341	44	-90	161	46	-90	19.65	80.35	0
6	-25	-50	0.0698	120	45	-90	300	45	-90	16.7	83.3	0
7	-25	-25	0.1969	341	45	-90	162	45	-90	23.53	76.47	0
8	-25	0	0.1997	145	45	90	325	45	90	22.78	77.22	0
9	-25	25	0.0438	110	46	90	290	44	90	16.8	83.2	0
10	-25	50	0.0317	356	44	-90	177	46	-90	16.2	83.8	0
11	0	-50	0.0431	118	46	-90	298	44	-90	15.75	84.25	0
12	0	-25	0.108	331	45	-90	151	45	-90	36.85	63.15	0
13	0	0	0.372	154	45	90	334	45	90	26.27	73.73	0
14	0	25	0.0977	344	44	-91	165	46	-89	32.63	67.37	0
15	0	50	0.0232	154	45	91	333	45	89	35.73	64.27	0
16	25	-50	0.0235	115	46	-90	296	44	-90	15.99	84.01	0
17	25	-25	0.0573	325	45	-90	145	45	-90	32.25	67.75	0
18	25	0	0.0141	148	45	90	328	45	90	29.79	70.21	0
19	25	25	0.0012	325	45	-90	144	45	-90	38.16	61.84	0
20	25	50	4.00E-04	330	45	-90	149	45	-90	27.77	72.23	0
21	50	-50	0.0095	114	46	-90	295	44	-90	15.12	84.88	0
22	50	-25	0.0016	152	45	90	333	45	90	31.55	68.45	0
23	50	0	0.0011	158	45	90	338	45	90	33.08	66.92	0
24	50	25	0.0012	152	45	90	332	45	90	42.8	57.2	0
25	50	50	1.00E-04	346	44	-94	171	46	-86	18.21	81.79	0

Table C.135: Full-wavefield moment tensor inversion results for location 3e, ISO input mechanism, isotropic medium, and dominant source frequency of 175 Hz with a DC constraint applied to the inversion. The bolded row is the location with the highest correlation in the grid search and thus the final ouputted result. Refer to Figure C.15i for visual.

Location Number	X Coord (m)	Y Coord (m)	Correlation	Strike 1 (°)	Dip 1 (°)	Rake 1 (°)	Strike 2 (°)	Dip 2 (°)	Rake 2 (°)	DC %	CLVD %	ISO %
1	-50	-50	0.1251	128	45	-90	308	45	-90	17.85	82.15	0
2	-50	-25	0.0333	149	46	90	329	44	90	93.67	6.33	0
3	-50	0	0.0551	136	46	89	318	44	91	92.47	7.53	0
4	-50	25	0.0361	140	45	91	318	45	89	97.24	2.76	0
5	-50	50	0.0323	341	44	-90	161	46	-90	19.65	80.35	0
6	-25	-50	0.0698	120	45	-90	300	45	-90	16.7	83.3	0
7	-25	-25	0.1969	341	45	-90	162	45	-90	23.53	76.47	0
8	-25	0	0.1902	149	45	90	329	45	90	97.9	2.1	0
9	-25	25	0.0438	110	46	90	290	44	90	16.8	83.2	0
10	-25	50	0.0317	356	44	-90	177	46	-90	16.2	83.8	0
11	0	-50	0.0431	118	46	-90	298	44	-90	15.75	84.25	0
12	0	-25	0.1056	334	45	-90	154	45	-90	94.29	5.71	0
13	0	0	0.3563	154	45	90	334	45	90	97.52	2.48	0
14	0	25	0.0977	344	44	-91	165	46	-89	32.63	67.37	0
15	0	50	0.0227	152	46	91	330	44	89	98.92	1.08	0
16	25	-50	0.0212	331	44	-89	150	46	-91	95.81	4.19	0
17	25	-25	0.0557	331	44	-89	151	46	-91	92.75	7.25	0
18	25	0	0.0135	152	45	90	332	45	90	94.41	5.59	0
19	25	25	0.0012	328	45	-90	147	45	-90	91.31	8.69	0
20	25	50	4.00E-04	330	45	-90	149	45	-90	27.77	72.23	0
21	50	-50	0.0082	326	44	-87	142	46	-93	99.27	0.73	0
22	50	-25	0.0015	156	45	90	337	45	90	96.89	3.11	0
23	50	0	0.0011	157	45	90	337	45	90	94.81	5.19	0
24	50	25	0.0011	153	45	90	333	45	90	90.45	9.55	0
25	50	50	1.00E-04	346	44	-94	171	46	-86	18.21	81.79	0

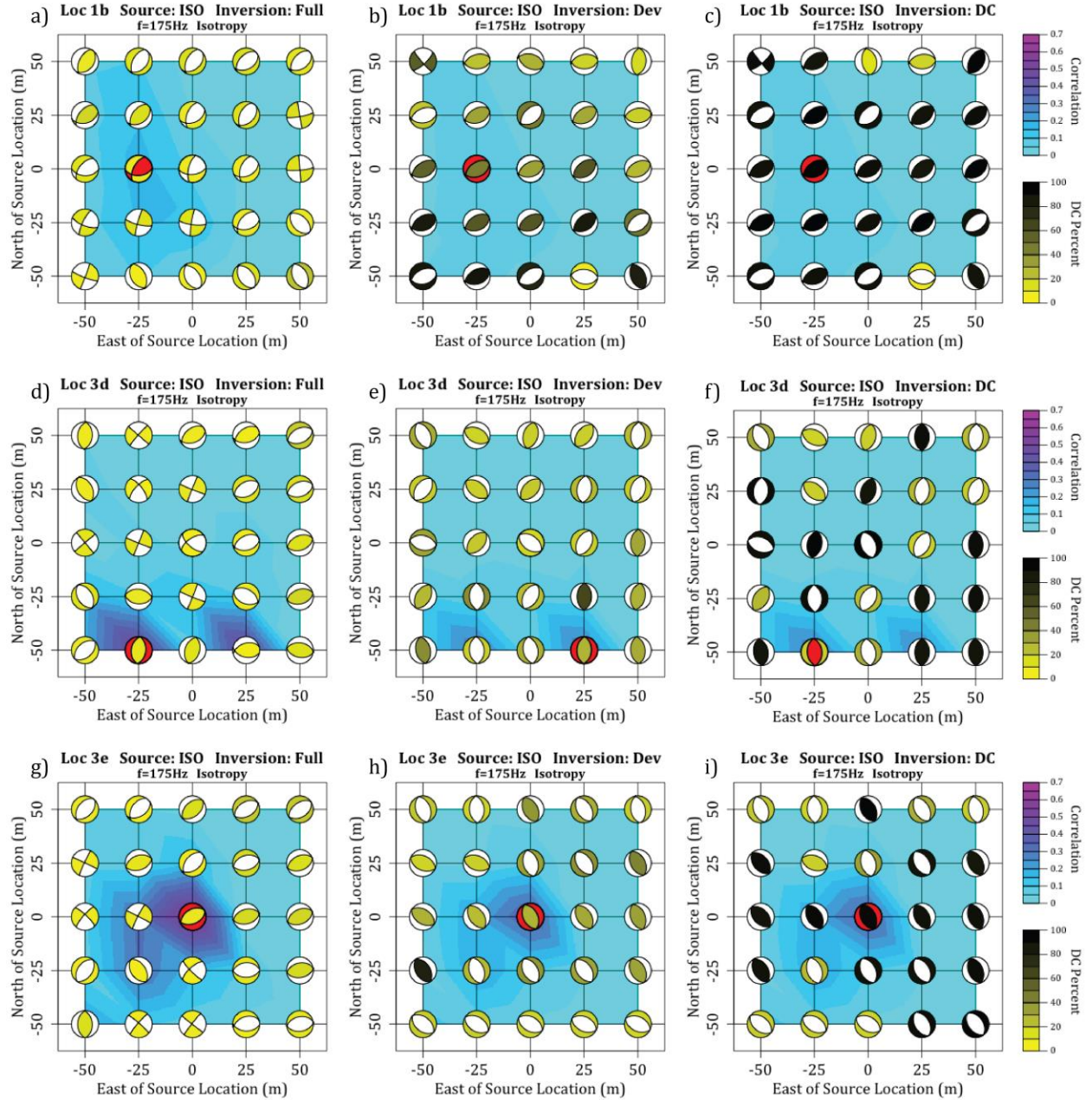


Figure C.15: Full-wavefield moment tensor inversion results for an ISO source mechanism in an isotropic medium and source frequency of 175 Hz for a) location 1b with no constraints on the inversion, b) location 1b with a deviatoric constraint, c) location 1b with a DC constraint, d) location 3d with no constraints, e) location 3d with a deviatoric constraint, f) location 3d with a DC constraint, g) location 3e with no constraints, h) location 3e with a deviatoric constraint, and i) location 3e with a DC constraint. The red beach-ball is the location and source mechanism with the highest correlation to the input seismograms. Refer to Tables C.127-C.135 for numerical values of results.

Vita

Trudy L. Watkins is from Houston, TX and completed her B.S. in Geophysics and Mathematics at Texas Tech University. She was a geophysics intern at Alta Mesa in Houston, TX after completion of her undergraduate studies. She chose to further her desire to learn more about geophysics and attended graduate school in the Department of Geology and Geophysics at Louisiana State University. For two summers during graduate school, she was a geophysics intern at Occidental Petroleum in Houston, TX and will work there full-time after completion of her Master's.